

Physicochemical Problems of Mineral Processing

**Volume 49, Issue 1
2013**

www.minproc.pwr.wroc.pl/journal
www.dbc.wroc.pl/dlibra/publication/11251



Oficyna Wydawnicza Politechniki Wrocławskiej
Wrocław 2013

Editors

Jan Drzymala editor-in-chief

Adriana Zalewska

Paweł Nowak

Editorial Board

Ashraf Amer, Wiesław Blaschke, Marian Brożek, Stanisław Chibowski, Tomasz Chmielewski,
Beata Cwalina, Janusz Girczys, Andrzej Heim, Jan Hupka, Andrzej Konieczny, Teofil Jesionowski,

Janusz Laskowski, Andrzej Łuszczkiewicz, Kazimierz Małysa, Andrzej Pomianowski,
Stanisława Sanak-Rydlewska, Jerzy Sablik, Kazimierz Sztaba, Barbara Tora, Kazimierz Tumidajski,
Zygmunt Sadowski

Production Editor

Marek J. Battek

The papers published in the Physicochemical Problems of Mineral Processing journal are abstracted
in BazTech, Chemical Abstracts, Coal Abstracts, EBSCO, Google Scholar, Scopus, Thomson Reuters
(Science Citation Index Expanded, Materials Science Citation Index, Journal Citation Reports)
and other sources

This publication was supported in different forms by

Komitet Górnictwa PAN (Sekcja Wykorzystania Surowców Mineralnych)

Akademia Górniczo-Hutnicza w Krakowie

Politechnika Śląska w Gliwicach

Politechnika Wroclawska

©Copyright by Oficyna Wydawnicza Politechniki Wroclawskiej, Wrocław 2013

ISSN 1643-1049 (print)

previously 0137-1282

ISSN 2084-4735 (online)

OFICyna WYDAWNICZA POLITECHNIKI WROCLAWSKIEJ

Wybrzeże Wyspiańskiego 27, 50-370 Wrocław, Poland

CONTENTS

B. Rewerski, S. Mielnicki, I. Bartosiewicz, H. Polkowska-Motrenko, A Sklodowska, <i>Uranium post-mining wastes as a potential reserve source of uranium for nuclear energy plants</i>	5
T. Suponik, <i>Groundwater treatment with the use of zero-valent iron in the permeable reactive barrier technology</i>	13
A. Lutynski, T. Suponik, M. Lutynski, <i>Investigation of coal slurry properties deposited in impoundments located in the upper silesian coal basin</i>	25
A. Stefanova, J. Aromaa, O. Forsen, <i>Alkaline leaching of zinc from argon oxygen decarbonization dust from stainless steel production</i>	37
A. Holda, E. Kisielowska, <i>Biological removal of Cr(VI) ions from aqueous solutions by Trichoderma viride</i>	47
M.G. Hasab, F. Rashchi, S. Raygan, <i>Chloride–hypochlorite oxidation and leaching of refractory sulfide gold concentrate</i>	61
J.A. Baranska, Z. Sadowski, <i>Bioleaching of uranium minerals and biosynthesis of UO₂ nanoparticles</i>	71
R. Modrzewski, P. Wodzinski, <i>Analysis of screening process of crushed basalt performed by a double-frequency screen</i>	81
A. Rapacz-Kmita, E. Stodolak-Zych, M. Dudek, B. Szaraniec, A. Rozycka, M. Mosialek, L. Mandecka-Kamien, <i>Degradation of nanoclay-filled polylactide composites</i>	91
L. Rusanen, J. Aromaa, O. Forsen, <i>Pressure oxidation of pyrite-arsenopyrite refractory gold concentrate</i>	101
M. Kotyczka-Moranska, G. Tomaszewicz, <i>Application of Polish calcium sorbents in carbonate looping</i>	111
D. Saramak, <i>Mathematical models of particle size distribution in simulation analysis of high-pressure grinding roll operations</i>	121
L. Gotfryd, G. Pietek, <i>Contaminants of post-leaching copper solutions and their behavior during extraction with industrial extractants</i>	133
A. Mehdilo, M. Irannajad, H. Zarei, <i>Flotation of zinc oxide ore using cationic and cationic-anionic mixed collectors</i>	145
A. Tasdemir, <i>Analysis of chromite processing plant data by first order autoregressive model</i>	157
T. Niedoba, <i>Statistical analysis of the relationship between particle size and particle density of raw coal</i>	175
A. Konieczny, W. Pawlos, M. Krzeminska, R. Kaleta, P. Kurzydlo, <i>Evaluation of organic carbon separation from copper ore by pre-flotation</i>	189
A. Gul, G. Bulut, A.A. Sirkeci, <i>Beneficiation of an arsenic bearing complex sulphide ore by flotation</i>	203
J. Konczyk, C. Kozłowski, W. Walkowiak, <i>Lead(II) removal from aqueous solutions by solvent extraction with tetracarboxylresorcin[4]arene</i>	213
R. Matlakowska, D. Ruszkowski, A. Sklodowska, <i>Microbial transformations of fossil organic matter of Kupferschiefer black shale – elements mobilization from metalloorganic compounds and metalloporphyrins by a community of indigenous microorganisms</i>	223
M. Gharabaghi, M. Irannajad, A.R. Azadmehr, <i>Separation of nickel and zinc ions in a synthetic acidic solution by solvent extraction using D2EHPA and Cyanex 272</i>	233
D. Saramak, Z. Naziemiec, <i>Determination of the nip zone angle in high-pressure grinding rolls</i> ...	243

F. Nakhaei, M. Irannajad, <i>Comparison between neural networks and multiple regression methods in metallurgical performance modeling of flotation column</i>	255
M. Kolodziejska, C. Kozłowski, M. Ulewicz, <i>Separation of lead(II) and copper(II) by plasticizer membranes with sulphur analogus of phosphinic acids as carriers</i>	267
M. Poleski, J. Luczak, R. Aranowski, C. Jungnickel, <i>Wetting of surfaces with ionic liquids</i>	277
I. Cichowska-Kopczynska, M. Joskowska, A. Wojciechowska, R. Aranowski, <i>Preparation and physicochemical characterisation of ceramic supports for supported liquid membranes</i>	287
P. Otremska, J. Gega, <i>Kinetic studies on sorption of Ni(II) and Cd(II) from chloride solutions using selected acidic cation exchangers</i>	301
A. Rogala, J. Krzysiek, M. Bernaciak, J. Hupka, <i>Non-aqueous fracturing technologies for shale gas recovery</i>	313
T. Marciniszyn, <i>Unusual application of porous matrix made from quartzite schist</i>	323
K. El Amari, E.-A. Jdid, P. Blazy <i>Copper recovery from chalcopyrite concentrate acid leach solutions by Acorga M5397</i>	329
M. Brozek, A. Mlynarczykowska, <i>An analysis of effect of particle size on batch flotation of coal</i>	341
K. Ochromowicz, T. Chmielewski, <i>Solvent extraction of copper(II) from concentrated leach liquors</i>	357
R.O. Ajemba, O.D. Onukwuli, <i>Adsorptive removal of colour pigment from palm oil using acid activated Nteje clay. Kinetics, equilibrium and thermodynamics</i>	369

Received April 16, 2012; reviewed; accepted May 13, 2012

URANIUM POST-MINING WASTES AS A POTENTIAL RESERVE SOURCE OF URANIUM FOR NUCLEAR ENERGY PLANTS

**Bartosz REWERSKI¹, Sebastian MIELNICKI¹, Iwona BARTOSIEWICZ²,
Halina POLKOWSKA-MOTRENKO², Aleksandra SKLODOWSKA¹**

¹ Laboratory of Environmental Pollution Analysis, Faculty of Biology, University of Warsaw, Miecznikowa 1, 02-096 Warsaw, Poland; corresponding author: asklodowska@biol.uw.edu.pl

² Laboratory of Nuclear Analytical Methods, Institute of Nuclear Chemistry and Technology, Dorodna 16, 03-195 Warsaw, Poland

Abstract: Biotechnology is an effective and environmental friendly method of waste utilization and poor refractory ores exploitation, well known since 1949 and successfully developed in many countries: Spain, Bulgaria, USA, and Sweden. Biotechnology opens the possibility to obtain uranium as by-product in rare element recovery process (eg. Co, Au, Re, Rh, Pt) and positively affects the economic efficiency of technology. The research program of biological exploitation of waste and poor ores in Poland is presented. Microbial consortia able to oxidize iron under neutral and acidic conditions (Fe concentration in ore is 1.8–3.4%) are isolated and developed during project realization.

Key words: *uranium, bacteria, bioleaching, solid waste*

Introduction

Uranium is commonly found in very small amounts in environment. All isotopes and compounds of U are toxic and radioactive. The average U concentration in the earth's crust is about 1.7–2.0 mg/kg (Kabata-Pendias and Mukherjee, 2007) and can be released to the surface and ground waters from rocks and ores by dissolution and desorption or by diffusion.

Soils of Poland contain average amounts of U at the value of 1.6 mg/kg (lowland) and up to >10 mg/kg in the mountain soils (Sudety Mts). Uranium is a basic fuel for nuclear power plants and U production was estimated at the level of 53.66 Gg (giga-grams) (ESA Annual Report 2010).

The uranium exploration and exploitation in the South-West Poland (Lower Silesia District) was carried out since 1925 when the first 9 Mg of uranium ore were mined of

which 690 mg of radium was extracted and mining was developing to 1962 and about 704 Mg of U was derived (Adamski, 2000). Nevertheless the old subsurface mines, piles and dumps are still involved in the geochemical cycle of the area. The dumping of mineral wastes containing 11 mining residues of radionuclides and heavy metals and their influence on the environment is a problem in many mining regions. Leaching of uranium and radionuclides is a serious environmental problem in many countries (Baranowski and Bozau, 2006; Kalinowski et al., 2004; 2006).

According to Piestrzynski et al. (1996) mined uranium ores explored in the Lower Silesia region were polymetallic and contained: pitchblende, uraninite, autunite, metautunite, uranocircite, torbernite, metatorbernite, uranophane, sklodowskite, gummite, fourmarierite and libegite. Investigations of the influence of mining activity on the natural environment revealed the local-scale radioactive contamination limited to the dumps and their nearest vicinity at four localities: Kowary-Podgorze, Radoniów, Kopaniec and Kletno. It is worth mentioning that some fragments of uranium ores contain up to 0.15 wt.% of U in the dump material. However, the content of uranium deposited in piles and dumps remains completely unrecognized although it may be a source of this element recovered by biotechnology.

Exploitation of refractory ores and uranium post-mining wastes in Poland is considered as reserve source of uranium for nuclear power plants. The Frame Program of Activities for Nuclear Energy predicts the recognition of different way of uranium source exploitation including the use of biotechnology. Uranium ores in Poland contain approximately 250 to 1100 mg/kg U and the total hypothetical amount of uranium in Poland was estimated at 0.1 Gg. Average demand of uranium for 1 GW energy is calculated at the level 180 Mg and it was estimated that projected Polish nuclear plants need about 32.4 Gg uranium during sixty years of exploitation (Miecznik et al., 2011)

Upper Carboniferous and Lower Permian rocks (Grzmiąca, Wambierzyce and Okrzeszyn deposits) and origin of sandstone type uranium deposits are located in the Lower Zechstein mineralization in Fore-Sudetic Monocline, Poland and in the Region of Wałbrzych and Jelenia Góra. The studies revealed that in the Lower Zechstein mineralization the chief carriers of radioactive elements (U and Th) are organic compounds occurring in shale (Kupferschiefer) and shale in Zechstein sandstone conglomerate, and that thorium appears only in trace amounts. Maximum U contents in shale are 163 ppm. The only exceptions are samples with large secretion-type concentrations of thucholite. In one of them the U content was as high as 0.89%. Average uranium concentration in Grzmiąca deposit is 540 mg/kg and the total uranium content is calculated at the level of 670–820 Mg and in Okrzeszyn deposit about 937 Mg (Solecki et al., 2011). Uranium content in other sandstone type deposits was calculated at the level of 1.1 Gg.

Preliminary studies carried out in the first stage of project “Meeting the Polish nuclear power engineering’s demand for fuel – fundamental aspects” which is realized in the frame of strategic research program “Technologies Supporting Development of Safe Nuclear Power Engineering” were focused on sampling of refractory ores and

uranium post-mining wastes deposited in dumps and piles in Lower Silesia region. The concentration of U and Th, Cu, Co, Mn, Zn, La, Yb, Mo, Ni, Sb and Fe was estimated using ICP-MS technique after acid digestion of mineral sample in high pressure microwave digestion system or alkali fusion. Results received for uranium and iron from the richest dumps are presented in Table 1.

Table 1. Uranium concentration, pH and dose rate in materials deposited in selected piles of Kłodzko and Jelenia Góra Valleys

No.	Sample	pH	$\mu\text{S/h}$	Background $\mu\text{S/h}$	U mg/kg	Fe mg/kg
1.	Grzmiąca	4.2–5.8	0.51–1.94	0.14	20.5–112,8	23978–35556
2.	Okrzyszyn	6.1	2,5	0.22	86,3–130	20300–3600
3.	Kletno	5.8–7.0	0.20–0.61	0.22	4.82–62.3	46000
4.	Bobrowniki	5.2	1	0.22	143	58500
5.	Dziecmorowice	6.9	0.77	0.22	195	26900
6.	Radoniów	5.8–6.0	1.5–4.4	0.22	306–801	18700–25200
7.	Kromnów	5.7	4.2–16.8	0.22	2261	20200
8.	Kopaniec	6.1	2.8	0.22	733–2400	65800
9.	Wojcieszyce	4.6	1.7	0.22	193	27800

These preliminary results clearly show that material deposited in dumps may be useful for bioleaching (biotechnological) processes.

Biotechnology is an effective and environmental friendly method of waste utilization and poor refractory ores exploitation, well known since 1949 and successfully developed in many countries: Spain, Bulgaria, USA and Sweden. Biotechnology opens the possibility to obtain uranium as by-product in rare element recovery process (eg. Co, Au, Re, Rh, Pt) and positively affects the economic efficiency of technology (Chmielewski et al., 2002).

The known industrial applications of uranium ores/waste bioleaching are based on chemical-bacterial leaching, percolation leaching, mine waters biotransformation and heap/dump leaching. Bioleaching technique could be and practically is economic on an industrial scale when using materials containing below 0.03% U_3O_8 .

Bacterial leaching of uranium is a two-step process (Figs 1 and 2). First, pyrite bioleaching is carried out, then the product of this process leaches the uranium ore/material. All applied industrial technologies are carried out in acidic environment but bioleaching processes on large laboratory scale in neutral or slightly alkaline pH were described. The main microorganisms used in these processes belong to the genus *Acidithiobacillus*, *Leptospirillum* and *Sulfobacillus*. Other microorganisms including

heterotrophs, fungi (e.g. *Penicillium* sp.) and yeasts (e.g. *Rhodotorula* sp.) are useful in this process. All mentioned microorganisms show high tolerance to heavy metals ions as well as uranyl ions (Munioz et al., 1995; Chmielewski et al., 2002).

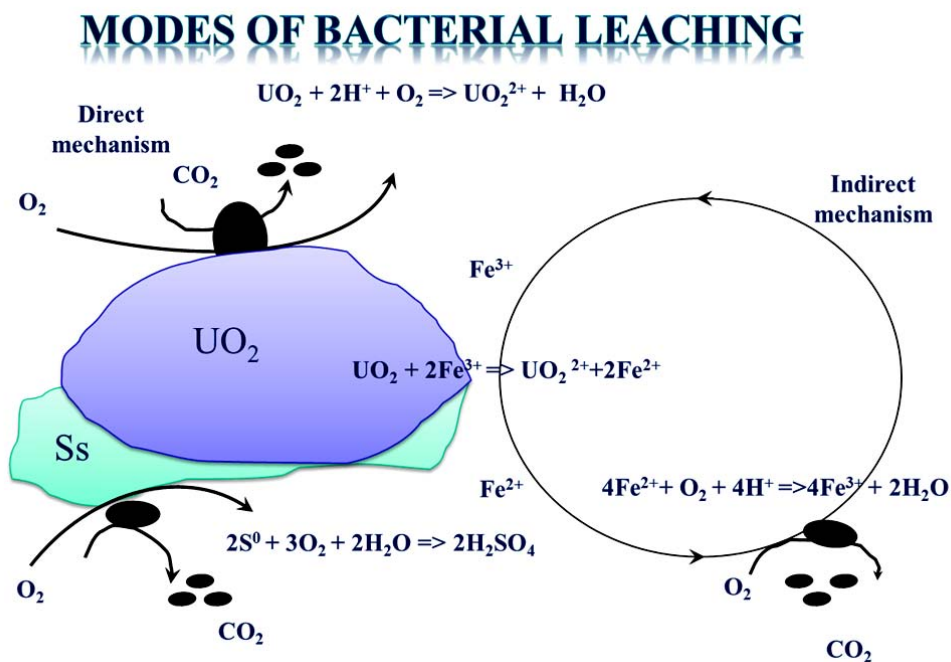


Fig. 1. Direct and indirect bacterial leaching of uranium

The efficiency of bacterial bioleaching processes can reach 98% of metal content. Some species of fungi are able to leach uranium in indirect way (Fig. 1). This process was described by Mishra et al. (2009) for the ore of Jaduguda, Bhatin and Nawapahar of UCIL India. The strains isolated from mine water were used for *in situ* leaching of mainly oxide low grade uranium ore of Turamdih mine containing 0.03% U_3O_8 . The maximum recovery of 71% uranium was obtained with the strain *Cladosporium oxysporum*. The other two strains belonging to *Aspergillus flavus* and *Curvularia clavata* gave 59% and 50% of metal recovery, respectively, from the same ore.

We have isolated and developed 25 microbial consortia able to oxidize iron under neutral and acidic conditions (Fe concentration in ore is 1.8–3.4%) during realization of the mentioned strategic project. Microbial consortia active in neutral pH were able to acidification of culture. The 8 most active consortia were chosen for further experiments and they were able to acidify the environment from pH =7.0 to < 3.0 in 14 days.

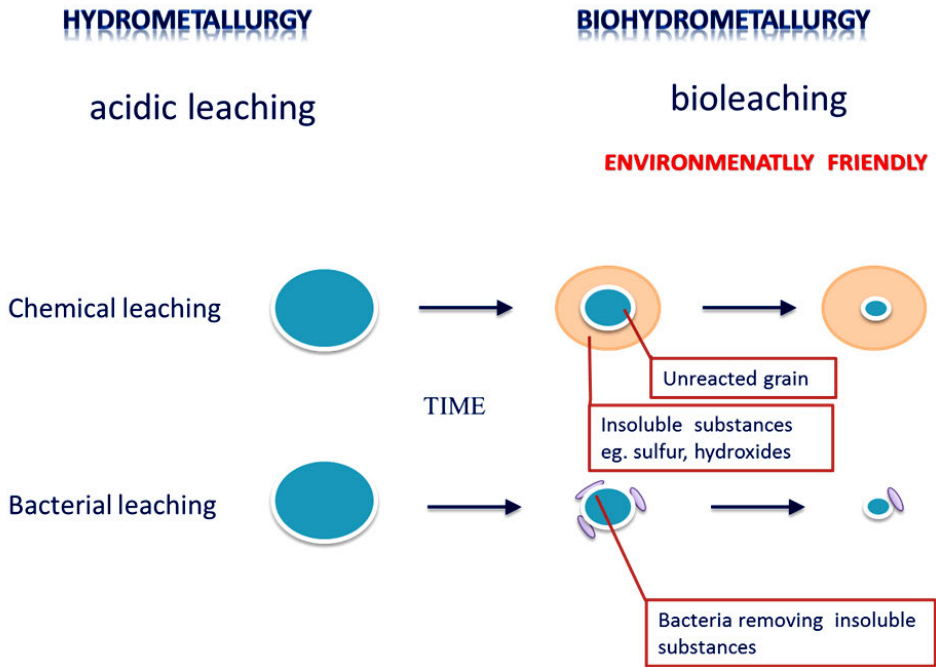


Fig. 2. Comparison of chemical and bacterial leaching process

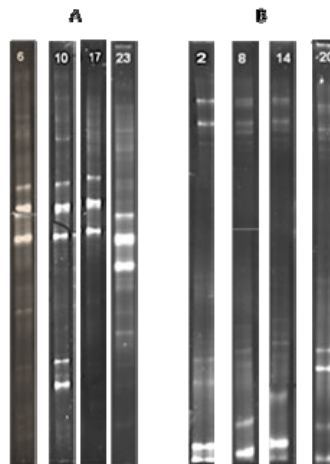


Fig. 3. The 8 most active consortia after Denaturing Gradient Gel Electrophoresis (DGGE). **A** – Microbial consortia active in neutral pH were able to acidification of culture and acidify ore/waste suspension from pH =7.0 to < 3,0 in 14 days. **B** – Consortia able to grow in acidic condition in pH 1.5–2.5

The most active consortia in both acidic and neutral pH were isolated from the Kromnów dump which contains the richest uranium material (up to 2261 mg/kg, Ta-

ble 1). Three unidentified species can be distinguished in microbial consortia active in neutral pH and 4–6 species in consortia growing in acidic conditions (Fig. 3).

Biorecovery efficiency reached during preliminary experiments was:

- in neutral pH – up to 30% of uranium content in ore/waste,
- in acidic conditions without any amendments 90%

and efficiency of chemical leaching with sulphuric acid was 10–60% of uranium content in ore/waste without bacteria.

Conclusions

The presented results are preliminary and they were received during the first 4 months of project realization. However, they seem to be very promising for biotechnological application. The biometallurgy technique has to be considered for some low small and specific grade sources because of its efficiency and low environmental impact if it is used cautiously under well described environmental condition. Moreover, this technique may be used for environment reclamation in post-mining areas. The economic efficiency may be significantly improved by the recovery of rare metals present in wastes and ores. The economic risk of development of new biotechnology of microbial leaching of the substrate for nuclear fuel production is lowered by the alternative use of recovered uranium for production of UO_2/UO_3 catalyst based on nanoparticles produced by microorganisms under anaerobic conditions.

Acknowledgement

This work was supported by strategic research project No. SP/J/3/143045/11 from The National Centre for Research and Development (NCBiR), Poland.

References

- ADAMSKI W., 2000, *Wpływ pouranowych wyrobisk górniczych na środowisko człowieka*, in: *Człowiek Środowisko Zagrożenia*, pod red. M. Zdulskiego, Wydawnictwo Nauczycielskie, Jelenia Góra.
- BABOROWSKI M., BOZAU E., 2006, *Impact of former mining activities on the uranium distribution in the River Saale (Germany)*, *Applied Geochemistry* 21, 1073–1082.
- CHMIELEWSKI T., FARBISZEWSKA T., FARBISZEWSKA-KICZMA J., KARAŚ H., MORIN D., MUSZER A., SADOWSKI Z. SKŁODOWSKA A., 2002, *Biometalurgia metali nieżelaznych – podstawy i zastosowanie*, pod redakcją Charewicza W., Wyd. CBPM „Cuprum”, Uniwersytet Wrocławski, Instytut Nauk Geologicznych, Wrocław.
- EURATOM SUPPLY AGENCY (ESA), Annual Report 2010, Luxembourg.
- KABATA-PENDIAS A., MUKHERJEE A.B., 2007, *Trace Elements from Soil to Human*, Springer-Verlag, Berlin, Heidelberg, New York.
- KALINOWSKI B. E., OSKARSSON A., ALBINSSON Y., ARLINGER J., ÖDEGAARD-JENSEN A., ANDLID T., PEDERSEN K., 2004, *Microbial leaching of uranium and other trace elements from shale mine tailings at Ranstad*, *Geoderma*, 122, 177–1944.
- KALINOWSKI, B. E., JOHNSON, A. A., ARLINGER, J., PEDERSEN, K., 2006, *Microbial Mobilization of Uranium from Shale Mine Waste*, *Geomicrobiology Journal*, 23, 157–164.

- MIECZNIK J.B., STRZELECKI R., WOŁKOWICZ S., 2011, *Uran w Polsce – historia poszukiwań i perspektywy odkrycia złóż*, Przegląd Geologiczny, 59, 688–697.
- MISHRA A., PRADHAN N., KAR R.N., L.B. SUKLA, MISHRA B.K., 2009, *Microbial recovery of uranium using native fungal strains*, Hydrometallurgy, 95, 175–177.
- MUNOZ J.A., GONZALEZ F., BLAZQUEZ A., BALLISTER A., 1995, *A study of the bioleaching of a Spanish uranium ore. Part I: A review of the bacterial leaching in the treatment of uranium ores*, Hydrometallurgy, 38, 39–57.
- MUNOZ J.A., GONZALEZ F., BLAZQUEZ A., BALLISTER A., 1995, *A study of the bioleaching of a Spanish uranium ore. Part II: Orbital shaker experiments*, Hydrometallurgy, 38, 59–78
- MUNOZ J.A., GONZALEZ F., BLAZQUEZ A., BALLISTER A., 1995, *A study of the bioleaching of a Spanish uranium ore. Part III: Column experiments*, Hydrometallurgy, 38, 79–97.
- PIESTRZYŃSKI J., PIECZONKA W., MIELNICZUK E., CHRUŚCIEL P., JODŁOWSKI P., 2006, *Effects of uranium mining on the contamination of some areas in Poland*, in: *Planning for environmental restoration of radioactively contaminated sites in central and eastern Europe*, Volume 1; Identification and characterization of contaminated sites, IAEA-Vienna 2006, TECDOC-865, 193–216.
- SOLECKI A., ŚLIWIŃSKI W., WOJCIECHOWSKA I., TCHÓRZ-TRZECIAKIEWICZ D., SYRYCZYŃSKI P., SADOWSKA M., MAKOWSKI B., 2011, *Ocena możliwości występowania mineralizacji uranowej w Polsce na podstawie wyników prac geologiczno-poszukiwawczych*, Przegląd Geologiczny, 59, 93–110.

Received May 1, 2012; reviewed; accepted May 12, 2012

GROUNDWATER TREATMENT WITH THE USE OF ZERO-VALENT IRON IN THE PERMEABLE REACTIVE BARRIER TECHNOLOGY

Tomasz SUPONIK

Politechnika Śląska, Wydział Górnictwa i Geologii, ul. Akademicka 2; 44-100 Gliwice, Poland
Tomasz.Suponik@polsl.pl

Abstract: The industrial dumping sites located in the southern provinces of Poland pollute groundwaters with metals. In the article, the possibility of groundwater (polluted by metals) treatment with the use of Permeable Reactive Barrier Technology has been presented. In this technology, the contaminants are removed from the aquifer by a flow of the groundwater through a PRB filled with a special reactive material. The wastewater (which simulated groundwater) circulated through the column filled with zero-valent iron in the laboratory tests. During the tests, the treatment processes proceeded. Chromium, copper, nickel, cobalt, lead, cadmium and zinc, occurring in the water as cations and anions, have been removed in the iron bed. The rapid metal removal has likely occurred due to the reduction and precipitation/co-precipitation and/or due to adsorption onto the iron metal surface or/and onto the iron corrosion products. Barium Ba^{2+} was the only metal, which has not been removed from the wastewater in the column. A rapid decrease of the redox potential and oxygen concentration as well as an increases of the pH value and stabilizations have also been observed during the flow of water through the column. Due to the Fe/Fe^{2+} half reaction during the treatment processes, the iron concentration has increased as well.

Key words: *remediation, dumping site, groundwater, PRB Technology, metals*

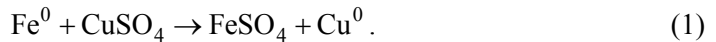
Introduction

In the southern provinces of Poland, there are plenty of industrial dumping sites for the hard coal and non-ferrous metal ores mining as well as dumps resulting from the manufacture of non-ferrous metals. They affect the quality of ground and surface water. The leachate from these dumping sites may contain following elements: As, Ba, B, Cd, Cu, Cr, Pb, Li, Mo, Ni, Rb, Sr, Tl, U, Zn (Twardowska et al., 2004; Pasieczna et al., 2008; 2010a; 2010b; Pasieczna and Kowalska, 2010; Nowak, 2008; Jarosiński et al., 2006, Suponik, 2012). An efficient removal of heavy metals as well as radionu-

clides and arsenic was achieved by the multibarrier presented in the study of Groudev et al. (2007).

In the article the possibility of the removal of Ni, Ba, Zn, Co, Cr, Cd, Pb and Cu from the groundwater with the use of zero-valent iron (ZVI, Fe^0) using Permeable Reactive Barrier (PRB) Technology has been presented. The application of ZVI for cationic and anionic metals removal has been investigated (Wilkin and McNeil, 2003; Rangsviek and Jekel 2005; Li and Zhang 2007; Fiore and Zanetti 2009; Puls et al., 1998; Meggyes et al., 1998). The main mechanisms suggested in these papers are reduction and precipitation/co-precipitation, and adsorption.

The results of the research on the copper removal from wastewater has also been presented elsewhere (Suponik, 2009). Cu^{2+} is characterized by a higher standard electrode potential than Fe^0 , hence iron displaces this hazardous cation from groundwater:



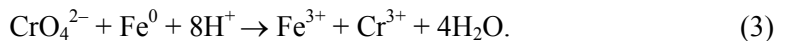
This reaction (called cementation) is a well known in hydrometallurgy (Ekmekyapar et al., 2012). The reaction proceeds under condition that:

$$U_{\text{Fe}/\text{Fe}^{2+}} < U_{\text{Cu}/\text{Cu}^{2+}} \quad (2)$$

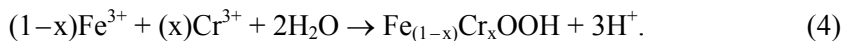
where $U_{\text{Fe}/\text{Fe}^{2+}}$ is the standard electrode potential (ORP), V.

It was assumed in the paper that, cationic and anionic metals such as Ni^{2+} , Cd^{2+} , Pb^{2+} , Co^{2+} and $\text{Cr}_2\text{O}_7^{2-}$, HCrO_4^- , CrO_4^{2-} , may probably be removed from groundwater when the zero-valent iron is used as a reactive material in a permeable reactive barrier, as all these ions are characterized by a higher standard electrode potential than iron (Fe^0). Finally, these metals may be precipitated out by a reactive material as Ni^0 , Cd^0 , Pb^0 , Co^0 and $\text{Cr}_x\text{Fe}_{(1-x)}\text{OOH}$ (see reaction 4) (Puls et al., 1998), $\text{Cr}(\text{OH})_3$ and Cr_2O_3 (ITRC, 2011).

Chromium(VI) is very toxic, whereas chromium(III) is slightly toxic and is easy to precipitate. Hence, the reduction of chromium(VI) into chromium(III) is the reaction which allows to remove it from groundwater (Suponik, 2011). The overall reaction for the hexavalent chromium, which occurs in water (under typical ground water pH and ORP conditions) as an oxyanion in the form of CrO_4^{2-} or as $\text{Cr}_2\text{O}_7^{2-}$ can be presented as (Meggyes et al., 1998):



In a further step, iron and chromium are precipitated as chromium(III) hydroxides or chromium-iron hydroxide solid solutions (Puls et al., 1998):



In accordance with Wilkin and McNeil (2003), when the value of pH is lower than 7, the process which causes the cationic metals removal is the adsorption onto the iron

surface or onto the iron corrosion products, whereas if a neutral or an alkaline pH condition occurs in the groundwater, the precipitation of carbonate species will provide different types of sorption surfaces and a potential for metals coprecipitation.

According to the study of Li and Zhang (2007), the sorption/surface complex formation is the removal mechanism for metal ions with a standard potential very close to, or more negative, than that of iron. The predominant removal mechanism, for metals with a greatly more positive and slightly more positive ORP than that of iron, is respectively the reductive precipitation, and the sorption and/or reductive precipitation. In the research presented in the paper of Li and Zhang (2007), the nanoscale zero-valent iron has been used as a reactive material for the removal of metal cations in water. The article also includes a claim that as the pH of the groundwater passing through zero-valent iron substantially increases (e.g. reactions 5 and 6), the precipitation of metal hydroxides may play an important role in the immobilization of metals – the following hydroxides are characterized by low solubility product: $\text{Cu}(\text{OH})_2$, $\text{Pb}(\text{OH})_2$, $\text{Cd}(\text{OH})_2$, $\text{Ni}(\text{OH})_2$, $\text{Co}(\text{OH})_2$, $\text{Zn}(\text{OH})_2$, $\text{Ba}(\text{OH})_2$.

The primary goal of this study was to assess the possibility of the treatment of the groundwater, contaminated by dumping sites located in the provinces of southern Poland. The zero-valent iron used as a reactive material in PRB Technology has been applied for that purpose.

Materials and methods

The laboratory tests carried out to determine the possibility of groundwater treatment were conducted in a glass column (Fig. 1) packed with scrap iron taken from a machining plant and with coarse sand located at the bottom of the column. The wastewater has been made to circulate through the column from bottom to top with the use of a peristaltic pump (type ZALIMP PP1B-05A) and during that time the treatment processes occurred. Fabric filters made by TAMFELT Co., were placed between the sand and the iron, on the bottom of the column and on the top of the iron bed (between iron and cork). The wastewater Darcian velocity used in the tests amounted to 0.02 m/day, 0.19 m/day and 0.50 m/day. These values corresponded to the groundwater velocity under industrial dumping sites located in southern Poland (the information has been obtained from the technical documentations of several dumping sites). This way, the conditions in column corresponded to the aquifer under the dumping sites in southern Poland.

Since the results of the tests for each velocity were similar the values for the Darcian velocity amounting to 0.50 m/day, were presented in the article.

There were seven sampling points in the installation in order to draw wastewater out and to take measurements. The wastewater (synthetic) was prepared by mixing distilled water (20 dm^3) with 108 mg $\text{CuSO}_4 \cdot 5\text{H}_2\text{O}$, 82 mg CoCl_2 , 84 mg $\text{NiSO}_4 \cdot 7\text{H}_2\text{O}$, 140 mg $\text{BaCl}_2 \cdot 2\text{H}_2\text{O}$, 228 mg $\text{ZnSO}_4 \cdot 7\text{H}_2\text{O}$, 20 mg K_2CrO_4 , 36 mg $\text{CdSO}_4 \cdot 8/3\text{H}_2\text{O}$ and

28 mg PbCl_2 . This way, the allowable concentration of chemicals in the simulated

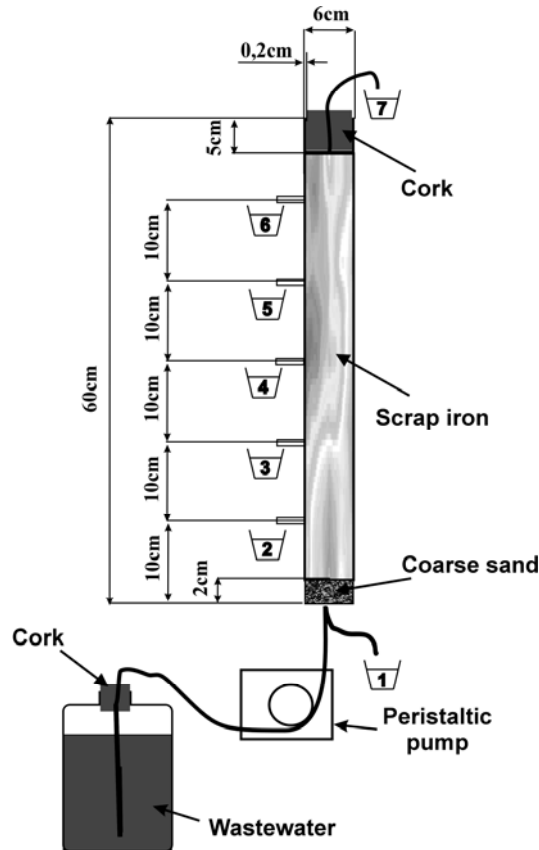


Fig. 1. Installation for simulation of flow and treatment processes of contaminated groundwater in reactive barrier; 1, 2, 3, 4, 5, 6, 7 – sampling points

groundwater has been exceeded within the meaning of legal regulations (Journal of Laws of 2009 No. 27 item 169). Since the pH of the groundwater under the dumping sites for the hard coal mining and non-ferrous metal ores mining, and for the manufacture of non-ferrous metals is respectively slightly acidic and rather neutral or alkaline (in southern Poland), it has not been purposely changed in the laboratory tests. The quantitative analysis of chemicals were carried out for:

- Cr^{6+} , UV-Vis Spectrophotometer DR5000 HachLange – 1,5-diphenylcarbohydrazide method; method 8023 of Hach Co.; test results are measured at 540 nm;
- Cu_{total} , UV-Vis Spectrophotometer DR5000 HachLange – bicinchoninate method; method 8506 of Hach Co.; test results are measured at 560 nm;

- Co_{total} , UV-Vis Spectrophotometer DR5000 HachLange – 1-(2-pyridolozo)-2-naphthol (PAN) method; method 8078 of Hach Co.; test results are measured at 620 nm;
- Ni_{total} , UV-Vis Spectrophotometer DR5000 HachLange – 1-(2-pyridolozo)-2-naphthol (PAN) method; method 8150 of Hach Co.; test results are measured at 560 nm;
- Ba^{2+} , UV-Vis Spectrophotometer DR5000 HachLange – turbidimetric method; method 8014 of Hach Co.; test results are measured at 450 nm;
- Zn_{total} , UV-Vis Spectrophotometer DR5000 HachLange – zincon method; method 8009 of Hach Co.; test results are measured at 620 nm;
- Cd_{total} , JY 2000 Spectrometer – Inductively Coupled Plasma Atomic Emission Spectroscopy method (ICP-AES);
- Pb_{total} , 2000 Spectrometer – Inductively Coupled Plasma Atomic Emission Spectroscopy method (ICP-AES);
- Fe_{total} , UV-Vis Spectrophotometer DR5000 HachLange – FerroVer method; method 8008 of Hach Co.; test results are measured at 510 nm;
- SO_4^{2-} , UV-Vis Spectrophotometer DR5000 HachLange – SulfaVer 4 method; method 8051 of Hach Co.; test results are measured at 450 nm;
- Cl^- , UV-Vis Spectrophotometer DR5000 HachLange – Mercuric Thiocyanate method; method 8113 of Hach Co.; test results are measured at 455 nm.

Concentrations of the Ni, Co, Cu, Zn, Cd, Pb metals in the wastewater, which was prepared by adding metal compounds to distilled water, were measured in a spectrophotometer and a spectrometer as a total value: Ni_{total} , Co_{total} , Cu_{total} , Zn_{total} , Cd_{total} , Pb_{total} . Since there were no metals speciation (at the beginning) in the wastewater other than the Ni^{2+} , Co^{2+} , Cu^{2+} , Zn^{2+} , Cd^{2+} , Pb^{2+} cations, the removal of the metals in the second oxidation state has been assessed in the article.

The pH, ORP, dissolved oxygen (DO), conductivity and temperature are important parameters that are easily monitored during column tests and are good indicators of conditions created by ZVI. They were measured for: a) pH, PORTAMESS 913 pH with SenTix 4 electrode; b) ORP, PORTAMESS 913 pH with POLYPLAST ORP electrode; c) conductivity and temperature, PORTAMESS 913 Cound, d) concentration of DO, PORTAMESS 913Oxy with oxygen SE 302 probe.

The scrap iron is easily available in large quantities at a reasonable price. It should have a high content of iron metal (>90%), low carbon content (<3%), and nonhazardous levels of leachable trace metal impurities (ITRC, 2011). It must be free of any surface coating (oils or grease) that inhibit its reactivity.

Both sand and iron (in the form chips and swarf, Fig. 2) were cleaned before using them to fill the column. The sand was cleaned with the use of distilled water, whereas iron was first cleaned with a thinner (painter's naphtha), dried in the moisture teller, and then, just before the application, cleaned with distilled water. Both materials were then carefully packed into the column.

The measurements have begun just after the achievement of a steady state in the column, i.e. after the wastewater in the column had been changed ten times.

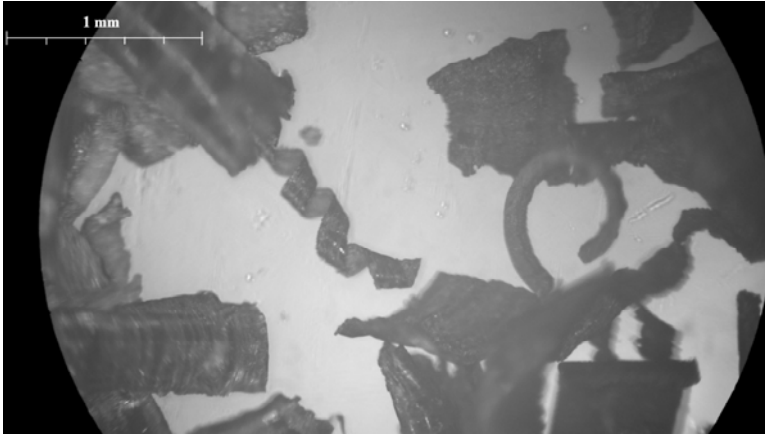


Fig. 2. Zero-valent iron Fe(0) used in laboratory tests

Table 1 presents the grain-size distribution of scrap iron used in the column test. The maximum size of the iron grain amounted to 4 mm. The material used in the size determination and in the measurements of the hydraulic parameters (Table 2) has also been cleaned with thinner (painter's naphtha) and dried in a moisture teller.

For a correct measurement of iron density (according to Polish Standard PN-88/B-04481), benzene (analytically pure) was applied in the test and a pycnometer with a sample was heated in a water bath (distilled water did not penetrate the measured material and lumps of iron were created in the pycnometer). The hydraulic conductivity of the reactive material was measured with the use of Kaminski's pipe method, while the bulk density and the effective porosity were determined in accordance with the Polish PN-88/B-04481 standard and King's method respectively (Pazdro et al., 1990; Wieczysty, 1982).

Table 1. Particle size distribution of zero-valent iron used in column test

Particle size, mm	4.0–2.0	2.0–1.6	1.6–1.0	1.0–0.71	0.71–0.5	<0.5
Mass fraction, %	1.77	1.28	7.26	38.79	36.57	14.33

Table 2. Parameters of zero-valent iron

Reactive material parameters, unit	Value
Hydraulic conductivity, m/s	$4.47 \cdot 10^{-4}$
Density, g/cm ³	7.85
Bulk density, g/cm ³	1.96
Effective porosity, –	0.46

Results and discussion

The scrap iron used in the tests shows an ability to create reductive conditions in a glass column and as a result, to remove cationic and anionic metals present in wastewaters in the following oxidation states: Cr^{6+} , Cu^{2+} , Ni^{2+} , Co^{2+} , Pb^{2+} , Cd^{2+} , Zn^{2+} (Table 3). In the present of iron, between the 1st and 2nd sampling point, the pH increased quickly as a result of the reactions 5 and 6 (reaction 6 proceeds slowly):



This potential increased from 6.44 in the first sampling point to reach 7.98 in the second point. Following that, it slowly decreased at the remaining points.

Similar values of sulphates (SO_4^{2-} decreased very slowly in the iron bed, Table 3) and a small increase of pH in the column showed that the metals did not precipitate (or they precipitated to a small degree) in the form of sulphides or hydroxides. Therefore, the reductive precipitation and/or the adsorption on iron surface or on the iron corrosion products were probably the groundwater (contaminated with metals) treatment mechanisms.

In accordance with Table 3, reaction 5 proceeded quickly, evidenced by the fact that both DO and the ORP dropped quickly as the wastewater entered the iron material. The value of ORP and DO for the 1st and the 7th sampling points amounted to $\text{ORP}_1 = 186 \text{ mV}$; $\text{DO}_1 = 7.25 \text{ mg/l}$ and $\text{ORP}_7 = -70 \text{ mV}$; $\text{DO}_7 = 4.59 \text{ mg/dm}^3$ respectively. These parameters decreased gradually.

The significant decrease of metals occurred already at the lower part of the iron bed – between the 1st and the 2nd sampling points. Low concentrations of the metals were still observed at the second point, while there was no evidence of any of the observed metals – except barium – at the 3rd sampling point. Its concentration kept a similar value at all points of the installation presented in Fig. 1. The half reaction of barium Ba/Ba^{2+} is characterized by a lower standard electrode potential than Fe/Fe^{2+} , which explains the treatment difficulty of water contaminated with barium in the 2nd oxidation state. Zinc, at the same time, is also characterized with a lower standard electrode potential than Fe^0 and was completely removed in the lower part of the iron bed. It might have been precipitated out in the form of hydroxide – $\text{Zn}(\text{OH})_2$ (pH increased slightly, Table 3) or, more probably, adsorbed on the iron surface, what was suggested by Li and Zhang (2007):



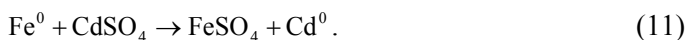
According to reactions 1 taking place in the system, and also reaction 7, the wastewater should be richer in Fe^{2+} and Fe^{3+} respectively, at the next sampling points.

Table 3. The results of the research carried out in the installation presented in Fig. 1

Parameter, unit	Values for the following sampling points						
	1	2	3	4	5	6	7
pH	6.44	7.98	7.83	7.90	7.80	7.66	7.74
ORP, mV	186	121	95	64	-3	-38	-70
Conductivity, mS/cm	0.1507	0.1621	0.1999	0.381	0.720	0.904	1.040
DO, mg/dm ³	7.25	6.13	5.26	5.09	4.54	4.77	4.59
Temp., °C	17.8	18.2	18.3	17.7	17.8	17.8	17.6
Cr ⁶⁺ , mg/dm ³	0.202	0.005	<0.001	<0.001	<0.001	<0.001	<0.001
Cu ²⁺ , mg/dm ³	1.27	0.05	<0.04	<0.04	<0.04	<0.04	<0.04
Ni ²⁺ , mg/dm ³	0.841	0.013	<0.006	<0.006	<0.006	<0.006	<0.006
Co ²⁺ , mg/dm ³	1.772	<0.006	<0.006	<0.006	<0.006	<0.006	<0.006
Ba ²⁺ , mg/dm ³	5.0	5.5	4.5	5.0	6.0	5.5	5.0
Pb ²⁺ , mg/dm ³	0.985	0.122	<0.005	<0.005	<0.005	<0.005	<0.005
Cd ²⁺ , mg/dm ³	0.695	0.005	<0.001	<0.001	<0.001	<0.001	<0.001
Zn ²⁺ , mg/dm ³	2.79	<0.01	<0.01	<0.01	<0.01	<0.01	<0.01
Fe _{total} , mg/dm ³	<0.02	5.05	6.89	7.60	10.80	14.51	15.84
SO ₄ ²⁻ , mg/dm ³	14	13	12	13	12	11	12
Cl ⁻ , mg/dm ³	8.8	8.2	9.5	8.2	9.1	9.9	8.2

The total concentration of iron increased from <0.02 mg/dm³ (detection limit in the spectrophotometer) in the untreated water, to 15.84 mg/dm³ at the 7th sampling point. A higher value of conductivity at successive points has also confirmed the increase of the iron concentration. The conductivity increased from 0.1507 mS/cm in the raw wastewater to 1.040 mS/cm at last measuring point (Table 3). The above means that reactions 1, 5, 6 and probably others, proceeded quickly while the wastewater has been flowing through the column.

To some degree, the temperature increase in the wastewater flowing through ZVI has also confirmed the occurrence of the 1, 3, 5, 7, and probably 8, 9, 10, 11 reactions:



The temperature of the wastewater in the column increased from 17.8°C at the 1st sampling point to 18.3°C at the 3rd point, and then dropped to the value of 17.8°C ± 0.1°C at the remaining points (4, 5, 6, 7). The increase of the temperature in the lower

part of the column probably occurred due to the negative enthalpy of reactions 1, 3, 5, 7 as well as 8, 9, 10 and 11, which could have caused (among others) the removal of cationic and anionic metals (Ni, Co, Cr, Cd, Pb, Cu) from the water and the increase of the iron concentration (Fe^{2+} , Fe^{3+}) in it. The decrease of temperature at remaining sampling points (4, 5, 6, 7) occurred due to the air temperature in the laboratory which was $17.6^{\circ}\text{C} \pm 0.2^{\circ}\text{C}$.

Conclusions

The industrial dumping sites in the southern provinces of Poland pollute groundwater with metals. Most of them may be removed with the use of zero-valent iron in the PRB Technology. In accordance with the results presented in the article, the cationic and anionic forms of Cr^{6+} , Cu^{2+} , Ni^{2+} , Co^{2+} , Pb^{2+} , Cd^{2+} , Zn^{2+} have been removed. Barium (Ba^{2+}) was the only assessed metal which remained in the wastewater after the treatment processes in the column. Rapid metals removal occurs most likely due to the reductive precipitation/coprecipitation and/or due to the adsorption onto the iron metal surface or/and onto the iron corrosion products.

As a result of the treatment processes in the column, a significant decrease of ORP (from 186 mV to -70 mV) and DO (from 7.25 mg/dm³ to 4.59 mg/dm³) and an increase of pH from ca. 6.5 up to ca. 7.8 occurred in the wastewater. At the same time, due to the Fe/Fe^{2+} and Fe/Fe^{3+} half reactions, the iron concentration (and the conductivity) increased. These reactions to a some degree, have confirmed the reduction and precipitation/coprecipitation of metals (reactions 1, 3, 8, 9, 10, 11), while also confirming the reduction of O_2 and H_2O (reactions 5, 6). Moreover, a significant increase of conductivity between the 1st and 7th sampling point showed that when iron was oxidized, the reductions of substances other than metals occurred (e.g. O_2).

Since the temperature of wastewater increased (from 17.8°C to 18.3°C) in the lower part of the iron bed, the exothermic processes in the wastewater can be assumed to occurred. The reactions of cationic and anionic forms of metals (Ni, Co, Cr, Cd, Pb, Cu) removal and the reactions of oxygen reduction have a negative enthalpy.

In order to check the mechanisms of the groundwater treatment with zero valent-iron and to assess the type of the treatment processes (reductive precipitation/coprecipitation or adsorption), the changes in the oxidation states of metals in the wastewater flowing through the column should be analysed.

References

- EKMEKYAPAR A., TANAYDIN M., DEMIRKIRAN N., 2012, *Investigation of copper cementation kinetics by rotating aluminum disc from the leach solutions containing copper ions*, Physicochemical Problems of Mineral Processing, vol. 48, issue 2, 355–367.
- FIORE, S., ZANETTI M. C., 2009, *Preliminary Tests Concerning Zero-Valent Iron Efficiency in Inorganic Pollutants Remediation*, American Journal of Environmental Sciences 5(4), 556–561.

- GROUDEV S., SPASOVA I., NICOLOVA M., GEORGIEV P., 2007, *Acid mine drainage cleanup in a uranium deposit by means of a passive treatment system*, Physicochemical Problems of Mineral Processing, vol. 41, 265–274.
- ITRC (Interstate Technology & Regulatory Council), 2011, *Permeable Reactive Barrier: Technology Update*, PRB-5. Washington, D.C.: Interstate Technology & Regulatory Council, PRB: Technology Update Team. Washington: <http://www.itreweb.org>.
- JAROSIŃSKI A., NOWAK A. K., WŁODARCZYK B., 2006, *Charakterystyka odpadów i ścieków z ZG „Trzebieńka” SA*, Ekotechnika nr 1/37, 43–45.
- JOURNAL OF LAWS OF 2009, NO. 27, ITEM 169; Rozporządzenie Ministra Środowiska z dnia 28 stycznia 2009 r. zmieniające rozporządzenie w sprawie warunków, jakie należy spełnić przy wprowadzaniu ścieków do wód lub do ziemi oraz w sprawie substancji szczególnie szkodliwych dla środowiska wodnego.
- LI, X.-Q., ZHANG W. X., 2007, *Sequestration of Metal Cations with Zerovalent Iron Nanoparticles: A Study with High Resolution X-Ray Photoelectron Spectroscopy (HRXPS)*, Journal of Physical Chemistry 111(19), 6939–6946.
- MEGGYES T., HOLZLOHNER U., AUGUST H., 1998, *A multidisciplinary approach to improving the safety and durability of landfill barriers*, in: *Contaminated and derelict land*, Sarsby R.W. (ed), Kraków. Thomas Telford, London, 413–420.
- NOWAK A. K., 2008, *Ekologiczno-techniczne aspekty pozyskiwania koncentratów cynku i ołowiu*, Praca doktorska. Wydział Inżynierii i Technologii Chemicznej Politechnika Krakowska. Kraków.
- PASIECZNA A., DUSZA-DOBEK A., KOWALSKA Z., 2010a, *Szczegółowa mapa geochemiczna Górnego Śląska 1:25000. Arkusz Katowice*. Państwowy Instytut Geologiczny, Warszawa. www.mapgeochem.pgi.gov.pl (dostęp: 24.02.2012).
- PASIECZNA A., KOWALSKA Z., 2010, *Szczegółowa mapa geochemiczna Górnego Śląska 1:25000. Arkusz Mysłowice*. Państwowy Instytut Geologiczny, Warszawa. www.mapgeochem.pgi.gov.pl (dostęp: 24.02.2012).
- PASIECZNA A., BIEL A., PAULO A., 2010b, *Szczegółowa mapa geochemiczna Górnego Śląska 1:25 000. Arkusz Imielin*, Państwowy Instytut Geologiczny, Warszawa. www.mapgeochem.pgi.gov.pl (dostęp: 24.02.2012).
- PASIECZNA A., LIS J., SZUWARZYŃSKI M., DUSZA-DOBEK A., WITKOWSKA A., 2008, *Szczegółowa mapa geochemiczna Górnego Śląska 1:25 000, Arkusz Chrzanów*, Państwowy Instytut Geologiczny, Warszawa.
- POLISH STANDARD PN-88/B-04481, 1988, Grunty budowlane – Badania próbek gruntu. Polski Komitet Normalizacji, Miar i Jakości.
- PULS R.W., POWELL M.R., BLOWES D.W., GILLHAM R.W., SCHULTZ D., SIVAVEC T., VOGAN J.L., POWELL P.D., 1998, *Permeable reactive barrier technologies for contaminant remediation*, Washington: United States Environmental Protection Agency.
- PAZDRO Z., KOZERSKI B., 1990, *Hydrogeologia ogólna*, wyd. Geologiczne, Warszawa.
- RANGSIVIEK, R., JEKEL M. R., 2005, *Removal of Dissolved Metals by Zero-Valent Iron (ZVI): Kinetics, Equilibria, Processes and Implications for Stormwater Runoff Treatment*, Water Research 39, 4153–4163.
- SUPONIK T., 2009, *Zastosowanie żelaza metalicznego w technologii PRB*, rozdział w monografii *Rekultywacja i rewitalizacja terenów zdegradowanych*, ed. Grzegorz Malina. Wydawnictwo Polskiego Zrzeszenia Inżynierów i Techników Sanitarnych, Oddział Wielkopolski (Inżynieria na rzecz ochrony środowiska, red. Jan F. Lemański, Sergiusz Zabawa, nr 866), Poznań, 161–172.

- SUPONIK T., 2011, *Optimization of the PRB (Permeable Reactive Barriers) parameters for selected area of dumping site*, The Publishing House of the Silesian University of Technology (monographs no 328), Gliwice.
- SUPONIK T., 2012, *Removing contaminants from groundwater polluted by the Trzebionka Mine Settling Pond located in Upper Silesia (Poland)*, Physicochemical Problems of Mineral Processing, vol. 48, issue 1, 169–180.
- TWARDOWSKA I., ALLEN H.E., KETTRUP A.A.F., LACY W.J. (eds.), 2004, *Solid waste: assessment, monitoring and remediation*, Waste Management Series 4; Elsevier.
- WILKIN R. T., MCNEIL M. S., 2003, *Laboratory evaluation of zero-valent iron to treat water impacted by acid mine drainage*, Chemosphere 53, 715–725.
- WIECZYSTY A., 1982, *Hydrogeologia inżynierska*, PWN, Warszawa.

Received April 22, 2012; reviewed; accepted May 12, 2012

INVESTIGATION OF COAL SLURRY PROPERTIES DEPOSITED IN IMPOUNDMENTS LOCATED IN THE UPPER SILESIAN COAL BASIN

Aleksander LUTYNSKI, Tomasz SUPONIK, Marcin LUTYNSKI

Silesian University of Technology, Faculty of Mining and Geology, Gliwice, Poland
e-mail: Aleksander.Lutyński@polsl.pl

Abstract: Results of investigation of physical, chemical and energetic properties of steam and coking coal slurries deposited in twenty Polish impoundments are presented in the paper. Coal slurry was sampled in accordance with a certain procedure from different locations and depths at each impoundment whereas laboratory investigation was performed on averaged samples. The performed investigation include determination of chemical composition, moisture content, volatile matter, sulfur and calorific value at various states. Additionally, properties of coal slurry of particle size below 0.1 mm are presented. The average content of this fraction is approximately 62% and ranges at individual impoundments from 28 to 79%. An average calorific value in analytical state of coal slurries deposited in impoundments in the fraction below 0.1 mm is rather high (12.01 MJ/kg on average) in comparison to the average calorific value of impoundments in analytical state i.e. 16.4 MJ/kg. Average ash and sulfur contents of the coal slurries in analytical state is on average: 42.5% and 1.0% respectively. Transient moisture content of coal slurries in the analytical state is on average 22%, whereas the average volatile matter content is 20.0%. Chemical composition is typical for coal tailings with low Al₂O₃ and TiO₂ content. The results indicate considerable variations in the quality of coal slurries deposited in different impoundments due to different geology of coal deposits of the mines. For individual impoundment these differences are smaller which is demonstrated by a lower variation in the standard deviation.

key words: *coal slurry, tailings, chemical composition, impoundments*

1. Introduction

Coal industry generates wastes during exploration, mining and processing of coal. Several studies indicate that the waste generated during coal production accounts for 40% of the total amount which is extracted. The amount of waste which is produced depends on the type of deposit, mining technology, mine planning, processing technology and increasing customers quality requirements for the final product. In the case

of coal, 94% of the waste consists of tailings i.e. waste which is generated during coal preparation. Such material is separated in coal preparation plants.

As a result of coal beneficiation, the following wastes are produced: coarse (200–20 mm), fine (20–0.5 mm), coal slurry and post-flotation mud with particle size of <1 (0.5) mm. Up to the thirties, i.e. the time of development and introduction of froth flotation technology, small size gangue was difficult to remove using conventional beneficiation methods. Its presence was significantly lowering the quality of coke. Therefore, particles smaller than 1 mm were treated as waste. The same situation was observed in the case of steam coal as it was impossible to burn small particles in stoker-fired boilers. Due to that fact coal slurry was stored on the surface in impoundments or ponds. Studies to recover coal from the waste material deposited in such impoundments are currently a subject of investigation due to high energetic potential (Miao et al. 2010, Anaç and Gitmez 2010). Coal slurries deposited in impoundments are hazardous for the environment as well. A recent helicopter electromagnetic surveys to identify potential hazards at coal waste impoundments in West Virginia was conducted by Hammack et al. (2010). The present paper concerns investigation of fine particle size tailings which were deposited in impoundments years ago. Fifty nine impoundments were identified and twenty nine were selected for thorough investigation of steam and coking coal slurry quality. Sample from the impoundments were collected according to the methodology developed at the initiation of the work. Sampling was done from the bore-holes drilled in the impoundments.

2. Investigation of coal slurry properties

Identification of coal slurry properties is crucial for the selection of a proper separation method (O'Brien et al. 2010). First stage of tests for averaged samples, i.e. samples that were mixed from all of the bore-holes in one impoundment was devoted to chemical composition analysis of the coal slurry. In the project, determination of the selected metals content as well as water leachate composition derived from compressive strength tests was done. After that, for each delivered sample, the following quality analysis were performed:

- transient moisture content W_{ex} and hygroscopic moisture content W_h ,
- ash content: analytical A^a , as received A^r and on dry basis A^d ,
- sulfur content: analytical S_i^a , as received S_i^r and on dry basis S_i^d ,
- volatile matter content: analytical V^a , as received V^r and on dry basis V^d ,
- calorific value: analytical Q^a , as received Q^r and on dry basis Q^d .

After quality analysis, the particle size and density analysis were performed for averaged samples. For each particle size fraction and density fraction, the following parameters were determined:

- fraction yield,
- hygroscopic moisture content W_h ,
- ash content: analytical A^a and on dry basis A^d ,

- sulfur content: analytical S_t^a and on dry basis S_t^d ,
- volatile matter content: analytical V^a and on dry basis V^d ,
- calorific value: analytical Q^a and on dry basis Q^d .

The tests were performed in accordance with appropriate standards and procedures (Szpyrka and Lutyński 2012, Witkowska-Kita et al. 2012)

3. Results of coal slurry analysis

Sample chemical composition tests results are shown in Table 1. The rest of quality analysis results are presented in Tables 2 to 7.

Table 1. Results of basic chemical composition analysis of coal slurries deposited in impoundments

Impoundment	Content, %									
	SiO ₂	Al ₂ O ₃	TiO ₂	Fe ₂ O ₃	CaO	MgO	K ₂ O	Na ₂ O	C	P ₂ O ₅
1	49.26	5.32	0.02	0.46	0.02	0.84	1.86	0.32	22.50	0.001
2	49.23	5.91	0.12	1.29	0.03	0.53	1.86	0.32	22.50	0.001
3	54.16	9.09	0.04	1.00	0.03	0.72	2.79	1.34	19.00	0.008
4	55.69	9.28	0.02	0.84	0.03	0.77	2.98	0.79	15.53	0.003
5	40.79	7.22	0.07	0.81	0.01	0.88	2.52	1.31	26.50	0.015
6	28.88	7.70	0.17	0.95	0.03	0.97	2.66	0.90	25.45	0.006
7	33.16	5.69	0.026	1.03	0.03	0.99	2.57	0.81	23.05	0.007
8	42.49	6.32	0.03	0.73	0.02	1.20	1.35	0.81	11.15	0.001
9	45.16	6.89	0.03	0.70	0.01	0.93	1.23	0.81	11.58	0.002
10	53.48	7.26	0.04	0.64	0.02	0.44	1.93	0.67	31.6	0.001
11	51.23	6.74	0.03	0.71	0.02	0.35	1.93	0.66	30.25	0.002
12	58.96	6.24	0.04	0.68	0.02	0.40	1.35	0.66	31.80	0.001
13	54.60	5.66	0.02	1.42	0.09	0.49	1.34	0.44	26.05	0.002
14	63.96	5.61	0.01	1.13	0.12	0.48	2.77	0.62	17.54	0.001
15	54.66	7.10	0.01	1.46	0.12	0.90	1.83	0.48	21.50	0.003
16	43.05	9.22	0.02	1.77	0.03	0.56	1.23	0.40	25.00	0.003
17	51.46	6.68	0.02	0.81	0.10	0.99	1.49	0.48	25.04	0.001
18	42.77	5.57	0.02	1.43	0.14	1.12	1.35	0.41	23.25	0.003
19	42.57	4.80	0.02	1.46	0.13	1.20	1.19	0.39	30.05	0.001
20	33.57	6.38	0.02	1.61	0.11	0.74	1.23	0.41	25.65	0.002
average	47.46	6.73	0.04	1.05	0.06	0.77	1.87	0.65	23.25	0.04
Standard dev.	9.11	1.29	0.04	0.38	0.05	0.27	0.82	0.29	5.94	0.01

In Tables 2 and 3 the results of analysis of sixteen and twenty two samples collected from two impoundment are presented. Samples were collected from different locations and depths of the impoundment.

Table 2. Properties of coal slurry from KX impoundment

Sample	Transient moisture content [%]	Hydroscopic moisture content [%]	Ash content [%]		Sulfur content [%]		Volatile matter content [%]		Calorific value [MJ/kg]				
			A^r	A^d	S_r^r	S_r^d	V^r	V^d	Q^r	Q^d			
1	24.77	1.31	37.75	28.89	38.25	0.89	0.68	19.85	15.19	20.11	19.06	14.59	19.32
2	25.35	1.25	37.19	28.23	37.66	0.87	0.66	20.36	15.45	20.62	19.41	14.74	19.66
3	23.83	1.40	37.87	29.37	38.41	0.85	0.66	20.43	15.85	20.72	18.68	14.49	18.94
4	23.41	1.44	39.47	30.80	40.05	0.84	0.66	19.92	15.54	20.21	17.22	13.44	17.48
5	25.81	1.23	35.38	26.68	35.82	1.07	0.81	21.09	15.91	21.35	20.40	15.38	20.65
6	23.09	1.46	35.59	27.89	36.12	1.01	0.79	20.97	16.43	21.28	19.80	15.52	20.09
7	24.63	1.33	35.46	27.20	35.94	0.86	0.66	20.27	15.55	20.54	19.76	15.16	20.03
8	22.16	1.35	43.25	34.25	43.84	0.76	0.60	19.73	15.62	20.00	17.25	13.66	17.49
9	21.46	1.31	37.90	30.26	38.40	0.76	0.61	20.87	16.67	21.15	19.23	15.36	19.49
10	24.26	1.28	37.76	29.08	38.25	0.87	0.67	21.15	16.29	21.42	19.55	15.06	19.80
11	23.20	1.26	36.03	28.13	36.49	0.93	0.73	21.17	16.53	21.44	19.86	15.50	20.11
12	23.34	1.21	37.44	29.15	37.90	0.89	0.69	21.19	16.50	21.45	19.05	14.83	19.28
13	20.15	0.74	59.52	47.97	59.96	1.35	1.09	12.46	10.04	12.55	13.10	10.56	13.20
14	26.18	1.10	34.54	25.88	34.92	0.97	0.73	21.05	15.77	21.28	21.21	15.89	21.45
15	22.56	1.24	37.79	29.73	38.26	0.91	0.72	21.14	16.63	21.41	19.42	15.28	19.66
16	24.56	1.11	38.40	29.40	38.83	1.15	0.88	20.88	15.98	21.11	19.21	14.70	19.42

Table 3. Properties of coal slurry from KY impoundment

Sample	Transient moisture content [%]		Hydroscopic moisture content [%]		Ash content [%]		Sulfur content [%]		Volatile matter content [%]		Calorific value [MJ/kg]			
	W_{ex}	W_h	A^a	A^d	A^r	A^d	S_t^a	S_t^r	S_t^d	V^a	V^r	V^d	Q^a	Q^r
1	22.77	5.80	55.53	46.11	58.95	0.73	0.61	0.77	16.85	13.99	17.89	9.84	8.17	10.45
2	25.86	4.74	53.60	42.28	56.27	0.63	0.50	0.66	18.05	14.24	18.95	10.78	8.50	11.32
3	17.83	7.11	46.74	41.73	50.32	0.90	0.80	0.97	19.11	17.06	20.57	12.13	10.83	13.06
4	22.40	7.42	40.98	34.84	44.26	1.01	0.86	1.09	21.41	18.20	23.13	14.11	12.00	15.24
5	16.45	6.04	48.90	43.81	52.04	0.99	0.89	1.05	18.69	16.75	19.89	13.21	11.83	14.06
6	17.55	6.19	50.12	44.43	53.43	1.04	0.92	1.11	18.24	16.17	19.44	13.02	11.54	13.88
7	27.87	6.09	47.77	37.36	50.87	0.83	0.65	0.88	19.26	15.06	20.51	13.33	10.43	14.20
8	28.05	5.49	52.87	40.94	55.94	0.84	0.65	0.89	17.66	13.68	18.69	12.25	9.49	12.96
9	25.95	6.69	42.73	34.50	45.79	0.72	0.58	0.77	20.93	16.90	22.43	14.65	11.83	15.70
10	15.70	6.09	48.29	43.65	51.42	1.17	1.06	1.25	18.76	16.96	19.98	11.99	10.84	12.77
11	19.92	5.91	50.23	43.19	53.39	0.95	0.82	1.01	18.44	15.86	19.60	12.86	11.06	13.67
12	27.54	6.46	44.59	35.19	47.67	0.73	0.58	0.78	20.49	16.17	21.91	15.08	11.90	16.13
13	27.53	4.82	56.46	43.64	59.32	0.56	0.43	0.59	16.69	12.90	17.54	10.70	8.27	11.24
14	28.47	4.96	56.59	43.28	59.54	0.76	0.58	0.80	16.12	12.33	16.96	11.78	9.01	12.40
15	18.94	5.95	51.05	44.42	54.28	0.76	0.66	0.81	18.40	16.01	19.56	12.88	11.20	13.69
16	25.20	5.29	55.24	44.24	58.33	0.65	0.52	0.69	17.51	14.02	18.49	11.33	9.07	11.96
17	14.29	7.11	40.97	38.03	44.11	1.13	1.05	1.22	21.00	19.49	22.61	16.74	15.53	18.02
18	22.51	5.69	51.08	42.49	54.16	0.91	0.76	0.96	17.99	14.96	19.08	15.62	12.99	16.56
19	15.26	1.39	41.07	35.37	41.65	2.14	1.84	2.17	15.55	13.39	15.77	19.72	16.98	19.99
20	26.26	5.46	58.76	46.54	62.15	0.39	0.31	0.41	15.85	12.55	16.77	10.31	8.16	10.90
21	22.46	5.11	44.64	36.90	47.04	0.90	0.74	0.95	21.61	17.86	22.77	16.96	14.02	17.87
22	28.58	5.93	50.36	38.95	53.53	0.63	0.49	0.67	18.44	14.26	19.60	13.25	10.25	14.09

In Tables 4, 5 and 6 a summary of coal slurry properties is presented as statistical average and their standard deviations for twenty two impoundments. Table 4 shows results of transient and hydroscopic moisture content analysis of coal slurries. In Table 5 quality parameters for analytical state are presented, whereas in Table 6 these parameters are presented on the “as received” basis.

The particle size analysis of coal slurries confirmed previous investigations that the majority of particles is in the fraction below 0.1 mm. In the case of coal slurries from each impoundment, 62.27% of particles is in the fraction below 0.1 mm and ranges for particular impoundments from 27.90 to 78.93% with standard deviation of 14.26%. In three impoundments the share of this fine fraction was below 50%.

Due to that fact, an in-depth analysis of this fraction was performed. Results of these analyses (see Table 7) are crucial due to the possibility of upgrading of this fraction as a high quality component of coal mixes (Figure 1). An in-depth study of coal slurry beneficiation from these impoundments was investigated by Szpyrka and Lutyński, 2012.

Table 4. Transient moisture content and hydroscopic moisture content in coal slurries at impoundments

Impoundment	Transient moisture content [%]	Standard dev. of transient moisture content [%]	Hydroscopic moisture content [%]	Standard dev. of hydroscopic moisture content [%]
1	24.75	3.94	7.00	0.29
2	27.69	1.32	7.92	0.40
3	23.05	1.79	5.25	0.73
4	20.69	1.99	3.73	0.97
5	19.47	2.42	4.66	2.40
6	22.61	4.86	5.71	1.21
7	27.25	4.19	2.15	0.40
8	11.69	6.79	1.77	1.60
9	17.66	3.58	1.27	0.19
10	18.57	3.66	1.69	0.22
11	18.77	2.46	1.58	0.11
12	17.28	4.72	1.66	0.11
13	25.01	0.92	1.14	0.12
14	24.53	2.57	2.23	0.22
15	34.48	3.85	3.17	0.77
16	22.45	3.98	1.23	0.31
17	24.67	1.58	1.29	0.07
18	25.45	1.36	1.04	0.08
19	24.63	1.07	1.20	0.12
20	23.67	1.60	1.25	0.17
average	22.70	–	2.85	–
standard dev.	4.92	–	2.13	–

Table 5. Quality parameters summary for analytical state of coal slurry at impoundments

Impoundment	Ash content [%]	Ash content standard deviation [%]	Sulfur content [%]	Sulfur content standard deviation [%]	Volatile matter content [%]	Volatile matter content standard deviation [%]	Calorific value [MJ/kg]	Calorific value standard deviation [MJ/kg]
1	27.47	2.99	1.90	0.84	28.50	4.32	15.10	1.51
2	32.98	2.58	0.72	0.03	23.85	0.41	15.65	0.83
3	41.36	1.41	0.86	0.10	21.31	1.25	14.81	0.58
4	63.96	9.06	0.57	0.16	14.38	2.55	9.33	2.05
5	63.04	17.76	0.64	0.25	14.39	5.47	10.07	2.75
6	49.48	5.39	0.88	0.34	18.50	1.76	13.30	2.41
7	60.43	10.56	0.70	0.20	16.41	3.13	9.27	3.50
8	45.90	12.59	2.98	1.27	18.01	2.23	14.88	5.98
9	58.34	8.24	2.26	0.67	14.29	1.17	12.30	2.80
10	28.41	4.23	0.95	0.11	23.47	1.33	22.81	1.54
11	26.98	3.46	0.95	0.15	23.77	0.75	23.29	1.44
12	27.89	0.32	0.97	0.13	23.79	0.71	22.94	0.59
13	47.22	2.55	0.59	0.11	18.89	0.29	15.81	0.94
14	31.84	4.51	0.79	0.13	23.85	1.25	20.83	2.07
15	53.79	5.17	1.21	0.19	16.99	1.52	12.05	1.50
16	42.86	13.10	1.09	0.38	16.89	2.30	17.80	5.35
17	37.59	1.44	0.94	0.08	20.64	0.87	19.40	0.65
18	35.22	1.28	0.97	0.02	21.54	0.40	20.35	0.84
19	37.33	1.29	0.92	0.06	20.72	0.54	19.67	0.77
20	38.83	5.88	0.94	0.15	20.16	2.12	18.89	1.83
average	42.55	–	1.09	–	20.02	–	16.43	–
standard deviation	12.28	–	0.60	–	3.85	–	4.52	–

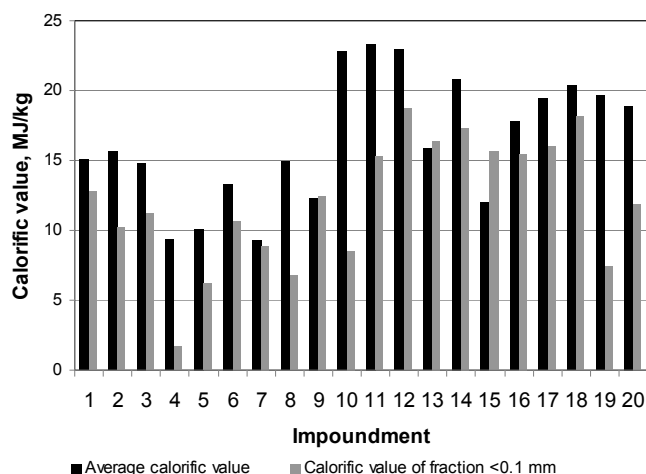


Fig. 1. Average calorific value (at analytical state) of coal slurry at individual impoundment in comparison with fraction <0.1 mm

Table 6. Quality parameters summary on “as received” basis of coal slurry at impoundments

Impoundment	Ash content [%]	Ash content standard deviation [%]	Sulfur content [%]	Sulfur content standard deviation [%]	Volatile matter content [%]	Volatile matter content standard deviation [%]	Calorific value [MJ/kg]	Calorific value standard deviation [MJ/kg]
1	24.31	3.37	1.58	0.73	23.49	4.25	12.38	0.67
2	26.46	1.94	0.58	0.01	19.14	0.61	12.55	0.61
3	34.01	1.69	0.70	0.07	17.53	1.33	12.18	0.57
4	53.11	7.60	0.48	0.14	11.95	2.14	7.74	1.67
5	53.68	15.08	0.55	0.22	12.26	4.70	8.59	2.37
6	40.99	3.88	0.74	0.31	15.40	1.94	11.09	2.32
7	45.46	10.20	0.52	0.13	12.24	1.73	6.87	2.27
8	41.91	13.53	2.71	1.26	16.22	2.59	13.12	4.66
9	49.00	8.53	1.91	0.62	11.92	0.71	10.21	1.98
10	23.55	3.20	0.79	0.10	22.47	1.33	18.98	1.73
11	22.36	3.05	0.79	0.13	19.69	0.87	19.29	1.29
12	23.55	1.62	0.81	0.06	20.05	0.70	19.35	1.06
13	35.95	1.95	0.45	0.09	14.38	0.30	12.04	0.73
14	24.81	4.26	0.61	0.12	18.51	0.78	16.16	1.39
15	37.00	4.78	0.83	0.16	11.65	1.04	8.26	0.97
16	33.62	11.40	0.86	0.35	13.05	1.58	13.65	3.63
17	28.79	1.08	0.72	0.06	15.82	0.89	14.87	0.68
18	26.62	0.89	0.73	0.02	16.28	0.57	15.39	0.76
19	28.59	1.25	0.70	0.04	15.87	0.47	15.06	0.46
20	30.18	5.11	0.73	0.12	15.62	1.56	14.63	1.27
average	34.19	–	0.88	–	16.18	–	13.12	
standard deviation	10.12	–	0.55	–	3.54	–	3.72	

4. Conclusions

The following can be concluded taking into account the obtained results:

- chemical composition of coal slurries is typical for fine particle tailings of coal (Blaschke, 2005; Grudziński, 2005; Strzyszc and Łukasik, 2008). Low Al_2O_3 and TiO_2 content is a departure from the literature data,
- average calorific value in analytical state of coal slurries deposited in impoundments ranges from 9.26 to 23.29 MJ/kg with standard deviation ranging from ± 0.58 to ± 5.98 MJ/kg,
- average ash content in analytical state of coal slurries deposited in impoundments ranges from 26.98 to 63.96% with standard deviation ranging from ± 1.28 to $\pm 17.76\%$,

Table 7. Physicochemical analysis of coal slurries from all impoundments for particle size fraction <0.1 mm for analytical state and dry basis

Impoundment	Fraction <0.1 mm yield [%]	Hydroscopic moisture content [%]	Ash content [%]		Sulfur content [%]		Volatile matter content [%]		Calorific value [MJ/kg]	
			A ^a	A ^d	S ^a	S ^d	V ^a	V ^d	Q ^a	Q ^d
	γ	W _h	A ^a	A ^d	S ^a	S ^d	V ^a	V ^d	Q ^a	Q ^d
1	27.90	4.30	53.00	55.38	1.21	1.26	17.21	17.98	12.75	13.33
2	60.79	3.97	55.64	57.94	0.66	0.69	12.66	13.19	10.19	10.61
3	70.16	4.61	53.02	55.58	0.86	0.90	15.20	15.94	11.22	11.77
4	69.33	2.99	73.49	75.75	0.44	0.45	10.60	10.93	1.68	1.74
5	54.75	2.13	77.23	78.91	0.47	0.48	7.92	8.09	6.20	6.33
6	67.87	4.07	58.94	61.44	0.74	0.77	16.25	16.94	10.68	11.13
7	28.43	1.51	57.73	58.62	4.15	4.21	15.62	15.86	8.91	9.05
8	48.36	1.38	67.20	68.14	2.49	2.52	13.56	13.75	6.79	6.89
9	57.23	2.56	52.49	53.87	0.67	0.69	16.21	16.63	12.39	12.71
10	77.58	2.87	64.43	66.33	1.29	1.33	14.37	14.80	8.54	8.79
11	65.75	1.57	49.91	50.71	1.36	1.38	16.15	16.40	15.27	15.52
12	67.76	2.07	37.03	37.81	0.21	0.21	22.27	22.74	18.70	19.10
13	54.80	1.92	41.19	42.00	0.38	0.39	20.02	20.41	16.41	16.73
14	57.57	1.83	39.75	40.49	1.36	1.39	19.91	20.29	17.27	17.59
15	75.76	1.64	45.53	46.29	0.96	0.98	17.83	18.13	15.68	15.94
16	72.87	2.03	44.20	45.12	1.00	1.02	18.00	18.37	15.46	15.78
17	68.53	1.24	42.58	43.11	1.05	1.06	17.98	18.21	16.06	16.26
18	68.12	2.08	43.01	43.92	1.04	1.06	18.42	18.81	18.12	18.50
19	78.93	2.57	63.13	64.80	0.69	0.71	14.30	14.68	7.39	7.58
20	72.97	1.33	57.24	58.01	0.61	0.62	16.36	16.58	11.86	12.02
average	62.27	2.43	53.84	55.21	1.09	1.11	16.04	16.44	12.08	12.37
standard deviation	14.26	1.05	11.31	11.71	0.88	0.89	3.30	3.34	4.58	4.66

- average sulfur content in analytical state of coal slurries deposited in impoundments ranges from 0.57 to 2.98%. with standard deviation ranging from ± 0.03 to $\pm 1.27\%$,
- average transient moisture content of coal slurries deposited in impoundments ranges from 11.69 to 34.48%. with standard deviation ranging from ± 1.07 to $\pm 4.89\%$,
- average hygroscopic moisture content of coal slurries deposited in impoundments ranges from 1.04 to 7.92%. with standard deviation ranging from ± 0.07 to $\pm 2.40\%$,
- average volatile matter content in analytical state of coal slurries deposited in impoundments ranges from 14.29 to 28.50%. with standard deviation ranging from ± 0.40 to $\pm 5.47\%$,
- particle size analysis of coal slurries revealed that the majority of particles is in the fraction below 0.1 mm. On average, 62.27% of particles has a size below 0.1 mm and ranges from 27.90 to 78.93% for particular impoundments with standard deviation of $\pm 14.26\%$. In three impoundments this share is below 50%,
- average calorific value in analytical state of coal slurries deposited in impoundments in fraction below 0.1mm is rather high (12.01 MJ/kg on average) and ranges from 1.68 to 18.70 MJ/kg with standard deviation of ± 4.58 MJ/kg,
- particle size fraction < 0.1 mm has a higher ash and sulfur content.

Presented results indicate considerable variations in the quality of coal slurries deposited in different impoundments which is obvious taking into account different geology of coal deposits of the mines. At individual impoundment these differences are smaller which is demonstrated by the lower variation in the standard deviation.

Qualitative and quantitative analyses of coal slurries deposited in impoundments demonstrate a significant energetic potential which can be utilized by applying proper upgrading technology.

Acknowledgments

This investigation is performed within the frame of development project Nr N R09 0006 06/2009 entitled "Identification of energetic potential of coal slurries in the national fuel balance and technological development strategy of their usage". The project is implemented by the Institute of Mechanized Construction & Rock Mining in Warsaw in cooperation with the Department of Mineral Processing and Waste Utilization of the Silesian University of Technology.

References

- BLASCHKE W., 2005, *Określenie wartości mulów węglowych zdeponowanych w osadnikach ziemnych*. Materiały VII Ogólnopolskiej Konferencji Naukowej pt. „Kompleksowe i szczegółowe problemy inżynierii środowiska”. Politechnika Koszalińska. Koszalin.
- ÇIÇEK. T., CÖCEN. I., ENGIN V.T. and CENGİZLER H., 2008, *An efficient process for recovery of fine coal from tailings of coal washing plants*. Energy Sources. Part A: Recovery. Utilization and Environmental Effects, vol. 30, no. 18, 1716–1728
- GRUDZIŃSKI Z., 2005, *Analiza porównawcza jakości mulów węgla kamiennego pochodzących z bieżącej produkcji i zdeponowanych w osadnikach ziemnych*. Materiały VII Ogólnopolskiej Konferencji Naukowej pt. „Kompleksowe i szczegółowe problemy inżynierii środowiska”. Politechnika Koszalińska, Koszalin.

- HAMMACK. R., KAMINSKI. V., HARBERT W., VELOSKI. V., LIPINSKI. B., 2010, *Using Helicopter Electromagnetic (HEM) Surveys to Identify Potential Hazards at Coal-waste Impoundments: Examples from West Virginia*. Geophysics, Vol. 75; no. 6; B221–B229.
- MIAO Wu, XUEDI Hao, WU Jing, DAKE Zhu, 2010, *Pipeline Transport and Utilization of Coal Sludge*. XVI International Coal Preparation Congress. Conference Proceedings, 826–836.
- O'BRIEN. G., FIRTH. B., ADAIR. B., 2010, *The application of the coal particle analysis method to coal liberation studies*, International Coal Preparation Congress 2010. Conference Proceedings, 922
- ANAÇ S., GITMEZ A., 2010, *A New Plant Design Intended to Recover Coal from the Thickener Tailings to Prevent New Waste Dams*, International Coal Preparation Congress 2010. Conference Proceedings, 822.
- STRZYSZCZ Z., ŁUKASIK A., 2008, *Zasady stosowania różnorodnych odpadów do rekultywacji biologicznej terenów poprzemysłowych na Śląsku*, Gospodarka Surowcami Mineralnymi, vol. 24, no. 2/3, 41–49.
- SZPYRKA J., LUTYŃSKI A., 2012, *Właściwości fizyko-chemiczne mulów węglowych zdeponowanych w osadnikach ziemnych*, rozdział monografii: *Innowacyjne i przyjazne dla środowiska techniki i technologie przeróbki surowców mineralnych. Bezpieczeństwo – jakość – efektywność*, Instytut Techniki Górniczej KOMAG, Gliwice.
- SZPYRKA J., LUTYŃSKI M., 2012, *Analysis of selected methods of beneficiating coal slurries deposited in impoundments*, Physicochemical Problem of Mineral Processing, Vol. 48, Issue 2.
- WITKOWSKA-KITA B., BAIC I., LUTYŃSKI A., SUPONIK T., 2012, *Identyfikacja depozytów mulów węglowych – właściwości chemiczne. Baza Danych (DMW)*, rozdział monografii: *Innowacyjne i przyjazne dla środowiska techniki i technologie przeróbki surowców mineralnych. Bezpieczeństwo – jakość – efektywność*. Instytut Techniki Górniczej KOMAG. Gliwice.

Received April 13, 2012; reviewed; accepted May 28, 2012

ALKALINE LEACHING OF ZINC FROM ARGON OXYGEN DECARBONIZATION DUST FROM STAINLESS STEEL PRODUCTION

Anna STEFANOVA, Jari AROMAA, Olof FORSEN

Aalto University, Department of Materials Science and Engineering
PO Box 16200, FI-00076, Aalto, Finland; email: anna.stefanova@aalto.fi

Abstract: Stainless steel production generates solid wastes such as dust and sludge that are considered as harmful in most industrial countries. Today dusts are recycled in separate treatment plants as these dusts contain valuable metals such as alloying elements. A direct recycling of dust back to steel production is hindered due to the presence of elements, especially zinc, that cause operational difficulties in the stainless steel making process. In this paper two different stainless steel converter argon oxygen decarbonization dusts (AOD1 and AOD2), from Outokumpu Stainless (Tornio, Finland), were leached using NaOH solutions. The purpose was to selectively leach zinc out from the dusts and to find factors that affected most dissolution of zinc. The dust samples were leached under atmospheric pressure and the factors tested were temperature, sodium hydroxide concentration, liquid to solid ratio (L/S), stirring rate and oxygen or nitrogen gas bubbling. All the studied factors had statistically significant effect on the dissolution of zinc. The maximum zinc extraction was achieved at 95°C, with 8M NaOH solution, stirring rate of 400 rpm and L/S ratio of 30 and was around 80% for AOD1 dust and around 50% for AOD2 dust. Difference in maximum zinc extraction arose from the mineralogical differences of the dusts. Zinc was leached selectively. Among alloying elements only molybdenum was leached and practically no iron, chromium and nickel were dissolved.

Key words: *AOD dust, stainless steel, zinc, leaching, sodium hydroxide*

Introduction

Stainless steel production generates quantities of various solid wastes in form of dust and sludge. During the production of stainless steel, between 30 and 70 kg of dust and fine waste is generated per ton (megagram) of steel produced (Denton, 2005). In most industrial countries stainless steel dusts are considered as harmful waste, on the other hand, these dusts also contain valuable metals such as alloying elements and zinc. From economic and environmental point of view it is desirable to recover the valuables and utilize these wastes (Majuste, 2009). However, a direct recycling of dust

back to stainless steel production is hindered because they contain considerable amounts of elements, especially zinc, that cause operational difficulties in the steel making process (Palencia, 1999). Zinc vaporizes easily and condenses into steel production fumes ending up in the flue dust or sludge usually as an oxide or ferrite and its content in stainless steel dusts is in the range of 1.0–16.4 wt% (Atkinson, 2001; Leclerc, 2002; Nyirenda, 1992).

Various pyrometallurgical, hydrometallurgical and combined processes have been developed to allow better utilization of steel making dusts in primary operations (Jha, 2000; Orhan, 2005; Rao, 2006; Xia, 1999; Youcai, 2000) but only few of them have reached commercialization. Today the dust treatment processes are predominantly pyrometallurgical and dusts are recycled in separate treatment plants to recover metals. There are still significant problems associated with treating this material and the developed processes have not been entirely satisfying (Xia, 1999). The drawbacks with pyrometallurgical processes are the high consumption of energy and a need of relatively large tonnage of dust to be economically competitive. Hydrometallurgical processes are considered suitable for an on-site treatment (Nakamura, 2007) as they can fit on small scale (Dutra, 2006), but the major obstruction in the hydrometallurgical extraction of zinc is the ferrite form of zinc. Zinc ferrite (ZnFe_2O_4) is insoluble in many solutions (Xia, 2000) and usually 30–70% of zinc is in ferrite form (Leclerc, 2002).

Metal extraction from the dusts is difficult due to their complex composition. Stainless steel dust consists mainly of oxide phases that are rich in Fe, Cr, Ca, Zn, Mg, Mn and Ni, with minor amounts of phases that contain alkaline metals (K, Na), halogens (Cl, F), Si, Mo, Pb and S (Ma, 2006). However, the chemical compositions and crystalline phases present in the dusts vary considerably depending on the steel grade produced, raw materials used, and operation conditions and procedures (Rao, 2006). Finding a suitable process is complicated as each dust is unique. Hydrometallurgical processes can offer an interesting alternative for zinc recycling if iron dissolution can be controlled. The major advantage of alkaline leaching is its selectiveness in leaching zinc compared to iron compounds. Thus, a relatively clean and iron-free solution is obtained and the complicated iron removal processes are avoided.

Previous studies on hydrometallurgical methods have concentrated on the leaching of zinc from carbon steel dusts and mainly from the electric arc furnace (EAF) dusts. In this paper two different argon oxygen decarbonization converter dusts (AOD1 and AOD2) from stainless steel production (Outokumpu Stainless Oy Tornio, Finland) were leached using NaOH solutions. The target was to selectively leach zinc out of stainless steel making dusts and to minimize the zinc content in the dust. This would provide an opportunity to effectively recycle the dust back to the steel making process and to recover zinc from the dust.

Experimental

Argon oxygen decarburization converter dust samples (AOD1 and AOD2) from stainless steel production were received from Outokumpu Tornio Works for the leaching experiments. AOD1 represents dust from line 1 and AOD2 from line 2. On line 1 ferrochrome is fed as melt into AOD converter whereas on line 2 solid ferrochrome is melted along with the charge. The dusts are a mixture of different production batches thus representing an average dust composition.

The chemical and mineralogical analysis of dust samples was done with optical microscopy, Scanning electron microscopy (SEM), Electron probe micro-analyzer (EPMA), X-ray diffraction (XRD), Atomic absorption spectroscopy (AAS), and Inductively coupled plasma atomic emission spectroscopy (ICP-AES) with molten sodium peroxide or nitro-hydrochloride acid leaching pre-treatment. The results of the chemical analyses are presented in Table 1. The main components in the dusts are iron, zinc, chromium and calcium. The zinc content is on average 9.762% for AOD1 and 4.650% for AOD2. The identified phases in the AOD1 and AOD2 dusts, according to qualitative phase analysis, are presented in Table 2. Zinc was found to be present as zincite (ZnO) in AOD1 as franklinite (ZnFe_2O_4) and zincite in AOD2. In the AOD2 dust, there were phases that contained a significant amount of molybdenum.

Table 1. The chemical composition of dust samples (in %)

	Fe	Cr	Zn	Ca	Mn	Mg	Ni	Pb	Si	Mo
AOD1	26.9–37.8	4.39–18.56	8.96–10.8	4.74–5.56	0.95–2.87	0–1.38	0.4–0.72	0.08–0.1	0–0.89	0–0.075
AOD2	13.8–26.4	2.18–13.39	3.52–5.91	13.08–17.2	0.9–3.4	0–2.53	1.88–2.92	0.39–0.56	0–2.76	0–1.4
Minor amounts 0–< 1% in both dusts	Al, B, Ba, C, Cd, Co, Cu, F, K, Na, P, S, Sr, V									

Table 2. The identified phases according to qualitative phase analysis

Element	AOD1	AOD2
Fe, Cr, Mg	FeCr_2O_4 (chromite), MgFe_2O_4 (magnesioferrite), Fe_3O_4 (magnetite), $(\text{NiFe})\text{Fe}_2\text{O}_4$ (trevorite), MgFe_2O_4 (magnesioferrite), Fe_2O_3 (maghemite)	MgFe_2O_4 (magnesioferrite), Fe_3O_4 (magnetite), FeCr_2O_4 (chromite), ZnFe_2O_4 (franklinite), $(\text{NiFe})\text{Fe}_2\text{O}_4$ (trevorite), Fe_2O_3 (maghemite), $(\text{FeMg})(\text{CrFe})_2\text{O}_4$ (donathite)
Zn	ZnO (zincite)	ZnFe_2O_4 (franklinite), ZnO (zincite)
Ni	NiO (bunsenite), $(\text{NiFe})\text{Fe}_2\text{O}_4$ (trevorite)	$(\text{NiFe})\text{Fe}_2\text{O}_4$ (trevorite)
Ca	CaO (lime)	CaO (lime), CaCO_3 (calcite)
Si	$(\text{NH}_4)_2\text{SiF}_6$ (cryptohalite)	$(\text{NH}_4)_2\text{SiF}_6$ (cryptohalite)
Mn		$\text{KMn}_8\text{O}_{16}$ (cryptomelane)
Mo		MoO_2 (tugarinovite)

The microstructure of the dusts consists of bigger particles and grains surrounded by finer fraction. Also agglomeration of finer fraction was noticed. The particle size analysis of dust samples was done with laser diffraction (Beckman Coulter) and by Scanning-Foto-Sedimentograf. All particles measured by Scanning-Foto-Sedimentograf were under $47\ \mu\text{m}$ for both AOD1 and AOD2 dusts with smallest particles under $1\ \mu\text{m}$. Analyses by laser diffraction showed that all particles were less than $4\ \mu\text{m}$ for AOD1 dust and $20\ \mu\text{m}$ for AOD2 dust. Larger particles consist of several phases and some phases were encapsulated inside of particles. For the finer fraction no encapsulation phenomenon was found. Zinc occurred mainly in the fine fraction in which the maximum ZnO content is around 14% in both AOD1 and AOD2 dusts.

The leaching experiments were carried out in the apparatus shown in Figure 1. The experimental setup for the leaching test consisted of a termobath (Lauda AquaLine AL25), glass reactor and motor driver stirrer (VWR VOS16). The cover of the glass reactor provided through holes for mercury thermometer, gas bubbling, stirrer and sampling/feeding. A water-cooled condenser was added to the structure at higher temperatures.

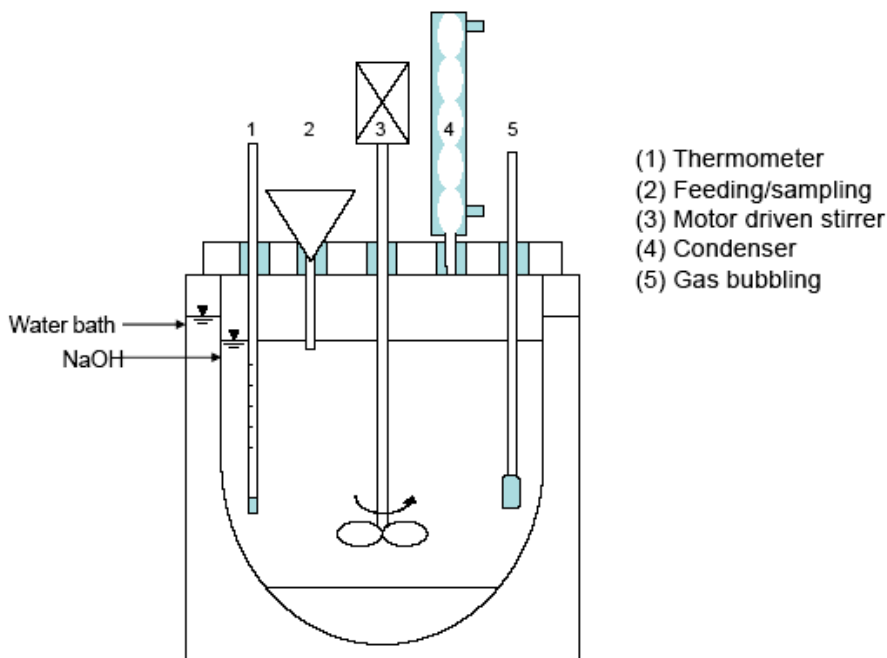


Fig. 1. Leaching reactor in water bath

Volume of $800\ \text{cm}^3$ of NaOH solution (prepared by technical grade grains and distilled water) was set into the reactor, which was put in a water bath in order to control the temperature in the reactor. For adjusting the oxidative or reductive conditions,

oxygen or nitrogen gas was fed into the reactor for 1 hour and after that the dust was charged and stirring rate was adjusted. A liquid sample was taken off and filtered in the chosen time intervals of 5, 10, 15, 20, 25, 30, 60 and 120 minutes for AOD1 dust and 5, 15, 30, 60 and 120 minutes for AOD2 dust. The stirring was stopped 30 seconds before each sampling.

The leaching tests were done using factorial test series (Table 3) with two replicates where a high and a low level of a factor were used. The studied factors were temperature, NaOH concentration, liquid-solid ratio (cm^3/g), stirring rate and oxygen or nitrogen gas bubbling. In the experiments temperature of 25°C or 95°C and NaOH concentrations of 2 M and 8 M were used. The chosen liquid/solid (cm^3/g) ratios were 5 and 30 and for this 160 g or 26.67 g of dust was added to the reactor. The stirring rate was adjusted to 100 or 400 rpm and the oxidative or reductive conditions were adjusted using oxygen or nitrogen gas bubbling.

Table 3. Factorial (2^{5-2}) test series used in the leaching experiments

Std Order	NaOH (M)	L/S Ratio	Temp. Deg C	Bubbling with	Agitation rpm
1	2	5	25	O ₂	400
2	8	5	25	N ₂	100
3	2	30	25	N ₂	400
4	8	30	25	O ₂	100
5	2	5	95	O ₂	100
6	8	5	95	N ₂	400
7	2	30	95	N ₂	100
8	8	30	95	O ₂	400

After filtering the leach samples were analysed for the amount of leached Zn, with the Perkin Elmer 372 AAS device. The standard solutions were prepared by using an Atomic Absorption Standard zinc $1000 \mu\text{g}/\text{cm}^3$ Baker 6827 solution. Part of the samples after 120 min of leaching was analyzed more precisely with multi-element ICP-AES analysis in order to investigate that the unwanted iron and other elements were not leached.

Results and discussion

The main response under investigation was the percentage of zinc extraction from the AOD1 and AOD2 dusts in the leach liquor. The leaching curves of zinc are presented in Figs 2 and 3. Figure 2 shows the leaching curves of the four experimental conditions with best zinc recovery. In Fig. 3 the four leaching conditions of lower zinc extractions are shown. From the shape of the leaching curves can be observed that the dissolution of zinc is fast (in the both high and low recoveries of zinc) and occurs in a

few minutes. Usually, the maximum recovery was achieved at the longest leaching time (120 min), however, in some experiments the maximum yield of zinc was achieved earlier and then it decreased, which may indicate that part of zinc was pre-precipitated back.

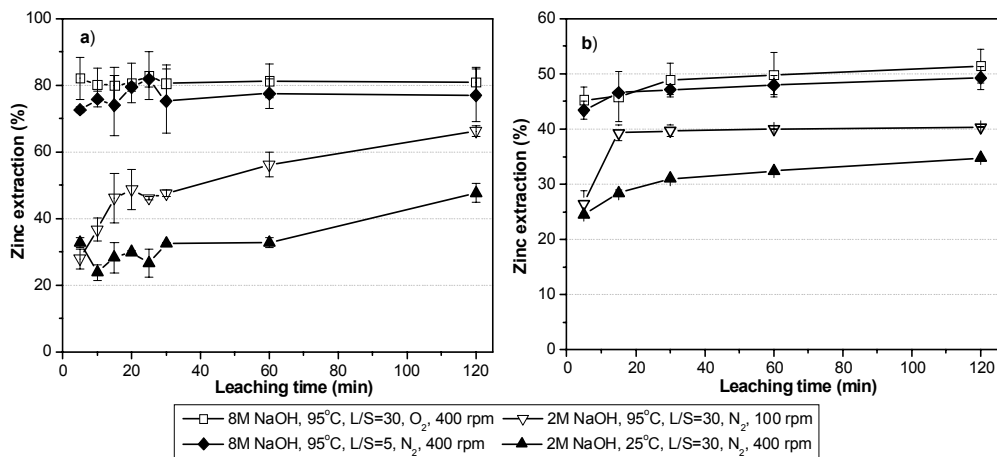


Fig. 2. The four leaching conditions that gave better zinc extractions for a) AOD1 and b) AOD2 dust

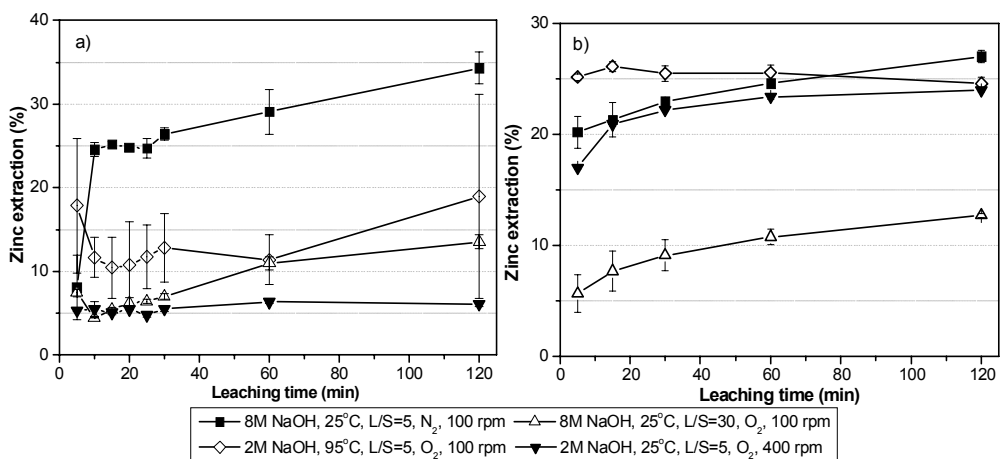


Fig. 3. The four leaching conditions that gave poorer zinc extractions for a) AOD1 and b) AOD2 dust

Under the present experimental conditions, zinc extraction varied from 6% to around 80% for the AOD1 dust. The extractions were on the average lower for AOD2 dust and varied from 13% to around 50%. Difference in maximum zinc extraction arose from the mineralogical differences of the dusts. In the AOD2 dust zinc was found to be present also in ferrite form that is difficult to dissolve in alkaline solutions.

For both dusts the maximum value of extracted zinc was obtained by using 8 M NaOH solution and stirring rate of 400 rpm at the temperature of 95°C. The liquid-solid ratio was 30 and oxygen bubbling was used. According to the results the dissolution of zinc was greater when high temperature and stirring rate, strong NaOH solution and lower liquid-solid ratio were used.

To study the effects and possible interactions of the leaching factors on zinc dissolution, the analysis was done using the Minitab 16 software. Figure 4 represents the normal plot of the standardized effects of the studied factors after 120 min leaching.

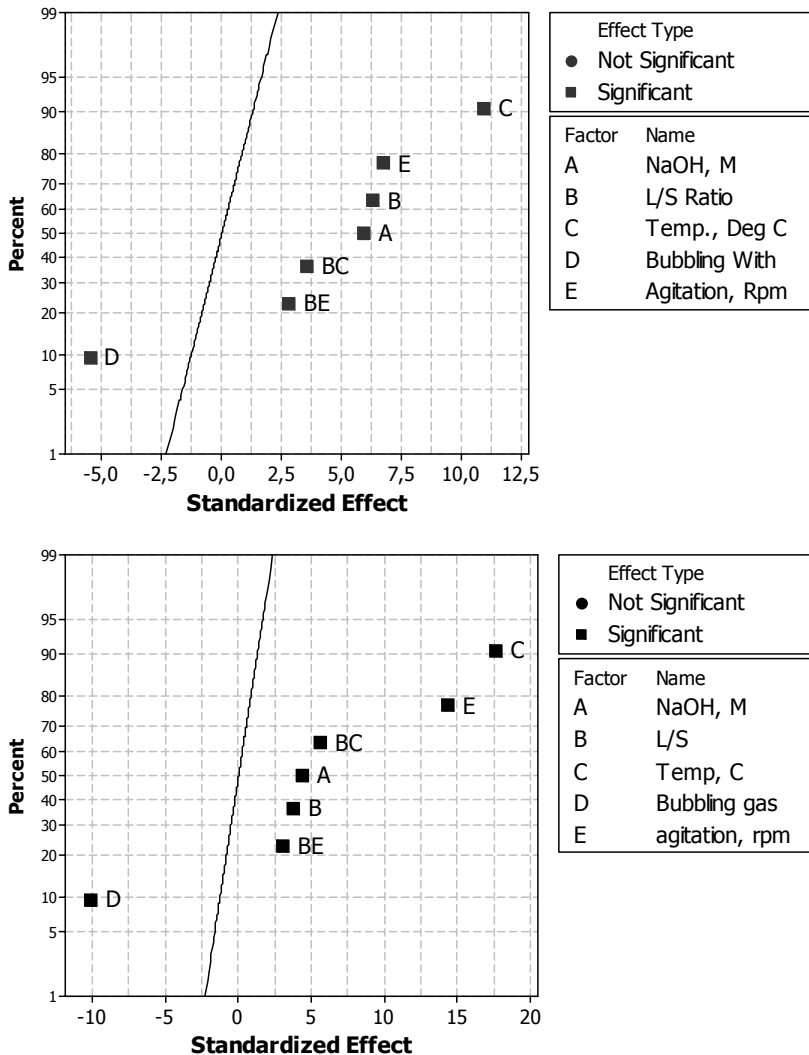


Fig. 4. Normal plot of the standardized effects of studied factors (response is Zn extraction %, alpha = 0.05). Above: AOD1 dust. Below: AOD2 dust

Mainly, the same trends can be observed for both dusts. All leaching factors studied in this work had statistically significant effect on the dissolution of zinc. Temperature affected the zinc extraction preferentially in both dusts and the other factors were nearly equally significant for the AOD1 dust. For AOD2 dust, temperature, agitation and bubbling gas were more significant factors when NaOH concentration and L/S ratio were less significant. For both dusts, temperature, NaOH concentration, stirring rate and liquid-solid ratio had a positive response on zinc dissolution and increasing values of these factors increased the dissolution of zinc. Oxygen bubbling had a negative response and the dissolution of zinc was enhanced with nitrogen gas bubbling although the highest zinc extraction was achieved under conditions in which oxygen bubbling was used.

The interactions of all factors were not easy to observe, nevertheless, two-factor interactions were found between NaOH concentration and other studied factors in both dusts (Fig. 5). The interactions with NaOH concentration, stirring rate and temperature are explained by the high viscosity of strong NaOH solution. The increase of temperature and/or stirring rate enhanced the extraction of zinc in strong viscous NaOH solution. Also a strong 8 M NaOH solution is needed for leaching zinc when the amount of solids was larger. The reason for interaction between NaOH concentration and bubbling gas is unclear. It is possible that there is not significant electrochemical dissolution, where the oxidant could have an effect. To find out the possible interactions between the other factors more experiments are needed.

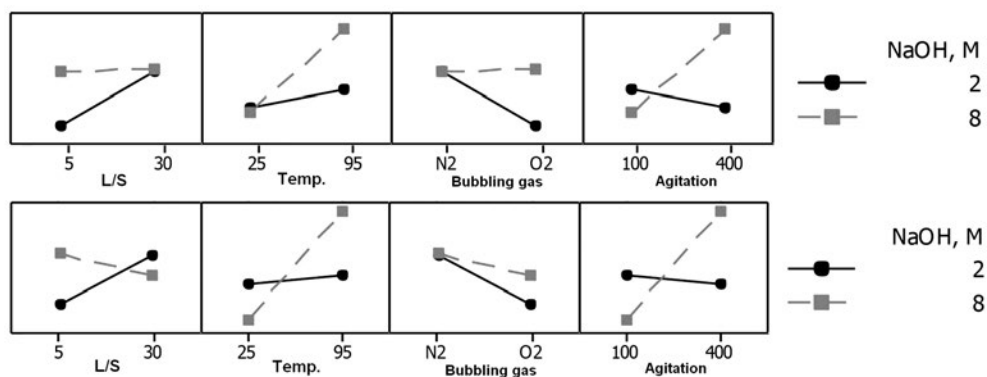


Fig. 5. Two-factor interactions between NaOH concentration and other studied factors after 120 min of leaching. Above: AOD1 dust. Below: AOD2 dust

Some of the samples after 120 min of leaching were analyzed with ICP-AES in order to investigate that iron and other elements such as alloying elements were not leached. The results for iron, chromium, nickel and molybdenum are presented in Table 4. Practically no iron ($< 1.5 \text{ mg/dm}^3$) or nickel ($< 0.1 \text{ mg/dm}^3$) was dissolved. Chromium was dissolved less than 4% at most. Solubility of molybdenum in strong NaOH solutions differed from the other alloying elements. Molybdenum dissolved

well and its amount (mg/dm^3) was almost the same as zinc in the leachates from the AOD2 dust. In couple of samples it was even slightly higher. In the AOD1 dust the amount of Mo was low compared to the AOD2 dust and thus also its amount (mg/dm^3) was low in relation to zinc in the leachate from the AOD1 dust.

Table 4. Amount of certain elements in leachate after 120 min leaching

	Amount in leachate (mg/dm^3)							
	Zn	Fe	Cr	Ni	Mo	Ca	Pb	Cd
AOD1	394–14950	< 1.5	27–484	< 0.1	3–56	< 5–21	< 2.5–24	< 0.25
AOD2	194–3722	< 1.5	< 1–258	< 0.1- 0.11	193–2834	< 5–10	< 2.5–61	< 0.25

Conclusions

Two different AOD dust samples from stainless production, delivered from Outokumpu Stainless (Tornio, Finland), were leached in NaOH solution using different leaching conditions. The purpose was to selectively leach zinc out from the dusts and to find factors that affected most on dissolution of zinc. The leaching experiments were done using factorial (2^{5-2}) test series and the studied factors were NaOH concentration, temperature, solid-to-liquid ratio, stirring rate and oxygen or nitrogen gas bubbling. All factors had statistically significant effect on the dissolution of zinc in both dusts and the effect of temperature was emphasized. All factors had positive response except oxygen gas bubbling, that had negative response. In both dusts the maximum zinc extraction was achieved at 95°C , with 8M NaOH solution, stirring rate of 400 rpm and L/S ratio of 30. Maximum zinc extraction was 80% from the AOD1 dust and 50% from the AOD2 dust. Difference in maximum zinc extraction arose from the mineralogical differences of the dusts. In the AOD2 dust zinc was found to be present also in ferrite. The experiments showed that leaching of zinc using NaOH solutions is selective, among alloying elements only molybdenum was leached and practically no iron, chromium and nickel were dissolved.

Acknowledgement

This work has been done in the METDUST project of the ELEMET research program funded by FIMECC Oy. The financial support of TEKES, Outokumpu Stainless Oyj and Outotec Oyj is gratefully acknowledged. The analytical work in characterizing the dusts done by the group of Professor Tomas Havlik in Technical University of Kosice and M.Sc. Hannu Makkonen from Oulu University is gratefully acknowledged. The authors are grateful to Mr. Terry Russell for the valuable guidance in data analysis.

References

- ATKINSON, M., KOLARIK, R., 2001, Chapter 4: Environmental Leadership. Steel Technology Roadmap, 83–120. Available: http://www1.eere.energy.gov/manufacturing/industries_technologies/steel/pdfs/roadmap_chap4.pdf [13.04.2012]

- DENTON, G.M., BARCZA, N.A., SCOTT, P.D., FULTON, T., 2005, *EAF Stainless Steel Dust Processing*, in: Sustainable developments in metals processing, eds. Nilmani M., Rankin W.J., Melbourne, Australia, 273–283.
- DUTRA, A.J.B., PAIVA, P.R.P., TAVARES, L.M., 2006, *Alkaline leaching of zinc from electric arc furnace steel dust*, Minerals Engineering, 19, 478–485.
- JHA, M.K., KUMAR, V., SINGH, R.J., 2000, *Review of hydrometallurgical recovery of zinc from industrial wastes*, Resources Conservation & Recycling, 33(2001), 1–22.
- LECLERC, N., MEUX, E., LECUIRE, J.-M., 2002, *Hydrometallurgical recovery of zinc and lead from electric arc furnace dust using monitrolotriacetate anion and hexahydrated ferric chloride*, Journal of Hazardous Material, B91, 257–270.
- MA, G., GARBERS-CRAIG, A.M., 2006, *A review on the characteristics, formation mechanism and treatment processes of Cr (VI)-containing pyrometallurgical wastes*, The Journal of Southern African Institute of Mining and Metallurgy, 106, 753–763.
- MAJUSTE, D., MANSUR, M.B., 2009, *Leaching of the fraction of the argon oxygen decarburization with lance (AOD-L) sludge for the potential removal of iron*, Journal of Hazardous Material, 153(1–2), 89–95.
- NAKAMURA T., S.E., TAKASU T., ITOU H., 2007, *Basic Consideration on EAF Dust Treatment Using Hydrometallurgical Processes*. 47–53.
- NYIRENDA, R.L., 1992, *The Reduction of Zinc-rich Ferrites and its Implication for a Caron-type Process for Carbon Steelmaking Dust*. Dissertation Thesis, Delft University of Technology.
- ORHAN, G., 2005, *Leaching and cementation of heavy metals from electric arc furnace dust in alkaline medium*, Hydrometallurgy, 78, 236–245.
- PALENCIA, I., ROMERO, R., IGLESIAS, N., CARRANZA, F., 1999, *Recycling EAF Dust Leaching Residue to the Furnace: A Simulation Study*, JOM: 28-32.
- RAO, S.R., 2006. Chapter 8: Metallurgical slags, dust and fumes, Waste Management Series: Resource Recovery and Recycling from Metallurgical Wastes, 269–327.
- XIA, D.K., PICKLES, C.A., 1999, *Caustic roasting and leaching of electric arc furnace dust*. Canadian Metallurgical Quarterly, 38(3), 175–186.
- XIA, D.K., PICKLES, C.A., 2000, *Microwave caustic leaching of electric arc furnace dust*, Minerals Engineering, 13(1): 79–94.
- YOUCAI, Z., STANFORTH, R., 2000, *Integrated hydrometallurgical process for production of zinc from electric arc furnace dust in alkaline medium*, Journal of Hazardous Material, B80, 223–240.

Received March 19, 2012; reviewed; accepted May 13, 2012

BIOLOGICAL REMOVAL OF Cr(VI) IONS FROM AQUEOUS SOLUTIONS BY *TRICHODERMA VIRIDE*

Anna HOLDA, Ewa KISIELOWSKA

AGH University of Science and Technology, Faculty of Mining and Geoengineering, turno@agh.edu.p

Abstract: The paper presents biological removing of Cr(VI) ions from aqueous solution by applying autochthonic fungi seedling of *Trichoderma viride* originated from chromium mud samples. The growth of organism and removing of chromium(VI) was performed in aqueous solution of various chromium(VI) contents and at optimal value of pH. During 14 days of incubation, samples of 5 cm³ each were collected every day for determination of chromium(VI) in solution and the efficiency of biological removal was specified. Since removal of chromium(VI) from aqueous solution may occur because of reduction, bio-sorption or bioaccumulation processes, to determine which one occurred, the Cr(III) contents were determined in samples of the medium as well in ooze after mycelium irrigating and in mycelium.

Key words: *bioaccumulation, chromium, Cr(VI), microscopic fungi, Trichoderma viride*

Introduction

Chromium occurs widely in earth's crust as a natural component of rocks, minerals, soils and water. On a worldwide basis, about 80% of the chromium mined goes into metallurgical applications (particularly for manufacture of stainless steel). Only about 15% is used in chromium chemicals manufacture and the remainder is used in refractory applications. In environment, the most often occurred valences of chromium are Cr(III) and Cr(V). The more toxic and harmful, both for environment and human beings, is Cr(VI). Because of its toxic properties and high mobility, effluents and wastes containing this element are treated as highly dangerous. Even relatively small amounts of this element may be a source of danger for ecosystem because of the persistence of its compounds and possibility of multiplying its concentration (Badura, 1993; Barnhart, 1997; Wolak et al., 1997).

The currently applied chemical methods of treatment of effluents containing chromium, which results are not satisfying, require significant financial costs (Kowalski, 2002). The alternative for them may be biotechnological processes (Bai et al., 2003; Chen et al., 1997; Sen et al., 2007). The application of selectively chosen microorgan-

isms may significantly limit the amount of chromium introduced to the environment. The main advantage of biotechnological methods is the fact that these methods are economic and environmentally friendly. Chromium is removed by a cellular metabolism of microorganisms mainly by bioaccumulation, biosorption and biotransformation.

Previous investigations describe the applications of living and dead microorganisms cells to remove Cr(VI) from aqueous solutions by biosorption (Dönmez and Koçberber, 2005; 2007; Dursan et al., 2003; Ksheminska et al., 2005; Saxena et al., 2000; Srinath et al., 2002) and bioaccumulation (Anjana et al., 2007; Deepa et al., 2006; Donghee Park et al., 2005; Kapoor and Viraraghavan, 1995; Kumar et al. 2008; Ming Zhou et al., 2007; Morales-Barrera and Cristiani-Urbina, 2006; Parka et al., 2005; Srinath et al., 2002; Srivastavaa, Thakurb, 2006; Ziagova et al., 2007). Each of these methods has advantages and disadvantages. The application of dead biomass removes problems of toxic metal concentration in solutions and requirements connected with growth environment – nourishment. Furthermore, the adsorbed metal may be easily removed and the remaining biomass may be applied again. However, the limitation of this method is the fact that no reactions are being continued in the dried cells.

The application of living biomass makes it possible to remove metals during its growth allowing to avoid processes of its reproduction, drying and storage. Unfortunately, in this case the metal concentration in environment is highly important since too high concentration may be toxic for the growing biomass. This problem can be avoided by applying the microorganisms of high tolerance to high concentrations of Cr(VI) or getting it by adaptive processes.

The purpose of the investigation presented in the paper is to optimize the biological process of removing Cr(VI) by application of indigenous microorganisms isolated from chromium mud samples (Holda et al., 2009).

Materials and methods

The autochthonic fungi seedling *Trichoderma viride*, originating from a chromium mud was selected to research on removing Cr(VI).

Investigation of process dependency on pH

Strains of fungi were grown aerobically at 28 °C in accumulating medium prepared by mixing Cr(VI) solution autoclaved separately (at 120 °C for at least 20 min) and sterilized solution according to Waksman. The pH of medium was adjusted to the desired value by using 0.5 M sulfuric acid(VI) solution. Cultures were formed in a 300 cm³ Erlenmeyer flask with 100 cm³ of accumulation medium containing 50 mg of ions of Cr⁶⁺/dm³. The 2.5 cm³ samples of medium were collected from each Erlenmeyer flasks daily, during 14 days, then transferred to flasks of 25 cm³ volume each. Then, solutions of 2 M sulfur acid(VI) and 1.5-difenylocarbaside(I) were added to the 25

cm³ flasks. After 5 minutes, the flasks were filled up to the line with medium according to Waksman. Residual chromium(VI) ions concentrations in the bioaccumulation medium were determined by measuring the absorption at 540 nm by means of spectrophotometer Cadas 200 type LPG 392 (Gajkowska-Stefańska et al., 2001; Hermanowicz et al., 1999; Marczenko and Balcerzak, 1998; PN-C-04604:1977; PN-EN ISO 18412:2007).

Determination of chromium(VI) contents

Agents used for determination of chromium contents, that is 1.5-difenylocarbaside(I) and 2 M sulfuric acid(VI), were prepared according to the Polish standard (PN-EN 12441-10).

Before starting the measurements, the standard line was prepared. To this purpose, solutions of sulfuric acid(VI), 1.5-difenylocarbaside(I) and certain volumes of standard solution of chromium(VI) were introduced to 100 cm³ flasks to get the Cr⁶⁺ ions concentrations of 0, 0.1, 0.2, 0.4, 0.6, 0.8 and 1 mg/dm³.

The analytical samples were prepared by mixing solutions of sulfuric acid(VI), 1.5-difenylocarbaside(I) and sample solution in 25 cm³ flask.

Dependence of the process of chromium (VI) concentration in nourishment

The investigation of Cr(VI) ions concentration in medium in relation to pH allowed to determine the best reaction by which the fungi grow the best. It was found to be 4.5.

A certain amount of medium and K₂Cr₂O₇ (1g of Cr⁶⁺ ions/dm³) were transferred to Erlenmeyer flasks to get the required chromium concentration in certain sample in the volume of 100 cm³ of the bed.

The determination of chromium(VI) contents was conducted every day at the same hour. The samples of 2.5 cm³ of medium were collected, which were then transferred to 25 cm³ flasks (10-fold dilution). Next, the solutions of 2M sulfuric acid(VI) and 1.5-difenylocarbaside(I) were added. After 5 minutes, the sample was filled up to the line with the Waksman medium. Chromium(VI) ions concentration in the sample was determined by measuring absorption at 540 nm using spectrophotometer Cadas 200, type LPG 392 (Gajkowska-Stefańska et al., 2001; Hermanowicz et al., 1999; Marczenko, Balcerzak, 1998; PN-C-04604:1977; PN-EN ISO 18412:2007).

In case of the concentration higher than the standard scale range, the samples were adequately diluted.

Determination of biological type of Cr(VI) ions removal

The removal of chromium(VI) from the aqueous solution may occur because of reduction, biosorption or bioaccumulation processes. To determine which of them occurred during the investigation, the Cr(III) contents were determined in samples of medium as well chromium contents in ooze after the mycelium irrigating and in mycelium.

Determination of Cr(III) in medium

The Cr(III) ions contents were determined on the basis on the difference between total chromium and chromium(VI) contents in the medium after 14 days of incubation.

For total chromium contents determination, the samples of the medium with volume assuring the concentration of Cr within the standard scale range, were introduced to a beaker of 200 cm³ in volume and were filled up to the volume of 50 cm³. Next, for oxidation of Cr(III) ions to Cr(VI) the solutions of sulfuric acid(VI) and ammonium persulfate were added to the sample and then it was boiled and maintained in this state during 20-25 minutes. After cooling, the samples were transferred to flask of 50 cm³ in volume and the solution of 1.5-difenylocarbaside(I) was added. After 5 minutes the sample was filled up to the line with the Waksman medium. Chromium(VI) ions concentration in the sample was determined by measuring absorption at 540 nm using spectrophotometer Cadas 200, type LPG 392 (Gajkowska-Stefańska et al., 2001; Hermanowicz et al., 1999; Marczenko, Balcerzak, 1998; PN-C-04604:1977; PN-EN ISO 18412:2007).

Determination of chromium contents in ooze after mycelium irrigating

Mycelium was investigated after 14 days of incubation. To determine the presence of chromium adsorbed on the surface, the mycelium was irrigated. The obtained ooze was then analyzed to find the total chromium content (Gajkowska-Stefańska et al., 2001; Hermanowicz et al., 1999; Marczenko, Balcerzak, 1998; PN-C-04604:1977; PN-EN ISO 18412:2007).

Determination of chromium contents in mycelium

After 14 days of incubation, dried fungi at 105 °C were inserted into oven at temperature of 600 °C. Next, the chromium compounds were transformed into dilatable nitrates by means of concentrated nitric acid(V). The content of Cr(VI) in the mineralized sample was determined by the spectrophotometric method (Gajkowska-Stefańska et al., 2001).

Results and discution

Investigation of process dependency on pH

On the basis of experimental results graphs were created with dependency of chromium(VI) ions concentration in the medium on pH.

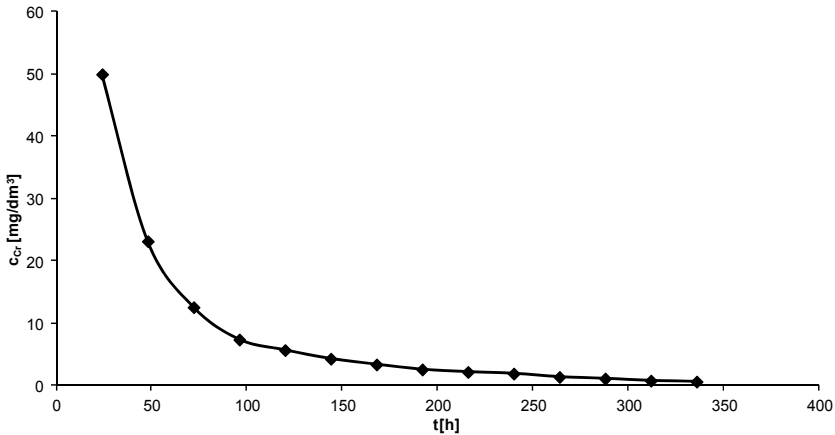


Figure 1. $c_{Cr} = f(t)$ at pH=4.0. Initial concentration of chromium(VI) was 50 mg/dm³

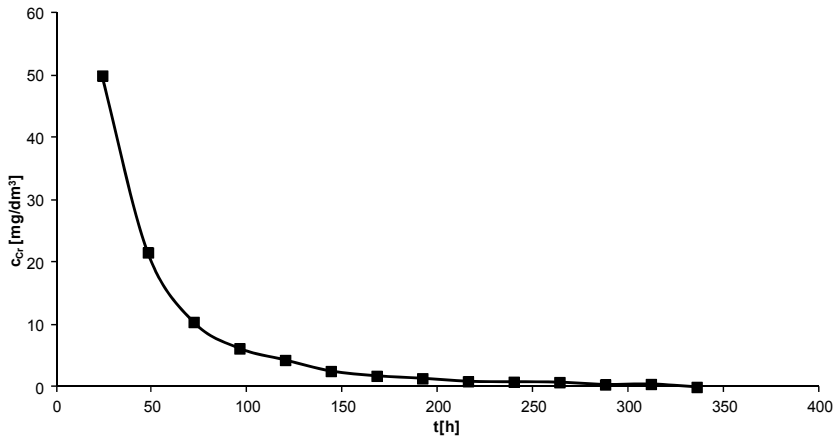


Figure 2. $c_{Cr} = f(t)$ for pH = 4.5. Initial concentration of chromium(VI) was 50 mg/dm³

Figures 1–7 show the change of Cr(VI) concentration in the medium with different initial pH, ranging from 4.0–6.5. Based on our study, the optimal pH for *Trichoderma viride* was found. At pH = 4.5, chromium(VI) ions were removed the most efficiently and the mildew fungi developed the best.

The optimum initial pH value for *Trichoderma viride* was 4.5. Morrales-Barrera et al. (2006) studied Cr(VI) removal by *T. viride* in a pneumatically agitated bioreactor. In the experiments the initial pH of the culture media was 6.0 ± 0.1 and the pH was not controlled during the experiments. In the case of biosorption by immobilized to Ca-alginate *T. viride* biomass, the optimum pH was 2.5 (Kumara et al., 2011) was determined.

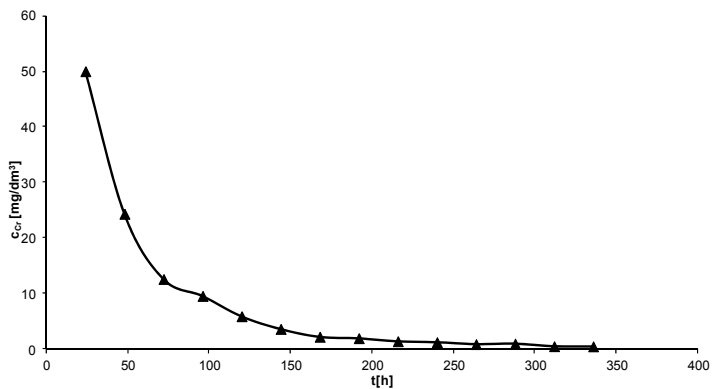


Figure 3. $c_{Cr} = f(t)$ for pH = 5.0. Initial concentration of chromium(VI) was 50 mg/dm^3

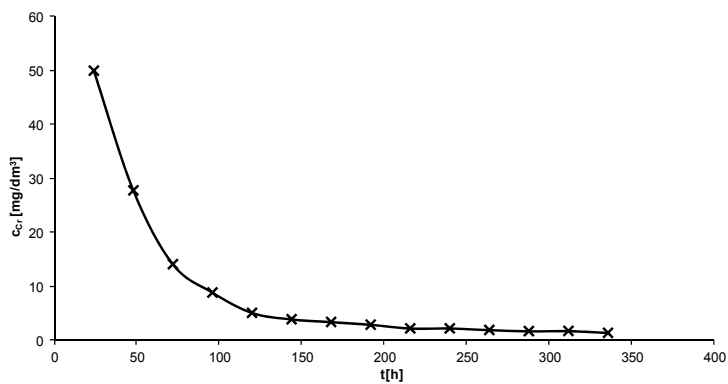


Figure 4. $c_{Cr} = f(t)$ for pH = 5.5. Initial concentration of chromium(VI) was 5 mg/dm^3

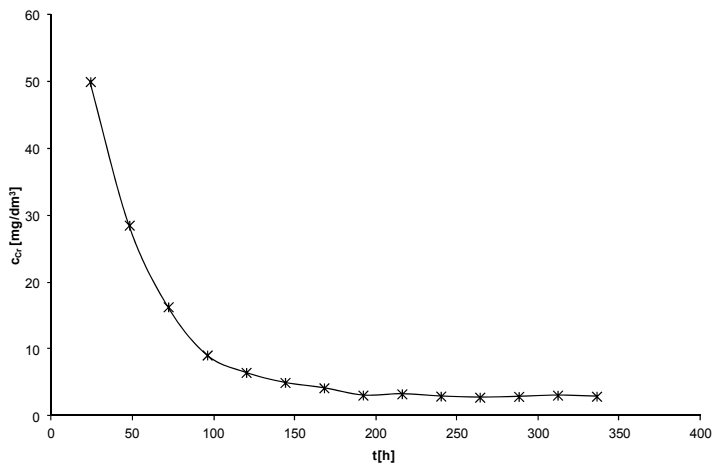


Figure 5. $c_{Cr} = f(t)$ for pH = 6.0. Initial concentration of chromium(VI) was 50 mg/dm^3

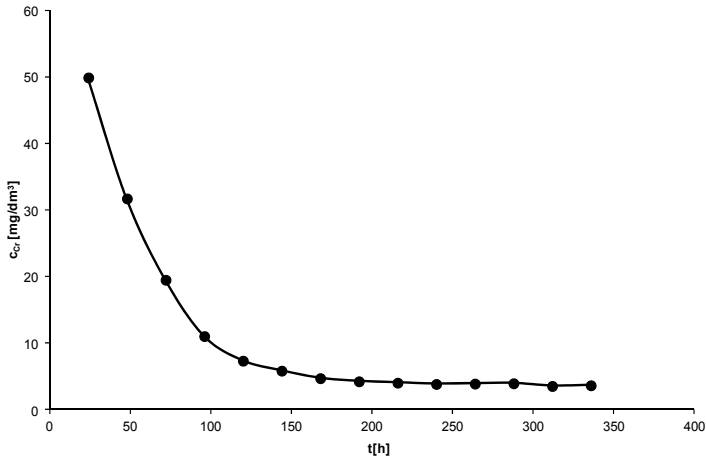


Figure 6. $c_{Cr} = f(t)$ for pH = 6.5. Initial concentration of chromium(VI) was 50mg/dm³

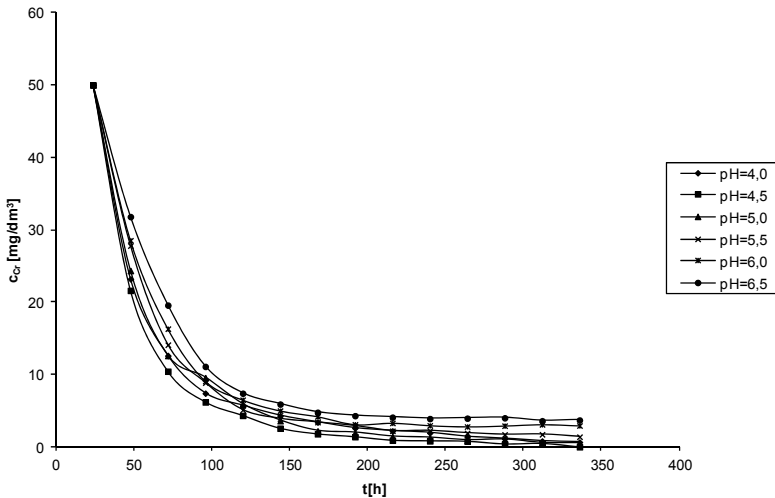


Figure 7. $c_{Cr} = f(t)$ by various values of pH, initial concentration of chromium(VI) 50 mg/dm³

The determined optimal pH was the basis for further research, where the relation between chromium(VI) ions concentration and initial concentration of chromium(VI)

Dependency on chromium(VI) concentration in the sample

On the basis of measurement results Figures 8–14 present the dependency of chromium(VI) ions concentration in medium on the process time. The effect of initial Cr(VI) concentration was investigated over a range of about 10–125 mg/dm³.

Obtained results suggested that Cr(VI) removal by *Trichoderma viride* occurred even at the highest concentration of 125 mg/ dm³, but complete Cr(VI) removal was

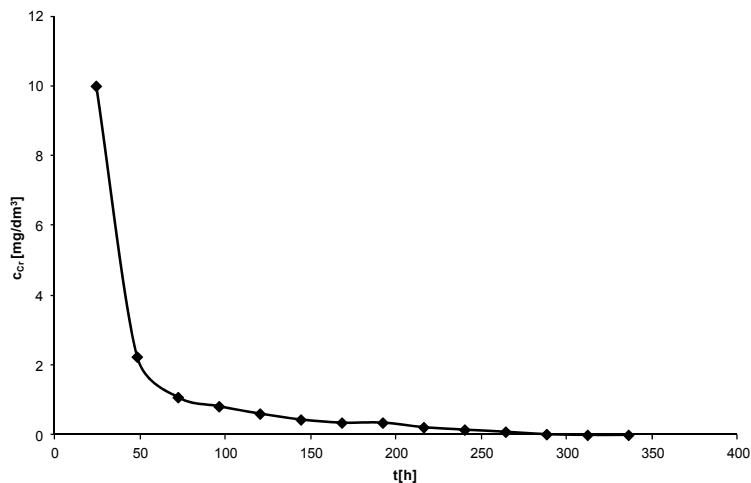


Figure 8. $c_{Cr} = f(t)$. Initial concentrations of chromium(VI) was 10 mg/dm³; pH = 4.5

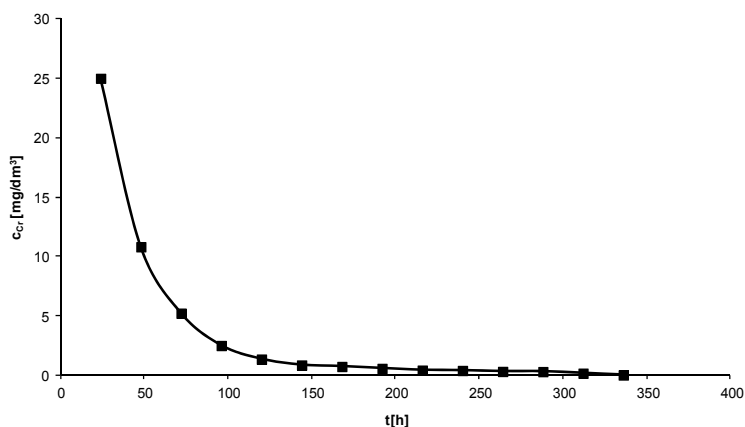


Figure 9. $c_{Cr} = f(t)$. Initial concentrations of chromium(VI) was 25 mg/dm³; pH = 4.5

observed for 10, 25, 50 and 75 mg/dm³ after 9, 11, 12 and 14 days, respectively. However the change of Cr(VI) concentration indicates that at the same incubation time, more Cr(VI) was reduced at higher initial Cr(VI) concentration.

Morrales-Barrera and Cristiani-Urbina (2006) have studied Cr(VI) removal by a microbial culture in a pneumatically agitated bioreactor. In an airlift bioreactor they reported a complete Cr(VI) removal at 1.3 and 1.6 mM initial chromium(VI) concentration after 30 and 80 h of incubation, respectively. Also a very high overall efficiency of Cr(VI) removal was achieved (94.3%) after more than 160 h of incubation at an initial Cr(VI) concentration of 1.94 mM. When *T. viride* was cultivated in unbaffled flasks containing culture medium with initial Cr(VI) concentrations of 1.0, 1.5 and 2.0 mM, the Cr(VI) removal efficiency was from 97 to 100%, respectively.

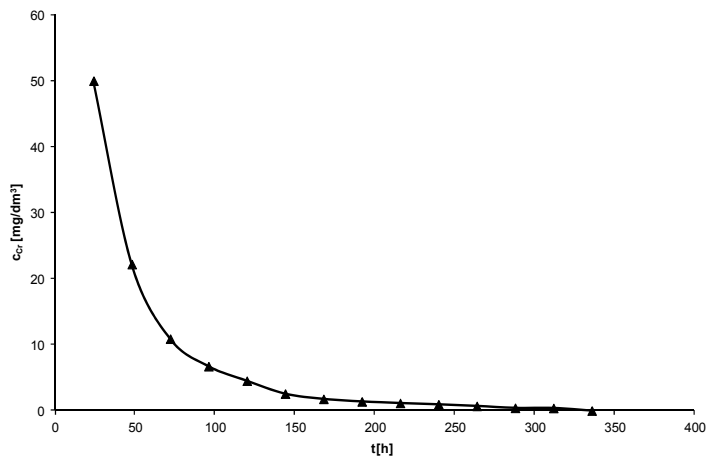


Figure 10. $c_{Cr} = f(t)$. Initial concentrations of chromium(VI) was 50 mg/dm³; pH = 4.5

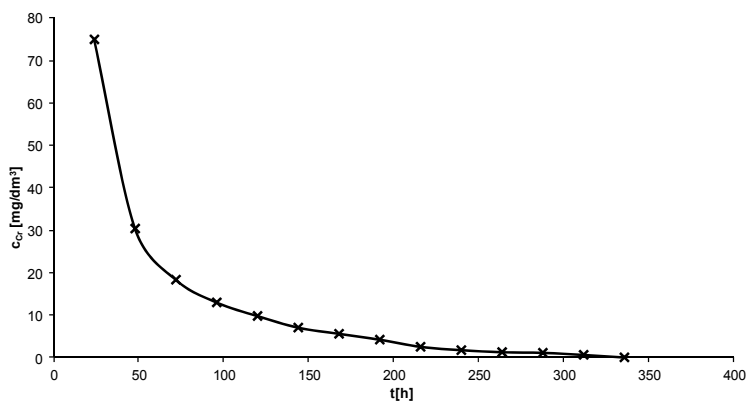


Figure 11. $c_{Cr} = f(t)$. Initial concentrations of chromium(VI) was 75 mg/dm³; pH = 4.5

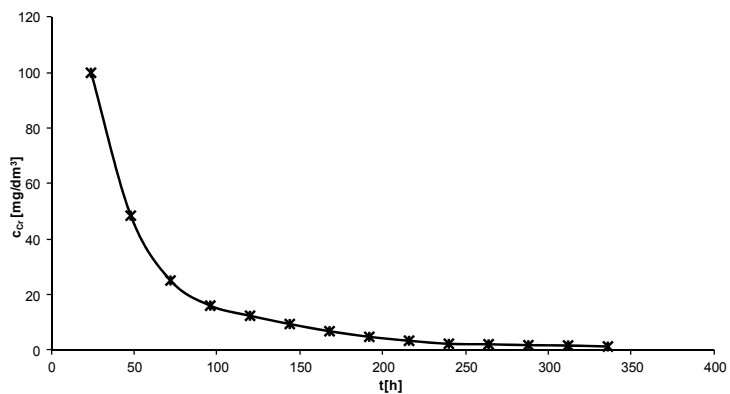


Figure 12. $c_{Cr} = f(t)$. Initial concentrations of chromium(VI) was 100 mg/dm³; pH= 4.5

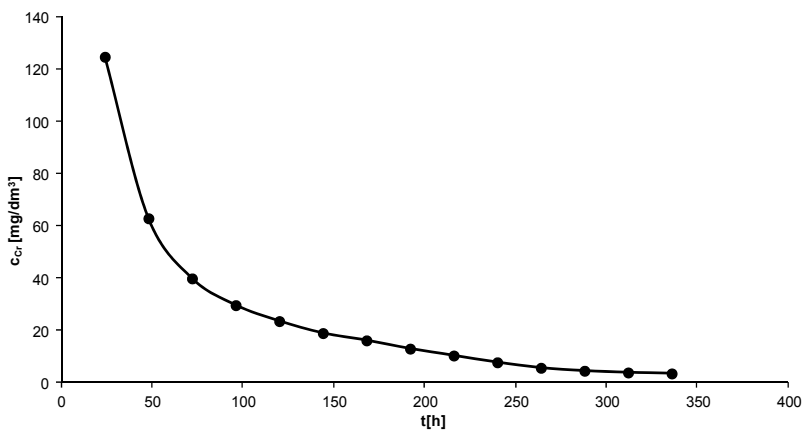


Figure 13. $c_{Cr} = f(t)$. Initial concentrations of chromium(VI) was 125 mg/dm^3 ; $\text{pH} = 4.5$

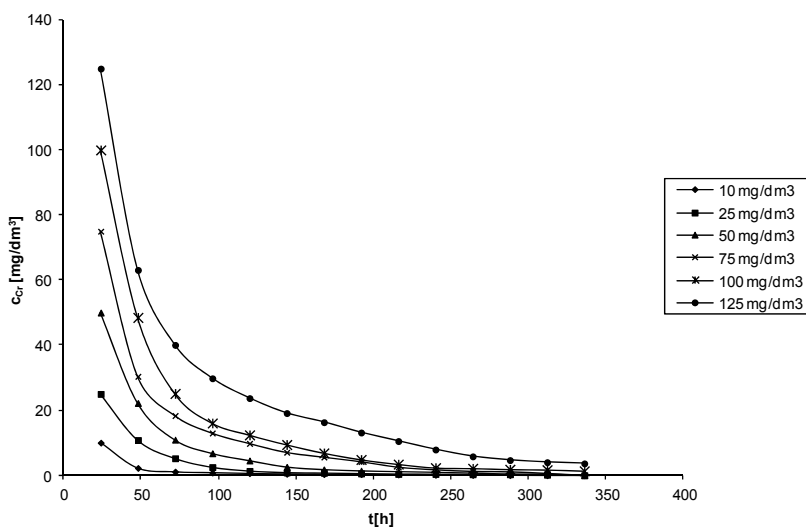


Figure 14. $c_{Cr} = f(t)$ for various initial concentrations of chromium(VI); $\text{pH} = 4.5$

Determination of type of biology Cr(VI) ions removing process

Determination of Cr(III) contents in medium

The results of analysis of total chromium presence in medium and initial chromium(VI) contents were presented in Table 1. The Cr(III) ions contents were determined on the basis on differences between the total chromium content and chromium(VI) content in the medium after 14 days of incubation.

Table 1. Results of analysis of Cr(III) presence in medium

Initial concentration Cr(VI) [mg/dm ³]	Total chromium concentration in medium [mg/dm ³]	Cr(III) concentration in medium [mg/dm ³]
10	0	0
20	0.15	0.15
50	0.408	0.408
75	0.625	0.605
100	2.15	0.806
125	4.012	0.376

Modest amounts of Cr(III) in the medium might occur because of acidification of environment by products of fungi metabolism in the final stage of 14-days period of culture. Such a small chromium(III) concentration proves also that the reduction process is not a cause of biological removal of Cr(VI) ions by application of the mildew fungi.

Determination of overall chromium contents in ooze after mycelium irrigating

The results of the analysis of total chromium presence in ooze, which depends on the initial chromium(VI) contents, were presented in Table 2.

Table 2. Results of analysis of overall chromium presence in the ooze

Initial concentration Cr(VI) [mg/ dm ³]	Total chromium concentration in ooze [mg/ dm ³]
10	0
20	0
50	0.02
75	0.092
100	0.131
125	0.3

Trace amounts of total chromium in ooze rather eliminates ion adsorption of this element on the surface of mycelium. This process could occur at the initial phase of the mycelium growth and was the first stage of the intracellular accumulation.

Determination of chromium contents in mycelium

Table 3 presents the results of total chromium contents in mycelium as a function of initial Cr(VI) ions concentration in the medium.

Table 3. Results of analysis of overall chromium presence in mycelium

Initial concentration Cr(VI) [mg/dm ³]	Total chromium concentration in mycelium [mg/ dm ³]
10	9.92
20	19.52
50	49.18
75	74.01
100	97.61
125	120.31

The results indicate that the increase of Cr(VI) ions in mycelium occurred in comparison with these ions concentration in surrounding environment. This may prove that the removal of Cr(VI) from aqueous solutions by macroscopic fungi occurs by intracellular bioaccumulation.

Conclusions

On the basis of presented results the following conclusions can be made:

- removal of Cr(VI) from water solutions by application of microscopic fungi *Trichoderma viride* occurs by intracellular bioaccumulation
- process of intracellular chromium absorption with alimentary substances is the largest during the first 5 days of mycelium growth
- bioaccumulation of chromium(VI) is dependent on environmental pH and is the most efficient at pH 4.5 for *Trichoderma viride*
- the greater is chromium(VI) concentration the smaller is accumulation of this element from the environment and the growth of mycelium is slower.

Application of mildew fungi to biological removing of chromium(VI) may be a suitable alternative to expensive chemical methods. Its disadvantages are longer time of bioaccumulation and lack of possibility of metal recovery without destruction of the mycelium. This causes that the application of these microorganisms is possible only once.

Acknowledgements

The paper has been supported by the University of Science and Technology AGH, work No. 11.11.100.196.

References

- ANJANA K., KAUSHIK A., KIRAN B., NISHA R., 2007, *Biosorption of Cr(VI) by immobilized biomass of two indigenous strains of cyanobacteria isolated from metal contaminated soil*. Journal of Hazardous Materials 148, 383–386.
- BADURA L., 1993, *Chrom w środowisku i jego oddziaływanie na organizmy żywe*. Zeszyty Naukowe PAN 5.

- BAI RS, ABRAHAM T.E., 2003, *Studies on chromium (VI) adsorption–desorption using immobilized fungal biomass*. *Bioresour Technol.* 87, 17–26.
- BARNHART J., 1997. *Occurrences, Uses, and Properties of Chromium*. *Regulatory toxicology and pharmacology* 26, 3–7.
- CHEN J.M., HAO O.J., 1997, *Biological removal of aqueous hexavalent chromium*. *J. Chem. Technol. Biotechnol.* 69, 70–76.
- DEEPA K.K., SATHISHKUMAR M., BINUPRIYA A.R, MURUGESAN G.S., SWAMINATHAN K., YUN S.E., 2006, *Sorption of Cr(VI) from dilute solutions and wastewater by live and pretreated biomass of Aspergillus flavus*. *Chemosphere* 62, 833–840.
- DONGHEE PARK, YEOUNG-SANG YUN, JONG MOON PARK, 2005, *Use of dead fungal biomass for the detoxification of hexavalent chromium: screening and kinetics*. *Process Biochemistry* 40, 2559–2565.
- DÖNMEZ G, KOÇBERBER N., 2005, *Bioaccumulation of hexavalent chromium by enriched microbial cultures obtained from molasses and NaCl containing media*. *Process Biochem.* 40, 2493–2498.
- DÖNMEZ G, KOÇBERBER N., 2007, *Chromium(VI) bioaccumulation capacities of adapted mixed cultures isolated from industrial saline wastewaters*. *Bioresource Technology* 98, 2178–2183.
- DURSAN AY, ULSU G, CUCI Y, AKSU Z., 2003, *Bioaccumulation of copper(II), lead(II) and chromium(VI) by growing Aspergillus niger*. *Process Biochem.* 38, 1647–1651.
- FASSATIOVA O., 1983, *Grzyby mikroskopowe w mikrobiologii technicznej*. WNT, Warszawa.
- GAJKOWSKA-STEFANŃSKA L. and others, 2001, *Laboratoryjne badania wody, ścieków i osadów ściekowych*. PW Publishing, Warszawa.
- GUPTA V.K., RASTOGI A., 2008. *Sorption and desorption studies of chromium(VI) from nonviable cyanobacterium Nostoc muscorum biomass*. *Journal of Hazardous Materials* 154, 347–354.
- HERMANOWICZ W. and others, 1999. *Fizyczno-chemiczne badanie wody i ścieków*. Arkady, Warszawa.
- HOLDA A., KISIELOWSKA E., NIEDOBA T., 2009, *Chemical and biological analysis of chromium waste*. *Górnictwo i Geoinżynieria* 33, 113–119.
- KAPOOR A., VIRARAGHAVAN T., 1995. *Fungal biosorption – an alternative option for heavy metal bearing wastewaters*. *Bioresource Technology* 53, 195–206.
- KOWALSKI Z., 2002. *Technologie związków chromu*, Wydawnictwo Politechniki Krakowskiej, Kraków.
- KSHEMINSKA H., FEDOROVYCH D., BABYAK L., YANOVYCH D., KASZYCKI P., KOLOCZEK H., 2005. *Chromium(III) and (VI) tolerance and bioaccumulation in yeast: a survey of cellular chromium content in selected strains of representative genera*. *Process Biochemistry* 40, 1565–1572.
- KUMAR R., NARSI R. BISHNOI, GARIMA, KIRAN BISHNOI, 2008. *Biosorption of chromium(VI) from aqueous solution and electroplating wastewater using fungal biomass*. *Chemical Engineering Journal* 135, 202–208.
- KUMARA R., BHATIAB D., SINGHA R., RANIA S., BISHNOIA N.R., 2011, *Sorption of heavy metals from electroplating effluent using immobilized biomass Trichoderma viride in a continuous packed-bed column*. *International Biodeterioration and Biodegradation* 65, 1133.
- MARCZENKO Z., BALCERZAK M., 1998, *Spektrofotometryczne metody w analizie nieorganicznej*. PWN, Warszawa.
- MING ZHOU, YUNGUO LIU, GUANGMING ZENG, XIN LI, WEIHUA XU, TING FAN, 2007, *Kinetic and equilibrium studies of Cr(VI) biosorption by dead Bacillus licheniformis biomass*. *World J Microbiol Biotechnol.* 23, 43–48.

- MORALES-BARRERA L., CRISTIANI-URBINA E., 2006, *Removal of hexavalent chromium by Trichoderma viride in an airlift bioreactor*. Enzyme and Microbial Technology 40, 107–113.
- PARKA D., YEOUNG-SANG YUNB, JI HYE JOA, JONGMOON PARKA, 2005, *Mechanism of hexavalent chromium removal by dead fungal biomass of Aspergillus niger*. Water Research 39, 533–540.
- PN-C-04604:1977, Polish Standards.
- PN-EN 12441-10, Polish Standards.
- PN-EN ISO 18412:2007, Polish Standards.
- SAXENA D., LEVIN R., FIRER M.A., 2000. Removal of chromate from industrial effluent by a new isolate of *Staphylococcus cohnii*. Water Sci Technol. 42, 93–98.
- SEN M., DASTIDAR M.G., ROYCHOUDHURY P.K., 2007, *Biological removal of Cr(VI) using Fusarium solani in batch and continuous modes of operation*. Enzyme and Microbial Technology 41, 51–56.
- SRINATH T., VERMA T., RAMTEKA P.W., GARG S.K., 2002, *Chromium(VI) biosorption and bioaccumulation by chromate resistant bacteria*. Chemosphere 48, 427–435.
- SRIVASTAVAA S., THAKURB I.S., 2006, *Evaluation of bioremediation and detoxification potentiality of Aspergillus niger for removal of hexavalent chromium in soil microcosm*. Soil Biology & Biochemistry 38, 1904–1911.
- WOLAK W., LEBODA R., HUBICKI Z., 1995, *Metale ciężkie w środowisku i ich analiza*. Biblioteka Monitoringu Środowiska, Chełm.
- ZIAGOVA M., DIMITRIADIS G., ASLANIDOU D., PAPAIOANNOU X., LITOPOULOU TZANNE-TAKI E., LIAKOPOULOU-KYRIAKIDES M., 2007. *Comparative study of Cd(II) and Cr(VI) biosorption on Staphylococcus xylosus and Pseudomonas sp. in single and binary mixtures*. Bioresource Technology 98, 2859–2865.

Received May 28, 2012; reviewed; accepted June 4, 2012

CHLORIDE–HYPOCHLORITE OXIDATION AND LEACHING OF REFRACTORY SULFIDE GOLD CONCENTRATE

Mehdi Ghobeiti HASAB, Fereshteh RASHCHI, Shahram RAYGAN

School of Metallurgy and Materials, College of Engineering, University of Tehran, Tehran, Iran
rashchi@ut.ac.ir

Abstract.: In this research, oxidation of sulfide minerals and leaching of gold from a gold-bearing sulfide concentrate using chloride–hypochlorite solution was investigated. The effects of calcium hypochlorite concentration, sodium chloride concentration and initial pH of leachant on changes of the slurry pH and Eh were examined. Then, considering the stability range of the gold complex (Eh ~ 1000 mV) and formation of chlorine gas (pH < 3.5), the optimum leaching parameters were determined. The optimum conditions were obtained at 200 g/dm³ calcium hypochlorite, 200 g/dm³ sodium chloride and initial pH 11 (with 200 g/dm³ concentrate, stirring speed 600 rpm and temperature 25°C) at which about 82% gold was extracted in 2 h.

Keywords: *refractory gold ore, oxidative pre-treatment, non-cyanide leaching*

Introduction

Although cyanide has been used commercially for the extraction of gold, investigations are being made on alternative non-toxic lixivants, such as thiosulfate (Abbruzzese et al., 1995; Aylmore and Muir, 2001), thiourea (Farinha et al., 1992; Ubaldini et al., 1998; Murthy et al., 2003), thiocyanate (Kholmogorov et al., 2002; Li et al., 2012) and halides (Davis et al., 1993; Van Meersbergen et al., 1993; Pangum and Browner, 1996; Vinals et al., 2006; Baghalha, 2012), mainly due to the failure of cyanidation for extracting gold from the refractory ores, long leaching times (more than 24 hours) and the environmental and safety issues (Senanayake, 2004). These lixivants have not been widely used, because they also have disadvantages (Kai et al., 1997; Aylmore, 2005; Feng and Van Deventer, 2007; Li et al., 2012). The use of chloride is a proven technology in gold refining (Feather et al., 1997). However, no current large scale applications of leach plants are known. The use of the halogen of the halide

itself as oxidant (chlorine gas), would lead to higher capital investment costs for the prevention of corrosion and the use of a closed system. Perhaps the biggest drawback in the use of the chloride/chlorine lies in the handling. Thus, it is important to select an effective substitute for chlorine.

For extraction of gold from the refractory ores in which gold is surrounded by sulfide minerals, oxidative pretreatment of the ore is essential to oxidize the sulfides and expose gold. Pyrometallurgical oxidation by roasting is encountered with environmental limitations; thus hydrometallurgical methods are preferred. These methods include pressure oxidation (Long and Dixon, 2004), bio-oxidation (Hansford and Chapman, 1992), oxidation by nitric acid (Gao et al., 2009) and chlorine species (Ikiz et al., 2006). Chlorine gas in aqueous solutions, depending on pH, can form three oxidizing species: aqueous chlorine ($\text{Cl}_2(\text{aq})$), hypochlorous acid (HOCl) and hypochlorite ion (OCl^-). These three species also can be generated by the addition of sodium hypochlorite (NaOCl) or calcium hypochlorite ($\text{Ca}(\text{OCl})_2$) to an aqueous solution (Puvvada and Murthy, 2000). Calcium hypochlorite is more stable than sodium hypochlorite and contains a higher chlorine concentration. These salts are ionized in water, Under acidic conditions ($\text{pH} < 7.5$) the hypochlorite ion is converted to hypochlorous acid. Under highly acidic condition ($\text{pH} < 3.5$) and in the presence of chloride ion, aqueous chlorine is formed. All of the chlorine species are powerful oxidants but HOCl is the most effective. Thus, pH should be maintained in the range of HOCl stability (Black and Veatch Corporation, 2010).

Hypochlorite solutions within the pH range at which hypochlorous acid dominates, will readily oxidize all sulfides commonly associated with gold. Pyrite is more stable than other metallic sulfides. It means that when in the aqueous media pyrite is oxidized, other sulfides are surely oxidized. The Pourbaix diagram of Fe-S shows that pyrite is decomposed to iron hydroxide and sulfate in the range of hypochlorous acid (grey area in Fig. 1). Oxidation of sulfides by hypochlorite solutions has an advantage of sulfate formation instead of elemental sulfur; since elemental sulfur causes passivation of minerals surfaces (Marsden and House, 2005). In hypochlorous acid solutions, gold is also dissolved as the $[\text{AuCl}_4]^-$ complex. Therefore it is possible to oxidize sulfides and leach gold simultaneously by this oxidant (Welham and Kelsall, 2000). Leaching of gold with hypochlorous acid follows reaction (1) (Jeffrey et al., 2001):



Controlling solution pH and Eh is important for stabilizing the gold complex. Failing to do this would cause the gold to reprecipitate, after it is dissolved from the ores (Baghalha, 2007; Soo Nam et al., 2008). The stability region of $[\text{AuCl}_4]^-$ is determined by the Pourbaix diagram of the Au-Cl system.

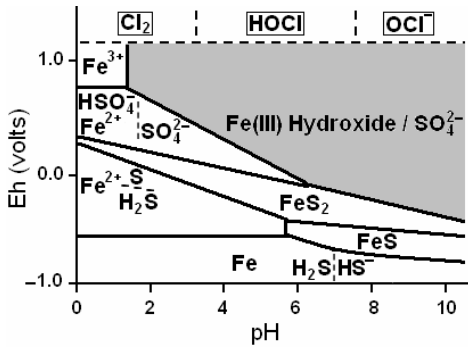


Fig. 1. The Pourbaix diagram of Fe–S at $[Fe] = 10^{-4} M$, $[S] = 10^{-4} M$ and $25^{\circ}C$ (the chlorine species regions are also marked) (Marsden and House, 2005)

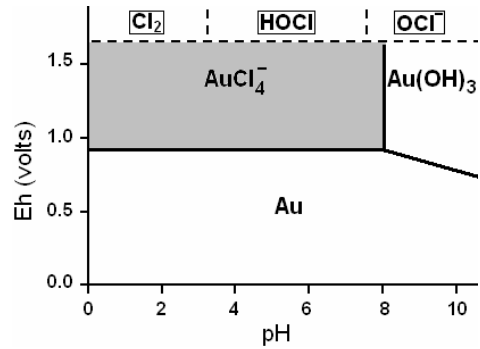
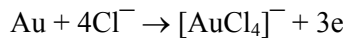


Fig. 2. A part of the Au–Cl Pourbaix diagram in the $[AuCl_4]^{-}$ domain at $[Au(III)] = 10^{-6} M$, $[Cl^{-}] = 1 M$ and $25^{\circ}C$ (Marsden and House, 2005)

A part of the Pourbaix diagram of Au–Cl in the $[AuCl_4]^{-}$ domain is shown in Fig. 2. This region is bounded by equations (2) and (3). According to these equations, increasing the Cl^{-} concentration results in the extension of $[AuCl_4]^{-}$ domain to the lower Eh and higher pH. The $[AuCl_4]^{-}$ is stable in the 0–8 pH range and in potentials greater than 0.9 volts, depending on the concentration of gold and chloride ion (Nesbitt et al., 1990; Welham and Kelsall, 2000).



$$Eh = 1.00 + 0.02 (\log [AuCl_4]^{-} - 4 \log [Cl^{-}]) \quad (2)$$



$$pH = (18.38 - \log [AuCl_4]^{-} + 4 \log [Cl^{-}])/3 \quad (3)$$

The present paper is a study about the changes of slurry pH and Eh during simultaneous oxidative pretreatment and gold leaching of a sulfide concentrate using the chloride/hypochlorite solution at various conditions of calcium hypochlorite concentration, sodium chloride concentration and initial pH. Then considering the suitable pH and Eh, optimum conditions are determined.

Experimental

The concentrate used in this study was obtained by flotation of an ore located in north-western Iran (Barika Mine in Sardasht). Flotation was conducted at $25^{\circ}C$ with a laboratory flotation machine at 25% solid by weight, 40 g/Mg of PEX (potassium ethyl xanthate as collector) and 25 g/Mg of MIBC (methyl isobutyl carbinol as frother). The pH of the slurry was about 7 and agitation rate was set at 1200 rpm. The

slurry was conditioned in the flotation cell for 5 minutes before air was introduced. Concentrate collecting time was set at 5 minutes. About 200 g concentrate was obtained from each 1 kg sample. The particles size of the concentrate was examined with a laser particle size analyser. Mineralogical studies were also carried out with an optical microscope (polished and thin sections) and X-ray diffractometer (XRD). Major elements analysis was determined by X-ray fluorescence (XRF). Gold and silver were analysed by Fire Assay and Atomic absorption spectroscopy (AAS), respectively. For leaching experiments the required reagents were added to a beaker containing deionized water (all the reagents used such as sodium chloride, calcium hypochlorite and sulfuric acid (H_2SO_4) were of analytical grade, purchased from Merck). Then, the concentrate was added into the leachant solution in the beaker and stirred by a magnetic stirrer at 600 rpm at 25°C for 2 h. The solid–liquid ratio was maintained at 1:5. During the leaching, slurry pH and Eh were controlled by two multi–meters with pH and ORP electrodes. Before starting every test, pH and ORP electrodes were calibrated. Solution samples were taken at different intervals by a syringe and filtered. Then clear solutions were analysed for gold by Inductively coupled plasma (ICP). The solid residues were washed and then dried in an oven at 80°C for 2 h and after drying, they were ground, then analysed by XRF, AAS and Fire Assay.

Results and discussion

Particles size analysis of the concentrate showed that 90% of particles are smaller than $37.4\ \mu\text{m}$ (~ 400 mesh) in size (Fig. 3). Mineralogical studies by optical microscope on polished and thin sections showed that the major components of the concentrate are quartz (SiO_2), pyrite (FeS_2), muscovite ($\text{H}_2\text{KAl}_3(\text{SiO}_4)_3$) and barite (BaSO_4). Sphalerite (ZnS), calcite (CaCO_3) and galena (PbS) constitute the minor phases of the concentrate. Small amounts of pyrrhotite (FeS), chalcopyrite (CuFeS_2), bornite (Cu_5FeS_4), tetrahedrite ($(\text{Cu,Fe})_{12}\text{Sb}_4\text{S}_{13}$) and arsenopyrite (FeAsS) were also detected. More than 90% of the minerals were separated from each others. Gold was not observable in this concentrate because of its small amount. The XRD analysis of the concentrate showed main phases of quartz and pyrite along with minor phases of muscovite and barite (Fig. 4). Major elements composition of the ore and floated concentrate are presented in Table 1. As shown in this table, by flotation of the ore with 3.770 g/Mg gold, a concentrate containing 20.451 g/Mg gold was obtained.

After 24 hours, direct cyanide leaching of the initial ore resulted in only 54.8% gold recovery. However, cyanidation after dissolving the ore sample in hydrochloric acid (HCl), sulfuric acid (H_2SO_4), ferric chloride (FeCl_3) and nitric acid (HNO_3), respectively, increased the gold recovery to 98.1%. This shows that the ore is a sulfide refractory gold ore (Saba et al., 2011).

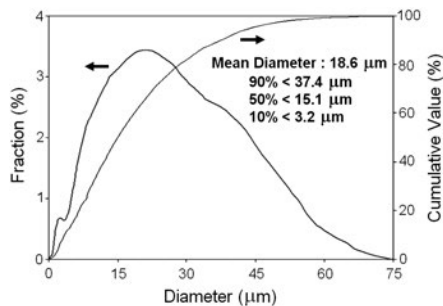


Fig. 3. Particles size analysis of gold concentrate

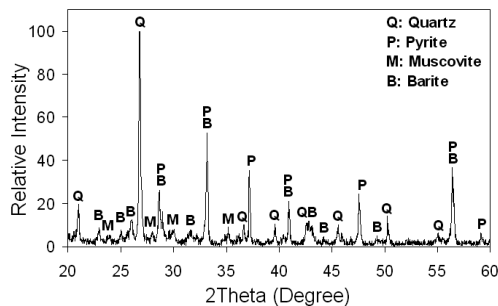


Fig. 4. XRD analysis of gold concentrate obtained by flotation

Table 1. Major elements composition of the ore and floated concentrate

Analysed Sample	Si (%)	S (%)	Al (%)	K (%)	Ba (%)	Ca (%)	Fe (%)	Zn (%)	Pb (%)	Cu (ppm)	Sb (ppm)	As (ppm)	Ag (ppm)	Au (ppb)
Ore	23.89	5.87	8.07	3.87	7.75	0.99	5.81	0.76	0.31	981	771	751	364	3770
Concentrate	17.76	13.68	5.93	2.26	1.84	0.75	12.79	1.79	0.51	3994	1870	1689	1650	20451

During leaching of concentrate by the chloride/hypochlorite solution, the changes of pH and ORP were detected to determine the optimum calcium hypochlorite concentration, sodium chloride concentration and initial pH.

Effect of hypochlorite concentration

The calcium hypochlorite powder, at various amounts of 2.5, 5, 10, 15, 20 and 25 g, was placed in a beaker containing 10 g of sodium chloride powder. Then, deionized water was added and the mixture was stirred to form a homogenous milky solution with a volume of 100 cm³. Initial pH of all these solutions was about 11. Then, a 20 g of concentrate was added into the stirring solution. Changes in the slurries pH and Eh during leaching are shown in Fig. 5 (a) and (b).

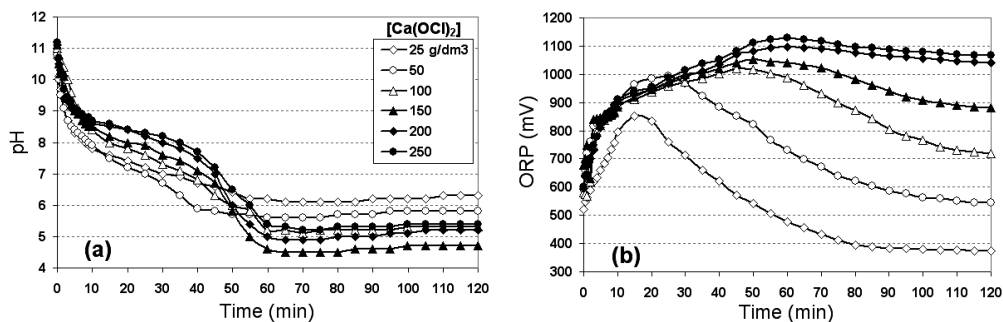


Fig. 5. Changes of (a) pH and (b) Eh of the slurries containing 100 g/dm³ sodium chloride and 25, 50, 100, 150, 200 and 250 g/dm³ calcium hypochlorite during 2 h

According to the results of Fig. 5a it was clear that for all the samples when the concentrate was added, pH decreased during the dissolution. Decreasing the pH is due to the oxidation of sulfides and generation of sulfuric acid. The rate of sulfides oxidation is indicated by the rate of the pH drop. With decreasing pH to below 7.5, hypochlorous acid becomes dominant oxidant and Eh is at its highest value. Due to the hypochlorous acid consumption in reaction with sulfides, its concentration in the slurry reduces and Eh drops (Fig. 5b). According to Fig. 5a and b, it seems that the 200 g/dm³ calcium hypochlorite is adequate for obtaining an oxidizing media with Eh about 1000 mV to stabilize the gold complex during 2 h. Higher concentration of calcium hypochlorite (250 g/dm³) has not significant effected changes of pH and Eh. At high hypochlorite concentrations, pH drops slowly due to hypochlorite/hypochlorous acid buffer solution.

Effect of initial pH

To investigate the effect of the initial pH, solutions with 100 g/dm³ sodium chloride and 200 g/dm³ calcium hypochlorite were prepared and their pH were adjusted to 10, 9, 8 and 7, by adding sulfuric acid. Figures 6a and b shows the changes of pH and Eh of these slurries during 2 h leaching. As shown, at initial pH of below 11, pH and Eh drop are faster and higher. It was found that the optimum initial pH was 11. In other words, decreasing the initial pH is not useful, neither for the desired reaction nor for the safety issues.

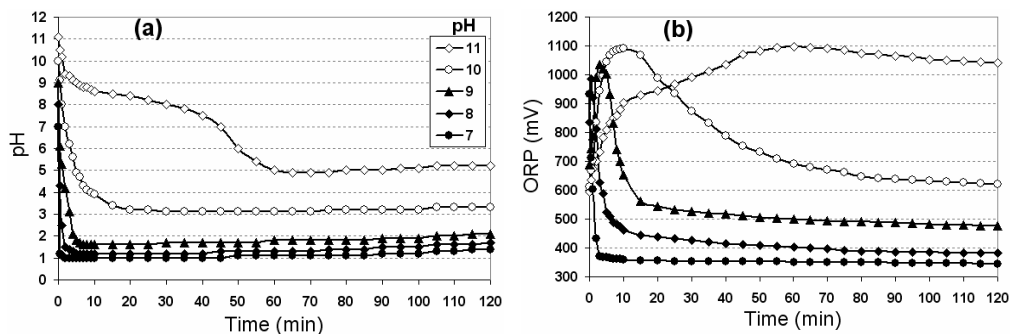


Fig. 6. Changes of (a) pH and (b) Eh of the slurries containing 100 g/dm³ sodium chloride and 200 g/dm³ calcium hypochlorite at various initial pH during 2 h

Effect of chloride concentration

Various quantities of sodium chloride in solution (100, 150, 200, 250 and 300 g/dm³) were used to determine the effect of chloride concentration on pH and Eh. The obtained results are given in Figs 7a and b. Higher levels of sodium chloride were found to significantly enhance the rate of pH drop, i.e. the rate of sulfides oxidation reaction. When the sodium chloride concentration was increased, conversion reaction of hy-

pochlorous acid species to chlorine species occurred at higher pHs. Thus, chlorine gas could be formed easier, and due to escaping of the chlorine oxidant from the solution, Eh drops rapidly.

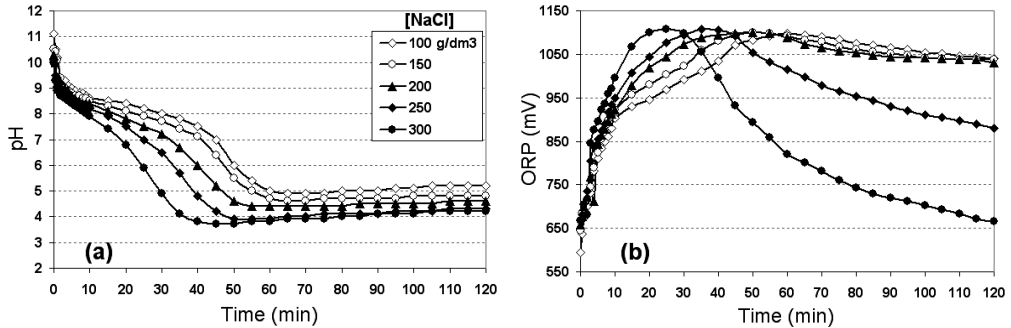


Fig. 7. Changes of (a) pH and (b) Eh of the slurries containing 200 g/dm³ calcium hypochlorite at initial pH 11 and various concentrations of sodium chloride during 2 h.

In all the experiments, it was observed that after the pH drop, it slowly increased again since the acid generated from the oxidation reaction was consumed by minerals such as CaCO₃, which could also increase the slurry viscosity (Marsden and House, 2005). Other gangue minerals such as quartz, muscovite and barite have a low reactivity in the chloride/hypochlorite system. Based on the results at the pH range of 4–7, Eh is at high levels. This indicates that the hypochlorous acid is the dominant oxidant in this pH range. Due to the oxidant consumption at dissolution reactions, Eh drops again. Two important points should be notified here. Dropping of the pH to the values below 3.5 and thus the formation of chlorine gas; dropping of the Eh to the values less than ca. 1000 mV and thus the instability of the gold complex. Therefore 200 g/dm³ sodium chloride is the optimum amount required.

Analysis of the resulting leach solution and the solid residue

Three clear filtrate solutions (with calcium hypochlorite–sodium chloride concentrations of 200–100, 250–100 and 200–200 g/dm³) were analyzed by ICP to determine the amount of leached gold. The results are presented in Fig. 8. It is evident that increasing the concentration of calcium hypochlorite had no significant effect on the recoveries of gold. However, increasing the concentration of sodium chloride had a considerable effect. Approximately 82% of gold had been leached during 2 h under experimental conditions of 200 g/dm³ calcium hypochlorite, 200 g/dm³ sodium chloride, 200 g/dm³ concentrate, initial pH 11, stirring speed 600 rpm and temperature 25°C. For this sample, after 30, 60, 90 and 120 min, the filter cake was analysed by XRF, AAS and Fire assay. The results are shown in Table 2, where it is evident that most of sulfides and gold have been extracted from concentrate during leaching. Remained sulfur in solid residue is related to BaSO₄ which was not dissolved during

leaching and CaSO_4 which can form during reaction of Ca(II) with generated sulfate. After 2 h, the slurry colour was converted from dark–grey to light–creamy, which is due to the metal sulfides removal.

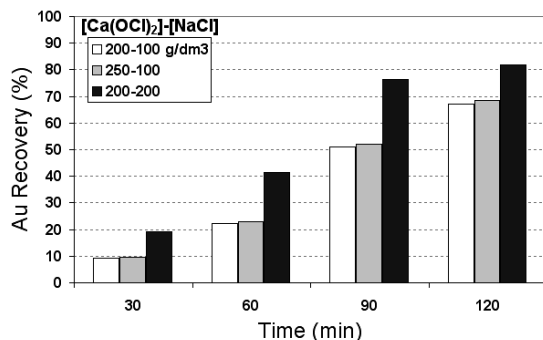


Fig. 8. Percentage recoveries of gold obtained at different concentrations of calcium hypochlorite and sodium chloride during 2 h (concentrate 200 g/dm^3 , initial pH 11, 600 rpm and 25°C)

Table 2. Major elements composition of filtrate cake after leaching at different times (200 g/dm^3 calcium hypochlorite, 200 g/dm^3 sodium chloride, 200 g/dm^3 concentrate, initial pH 11, 600 rpm and 25°C)

Time of leaching	Si (%)	S (%)	Al (%)	K (%)	Ba (%)	Ca (%)	Fe (%)	Zn (ppm)	Pb (ppm)	Cu (ppm)	Sb (ppm)	As (ppm)	Ag (ppm)	Au (ppb)
30 min	20.72	8.03	7.58	3.46	2.38	4.80	10.35	6317	4697	3430	1265	1214	1320	16019
60 min	21.54	5.76	7.83	3.68	2.64	6.59	9.27	173	4659	2846	137	57	988	11732
90 min	21.53	5.79	7.91	3.71	2.71	6.63	9.22	67	4571	2673	78	38	403	4631
120 min	21.54	5.81	7.93	3.72	2.73	6.66	9.21	44	4563	2648	51	36	274	3065

Conclusions

Combining sulfides oxidation and gold leaching processes using chloride/hypochlorite solution was a successful method for leaching of a refractory sulfide concentrate containing 20.451 g/Mg gold. Leaching tests at different concentrations of calcium hypochlorite and sodium chloride and also various initial pHs were performed. It was observed that for 200 g/dm^3 concentrate, initial pH 11, stirring speed 600 rpm and temperature 25°C , at least 200 g/dm^3 calcium hypochlorite is required to achieve high potential values for the gold leaching. Increasing the sodium chloride concentration from 100 to 200 g/dm^3 resulted in an increase in the sulfide oxidation rate as well as the extent of extracted gold. Under optimum conditions (200 g/dm^3 calcium hypochlorite, initial pH = 11 and 200 g/dm^3 sodium chloride), the recovery of gold after 2 h of leaching was about 82%.

References

- ABBRUZZESE C., FORNARI P., MASSIDDA R., VEGLIO F., UBALDINI S., 1995, *Thiosulphate leaching for gold hydrometallurgy*, *Hydrometallurgy*, 39, 265–276.
- AYLMORE M.G., 2005, *Alternative lixiviants to cyanide for leaching gold ores*, in: *Advances in Gold Ore Processing* (Adams, M.D., Ed.), *Developments in Mineral Processing*, 15, 501–539.
- AYLMORE M.G., MUIR D.M., 2001, *Thiosulfate leaching of gold – A review*, *Minerals Engineering*, 14, 135–174.
- BAGHALHA M., 2007, *Leaching of an oxide gold ore with chloride/hypochlorite solutions*, *International Journal of Mineral Processing*, 82, 178–186.
- BAGHALHA M., 2012, *The leaching kinetics of an oxide gold ore with iodide/iodine solutions*, *Hydrometallurgy* 113–114, 42–50.
- BLACK and VEATCH CORPORATION, 2010, *White's handbook of chlorination and alternative disinfectants*, 5th Edition, John Wiley & Sons, New York, 68–131.
- DAVIS A., TRAN T., YOUNG D.R., 1993, *Solution chemistry of iodide leaching of gold*, *Hydrometallurgy*, 32, 143–159.
- FARINHA P.A., CORREIA M.J.N., CARVALHO J.R., 1992, *Leaching of gold from a Portuguese concentrate with thiourea*, *Minerals Engineering*, 5, 953–959.
- FEATHER A., SOLE K.C., BRYSON L.J., 1997, *Gold refining by solvent extraction – the Minataur Process*, *The Journal of The South African Institute of Mining and Metallurgy*, 97, 169–174.
- FENG D., VAN DEVENTER J.S.J., 2007, *The role of oxygen in thiosulphate leaching of gold*, *Hydrometallurgy*, 85, 193–202.
- GAO G., LI D., ZHOU Y., SUN X., SUN W., 2009, *Kinetics of high-sulphur and high-arsenic refractory gold concentrate oxidation by dilute nitric acid under mild conditions*, *Minerals Engineering*, 22, 111–115.
- HANSFORD G.S., CHAPMAN J.T., 1992, *Batch and continuous biooxidation kinetics of a refractory gold-bearing pyrite concentrate*, *Minerals Engineering*, *Minerals Engineering*, 5, 597–612.
- IKIZ D., GULFEN M., AYDIN A.O., 2006, *Dissolution kinetics of primary chalcopyrite ore in hypochlorite solution*, *Minerals Engineering*, 19, 972–974.
- JEFFREY M.I., BREUER P.L., CHOO W.L., 2001, *A kinetic study that compares the leaching of gold in the cyanide, thiosulfate, and chloride systems*, *Metallurgical and Materials Transactions B*, 32B, 979–986.
- KAI T., HAGIWARA T., HASEBA H., TAKAHASHI T., 1997, *Reduction of thiourea consumption in gold extraction by acid thiourea solutions*, *Industrial & Engineering Chemistry Research*, 36, 2757–2759.
- KHOLMOGOROV A.G., KONONOVA O.N., PASHKOV G.L., KONONOV Y.S., 2002, *Thiocyanate solutions in gold technology*, *Hydrometallurgy*, 64, 43–48.
- LI J., SAFARZADEH M.S., MOATS M.S., MILLER J.D., LEVIER K.M., DIETRICH M., WAN R.Y., 2012, *Thiocyanate hydrometallurgy for the recovery of gold. Part I: Chemical and thermodynamic considerations*, *Hydrometallurgy*, 113–114, 1–9.
- LI J., SAFARZADEH M.S., MOATS M.S., MILLER J.D., LEVIER K.M., DIETRICH M., WAN R.Y., 2012, *Thiocyanate hydrometallurgy for the recovery of gold. Part II: The leaching kinetics*, *Hydrometallurgy*, 113–114, 10–18.
- LONG H., DIXON D.G., 2004, *Pressure oxidation of pyrite in sulfuric acid media: a kinetic study*, *Hydrometallurgy*, 73, 335–349.
- MARSDEN J.O., HOUSE C.I., 2005, *The chemistry of gold extraction*, 2nd Edition, Society for mining, metallurgy and exploration, Colorado, USA, 185–190.

- MURTHY D.S.R., KUMAR V., RAO K.V., 2003, *Extraction of gold from an Indian low-grade refractory gold ore through physical beneficiation and thiourea leaching*, Hydrometallurgy, 68, 125–130.
- NESBITT C.C., MILOSAVLJEVIC E.B., HENDRIX J.L., 1990, *Determination of the mechanism of the chlorination of gold in aqueous solutions*, Industrial & Engineering Chemistry Research, 29, 1696–1700.
- PANGUM L.S., BROWNER R.E., 1996, *Pressure chloride leaching of a refractory gold ore*, Minerals Engineering, 9, 547–556.
- PUVVADA G.V.K., MURTHY D.S.R., 2000, *Selective precious metals leaching from a chalcopyrite concentrate using chloride–hypochlorite media*, Hydrometallurgy, 58, 185–191.
- SABA M., YOUSEFI A.M., RASHCHI F., MOGHADDAM J., 2011, *Diagnostic pre-treatment procedure for simultaneous cyanide leaching of gold and silver from a refractory gold/silver ore*, Minerals Engineering, 24, 1703–1709.
- SENANAYAKE G., 2004, *Gold leaching in non-cyanide lixiviant systems: critical issues on fundamentals and applications*, Minerals Engineering, 17, 785–801.
- SOO NAM K., HI JUNG B., WOONG AN J., JUN HA T., TRAN T., JUN KIM M., 2008, *Use of chloride–hypochlorite leachants to recover gold from tailing*, International Journal of Mineral Processing, 86, 131–140.
- UBALDINI S., FORNARI P., MASSIDDA R., ABBRUZZESE C., 1998, *An innovative thiourea gold leaching process*, Hydrometallurgy, 48, 113–124.
- VAN MEERSBERGEN M.T., LORENZEN L., VAN DEVENTE J.S.J., 1993, *The electrochemical dissolution of gold in bromine medium*, Minerals Engineering, 6, 1067–1079.
- VINALS J., JUAN E., RUIZ M., FERRANDO E., CRUELLES M., ROCA A., CASADO J., 2006, *Leaching of gold and palladium with aqueous ozone in dilute chloride media*, Hydrometallurgy, 81, 142–151.
- WELHAM N.J., KELSALL G.H., 2000, *Recovery of gold from pyrite (FeS₂) by aqueous chlorination, 1. Oxidation rates of gold and pyrite in aqueous chlorine solutions*, in: *Electrochemistry in Mineral and Metal Processing V* (Woods, R., Doyle, F.M., Eds.), The Electrochemical Society, Pennington N.J., 141–151.

Received May 19, 2012; reviewed; accepted June 10, 2012

BIOLEACHING OF URANIUM MINERALS AND BIOSYNTHESIS OF UO_2 NANOPARTICLES

Joanna A. BARANSKA, Zygmunt SADOWSKI

Wroclaw University of Technology, Chemical Engineering Department, Wybrzeze Wyspianskiego 27,
50 370 Wroclaw, POLAND; joanna.a.baranska@pwr.wroc.pl ; zygmunt.sadowski@pwr.wroc.pl

Abstract: Uranium mining has resulted in generation of significant amounts of solid wastes. The mechanism and chemical conditions of uranium waste bioleaching were considered. The initial results of bioleaching of solid waste from closed Kowary mine were presented. The process of U(VI) bioreduction by anaerobic reduction microorganisms was described. The factors that contributed to UO_2 nanoparticles fabrication were discussed. The obtained UO_2 particles are promising for development of novel catalysts.

Keywords: *bioleaching, U(VI) reduction, Acidithiobacillus ferrooxidans, Shewanella, nanoparticles, UO_2 precipitation*

Introduction

During the last decades the mining activities created significant amounts of uranium solid wastes. For instance, in the south-east part of Germany (Saxony and Thuringia) the intensive uranium mining has resulted in generation of significant amounts of mining waste piles (Pollmann et al., 2006).

Uranium is produced conventionally using a process that employs a strong acid and large amounts of energy. This technology creates environmental problems. Autochthonic microorganisms are able to mobilize metal ions through autotrophic and heterotrophic leaching. The important environmental goal is to prevent uranium transport. One potential method is to use iron-reducing bacteria for multivalent metals and radionuclides transport halt [Sani et al., 2008]. The objective of this paper is to obtain information on the bioleaching of uranium solid wastes and microbial reduction of U(VI) to U(IV) and UO_2 precipitation.

Bioleaching uranium minerals

Bioleaching of uranium from natural sources was applied to uranium-bearing ores from Daejeon and Okchen districts of South Korea (Choi et al., 2005). The quantity of uranium in these ores is estimated to be over 100 million megagrams. The average content of U_3O_8 in these deposits is below 0.1% by weight.

One of the most widely employed bacteria in the bioleaching process is *Acidithiobacillus ferrooxidans*. This acidophilic bacteria oxidizes ferrous ions (Fe^{2+}) to ferric ions (Fe^{3+}) which can act as a strong oxidant capable oxidizing uranium minerals. Bioleaching experiments were carried out with 10g of ground and sieved black schist in a 250 cm³ Erlenmeyer flask and 100 cm³ of 9 K medium (medium contains 9 g/dm³ $FeSO_4$). The uranium transfer from the schist into the solution increases as the Fe^{2+} ions oxidation was increased. The highest uranium leaching efficiency increased from 18% in the absence of bacteria to almost 80% following the introduction of *A. ferrooxidans*.

The effect of *A. ferrooxidans* on uranium leaching from the black shale ore has also been investigated by Lee and coworkers (2005). The black shale ore was taken from Deokpyeong area (Korea). The ore contains 349 mg uranium per kg. Uranium in the ore was associated with carbonates (58%) and organic matter and sulfides (42%). The pH of mineral suspension was systematically decreases to the level of pH = 2.5. The redox potential was mainly due to bacteria oxidation of Fe^{2+} to Fe^{3+} . After 250 h of the bioleaching process the redox potential has value of 0.59 V.

Initial bioleaching experiments were carried out using solid waste from the closed Kowary mine. Figure 1 presents bioleaching data using *Acidithiobacillus ferrooxidans*.

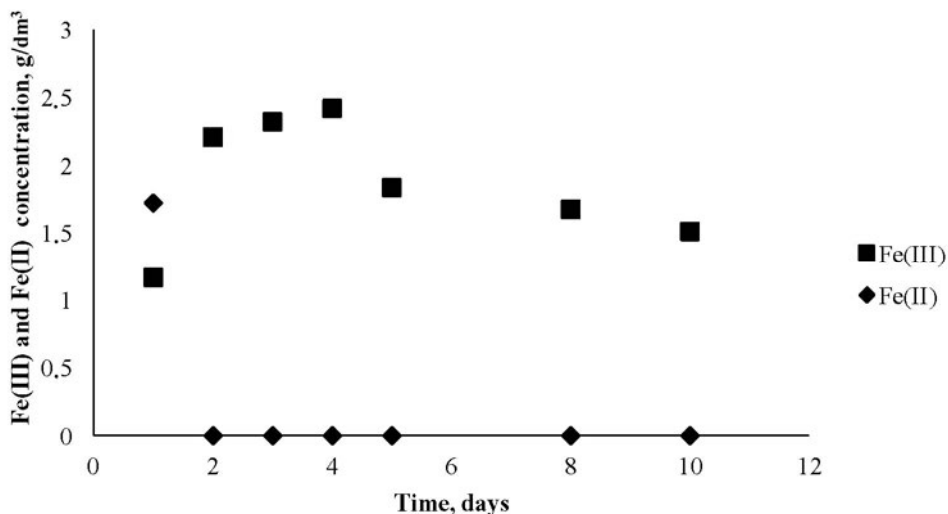


Fig. 1. Bioleaching of solid waste from Kowary by *Acidithiobacillus ferrooxidans*

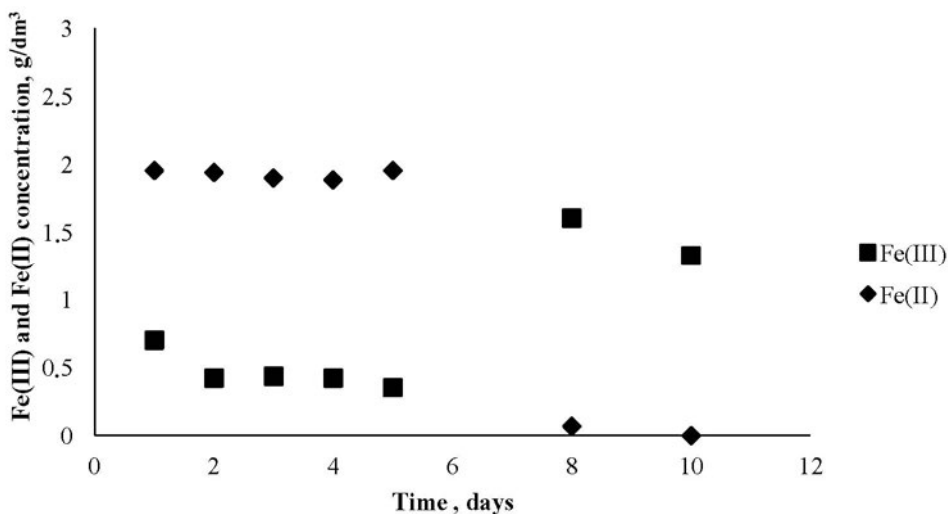


Fig. 2. Bioleaching of solid waste from Kowary using autochthonic bacteria

The bioleaching results using indigenous bacteria are presented in Fig. 2. As can be observed, an intensive oxidation of Fe(II) ions occurred after a 6 days period. Such behavior is in contrast to the literature report of Pal et al., 2010 and it will be investigated.

Since uranium dissolution from the solid wastes requires a strong oxidant therefore the bioleaching experiments are carried out in the presence of ferrous sulfate. The bioleaching path can be composed of three stages within 32 days. In the first stage up to 7 days, the oxidation rate was very fast. From the seventh to the twentieth day the rate of biooxidation was slowly decreased. After the twentieth day the rate of biooxidation was parallel to the rate of biooxidation without iron (Pal et al., 2010).

Leaching of uranium-bearing minerals is accomplished by oxidation of the insoluble U^{4+} form to the acid soluble U^{6+} form in an acid environment. The indirect mechanism by using ferric (Fe^{3+}) ions as an oxidant is proposed for the uranium bioleach process (Lottering et al., 2008; Abhilash et al., 2011). The uranium bioleaching process has an electrochemical nature. It is confirmed by Eh changes during biooxidation.

Figure 3 presents the Eh changes during uranium waste biooxidation. An increase of Eh corresponds to an increase of Fe(III) ions concentration. From the data present in Fig. 3 the efficiency of Fe(II) biooxidation was better for *Acidithibacillus ferrooxidans*.

Gold deposits located at Vaal Rever (South Africa) also contain uranium-bearing minerals. The brannerite-type minerals ($U_{1-x}Ti_{2+x}O_6$) are a major source of uranium in these ores. The insoluble uranium(IV) is oxidized to the water soluble uranium(VI) sulfate as follows:

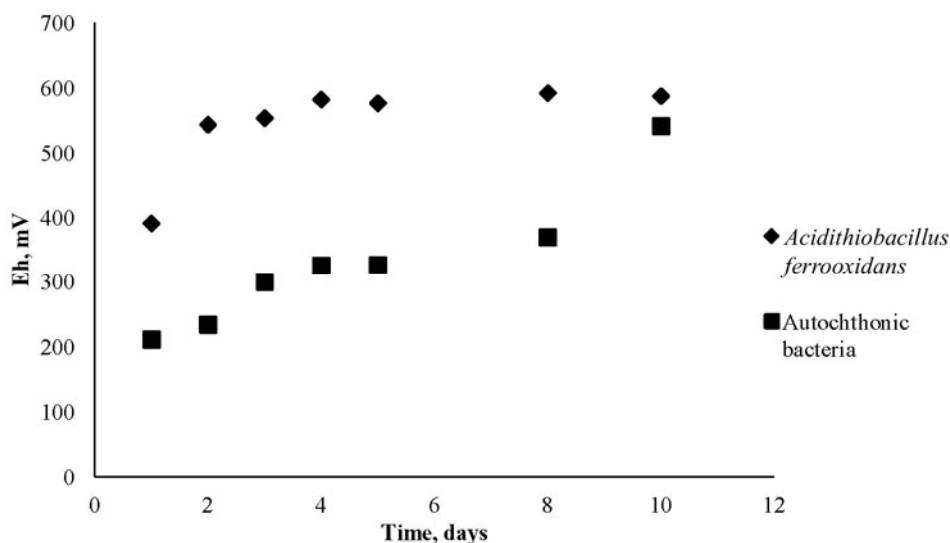
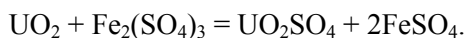


Fig. 3. Changes of Eh during bioleaching of Kowary solid waste by *Acidithiobacillus ferrooxidans* and autochthonic bacteria



A model for uranium minerals bioleaching was developed (Rashidi et al., 2012). The material balances of three reactions provided a correlation between the chemical and biological phenomena.

The efficiency of uranium recovery is depended on the mineralogical characteristics of the ore. In the case of the Vaal River ores 90% uranium dissolution was maximum (Lottering et al., 2008).

A high biosorption of toxic metals such as U, Cu, Pb, Al and Cd accompany to the bioleaching process. For instance, *Acidithiobacillus ferrooxidans* is able to accumulate uranium ions. The ability of *A. ferrooxidans* to bind uranium decreased from 44.62 to 33.81 (mg/g dry weight) when the pH was reduced from 4 to 1.5 (Merroun Selenska-Pobell, 2001).

The Curilo uranium deposit is located in Western Bulgaria. This deposit is a permanent source of acid mine drainage. The generation of drainage water is connected with biooxidation of pyrite and other sulphide minerals. The drainage water was treated by natural and constructed wetlands and alkalized limestone drains (Groudev et al., 2008).

The migration of soluble U(VI) forms can be realized by the reaction of soluble U(VI) to quite insoluble U(VI). Anaerobic microbial activity may lead to U(VI) reduction coupled with oxidation of organic carbon.

Some photosensitive cyanobacteria and algae as *Porphyridium cruentum*, *Spirulina platensis* and *Nostoc linkia* were used for uranium leaching from ores content less than

0.5% of uranium(VI) (Cecal et al., 2000). The bioleaching data showed that the leaching process is more evident in the presence of cyanobacteria (40-90%).

Removing uranium from pregnant solution

Interest is in removing uranium from the acid mine drainage solution in a cost efficient way. During the last two decades, different groups of microorganisms, such as *Actinomyces* and other bacteria demonstrated the ability to remove uranium from the leaching solution. The capacity to enzymatically reduce U(VI) has been demonstrated for sulphate reducing bacteria (SRB) (Martins et al., 2010). This process can be realized by sulfate and iron reducing bacteria under anaerobic conditions (Gargarello et al., 2010). Microbial reduction of U(VI) to sparingly soluble and immobile U(VI) compounds is a promising method for uranium migration control. However, under anaerobic conditions many iron reducing and sulfate-reducing bacteria can participate in the uranium(VI) reduction process. These bacteria must compete with the bacteria which did not participate in U(VI) reduction, for instance methanogenes bacteria.

Clastridium spheroids bacteria are able to reduce Fe(III) to Fe(II), Mn(IV) to Mn(II), U(VI) to U(IV), Pu(IV) to Pu(III) and Tc(VI) to Tc(IV) (Francis, Dodge, 2008). Under anaerobic conditions (pH = 6) uranium complexed with organic ligand (citric acid) was reduced to uranium(IV)-citrate. The reduced uranium remained in the solution as a complex of citric acid. The above results indicate that selection of an appropriate electron donor (organic compound) is important for uranium bioreduction and immobilization.

Rate of bioreduction

Reduction rates did not vary for the bacteria grown under aerobic and anaerobic conditions. Among the microbial reduction processes that can be determined the environmental behavior of radionuclides, biosorption of uranium and other radionuclides is important for the bioremediation strategic (Kazy et al., 2009). Microbial synthesis of nanoparticles is another very promising aspect of microbial interaction with metal ions. Initial works showed that uranium and thorium biosorption by *Rhizopus* sp. consists of the three processes such as: coordination, adsorption and precipitation. Also, the role of phosphate and carboxylic groups in a complexation phenomenon was considered. The X-ray microanalysis strongly indicated the possibility of uranium and thorium binding with the biomass (*Pseudomonas*) by displacing cellular potassium through ion-exchange mechanism (Kazy et al., 2009). FTIR spectroscopy data showed that after U and Th biosorption, the spectra exhibited changes in peak position further indicating a strong role of carboxyl groups in radionuclide bonding.

Topography analyses using the AFM tapping method, of the cells before and after uranium and thorium sorption revealed an enlargement of bacteria cells and increase in surface roughness. It is interesting that *Acidithiobacillus ferrooxidans* bacteria can

grow under anaerobic condition using iron(III) as the electroacceptor and sulfur as substrate.

Biosynthesis of UO_2 nanoparticles

The most stable forms of uranium at ambient temperature are U_3O_8 and UO_2 . However, UO_2 will gradually convert to U_3O_8 (Gavrilescu et al., 2009). The bioreduction of U(VI) to U(IV) by abiotic and biotic processes has a significant effect on the uranium ions mobility in the natural environment. $[\text{UO}_2]^{2+}$ ions can be enzymatically reduced to UO_2 by sulfate reducing bacteria such as *Shewanella*, *Geobacter* and *Desulfovibrio*.

Shewanella species belong to a relatively well-characterized group of U(VI)-reducing bacteria (Burgos et al., 2008). They have a complex and apparently electron transfer system for the reduction of U(VI) ions. For instance, *Shewanella putrefaciens* was grown aerobically on soy broth and harvested by centrifugation. Biomass was resuspended and washed three times in anoxic bicarbonate buffer. The pure cell suspension (approximately $1.1 \cdot 10^{10}$ cell/dm³) was used to bioreduction of U(VI). The medium contains 5 mM of sodium lactate and 1.4 mM uranyl acetate. pH solution was equal to 6.8. Bioreduction was maintained at 23°C in darkness (Senko et al., 2007).

Upon complete bioreduction of U(VI) by *Shewanella putrefaciens*, UO_2 nanoparticles were located in the periplasm or extracellularly. The localization of UO_2 particles suggests that U(VI) may be reduced in the periplasm and exported out of the cell via active or passive processes.

The rate of U(VI) reduction is determined by the geochemical conditions under which U(VI) reduction takes place, and the physiological state of the microorganisms used. For example, the presence of Ca^{2+} ions may inhibit U(VI) bioreduction (Burgos et al., 2008). The kinetics of U(VI) bioreduction process was observed to be first-order with respect to the concentration of U(VI) ions according to following equation:

$$R_{red} = \frac{d[U(VI)]}{dt} = -k_{red} [U(VI)_{solution}]$$

where: k_{red} is the first-order bioreduction rate constant [d^{-1}].

The rate of U(VI) bioreduction was also depended on the lactase concentration, cell/U(VI) ration, cell/lactase ration and temperature. The obtained results suggested that careful manipulation of addition of electron donor (lactase) could give rise to UO_2 precipitation (Burgos et al., 2008).

The U(VI) bioreduction rate constants were dependent on the used buffer solution and are presented in Table 1.

Table 1. First-order rate constants for U(VI) bioreduction by *Shewanella oneidensis* (Burgos et al., 2008)

Buffer solution	k_{red} [d ⁻¹]	Cell concentration [cell ml ⁻¹]	Temperature [°C]	r^2
NaHCO ₃ “fast”	11	2 10 ⁸	37	0.97
NaHCO ₃ “slow”	0.45	1 10 ⁸	20	0.87
PBAGW “fast”	0.99	2 10 ⁸	37	0.98
PBAGW “slow”	0.13	1 10 ⁻⁸	20	0.86

PBAGW-buffer contains piperazine-NN-bis-2 ethansulfonic acid.

For uranium reduction under iron reducing conditions, the nanoparticles of hematite, as the Fe(III) substrate, and the facultative anaerobic bacterium *Shewanella putrefaciens* were used. The reduction of U(VI) in the bacteria+hematite experiments run was fast (Behrends, van Cappellen 2005). In this case, the competition between abiotic and enzymatic reduction of U(VI) can be explained as a competition between the adsorption onto the hematite surface or the bacterial cell walls.

The redox potential of the U(VI)/U(VIV) couple strong by depends on the chemical and geochemical conditions. Table 2 presents two examples of the uranium couple.

Table 2. Standard stage reduction potential E[V] for uranium (Zhang et al., 2009)

Redox couple	E [V]
Uranyl carbonate $UO_2(CO_3)_3^{4-}$ $0.5 UO_2(CO_3)_3^{4-} = 1.5 H^+ + e^- \rightarrow 0.5 UO_2 + 1.5 HCO_3^-$	0.687
Ca-U(VI)-CO ₃ complex $CaUO_2(CO_3)_3$ $0.5CaUO_2(CO_3)_3^{2-} + 1.5 H^+ + e^- \rightarrow 0.5 UO_2 + 1.5 HCO_3^- + 0.5 Ca^{2+}$	0.424

SEM images of biogenic nanoparticles of UO_2 are presented in Fig. 4. As can see the majority of UO_2 particles were located outside of the cells.

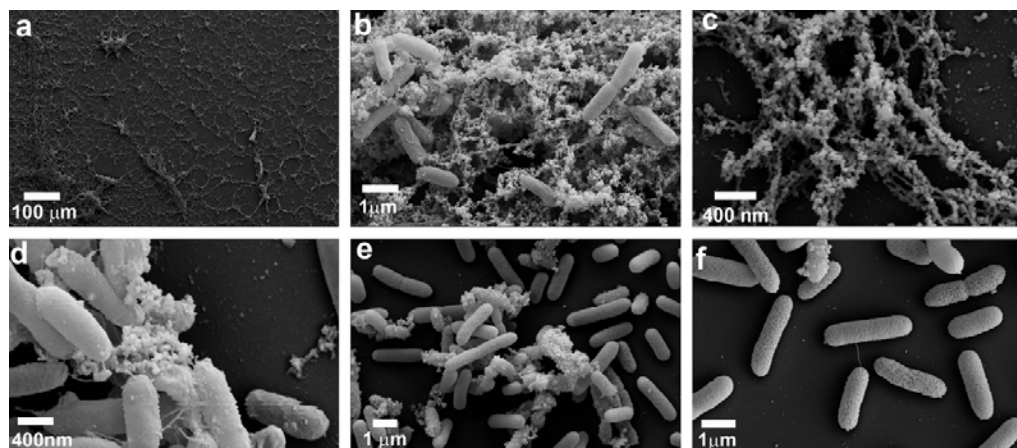


Fig.4. Scanning electron micrographs of UO_2 particles and *Shewanella oneidensis* cells (a–d) NaHCO₃ buffer and (e–f) PBAGW buffer, from (Burgos et al., 2008)

The uranium ions can be adsorbed by carbon nanotubes. The adsorption isotherms of uranium(VI), preferentially the UO_2^{2+} and UO_2OH^+ ions on the carbon nanotube surfaces were presented by Schierz and Zanker (2009). An increase from 18 mmole/g to 193 mmole/g in uranium ions sorption was observed at pH 5. Such behavior was caused by the increases number of functional groups on the modified surface of carbon nanotubes.

A promising alternative for removing palladium from solution can be use of bacteria for bioreductive deposition of Pd(0) nanoparticles. The formation of Pd(0)-nanoclusters using *Bacillus sphaericus* JG-A12 isolated from the uranium mining pile was investigated (Pollmann et al., 2006). Initial studies showed that the Pd-nanoparticles produced by the cell and deposited onto the cell surfaces are able to catalyze various chemical processes.

Summary

Biobleaching is a profitable alternative to the conventional chemical process of uranium recovery. The leaching of U from low-grade ores and solid wastes is realized by chemoautotrophic bacteria such as *Acidithiobacillus ferrooxidans*. The initial results demonstrated that biobleaching of uranium solid wastes, located at Kowary, is an effective method for uranium removal. Uranium reducing bacteria, particularly *Shewanella putrefaciens* and *Shewanella oneidensis*, can be used for UO_2 particles synthesis. The rate of U(VI) bioreduction is first order with respect to the concentration of U(VI) ions. The bioreduction of U(VI) in the presence of hematite particles can be a way to new catalyst fabrication.

Acknowledgment

The work was financed by a statutory activity subsidy from the Polish ministry of Science and Higher Education for the Faculty of chemistry of Wroclaw University of Technology

References

- ABHILASH, MEHTA K.D., KUMAR V., PANDEY D.B., TAMRAKAR K.P., 2011, *Biobleaching – An alternate uranium ore processing technology for India*, Energy Procedia 7, 158–162.
- BEHRENDTS T., VAN CAPPELLEN P., 2005, *Competition between enzymatic abiotic reduction of uranium(VI) under iron reducing conditions*, Chemical Geology, 220, 315–327.
- BURGOS D.W., MCDONOUGH T.J. SENKO M.J., ZHANG G., DOHNALKOVA G.A., KELLY D.S., GORBY Y., KEMNER M.K., 2008, *Characterization of uraninite nanoparticles produced by Shewanella oneidensis MR-1*, Geochimica et Cosmochimica Acta, 72, 4901–4915.
- CECAL A., HUMELNICU D., POPA K., RUDIC V., GULEA A., PALMARU I., NEMTOI G., 2000, *Biobleaching of UO_2^{2+} ions from poor uranium ores by means of cyanobacteria*, J. Radioanalytical Nuclear Chemistry, 245, 427–429.
- CHOI M-S., CHO S-K., KIM S-D., RYU W-H., 2005, *Biobleaching of uranium from low grade black schists by Acidithiobacillus ferrooxidans*, World J. Microbiology Biotechnology, 21, 377–380.

- FRANCIS J.A., DODGE J.C., 2008, *Bioreduction of uranium(VI) complexed with citric acid by Clostridia affects its structure and solubility*, Environ. Sci. Technol., 42, 8277–8282.
- GARGARELLO M.R., DI GREGORIO D., HUCK H., FERNANDEZ NIELLO J., CURUTCHET G., 2010, *Reduction of uranium(VI) by Acidithiobacillus thiooxidans and Acidithiobacillus ferrooxidans*, Hydrometallurgy, 104, 529–532.
- GAVRILESCU M., PAVEL V.L., CRETESCU I., *Characterization and remediation of soils contaminated with uranium*, J. Hazardous Materials, 163, 475–510.
- GROUDEV S., GEORIEV P., SPASOVA I., NICOLOVA M., 2008, *Bioremediation of acid mine drainage in uranium deposit*, Hydrometallurgy, 94, 93–99.
- KAZY K.S., D'SOUZA F.S., SAR P., 2009, *Uranium and thorium sequestration by a Pseudomonas sp.: mechanism and chemical characterization*, J. Hazardous Materials, 163, 65–72.
- LEE J-U., KIM S-M., KIM K-W, KIM S.I., 2005, *Microbial removal of uranium in uranium-bearing black shale*, Chemosphere, 59, 147–154.
- LOTTERING J.M., LORENZEN L., PHALA S.N., SMIT T.J., SCHAKWYK C.A.G., 2008, *Mineralogy and uranium leaching response of low grade South African ores*, Minerals Engineering, 21, 16–22.
- MARTINS M., FALEIRO L.M., CHAVES S., TENREIRO R., COSTA M.C., 2010, *Effect of uranium (VI) on two sulphate-reducing bacteria culture from a uranium mine site*, Science Total Environment, 408, 2621–2628.
- MARTINS M., FALEIRO L.M., CHAVES S., TENREIRO R., SANTOS E., COSTA M.C., 2010, *Anaerobic bio-removal of uranium (VI) and chromium (VI): Comparison of microbial community structure*, J. Hazardous Materials, 176, 1065–1072.
- MERROUN L.M., SELENSKA-POBELL S., 2001, *Interactions of three eco-types of Acidithiobacillus ferrooxidans with U(VI)*, BioMetals, 14, 171–179.
- PAL S., PRADHAN D., DAS T., SUKLA B.L., CHAUDHURY R.G., 2010, *Bioleaching of low-grade uranium ore using Acidithiobacillus ferrooxidans*, Indian J. Microbiol, 50, 70–75.
- POLLMANN K. RAFF J., MERROUN M., FAHMY K., SALENSKA-PODELLI S., 2006, *Metal binding by bacteria from uranium mining waste piles and its technological applications*, Biotechnology Advances, 24, 58–68.
- RASHIDI A., SAFDARI, ROOSTA-AZAD R., ZOKAEI-KADIJANI. 2012, *Modeling of uranium bioleaching by Acidithiobacillus ferrooxidans*. Annales Nucler Energy, 43, 13–18.
- SCHIERZ A., ZANKER H., 2009 *Aqueous suspension of carbon nanotubes . Surface oxidation, colloid stability and uranium sorption*, Environmental Pollution, 157, 1088–1094.
- SENKO M.J., KELLY D.S., DOHNALKOVA C.A., MC DONOUGH T.J., KEMNER M.K., Durgos D.W., 2007 *The effect of U(VI) bioreduction kinetics on subsequent reoxidation of biogenic U(IV)*, Geochimica et Cosmochimica Acta, 71, 4644–4654.
- ZHANG G., SENKO M.J., KELLY D.S., TAN H., KEMNER M.K., BURGOS D.W., 2009, *Microbial reduction of iron(III)-rich nontronite and uranium(VI)*, Geochimica et Cosmochimica Acta, 73, 3523–3538.

Received March 3, 2012; reviewed; accepted June 16, 2012

ANALYSIS OF SCREENING PROCESS OF CRUSHED BASALT PERFORMED BY A DOUBLE-FREQUENCY SCREEN

Remigiusz MODRZEWSKI, Piotr WODZINSKI

Łódź University of Technology, ul. Wólczajska 175, 90-942 Łódź, Poland; wodzinsk@wipos.p.lodz.pl

Abstract: This work presents the results of the investigations, devoted to multi-frequency screens, devices being used for the screening process and equipped with two drive vibrators operating at various rotation speeds. The object of this research was to evaluate the efficiency and capacity of a newly designed double-frequency screen to sieve the grained materials, especially those difficult to separate. The experimental double-frequency screen is driven by two inertial drive vibrators operating at various rotation speed, providing complex shaking movement of the screen. In comparison to conventional devices containing vibrators operating at constant rotation speed, the application of this modern double-frequency screen resulted in improving parameters of the screening process.

Keywords: *screening, screen, sieve, grained material, double-frequency screen*

Introduction

The most difficult problem that arises during the screening process is classification of the fine-grained materials containing small grains with cut size (d_{50}) lower than 1 mm. Small grains most easily block the sieve holes lowering the surface area of the sieve (effective area) and also causing difficulties in obtaining a homogeneous and thin enough layer of the material above the sieve. It is usually assumed, that the screening process can be efficient if the layer of grains on the sieve is not thicker than 5-10 average grain diameters (Kanzleiter, 1971; Fischer, 1982). Similar problem arises during the screening process of the grained materials containing large quantities of grains with dimensions approximately equal to the dimensions of the sieve openings, called grains-difficult-to-separate.

The shape of the grains also plays an important role in the screening process of the grained materials. For instance grains with sharp edges can more easily block the sieve holes, than those spherical in shape. Moreover, the sharp-edged grains can be firmly

fixed in the sieve holes and resist the intense movements of the screen. In addition, the motion of the sharp-edged grains in the layer of the material on the sieve is hampered, which reduces moving of the grains of the bottom class to the sieve level and passing through the sieve holes. As a result, the efficiency of the screening process of the materials containing grains with sharp edges decreases comparing to those containing grains with other shapes (Rogers, 1982; Schmidt, 1984). It is illustrates in Fig. 1, where the results of the screening process of variously grained materials with the use of a conventional industrial screen equipped with a single-frequency inertial drive vibrator are showed. The lowest efficiency is observed for crushed basalt stone containing sharp-edged grains, whereas higher efficiencies are observed for both sand being composed of irregular grains and agalut composed of spherical grains.

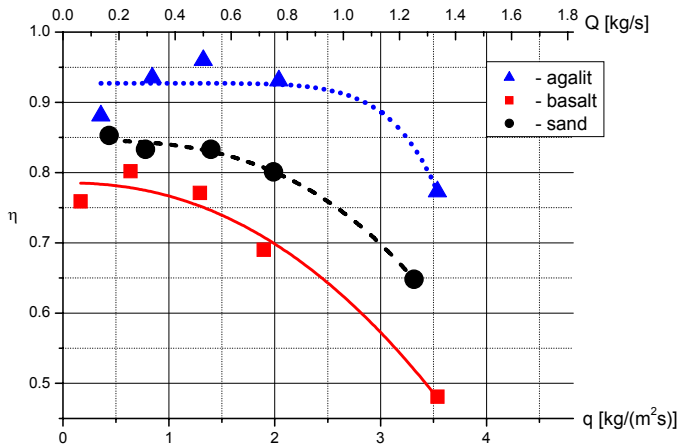


Fig. 1. The efficiency of the screening process performed for the grained materials containing grains with various shapes (q – specific capacity, Q – total capacity, η – efficiency)

The goal of the invention of a new double-frequency screen was to solve the problems mention above by improving conditions of the screening process. Our intention was to find such oscillation paths of the sieve which provide the most efficient separation of grains in the layer on the sieve.

Figure 2 shows the schematic representation of the double-frequency screen offering a wide range of oscillations of the screen with various movement trajectories. Types of movement trajectories and methods of their characterization were already published (Modrzewski and Wodziński, 2010; 2011), whereas this paper describes a continuation of those investigations devoted to the screening process of basalt crushed stone. Basal crushed stone is known to be difficult for the classification by means of a screen as showed above. However, it seems that by using the double-frequency screen possessing unique properties it should be possible to obtain satisfying results.

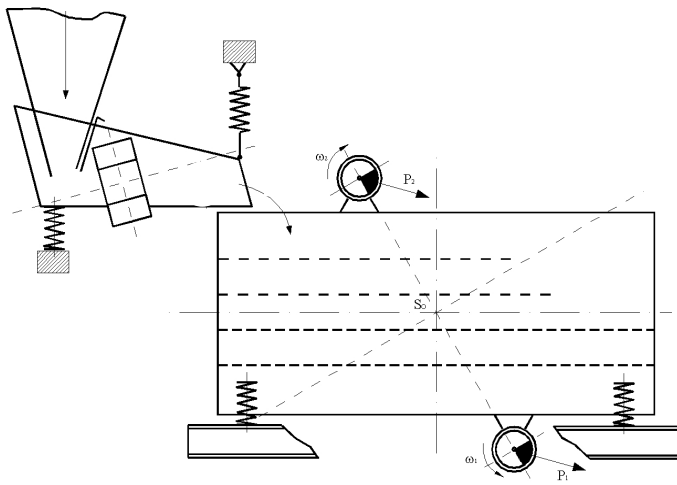


Fig. 2. The double-frequency screen with a feeder

The problems occurring during the application of the double-frequency screen

The construction of the double-frequency screen allows the control of the most of technical parameters of the device including inclination of the sieve (α), driving forces of the vibrators (P_1 and P_2), location of the vibrators (S_0) and, first of all, their rotation speeds (ω_1 and ω_2). By changing the configuration setting a wide range of operating conditions may be applied (Modrzewski and Wodziński, 2011). The best combinations of parameters were selected basing on the results of the measurements.

It is worth to mention that apart from the advantages, application of the double-frequency screens may cause some problems, which are not observed when using a single-frequency screens (Banaszewski, 1990). However in many cases, despite apparently beneficial kinematic conditions (high throwing coefficient, high amplitudes of the screen etc.) the screening process with the application of the double-frequency screens does not occur correctly.

According to the electronic measurements of the screen movements those problems arise when the torsional vibrations of the riddle appear. Those vibrations cannot be seen with naked eyes, however, they can be simply determined by measuring the amplitude of the screen at three different points (Fig. 3 and Fig. 4) (e.g. at the beginning a1, in the middle a2 and at the end a3) in a direction perpendicular to the surface of the screen using the same time scale. When the amplitudes are synchronized no torsional vibrations occur and the screen moves equally along its whole length, and both ends (a1, a3) of the screen have the same amplitudes and trajectories as the centre of the screen (a2). The lack of synchronisation (Fig. 3) means that the amplitudes of the end (a3) and beginning of the screen (a1) are opposite and causes torsional vibrations.

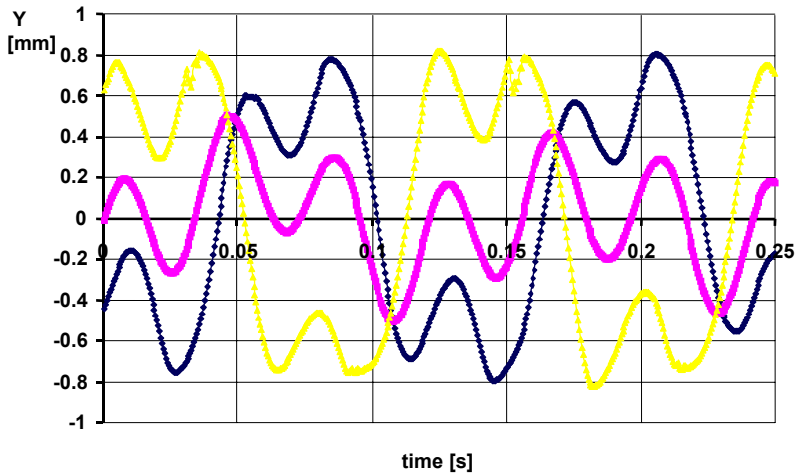


Fig. 3. The amplitudes of the screen in the presence of torsional vibrations

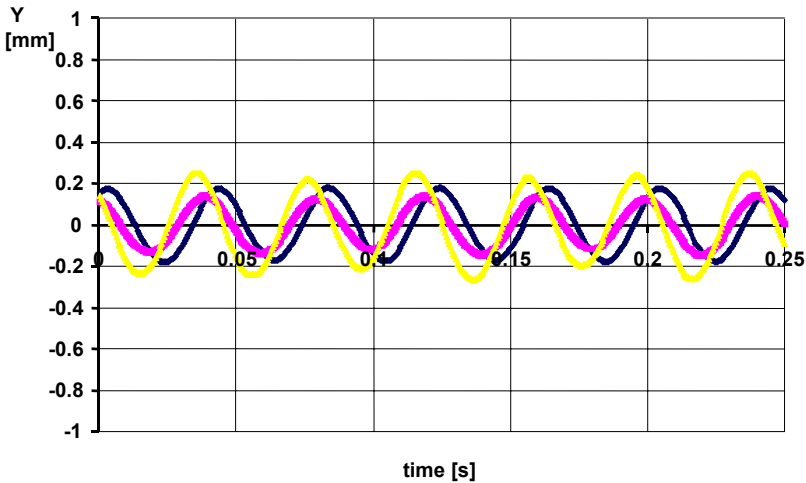


Fig. 4. The amplitude of the screen in the absence of torsion vibrations

Based on experimental data collected for the screening process of basalt crushed stone, one may conclude that even a small contribution of torsional vibrations to the screen motion can cause significant problems. As a consequence of the presence of torsional vibrations the grained material is accumulated in the central part of the screen causing a partial or complete blockage of the screening process.

In the less serious case the layer of the grained material formed at the presence of torsional vibrations becomes thicker in the central part of the screen (Fig. 5) than in other parts and vividly differs from an optimal profile forming in the absence of torsional vibrations (Fig. 6), described by an exponential curve. The accumulation of the

grained material in the central part of the screen, even if does not lead to the stopping of the process, causes the lowering of the overall efficiency of the screening. So, those parameter combinations that cause torsional vibrations were discarded at the stage of the process investigation.

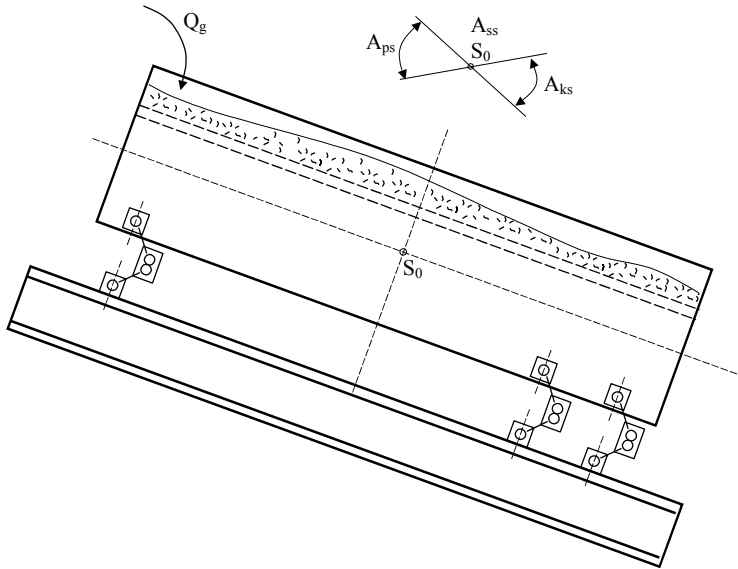


Fig. 5. The layer of the grained material formed on the double-frequency screen in the presence of torsional vibrations

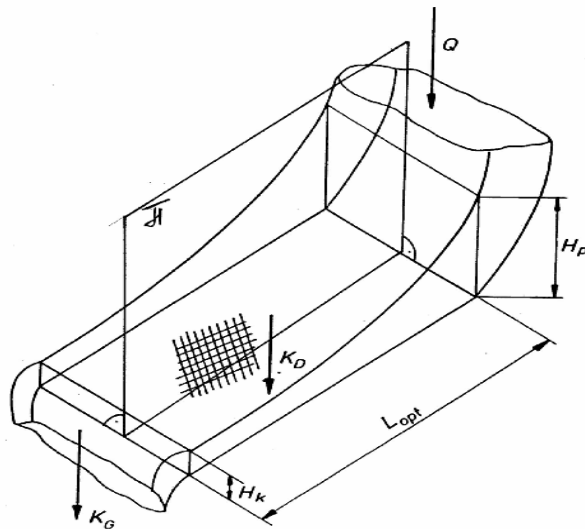


Fig. 6. The profile of the layer of the grained material on the screen in the absence of torsional vibrations

The screening process of basalt crushed stone

Basalt crushed stone with grain size ranging from 0 to 2 mm (Table 1) was selected for the examination of the double-frequency screen. The cut size (d_{50}) of the sieved material was equal to 0.63 mm. The fraction of grains difficult to sieve, i.e. with the dimensions approximately equal to 0.63 mm, in the initial grained material was ca. 45% (including upper and bottom classes). Besides a large content of grains difficult to sieve, the grained material was also composed of grains with sharp edges, therefore it had to be classified as an exceptionally difficult to sieve.

Preliminary experiments on the examination of the double-frequency screen using different grained materials, e.g. sand were described in previous papers (Modrzewski and Wodziński, 2010; 2011), where a detailed information on the parameters of the double-frequency screen was also included. Current experiments were conducted using basalt crushed stone and applying the same operating conditions, such as:

- inclination of the screen 0–20° (α),
- alignment of the vibrators (S_0),
- driving force generated by the vibrators (P_1 and P_2),
- rotation speed of the drive vibrators (ω_1 and ω_2).

Table 1. Granulometric composition of the initial grained material

Grain size d [mm]	Percentage share U [%]	
0.2	11.25	
0.4	16.25	50
0.63	22.5	
0.85	22.5	
1	16.25	50
2	11.25	

The screening process was tested by changing the configuration of operating conditions. The mass of the upper and bottom parts was measured for each configuration. Then, the efficiency (η), total capacity (Q) and specific capacity (q) (per unit of screen surface area) (Sztaba 1993) of the screening process were calculated. The efficiency of the screening process was calculated according to the equation:

$$\eta = \frac{m_d}{m_n K_d} \quad (1)$$

where: m_d – the mass of the product collected under the sieve [kg],

m_n – the mass of the initial grained material [kg],

K_d – the percentage of the bottom class in the initial grained material

The results of investigations were presented as the relation between efficiency and capacity. About two hundred various experiments were carried out changing the configuration, which however was only a part of possible combinations of parameters. Unpromising results, especially those obtained in the presence of torsional vibrations were not taken into consideration.

A major criterion for the evaluation of the efficiency-capacity relations was the efficiency of the screening process, which should be naturally as high as possible. The most representative results are displayed in Figure 7 which shows how the efficiency, capacity and specific capacity changes with various speed ratios of both vibrators, e.g. 1:1, 2:3, 1:2, 1:3.

The curves were plotted using experimental data recorded for applying rotations in the same direction. The rotations in the opposite directions caused torsional vibrations. Therefore the results were not taken into consideration for the reason described above. High efficiency, about 0.9 was achieved using the optimal gear ratio of 2:3, which may fully satisfy industry standards.

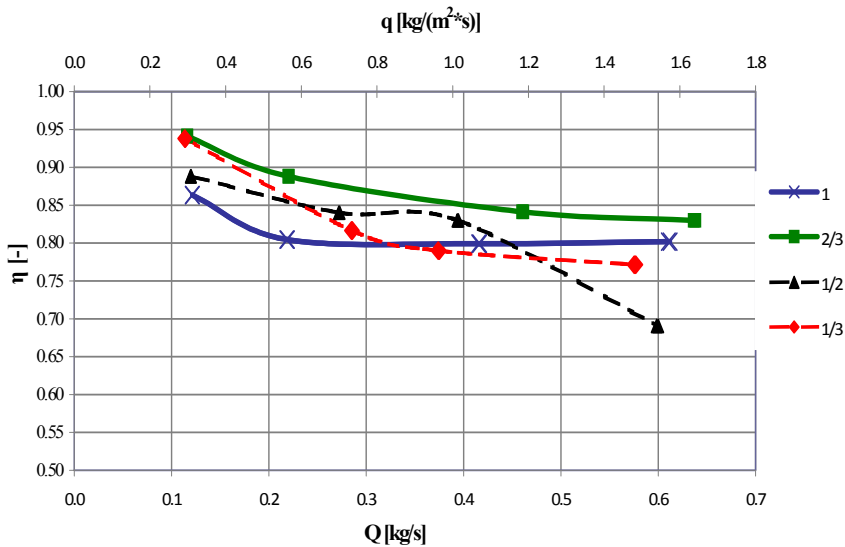


Fig. 7. The comparison of the efficiency (η), capacity (Q) and specific capacity (q) calculated for various gear ratios

Figure 8 displays the comparison of results obtained for various arrangements of the vibrators on the screen, e.g. keeping minimum distance (the vibrators positioned one over the other) or maximum distance between vibrators. It shows that the location of the vibrator on the screen had no influence on the efficiency of the screening process. The values obtained for the minimum distance between vibrators were similar to those obtained for the maximum distance.

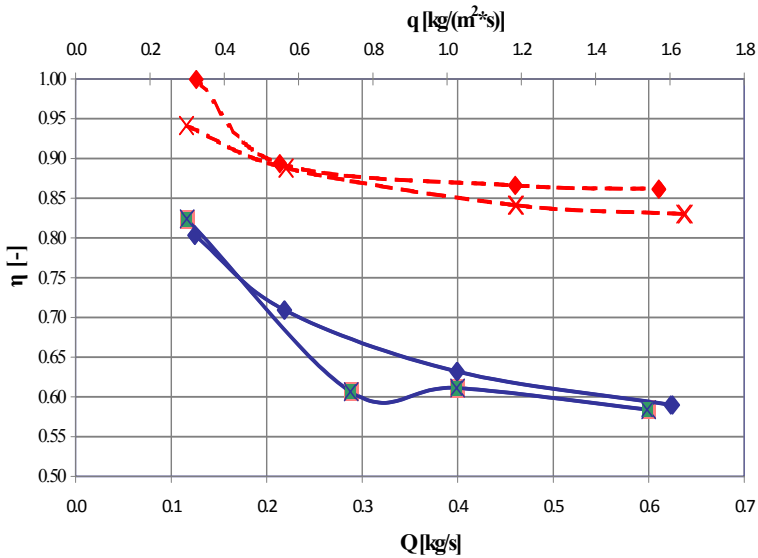


Fig. 8. The influence of location and rotation direction of the vibrators on the efficiency of the screening process

Figure 8 also shows the influence of various rotation directions of the vibrators on the efficiency of the screening process. Dashed red lines represent the data collected using rotations in the same direction, whereas solid blue lines are related to the data collected using rotations in the opposite direction. A high efficiency (ca. 0.9) was achieved setting the rotations in the same direction. By applying the rotations in the opposite directions a low efficiency (ca. 0.6–0.7) was achieved, which is insufficient for industry standards. All results shown in Figure 8 are based on the data collected using gear ratio of 2:3.

Conclusions

Based on experimental results obtained for basalt crushed stone one may conclude that the double-frequency screen can be successfully applied for the screening process of the grained materials especially those difficult to separate. However, certain unfavourable operating conditions described above must be avoided whilst using this device.

However, the regression analysis of the process, for the applied process evaluation criterion, the efficiency, does not lead to the unequivocal conclusions, because of large number of complicated dynamic parameters that also influence each other. For example, it is impossible to determine solely the effect of inclination of the screen on efficiency of the screening process because such effect may differ or even be opposite for different sets of parameters, depending on dynamic factors. Similar mutual interferences may be observed for other operating conditions and dynamic factors.

The results for all investigated sets of parameters cannot be fully presented in so this paper, however a few basic suggestions for designing and operating the double-frequency screen may be provided:

- both vibrators should rotate in the same direction to avoid the appearance of torsional vibrations,
- the vibrators should be fixed with a minimum distance, e.g. one should be located above the other, to reduce the risk of generating torsional vibrations,
- depending on the type of the vibrator, driving force should be set to a maximum possible value,
- it is strongly recommended to apply the speed ratio of 2:3, which offers stable trajectories and high efficiency.

Acknowledgments

This study was performed as a part of chartered assignment W-10/16/2012/Dz.St.

References

- BANASZEWSKI T., 1990, *Przesiewacze*; Wydawnictwo Śląsk.
- FISCHER M., 1982, *Doppel-Frequenz-Siebmaschinen in der Bewahrung*, *Aufbereitungs Technik.*, 12, 687–693.
- KANZLEITER T., 1971, *Die Taumelsiebmaschine. Maschinendynamik und Guttransport*, *Aufbereitungs Technik*, 3, 7–12.
- MODRZEWSKI R., WODZIŃSKI P., 2010, *The results of process investigations of a double-frequency screen*, *Physicochem. Probl. Miner. Process.*, 44, 169–178.
- MODRZEWSKI R., WODZIŃSKI P., 2011, *Grained material classification on a double-frequency screen*, *Physicochem. Probl. Miner. Process.*, 46, 5–12.
- ROGERS R.S.C., 1982, *A classification function for vibrating screens*, *Powder Technology*, 1, 135-137.
- SCHMIDT P., 1984, *Das Siebklassieren*, *Chem. Ing. Techn.*, 56, nr 12.
- SZTABA K., 1993, *Przesiewanie*; Śląskie Wydawnictwo Techniczne.

Received April 13, 2012; reviewed; accepted June 15, 2012

DEGRADATION OF NANOCLAY-FILLED POLYLACTIDE COMPOSITES

Alicja RAPACZ-KMITA¹, Ewa STODOLAK-ZYCH², Magdalena DUDEK²,
Barbara SZARANIEC¹, Agnieszka ROZYCKA¹, Michał MOSIALEK³,
Lucjana MANDECKA-KAMIEN¹

¹ AGH – University of Science and Technology, Faculty of Materials Science and Ceramics, Mickiewiczza 30, 30-059 Cracow, Poland, kmita@agh.edu.pl, stodolak@agh.edu.pl, szaran@agh.edu.pl, ar@agh.edu.pl, mandecka@agh.edu.pl

² AGH – University of Science and Technology, Faculty of Energy and Fuels, Mickiewiczza 30, 30-059 Cracow, Poland, potoczek@agh.edu.pl (corresponding author)

³ J. Haber Institute of Catalysis and Surface Chemistry PAS, Niezapominajek 8, 30-239 Cracow, Poland and Institute of Physical Chemistry PAS, Kasprzaka 44/52, 01-224 Warsaw, Poland; nbmosial@cyfronet.pl

Abstract: Nanoclay-filled polylactide (PLA 3051D) composite materials were tested in this study and their capacity for degradation was investigated. Activated and lyophilized smectite clay was used. The filler, its morphology, and grain size distribution were characterized by the use of transmission electron microscopy, scanning electron microscopy, and the dynamic light scattering technique. Samples of pure polylactide and polylactide filled with 3% wt., 5% wt., and 10% wt. of nanoclay in subsequent series were obtained by injection molding. The optimum amount of the filler in the nanocomposites was evaluated based on an assessment of mechanical properties as well as capacity to degrade. The 3% wt. mass fraction of nanofiller in the polylactide matrix was found to be the most effective in enhancement of both tensile strength (R_M) and Young's Modulus (E). It was also reported that polylactide nanocomposites filled with 3% wt. of smectite clay were characterized by the highest decrease in molecular mass of the matrix polymer after degradation tests (6 weeks incubation in water at 80°C). The observed decrease in degradation time and the overall changes distinguished in the nanocomposite structure suggest the potential for application of the material in the packaging industry.

Keywords: *nanocomposite materials, food packaging, polymer, smectite clay*

Introduction

Polymers, polymer blends, and polymer composites (i.e. polymers filled with fibers or particles) are very often used as conventional food packaging materials. However, some drawbacks related to their use, such as quality of packaging (mechanical proper-

ties, suitability, and durability in operating conditions), potential influence on food, and total costs of production, guarantee an ever-growing need for new kinds of materials with improved properties (Appendini and Hotchkiss, 2002; Auras et al., 2004; Drumright et al., 2000; Platt, 2006). Polymer-based nanocomposites are among the most promising materials, which nowadays are subjected to a great deal of research all over the world. A relatively small amount of nanofiller (up to 10%) with a high level of refinement (at least one dimension below 100 nm) results in the creation of a filler-matrix interface with surface development several times higher than traditional composite materials. This enables either second-order bonding or electrostatic interactions, and influences physicochemical/mechanical (higher stiffness and strength), thermal (better stability), and chemical (resistance to solvents) properties of materials and their capacity for controlled degradation. All these features argue for the extension of their range of application in the packaging industry (Alexandre and Dubois, 2000; Pfaendner, 2010; Sinha Ray and Bousmina, 2005; Sorrentino et al., 2007).

The use of nanocomposite materials for food packaging applications enables the design and manufacture of materials with improved properties compared to conventional materials (Avella et al., 2005; Murariu et al., 2010). Enhancements include improved stability over time (*in vitro* condition), better barrier properties, and lower spoilage (Matusik et al. 2011). Among others, one may name improved mechanical properties and durability. The first may be achieved by the introduction of nanofiller into a polymer matrix and by very good overall homogenization of the material. The second feature, durability, is the result of the limited release of water into the bulk of the polymer matrix, considered a step in promoting the hydrolysis process (Solarski et al., 2008; Tsuji and Ikarashi, 2004). This promotion is decelerated due to the presence of nanoparticles such as clays, silica, carbon nanotubes and others in the polymer matrix. The most promising nanofillers acting as water storage materials in this case are clays: montmorillonite (MMT), bentonite, kaolinite (Fukushima et al., 2010; Sinha Ray et al., 2003; Tsuji et al., 1998).

This paper presents the results of the study on properties of nanocomposite materials based on degradable polylactide modified by different amount of nanofillers (smectite clay).

Experimental

As a degradable matrix for preparation of nanocomposite samples, poly-L-lactide (PLA 3051D), manufactured by Nature Works, was used. The manufacturer has provided typical parameters of PLA pertinent to the molding process, as shown in Table 1. The PLA was modified with a nanometric smectite clay filler (SM), Veegum F, manufactured by R.T. Vanderbilt Company, Inc.

Table 1. Producer data sheet for PLA

Properties of PLA 3051D	
Melt temperature	200°C
Feed temperature	165°C
Glass transition temperature	55–65°C
Screw speed	100–175 rpm
Density	1.24 g/dm ³
Relative viscosity	3–3.5
Molecular mass	25 kDa

Nanocomposite samples were prepared in two stages. The initial stage of the experiment consisted of modifying smectite clay by chemical treatment, followed by exfoliation. The effects of this procedure were analyzed by the DLS method. Smectite was treated with ionic activation in 2 M NaCl solution, centrifuged, and rinsed up to the extinction of chlorine ion reaction. The obtained nanofiller product was lyophilized in the subsequent step, and the morphology of the particles was characterized using the transmission electron microscope TEM (JEOL JEM-1011). Both types of powders, i.e. pure and modified smectite, were dispersed in isopropanol and covered with a carbon layer prior to observation. Samples prepared for SEM observations (Nova NanoSEM 200, FEI) were also covered with a carbon layer. The smectite particle size distribution was evaluated by the dynamic light scattering method (Zetasizer Nano ZS, Malvern Instruments) in a water suspension at 25°C. Prior to measurement, the powder was mixed with water and homogenized with an ultrasonic horn.

In the next stage of the experiment, smectite clay powder was homogenized with PLA pellets. The nanoadditive, in amounts of 3, 5 or 10% wt., was added to a charge of polymer pellets and milled in a roller mill for 48 h. As a result, the smectite particles covered the polymer pellets, which then were used as a charge for the injection molding process. The nanocomposite samples (paddle-shaped 75×5×2 mm, following Polish Standard PN-EN ISO 527) were manufactured by the use of injection molding. The injection was carried out at 165°C under a pressure of 60 kg/cm² in a vertical injection molding machine (Multiplas).

The mechanical properties and the degradation ability of the nanocomposite were investigated. A standardized tensile test was used for determining mechanical properties such as tensile strength and Young's modulus according to ISO 527 standards by using the Instron 3367 testing machine. The extensometers were used for precise measurements of strain.

The degradation capacity of the nanocomposite materials filled with smectite clay in water environment was observed during the incubation (6 weeks/80°C/H₂O with an initial water pH of 6.35). Pure polylactide was used as a reference material in the study. All the samples were monitored for changes of pH in the immersion solution and viscosity of the polymer. The viscosity coefficient (η) of the materials was measured by the Hoppler method and calculated by equation (1) (Lunt, 1998; Tsuji, 2002).

$$\eta = k(\rho - \rho') \cdot t \quad (1)$$

where: η – viscosity coefficient,
 k – constant describing conditions of the experiment,
 ρ – density of the ball material,
 ρ' – density of the liquid phase,
 t – flow time of the ball.

The nanocomposite materials were dissolved in DCM (dichloromethane, POCh Gliwice) without separating the nanofiller from the polymer solution. The initial concentration of the polymer solution was 0.1 g/cm^3 .

The molecular mass of the polymer was evaluated according to the Mark-Houwink equation (2) for a given polymer-solvent system (PLA/DCM; $K = 2.21 \cdot 10^{-4} \text{ cm}^3/\text{g}$, $a = 0.77$) (Lunt, 1998; Tsuji, 2002):

$$\eta = K \cdot M_n^a \quad (2)$$

where: K – coefficient characteristic for the PLA/DCM system,
 M_n – molecular mass of the polymeric material,
 a – constant describing conditions of the experiment.

Results and discussion

The base smectite powder was characterized by a strong tendency both to agglomerate and aggregate, which was clearly visible in SEM images (Fig. 1). The grain size distribution analysis showed monomodal distribution, in which aggregates of 600-750 nm in size dominate rather than separate single particles (Fig. 2).

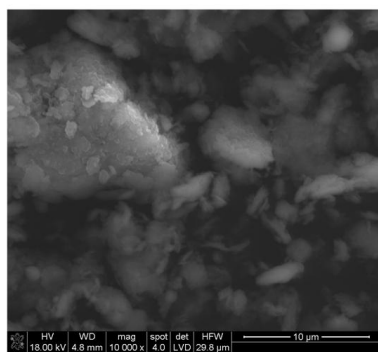


Fig. 1. SEM microphotograph of smectite clay powder before activation

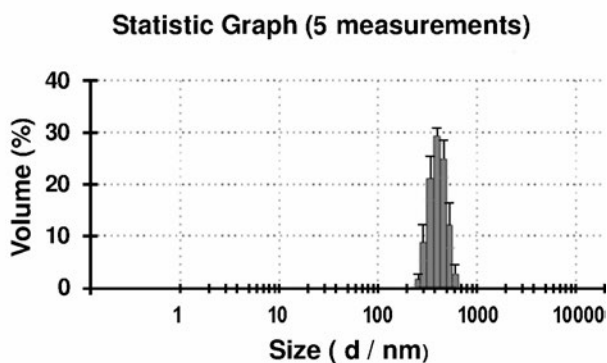


Fig. 2. Particle size distribution of smectite clay powder before activation

The thermal treatment process, followed by the lyophilization of the nanofiller, led to its activation and to the decomposition of the aggregates. A noticeable change in grain size distribution was reported after the activation process, with the resulting size of the filler particles estimated at about 80–100 nm (Fig. 4).

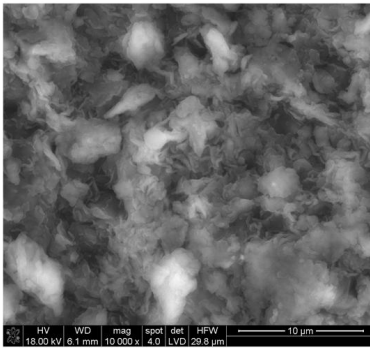


Fig. 3. SEM microphotograph of smectite

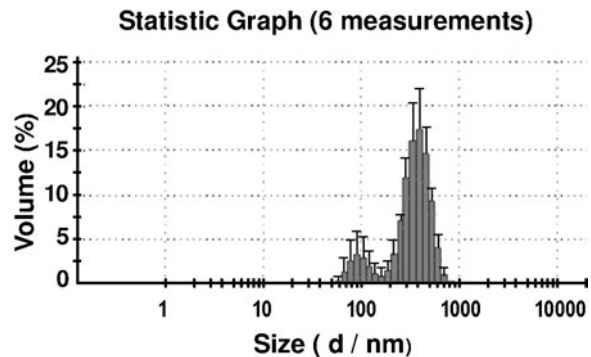


Fig. 4. Particle size distribution of smectite clay powder after activation

The bimodal distribution of the filler confirmed that aggregates were still present but their frequency was lowered by 30% compared to the base unmodified smectite clay powder. This was due to the lyophilization process which leads to “freezing” the chaotic structure of montmorillonite tiles. As a result, the grain morphology also changed (Fig. 3), leading to the appearance of the so-called texturization effect (the tendency of montmorillonite tiles to align parallel to one another) (Fukushima et al., 2009).

Thus, modification of the smectite powder influenced both powder morphology and powder grain size distribution. These changes were confirmed by TEM analysis, and the grain size distribution was reported to have become nanometric in its major dimensions, which had not been observed for the unmodified smectite powder before activation (Fig. 5).

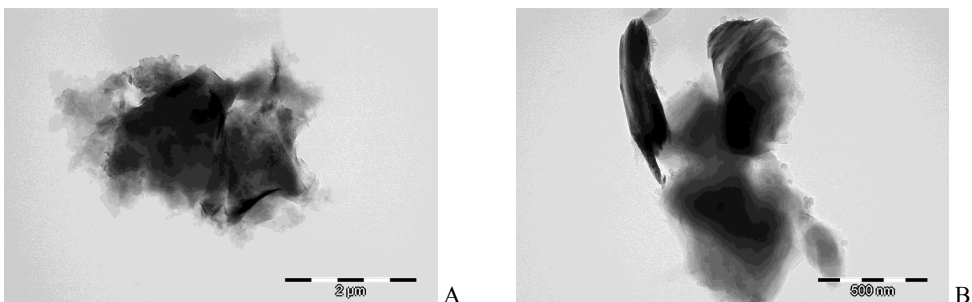


Fig. 5. TEM image of smectite clay powder before (A) and after (B) activation

Different mass fractions of smectite were used to evaluate its influence on the mechanical properties of the composites. This procedure was also designed to optimize the amount of smectite along with the mechanical performance. The results of mechanical tests indicated that 3% wt. of smectite in the polylactide matrix can be considered the optimum value. Addition of 5% wt. in the matrix resulted in mechanical performance similar to that of the unfilled polylactide, while 10% wt. led to a reduction of the mechanical strength reported during the tests. This behavior can be explained by the presence of agglomerates in the matrix which act as inclusions and can be treated as stress concentrators rather than reinforcements (Fig. 6). Considering changes in the overall stiffness, it can be stated that the presence of smectite filler in the matrix increases the value of Young's modulus of composites by about 10% compared to unfilled polylactide (PLA) (Fig. 7). This can be explained by the likely occurrence of electrostatic and/or second-order interactions between the filler and matrix. However, this must be clarified by further research.

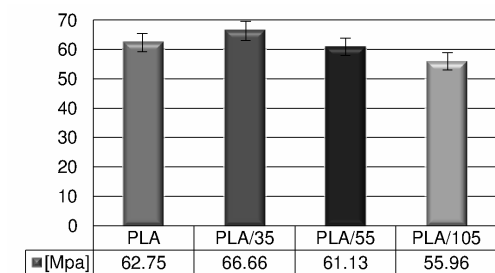


Fig. 6. Tensile strength results of nanocomposites and reference polylactide samples

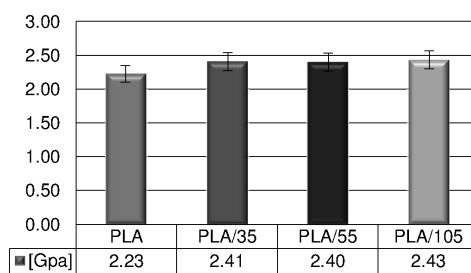


Fig. 7. Young's modulus results of nanocomposites and reference polylactide samples

Due to its potential application as degradable packaging material, the impact of filler content on degradation time of the composites was also evaluated. After 6 weeks of incubation in water at 80°C, structural degradation of all composites filled with smectite (excluding pure polylactide) was observed (Fig. 8). According to the literature, PLA degradation is a two-step process. In the initial step the polymer molecular weight decreases (bulk degradation) and in the second step degradation is observed both in bulk and on the surface of the PLA. During this step the molecular weight remained constant, but a weight loss in the material could be measured. For this reason a change in the coefficient of viscosity was also reported for all nanocomposite materials. It was shown that viscosity was strongly dependent on the amount of nanofiller. The most noticeable decrease in viscosity was observed for materials with 5% wt. and 3% wt. of nanofiller. This may indicate accelerated degradation in materials filled with 5% wt. and 3% wt. smectite, both in comparison to the pure polymer material and the composite filled with 10% wt. smectite (Table 2). This phenomenon was due to the modified (i.e. activated and lyophilized) nanofiller's strong absorption of water, so that hydrolytic degradation of the material (hydrolysis of polylactide) occurred not

only at the surface but also within the bulk polymer matrix (Nakamura et al, 1989; Padua and Wang, 2012). This resulted in a decrease of the molecular weight of the polymer, which led in turn to a reduction in the durability and consistency of the material. The rate of hydrolysis strongly depends on environmental conditions: ions, pH and temperature. It was expected that the nanofiller present in the polymer matrix would serve as a reservoir of water. Additionally, degradation would be faster because of chlorine ions which might be present in the smectite after its chemical modification (NaCl). The nanofiller present in the polylactide matrix also changed the crystallinity of the nanocomposite materials, mostly by disordering the polymer chain. This effect hydrolyzed amorphous regions significantly faster than crystalline regions. An exceedingly low concentration of the polymer solution made it difficult to note results of viscosity correctly, so all samples were measured in the same way.

Table 2. Viscosity and molecular weight of the nanocomposite materials and the reference polymer after incubation in *in vitro* conditions

Materials	Initial polymer concentration [g/100 dm ³]	Viscosity coefficient, η [Pa·s]	Molecular weight, Mn [kDa]
PLA	0.01	0.78	20.0
PLA/3SM	0.01	0.45	12.0
PLA/5SM	0.01	0.55	7.7
PLA/10SM	0.01	0.74	4.4

During the durability experiment, the immersion medium (water) of the nanocomposite samples significantly changed pH, from a starting value of 6.35 to 6.05 by the end of the test. Probably hydroxyl ions migrated inside the smectite structure, or chlorine ions were released from the smectite and influenced the pH of the medium. The degradation of the polymer matrix was much more significant above its glass transition temperature, i.e. 65°C (an incubation in *in vitro* conditions was performed at 80°C). The duration time of the experiment (6 weeks/80°C) was enough to destroy the nanocomposite materials, a phenomenon not observed in the case of the pure polymer samples (Fig. 8). During the test all nanocomposite materials were completely degraded. Hence the weight loss could not be measured.

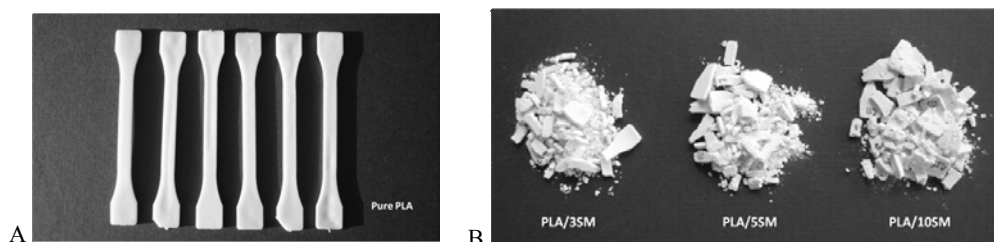


Fig. 8. Macroscopic changes after 6 weeks incubation: (A) limited degradation of pure polylactide samples, (B) excessive degradation of smectite-filled polylactide

Conclusions

Chemical modification, i.e. the activation and the lyophilization of a nanofiller (smectite), favorably affected its structural form by increasing its surface development and the number of active chemical groups, which led to improved dispersion within the polymer matrix (PLA). The presence of the activated nanofiller improved the strength of the nanocomposite materials and their Young's modulus (overall stiffness). The best material properties were achieved for the nanocomposite material filled with 3% wt. of smectite. The greater the amount of the nanofiller, the faster their hydrolysis was, but the presence of the nanofiller accelerated the overall degradation of the material. The nanofiller's presence accelerated the overall degradation of the material. As a result, a dramatic decrease was observed in the mass of material, followed by macroscopic disintegration. Good strength, in combination with a shorter disintegration time, make the nanocomposites potential candidates for an application in the packaging industry.

Acknowledgments

Work was done within the framework of funding for statutory activities of AGH – University of Science and Technology in Krakow, Faculty of Materials Science and Ceramics (11.11.160.603).

References

- ALEXANDRE M., DUBOIS P., 2000. *Polymer layered silicate nanocomposite: preparation, properties and use of new class of materials*. Materials Science Engineering, 28 (1–2), 1–63.
- APPENDINI P., HOTCHKISS J.H., 2002. *Review of antimicrobial food packaging*. Innovative Food Science and Emerging Technologies 3, 113–126.
- AURAS R., HARTE B., SELKE S., 2004. *An overview of polylactides as packaging materials*, Macromol. Biosci. 4 (9), 835–839.
- AVELLA M., De VLIENER J.J., ERRICO M.E., FISCHER S., VACCA P., VOLPE M.G., 2005. *Biodegradable starch/clay nanocomposite films for food packaging applications*. Food Chemistry 93, 467–474.
- DRUMRIGHT R.E., GRUBER P.R., HENTON D.E., 2000. *Polylactic acid technology*. Advances Materials 12 (23), 1841–1846.
- FUKUSHIMA K., TABUANI D., ABBATE C., ARENA M., FERRERI L., 2010. *Effect of sepiolite on the biodegradation of poly(lactic acid) and polycaprolactone*. Polymer Degradation and Stability 95, 2049–2056.
- FUKUSHIMA K., TABUANI D., CAMINO G., 2009. *Nanocomposites of PLA and PCL based on montmorillonite and sepiolite*. Materials Science Engineering C 29, 1433–1441.
- LUNT J., 1998. *Large-scale production, properties and commercial applications of polylactic acid polymers*. Polymer Degradability Stability 59, 145–152.
- MATUSIK J., STODOLAK E., BAHRANOWSKI K., 2011. *Synthesis of polylactide/clay composites using structurally different kaolines and kaolinite nanotubes*. Applied Clay Science 51, 102–109.
- MURARIU M., DECHIEF A., BONNAUD L., PAINT Y., GALLOS A., FONTAINE G., BOURBIGOT S., DUBOIS P., 2010. *The production and properties of polylactide composites filled with expanded graphite*. Polymer Degradation and Stability 95, 889–900.

- NAKAMURA T., HITOMI S., WATANABE S., SHIMIZU Y., JAMSHIDI K., HYON S.H., IKADA Y., 1989. *Bioabsorption of polylactides with different molecular properties*. J. Biomed. Mater. Res. 23, 1115.
- PADUA G.W., WANG Q., 2012. *Nanotechnology research methods for foods and bioproducts*. Wiley-Blackwell.
- PFAENDNER R., 2010. *Nanocomposite: Industrial opportunity or challenge*. Polymer Degradation and Stability 95, 369–373.
- PLATT D., editor., 2006. *Biodegradable polymers – market reports*. Shawbury, Shrewsbury, Shropshire: UK: Smithers Rapra Limited.
- SINHA RAY S., BOUSMINA M., 2005. *Biodegradable polymers and their layered silicate nanocomposites: in greening the 21st century materials world*. Prog. Materials Science 50 8, 962–1079.
- SINHA RAY S., OKAMOTO K., OKAMOTO M., 2003. *Structure-property relationship in biodegradable poly(butylenes succinate)/layered silicate nanocomposites*. Macromolecules 36, 2355–2367.
- SOLARSKI S., FERREIRA M., DEVAUX E., 2008. *Ageing of polylactide and polylactide nanocomposite filaments*. Polymer Degradation and Stability 93, 707–713.
- SORRENTINO A., GORRASI G., VITTORIA V., 2007. *Potential perspectives of bio-nanocomposites for food packaging applications*. Trends in Food Science and Technology 18, 84–95.
- TSUJI H., 2002, *Poly lactides*, in *Biopolymers*, Wiley-VCH, chap. 5.
- TSUJI H., IKARASHI K., 2004. *In vitro hydrolysis of poly(L-lactide) crystalline residues as extended-chain crystallites*. Effects of pH and enzyme. Polymer Degradation Stability 85, 647–656.
- TSUJI H., MIZUNO A., IKADA Y., 1998. *Blends of aliphatic polyesters III. Biodegradation of solution-cast blends from poly(L-lactide) and poly(caprolactone)*. Journal Applied Polymer Science 70, 11, 2259–2268.

Received April 15, 2012; reviewed; accepted June 15, 2012

PRESSURE OXIDATION OF PYRITE-ARSENOPYRITE REFRACTORY GOLD CONCENTRATE

Lauri RUSANEN, Jari AROMAA, Olof FORSEN

Aalto University, Department of Materials Science. P.O. Box 16200, Aalto, Espoo, Finland, jari.aromaa@aalto.fi

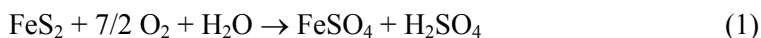
Abstract: Refractory gold ores have poor gold recoveries with direct cyanide leaching. Typically the refractoriness is due to encapsulation of the gold particles inside the host mineral. To liberate gold for leaching the host mineral must be broken by mechanical or chemical means. The aim of this study was to study the effect of temperature, oxygen partial pressure and slurry density on pressure oxidation of pyrite-arsenopyrite gold concentrate. Batch oxidation tests in an autoclave were done using a factorial design. Different responses were measured and analysed to study effect of the three factors and oxidation kinetics. Generally, high slurry density required high temperature and oxygen partial pressure to reach complete oxidation. Oxidation kinetics at 225°C temperature, with 1050 kPa oxygen partial pressure and 15% slurry density was found to be fastest resulting in complete conversion of sulfides in 30 minutes. At 195°C, 700 kPa oxygen partial pressure and 10% slurry density, the oxidation kinetics for complete sulfide conversion was about 60 minutes. Slurry densities above 10% had an adverse effect on the oxidation rate, when the temperature was below 225°C and oxygen partial pressure below 1050 kPa.

Keywords: *gold ore, hydrometallurgy, leaching, factorial design*

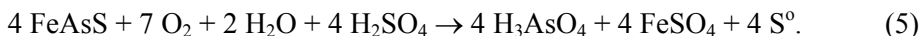
Introduction

Many of the gold deposits today contain gold finely disseminated in iron sulfide minerals, such as pyrite and arsenopyrite. Such deposits are known as refractory gold ores due to encapsulation of fine gold particles in the host mineral (Iglesias and Carranza 1994; Fleming 1992; Corrans and Angove 1991). A clear border between refractory and non refractory ore in terms of gold recovery is not given, but several authors have stated that less than 80% gold recovery by direct cyanide leaching after fine grinding of the ore indicates a refractory ore (Iglesias and Carranza 1994; Fleming 1992; Corrans and Angove 1991; Pangum and Browner 1996). The refractory ore must be broken down by chemical means, with utilization of oxidative processes, such as roasting, pressure oxidation or bacterial leaching. These expose the valuable metals to subsequent cyanidation.

Leaching of metal sulfide minerals is commonly considered as an electrochemical reaction between sulfide ion and oxygen. Sulfide sulfur is oxidized either into elemental sulfur, sulfite or sulfate ions. Oxygen undergoes a reduction reaction with water formation (Bailey and Peters 1976; Rimstidt and Vaughan 2003; Papangelakis and Demopoulos 1990; Long and Dixon 2004). All these studies present two competing reactions to occur as the anodic oxidation reaction of pyrite, one producing sulfate and sulfuric acid (1) and the other sulfate and elemental sulfur (2). Oxygen can also oxidize pyrite directly producing Fe^{3+} and thiosulfate (3) followed by thiosulfate decomposition and oxidation of the resulting sulfite ion to sulfate (Long and Dixon 2004).



The proposed reactions of arsenopyrite are quite identical (Eqs (4) and (5)) (Papangelakis and Demopoulos 1990)



Pressure oxidation is typically operated in temperatures of 190 to 230°C and oxygen overpressure of 350 to 700 kPa (Fleming 2010). Under these conditions sulfide sulfur is oxidized into sulfates and bisulfates and iron dissolves as ferrous iron or ferric iron. Ferric iron can hydrolyse and precipitate as hematite, basic iron sulfate or jarosite, and also formation of elemental sulfur as oxidation product is possible. High temperatures are required to avoid formation of elemental sulfur, which is detrimental for cyanidation due to excess consumption of cyanide. In this work the effect of temperature, oxygen partial pressure and slurry density on oxidation kinetics and conversion were studied using batch tests in an autoclave.

Experimental

Refractory gold concentrate was supplied from pyrite-arsenopyrite mineralization in northern Finland. Minerals recognized from the concentrate with XRD were pyrite 24.7%, arsenopyrite 27.1%, quartz 10.7%, and less than 10% each of albite, dolomite, microcline, anorthite and chlorite. Coulter Counter analysis showed that majority of the particles were 1 to 300 μm . Chemical analysis of the concentrate in wt-% was As 6.0%, Fe 21.6%, C 3.3%, S 19.5%, elemental S 0.25%, sulphate 0.42%, and Cl 0.007%. For the pressure oxidation experiments 99.5% pure oxygen was used. A 20 g/dm^3 sulfuric acid solution was prepared from laboratory grade 95–97% sulfuric acid and distilled water.

Autoclave oxidation tests were conducted in Büchi ecoclave model 075 titanium autoclave. The total volume of the autoclave vessel was about 1.1 dm³ and it was equipped with magnetic agitation unit, gas inlet and outlet, and sampling system with nitrogen flush that was also used for nitrogen feed into the vessel. The jacket of the reactor had inbuilt electric heating and cooling water circulation for temperature control. Pitched blade propeller and agitation speed 650 rpm were used in all experiments. Oxygen pressure was adjusted with pressure drop valve and oxygen flow was measured with oxygen mass flow meter.

Dried and homogenized sample was used in all of the experiments. For each test a sample of concentrate and 750 cm³ sulfuric acid were loaded into the reactor. Nitrogen was purged to remove oxygen. Reactor was then heated with the heating resistors in the reactor jacket. Each test was started when oxygen feed was started. Oxygen feed pressure was adjusted before the experiment start as a sum of the water vapour pressure at experiment temperature and the desired oxygen overpressure. Every experiment was run for sixty minutes and the end of experiment was closing the oxygen inlet valve. Immediate cooling of the reactor was started. Slurry drain was done at temperature of about 80°C. Slurry was left for decantation, and in two hours from the draining pH and redox potential of the solution versus a calomel electrode were measured. Dried solids were analysed for total sulfur content, elemental sulfur and sulfate sulfur. Filtered solutions were analysed for dissolved iron. Total amount of consumed oxygen was integrated using the measured oxygen mass flow. Conversion of iron was calculated by dividing the amount of dissolved iron by the amount of iron charge. Conversion of sulfide was calculated as difference between residual sulfide amounts and initial sulfide amount in relation to the initial sulfide amount.

Table 1. Factorial design of experiments

Test Std number	Temperature, °C	Oxygen partial pressure, kPa	Slurry density, %
1	165	350	15
2	225	350	5
3	165	1050	5
4	225	1050	15
5	165	350	15
6	225	350	5
7	165	1050	5
8	225	1050	15
9	195	700	10

This study was planned as half factorial to ensure the reliability of the main factor analysis. Experimental setup was four different combinations of selected three factors with two replicates (Table 1). The centre point was replicated three times. Replication gives more reliability on the analysis of the main factors, but a half factorial setup lacks on the analysis of the interactions of the factors. Factorial analysis of the vari-

ables was made with MINITAB 16 statistic calculation software. Three major analyses were conducted. Pareto analysis shows the significance of the factor to the measured response. Main factor analysis shows the effect of each individual factor on the measured response. Interaction plot shows how two factors affect the response together.

Results

The oxidation of concentrate was followed during the test by measuring oxygen consumption. The experiment had a set value for oxygen partial pressure and that pressure was maintained by controlling oxygen feed. The oxygen was consumed in the oxidation reactions and therefore oxygen flow is a measure of reactions proceeding. The effect of temperature, oxygen pressure and slurry density were measured using a factorial experimental design. The effect of these factors was estimated from the solution redox potential and iron concentration and solids sulfur concentration after completing the experiment.

Oxidation kinetics

Oxygen consumption was measured online during the oxidation test. It was assumed that the oxidation is complete when oxygen feed is no longer needed to maintain reactor pressure. This is reasonable if the reaction proceeds with direct oxidation of the sulfides as suggested for pyrite in Eq. (3) (Long and Dixon 2004). Figure 1 shows four different types of oxygen consumption curves noticed in the tests. When using

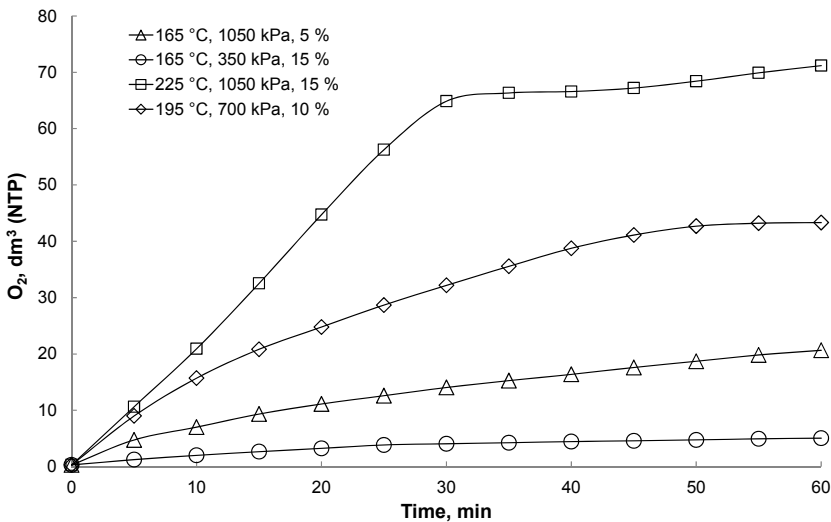


Figure 1. Examples of calculated oxygen consumptions

low temperature and low oxygen pressure the oxygen consumption was small and either reached a very low steady level soon after the beginning (test 5, 165°C,

350 kPa, 15%) or increased very slowly (test 3, 165°C, 1050 kPa, 5%). At higher temperature and oxygen pressure the oxygen consumption was more rapid and reached a steady level in 55–60 minutes (test 9 I, 195°C, 700 kPa, 10%). At highest temperature and oxygen pressure the oxygen consumption was even more rapid and reached a high steady level in 30 minutes (test 8, 225°C, 1050 kPa, 15%).

The oxygen consumption rates at the beginning of the test were estimated from curves like shown in Figure 1. They varied from 0.14 dm³/min in test 5 (165°C, 350 kPa, 15%) to 2.2 dm³/min in test 8 (225°C, 1050 kPa, 15%). Some of the experiments showed clear changes in cumulative oxygen consumption and these were taken as points where sulfide conversion had reached its maximum value. This was taken as the endpoint of the oxidation. Table 2 shows the initial oxygen consumption rates, endpoints and the cumulative oxygen consumption to the endpoint. Note that test number four is missing due to equipment malfunction.

Table 2. The initial oxygen consumption rates, endpoints and the cumulative oxygen consumption to the endpoint determined from online oxygen flow measurements

Test	Initial O ₂ , dm ³ /min	Endpoint, min	Cumulative O ₂ , dm ³
Std1 (165°C, 350 kPa, 15%)	0.19	No endpoint	Not estimated
Std2 (225°C, 350 kPa, 5%)	0.84	60	47.6
Std3 (165°C, 1050 kPa, 5%)	0.52	No endpoint	Not estimated
Std4 (225°C, 1050 kPa, 15%)	–	–	–
Std5 (165°C, 350 kPa, 15%)	0.14	25	3.85
Std6 (225°C, 350 kPa, 5%)	0.35	30	11.9
Std7 (165°C, 1050 kPa, 5%)	0.59	No endpoint	Not estimated
Std8 (225°C, 1050 kPa, 15%)	2.20	30	64.9
Std9 (195°C, 700 kPa, 10%)	0.95	No endpoint	Not estimated
Std9 I (195°C, 700 kPa, 10%)	1.0	55	42.0
Std9 II (195°C, 700 kPa, 10%)	0.93	60	43.1

The results in Table 2 indicate that oxygen consumption at the beginning of oxidation increases with increasing temperature, oxygen pressure and slurry density. A bigger charge requires more oxygen and it is delivered sufficiently only in experiments with high temperature and oxygen pressure. The appearance of an endpoint indicates that no further oxidation happens but it does not necessarily mean that the sulfide conversion is complete.

The effect of oxidation factors

The conversion of sulfides after the test was estimated using redox potential of the solution, iron concentration of the solution and remaining sulfur in the residue. The effect of temperature, oxygen pressure and slurry density were analysed using factorial setup. Measurements and values of the calculated responses are presented in Table 3.

The oxygen columns refer to oxygen consumed in the first 20 minutes and during the whole 60 minutes. Due to agitation problems at high temperatures test number 4 failed and for conducting the factorial analysis its results were copied from the replicate test number 8. For the same reason during test 6 the agitation stopped after about 30 minutes from the start of the experiment and did not return until the end of the experiment. The reason was later identified as thermal expansion of the bearings that resulted in seizing.

Table 3. Measured pH, redox and oxygen consumption values and calculated iron and sulfide conversion

Test	pH _{init.}	pH _{fin.}	E _{redox} , mV SCE	O ₂ /20, dm ³	O ₂ /60, dm ³	Fe _{conv.} , %	S _{conv.} , %
Std1 (165°C, 350 kPa, 15%)	0.67	7.38	247	4.7	10.9	0.003	-3.4
Std2 (225°C, 350 kPa, 5%)	0.70	0.51	562	19.4	47.6	29.6	100.0
Std3 (165°C, 1050 kPa, 5%)	0.86	0.81	497	11.1	20.7	62.6	83.0
Std4 (225°C, 1050 kPa, 15%)	--	--	--	--	--	--	--
Std5 (165°C, 350 kPa, 15%)	0.76	7.14	237	3.2	5.1	0.005	-1.7
Std6 (225°C, 350 kPa, 5%)	0.59	0.93	442	9.9	15.5	18.3	9.1
Std7 (165°C, 1050 kPa, 5%)	0.74	0.52	501	12.8	20.1	59.9	85.3
Std8 (225°C, 1050 kPa, 15%)	0.88	0.47	621	44.6	71.2	40.8	99.6
Std9 average (195°C, 700 kPa, 10%)	0.60	0.24	580	23.5	43.3	41.0	100.0

Calculated constant and coefficients for regression equations for each response are presented in Table 4. The R² values show that three responses, oxygen consumption after 20 minutes, discharge solution redox potential and iron conversion at the end of the experiment, have good fitting of the regression model with over 90% goodness of fit. Two other responses, total oxygen consumption and conversion are less well modelled by the regression equation.

Table 4. Regression equation constant and coefficients α for each response

Response	Constant	$\alpha(T)$, °C	$\alpha(pO_2)$, kPa	$\alpha(\text{slurry density})$, %	R ²
O ₂ 20 min, dm ³	-81.6	0.36	0.03	1.10	0.92
O ₂ 60 min, dm ³	-128	0.62	0.04	1.36	0.81
E _{redox} , mV SCE	-274	3.18	0.27	-6.87	0.93
Fe _{conv.} , %	31.5	0.87	19.5	-11.1	0.97
S ²⁻ _{conv.} , %	-76.3	0.46	0.09	-2.46	0.66

In Table 4 the trends in oxygen response are the same as were found for initial oxygen consumption rate. An increase in the redox potential and higher conversions indicate that more of the sulfide has been oxidized. For these responses the increases in temperature and oxygen pressure are beneficial whereas increase in slurry density

decreases the response value. According to the Tromans model (Tromans 1998) oxygen solubility increases both with increasing temperature and oxygen pressure and so the dissolution reactions (1)–(5) will proceed further. When the temperature and oxygen pressure are too low and slurry density is too high there is not enough dissolved oxygen to oxidize sulphide completely.

Discussion

Analysis of Tables 3 and 4 show that discharge solution redox potential is clearly correlated with consumed oxygen (Fig. 2). Assuming that the sulfide oxidation proceeds with direct oxidation by dissolved oxygen and produces ferric ions (Long and Dixon 2004) the more oxygen is consumed the higher is the amount of ferric iron. According to Nernst equation increasing ferric iron concentration increases the redox potential logarithmically. In the experiments done at 195°C and 225°C redox potential was higher and at 165°C lower than the standard electrode potential of $\text{Fe}^{3+}/\text{Fe}^{2+}$ equilibrium. At the lowest temperature there is not enough oxidizing power to convert iron to ferric iron or the ferric iron produced has been reduced to ferrous iron in oxidation of concentrate. Sulfur compounds in the solution can also reduce ferric iron. For example decomposition of thiosulfate produces elemental sulfur and sulfite, which is oxidized by ferric iron to sulfate (Long and Dixon 2004).

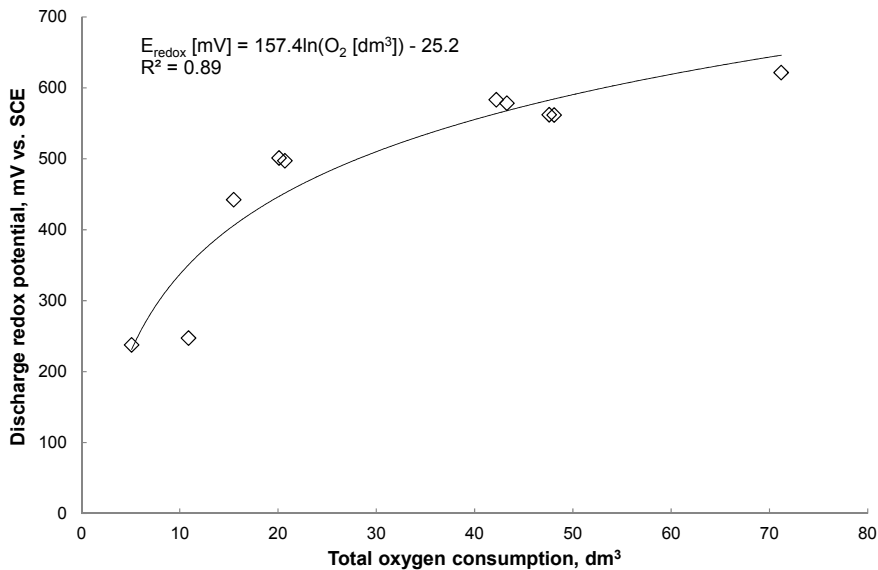


Figure 2. Discharge solution redox potential after the experiment as a function of oxygen consumed during the oxidation test

The iron and sulfide conversions describe how much of the concentrate charge iron has dissolved in the solution and how much of the sulfide sulfur remained in the leaching residue. The iron and sulfide conversions as function of oxygen consumed during the test are shown in Fig. 3. The conversion of sulfide is quite well described with a logarithmic equation. Using a high temperature and oxygen pressure the conditions are suitable for oxidation and complete conversion can be achieved. The iron conversion is less well described with a logarithmic equation. As shown by equations (1)–(5) iron should produce soluble sulfates. The low conversion values indicate that iron has been precipitated back. Especially the tests with high oxygen consumption suggest that iron has been oxidized to ferric iron, hydrolysed and converted to solid iron compounds.

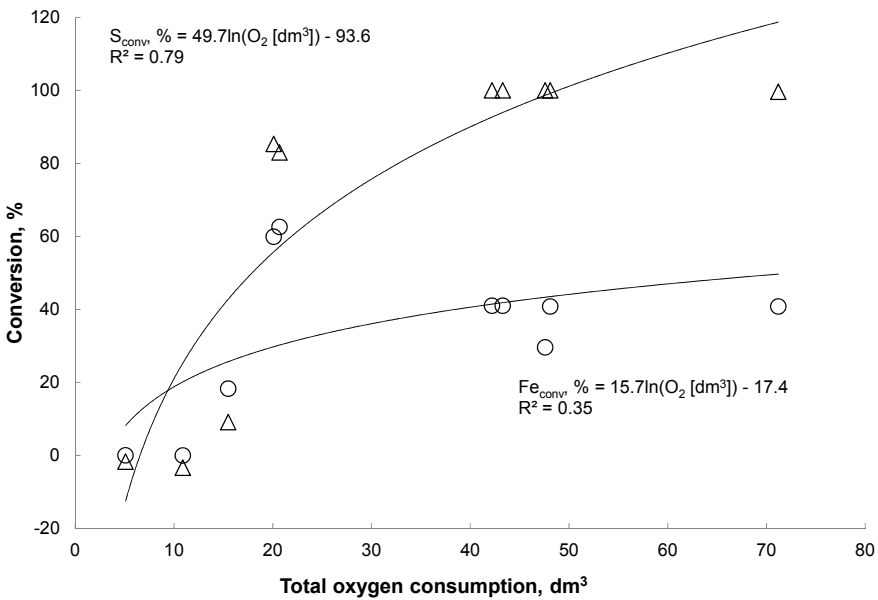


Figure 3. Iron and sulfur conversions after the experiment as a function of oxygen consumed during the oxidation test

Conclusions

Oxidation of the pyrite-arsenopyrite concentrate is improved by higher temperature and oxygen pressure and these are linked to the amount of dissolved oxygen. If these factors are high enough and charge size small enough, oxidation is completed in 30–60 minutes. The higher are temperature and oxygen pressure the more rapid is oxidation.

Factorial testing indicates that all three studied factors affect conversion of the concentrate minerals. Oxygen pressure is the most important. It is possible that the effect

of temperature is not shown clearly as it is linked to the concentration of dissolved oxygen.

The conversion of the concentrate minerals was estimated using discharge redox potential describing $\text{Fe}^{3+}/\text{Fe}^{2+}$ equilibrium, iron conversion using discharge iron concentration and sulfur conversion using leaching residue sulfide concentration. Of these responses the sulfide conversion is most useful as ferric iron can react to insoluble compounds.

Acknowledgements

This work has been done in the LOWGRADE project of the ELEMET research program funded by FIMECC Oy. The financial support of TEKES and Outotec Oyj is gratefully acknowledged.

References

- IGLESIAS, N., CARRANZA, F., 1994, *Refractory gold-bearing ores: a review of treatment methods and recent advances in biotechnological techniques*. Hydrometallurgy 34, 3, 383–395.
- FLEMING, C.A., 1992, *Hydrometallurgy of precious metals recovery*. Hydrometallurgy 30, 1–3, 127–162.
- CORRANS, I.J., ANGOVE, J.E., 1991, *Ultra fine milling for the recovery of refractory gold*. Minerals Engineering 4, 7–11, 763–776.
- PANGUM, L.S., BROWNER, R.E., 1996, *Pressure chloride leaching of a refractory gold ore*. Minerals Engineering 9, 5, 547–556.
- BAILEY, L.K., PETERS, E., 1976, *Decomposition of pyrite in acids by pressure leaching and anodization: the case for an electrochemical mechanism*. Canadian Metallurgical Quarterly 15, 4, 333–344.
- RIMSTIDT, J.D., VAUGHAN, D.J., 2003, *Pyrite oxidation: a state-of-the-art assessment of the reaction mechanism*. Geochimica et Cosmochimica Acta 67, 5, 873–880.
- PAPANGELAKIS, V.G., DEMOPOULOS, G.P., 1990, *Acid Pressure Oxidation of Arsenopyrite: Part I, Reaction Chemistry*. Canadian Metallurgical Quarterly 29, 1, 1–12.
- LONG, H., DIXON, D.G., 2004, *Pressure oxidation of pyrite in sulfuric acid media: a kinetic study*. Hydrometallurgy 73, 3–4, pp. 335–349.
- FLEMING, C.A., 2010, *Basic iron sulfate – a potential killer in the processing of refractory gold concentrates by pressure oxidation*. Minerals & Metallurgical Processing 27, 2, 81–88.
- TROMANS, D., 1998, *Oxygen solubility modeling in inorganic solutions: concentration, temperature and pressure effects*. Hydrometallurgy 50, 3, 279–296.

Received April 13, 2012; reviewed; accepted June 15, 2012

APPLICATION OF POLISH CALCIUM SORBENTS IN CARBONATE LOOPING

Michalina KOTYCZKA-MORANSKA, Grzegorz TOMASZEWICZ

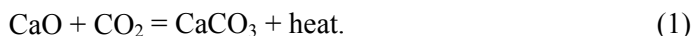
¹ Institute for Chemical Processing of Coal, Zamkowa 1 41-801 Zabrze, mmoranska@ichpw.zabrze.pl

Abstract: The purpose of this work was the investigation of behaviour of three Polish CaO-based sorbents during calcium looping cycles. All investigations were conducted with a Netzsch STA 409PG Luxx thermogravimetric analyser. Samples weighing $m_s = 10.0(1)$ mg were placed in an Al_2O_3 crucible. The calcium looping processes were performed at two carbonation temperatures (650°C and 680°C) and three calcination temperatures (880°, 900° and 920°C). Additionally, calcination-carbonation cycles with different gas flows were explored. We investigated the influence of CO_2 concentration and total gas flow on carbonation conversion.

Keywords: *calcium looping, CO₂ capture, CaO-based sorbents*

Introduction

The emission of CO_2 from fossil fuel combustion is the major contributor to anthropogenic greenhouse gas emissions. During the last several years, CaO-based sorbents have been intensively investigated for their possible applications in CO_2 capture. Among the various options for the separation of CO_2 from flue gases, high-temperature CO_2 absorption by mineral sorbents such as Ca-sorbents appears promising. The main reaction in this process is the carbonation reaction:



The sorbent can be regenerated via calcination, which entails heating the carbonate until it decomposes into CaO and CO_2 . In this process, pure CO_2 is obtained for sequestration. The regenerated sorbent can then undergo another round of carbonation. This process is based on a looping cycle in which the two reactions, carbonation and calcination, are alternated. The carbonation reaction is exothermic, whereas calcination reaction is endothermic. Carbonation is characterised by a rapid initial rate and a very slow final reaction rate. Calcination is a rapid process that occurs over a wide

temperature range (Blamey et al., 2010). Thus, the carrying capacity of the sorbent is the number of moles of CO_2 reacted in the period of fast reaction rate with respect to that of the reaction stoichiometry for complete conversion of CaO to CaCO_3 . The main disadvantage of CaO -based sorbents is the decay of activity with an increasing number of cycles. This decay trend was summarised by Abanades and Alvarez (2003) as the following first-order formula:

$$X_N = f_m^N (1 - f_w) + f_w \quad (2)$$

where X_N is the carbonation conversion in the N th cycle, and f_m and f_w are empirical parameters.

The optimal values of these parameters were calculated from a data series found in the literature as $f_m = 0.77$ and $f_w = 0.17$. This equation was fitted to carbonation/calcination data from over 50 cycles, and an excellent regression coefficient of approximately 0.99 was obtained, indicating that fresh sorbent is needed in the calcium looping process due to its deactivation, which increases the cost of the process. For this reason, it is necessary to mitigate natural sorbent deactivation (Li, 2011). The largest deviation from the optimum value given by equation 2 is found in processes where in a considerable sintering was observed, and the deactivation rate of the sorbents increased accordingly. Fennell et al. (2007) found that equation 2 does not describe sorbent activity in a fluidised bed environment because increasing the calcination period reduces f_m . This parameter can be interpreted as a residual reactivity. Mess et al. (1999) observed that sorbent particles remained capable of forming a CaCO_3 layer despite undergoing numerous cycles. For this reason, the term f_m and equation 2 are more applicable in systems where attrition and friability are less significant. An alternative formula was developed by Wang and Anthony for carbonation conversion activity (Wang and Anthony, 2005):

$$a_N = a_{N-1}(1 - ka_{N-1}) \quad (3)$$

where k is a proportionality coefficient, and a_N is the activity of the sorbent in the N th cycle.

These authors reported that activity decay depends on the activity of the sorbent in the $(N - 1)$ cycle. Their formula describes the data quite well with $k = 0.23$. The disadvantage of this formula is its limitation in N , becoming useless when N is large. As an alternative for large N , Wang and Anthony (2005) proposed equation (4):

$$a_N = \frac{1}{1 + kN} \quad (4)$$

In this equation, the parameter k is the rate of decay of sorbent activity. This equation is reminiscent of the formula for catalyst deactivation by sintering as function of time t :

$$a_N = \frac{1}{1 + kt} \quad (5)$$

Equation (5) suggests that sintering is the cause of decay. The equation proposed by Wang and Anthony does not include residual reactivity. Grasa and Abanades (2006) developed Eq. 4 to account for the residual activity:

$$a_N = \left[\frac{1}{\frac{1}{1 - a_\infty} + kN} + a_\infty \right] \times 100 \quad (6)$$

where a_∞ is the residual activity, with a value of approximately 7%.

This equation is useful for data for up to approximately 500 cycles, where $a_\infty = 0.075$. Another formula was subsequently proposed by Lysikov et al. (2007):

$$a_N = \left[\frac{1 - a_\infty}{(1 + kN)^\alpha} + a_\infty \right] \times 100 \quad (7)$$

where a_∞ is the residual activity, and α is a parameter that depends on the sintering mechanism. This formula is especially useful for synthetic sorbents but requires an additional parameter α . Wang and Anthony (2007) later proposed a formula that includes residual reactivity:

$$a_N = a_{N-1} [1 - k(a_{N-1} - a_\infty)] \times 100 \quad (8)$$

which, for large number of cycles, reduces to the following:

$$a_N = \left[\frac{a_\infty}{1 - (1 - a_\infty)e^{-ka_\infty N}} \right] \times 100 \quad (9)$$

This equation also describes decay behaviour in systems where sintering occurs. There are numerous equations in the literature that can fit experimental data, but there is no ready correlation between their parameters, sorbent characteristic and process conditions. Therefore, the final sorbent capacity after an “infinite” number of cycles is not predictable. This situation demonstrates that the influence of different process parameters on sorbent activity requires additional investigation. Manovic and Anthony (2008) examined the influence of temperature on sorbent activity using the same temperatures for calcination and carbonation and found that sorbent sintering is masked at higher temperatures by enhanced carbonation due to increased CO₂ diffusion through the CaCO₃ layer. These authors concluded that a long carbonation period led to a faster loss of sorbent activity and further showed that a longer calcination period

increases sorbent conversion. Their results stand in contrast to those presented by Grasa and Abanades (2006) and Lysikov (2007), who reported that calcination time is not an important parameter.

The aim of this work was to determine the carbonation/calcination process parameters that allow for the most efficient use of the sorbent in a calcium looping installation. For this purpose, we studied the influence on sorbent activity of parameters such as carbonation and calcination temperatures, the CO_2/CaO ratio in the reactor and the choice of mineral sorbent.

Experimental system

We investigated three natural Polish mineral sorbents: limestone from Czatkowice and dolomites from Siewierz and Sandomierz. All investigations were conducted in an STA 409PG Luxx thermogravimetric analyser (Netzsch). Samples of mass $m_s = 10.0(1)$ mg were placed in an Al_2O_3 crucible. The measurements were conducted at various carbonation and calcination temperatures, gas flows and CO_2 concentrations.

Results and discussion

Figure 1 presents a comparison of these three mineral sorbents during ten calcination/carbonation cycles.

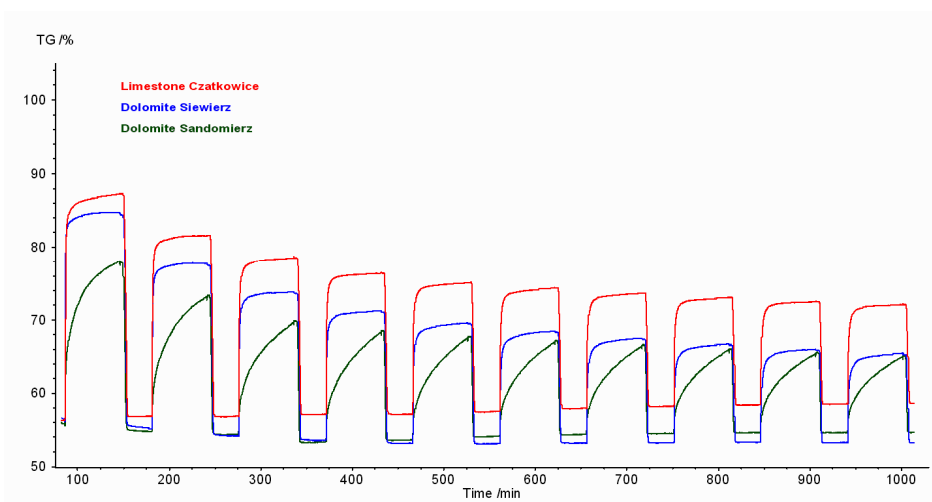


Fig. 1. Comparison of three mineral sorbents during ten calcination/carbonation cycles

All the measurements were conducted under the same conditions: carbonation at 650°C , calcination at 900°C and a CO_2 flow of $25\text{ cm}^3/\text{min}$ during carbonation. The simple comparison of the two dolomites shows that the dolomite from Sandomierz

displays worse sorbent properties because the period of fast reaction rate during the carbonation process is less than that of the dolomite from Siewierz. Therefore, we used the dolomite from Siewierz and the limestone from Czatkowice in our subsequent investigations.

The first stage of our measurements involved conducting carbonation/calcination cycles at different carbonation temperatures. We investigated two temperatures: 650°C and 680°C. These temperatures were chosen because their application in a calcium looping installation can be economically justified. Furthermore, we chose not to apply a higher temperature during carbonation to prevent sorbent sintering (Manovic and Anthony, 2008). Figure 2 presents the results for the limestone from Czatkowice. The calcination temperature was 900°C, and the gas flows consisted of 25 cm³/min CO₂ plus 25 cm³/min N₂ during carbonation and 25ml/min N₂ during calcination. We observed no difference between the results for this sorbent at these two temperatures.

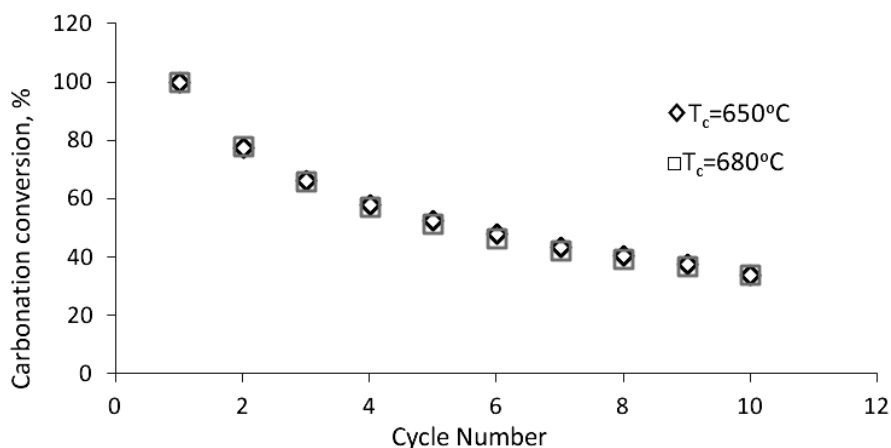


Fig. 2. Comparison of carbonation conversion of limestone for two carbonation temperatures

The second part of our study consisted of investigating the influence of calcination temperature on sorbent activity. For the limestone, we compared three calcination temperatures: 880, 900 and 920°C. The cycles were performed at a carbonation temperature of 650°C and the gas mixtures consisted of 25 cm³/min CO₂ plus 25 cm³/min N₂ during carbonation and 25 cm³/min N₂ during calcination.

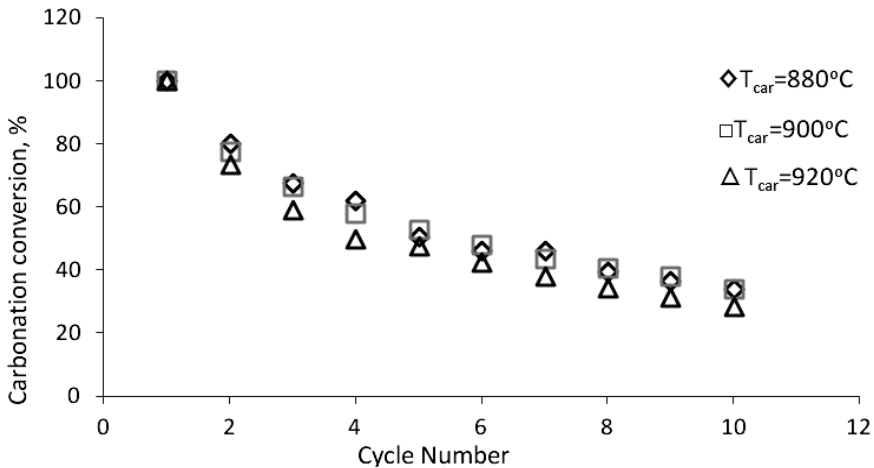


Fig. 3. Comparison of the carbonation conversion of limestone at three calcination temperatures

Figure 3 presents a comparison of the carbonation conversion for limestone at the three studied temperatures. There was no difference observed between carbonation conversions at 880°C and 900°C, but carbonation conversion was lower at 920°C. These results are in accordance with the results presented by Manovic and Anthony (2008), who reported that samples cycled at higher temperature were more sintered and, hence, less active. However, the calcination temperature in an industrial reactor should be at least 900°C to achieve calcination yielding a concentrated CO₂ stream. Thus, it appears appropriate to conduct further investigations at a calcination temperature of 900°C and a carbonation temperature of 650°C. The second investigated sorbent was the dolomite from Siewierz. We conducted measurements in the same way as for the limestone, and the results were the same as for the limestone. Regarding the first variable (carbonation temperature), there was no difference between the results obtained with carbonations at 650°C and 680°C. In processes with different calcination temperatures, the results were also similar to the limestone results. The worst carbonation conversion was obtained for calcination conducted at 920°C.

The last part of our investigation consisted of calcination/carbonation processes conducted using several different gas flows with various CO₂ concentrations. These measurements were all conducted at a calcination temperature of 900°C and a carbonation temperature of 650°C.

Figure 4 presents the data obtained in four limestone calcination/carbonation cycles conducted with four different gas flows during carbonation (24, 50, 100 or 150 ml/min) with a constant CO₂ concentration (50%). The partial gas flows are also presented in this figure. Nitrogen was used as a purge gas at a constant flow rate in each process (12, 25, 50, or 75 cm³/min). We observed that the carbonation conversion is better at lower gas flows than with the largest gas flow (150 cm³/min). The influence of CO₂ concentration on carbonation conversion was also investigated. Three proc-

esses with different CO₂ concentrations (25, 50 or 75%) but a constant total gas flow during carbonation (100 cm³/min) were evaluated with the limestone.

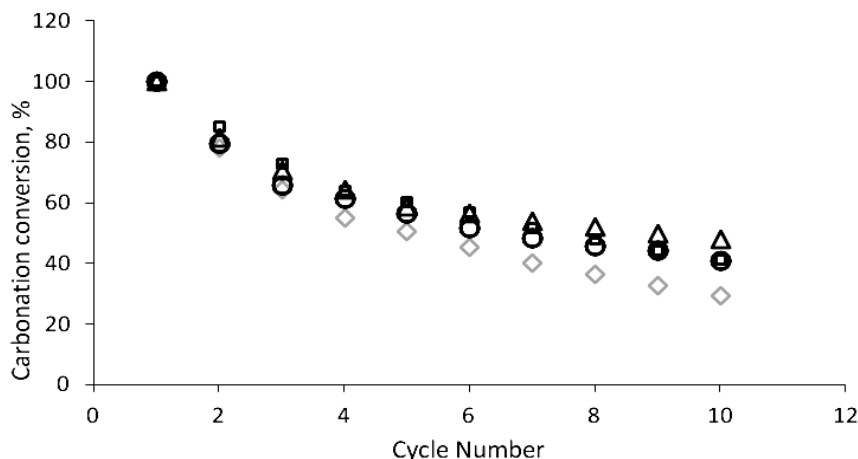


Fig. 4. Comparison of carbonation conversion of limestone for four gas flows:

- ◇ – N₂ 75 cm³/min/CO₂ 75 cm³/min; □ – N₂ 50 cm³/min/CO₂ 50 cm³/min;
- △ – N₂ 25 cm³/min/CO₂ 25 cm³/min; ○ – N₂ 12 cm³/min/CO₂ 12 cm³/min

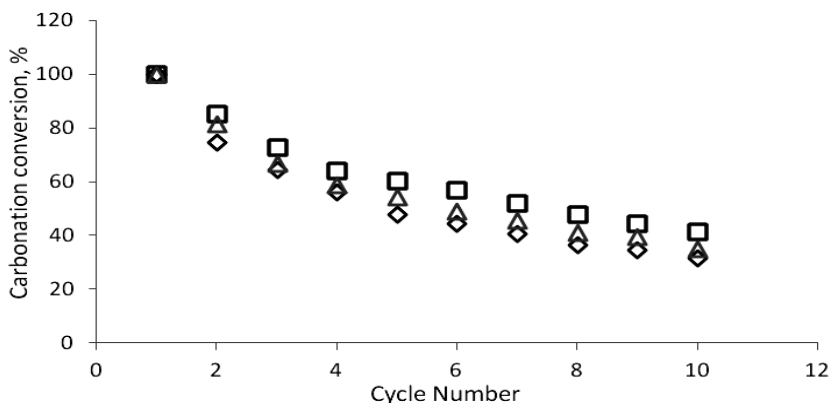


Fig. 5. Comparison of carbonation conversion of limestone for three CO₂ concentrations with the same gas flow: ◇ – N₂ 25 cm³/min/CO₂ 75 cm³/min; □ – N₂ 50 cm³/min/CO₂ 50 cm³/min; △ – N₂ 25 cm³/min/CO₂ 75 cm³/min

The data presented in Fig. 5 show that the carbonation conversion is slightly lower at 75% CO₂ than at the other CO₂ concentrations. This result may be related to the fact that an atmosphere of concentrated CO₂ also amplifies sintering, consequently reducing the sorbent activity with an increasing number of reaction cycles. This phenomenon can also be observed in Fig. 6.

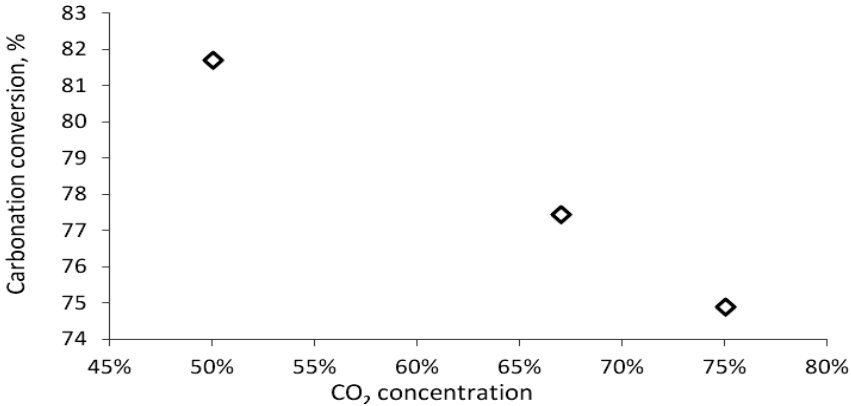


Fig. 6. Carbonation conversion of limestone for three CO₂ concentrations (purge gas flow 25 cm³/min)

This graph presents the relation between CO₂ concentration and carbonation conversion during the first cycle. In these processes, the purge gas flow was constant (25 cm³/min), and CO₂ concentration was varied (50, 67 and 75%). The same types of measurements were performed for the dolomite, and in both cases (constant CO₂ concentration and constant total gas flow), there were no differences between the data obtained. Figure 7 presents the data collected at a constant total gas flow; here, it can be observed that dolomite activity does not depend on CO₂ concentration in this range.

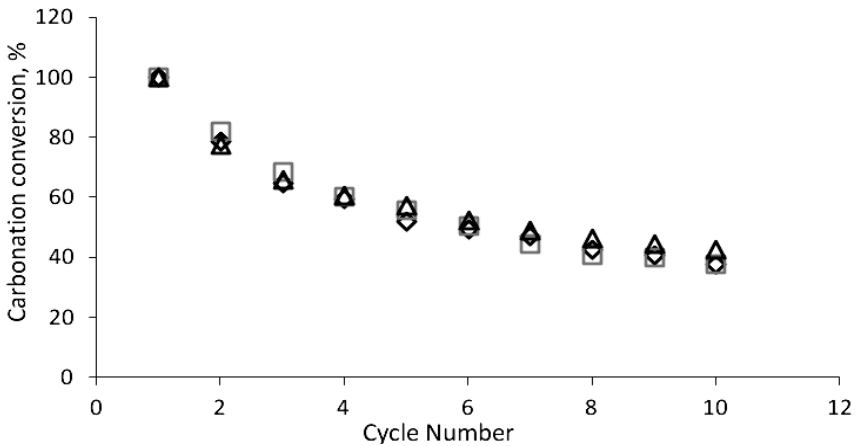


Fig. 7. Comparison of carbonation conversion of dolomite for three CO₂ concentrations with the same gas flow: ◇ – N₂ 25 cm³/min/CO₂ 75 cm³/min; □ – N₂ 50 cm³/min/CO₂ 50 cm³/min; △ – N₂ 25 cm³/min/CO₂ 75 cm³/min

Because the CO₂ concentration in typical flue gas is approximately 20%, we decided that the best data for further analysis were those obtained at 20% CO₂. Figure 8

presents a comparison of our data for limestone and dolomite in 10 carbonation/calcination cycles with three curves representing relations found in the literature (Eqs (2), (3), (8)). We observed that the activity of dolomite is slightly higher than that of limestone. All these equations describe carbonation conversion for limestone. As stated in the introduction, Eq. 2 does not consider sorbent sintering, and this equation did not describe our data. Furthermore, the equation developed by Wang and Anthony (Eq. (3); 2005) did not describe our data, but after the introduction of the factor for residual reactivity (Eq. (8)), corresponded to our data quite well.

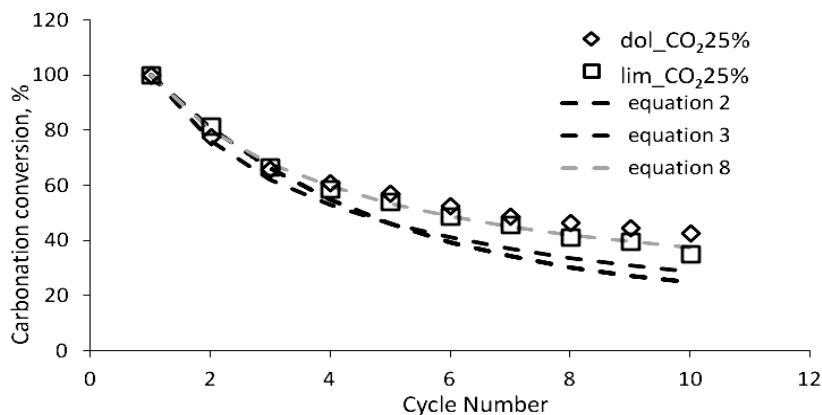


Fig. 8. Comparison of data obtained for limestone and dolomite in 10 carbonation/calcination cycles with the relations found in the literature

Conclusions

The purpose of our work was to determine the best parameters for calcium looping processes conducted with Polish mineral sorbents. We investigated three mineral sorbents: one limestone and two types of dolomite. We excluded one type of dolomite early in our experiments due to its weak carbonation conversion. The two other sorbents were investigated at various carbonation and calcination temperatures and at different CO₂ concentrations and gas flows. We found that the best process parameters for our sorbents are a calcination temperature of 900°C and a carbonation temperature of 650°C. Additionally, we observed that there was no difference in carbonation conversion for dolomite in the range 25–75% CO₂, and higher activity decay occurs with limestone at high CO₂ concentrations. We also found that the activity decay of the limestone from Czatkowice is well described by the equation developed by Wang and Anthony (Eq. 8). This relation is useful because it allows for the calculation of sorbent activity in a calcium looping installation after N cycles.

Acknowledgements

This research was conducted in the framework of the “Development of coal gasification technology for high-efficiency production of fuels and energy” project, Task No. 3 of the Strategic Programme for Research and Development: “Advanced energy generation technologies” funded by the National Centre for Research and Development, Poland.

References

- ABANADES J., ALVAREZ D., 2003, *Conversion Limits in the Reaction of CO₂ with Lime*, Energy & Fuels, 17, 308–315.
- BLAMEY J., ANTHONY E., WANG J., FENNELL P., 2010, *The calcium looping cycle for large-scale CO₂ capture*, Progress in Energy and Combustion Science, 36, 260–279.
- FENNELL P., PACCIANI R., DENNIS J., DAVIDSON J., HAYHURST A., 2007, *The effects of repeated cycles of calcination and carbonation on a variety of different limestones, as measured in a hot fluidized bed of sand*, Energy & Fuels;21, 2072–2081.
- GRASA G., ABANADES J., 2006, *CO₂ capture capacity of CaO in long series of carbonation/calcination cycles*, Industrial & Engineering Chemistry Research, 45, 8846–8851.
- LI Y., ZHAO Ch., CHEN H., REN Q., LUNBO D., 2011, *CO₂ capture efficiently and energy requirement analysis of power plant using modified calcium-based sorbent looping cycle*, Energy 36, 1590–1598.
- LYSIKOV A., SALANOV A., OKUNEV A., 2007, *Change of CO₂ carrying capacity of CaO in isothermal recarbonation–decomposition cycles*, Industrial & Engineering Chemistry Research 46, 4633–4638.
- MANOVIC V., ANTHONY E., 2008, *Parametric study on the CO₂ capture capacity of CaO-based sorbents in looping cycles*, Energy & Fuels, 22, 1851–1857
- MESS D., SAROFIM A., LONGWELL J., 1999, *Product layer diffusion during the reaction of calcium oxide with carbon dioxide*, Energy & Fuels, 13, 999–1005.
- WANG J., ANTHONY E., 2005, *On the decay behavior of the CO₂ absorption capacity of CaO-based sorbents*, Industrial & Engineering Chemistry Research, 44, 627–629.
- WANG J., ANTHONY E., 2007, *A common decay behavior in cyclic processes*, Chemical Engineering Communications, 194, 1409–1420.

Received June 5, 2012; reviewed; accepted July 4, 2012

MATHEMATICAL MODELS OF PARTICLE SIZE DISTRIBUTION IN SIMULATION ANALYSIS OF HIGH-PRESSURE GRINDING ROLL OPERATIONS

Daniel SARAMAK

AGH University of Science and Technology, Faculty of Mining and Geoengineering, Department of Environmental Engineering and Mineral Processing, Mickiewicza 30 Av., 30-059 Krakow, Poland, Fax: +48 12 617 21 98, Mobile: +48 692 597 032, Email: dsaramak@agh.edu.pl

Abstract: The high-pressure grinding roll (HPGR) technology is currently one of the most efficient methods of hard ore comminution from the scope of the energy consumption. Throughput and energetic models of performance are quite well developed, but technological models predicting the comminution effects still needs an in-depth research. In the paper author presents the method of modeling of HPGR products' particle size distribution by using suitable mathematical models. A basis of the HPGR performance assessment and HPGR-based crushing circuits design is a product's particle size distribution. In order to precisely determine the particle size distribution of a HPGR product, parameters of product's particle size distributions should be conditional on the main technical parameters of the roller press like operating pressure and the speed of rolls. The most accurate approximation of a distribution of size particle appears to be Weibull's truncated distribution and it is possible to obtain significant relationships between the approximation formula and the value of operating pressure, or feed characteristics. It makes possible a determination of mass recoveries of the product's respective size fractions and the productivity planning. Instead of pressure, the other HPGR operating parameters can be applied, but the pressure value appears to produce the most relevant relationship. A determination of HPGR product's particle size distribution is a basis of the press operation simulation analysis.

Keywords: *HPGR, comminution, particle size distribution, ore processing*

Introduction

Comminuting circuits constitute an integral part of mineral processing technology and a basis of the ore enrichment process. The work efficiency of ore pretreatment circuits for downstream upgrading processes determines in fact the effectiveness of the overall process because it enables proper liberation of useful minerals from the feed to take part. It is especially significant in base metals and non-ferrous ore processing, where liberation of useful components is achieved by obtaining the comminution ratio, suit-

able for a given type of ore, together with avoiding feed overgrinding, which increases the paymetal losses (Saramak et al. 2010; Tumidajski 2010).

High-pressure comminution is currently the one of most effective method of the material size reduction. Main advantages of the technology include:

- low unit energy consumption, from 0.8 to 3 kWh (2,880 to 10,800 kJ respectively) per tonne of treated material,
- micro-crack generation, which gives the benefit in downstream grinding processes (usually in ball mill). As a result of the micro-crack formation, the process energy-consumption, measured with using the Bond work index, can be reduced for up to 30%, according to various investigations,
- increasing of useful mineral grade in ore upgrading operations, improvement of the weight recovery index for the entire process,
- dry and wet crushing options, with the feed material moisture up to 10%,
- high availability ($T_e > 95\%$),
- low dust pollution, low noise and vibration emission,
- low footprint comparing to SAG mills or even vertimills

High-pressure comminution operations also affect the grinding kinetics in downstream milling stage, through shortening the grinding time. Another method of enhancing the grinding effectiveness is an increase of grinding media charge (Olejnik 2006), but here the gain is obtained with no extra cost of grinding media.

The application of the high-pressure grinding rolls (HPGR) in comminution circuits is currently a key issue in many mining and mineral processing sectors and HPGR principles are well presented in many works (Schoenert, 1988; Morley, 2003; 2010; Maxton et al., 2003; Daniel and Morell, 2004; Naziemiec and Saramak, 2009; van der Meer and Gruendken, 2010; Saramak, 2011a; 2012). HPGR devices are present in industrial circuits of cement production (Kurdowski, 1998; Gawenda, 2009) and in hard ore processing technology (Schoenert, 1988) since the mid-nineties and the development in HPGR applications in ore pretreatment technology is a current worldwide trend. The investigations of grinding processes in HPGR devices are still in progress and the technical level of current industrial presses was obtained at the beginning of this century (Morley, 2003). The HPGR technology is currently the most effective method, as far as energy consumption and hard minerals comminution are concerned and can be a good alternative for semi-autogenous (SAG) and even tower mills (Kalinowski, 2006).

Taking into consideration the above aspects, the main aim of the paper is a proposal of approximation of HPGR crushing products with using of specific theoretical distribution. All parameters of the selected theoretical particle size distribution will be combined with the main operating parameter – the operating pressure (P). A knowledge of the crushing product's quality described through a particle size distribution curve is significant in terms of the process description and optimization of crushing and grinding circuit's performance.

Crushing product particle size distributions

The feed for HPGR-based crushing circuits can be analyzed with regards to its physico-mechanical properties, mineralogical composition, particle size distribution and other features. These features, in turn, determine the effect of comminution process, assessed on the basis of the quality of grinding products, process energy consumption, process capacity and economic indices. The HPGR feed characteristics usually take into consideration only the d_{max} value (maximum particle size), and that appears to be insufficient for proper modeling of the HPGR comminution processes. Besides d_{max} , knowledge of individual size fraction participations in the feed (product particle size distribution), especially the mass recoveries of fines and coarsest particles, is required (Saramak 2011b).

Particle size distributions of grained material processed in mineral processing plants are important, because they generate distributions of other features of particles, which determine the course of enrichment operations. A modification of material particle size during the comminution process (size reduction), plays a key role in the assessment of process energy-consumption and susceptibility of the ore to downstream upgrading processes. Particle size distributions are also significant in heuristic modeling of various enrichment processes (Tumidajski and Saramak 2010).

A theoretical approach to determination of particle size distribution of crushing products was presented by Kolmogorow (1941) and Epstein (1947), who proved that for a multi-stage comminution process, the particle size distributions of products are log-normal. The product particle size distribution depends on the crushing process intensity (stage). Let's consider the comminution of crystalline particles. When a full liberation of these grains is achieved (the level of grain boundaries is reached), the size distribution of these particles should tend towards either log-normal or logistic distribution, because the content of very fine particles should be rather low, together with expected lack of coarser (uncrushed) grains. According to the nature of the grained material, the cumulative distribution proposed for description of the empirical data, should reach a value of 1 for the maximum particle size (d_{max}) and therefore there should be applied truncated distributions. A common modification of Rosin–Ramler–Bennets' distributions, is the truncated distribution, utilizing the expression

$$w = \left(\frac{d}{d_{max} - d} \right):$$

$$\Phi(d) = 1 - \exp \left[-c \left(\frac{d}{d_{max} - d} \right)^n \right], \quad 0 \leq d \leq d_{max} \quad (1)$$

where: d – particle size;

c , n , d_{max} – parameters determined on the basis of the empirical data (d_{max} – maximum particle size in crushing product)

$\Phi(d)$ – cumulative particle size distribution curve.

w – expression converting the regular (untruncated) distribution into truncated one

An advantage of the above formula is using of a third parameter, d_{\max} , which denotes the maximum particle size, and the particle size distribution function has its course within a range of $\langle 0, d_{\max} \rangle$, instead of the $\langle 0, +\infty \rangle$, which is used for regular Weibull's distribution. The application of d_{\max} parameter also increases the accuracy of approximation. Analogous truncated formulas utilizing the expression w , applied in description of particle size distribution curves, are the log-normal and logistic distributions (Tumidajski, 2012).

The approximation procedure utilizing formula (1) is carried out with using the least sum of squares method. After taking a double logarithm of formula (1) we obtain the following equation:

$$\ln \ln \frac{1}{1 - \Phi(d)} = n \ln \left(\frac{d}{d_{\max} - d} \right) + \ln c \quad (2)$$

which has a linear form and where c is a constant.

In order to determine n and c parameters, one should accepted such d_{\max} value for which the residual deviation value is minimal:

$$s_r = \sqrt{\frac{\sum_{i=1}^{p_s} (\Phi_e(d_i) - \Phi_t(d_i))^2}{p_s - 2}} \quad (3)$$

where: p_s – a number of sieves with aperture d_i ,

$\Phi_e(d_i)$ empirical cumulative distribution function

$\Phi_t(d_i)$ theoretical cumulative distribution function, determined by using formula (1).

Calculations should be carried out for all d_{\max} values greater from the maximum sieve aperture and the values of n , c and d_{\max} , which minimize the s_r value should be accepted in further analyses. When the approximation formula reveal a significant convergence with the empirical data, it is possible to combine its parameters with the feed material properties and the crusher operating parameters. The analysis of relationships between technological and technical operating parameters of the roller press makes it possible to divide them into four groups (Saramak, 2010):

- parameters controlled directly (operating pressure, speed of rolls),
- parameters controlled indirectly (gap, skew, torque),
- parameters combined with the feed material properties,
- indices (i.e. specific energy consumption, specific throughput).

The operating pressure (P) has the most significant importance on the roller press operating efficiency. The operating pressure level influences the gap width and, as a result, the d_{\max} value. Relationship between the gap (s) and operating pressure is presented in Fig. 1.

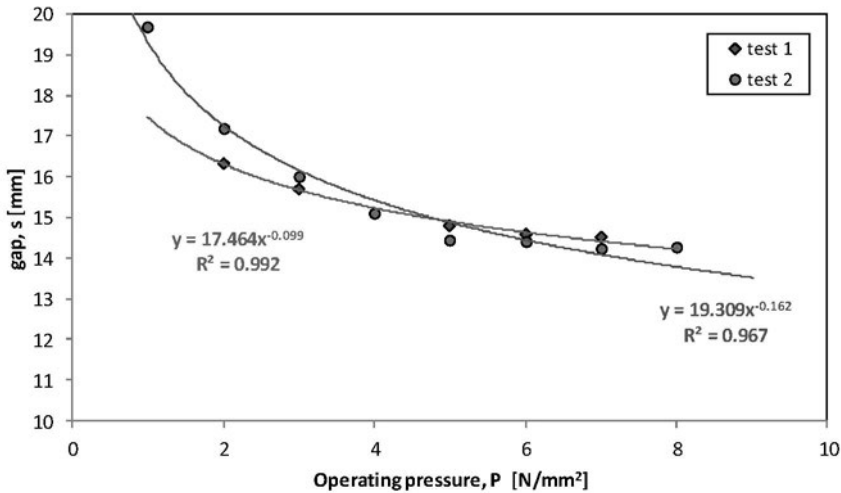


Fig. 1. Relationship between operating pressure and gap in roller press (tests for porphyry) (Saramak, 2011 c) for two series of similar laboratory tests denoted as “test 1” and “test 2”.

The shape parameter n can be directly combined with the operating pressure value, because the finer product, the lower n value in formula (1). The material size reduction, in turn, is directly proportional to pressure level. The scale parameter c is combined with the feed material physico-mechanical properties. Changes in c value cause a diverse run of the particle size curve approximated with using of formula (1), resulting in existence of the inflection point corresponding to material grindability. The d_{\max} parameter reflects the material size reduction, what can be combined with the gap width and, as a result similarly to n , with the operating pressure value. The HPGR crushing process efficiency assessment, considered from the scope of energy, technology or ecology, can be done utilizing the obtained approximation formulas.

Experimental programme

A series of HPGR laboratory crushing tests of copper ore for various operating pressure levels within the range from 1 to 8 N/mm² were run. A particle size distribution curve was determined for each crushing product, the results are presented in Fig. 2.

Theoretical cumulative distribution functions were calculated by using truncated Weibull's formula (1). Values of coefficients in the formula are presented in Table 1 and in Figs 3 and 4.

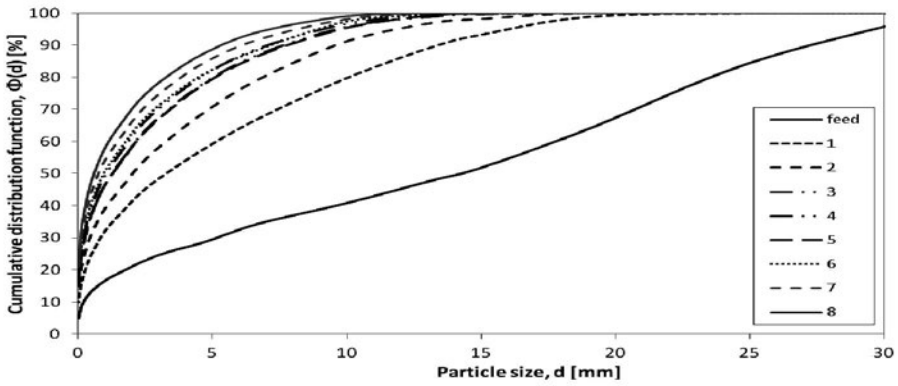


Fig. 2. Particle size distribution curves for all crushing products. Numbers from 1 to 8 denote single batch tests for respective value of operating pressure (from 1 to 8 N/mm²).

Table1. Values of coefficients in formula (1)

	Operating pressure, P [N/mm ²]							
	1	2	3	4	5	6	7	8
n	0.461	0.443	0.428	0.431	0.432	0.421	0.416	0.413
c	1.868	2.005	2.365	2.359	2.139	2.245	2.467	2.610
d_{max}	25.7	19.6	19.4	16.3	16.0	15.5	15.5	13.9
s_r	2.70	2.37	2.12	1.65	1.38	1.17	1.31	1.21

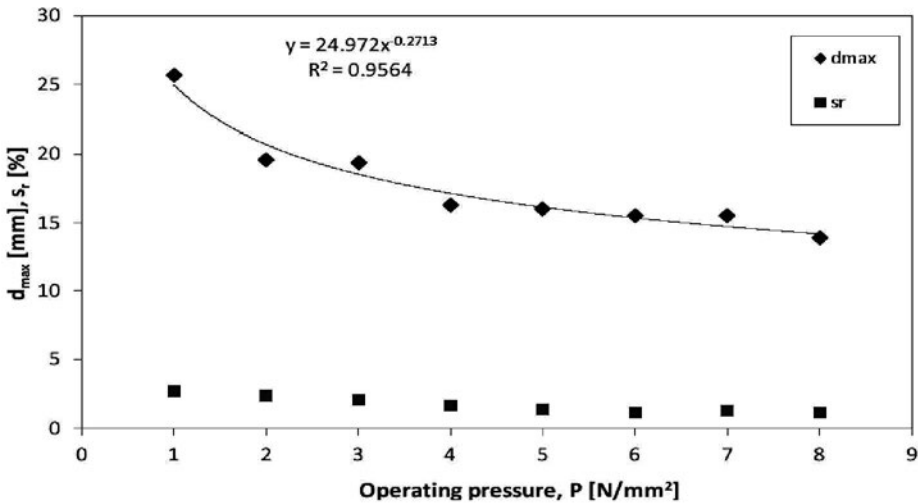


Fig. 3. Course of d_{max} and s_r parameters depending on the operating pressure P

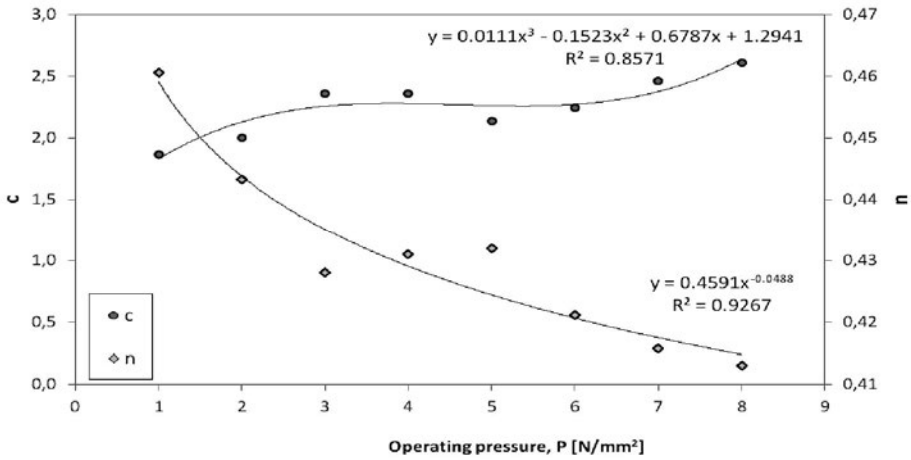


Fig. 4. Course of n and c parameters depending on the operating pressure P

The next stage included the approximation of n , c and d_{\max} parameters course. It was possible to determine an approximation function for each parameter on satisfactory accuracy level. The course of c parameter is well described by polynomial of third degree (Fig. 4) what has its practical justification. Following ranges can be distinguished in the course of c parameter approximation function:

- range from 1 to 4 N/mm², where c values increase – it illustrates the entire comminution process at relatively lower pressure values. Size reduction is directly proportional to the pressure, but comminution efficiency is less intense together with the further increase of P value,
- range from 4 to 6 N/mm², where c values are generally stable. In comminution process this stage corresponds to the situation where almost full liberation of particles, (up to the grain boundary) was achieved. The size of most particles was reduced along the grain boundaries, micro-cracks formation is also observable, but the pressure is not high enough to disintegrate a single grain structure,
- range above 6 N/mm². The highest pressure values cause crushing of single structures of grains, size reduction index increases again, until the maximum operating pressure for the device is achieved.

The d_{\max} parameter course is very well approximated by the hyperbolic function (Fig. 3). Significant decrease of d_{\max} for lower pressure values is observed, while for the higher P values, d_{\max} course stabilizes itself, reflecting relatively lower size reduction index for excessive pressure (maximum compression of the material bed between the rolls).

Values of the n parameter decrease together with an increase the operating pressure P values (Fig. 4). At the entire stage of the process (lower P values) the n values drop significantly (a relatively easy increase in finer size fractions of crushing product),

next a kind of stabilization is observed and finally, for highest P values, a further decrease on n can be noticed (renewed increase of finer particles in the product).

Practical implementations

It appears that the course of n , c and d_{\max} parameters can be described as functional relationships of pressure (Table 2). A selection of respective pressure level in press results in particular values of n , c and d_{\max} which, in turn, give us the information about the particle size distribution of crushing products.

Table 2. Coefficients of function (1) as functional relationships of pressure P

Parameter	Function	R ²
n	$n = 0.459 \cdot \frac{0.46}{P^{0.05}}$	0.956
c	$c = 0.01 \cdot P^3 - 0.15 \cdot P^2 + 0.68 \cdot P + 1.29$	0.857
d_{\max}	$d_{\max} = \frac{24.97}{P^{0.27}}$	0.927

As a result of the above it is possible to control the work of entire crushing and grinding circuit in terms of technological, economic or ecological effects. A general three-stage crushing and grinding circuit, under examination, is presented in Fig. 5.

Following variables can be regarded as controllable:

- crusher's outlet gap (s)
- press operating pressure (P)
- screening cut point (d_T)
- grinding time (t).

A generalized model (target function) from a technological (product size reduction) or economic (process energy consumption) scope will have a following form:

$$F = f(P, s, d_T, t) \quad (4)$$

where F (target function) can denote either S_{50} or S_{80} (average or eighty percent product's size reduction index), or E_{sp} (unit energy-consumption of the process) depends of the accepted point of view.

Determining the value of the target function (4) is possible after calculating the conditional extremum of multi-variable function within the constrained area. This area respects a changeability range of key-operational parameters of devices incorporated into the circuit and below relationship constitute the limitations supplementing the target function formula:

- $P < P_{\max}$
- $Q_{\min} < Q < Q_{\max}$
- $S_x > S_{x_{\min}}$

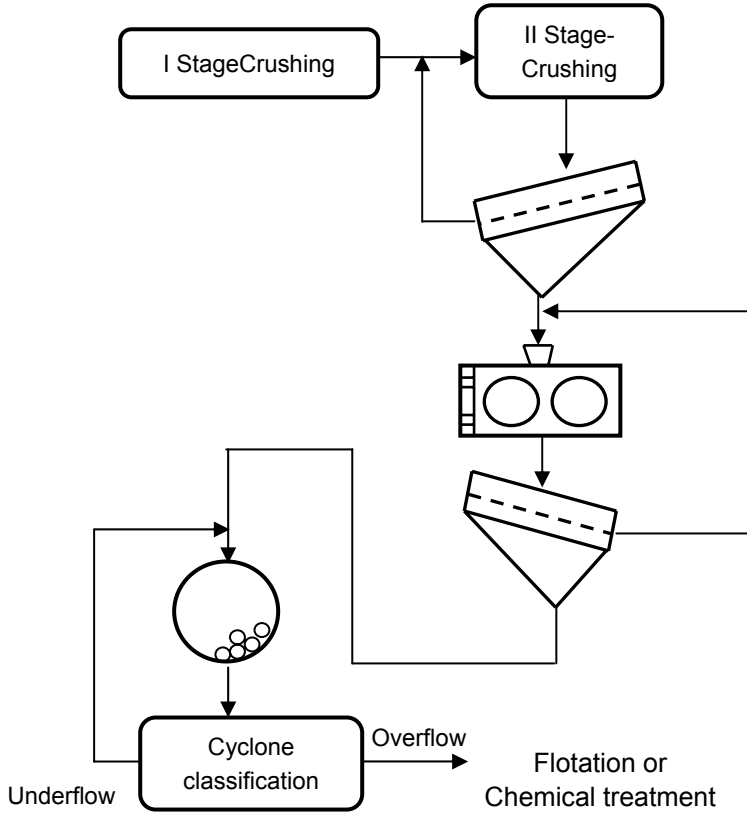


Fig. 5. Exemplary three-stage crushing and grinding HPGR based circuit

- $\gamma_x > \gamma_{x_min}$
- $E_{sp} < E_{sp_max}$

where S_x – given size reduction ratio (i.e. average or 80%), γ_x – the yield of given size fraction in crushing products, Q [Mg/h] – press throughput, E_{sp} [kWh/Mg] – unit energy-consumption.

The model built in the above manner is a classical issue of mathematical programming, i.e. finding the minimum (or maximum) of target function at presence of given limitations. The conditional extremum of the target function, in turn, gives us information of the controllable variables' values, which optimize the device's performance.

Summary and final conclusions

The issue of modeling the particle size distribution curves of HPGR crushing products, presented in the article, is significant from the point of view of both HPGR and the modern enrichment circuits work optimization. The methodology presented ap-

appears to be accurate, because the truncated distribution applied in the work, gives a very precise approximation, accuracy of which increases together with increasing the operating pressure value. The control of comminution results is then possible through a selection of particular value of the pressure which, in turn, is combined with parameters of the approximation formula (1) through equations presented in Table 2. It also appears that the major influence on the crushing process course has the operating pressure P . The process efficiency, measured with chosen indices, like the specific energy consumption, throughput or the content of desirable size fractions in product, can be then dependent on the operating pressure value. Conditioning the parameters of formula (1), approximating the particle size distribution function of crushing products, on the device work characteristics, permits the simulation to be carried out, which leads to determination the optimal operating conditions. It also enables the HPGR crushing process course to be better understood, as well as emphasizing the role of individual operating parameter of the device and the feed properties.

The investigations were carried out for copper ore and no additional analyses concerning the particle structure and the size of grain boundaries were made. Relationships obtained in the above investigations should have different values of coefficients depending the type of material, but it is accepted that the forms of functional relationships (presented in Table 2) are the same. It is obvious that the relationship $d_{\max} = f(P)$ is a hyperbole, $c = f(P)$ – polynomial of third degree, while $n = f(P)$ can be either the hyperbole or the straight line. Parameters n and c are responsible for the shape of distribution function (convexity) and it is claimed that the c parameter is connected with the material characteristics (structure). It might be accepted a hypothesis that the type of material determines a distribution type, i.e. either Weibull's distribution or the one of two others, namely log-normal or exponential, not considered in this work.

Acknowledgements

The article was written within the frames of Ministry of Science Research Grant N N524 466139.

References

- DANIEL M.J., MORRELL S., 2004, *HPGR model verification and scale-up*, Minerals Engineering, vol. 17.
- EPSTEIN B., 1948, *Logaritmico-normal distributions in breakage of solids*. Ind. Eng. Chem., 40.
- GAWENDA T., 2009, *Główne aspekty rozdrabniania twardych surowców mineralnych w wysokociśnieniowych prasach walcowych*. ZN AGH Górnictwo i Geoinżynieria, rok 33 (4).
- KALINOWSKI W., 2006, *Modernizacja procesów przemiałowych w przemyśle cementowym w świetle wymagań najlepszych dostępnych technik*. Surowce i Maszyny Budowlane, nr 1/2006.
- KOŁMOGOROW A.N., 1941, *O logaryfmiczieski normalnom zakonie raspriedielenija razmierow czastie pri drobleniji*, dokł. AN SSSR, 31.
- KURDOWSKI W., 1998, *Stan techniki w zakresie przemiatu cementu*. Cement Wapno Beton nr 3/1998.
- MAXTON D., MORLEY C., BEARMAN R., 2003, *A quantification of the benefits of high pressure rolls crushing in an operating environment*. Minerals Engineering, vol. 16.

- MORLEY C., 2003, *HPGR in hard rock applications*, Mining Magazine, IX/2003.
- MORLEY C., 2010, *HPGR-FAQ*, The Journal of Southern African Institute of Mining and Metallurgy, vol. 110.
- NAZIEMIEC Z., SARAMAK D., 2009, *Analiza zmian obciążenia materiału w strefie zgniotu pras walcowych*. ZN AGH Górnictwo i Geoinżynieria, rok 33 (4).
- OLEJNIK T.P., 2006, *Grinding kinetics of selected minerals with reference to the number of contact points*, Physicochemical Problems of Mineral Processing, vol. 40.
- SARAMAK D., TUMIDAJSKI T., BROŻEK M., GAWENDA T., NAZIEMIEC Z., 2010, *Aspects of comminution flowsheets design in processing of mineral raw materials*. Gospodarka Surowcami Mineralnymi, Mineral Resources Management, vol. 26 (4).
- SARAMAK D., 2012, *De-agglomeration in high pressure grinding roll based crushing circuits*, Physicochemical Problems of Mineral Processing vol. 48 (1).
- SARAMAK D., 2011c, *High-pressure comminution technology* (in Polish), Surowce i Maszyny Budowlane, 2011/3.
- SARAMAK D., 2011a, *Technological issues of High-Pressure Grinding Rolls operation in ore comminution processes*, Archives of Mining Sciences, vol. 56 (3).
- SARAMAK D., 2011b, *The influence of chosen ore properties on efficiency of HPGR-based grinding circuits*, Gospodarka Surowcami Mineralnymi Mineral Resources Management, vol. 27 (4).
- SCHOENERT K., 1988, *A first survey of grinding with high-compression roller mills*. International Journal of Mineral Processing, vol. 22.
- TUMIDAJSKI T., SARAMAK D., 2009, *Metody i modele statystyki matematycznej w przeróbce surowców mineralnych*, AGH University of Science and Technology Press, Krakow.
- TUMIDAJSKI T., 2010, *Actual tendencies in description and mathematical modeling of mineral processing* (in Polish), Gospodarka Surowcami Mineralnymi - Mineral Resources Management, vol. 26 (3).
- TUMIDAJSKI T., 2012, *Heuristic models of comminution processes as a basis for simulation and optimization of their course* (in Polish), Gospodarka Surowcami Mineralnymi - Mineral Resources Management, vol. 28.
- Van der MEER F.P., GRUENDKEN A., 2010, *Flowsheet considerations for optimal use of high pressure grinding rolls*, Minerals Engineering, Volume 23 (9).

Received March 16, 2012; reviewed; accepted July 9, 2012

CONTAMINANTS OF POST-LEACHING COPPER SOLUTIONS AND THEIR BEHAVIOR DURING EXTRACTION WITH INDUSTRIAL EXTRACTANTS

Leszek GOTFRYD, Grzegorz PIETEK

Institute of Non-Ferrous Metals, Sowińskiego 5; 44-100 Gliwice, Poland, leszekg@imn.gliwice.pl

Abstract: Several copper extractants have been examined in laboratory glassware with a special attention paid to their behavior towards cations others than copper(II). In the studies 25 vol. percent of hydrocarbon (Exxsol D80 AZ) solutions of six industrial copper extractants have been used. They were mainly reagents of hydrooxime type (LIX 860N-IC, LIX 984, LIX 984N, LIX 84-I, Acorga M5640) and diketone type LIX 54-100. Individual isotherms of independent extraction of copper(II) and selected cations (Fe^{3+} , Fe^{2+} , Co^{2+} , Ni^{2+} , Zn^{2+} , Mn^{2+} , Cd^{2+} , Mg^{2+}) versus equilibrium pH have been compared. Investigations have been conducted with synthetic 0.1 mol/L solutions of their sulfates. The values of $\text{pH}_{50\%}$ – parameter defined as an equilibrium pH at the moment of half-and-half extraction of the investigated cationic species have been presented. Also $\Delta\text{pH}_{50\%}$, that is differences between values of $\text{pH}_{50\%}$ for specific cation Me(II) and copper(II): $\Delta\text{pH}_{50\%} = \text{pH}_{50\%}(\text{Me}) - \text{pH}_{50\%}(\text{Cu})$, have been given. In addition to that 25% LIX 984 has been used in counter-current pilot trials for copper(II) extraction from naturally contaminated solutions produced by bioleaching of industrial sulfide copper concentrate to observe behavior of investigated contaminants such as correlations between their real co-extraction with copper(II) and the position of their extraction on the pH scale. Copper electrolyte/strip solution, working alternately within close loop of coupled stripping - electrowinning system, has been analyzed during consecutive cycles to observe building up of the contaminants concentrations in the course of test.

Keywords: industrial copper extractants, copper contaminants, copper extraction isotherms

Introduction

Dominant amounts of worldwide copper production come from copper ores which, after mining, crushing, grinding and enrichment by flotation to 20-30 % Cu, are processed pyrometallurgically into metallic copper. Also most of copper scrap is recovered by melting and pyrometallurgical refining. Crude blister copper is finally refined using hydrometallurgical electrolytic means to produce copper cathodes. A simpler, fully hydrometallurgical method to obtain electrolytic copper is based on the ion exchange solvent extraction technique. About 20% of the world copper production is processed

this way. Mostly poor and oxidized raw materials, unsuitable for flotation, are processed by means of extraction even though quite effective methods of bioleaching are available, which guarantee dissolution of rich sulfide copper concentrates by bioleaching (bacterial and/or fungal) and transforming them into copper(II) sulfate(VI) solutions and elemental sulfur. Generally, hydrometallurgical technology of copper production consists of raw material leaching (often using heaps or piles) with sulfuric acid solutions in the form of post-extraction raffinate or depleted copper electrolyte, solid/liquid separation (sedimentation and filtration) and final extractive treatment of the solution. The extracted copper is recovered as a stripped liquor being a moderately acidic copper sulfate solution and containing, for example, $55 \text{ g/dm}^3 \text{ Cu(II)}$ and $130 \text{ g/dm}^3 \text{ H}_2\text{SO}_4$). Next, it is subjected to electrolysis to obtain copper cathodes as the final product, with a simultaneous acid regeneration in amounts equimolar to deposited copper (e.g. $30 \text{ g/dm}^3 \text{ Cu(II)}$ and $179 \text{ g/dm}^3 \text{ H}_2\text{SO}_4$). Regenerated electrolyte is used again in cycles as a stripping factor.

Reagents for copper extraction

Currently there are two basic types of reagents capable to extract copper(II) from concentrated and/or acidic solutions which show high selectivity towards iron(III). They are of (hydroxy)oxime character – derivatives of aromatic ketones or aldehydes with elongated linear alkyl substituent attached – i.e. alkylaromatic ketoximes or aldoximes.

Commercially available are 2-hydroxy-5-nonylacetofoxime /LIX 84-I/, 5-dodecylsalicylaldoxime /LIX 860/ and 5-nonylsalicylaldoxime /LIX 860N or Acorga P-50/ (MTC Redbook, 2011, Cytec Industries technical brochures, 2011, Kordosky et al., 1983, 2003; Merigold, 1996, Agers, 1972). They contain basic ingredients which are used to compose extractants applied in industry by blending them with organic solvents (hydrocarbon) as well as with some supplementary additives (modifiers), e.g. phenoles (p-nonylphenol), higher alcohols (tridecanol), esters and similar. Those extra components have some influence on extraction characteristics (mitigating, decreasing extraction power causing softening of the stripping conditions), as well as on physical and chemical properties such as diminishing viscosity and increasing surface tension (Merigold, 1996).

Presently there are three companies manufacturing industrial amounts of reagents of the discussed types. Cognis Corporation (MTC Redbook, 2011) mainly produces LIX 84-I and LIX 860N-I, whereas Cytec Industries Inc. (Cytec Industries technical brochures, 2011) supplies a reagent called (Acorga) P50 while AllCo Chemicals provides aldoxime type reagent MOC 45. Due to these reagents numerous commercial products are available including LIX 984, 984N, 973N (blends of LIX 84-I and LIX 860), LIX 622N and 664N (LIX 860 with tridecanol or ester added); Acorga M 5640, PT 5050, P5100 (modified P-50); MOC 55TD. Evaluation of both types of extractants shows an advantage of the ketoxime type reagents. They are more resistant to hydrolysis under stripping conditions at elevated temperature than aldoximes. One of the rea-

sons is that they do not need to be blended with modifiers. They can be stripped with a typical copper electrolyte (Kordosky, 2003; Merigold, 1996).

To extract copper other chemical compounds can be used, e.g. β -diketones, having structure of $R^1COCH_2COR^2$, where $R^1 = -(CH_2)_6CH_3$, $R^2 = -C_6H_4-R$ and R is an alkyl substituent /LIX 54-100 = 1-phenyldecane-1,3-dion/. Their power of copper extraction is slightly lower. Additionally, they are not selective against iron(III), which presents an important disadvantage, limiting in practice their application to cuprammonium solutions (Kordosky, 2003; Agers, 1972; Jenkins et al., 1999).

Copper(II) can be extracted with many other reagents, including organic derivatives of acidic compounds of phosphorus /DEHPA = bis(2-ethylhexyl)phosphoric acid, PC88A = (2-ethylhexyl)2-ethylhexylphosphoric acid, Cyanex 272 = bis(2,4,4-trimethylpentyl)phosphinic acid/, carboxylic /naphthenic, versatic/ and sulphonic acids, and hydroxyquinolines. Quite often they present disadvantage of poor selectivity against many cations and/or very strong co-extraction of Fe(III), which in practice leads to a permanent poisoning of the extractant.

Contaminants of the post-leaching solution and selectivity of copper extraction

Leaching of copper-bearing materials with sulfuric acid solutions is not selective. Together with the main ingredient also its contaminants (Fe, Zn, Mg, Ni, Co, As) permeate to the solutions. Copper(II) extraction from such solutions, however, leads to production of relatively pure copper(II) sulfate(VI) solutions, which can be seen as a definite advantage of those extractants used for copper recovery. Requirements with respect to the contents of contaminants in copper electrolyte are not especially high (in comparison, for instance to zinc or manganese sulfate solutions prepared for electrolysis). Therefore, no special attention is paid to their level when they are present within relatively broad and acceptable limits. It is especially related to such ingredients as nickel, cobalt, arsenic, antimony, and to some lower degree also to iron. Some of them (Co) might be even desirable in the electrolyte, to prevent corrosion of insoluble lead anodes by causing their advantageous polarization. These facts, to a considerable degree, justify why there is scarcity of information in technical literature concerning levels of contaminants transferred to the electrolyte, except for iron, which is typically used to determine selectivity of copper extraction. It is suggested that selectivity of copper over iron defined as Cu/Fe in the stripped solutions (copper electrolytes) is from 2000 to ≥ 2500 (MTC Redbook, 2011; Cytec Industries technical brochures, 2011).

This study represents both an attempt to verify those data on iron(III) cation and also an effort to fill up the gap in information on the behavior of other elements. Therefore, it represents also an attempt to show potential differences between extractants, present on the market and in industry, considering their copper(II) extraction selectivity against iron(III) as well as against other ingredients of treated solutions.

How to compare particular extractants? Methodology of the research

In this respect the indicative quantitative information is defined by pH of half extraction of the examined cation denoted as $\text{pH}_{50\%}$, indicating pH at which, at thermodynamic equilibrium, half of the amount of the cation in the feed solution subjected to extraction was extracted to the organic phase of the extractant. The value of $\text{pH}_{50\%}$ depends on extractant concentration in the organic phase and cation concentration in the aqueous one. It depends on a volumetric ratio of reacting phases, temperature, and other factors. Generally, under established conditions, this parameter characterizes the pair of extractant and cation. Relative position on the pH scale of graphs presenting percent of extraction vs. equilibrium pH curves, and the $\text{pH}_{50\%}$ values in particular, for various extracted cations, that is an order of their extraction, is a characteristic feature of a particular extractant. It describes its behavior versus the ingredients of treated solution. The range and the slope of the essential part of the particular curve is also of some importance.

To create extractant/cation characteristics for comparison, very diluted salt solutions of investigated cations Me^{2+} ($0.001\text{--}0.01\text{ mol/dm}^3$) and from 2.5 to 3.0-fold concentrated organic solutions of extractants are tested. For more practical applications the extractants are prepared in a form and concentration used by industry and the cations in a form of their independent and still comparatively diluted ($0.05\text{--}0.1\text{ mol/dm}^3$) salt solutions. The second method has been applied in the presented study.

Experimental

Extractants and chemicals

The following solvent extraction reagents were used (main ingredients in parenthesis):

- LIX 860N-I (5-nonylsalicylaldoxime),
- Acorga M5640 (5-nonylsalicylaldoxime modified with TXIB /2,2,4-trimethyl-1,3-pentanediol di-isobutyrate/),
- LIX 84-I (2-hydroxy-5-nonyl-acetophenone oxime),
- LIX 54-100 (1-phenyldecane-1,3-dione),
- LIX 984N (blend of LIX 860N and LIX 84-I),
- LIX 984 (blend of LIX 860 /= 5-dodecylsalicylaldoxime/ and LIX 84-I).

Composition and typical properties of the reagents were available from Blue Line Technical Bulletins (Tech. Bull. 1996-2000) and/or their Safety Data Sheets, routinely provided by producers with the samples. They were used as received after dilution to 25 vol% with Exxsol D80 AZ dissolvent (Exxon Chemicals). Salts, bases, acids were delivered by POCH Gliwice, and were of AR grade.

Pregnant leaching solutions (PLS) – feed for copper extraction

The composition of the solutions from microbiological leaching of copper concentrate is shown in Table 1. They were used in extractive continuous and counter-current experiments.

Table 1. Composition of pregnant leach solutions from biological leaching of copper concentrate

Feed	pH	H ₂ SO ₄	Cu	Fe(II)	Fe(III)	Mg	Zn	Ni	Co	Ag	As	Cl	SO ₄	
PLS/1	1.78	15.1	44.91	0.27	5.50	6.00	2.99	0.22	0.42	< 0.0002	0.24	0.46	116.4	g/dm ³
PLS/2	1.68	17.4	28.6	0.29	6.25	4.30	2.09	0.17	0.32	< 0.0002	0.20	0.39	89.5	

Experimental methods

The characteristics of the extractants have been examined with reference to copper(II) and six other cations of non-ferrous metals, i.e. Cu²⁺, Co²⁺, Ni²⁺, Zn²⁺, Mn²⁺, Cd²⁺, Mg²⁺, and also to both Fe³⁺ and Fe²⁺ cations. During these trials individual synthetic solutions of metal sulfates of 0.1 mol/dm³ concentrations have been used, except for iron, which was used in a form of equimolar (0.1 + 0.1 mol/dm³) Fe(III) and Fe(II) solutions.

Determination of pH_{50%} for extractant/cation couples was performed by reading their values from the graphs relating extraction vs. equilibrium pH. The preparation of the curves was based on point-by-point collection of data on concentration of extracted cation in aqueous and organic solutions and corresponding equilibrium pH. The experiments consisted of mixing of reacting phases, i.e. the aqueous (A) solution of metal salt and the organic (O) solution of the extractant at their volumetric ratio A:O = 1:1, for the period of 10 minutes. Then, the phases were separated and sampled to analyze concentrations of the extracted cation. Gradual increase of pH of the reaction environment, and thereby progress of the reaction, was forced by a regular addition of a 5.0 mol/dm³ NaOH solution in small portions.

More advanced tests

Beside the described procedures for creation of pH_{50%}, to be used in a quasi-quantitative assessment of a particular extractant behavior versus copper(II) and cations of accompanying metals, in one case (LIX 984) a more advanced tests was performed during the pilot trials of copper extraction from the real feed solution. This test was conducted with a slightly excessive set of eight extractors of mixer-settler type, each of 0.5/1.5 dm³ in capacity, combined into 4/4 (extraction/stripping) counter-current system and fed by three membrane pumps. At the first stage the extractant (25% LIX 984/Exxsol D80) was saturated with copper(II) during the contact with the feed solution (PLS/1 or PLS/2) and at the second stage it released copper in favor of the sulfuric acid solution of 2.2 mol/dm³ initial concentration (in the first cycle) or in favor of depleted electrolyte from copper electrolysis. Operating media were provided by pumps and were flowing between particular extractors due to gravity, with some

support of sucking operation of the rotors of the mixer. The obtained strip solutions were collected and directed to electrolysis, after remaining organic phase removal with active carbon. The electrolytes depleted by electrolysis were used again as stripping agents. Samples of stripped solutions, taken from particular cycles, were analyzed for content of all impurities.

The extraction system was of 0-4-0-4 type, i.e. no extractant pretreatment, 4 steps of counter-current extraction, no scrubbing stage and 4 steps of counter-current stripping. Experiments were conducted at room temperature. Other conditions applied are listed in Table 2.

Table 2. Conditions of continuous counter-current copper(II) solvent extraction / stripping process

Process	Counter-current steps	Medium	Composition	Flow [dm ³ /h]	O:A ratio [vol./vol.]	Cycles
–	–	Organics	25 % vol. LIX 984 / Exxsol D80	4.12	–	–
Extraction	4	Feed 1	PLS/1 (table 1)	1.20	3.45	1
		Feed 2	PLS/2 (table 1)	1.88	2.20	2,3,4
		Strip 1	2.2 M H ₂ SO ₄	0.92	4.50	1
Stripping	4	Strip 2	Copper electrolyte 35 g/dm ³ Cu	3.10	1.35	2,3,4

The strip solution obtained in cycle 1 was gathered and directed to copper electrolysis, after removal of the remaining organic phase with active carbon. The depleted by electrolysis (to the level of 35 g/dm³ Cu) electrolyte was used again as a stripping agent in the second cycle. Four campaigns of such extraction – stripping – electrolysis cycles were performed. The circulating extractant performed a role of a copper carrier from the feed (PLS) to the strip solutions. A portion of about 70 dm³ of electrolyte/stripping solution was circulating as copper carrier from saturated organic extractant to the metal cathode. Samples of stripped solutions, taken from particular campaigns, were analyzed for content of acid, copper and all impurities.

Analytical procedures

All samples and solutions were processed and analyzed by modern instrumental methods: ASA or AES-ICP (Horizon or Perkin-Elmer Optima 5300 V) for determination of complex mixed solutions, and by more traditional titration methods for determination of pure single components.

Results and discussion

The studied extractants consisted of 25 vol% organic solutions of the following reagents: LIX 860N, LIX 984, LIX 984N, Acorga M5640, LIX 84-I and LIX 54-100 in Exxsol D80 AZ dissolvent. The results are presented in a graphical form as sets of

curves showing dependency of the degree of extraction and equilibrium pH curves (% of extraction – pH) for particular cations and each investigated extractant (Fig. 1 a–f), and also in a form of collected data in Table 3 with $\text{pH}_{50\%}$ values, as well as in Table 4 with characteristic differences between those values for particular cation and Cu(II) values.

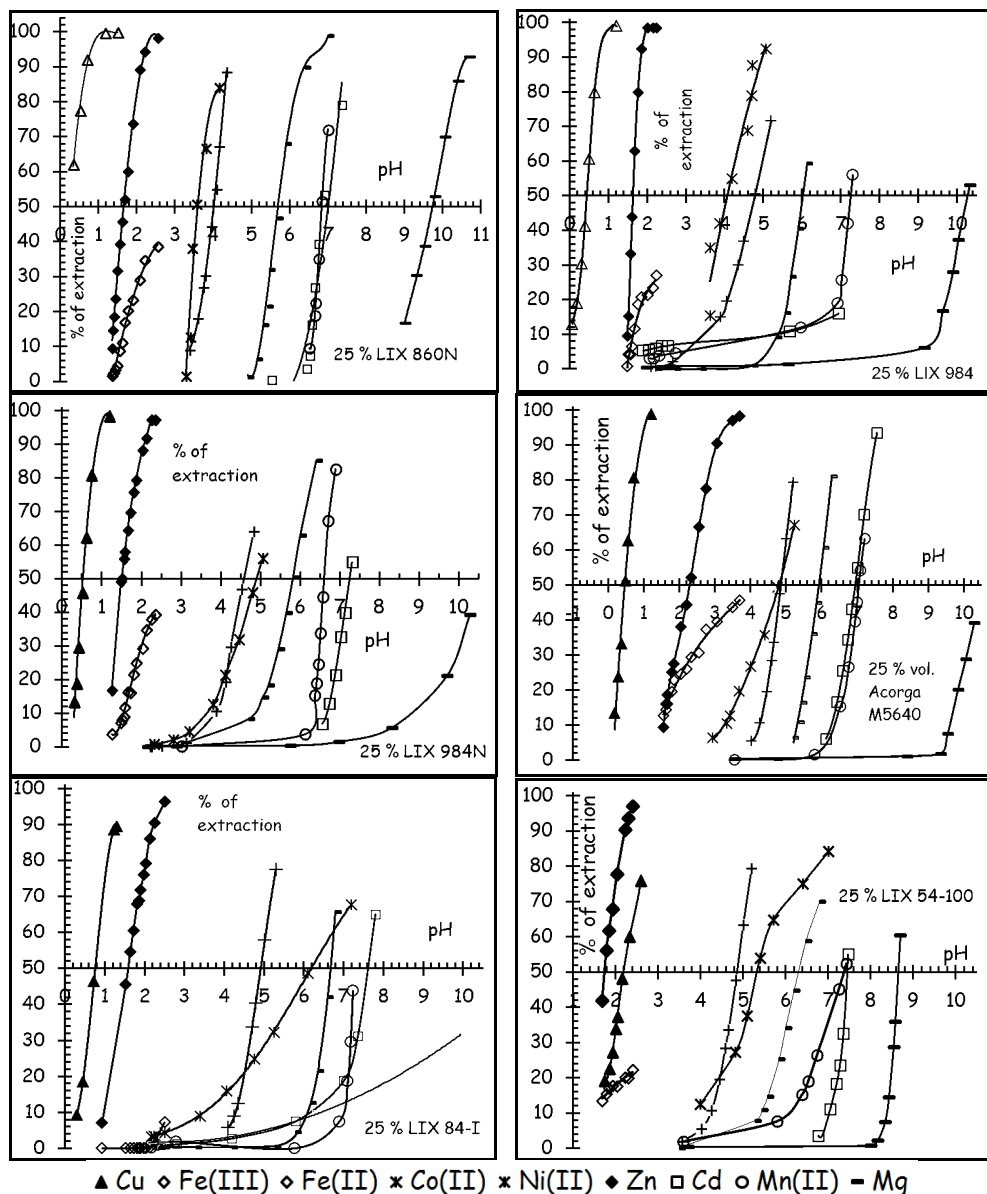


Fig. 1. Extraction of different cations with selected extractants intended for selective extraction of copper(II)

Table 3. $pH_{50\%}$ values for cations extraction with 25 vol% organic solutions (Exxsol D80 AZ) of selected industrial copper(II) extractants obtained during extractant contact with 0.1 mol/dm^3 aqueous solutions of metal sulfates

Extractant→	LIX	LIX	Acorga	LIX	LIX	LIX
Cation	860N-I	984	M5640	984N	84-I	54-100
Cu(II)	0.30	0.43	0.47	0.55	0.76	2.20
Fe(III)	1.66	1.64	2.22	1.53	1.62	1.75
Fe(II)	1.90	-	3.45	2.30	-	-
Co(II)	4.00	4.78	4.82	4.60	4.90	4.87
Ni(II)	3.60	4.10	4.74	4.80	4.00	5.35
Zn(II)	5.70	6.00	5.93	5.78	6.67	6.31
Mn(II)	6.84	7.24	7.05	6.60	7.21	7.34
Cd(II)	6.85	-	6.90	7.28	7.60	7.45
Mg(II)	9.72	10.27	10.50	10.5	-	8.65
$pH_{50\%}$ of cation extraction						

Table 4. Values of $\Delta pH_{50\%} = pH_{50\%}(\text{Me}) - pH_{50\%}(\text{Cu})$ for cation extraction with 25 vol% organic solutions (Exxsol D80 AZ) of industrial copper(II) extractants, obtained during extractant contact with 0.1 mol/dm^3 aqueous solutions of metal sulfates

Extractant→	LIX	LIX	Acorga	LIX	LIX	LIX
Cation	860N-I	984	M5640	984N	84-I	54-100
Cu(II)	0.00	0.00	0.00	0.00	0.00	0.00
Fe(III)	1.36	1.21	1.75	0.98	0.86	-0.45
Fe(II)	1.60	-	2.98	1.75	-	-
Co(II)	3.70	4.35	4.35	4.05	4.14	2.67
Ni(II)	3.30	3.67	4.27	4.25	3.24	3.15
Zn(II)	5.40	5.57	5.46	5.23	5.91	4.11
Mn(II)	6.54	6.81	6.58	6.05	6.45	5.14
Cd(II)	6.55	-	6.43	6.73	6.84	5.25
Mg(II)	9.42	9.97	10.03	9.95	-	6.45
$\Delta pH_{50\%} = pH_{50\%}(\text{Me}) - pH_{50\%}(\text{Cu})$						

Table 5 shows composition of a few strip solution samples produced during pilot trials of copper extraction with 25 vol% LIX 984/Exxsol D80 and, for comparison, composition of a typical electrolyte from industrial copper electrorefining process. These data confirm the general effectiveness of ion-exchange solvent extraction technique in providing a barrier for iron(II/III) and the cations of non-ferrous metals other than copper(II) as well as prove the meaning of the data in Tables 3 and 4. Indirectly they demonstrate a sequence of minimal co-extractions of some elements – especially

Fe and Zn, which are present in the feed solutions in slightly bigger amounts, but also Ni, Co or Mn, and that sequence is similar to the that of extractions on the pH scale. These elements find their way to the strip solutions at relatively low level of several dozen (Fe – about 100, Zn – about 20–30) and in further cases (Ni, Co, Mn) of merely a few milligrams per liter and per cycle, while the other components of the feed solution (As, Sb, Se, Te, Bi, Pb and especially Sn, Cd, Cr, Ag) are practically absent in the strip solutions. Additionally, regardless of cationic ingredients, small amounts of chlorides, phosphates and silica are observed in the strip solutions.

Essential cationic (Fe, Zn, Ni, Co) as well as some anionic (chlorides, phosphates) components increase their concentrations during subsequent cycles of copper(II) extraction, gradually accumulating in strip solution which circulates between systems of stripping and electrolysis.

Table 5. Composition of copper strip solutions, obtained during pilot trials of copper extraction from post-leaching solutions with 25 % LIX 984/Exxsol D80 AZ

Component	> H ₂ SO ₄	Cu	Ni	Co	Fe	As	Sb	Se	Cl	Zn
Electrolyte ^{*)}	172	43.2	7.56	0.10	0.13	4.0	0.37	0.095	0.046	0.029
Strip 1	135	55.5	< 0.001	0.002	0.090	< 0.001	< 0.001	< 0.001	0.020	0.030
Strip 2	140	50.2	0.0030	0.003	0.10	< 0.001	< 0.001	< 0.001	0.035	0.020 g/dm ³
Strip 3	148	53.7	0.0064	0.007	0.169	< 0.001	< 0.001	< 0.001	0.028	0.082
Strip 4	145	57.6	0.0054	0.010	0.267	–	–	–	0.014	0.098

continued	Si	P	Sn	Cd	Cr	Te	Bi	Mn	Pb	Ag
Electrolyte ^{*)}	16	9	2.9	1	0.6	< 0.5	< 0.5	0.4	–	–
Strip 1	6	26	< 0.1	< 0.1	< 0.1	< 1	< 1	3	< 2.5	< 0.1
Strip 2	3	30	< 0.1	< 0.1	< 0.1	< 1	< 1	3	0.5	< 0.1 mg/dm ³
Strip 3	5.9	50	< 0.1	< 0.1	< 0.1	< 1	< 1	5.9	2.6	< 0.1
Strip 4	3.5	41	–	–	–	–	–	7.7	1.0	–

^{*)} composition of typical electrolyte of copper electrolytic refining; the other solutions are strip liquors, obtained during pilot plant trials from feed solution PLS/2 (Strip 1) or PLS/1 (Strip 2, 3 & 4)

Conclusions

Six solvent extraction reagents – five of Cognis' LIX family: 860N-I, 84-I, 984N, 984 (hydroxyoximes), 54-100 (diketone) and Avecia's M5640 (modified salicylaldoxime of Acorga family), capable of selective extraction of copper(II), were characterized, with special attention paid to the selectivity of Cu(II) extraction against typical contaminants such as iron (Fe³⁺, Fe²⁺) and cations of other non-ferrous metals (Co²⁺, Ni²⁺, Zn²⁺, Mn²⁺, Cd²⁺, Mg²⁺). For the studies their 25 vol% solutions in hydrocarbon dis-

solvent Exxsol D80 AZ (ExxonMobil Chemical) were prepared. The most important our observations are:

- in most of the examined cases (except for LIX 54-100) copper(II) is the most strongly extracted cation ($\text{pH}_{50\%}$ from 0.30 to 0.76),
- extractants, claimed as highly selective against iron, proved to be effective within a very narrow pH range of acidic solutions; extraction of Fe(III) begins at $\text{pH} \geq 1.0$ –1.5, even with Acorga M5640, which was the best agent with $\text{pH}_{50\%}^{\text{Fe(III)}} = 2.22$
- the distance between extraction of copper(II) and iron(III) $\Delta\text{pH}_{50\%}^{\text{Fe(III)/Cu(II)}}$ is broad enough (≥ 1.0) with the four reagents (M5640, 860N-I, 984N, 984); in that respect Acorga M 5640 (1.75) is definitely the best one; the rest (/LIX 84-I (0.86) and LIX 54-100 (-0.45)/ should rather be applied to extraction of copper(II) from ammonia solutions,
- iron(II) is the third to be extracted with respect to its position on pH scale, but in all cases the extraction is naturally strongly hampered and raises to merely 20–40% in the conditions under which other cations reach close to 100 % extraction,
- next, the pair of cobalt/nickel is extracted with a great distance to copper(II) at $\text{pH}_{50\%}$ levels of 3.5-4.5 and 4.5-5.5 for Co(II) and Ni(II), respectively,
- cobalt(II) extraction is related to its partial oxidation and fractional permanent presence in organic phase (showing partial resistance to Co stripping), what was demonstrated by its permanent dark coloring; it seems that a similar situation takes place with all extractants,
- Mn(II) and Cd(II) form a similar ‘pair’ because they are extracted relatively close to each other and far from copper(II), at the level of 6.6-7.6 on the pH scale,
- zinc(II) extraction takes place earlier, between groups of Co(II)/Ni(II) and Mn(II)/Cd(II), at pH level about 5.5–6.0; slightly higher for LIX 54-100 and LIX 84-I.

Small co-extraction of some cations, in particular iron(III) and zinc(II), has a cumulative character. Therefore, when they are present in feed solutions in considerable amounts in the applied system of copper(II) extraction, a stage of organic phase scrubbing should be predicted.

References

- AGERS D.W. et al, 1972, *The evaluation of new LIX reagents for the extraction of copper and suggestions for the design of commercial mixer-settler plants*; AIME Annual Meeting, San Francisco, Calif. TMS Paper Selection A72-87.
- Cytec Industries technical brochures; www.cytec.com/specialty-chemicals, (accessed Sept. 30, 2011), Acorga Extractants; Acorga OPT Series Solvent Extraction Reagents.
- JENKINS J. et al: *Electrolytic copper – leach, solvent extraction and electrowinning world operating data*, Proc. of Copper 99 – Cobre 99 International Conference; Vol. IV – *Hydrometallurgy of Copper*; Ed. by S.K. Young.
- KORDOSKY G.A., 2003, *Copper SX circuit design and operation - current advances and future possibilities*; Technical Proceedings ALTA 2003 SK/IX World Summit, Perth, Australia.

- KORDOSKY G.A. et al, 1983, *The LIX 860 series: Unmodified copper extraction reagents*, Proc. of the International Solvent Extraction Conf., Denver, Colorado,
- MERIGOLD C.R., 1996, *Copper extractants – modified and unmodified oximes, a comparison*, MID, CNNMIEC – Yunnan Company, BGRIMM Annual Technical Seminar, Kunming, Yunnan Province, PR of China,
- MTC Redbook technical brochure; *Solvent Extraction Reagents and Applications*. Mining Chemicals Technology Division, Cognis Corporation /Cognis Group/; (from www.cognis.com, accessed Sept. 30, 2011);
- RITCEY G.M., 2006, *Solvent Extraction – Principles and applications to process metallurgy*, 2nd ed., Hong Kong,
- Tech. Bull. 1996-2000; LIX 860N-I, LIX 984, LIX 984N, LIX 84-I, LIX 54-100 particular Blue Line Technical Bulletins (accessed Sept. 30, 2011 at www.cognis-us.com)

Received May 31, 2012; reviewed; accepted July 10, 2012

FLOTATION OF ZINC OXIDE ORE USING CATIONIC AND CATIONIC-ANIONIC MIXED COLLECTORS

Akbar MEHDILO, Mehdi IRANNAJAD, Hossein ZAREI

Department of Mining and Metallurgical Eng., Amirkabir University of Technology, Tehran, Iran
Email: iranajad@aut.ac.ir

Abstract: Flotation of smithsonite coming from a cerussite flotation circuit was investigated using Armac C and Armac T as cationic collectors and their mixtures with potassium amyl xanthate (KAX) as an anionic collector. Under optimum condition using Armac T with sodium hexamethaphosphate as a depressant, a smithsonite concentrate with 42% Zn and 89.6% recovery is obtained while in the presence of sodium silicate depressant Armac C produces a concentrate containing 40.8% Zn with 92.5% recovery. However, Armac T acts a little more selectively than Armac C but their mixture with KAX act inversely. The KAX-Armac C mixed collector improves the Zn grade and recovery of the flotation concentrate while KAX-Armac T does not. At the mixture ratio of KAX - Armac C 2:1, the amine collector consumption is decreased and an optimal concentrate with 94% recovery and 43% Zn grade is obtained without any gangue depressant reagents.

Keywords: *flotation, smithsonite, collector, mixed collector, zinc*

Introduction

Nowadays, new technologies to produce zinc metal from oxidized zinc ores are being developed as it is becoming more difficult to find new sphalerite mines. Oxidized ores contain zinc in various carbonate and silicates minerals, such as smithsonite (ZnCO_3), hydrozincite ($2\text{ZnCO}_3 \cdot 3\text{Zn}(\text{OH})_2$), zincite (ZnO), willemite (Zn_2SiO_4) and hemimorphite ($\text{Zn}_4\text{Si}_2\text{O}_7(\text{OH})_2 \cdot \text{H}_2\text{O}$) and so on (Chen et al., 2009). In practice, the commonly used method for the recovery of oxidized lead and zinc minerals from ores at present is flotation (Onal G. et al., 2005). The flotation of oxidized lead and zinc minerals, particularly zinc minerals, is much more difficult than the flotation of corresponding sulfide minerals. Hexyl and amyl xanthates are capable of collecting smithsonite. However, the process is not selective enough in practice (Gaudin, 1957; Billi and Quai, 1963; Nagano et al., 1975; Yamada et al., 1976; Yamazaki et al., 1978; Herrera Urbina et al., 1999; Hosseini and Forssberg, 2006; Hosseini and Forssberg, 2007). The fatty acids are also

used to recover the zinc oxide minerals such as smithsonite, hemimorphite and calamine via froth flotation method (Rey, 1953; Nagano et al., 1974; Kiersznicki et al., 1981; Hosseini and Forssberg, 2006; Irannajad et al, 2009; Ejtemaei et al, 2011). Flotation using chelating agents is another alternative for beneficiation of zinc oxide minerals (Rinelli and Marabini, 1973; Fuerstenau and Palmer, 1976; Barbery et al., 1977; Marabini et al., 2007). The most common flotation technique used commercially for the treatment of zinc oxide minerals is sulfidization with Na_2S , followed by treatment with conventional cationic collectors, namely amine (Mckenna et al., 1949; Rey, 1979; Abramov, 1961; Onal et al., 2005; Pereira and Peres, 2005; Keqing et al., 2005; Hosseini and Forssberg, 2006; Irannajad et al., 2009). The amount of sulfidizing reagent and pH of the pulp must be carefully controlled in amine flotation (Hosseini and Forssberg, 2007; Salum et al, 1992). Either sodium sulfide or sodium hydrosulfide is used as a sulfidizing agent (Onal G. et al., 2005). When the pH value decreases, there is a drop in recovery (Hosseini and Forssberg, 2007; Salum et al, 1992). A mixture of amines and xanthates can be used as a collector. A system that contains two surfactants of different charge is called a catanionic system (Herrington et al., 1993; Hosseini and Forssberg, 2006; Hosseini and Forssberg, 2007; Ejtemaei et al, 2011).

The Angooran mine, located 100 km south west of Zanjan, is one of the largest lead and zinc oxide deposit in Iran. The major zinc mineral is smithsonite with hemimorphite and hydrozincite as minor minerals while the major lead mineral is cerrusite with mimetite as a minor one. Generally, the associated minerals are mainly calcite and quartz which are accompanied with minor amount of mica, hematite, goethite, kaolinite, and montmorolinite. The exploited ore is concentrated in Dandy Processing Plant which is located 20 km far from the mine with approximately 1 Gg (gigagram or 1000 ton) daily feed. The schematic flowsheet of present concentration process is shown in Fig. 1. The tailing of cerrusite flotation is the zinc concentrate containing 20-25% Zn, which is leached by sulfuric acid to extraction the zinc metal (Irannajad 2007; Mehdilo et al, 2010; Ejtemaei and Irannajad, 2008). In recent years by decreasing the Zn content of the ore, upgrading of tailing by froth flotation before acid leaching has been attracted considerably. In this work the cationic/anionic flotation of smithsonite from the tailing of cerrusite flotation circuit is studied.

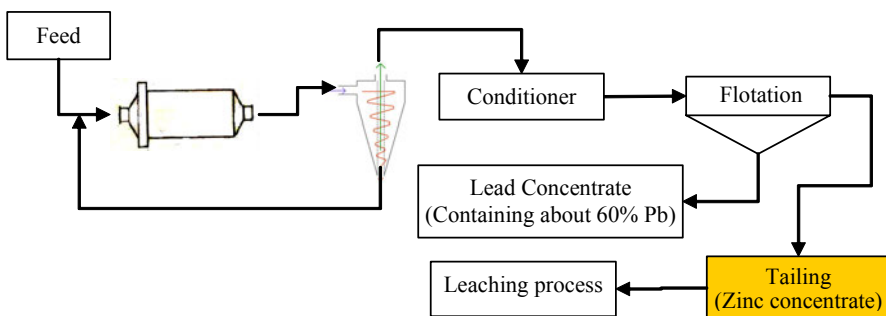


Fig. 1. Schematic flow diagram of Dandy Mineral Processing Plant

Materials and Methods

Materials

A representative sample containing 21.7% Zn was taken from tailing of the cerrusite flotation circuit. The chemical composition of the ore sample and pure smithsonite determined by XRF is presented in Table 1. The XRD (X-ray diffraction) pattern of the sample indicated that the associated minerals of smithsonite are calcite, quartz and minor amount of goethite, kaolinite, and montmorolinite. The reagents used in the study are shown in Table 2.

Table 1. Chemical composition of representative sample

Sample	Composition (wt. %)											
	ZnO	pbO	SiO ₂	CaO	Al ₂ O ₃	Fe ₂ O ₃	MgO	K ₂ O	CdO	NiO	SO ₃	L.O.I
ore sample	27.0	4.8	16.9	17.5	2.6	2.62	0.65	0.36	0.19	0.09	0.22	25.64
pure smithsonite	63.5	3.11	0.13	0.51	–	2.45	–	–	–	–	–	29.4

Table 2. Reagents used in flotation tests

Chemical	Concentration	Supplier	Role
Armac C (Cocoalkylamine) acetate)	99	Akzo Nobel	Collector
Armac T (Tallowalkylamine)	99	Akzo Nobel	Collector
Potassium amyl xanthate (KAX)	90	Cheminova	Collector
Sodium sulfide (Na ₂ S)	75	Merck	Sulfidizing reagent
Sodium silicate (SS)	97	Merck	Depressant
Sodium hexa methaphosphate (SH)	96	Scharlau	Depressant
NaOH	–	Merck	pH adjuster
Pine oil	99	Penn Chemical	Frother

Methods

Microflotation test

The samples were ground and then sieved to collect the $-150 + 75 \mu\text{m}$ fraction for the microflotation tests. Single mineral microflotation tests were performed in a 300 cm^3 Hallimond tube at a constant air flow rate. Experiments were carried out at varying pH and reagent concentrations. Sulphuric acid and sodium hydroxide solution were used for pH adjustment. For each test, 3 g of $-150 + 75 \mu\text{m}$ fractions were separately conditioned using reagents at the desired pH in a 400 cm^3 volumetric flask for a predetermined time (3 min). The collector was then added to the slurry and flotation was carried out in the Hallimond tube. After the flotation tests, the concentrate and tailings were filtered, dried and weighed.

Flotation tests

In the flotation tests carried out in 1 dm³ Denver cell according Fig. 2, the desired amount of sodium sulfide was added to the pulp and was conditioned for 10 min by adjusting the pH at 11. A depressant was then added and conditioned for 5 min, after which the slurry was conditioned with collectors for 5 min (conditioning time for mixed collectors was 10 min). Finally, pine oil was used as a frother (120 g/Mg) with a conditioning time of 2 min. The froth collection was performed for 10 min. The flotation concentrate and tailing were filtered, dried, weighed, and analyzed by atomic absorption technique.

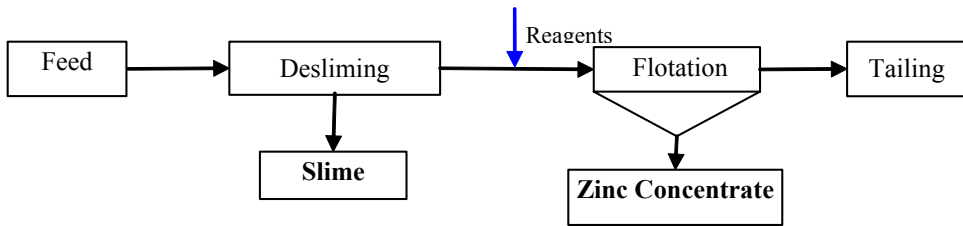


Fig. 2. Schematic diagram of flotation tests

Results and discussion

Microflotation tests

The microflotation tests were carried out in order to select the optimum amount of sulfidizer agent and pH value. The recovery of smithsonite flotation using 500 g/Mg Armac C and KAX as a function of pH value are shown in Fig. 3. The maximum recovery of smithsonite flotation occurred at pH = 9 and pH = 10.5–11 using KAX and Armac C, respectively. In the next experiments pH=11 was selected for cationic flotation by Armac C and Armac T. The effects of sodium sulfide on smithsonite flotation using 500 g/Mg Armac C, Armac T and KAX are shown in Fig. 4. The recovery of smithsonite was increased by increasing sodium sulfide concentration. The optimum dosage of sodium sulfide is 500 g/Mg which results in 82.6% and 83.7% recoveries using Armac C and Armac T, respectively, while its optimum amount is 1.25 kg/Mg for KAX with 73.4% recovery. The recovery of smithsonite decreases with the increasing sodium sulfide concentration. This is due to over-sulfidization of the pulp and a high content of HS⁻ ion in the flotation system (Malghan, 1986; Onal et al., 2005; Fa et al., 2005).

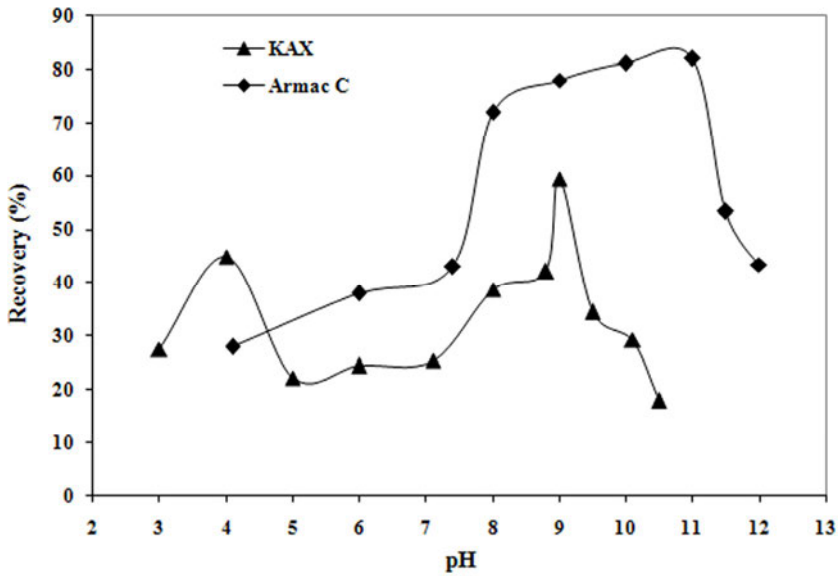


Fig. 3. Recovery of smithsonite flotation as a function of pH value (500 g/Mg Armac C, 500 g/Mg KAX, 500 g/Mg Na₂S)

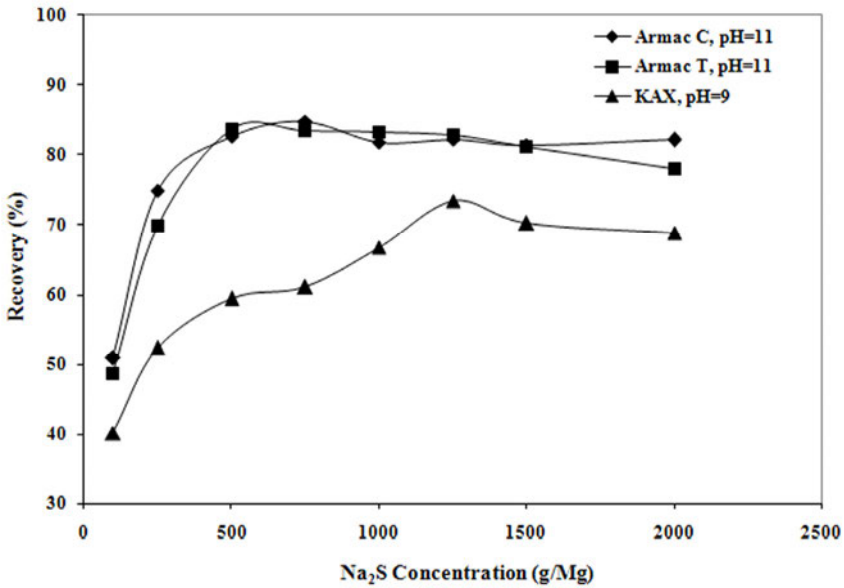


Fig. 4. Recovery of smithsonite as a function of Na₂S concentration (500 g/Mg Armac C, 500 g/Mg Armac T, 500 g/Mg KAX)

Ore sample flotation

Cationic flotation

Figure 5 shows smithsonite flotation from the ore sample as a function of the sodium sulfide dosage using Armac C. The results revealed that the smithsonite particle surface was not sufficiently sulfidized. The optimal dosage of sodium sulfide is up to about 7500 g/Mg. At a high dosage, the adsorption of S^{2-} ions increases with the increase of sodium sulfide, and the flotation of smithsonite is hence depressed. Marabini et al., 1984, found that the smithsonite recovery is not sensitive to the Na_2S concentration when the concentration of sodium sulfide is high. The reason for this observation is that at high concentration of Na_2S , the $ZnCO_3$ component disappears totally and a dense coating of ZnS is formed on the mineral surfaces. Essentially, the full formation of ZnS on the surface of ZnO minerals results in the amine adsorption less sensitive to the effects of concentration of Na_2S . However, the Na_2S dosage is relatively high but it also has the role of a pH adjuster, and no other pH adjusting reagent is required (Marabini et al., 1984).

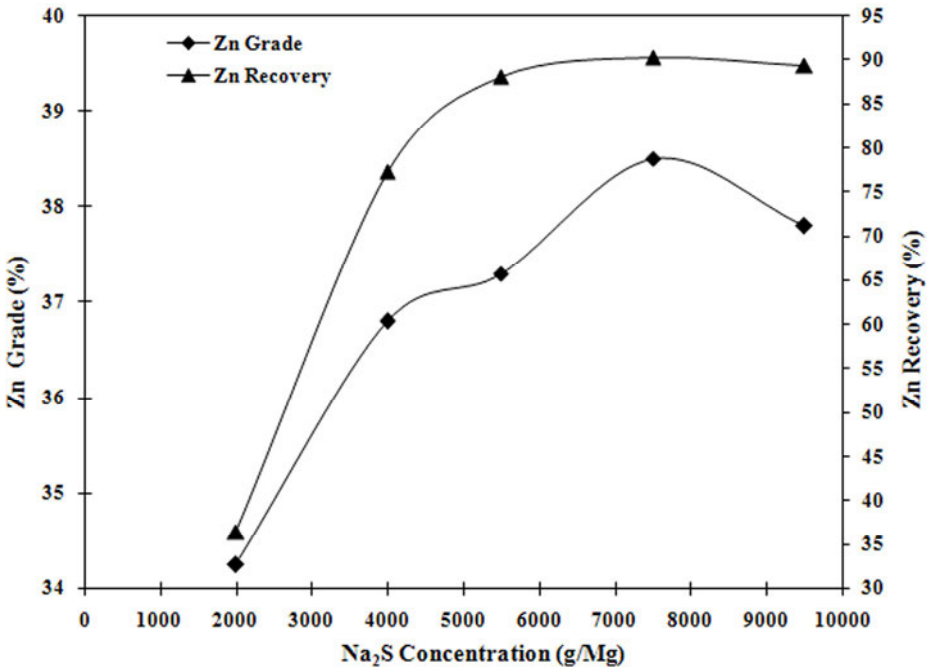


Fig. 5. Grade and recovery of zinc in smithsonite flotation concentrate as a function of sodium sulfide dosage using Armac C (Armac C 200 g/Mg, pH=11)

The flotation response of smithsonite as a function of Armac C or Armac T dosage in the presence of SS and SH as depressant reagents is shown in Figs 6 and 7. It is clear that the Zn grade of the concentrate obtained by Armac T is higher than that by

Armac C. The increase of both collectors dosage increases Zn recovery and decreases Zn grade in the smithsonite flotation concentrate. The reduction of Zn grade is attributed to the flotation of more gangue minerals due to high collector concentration.

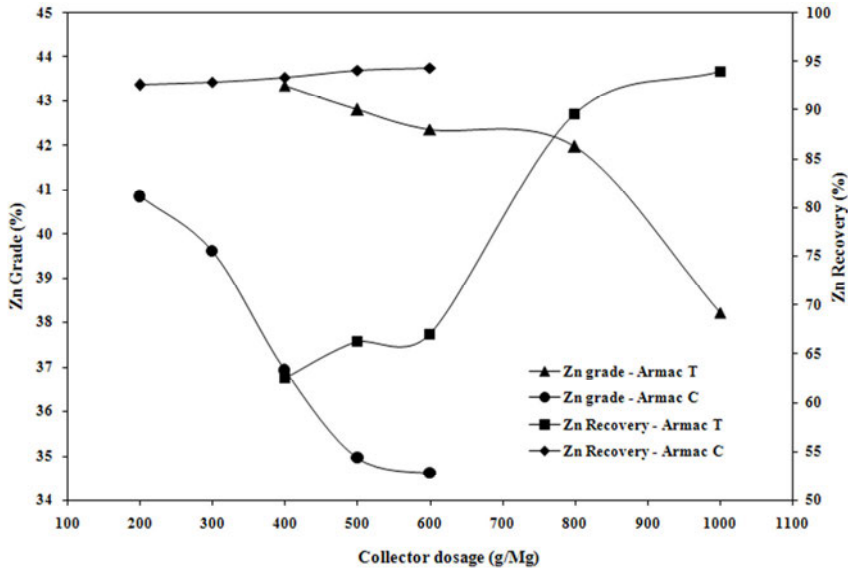


Fig. 6. Grade and recovery of zinc in smithsonite flotation concentrate as a function of collector dosage (7500 g/Mg Na₂S, 600 g/Mg SS, pH = 11)

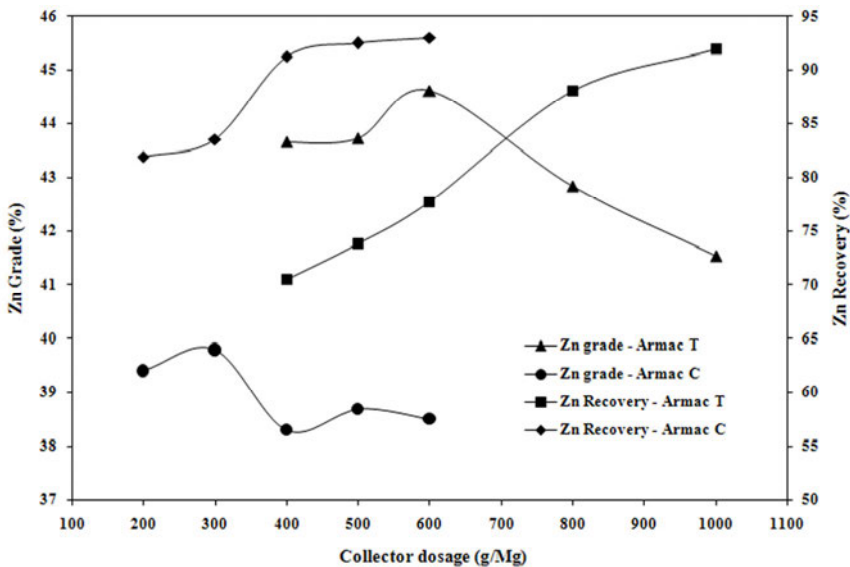


Fig. 7. Grade and recovery of zinc in smithsonite flotation concentrate as a function of collector dosage (7.5 kg/Mg Na₂S, 250 g/Mg SH, pH = 11)

In the presence of SS, the optimal dosage of Armac C is 200 g/Mg, which results in a smithsonite concentrate with 40.8% Zn and 92.5% recovery, while the optimum Zn grade and recovery in the concentrate produced by Armac T are about 42.0% and 89.6%, respectively which is obtained at dosage of 800 g/Mg. Using SH as depressant reagent increases the optimal dosage of Armac C to 300 g/Mg which results in a concentrate containing 39.8% Zn with 83.5% recovery. In the presence of SH, using 800 g/Mg as an optimal dosage of Armac T a concentrate with 42.8% Zn and 92.5% recovery is obtained.

Anionic–Cationic flotation

KAX–Armac C

The Zn grade – recovery curves of the bench flotation using mixed collectors depend on the mixture ratio and are shown in Fig. 8. At a fixed concentration of Armac C (50 g/Mg), the KAX concentration was increased from 150 to 900 g/Mg and the mixed collector ratio of KAX:Armac C was varied from 3:1, 6:1, 10:1, 14:1, to 18:1. The results (Fig. 8a) show that the increasing of KAX dosage or mixture ratio improves the Zn grade significantly but it decreases the Zn recovery from 92.5% (using Armac C only) to about 70%. The optimum mixture ratio of the mixed collector is KAX: Armac C, 6:1 (300 g/Mg KAX and 50 g/Mg Armac C) which results in a concentrate with 72.6% recovery and 47.5% Zn grade. For improving the recovery, at the optimum dosage of KAX (300 g/Mg) the dosage of Armac C was increased gradually according Fig. 8b. With increasing the concentration of Armac C, the Zn grade is decreased but the Zn recovery is improved significantly. The optimal ratio of collectors is KAX:Armac C, 2:1 (300 g/t KAX and 150 g/t Armac C) which results in a smithsonite concentrate with about 43% Zn and 94% recovery. At the optimal conditions the Zn grade and recovery of the concentrate obtained by mixed collector are 2.15% and 1.5% respectively higher than that obtained using Armac C alone. Furthermore, by using mixed collectors without any depressant reagents, the optimum consumption of amine collector is also decreased.

KAX–Armac T

The Zn grade – recovery curves of the bench flotation using the mixture of KAX and Armac T at the different mixture ratios are shown in Figure 9. At a fixed concentration of Armac T (300 g/Mg), the KAX concentration was increased from 90 to 1000 g/Mg and the mixed collector ratio of KAX:Armac T was varied from 0.3:1, 0.6:1, 1.2:1, 1.8:1, 2.3:1 to 3.3:1. As seen from Fig. 9a the increasing KAX concentration or mixture ratio improves the Zn grade and recovery and the optimum concentrate containing 43.3% Zn grade and 65.1% recovery are obtained at a mixture ratio of 1.2 : 1 (360 g/Mg KAX and 300 g/Mg Armac T). A further increase of the KAX concentration decreases the selectivity of the amine collector and Zn content of the concentrate but it does not have significant effect on the Zn recovery. At the KAX concentrations

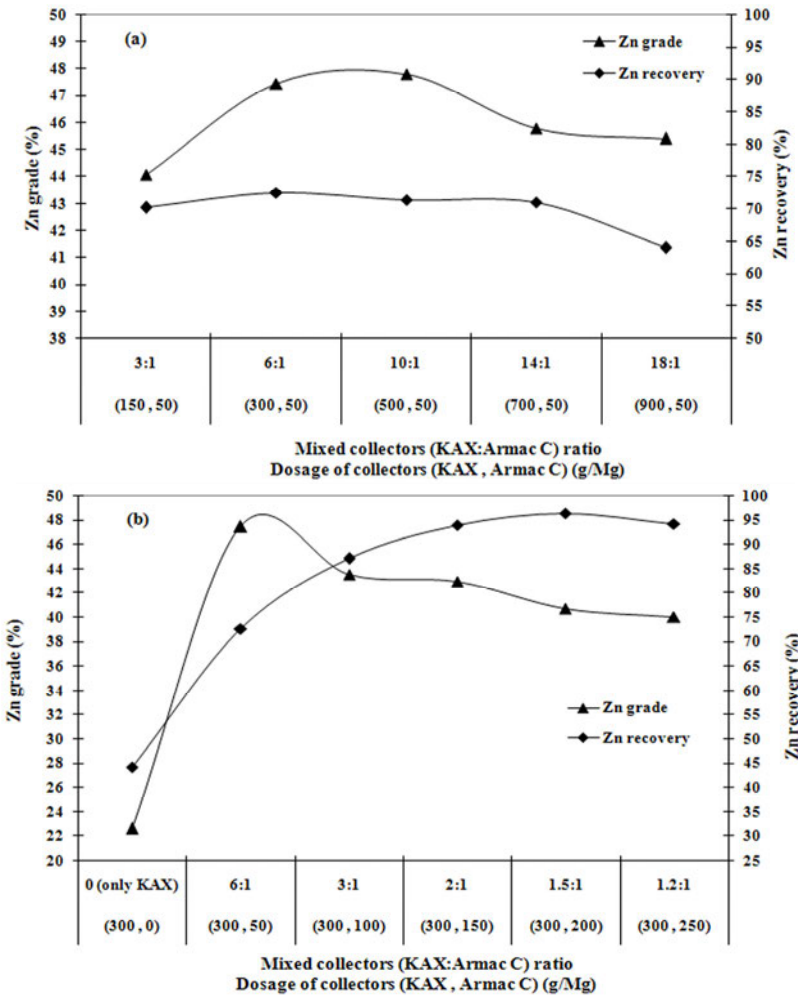


Fig. 8. Grade and recovery of Zn in smithsonite flotation concentrate as a function of mixed collectors ratio (Na_2S 7500 g/Mg, without depressant, pH = 11): (a) variation of KAX concentration, (b) variation of Armac C concentration

higher than 700 g/Mg with decreasing the Zn grade, the recovery is increased significantly. For improving the Zn grade and recovery of the concentrate, at the optimum fixed concentration of KAX (360 g/Mg) the concentration of Armac T is increased according Fig. 9b. The results show that the increasing of Armac T consumption increases the Zn recovery of the concentrate significantly but it decreases the Zn grade of the concentrate. The optimum mixture ratio of the mixed collector is KAX:Armac T as 0.6:1 (360 g/Mg KAX and 600 g/Mg Armac T) which results in a concentrate with

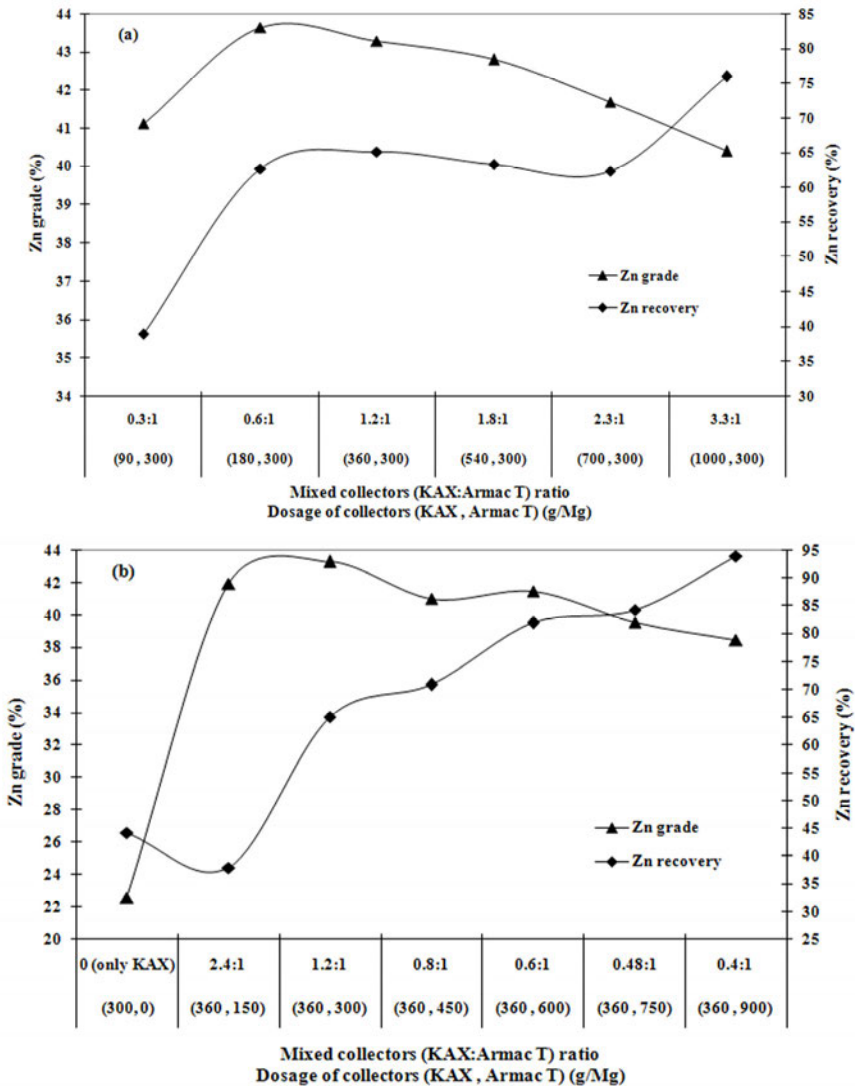


Fig. 9. Grade and recovery of Zn in smithsonite flotation concentrate as a function of mixed collectors ratio (Na_2S 7500 g/Mg, without depressant, pH = 11): (a) variation of KAX concentration, (b) variation of Armac T concentration

41.5% Zn grade and about 82% recovery. A comparison of results presented in Figs 6, 7 and 9 shows that the Zn grade and recovery of the concentrate obtained using mixed collector (KAX and Armac T) are lower than those produced by Armac T alone. However, more experiments indicated that using SH as a depressant reagent the Zn grade and recovery of the concentrate produced with mixed collector are improved a little but the results are not as good as obtained with Armac T alone.

Conclusion

From two amine collectors used in this study, Armac T acts a little more selectively than Armac C and results in smithsonite concentrate with higher Zn grade while Armac C is effective in enhancing the recovery of Zn. The KAX–Armac C mixed collector improves Zn grade and recovery of the smithsonite concentrate while the KAX–Armac T one does not. The best concentrate with 43% Zn and 94% recovery is obtained using the KAX–Armac C mixed collector at a mixture ratio of KAX:Armac C as 2:1 (300 g/Mg KAX and 150 g/Mg Armac C). The improvement of Zn grade and recovery is probably related to the co-absorption of KAX and Armac C when they are used as a mixed collector. The presence of KAX increases the Armac C adsorption due to the decrease in the electrostatic head–head repulsion between the surface and ammonium ions and increase in the lateral tail–tail hydrophobic bonds (Hosseini and Forsberg, 2007). The reason why the mixture of KAX with Armac T does not have positive effect on the smithsonite flotation concentrate should be investigated comprehensively. The decrease of collectors consumption and also no requirement of any depressant reagents are other advantages of the studied xanthate-amine (KAX-Armac C) mixed collector.

References

- ABRAMOV A.A., 1961. *Use of cationic agents for oxide lead–zinc minerals*. Chemical Abstracts 55, 26910f.
- BARBERY G., CECILE J.L., PLICHON V., 1977. *The use of chelates as flotation collectors*. In: Proceeding of XII International Mineral Processing Congress, Sao Polo, pp. 19–34.
- BILLI M., QUAI V., 1963. *Development and results obtained in the treatment of zinc oxide ores at AMMI mines*. In: XI International Mineral Processing Congress, Cannes, pp. 631–649.
- CHEN A., ZHAO Z.W., JIA X., LONG S., HUO G., CHEN X., 2009. *Alkaline leaching Zn and its concomitant metals from refractory hemimorphite zinc oxide ore*. Hydrometallurgy (97) 228–232.
- EJTEMAEI M., IRANNAJAD M., GHARABAGHI M., 2011. *Influence of important factors on flotation of zinc oxide mineral using cationic, anionic and mixed (cationic/anionic) collectors*; Minerals Engineering 24 (13), 1402–1408.
- EJTEMAEI M., IRANNAJAD M., 2008. *Recovery of Zinc Oxide Minerals from Angooran Mining Tailings by Flotation*. MSc Thesis, Amirkabir University of Technology, Iran.
- FUERSTENAU M.C., PALMER B.R., 1976. *Anionic flotation of oxides and silicates flotation*. In: Gaudin, A.M. (Ed.), Memorial Volume, vol. 1. American Institute of Mining, Metallurgical and Petroleum Engineers, New York, pp. 148–196.
- FUERSTENAU M.C., MILLER J.D., KUHN M.C., 1985, *Chemistry of Flotation*, SME, New York.
- GAUDIN A.M., 1957. *Flotation*. McGraw Hill Inc., New York. pp. 182–189.
- HERRINGTON K.L., KALER E.W., MILLER D.D., ZASADZINSKI J.A., CHIRUVOLU S., 1993. *Phase behaviour of aqueous mixtures of dodecyltrimethylammonium bromide (DTAB) and sodium dodecyl sulfate (SDS)*. Journal of Physical Chemistry 97 (51), 13792–13802.
- HERRERA URBINA R., SOTILLO F.J., FUERSTENAU D.W., 1999. *Effect of sodium sulfide additions on the pulp potential and amyl xanthate flotation of cerussite and galena*. International Journal of Mineral Processing 55 (3), 157–170.

- HOSSEINI S.H., FORSSBERG E., 2006a. *Adsorption studies of smithsonite flotation using dodecylamine and oleic acid*, Minerals and Metallurgical Processing, Processing SME 23 (2), 87–96.
- HOSSEINI S.H., FORSSBERG E., 2006b. *Flotation behaviour of oxide zinc ore from Angooran deposit, Iran in the presence of cationic/anionic and mixed (cationic/anionic) collectors*. European Journal of Mineral Processing and Environmental Protection 6 (3), 1–2.
- HOSSEINI S.H., FORSSBERG E., 2007. *Physicochemical studies of smithsonite flotation using mixed cationic/anionic collector*, Minerals Engineering 20 (6), 621–624.
- IRANNAJAD M., EJTEMAEI M., GHARABAGHI M., 2009. *The effect of reagents on selective flotation of smithsonite–calcite–quartz*. Minerals Engineering (20), 621–624.
- IRANNAJAD M., 2007. *Recovery of zinc from low grade zones of Angouran mine (research project)*, Department of Mining and Metallurgical Engineering, Amirkabir University of Technology.
- KEQING F.A., MILLER J.D., GUANG-HUI Li, 2005. *Sulfidization flotation for recovery of lead and zinc from oxide–sulfide ores*. Transactions of Nonferrous Metals Society of China (15), 1138–1147.
- KIERSZNICKI T., MAJEWSKI J.J., MZYK J., 1981. *5-Alkylsalicyladdoximes as collectors in flotation of sphalerite, smithsonite and dolomite in a Hallimond tube*. International Journal of Mineral Processing 7, 311–318.
- MARABINI A.M., CIRIACHI M., PLESCIA P., BARBARO M., 2007. *Chelating reagents for flotation*. Journal of Minerals Engineering 20, 1014–1025.
- MARABINI A.M., ALESSE V., GARBASSI F., 1984. *Role of sodium sulfide, xanthate and amine in flotation of lead–zinc oxidized ores*, Reagents in the mineral industry, The Institute of Mining and Metallurgy, 1984:125.
- MCKENNA W.J., LESSELS V., PETERSSON E.C., 1949. *Froth flotation of oxidized zinc ores*, United States, Patent: 2482859.
- MEHDILO A., ZAREI H. and IRANNAJAD M.; 2010. *Concentration of Iranian low grade zinc ore*, International Mining Congress and Exhibition. 18–21 October, Tehran, Iran.
- NAGANO J., TANAKA M., SAITO K., 1975. *Flotation of zinc oxide ore*. Chemical Abstracts 83, 31384.
- NAGANO J., TANAKA M., SAITO K., 1974. *Ore flotation*. Chemical Abstracts 82, 114571.
- ONAL G., BULUT G., GUL A., KANGAL O., PEREK K.T. and ARSLAN F.; 2005. *Flotation of Aladag^o oxide lead–zinc ores*, Minerals Engineering (18) 279–282.
- PEREIRA C.A., PERES A.E.C., 2005. *Reagents in calamine zinc ores flotation*, Minerals Engineering 18, 275–277.
- PERES A.E.C., BORGES A.M., GALERY R., 1994. *The effect of dispersion degree on the floatability of an oxidized zinc ore*. Minerals Engineering 7 (11), 1435–1439.
- REY M., 1953. *The flotation of oxidized ores of lead copper and zinc*. In: *Recent Developments in Mineral Dressing Symposium*. IMM, London, pp. 541–548.
- REY M., 1979. *Memoirs of milling and process metallurgy: 1 – flotation of oxide ores*. Institution of Mining and Metallurgy, Section C 88, 245–250.
- RINELLI G., MARABINI A.M., 1973. *Flotation of zinc and lead oxide-sulfide ores with chelating agents*, Inst. Min. Met. In: Proc. X International Mineral Processing Congress, London, pp. 493–521.
- SALUM M.J.G., DE ARAUJO A.C. and PERES A.E.C., 1992. *The role of sodium sulfide in amine flotation of silicate zinc minerals*; Minerals Engineering, 5, 411–419.
- YAMADA M., SHOJI T., ONADA T., SHIMOHIZAKA J., 1976. *Flotation of zinc carbonate*. Chemical Abstracts 84, 182894.
- YAMAZAKI S., MATUSI N., OHTSUBO E., 1978. Chemical Abstracts 89, 63078.

Received May 21; reviewed; accepted July 7, 2012

ANALYSIS OF CHROMITE PROCESSING PLANT DATA BY FIRST ORDER AUTOREGRESSIVE MODEL

Adem TASDEMİR

Department of Mining Engineering, Division of Mineral Processing, Eskişehir Osmangazi University, 26480, Eskişehir, Turkey. E-mail: atasdem@ogu.edu.tr, Tel: +90 222 239 37 50 ext: 3438.

Abstract: Many mineral processing data can be monitored by a time series model. This research presents results of analysis and simulations of a chromite processing plant data determined by time series model. The plant data obtained by shift to shift include feed grade, concentrate grade, tailing grade, Cr/Fe ratio in concentrate. All the chromite processing data were found stationary over time. The autocorrelation was high for feed grade and Cr/Fe ratio. Weaker autocorrelation was observed for concentrate grade and tailing grade. Autoregressive integrated moving average (ARIMA, 1,0,0) or first order autoregressive (AR, 1) model, was found to fit all data very well. The models obtained have been also shown to be used for the near future estimation of these data. The time constant which is an indicator of sampling frequency of the data sets were determined. It was found that sampling frequency was enough for concentrate and tailing grade and their original values can be used in process control charts for monitoring. On the other hand, the sampling frequency should be reduced for feeding grade and Cr/Fe ratio for the same aims hence ARIMA residual charts were more suitable to monitor their values.

Keywords: *time series, autoregressive model, time constant, process control, chromite processing*

Introduction

Although process data at any time are determined by process conditions, there are random or probabilistic data which can only be characterized by statistical methods (Gleit 1985). In mineral processing plants, many data are obtained over time. The performance of a mineral processing plant can be evaluated by analyzing these data. The analysis of the resulting data properly is a very important step in understanding plant's performance (Ketata and Rockwell, 2008). A set of observations in time sequence is defined as a time series (Ganguli and Tingling, 2001). The data from mineral processing plants may be evaluated by applying times series models since the data structure is identical to the time series form. In some processes, these observations are

correlated. Many quality characteristic values are a good example of a time series that is correlated in time domain (Ganguli and Tingling, 2001).

Time series analysis models are very useful in modeling dynamic systems in science and engineering applications (Capodaglio, et al., 1992). This class of models is in fact able to represent the dynamic features of physical systems that are subject to often uncontrollable inputs with random components. Mineral processing plants can also be considered as examples of dynamic systems, with inputs (ore characteristics, feeding and flow, organic loads, etc.) that vary stochastically within more or less wide ranges. The use of stochastic models allows a more detailed representation of the dynamic nature of these systems, while retaining the degree of information contained in most deterministic models (Capodaglio, et al., 1992). A fundamental utility of these models is their ability to forecast the level of the process into the future, accounting for its recent history and the underlying stochastic nature (Ganguli and Tingling, 2001).

In quality control, the production achieved can be collected under two headings by taking into consideration the type and nature of it. If production can be measurable, can be weighted and can be expressed in a unit with one or more of these feature, it can be mentioned that the production is continuous. Otherwise, there is a discrete manufacturing process. However, continuous and discrete concepts in time series are determined according to whether the observation values are obtained from equal time intervals or not. In other words, if the observation values making time series are obtained from unequal time intervals, the series occurred are defined as continuous time series. If the observations are obtained at equal or certain time intervals, they are known as discrete time series (Kaya, 1995). Even where the observations carried out continuously, the observation for the specific time intervals or based on the total value or can be converted by means of sampling to discrete continuous series.

Trybalski and Cieply (2000) stated that most mineral processing unit operations are in principle continuous processes but the majority of continuous processes such as mineral processing plants can be regarded as discrete. Therefore, the processes of mineral processing can be regarded as discrete processes which can be described with time series (Trybalski and Cieply, 2000). Some applications of time series models for mineral/metal processing plants have been reported in the literature for different aims. Examples can be given such as the investigation of dynamic characteristics of the flotation circuits (O'Keefe et al., 1981), the coal data from preparation plants (Cheng et al., 1982), the SO₂ stack emissions from coal boilers (Gleit, 1985), modeling of daily data of metal grade or recovery (Napier-Munn and Meyer, 1999), estimation of world copper production (Kutlar and Elevli, 1999), the copper ore flotation (Trybalski and Cieply, 2000), analyzing and modeling the behavior of operators of ilmenite reduction furnaces (Bazin et al., 2000), the coal segregation control (Ganguli and Tingling, 2001) and the variables of stream materials and sampling errors (Ketata and Rockwell, 2008). The time series models have been also used for the statistical process control charts of autocorrelated data of mineral processing/mining applications (Samanta and

Bhattacharjee, 2001; Bhattacharjee and Samanta, 2002; Samanta, 2002; Eleveli et al., 2009; Taşdemir, 2012)

The autoregressive integrated moving average, called as ARIMA time series models in short, are perhaps the most popular methods to evaluate a process variable and to make estimation for the future. The ARIMA time series models capture the stochastic characteristics of the fluctuations in a quality levels over time (Ganguli, and Tingle, 2001).

The purpose of this study was threefold. First aim was to determine if the first order autoregressive time series model, ARIMA(1,0,0) or AR(1), can be used an appropriate time series model in monitoring and analyzing the four types of data obtained from a chromite processing plant and to test the performance of models in the near future forecasting. The next purpose was to determine the time constants of data sets obtained from AR(1) models to test adequacy of sampling frequencies of data. The last aim was to show how weak and moderate autocorrelation of datasets affect the Shewhart charts of individual observations for the process control of these data sets.

Autoregressive (AR) time series models

Autoregressive (AR) time series models are called according to referring to the past period by the number of observations containing the value in the AR models. If AR model contains one observation values in the past period it is called as first order AR model. If it contains two value of the past period of observation, it is called the second order AR model. In general, p -order AR model contains p historical value of the observation period in question. Let X_1, X_2, \dots, X_t be stationary time series (such as feeding Cr_2O_3 grade, tailing Cr_2O_3 grade, concentrate Cr_2O_3 grade etc.) The object of this modeling approach is to derive an expression for X_t , the value of the series at time t , in terms of values of the series from the past, i.e at times $t-1, t-2$, etc. (Cheng at al., 1982). There must be some totally random shocks a_t entering the model at time t due to the random fluctuations in the series. General expressions of the AR (p) model are as follows (Montgomery et al., 2008):

$$X_t = \delta + \phi_1 X_{t-1} + \phi_2 X_{t-2} + \dots + \phi_p X_{t-p} + \varepsilon_t \quad (1)$$

$X_t, X_{t-1}, X_{t-2}, \dots, X_{t-p}$ are the observation values. The $\phi_1, \phi_2, \dots, \phi_p$ are the model parameters which are termed the autoregressive constants $\delta = \left(1 - \sum_{i=1}^p \phi_i\right) \mu$ with μ denot-

ing the process mean, p is the order of model, ε_t is a random shock which is independent error term which reflects the amount of variation in the data which is not explained by the AR model and is assumed to follow a normal distribution with mean zero and variance, σ_e^2 , which is termed white noise variance (WNV). A random shock is a random variable that is independent of all past history (Gleit, 1985). It accounts for any inherent variance in the data.

In practice, the first and second-order AR models commonly used as models and they are shown as AR (1) and AR (2) in short respectively. In AR (1) model, an observation value at t period of a time series is explained by observation value of X_{t-1} at $t-1$ period of time series and an error term. The variability associated with a chromite property, X , is subject to correlated and random elements. This stochastic process is modeled by autoregressive model of order one (i.e., an AR(1) process) with the equation:

$$X_t = \delta + \varphi X_{t-1} + \varepsilon_t \quad (2)$$

where: X_t – measurement at time t ,

X_{t-1} – measurement at time $t-1$,

$\delta - (1 - \varphi) \mu$, μ is the process mean

φ – autocorrelation coefficient ($-1 < \varphi < 1$),

ε_t – error term, normal random shock at time t .

The AR (1) model implies that each observation depends on the previous one to an extent defined by φ (Napier-Munn and Meyer, 1999). The autoregressive parameter, φ , is a measure of the autocorrelation between the past data point X_{t-1} and the current data point of X_t .

Autocorrelation

Autocorrelation in a time series, meaning the correlation between current observations (X_t) and observation from p periods before the current one (X_{t-p}) (Montgomery et al., 2008). In a given series, the autocorrelation at lag p which ranges from -1 to $+1$ is the correlation between the X_t , and X_{t-p} pairs and is given by:

$$r_p = \frac{\sum_{t=1}^{n-p} (X_t - \bar{X})(X_{t+p} - \bar{X})}{\sum_{t=1}^n (X_p - \bar{X})^2} \quad (3)$$

Theoretical autocorrelation functions (ACFs) and partial autocorrelation functions (PACFs) (autocorrelations versus lags) are available for the various models chosen. Many important conclusions about a time series can be made according to the correlograms which a plot of sample ACFs/PACFs versus lags obtained for a data set when choosing an appropriate time series model. More details can be found in Montgomery et al (2008). For example, ACF of a characteristic AR model slowly approaches zero and its PACF spikes at lag p . Therefore, the model is most probably characterized by ARIMA (1,0,0) or AR(1) when there is a significant spike only at lag 1 of the PACF (partial autocorrelation between X_t and X_{t-1}) and the ACF slowly declines.

The Time Constant (T)

Rius and Callao (2001) and Callao and Rius (2003) used the time constant (T) that is related to the behavior of AR(1). The T parameter is calculated by the following equation for the AR(1) model:

$$T = -\frac{1}{\ln \phi_1} . \quad (4)$$

The time constant is an indicator which controls the appropriateness of sampling frequency. It provides a time constant for eliminating autocorrelation if the frequency of analysis can be decreased. When it equals to 1, we can conclude that the sampling frequency might be enough. If T is equal to two, the sampling frequency can probably be cut by half. In case of its value 3, it means that it can probably be cut by a third. The data autocorrelation disappears when the sampling frequency decreases (Rius and Callao, 2001; Callao and Rius, 2003). The time constant of the system indicates the sampling frequency that must be reduced to apply control charts to the original data. In other words, the time constant of time series obtained by Eq. 4 is used to determine whether sampling frequency is correct (Rius and Callao, 2001).

Methodologies

The data sets were obtained from a chromite processing plant in Turkey to monitor changes shift by shift, in four dataset characteristics in 30 days time period. These are Cr_2O_3 per cent of feeding ore, concentrate Cr_2O_3 content, tailing Cr_2O_3 content and Cr/Fe ratio of concentrate. Three shifts in a day are applied at the plant. Therefore, 93 observations in total for each data set which was collected from December 1 to December 31, 2011 were obtained and used in the study.

Since the observation values obtained from chromite production process have occurred from the measurements in each shift, these observations have been obtained at equal time intervals. Therefore, the time series obtained was a series of discrete time series. However, the observation values that the continuous observation characteristic features carry measurable. The ARIMA model data sets can be used.

For each data set, the model parameters of time series were estimated by applying ARIMA time series model (known as Box-Jenkins model). Software of Minitab 16 and trial version of Statgraphics Centurion XVI were used for the statistical analyses of data sets. The time series models which have the lowest AIC (Akaike Information Criterion) values are selected for representing the best model for each data set. The residuals of the models were evaluated by residual analysis. The near future forecasting performances of the models were also performed by comparing the real data with estimated data. In addition, effect of Shewhart charts of individual observations were compared with the \bar{X} control charts based on ARIMA residuals to examine the effect of autocorrelation on the performance of the Shewhart chart. The time constants of

data sets required for the estimation of sampling frequency to reduce the autocorrelation for the usage of original data with control charts were also determined.

Results and discussions

Autocorrelation and Time Series Models

The time series of four data sets are shown in Fig. 1. Mineral processing plant production data often exhibit great variability with time (Napier-Munn and Meyer, 1999). Napier-Munn and Meyer (1999) stated that most mineral processing data moves around, both from day to day in an apparently random fashion and in short or long-term trends or cycles, even if over a long period the mean remains approximately constant. We can see all these statements on the time series plots presented in Fig. 1. There are two major kinds of time series. The one is the stationary time series which both the mean and variance of the values remain stable over time. The other one is the non-stationary time series which the mean or variance, or both, change with time. By applying a difference process, a non-stationary series can make a stationary series (Huang et al., 2002). As it can be seen clearly, all chromite data sets exhibit a stationary behavior over time and there is no trend and no need to a difference process to the data.

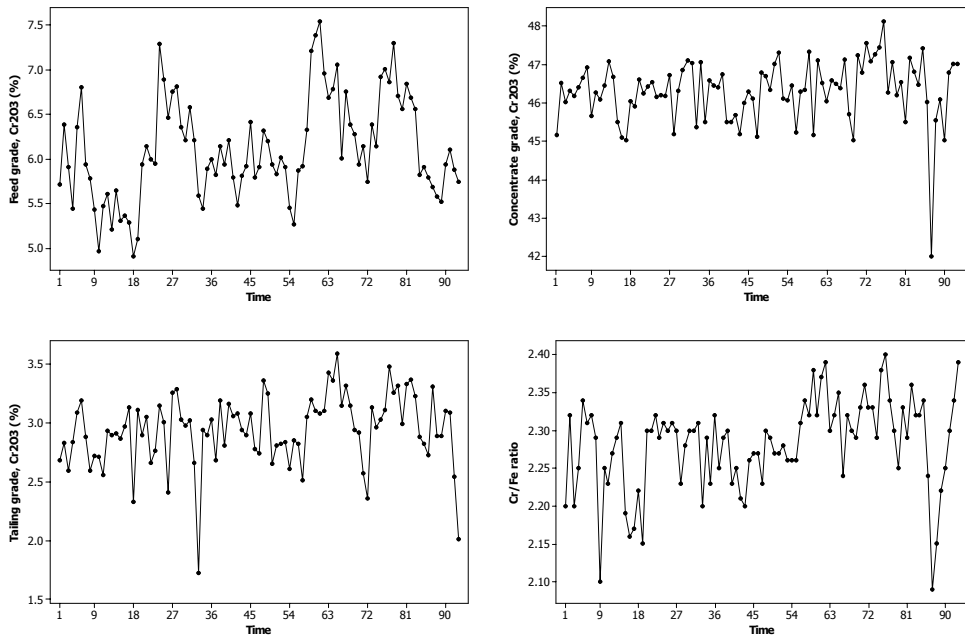


Fig. 1. Time series plots of four data sets of chromite processing plant

For the stationary control of the time series of four chromite data, their ACF plots are also generated and presented in Fig. 2. It is seen that these ACF patterns of data sets show typical stationary time series, because they are cutting off or tailing off near zero after a few lags. There are significant autocorrelations at first lag for feeding

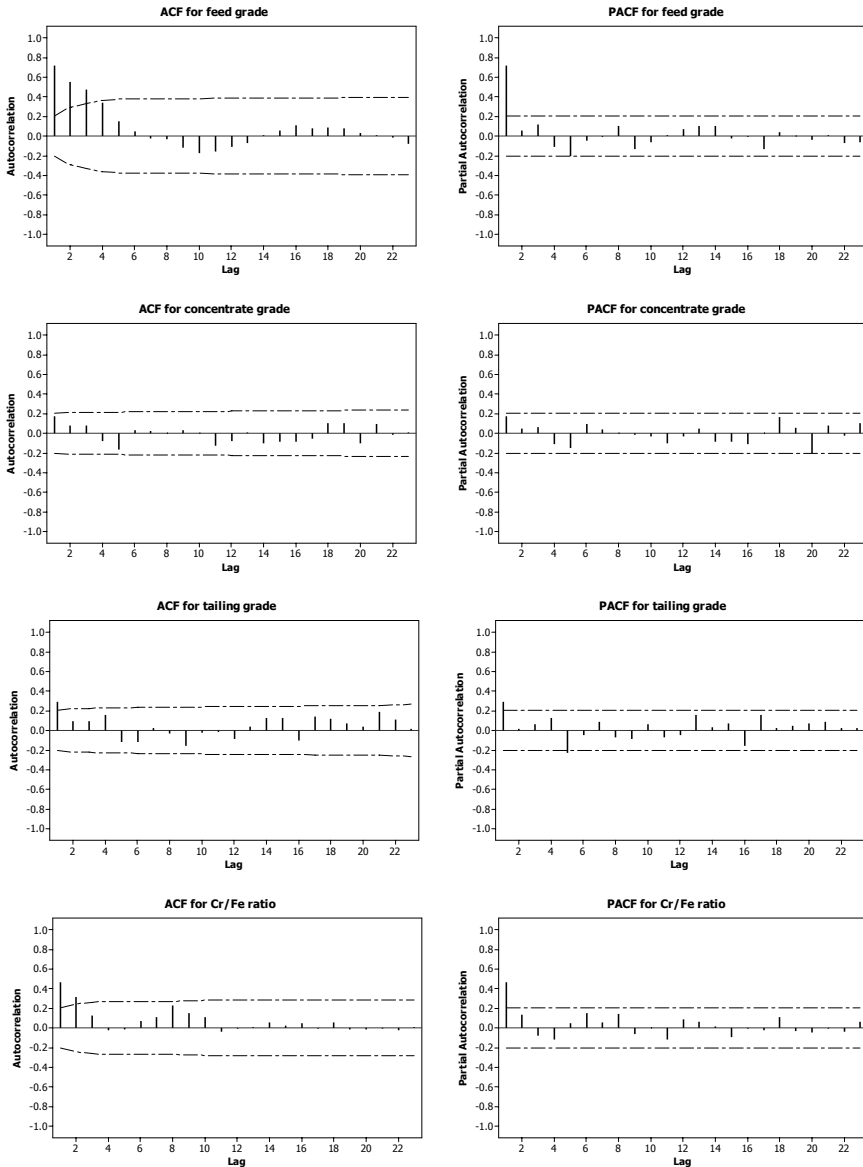


Fig. 2. Autocorrelation (ACF) and partial autocorrelation (PACF) functions for four chromite data sets with 5% significance limits

grade ($r_p = 0.728$) and Cr/Fe ratio ($r_p = 0.493$). The tailing grade ($r_p = 0.327$) and concentrate grade ($r_p = 0.178$) exhibited weaker autocorrelation compared to other two datasets. Moreover, ACF values of data sets decrease or decay very quickly (Fig. 2). In contrary, a non-stationary time series decay very slowly and exhibits sample autocorrelations that are still father large even at long lags (Montgomery et al., 2008). Therefore, it can be concluded that they are all may be considered as stationary time series. There exists serial autocorrelation of chromite processing data over one shift time intervals.

According to the PACF plots of datasets in Fig. 2, they all followed the AR(1) model since they all, except concentrate grade, show a significant spike (significant autocorrelation) at lag 1 followed by no apparent pattern meaning that all the higher-order autocorrelations are effectively explained by the lag 1 autocorrelation. When the PACF displays a sharp cutoff while the ACF decays more slowly as in the Fig. 2, the series displays an AR signature and the autocorrelation can be explained more easily by AR terms (Montgomery et al., 2008). The statistical test results also confirmed that the data sets except concentrate grade data, are best described by the AR(1) model according to the automatic time series model selection module of Statgraphics software taking into lowest AIC (Akaike Information Criterion) value.

The AIC is a function of the variance of the model residuals, penalized by the number of estimated parameters. In general, the model that minimizes the mean squared error without using too many coefficients is selected. As seen in Fig. 2, the concentrate grade data has little autocorrelation value which can be ignored. It is found to be best described by constant mean or ARIMA (0,0,0) time series model having an AIC value of -0.3942 . On the other hand, the AR (1) model which has an AIC value of -0.3936 was found the second best model for this data set. Considering the very small differences between the two AIC values, the AR(1) model which was the best for other data sets was also used in this study for the concentrate grade data. The parameters of the AR(1) models for the four datasets are summarized in Table 1. According to the t values and corresponding p values, all data sets have p -values smaller than 0.05 indicating the suitability of model parameters. Only p value of autocorrelation for concentrate grade was 0.089 but it was also accepted to use the AR(1) model to evaluate the results according to the reasons explained above.

We obtained the following AR(1) models for the four data sets in the form:

$$X_t = 0.726X_{t-1} + 1.669 \text{ (feed grade),}$$

$$X_t = 0.176X_{t-1} + 38.131 \text{ (concentrate grade),}$$

$$X_t = 0.325X_{t-1} + 1.981 \text{ (tailing grade),}$$

$$X_t = 0.485X_{t-1} + 1.175 \text{ (Cr/Fe ratio).}$$

Table 1. Parameters in AR(1) models for four datasets

Feed grade, Cr ₂ O ₃ %				
Parameter	Estimate	Std. Error	<i>t</i>	<i>p</i> -value
AR(1)	0.726	0.072	10.105	0.000
Mean, μ	6.101	0.145	42.109	0.000
Variance, σ	0.329			
WNV, σ_e^2	0.158			
Constant, δ	1.669			
Time constant, <i>T</i>	3.123			
Box-Pierce Test based on first 36 autocorrelations				0.949
Concentrate grade, Cr ₂ O ₃ %				
Parameter	Estimate	Std. Error	<i>t</i>	<i>p</i> -value
AR(1)	0.176	0.102	1.719	0.089
Mean, μ	46.297	0.100	460.308	0.000
Variance, σ	0.659			
WNV, σ_e^2	0.647			
Constant, δ	38.131			
Time constant, <i>T</i>	0.576			
Box-Pierce Test based on first 36 autocorrelations				0.609
Tailing grade, Cr ₂ O ₃ %				
Parameter	Estimate	Std. Error	<i>t</i>	<i>p</i> -value
AR(1)	0.325	0.105	3.097	0.003
Mean, μ	2.933	0.044	67.255	0.000
Variance, σ	0.092			
WNV, σ_e^2	0.084			
Constant, δ	1.981			
Time constant, <i>T</i>	0.889			
Box-Pierce Test based on first 36 autocorrelations				0.114
Cr/Fe ratio				
Parameter	Estimate	Std. Error	<i>t</i>	<i>p</i> -value
AR(1)	0.485	0.093	5.234	0.000
Mean, μ	2.282	0.010	221.911	0.000
Variance, σ	0.004			
WNV, σ_e^2	0.003			
Constant, δ	1.175			
Time constant, <i>T</i>	1.382			
Box-Pierce Test based on first 36 autocorrelations				0.930

WNV – White noise variance

Residual Analysis of AR(1) Models

Diagnostic checks of the residuals of four data sets through sample ACF plots and residuals plots are presented in Fig. 3 and in Fig. 4, respectively. Plots imply that we have a good fit for all the data sets. The Box-Pierce (*Q*-statistics) of the residuals for the data sets in Table 1 is based on the sum of squares of the first lag 36 autocorrelation coefficients. Since the *p*-values for this test are greater than 0.05 for all data sets,

we can conclude that the residual series are random at the 95% level. These results are confirmed by the ACF graphs of residuals for four data sets as shown in Fig. 3 since the examinations of ACF graphs of the residuals did not differ from the conclusions of Box-Pierce tests.

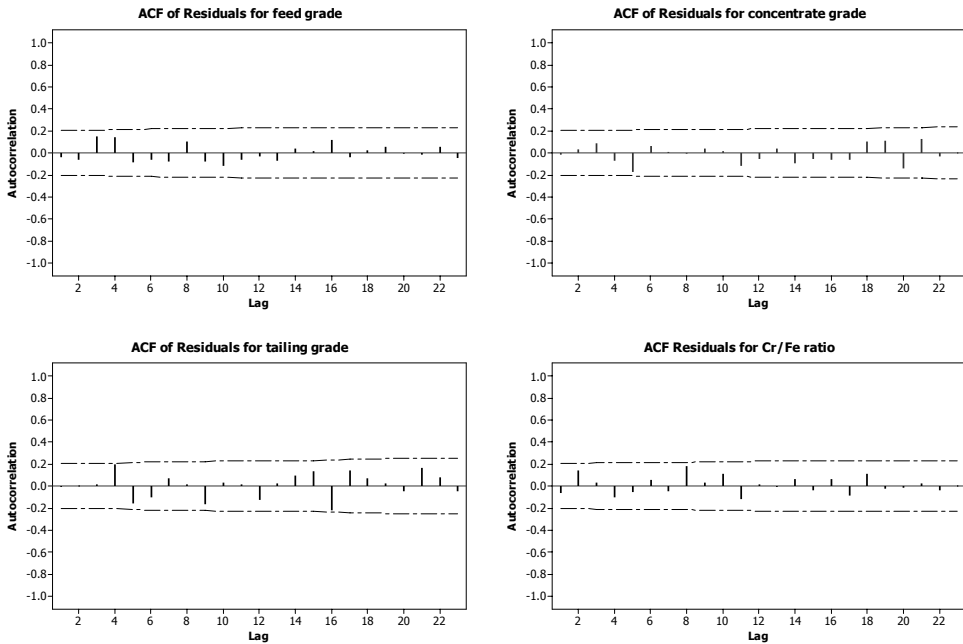


Fig. 3. Autocorrelation functions (ACF) for the residual values obtained from AR(1) models with 5% significance limits

Figure 4 plots the residuals for the time series models that fit the four chromite data. In these plots, four types of residual presentation format obtained by Minitab software are given. The plots in the upper left-hand portion of the display are a normal probability plot of the residuals. The residuals of data sets lie generally along a straight line, so the normality assumptions are satisfied properly. According to the histograms of the residuals presented in the lower left plots in Fig. 4, they do not give any serious indication of nonnormality. The upper right plots are the residuals versus the fitted values. These plots indicate the ideal patterns with essentially random scatter in the residuals. If these plots had exhibited a funnel shape, it could be indicate problems with the equality of variance assumption (Montgomery et al., 2008). The lower right plots are the plots of the observations in the order of the datasets. If these were of the order in which the data were collected, or if the data were a time series, this plot could reveal information about how the data may be changing over time.

According to the all results regarding to the residuals of the AR(1) models, the models can be used for the forecasting and process control charts.

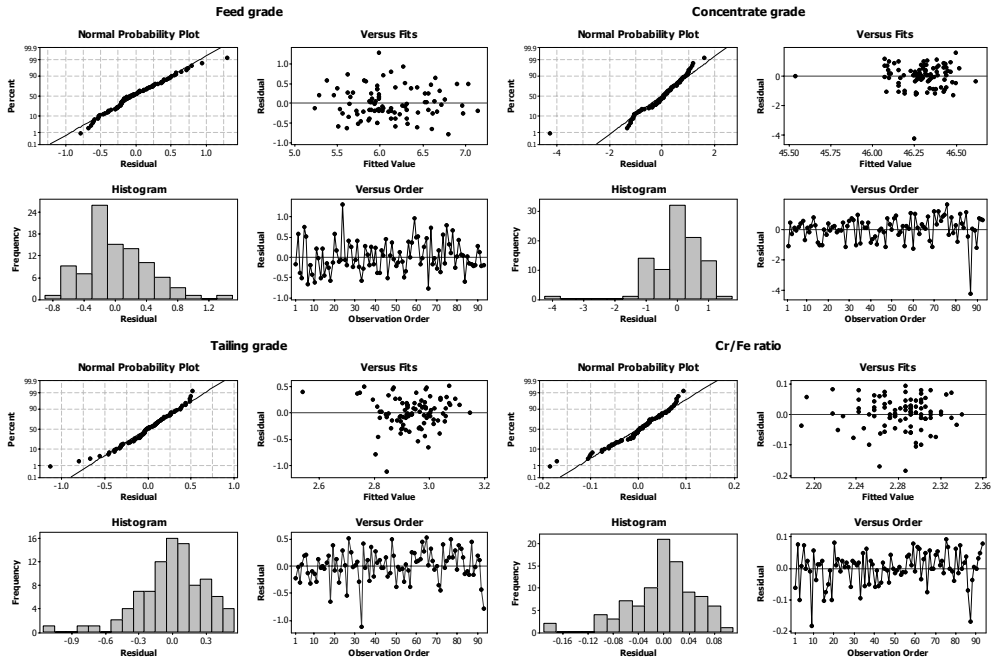


Fig. 4. Residual plots from AR(1) models for four chromite datasets

AR(1) Model Fits to Datasets and Forecasting Performances

The AR(1) time series models to capture the stochastic characteristics of the fluctuations in the four chromite data sets over time and their forecast values using these models are given in Fig. 5. As it can be seen in the actual versus fits plots, the selected AR(1) models of datasets follow the actual data closely. As a result, the plots do not reveal any problems with AR(1) model fits to the original data of chromite data sets. These results are consistent with literature. Some mineral and mineral processing data have been shown to be modeled by simple a AR(1) model. For example, Napier-Munn and Meyer (1999) showed that mineral processing plant performance data of daily metal recovery or concentrate grade followed a first order autoregressive time series model, AR(1), for a zinc flotation plant. Meyer and Napier-Munn (1999) have shown that dependence in the daily gold feed grade and gold recovery data can be described by the AR(1) model. Eleveli et al (2009) has also found recently that the AR(1) model was a suitable model for the contents of $B_2O_3\%$ at the two colemanite concentrator plants in Turkey. Similarly, Bhattacharjee and Samanta (2002) have shown that $Al_2O_3\%$ and $SiO_2\%$ constituents of a bauxite ore can be estimated by a simple AR(1) model. However, it does not mean that all mineral processing data can only be modeled by an universal AR(1) model since other time series models such as ARMA for flotation (Trybalski and Cieply, 2000), ARMA for SO_2 emissions (Gleit, 1985) and ARMA and ARIMA models for coal data (Taşdemir, 2012) have been also reported

depending on the nature of the data. Several coal data sets were found to fit often AR(1) models but not always (Cheng et al., 1982).

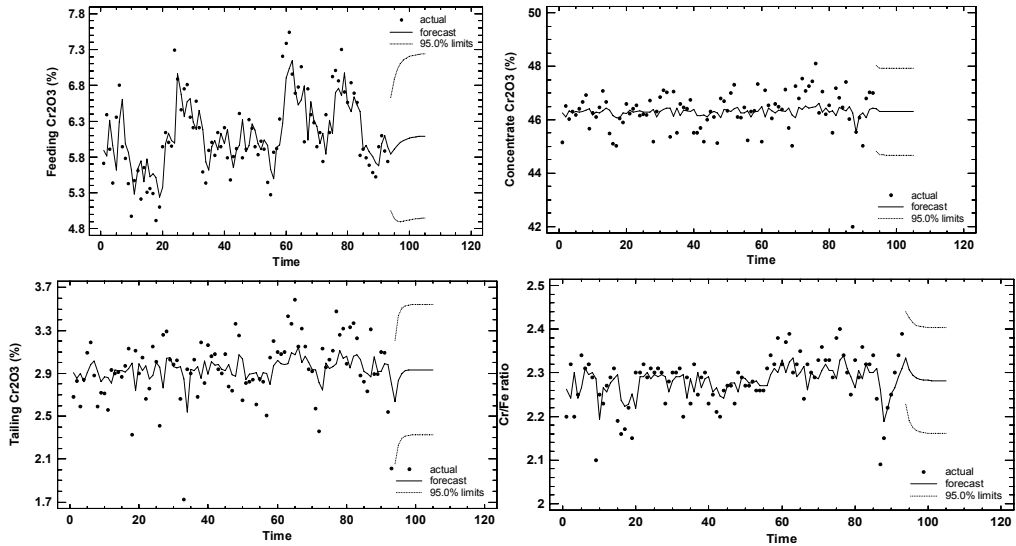


Fig. 5. Actual values versus fits plots by AR(1) models with four days estimation within 95% confidence limit

To test the performances of AR(1) models, the real data of last twelve shifts data values (observation values from 82 to 93 shifts) were estimated by the models for each data set and these results were compared to real data values. Shown in the plots of Fig. 6 are the results obtained within 95% confidence limits. As seen clearly from these plots, the results are very good for feed grade and tailing grade since most estimated data points are near to real values and all estimated points are within the 95% limits. The results can be also considered well for the other data sets. However, there is an unusual point in these plots exceeding the 95% limits. The unusual point at shift 87 is below the control limit for concentrate grade and Cr/Fe ratio. Since the variability of the chromite feeding grade does not change and within the confidence limits in the twelve shifts, this unusual point may be attributed to the measurement/analysis errors or unusual plant working conditions of plant at 87th shift rather than variability of the chromite.

In the plots in Fig. 5, we can also see the forecasting lines drawn from estimation points with their 95% confidence intervals for future 4 days (12 shifts) after 30 days (after shift 93). According to the above results, the estimation of near future values of four variables can be made conveniently by applying their AR(1) models. Therefore, it is possible to make any preventive and corrective actions for the quality characteristics of chromite by using AR(1) models since these models can also forecast for the near

future of any data using past data of the processes. Estimation for the future values of data sets can reduce the operating costs.

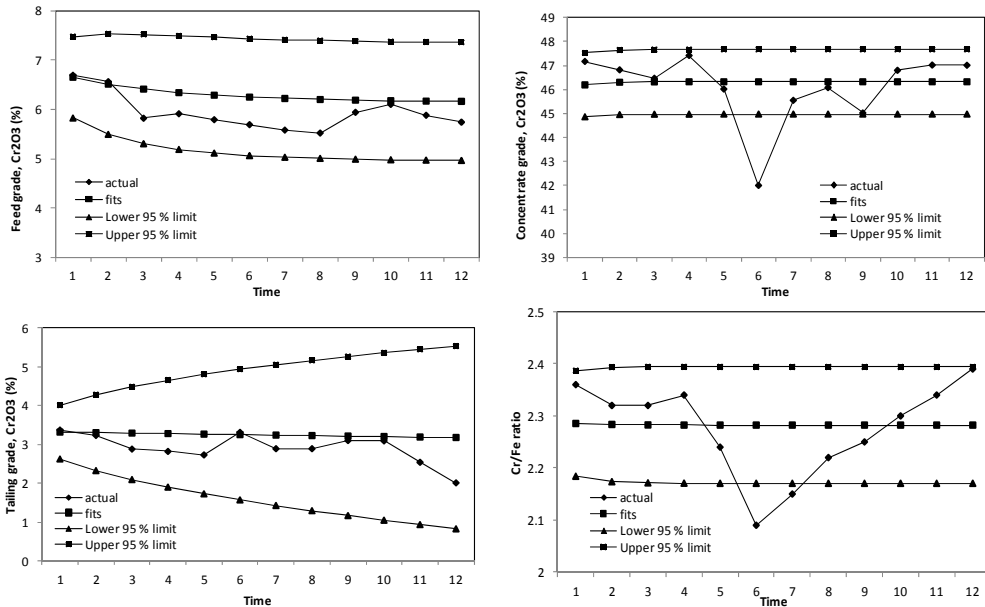


Fig. 6. Estimation of dataset values by AR(1) models versus actual values for the 82–93 shifts

Time Constant and Individual Control Charts of Original Data and ARIMA Residuals

The time constant (T) was found to be 3.123 for the feed grade implying that the frequency of measurements need to be reduced by dividing it by 3 to eliminate the autocorrelation. Other T values were found as 1.38, 0.889 and 0.576 for the Cr/Fe ratio (Table 1), tailing grade and concentrate grade respectively. These results revealed that sampling frequency needs to be reduced by dividing approximately by 1.5 for the Cr/Fe ratio. Since the T values are smaller than 1, there is no need to reduce sampling frequency for tailing grade and concentrate grade. For fast fluctuating processes as in the concentrate grade and tailing grade, T is small and simple ACF decays quickly to zero (Callao and Rius, 2003). However, fast fluctuations are more common in the concentrate grade data which has the smallest time constant.

The effect of autocorrelation may cause wrong decisions for the monitoring of data by statistical process control charts (SPCs). Its effect has been shown also important for many mineral processing/mining applications of SPCs (Samanta and Bhattacharjee, 2001; Bhattacharjee and Samanta, 2002; Samanta, 2002; Elevli et al., 2009; Taşdemir, 2012). Figure 7 compares the individual charts of Shewhart and ARIMA residuals (special cause charts) with additional Western Electric rules which are applied to improve the efficiency of control charts for small shifts. The number of Western

Electric rules applied was four as the same in our previous study (Taşdemir, 2012). The details of the method can be found elsewhere (Montgomery and Runger, 2011). The values of data sets were presented as normalized on the y axes these plots to make the comparisons easily. Since our data sets had different autocorrelation degree, this analysis showed the efficiency of the Shewhart charts of individual observations on the four data sets of chromite processing plant having from weak to moderate autocorrelations.

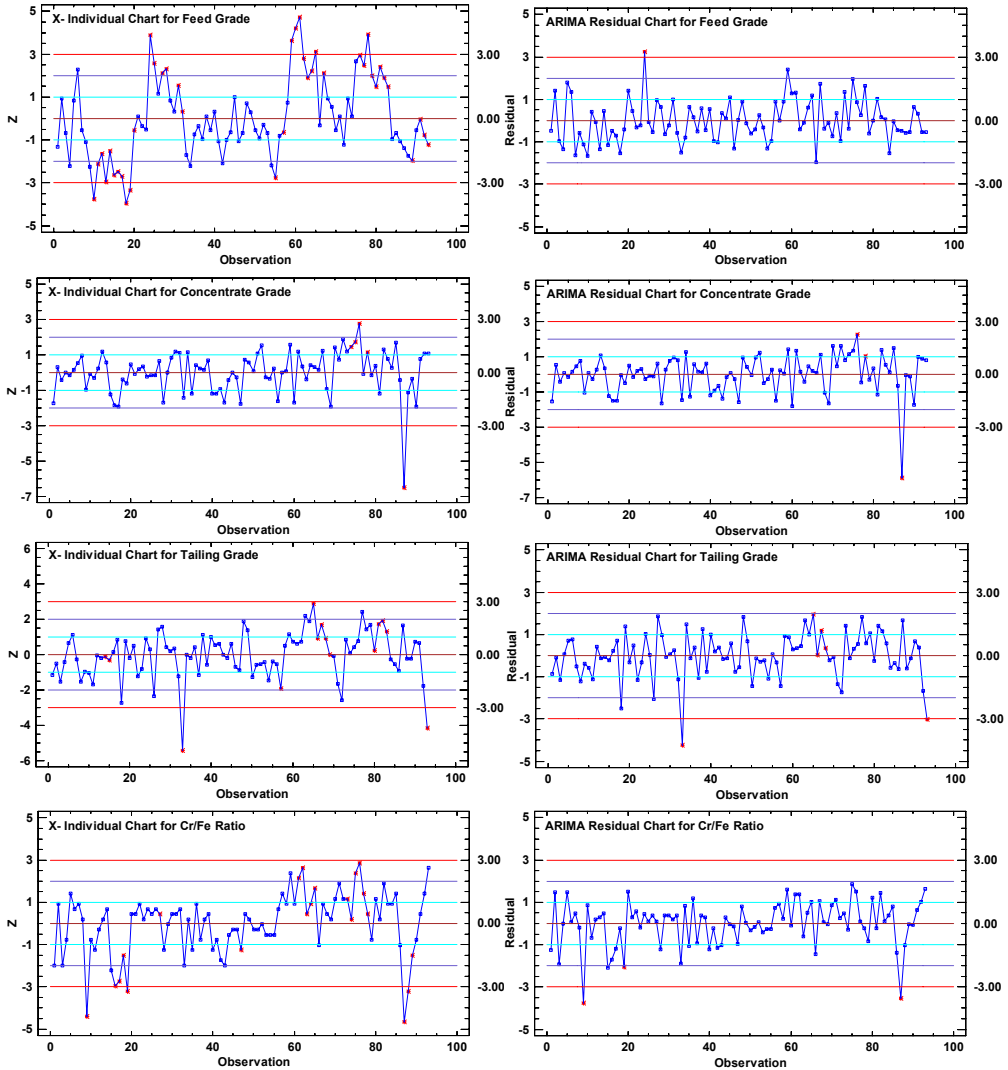


Fig. 7. Comparison of individual and ARIMA residual control charts of four chromite data sets

The Shewhart individual chart performs better when the datasets exhibit weak autocorrelation as in the case of concentrate grade and tailing grade. It shows almost the same results with ARIMA residual charts of individuals for these two data. However, when the autocorrelation increases, the number of wrong out of control points increases in the charts of original data compared to their ARIMA residual charts. These effects can be seen clearly on comparative charts of Cr/Fe ratio and feed grade variables. The Shewhart individual chart also performed weaker for Cr/Fe ratio data which has moderately autocorrelated data to catch the right out of control points. It showed the worst performance for the feed grade data which has the highest autocorrelation between the data sets when it is compared with its ARIMA residual chart. Only one point was out of control according to the residual chart while this number in original data was 39 points with Western Electric rules applied. This would cause wrong decisions about the homogeneity of chromite ore feed to plant. Almost the same wrong conclusion can be given when the Cr/Fe ratio with original data was evaluated by the Shewhart individual chart. The number of out of control points was 3 in the ARIMA residual chart of individual although it was 21 in the individual chart. The performance of the Shewhart individual chart has been shown better for weak positive and negative autocorrelation and got worse with increasing autocorrelation (Karaođlan and Bayhan, 2011). These results clearly indicate and reconfirm that autocorrelation must be taken into account when applying Shewhart individual chart whether the process is under control or not since wrong decisions can be given for the process control applications.

Meyer and Napier-Munn (1999) confirmed that the data dependence or autocorrelation can be reduced in mineral processing plants by increasing sampling frequency or sampling intervals. Reversely, the autocorrelation between the data obtained can be increased by decreasing the sampling frequency or sampling intervals. In this situation, time constants which are obtained by the AR(1) models may provide a tool for eliminating autocorrelation which is something that must be considered if we can decrease the frequency of the analysis (Rius and Callao, 2001). It has been suggested by the Rius and Callao (2001) and Callao and Rius (2003) that time constants can be used to reduce the autocorrelation for applying the Shewhart individual chart to the original data. It is seen that the original data of concentrate grade and tailing grade can be used for control charts. It was determined that sampling frequencies needs to be reduced for feed grade and Cr/Fe ratio variables by cutting 3 and 1.5, respectively, to use their original values with control chart. Rius and Callao (2001) concluded that sampling frequency is decreased in order to apply control charts to the original data. They also stated that the decrease in the sampling frequency has the advantage since there may not need to use time series models once the optimum frequency has been established. However, they also took attention that a drawback would be detected later. This finding is especially right for the mineral processing systems since there are many causes of the data variability including the error in sampling and grade and real variation in performance due to changes in ore mineralogy. Small changes in ore mineralogy of

feed material may not be determined by using long sampling intervals. As a result, reducing the sampling frequency may cause a drawback due to the inefficiency in homogeneity control of the feed grade properly since the feeding is made as a mixture of ores from different chromite mines. In conclusion, usage of autocorrelated data and AR(1) residuals seem to be a more suitable approach to control the homogeneity in the feed grade with control charts.

Conclusions

In this study, an analytical technique, time series, was used to quantify the correlated and random components of the variability in four variables of chromite data. The data of feed grade and Cr/Fe ratio values were found more moderately autocorrelated than the other data sets over time. The data from the concentrate grade exhibited weakest autocorrelation than the other data sets. The ARIMA (1,0,0) or AR (1) models were found to fit well for all data sets obtained from a chromite processing plant. The sample ACF plots as well as further residual plots of the AR(1) models of data sets revealed that no autocorrelation was left in the data and the models give reasonable fits for all data sets. AR(1) is the first order model indicating that their values are strongly dependent on their previous measurements. The model considers the autocorrelation between measurements and random shock error term that cannot be explained by the model.

The AR (1) time series models can accommodate the autocorrelated nature of chromite dataset levels when estimating parameters to characterize the process. It is shown that the AR(1) models can be used to forecast the near future estimation of data sets investigated. Only one point was out of 95% confidence limits on the actual and estimated plots for concentrate grade and Cr/Fe ratio. The reasons may be attributed to the operating conditions and to the measurement errors since the homogeneity of feed grade was supplied by the plant for this point. Moreover, they also provide forecasting capability to take preventive actions that will be useful in process control.

The AR(1) model have been also shown a potential applications to be used for homogeneity control of feed grade, concentrate grade, tailing grade and Cr/Fe ratio in a chromite processing plant. Whether original data can be used or not may be determined by the degree of autocorrelation during the application of the Shewhart charts of individual to detect the right out of control points. The number of out of control points increases with increasing autocorrelation and this causes no suitability usage of original values with Shewhart charts. Consistent with literature, when time constant obtained by the autocorrelation of AR(1) model is smaller than 1, we can use original data, otherwise it is suitable to use the ARIMA residual charts to detect right out of control points for the data sets having higher time constants.

References

- BAZIN C., GIRARD B., HODOUIN D., 2000, *Time Series Analysis: A Tool for Operators Training? Application to the Direct Reduction of Ilmenite Concentrate*, Powder Technology, 108, 155–159.
- BHATTACHERJEE A., SAMANTA B., 2002, *Practical Issues in the Construction of Control Charts in Mining Applications*, The Journal of The South African Institute of Mining and Metallurgy, 173–180.
- CAPODAGLIO A.G., NOVOTNY V., FORTINE L., 1992, *Modelling wastewater treatment plants through time series analysis*, Environmetrics, 3(1), 99–120.
- CALLAO M.P., RIUS A., 2003, *Time Series: A Complementary Technique to Control Charts for Monitoring Analytical Systems*, Chemometrics and Intelligent Laboratory Systems, 66, 79–87.
- CHENG B.H., WOODCOCK B., SARGENT D., GLEIT A., 1982, *Time Series Analysis of Coal Data from Preparation Plant*, Journal of Air Pollution Control Association, 32(11), 1137–1141.
- ELEVLİ S., UZGÖREN N., SAVAS M., 2009, *Control Charts for Autocorrelated Colemanite Data*, Journal of Scientific & Industrial Research, 68: 11–17.
- GLEIT A., 1985, *SO₂ Emissions and Time Series Models*, Journal of Air Pollution Control Association, 35(2), 115–120.
- GANGULI R., TINGLING J.C., 2001, *Algorithms to Control Coal Segregation Under Non-Stationary Conditions. Part II: Time Series Based Methods*, International Journal of Mineral Processing, 61, 261–271.
- HUANG Z., MUMAR R., YINGLING J., SOTTILE J., 2002, *Coal Segregation Control for Meeting Homogeneity Standards*, International Journal of Mineral Processing, (submitted manuscript, (<http://home.engineering.iastate.edu/~rkumar/PUBS/coal2.pdf>).
- KARAOĞLAN A.D., BAYHAN G.M., 2011, *Performance Comparison of Residual Control Charts for Trend Stationary First Order Autoregressive Processes*, Gazi University Journal of Science, 24(2):329–33.
- KAYA A., 1995, *Outlier Analysis in Time Series Used for Statistical Process Control*, MSc Thesis in Statistics of Ege University (in Turkish).
- KETATA C., ROCKWELL M.C., 2008, *Stream Material Variables and Sampling Errors*, Mineral Processing & Extractive Metall. Rev., 29, 104–117.
- KUTLAR A., ELEVLİ S., 1999, *Estimation of World Copper Production with Linear Time Series*, Madencilik, 38(4), 43–55 (in Turkish).
- MEYER D., NAPIER-MUNN T.J., 1999, *Optimal Experiments for Time-Dependent Mineral Processes*, Austral. & New Zeland J. Statist. 41(1), 3–17.
- MONTGOMERY D.C., JENNINGS C.L., KULAHÇI M., 2008, *Introduction to Time Series Analysis and Forecasting*, Wiley Series in Probability and Statistics.
- MONTGOMERY D.C., RUNGER G.C., 2011, *Applied Statistics and Probability for Engineers*, Fifth Edition, John Wiley&Sons, Inc.
- NAPIER-MUNN and MEYER D.H., 1999, *A Modified Paired t-Test for the Analysis of Plant Trials with Data Autocorrelated in Time*, Minerals Engineering, 12(9), 1093–1100.
- O'KEEFE K., SELBY W., SUTHERLAND D.N., 1981, *An Analysis of the Dynamic Characteristics of Flotation Circuits by Time-Series Analysis*, International Journal of Mineral Processing, 8(2), 147–163.
- RIUS A., CALLAO M.P., 2001, *Application of Time Series Models to the Monitoring of a Sensor Array Analytical System*, Trends in Analytical Chemistry, 20(4), 168–177.
- SAMANTA B., BHATTACHERJEE A., 2001, *An Investigation of Quality Control Charts for Autocorrelated Data*, Mineral Resources Engineering, 10: 53–69.

- SAMANTA B., 2002, *Multivariate Control Charts for Grade Control Using Principal-Component Analysis and Time Series Modelling*, Trans. Inst. Min. Metall. (Sect A: Min Technol), 307: 149–157.
- TAŞDEMİR A., 2012, *Effect of Autocorrelation on the Process Control Charts in Monitoring of a Coal Washing Plant*, Physicochemical Problems of Mineral Processing, 48(2), 495–512.
- TRYBALSKI K., CIEPLY J., 2000, *ARMA Type Model for Copper Ore Flotation*, Proceedings of the XXI International Mineral Processing Congress, C3(72–78).

Received May 13, 2012; reviewed; accepted July 7, 2012

STATISTICAL ANALYSIS OF THE RELATIONSHIP BETWEEN PARTICLE SIZE AND PARTICLE DENSITY OF RAW COAL

Tomasz NIEDOBA

AGH University of Science and Technology, al. Mickiewicza 30, 30–059 Kraków,
e-mail: tniedoba@agh.edu.pl.

Abstract: The paper presents a multidimensional analysis of mineral processing feeds consisting of different amounts of different size and density fractions. The considered feed was coal which was screened into size fractions which were subsequently separated into density fractions and their weights determined. The feed material was characterized with commonly used size and density frequency and cumulative distribution plots and next approximated with the Weibull (size) and logistic (density) mathematical functions. Having the contribution of each particle size and density fraction in the feed a two-dimensional analysis of the feed size/density properties was performed using two methods. The first one is based on the best chosen cumulative frequency function for two random variables and the second uses the so-called Morgenstern family functions. In the paper the undependability of the particles size and density was investigated using statistical approach based on the so-called χ^2 test, and the correlation between these parameters using the so-called *F*-Snedecor statistical test. In both cases it was found that particles size and density of the investigated coal particles were dependent what means that with growth of particle size its density grew too and there was correlation between them regardless of significance level assumed for the analysis.

Keywords: *approximation, coal, multidimensional analysis, statistical tests, particle size, density*

Introduction

In mineral processing operations particle properties influence separation results (Kelly and Spottiswood, 1989). In the case of coal the most important parameters are size and density. However, it is not easy to describe precisely properties of coal taking into account both properties simultaneously. Traditional methods of multidimensional statistical analysis are not always sufficient to describe well the material. Also, the data are not always complete and any kind of forecast is not precise. There is also a question regarding significance of the relation between coal particle size and density. In

this work an attempt was undertaken to answer this question, taking coal, type 31 in Polish classification system, as an example.

Experimental

Coal, type 31 in Polish classification, called also energetic coal, contained 66% C. It originated from one of the Polish coal mines and was screened on a set of sieves of following sizes: -1.00, -3.15, -6.30, -8.00, -10.00, -12.50, -14.00, -16.00 and -20.00 mm. Then, the size fractions were additionally separated into density fractions by separation in dense media using zinc chloride aqueous solution of various densities (1.3, 1.4, 1.5, 1.6, 1.7, 1.8 and 1.9 g/cm³). The fractions were used as a basis for further consideration.

Coal characteristics

The size fractions of investigated coal are presented in Table 1 while frequency and cumulative size distributions are presented in Figs 1a and 1b.

Table 1. Sieve analysis of investigated coal

Sieve number <i>i</i>	Size fraction $d_{i-1} - d_i$, mm	Average particle size d_{av} , mm	Percentage retained $f_i(d_{av})$	Cumulative percent retained $F_i(d_i)$	Calculated from Eq. (1) $\Phi_1(d_i)$
1	0-1.00	0.500	16.43	16.43	16.47
2	1.00-3.15	2.075	27.80	44.23	38.56
3	3.15-6.30	4.725	28.05	72.28	66.35
4	6.30-8.00	7.150	6.76	79.04	80.46
5	8.00-10.00	9.000	4.52	83.56	87.06
6	10.00-12.50	11.250	6.42	89.98	92.14
7	12.50-14.00	13.250	2.83	92.81	94.85
8	14.00-16.00	15.000	3.54	96.35	96.56
9	16.00-20.00	18.000	3.65	100	98.22

Table 1 and Fig. 1b also show approximation of the cumulative particle size distribution with the Weibull formulae:

$$\Phi_1(d) = 1 - \exp\left(-\left(\frac{d_i}{4.33}\right)^{0.978}\right) \quad (1)$$

where $\Phi_1(d)$ denotes cumulative percent of material weight passing a given mesh and d_i is the particle size expressed by the upper limit of size fraction. The contents 0.978

and 4.33 were found by least squared method. Figure 1a clearly shows that the distribution is asymmetrical.

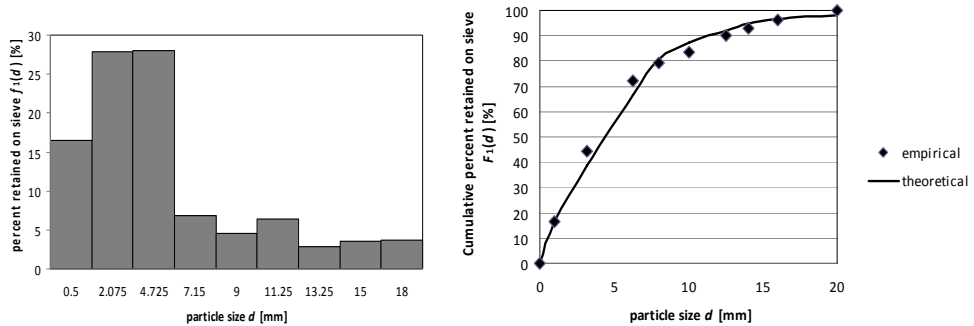


Fig. 1. Coal size distribution, a) frequency plot , b) cumulative plot

Each size fraction of coal was subjected to density analysis to determine content of different density fractions in each size fraction. The results are shown in Table 2 in the form of a matrix.

Table 2. Distribution (in weight %) of size and density fractions. The sum of all contributions is 100%

Size fraction $d_{i-1} - d_i$, mm	Density fraction $\rho_{j-1} - \rho_j$, g/cm ³						
	0–1.3	1.3–1.4	1.4–1.5	1.5–1.6	1.6–1.7	1.7–1.8	1.8–1.9
0–1.00	12.32	2.93	0.47	0.12	0.05	0.40	0.13
1.00–3.15	20.15	4.84	1.25	0.42	0.45	0.39	0.30
3.15–6.30	16.47	8.53	1.38	0.46	0.44	0.42	0.35
6.30–8.00	4.19	1.74	0.32	0.12	0.11	0.12	0.16
8.00–10.00	2.14	1.48	0.34	0.20	0.12	0.07	0.17
10.00–12.50	3.06	1.89	0.64	0.27	0.22	0.18	0.16
12.50–14.00	1.25	1.18	0.14	0.04	0.10	0.06	0.06
14.00–16.00	1.66	0.48	0.84	0.39	0.09	0.03	0.05
16.00–20.00	1.23	0.92	0.79	0.27	0.08	0.10	0.26

Having contributions of all size/density fractions it becomes possible to plot particle density distribution of the coal feed by summing up the contributions, for a given density fraction, different size fraction. The results of summation are shown in Fig. 2 and Table 3.

Table 3. Density analysis of investigated coal

$\rho_{j-1} - \rho_j$ [g/cm ³]	Average particle density ρ_{av} , mm	Fraction mass per- centage $f_2(\rho_{av})$	Cumulative mass percent $F_2(\rho_j)$	Calculated from Eq. (2) $\Phi_2(\rho_j)$
0–1.3	0.65	62.47	62.47	65.85
1.3–1.4	1.35	23.99	86.46	82.68
1.4–1.5	1.45	6.18	92.64	87.25
1.5–1.6	1.55	2.29	94.93	92.33
1.6–1.7	1.65	1.66	96.59	97.08
1.7–1.8	1.75	1.75	98.34	99.72
1.8–1.9	1.85	1.66	100	100

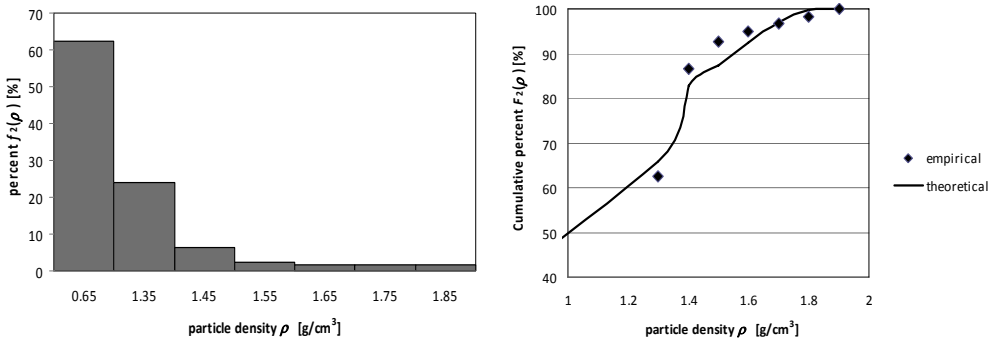


Fig. 2. Coal density fractions distribution, a) frequency plot , b) cumulative plot

The following logistic cumulative frequency function was used for approximation of the density cumulative distribution curve of investigated coal.

$$\Phi_2(\rho_j) = \left(\frac{1}{1 + 0.6616 \exp\left(-0.4687 \left(\frac{\rho_j}{1.9 - \rho_j}\right)\right)} \right) \quad (2)$$

where $\Phi_2(\rho_j)$ stands for cumulative percent of material mass and ρ_j denotes upper limit of a density fraction. The results of approximation are also shown in Table 3.

Two-dimensional cumulative frequency function

To find a relationship between particle size and particle density of investigated coal a two-dimensional cumulative frequency analysis is necessary. For this purpose it is convenient to modify Table 2 with the distribution of size and density fractions into cumulative form (Table 4).

Table 4. Cumulative contribution (content in weight %) of different size d_i and density ρ_j fractions in the coal feed (in statistics terms random variable of cumulative frequency function $F_0(d_i, \rho_j)$ describing the cumulative percent of fraction of size lower or equal d_i and density lower or equal ρ_j)

ρ_j $d_{i-1}-d_i$	ρ_{j-1}						
	0-1.3	1.3-1.4	1.4-1.5	1.5-1.6	1.6-1.7	1.7-1.8	1.8-1.9
0-1.00	12.32	15.25	15.72	15.84	15.89	16.30	16.42
1.00-3.15	32.47	40.24	41.90	42.49	42.99	43.77	44.23
3.15-6.30	48.94	62.54	68.34	69.34	70.27	71.47	72.28
6.30-8.00	53.13	71.15	74.57	75.69	76.73	78.04	79.05
8.00-10.00	55.26	74.77	78.53	79.85	81.02	82.41	83.55
10.00-12.50	58.32	79.72	84.12	85.70	87.09	88.66	89.98
12.50-14.00	59.57	82.15	86.70	88.33	89.92	91.45	92.80
14.00-16.00	61.23	84.29	89.68	91.71	93.29	94.95	96.32
16.00-20.00	62.46	86.46	92.64	94.93	96.59	98.34	100

The simplest way of approximation of two-dimensional cumulative frequency function $F_0(d, \rho)$ is its presentation as the product of two cumulative frequency functions for random variables d and ρ , what means that (Fisz, 1969; Hahn and Shapiro, 1994)

$$F_3(d, \rho) = \frac{F_1(d)F_2(\rho)}{100} \tag{3}$$

The results of distribution function $F_3(d, \rho)$ are presented in Table 5.

Table 5. Results of cumulative frequency function $F_3(d, \rho) = F_1(d)F_2(\rho)$

ρ_j $d_{i-1}-d_i$	ρ_{j-1}						
	0-1.3	1.3-1.4	1.4-1.5	1.5-1.6	1.6-1.7	1.7-1.8	1.8-1.9
0-1.00	10.26	14.20	15.22	15.60	15.87	16.15	16.43
1.00-3.15	27.63	38.24	40.97	41.98	42.72	43.50	44.23
3.15-6.30	45.15	62.49	66.96	68.62	69.81	71.08	72.28
6.30-8.00	49.38	68.33	73.22	75.03	76.34	77.72	79.04
8.00-10.00	52.19	72.24	77.40	79.31	80.70	82.16	83.55
10.00-12.50	56.21	77.80	83.36	85.42	86.91	88.49	89.98
12.50-14.00	57.96	80.22	85.96	88.08	89.62	91.25	92.79
14.00-16.00	60.17	83.28	89.06	91.43	93.03	94.72	96.32
16.00-20.00	62.47	86.46	92.64	94.93	96.59	98.34	100

To find the error of approximation the mean squared error was calculated using Eq. 4 (Dobosz, 2001)

$$s_r = \sqrt{\frac{\sum_{i=1}^k \sum_{j=1}^l (F_3(d_i, \rho_j) - F_0(d_i, \rho_j))^2}{N - 2}} \sqrt{2} \tag{4}$$

where N is number of fractions ($N = 63$), F_3 are values of calculated cumulative frequency function based on empirical values and F_0 are values of empirical cumulative frequency function. In this case the value of s_r was equal to 1,37. The small value of the error suggests that particle size d and density ρ may be independent, but as it occurred in the further part of the paper it is not true. When instead of empirical cumulative frequency functions $F_1(d)$ and $F_2(\rho)$ the approximations $\Phi_1(d)$ and $\Phi_2(\rho)$ will be used, given by equations (1) and (2) the function $\Phi_3(d, \rho)$ will be given by

$$\Phi_3(d_i, \rho_j) = \Phi_1(d_i) \Phi_2(\rho_j) \tag{5}$$

and

$$\Phi_3(d_i, \rho_j) = \left(1 - \exp\left(-\left(\frac{d}{4.33}\right)^{0.978}\right) \right) \left(\frac{1}{1 + 0.6616 \exp\left(-0.4687\left(\frac{\rho}{1,9 - \rho}\right)\right)} \right) \tag{6}$$

The results of distribution function $\Phi_3(d, \rho)$ are presented in Table 6.

Table 6. Results of cumulative frequency function $\Phi_3(d_i, \rho_j) = \Phi_1(d_i) \Phi_2(\rho_j)$

	ρ_{j-1}						
$\frac{\rho_j}{d_{i-1} - d_i}$	0–1.3	1.3–1.4	1.4–1.5	1.5–1.6	1.6–1.7	1.7–1.8	1.8–1.9
0–1.00	10.85	13.61	14.37	15.20	15.99	16.42	16.47
1.00–3.15	25.38	31.87	33.63	35.39	37.42	38.44	38.55
3.15–6.30	43.69	54.86	57.89	61.26	64.41	66.16	66.35
6.30–8.00	52.98	66.43	70.20	74.29	78.11	80.23	80.46
8.00–10.00	57.32	71.98	75.96	80.38	84.51	86.82	87.06
10.00–12.50	60.67	76.80	80.39	85.07	89.45	91.88	92.14
12.50–14.00	62.25	78.50	82.84	87.67	92.18	94.68	94.90
14.00–16.00	63.58	79.83	84.25	89.15	93.74	96.22	96.56
16.00–20.00	64.68	81.20	85.70	90.69	95.35	97.74	98.22

Comparing the results of empirical cumulative distribution function $F_0(d_i, \rho_j)$ and distribution function $\Phi_3(d_i, \rho_j)$ obtained by approximation, the mean standard error s_r value was equal to 4.18. A higher value of s_r is obvious because the errors of approximations of $\Phi_1(d)$ and $\Phi_2(\rho)$ influence the final result.

Application of the Morgenstern family of distribution functions

Another way to approximate cumulative frequency function F_0 is by using the so-called Morgenstern family functions, which are presented by equation (Balasubramanian and Beg, 1997; Firkowicz et al., 1977; Johnson and Kotz, 1972; Niedoba, 2009; 2011a; Niedoba and Tumidajski, 2008; Scaria and Nair, 1999; Tumidajski, 1997)

$$F_4(d, \rho) = F_1(d)F_2(\rho)(1 + \mu(1 - F_1(d))(1 - F_2(\rho))) \tag{7}$$

where μ is a fixing parameter, $\mu \in [-1, 1]$.

By using the least squared method (Firkowicz et al., 1977), by minimizing function $L(\mu) = \sum_{i=1}^n \sum_{j=1}^k [F_4(d_i, \rho_j) - F_0(d_i, \rho_j)]^2$, under condition that $\mu \in [-1, 1]$ it is possible

to calculate the value of μ

$$\mu = \frac{\sum_{i=1}^l \sum_{j=1}^k (F_0(d_i, \rho_j) - F_1(d_i)F_2(\rho_j)) F_1(d_i)F_2(\rho_j)(1 - F_1(d_i))(1 - F_2(\rho_j))}{\sum_{i=1}^l \sum_{j=1}^k (F_1^2(d_i, \rho_j)F_2^2(d_i, \rho_j)(1 - F_1(d_i))^2(1 - F_2(\rho_j))^2)} \tag{8}$$

Table 7. Results of cumulative distribution function $F_4(d, \rho)$ based on Eq. 7

ρ_j $d_{i-1} - d_i$	ρ_{j-1}						
	0-1.3	1.3-1.4	1.4-1.5	1.5-1.6	1.6-1.7	1.7-1.8	1.8-1.9
0-1.00	13.48	15.81	16.15	16.26	16.32	16.39	16.43
1.00-3.15	33.41	41.12	42.65	43.16	43.53	43.89	44.23
3.15-6.30	49.85	64.83	68.32	69.57	70.96	71.40	72.28
6.30-8.00	53.26	70.27	74.20	75.83	76.89	78.00	79.04
8.00-10.00	55.41	73.84	78.34	79.97	81.15	82.39	83.55
10.00-12.50	58.32	78.85	83.97	85.85	87.20	88.63	89.98
12.50-14.00	59.53	81.00	86.42	88.40	89.84	91.35	92.79
14.00-16.00	61.00	83.69	89.47	91.61	93.15	94.78	96.32
16.00-20.00	62.43	86.46	92.64	94.93	96.59	99.35	100

On the basis of the empirical data the value $\mu = 1$ was obtained what means that the cumulative frequency function is

$$F_4(d, \rho) = F_1(d)F_2(\rho)\left(1 + (1 - F_1(d))(1 - F_2(\rho))\right). \tag{9}$$

The results of approximation with $F_4(d, \rho)$ are presented in Table 7.

The error of approximation with $F_4(d_i, \rho_j)$ using the Morgenstern function was equal to 0.52. The application of the Morgenstern distribution function gave better results of approximation in comparison with the previous method. It suggests that there is a significant relation between particle size d_i and density ρ_j . When instead of empirical values the approximations functions $\Phi_1(d)$ and $\Phi_2(\rho)$ are applied the value of parameter μ is also equal to 1. The equation of function $\Phi_4(d, \rho)$ is given then by the following formulae

$$\Phi_4(d_i, \rho_j) = \Phi_1(d_i)\Phi_2(\rho_j)\left(1 + (1 - \Phi_1(d_i))(1 - \Phi_2(\rho_j))\right). \tag{10}$$

The values of cumulated frequency function $\Phi_4(d_i, \rho_j)$ are presented in Table 8.

Table 8. Results of cumulative frequency function $\Phi_4(d_i, \rho_j)$

ρ_j $d_{i-1} - d_i$	ρ_{j-1}						
	0–1.3	1.3–1.4	1.4–1.5	1.5–1.6	1.6–1.7	1.7–1.8	1.8–1.9
0–1.00	13.94	15.58	15.90	16.18	16.38	16.46	16.47
1.00–3.15	30.71	32.27	36.27	37.27	38.09	38.51	38.55
3.15–6.30	48.71	58.06	60.37	62.84	65.05	66.23	66.35
6.30–8.00	56.52	68.77	71.95	75.40	78.56	80.28	80.46
8.00–10.00	59.86	73.59	77.21	81.18	84.84	86.85	87.06
10.00–12.50	62.30	77.21	81.19	85.59	89.65	91.90	92.14
12.50–14.00	63.53	79.11	83.29	87.91	92.91	94.59	94.85
14.00–16.00	64.33	80.31	84.61	89.39	93.83	96.30	96.56
16.00–20.00	65.07	81.45	86.31	90.81	95.40	97.95	98.22

In this case the value of s_r is equal to 3.5. It is also smaller when compared to the approximation with function $\Phi_3(d_i, \rho_j)$. It also suggests that the particle size and density depend on each other. A comparison of all approximations is presented on Fig. 3.

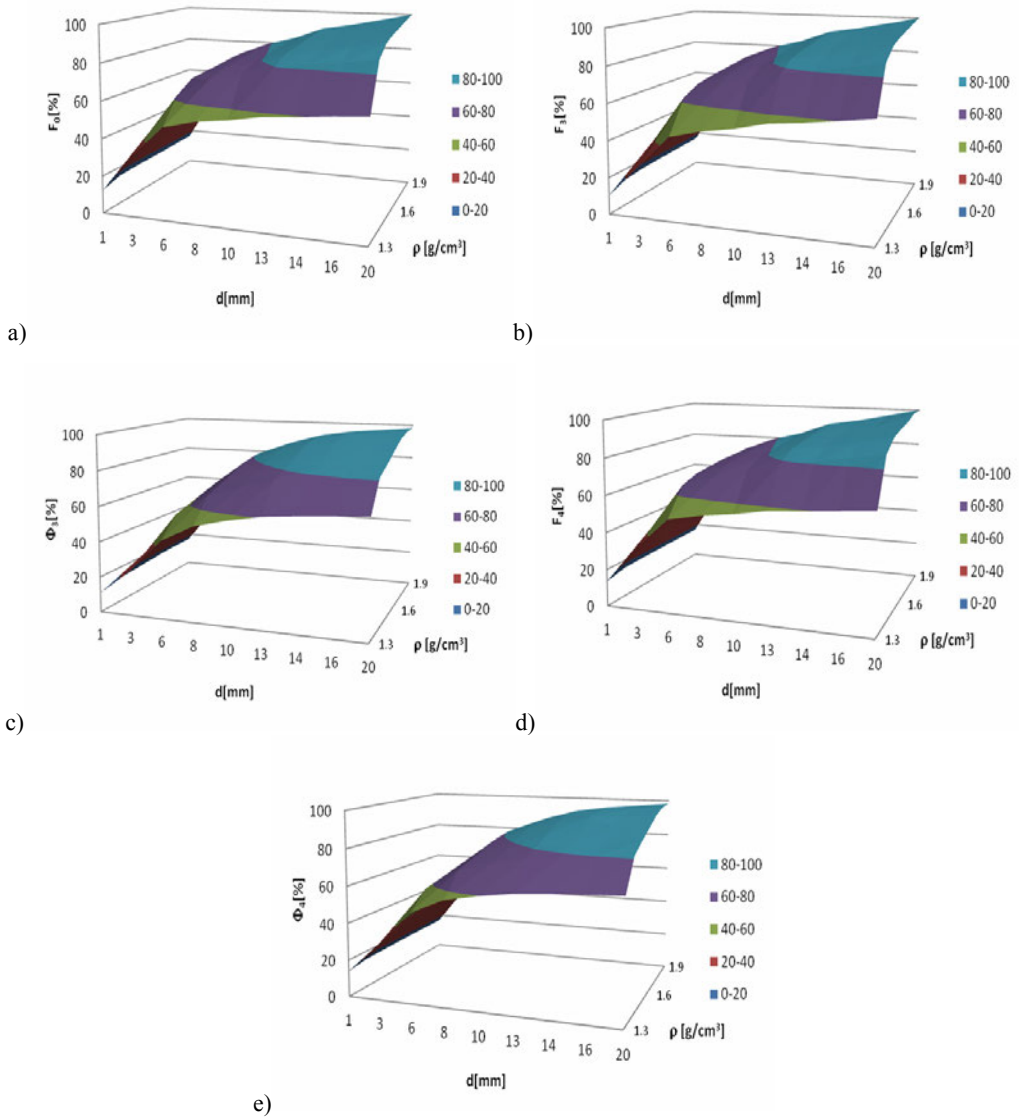


Fig. 3. A comparison of cumulative functions, a) empirical cumulative frequency function $F_0(d_i, \rho_j)$; b) cumulative frequency function $F_3(d_i, \rho_j)$; c) approximated function $\Phi_3(d_i, \rho_j)$; d) cumulative frequency function $F_4(d_i, \rho_j)$; e) approximated function $\Phi_4(d_i, \rho_j)$.

Verification of statistical hypotheses

By comparing the results of approximations it can be seen that they are quite similar. It is also proved by small values of s_r . There is a question regarding a potential relation between particle size and its density. It is not possible to apply directly known statisti-

cal independability tests to answer this question. Usually it must be assumed that all particles are cubic of length d . In this case the number of such particles N_{ij} in weight fraction ij , by density ρ_i is given by equation (11) (Saramak and Tumidajski, 2006).

$$N_{ij} = \frac{w_{ij}}{d_i^3 \rho_j} \tag{11}$$

where w_{ij} is the mass yield of fraction of size $d \in (d_{i-1}, d_i)$ and density $\rho \in (\rho_{j-1}, \rho_j)$.

The quantitative particle frequency for accepted assumptions and without the fraction of the finest particles is given by Table 9.

Table 9. Quantitative particle frequency without finest particles fraction

ρ_{j-1}, ρ_j	d_{i-1}, d_i							$n_j = \sum_{i=1}^5 N_{ij}$
	3.15–6.30	6.30–8.00	8.00–10.00	10.00–12.50	12.50–14.00	14.00–16.00	16.00–20.00	
1.4–1.5	910	160	79	56	11	36	16	1268
1.5–1.6	303	54	45	22	4	15	5	448
1.6–1.7	254	46	26	17	7	4	1	355
1.7–1.8	231	48	14	13	3	1	2	312
1.8–1.9	185	69	28	11	3	1	4	301
$n_i = \sum_{j=1}^7 N_{ij}$	1883	377	192	119	28	57	28	2684

where n_i is number of particles from i^{th} density fraction and n_j is number of particles from j^{th} size fraction.

To check the dependability of the random variables d and ρ the independability test χ^2 was used (Sobczyk, 2001), where

$$\chi^2 = \sum_{i=1}^5 \sum_{j=1}^7 \frac{(n_{ij} - np_{ij})^2}{np_{ij}} \tag{12}$$

and

$$p_{ij} = \frac{n_i \cdot n_j}{n^2} \tag{13}$$

where n is number of all particles and n_{ij} is number of particles in fraction (i, j) (according to Table 9), p_{ij} is theoretical probability for particles to be in certain fraction (i, j) . The statistics is based on χ^2 distribution function with $(j - 1)(i - 1)$ degrees of

freedom (Sobczyk, 2001), where j is a number of density fractions and i number of particle size fractions.

Due to the fact that the sample is large the statistics $U = \sqrt{2\chi^2} - \sqrt{2(i-1)(j-1)-1}$ can be applied, which is described by normal cumulative frequency function $N(0, 1)$ (Sobczyk, 2001).

On the basis of the empirical data $U = 3.7$ and the array values, given in normal cumulative frequency table (Sobczyk, 2001), $u_{\frac{\alpha}{2}} = 1.96$ for $\alpha=0.05$ and $u_{\frac{\alpha}{2}} = 2.58$ for $\alpha = 0.01$.

In both cases the inequality $U > u_{\frac{\alpha}{2}}$ is fulfilled what means that the hypothesis about undependability between random variables d and ρ should be rejected.

Let's check this conclusion on the basis of correlative relations between these variables, by means of equations (14) and (15) (Sobczyk, 2001).

$$\eta^2_{d|\rho} = \frac{\sum_i (\bar{d}(\bar{\rho}_i) - \bar{d})^2 n_i}{\sum_j (\bar{d}_j - \bar{d})^2 n_j} \tag{14}$$

$$\eta^2_{\rho|d} = \frac{\sum_j (\bar{\rho}(\bar{d}_j) - \bar{\rho})^2 n_j}{\sum_i (\bar{\rho}_i - \bar{\rho})^2 n_i} \tag{15}$$

where $\eta^2_{d|\rho}$ and $\eta^2_{\rho|d} \in [0, 1]$ are correlative relations. In case when the relation between investigated features is strong these values are close to 1, in case of lack of relation the values are close to 0; $\bar{\rho}$ – mean value of random variable P , \bar{d} – mean value of random variable D ; $\bar{\rho}(\bar{d}_j)$ – mean value of random variable P by condition that $d = \bar{d}_j$; $\bar{d}(\bar{\rho}_i)$ – mean value of random variable D by condition that $\rho = \bar{\rho}_i$.

The values of $\bar{\rho}(\bar{d}_j)$ and $\bar{d}(\bar{\rho}_i)$ were presented in Tables 10 and 11.

Table 10. The conditional mean values of particle density ρ (for chosen i^{th} particle size fraction)

\bar{d}_j	6.30	8.00	10.00	12.50	14.00	16.00	20.00
$\bar{\rho}(\bar{d}_j)$	1.62	1.65	1.63	1.61	1.64	1.55	1.6

Table 11. The conditional mean values of particle size d (for chosen j^{th} particle density fraction)

$\bar{\rho}_i$	1.5	1.6	1.7	1.8	1.9
$\bar{d}(\bar{\rho}_i)$	7.53	7.72	7.39	7.18	7.55

The mean values of random variables are $\bar{d} = 7.5$ and $\bar{\rho} = 1.62$ and the values of correlative relations are $\eta^2_{d|\rho} = 0.0056$ and $\eta^2_{\rho|d} = 0.0135$. To verify if there is correlation between random variables D and P the following statistical hypotheses can be checked:

$$H_0: \eta^2_{d|\rho} = 0 \text{ and } H_0: \eta^2_{\rho|d} = 0$$

The tests for these hypotheses are (Sobczyk, 2001), respectively:

$$G_I = \frac{\eta^2_{\rho|d}}{1 - \eta^2_{\rho|d}} \cdot \frac{n - i}{i - 1} \text{ and } G_{II} = \frac{\eta^2_{d|\rho}}{1 - \eta^2_{d|\rho}} \cdot \frac{n - j}{j - 1} \tag{16}$$

and are called the Snedecor tests (Sobczyk, 2011) which are described by the F -Snedecor cumulative frequency function with, respectively, $(i - 1, n - i)$ and $(j - 1, n - j)$ statistical degrees of freedom, where i is number of fractions for random variable d and j is number of fractions of random variable ρ . The values of calculated statistics and their respective array values are presented in Table 12.

Table 12. Values of F statistics compared with array values G_α

G_I	G_{II}	$G_{I\alpha}, \alpha = 0.05$	$G_{II\alpha}, \alpha = 0.05$	$G_{I\alpha}, \alpha = 0.01$	$G_{II\alpha}, \alpha = 0.01$
6.10	3.77	2.10	2.37	2.80	3.32

Because for both levels of significance level α the inequalities $G_I > G_{I\alpha}$ and $G_{II} > G_{II\alpha}$ occurred, the statistical hypotheses H_0 should be rejected so there is basis to state that between random variables ρ and d there is correlation. It can be then assumed that there is relation between these variables. In quantitative methods only the fractions of larger density were taken into consideration because for smaller fractions the number of particles would be too high (in millions) what would cause the use of the tests impossible. To take them into account in such investigation as our the fractions of small sizes and densities should be numerous and of small range. Similar cumulative frequency functions were obtained assuming that the particles have cubic shape. On the basis of the results of applied statistical methods it can concluded that for particles of larger sizes and densities there is a correlation between their density and size.

Conclusions

On the basis of investigation results the following conclusions can be made:

1. Only multidimensional statistical analysis of coal characteristics may give sufficiently full information about relations and influences caused by its certain fea-

tures. Apart from classical approach to this issue it is proposed to use many techniques to perform such analyzes, like applications of the Morgenstern family functions. The results of approximation proved that this is good way to get good description of the investigated material.

2. Apart from particle size and density taken into consideration in this paper as random variables also other coal features may be considered as ash contents or sulfur contents which are also very important from the coal quality point of view.
3. The obtained results may suggest that there is correlation between particle size and density of coal. The application of commonly used statistical tests proved that this hypothesis can be accepted.
4. Author suggests also to apply other multidimensional techniques as kriging method which was already applied to these purposes in other publications (Niedoba, 2010; 2011b).

Acknowledgements

The paper is the effect of scientific project No. 3390/B/T02/2011/40.

References

- BALASUBRAMANIAN K., BEG M.I., 1997, *Concominants of order statistics in Morgenstern type bivariate exponential distribution*, Journal of Applied Statistical Science, 54(4), 233–242.
- DOBOSZ M., 2001, *Statystyczna analiza wyników badań*, Akademicka Oficyna Wydawnicza Exit, Warszawa.
- FIRKOWICZ S. et al., 1977, *Metody statystyczne w sterowaniu jakością*, PWN, Warszawa.
- FISZ M., 1969, *Rachunek prawdopodobieństwa i statystyka matematyczna*, PWN, Warszawa.
- HAHN G.J., SHAPIRO S.S., 1994, *Statistical Models in Engineering*, John Wiley, New York.
- JOHNSON N.L., KOTZ S., 1972, *Distributions in Statistics, Continuous Multivariate Distributions*, John Wiley, New York.
- KELLY E.G., SPOTTISWOOD D.J., 1989, *The Theory of Electrostatic Separations, a Review, Part I. Fundamentals*, Minerals Engineering 2/1, 33–46.
- NIEDOBA T., 2009, *Wielowymiarowe rozkłady charakterystyk materiałów uziarnionych przy zastosowaniu nieparametrycznej aproksymacji funkcji gęstości rozkładów brzegowych*, Górnictwo i Geoinżynieria, 4, 235–244.
- NIEDOBA T., 2010, *Application of kriging in approximations of grained materials characteristics distribution functions*, in Proceedings of the XXV International Mineral Processing Congress, Brisbane, 3321–3326.
- NIEDOBA T., 2011a, *Three-dimensional distribution of grained materials characteristics*, in Proceedings of the XIV Balkan Mineral Processing Congress, Tuzla, 1, 57–59.
- NIEDOBA T., 2011b, *Zastosowanie krigingu zwyczajnego dla oszacowania zawartości popiołu i siarki w węgla w zależności od gęstości i rozmiaru ziarna*, Górnictwo i Geoinżynieria, 2, 159–166.
- NIEDOBA T., TUMIDAJSKI T., 2008, *Multidimensional analysis of coal separation processes*, in Proceedings of XXIV International Mineral Processing Congress, Beijing, 2, 2357–2364.
- SARAMAK D., TUMIDAJSKI T., 2006, *Rola i sens aproksymacji krzywych składu ziarnowego surowców mineralnych*, Górnictwo i Geoinżynieria, 3/1, 301–313.

- SCARIA J., NAIR N.U., 1999, *On concominants of order statistics from Morgenstern family*, Biometrical Journal, 41, 4, 483–489.
- SOBCZYK M., 2001, *Statystyka*, PWN, Warszawa.
- TUMIDAJSKI T., 1997, *Stochastyczna analiza własności materiałów uziarnionych i procesów ich rozdziałów*, Wydawnictwo AGH, Kraków.

Received July 9, 2012; reviewed; accepted August 10, 2012

EVALUATION OF ORGANIC CARBON SEPARATION FROM COPPER ORE BY PRE-FLOTATION

**Andrzej KONIECZNY, Witold PAWLOS, Małgorzata KRZEMINSKA,
Rafał KALETA, Paweł KURZYDŁO**

KGHM Polska Miedz S.A. Oddział Zakłady Wzbogacania Rud, Polkowice, Poland, r.kaleta@kghm.pl

Abstract: This paper describes possibilities of organic carbon matter separation during a pre-flotation stage in KGHM Polska Miedz, Division of Concentrators. The paper contains a survey of organic carbon removal technologies in worldwide plants as well as KGHM achievements in this field. Laboratory flotation testing results have also been described. Next, an industrial scale trial at Polkowice Concentrator has been conducted to confirm the previous laboratory results. The results have been discussed. They indicate a positive role of the pre-flotation stage on organic carbon removal using only frother as the flotation reagent.

Keywords: *flotation, carbonaceous matter, copper ore*

Introduction

The copper ore located in the for-Sudetic monocline, besides copper and silver, contains many other valuable chemical elements. The polymetallic character of the ore and produced by KGHM Polska Miedz SA flotation concentrates influences effectiveness of pyrometallurgical processes, mainly due to the presence of harmful impurities, for example lead and organic carbon (C_{org}).

The presence of shale, the source of carbonaceous matter in the ore, has also a negative effect on flotation and pyrometallurgical processes. The presence of clay minerals and organic carbon in shale makes the production of high quality flotation concentrates, without excessive loss of copper and other metals in the flotation tailing, difficult. The reason for the diminished concentrate quality is reporting of the shale particles into the concentrate leading to an increased yield and reduced concentrate quality. Therefore, the concentrate quality, represented by the copper content, is of great significance.

On the basis of technological indices it is possible to show that the increased amount of shale in the flotation concentrate leads to a decrease of beneficiation efficiency. This also leads to an increase of unwanted elements such as arsenic, lead, organic matter in the concentrate. Greater amounts of shale complicate copper ore concentration process and cause lower copper recovery at the assumed concentrate grade (Skorupska et al., 2011).

The increasing content of C_{org} , observed in the flotation concentrate throughout the years, is also of significant importance for effectiveness of subsequent pyrometallurgical processes. An increased organic carbon in the final flotation concentrate does not cause much problem for the copper production in the shaft furnace located in Legnica and Glogow, since its presence, due to energy release, is to some degree beneficial, while the C_{org} content exceeding 8% for the one-stage flash furnace disrupts the thermal balance of concentrate melting, effectively decreasing the flash furnace efficiency and increased production cost (Kijewski et al., 2010).

According to KGHM Polska Miedz S.A. strategy, the goal of copper production is a complete replacement of the shaft furnace with the flash smelting technology. Currently, there are two different, shaft furnace and flash smelting technologies, which complement each other, making concentrate management possible. However, due to the target implementation of only flash smelting furnaces in the plant, actions have been taken in order to match the chemical composition of the concentrate for the flash furnace with a focus on appropriate contents of C_{org} , Pb, and S, because the amount of concentrate processed is determined by its calorific value. This requires the furnace feed to have an appropriate composition. It is possible to increase the feed load to the furnace by using cooling aids, but such a technique has limitations. The amount of cooling additives is limited by the process economy, because the cooling additives increase the mass of the slag and generate copper losses in the slag.

Organic carbon removal technologies used throughout the world

Organic carbon removal in the Red Dog mine (Smith et al., 2008)

The Red Dog mine, located in the north part of Alaska near the Arctic Circle, is one of the greatest zinc-lead ore processing plants in North America. The Red Dog ore deposit features, other than its prime chemical elements (Pb, Zn), a great content of organic carbon ($C_{org} = 0.67\%$) which has an adverse effect on its lead and zinc recovery. The problem of organic carbon being present in the Red Dog mine ore was solved by using the so-called “carbon pre-float” process.

The idea behind the process is channeling the material, after grinding and classification in hydrocyclones, to pre-flotation, which results in two products: rich in organic carbon concentrate and poor in carbon waste material, which is the feed for further concentration processes. The pre-flotation process is conducted only in the presence of frother, which makes separation of naturally hydrophobic particles possible. Until 2006 carbon pre-flotation was conducted in flotation machines, however, in order to

increase the effectiveness of organic carbon separation currently Jameson cells are used. The change of the processing system has brought the expected results. The reject of about 70% organic carbon was accomplished.

Organic carbon removal in the Zinifex Century mine (Gredelj et al., 2009)

In the Zinifex Century mine, the main ore mineralization includes galena and sphalerite, while the gangue consists of a large amount of organic matter, which is the main carrier (~3%). The presence of organic carbon is not without consequences in the flotation separation of galena and sphalerite. Due to this, a pre-flotation process has been used in the aforementioned mine for its separation. The effectiveness of the process is conditioned by the application of the *MIBC* (methyl isobutyl carbinol) frother.

Organic carbon removal in the Kittila mine (Doucet et al., 2010)

The Kittila mine is an open-pit and underground gold mine and also a processing-hydrometallurgical complex. Gold is concentrated by flotation due to the fact that it occurs mainly in arsenopyrite in the processed material. The acquired concentrate is leached via a pressure filtering method in POX (Pressure Oxidation) autoclaves, and gold is separated from the solution by using active carbon through the CIL (carbon in leach) technology. There were significant losses of gold following the implementation of this technology caused by its absorption on the organic carbon surface. Its cause was the presence of C_{org} . The technical parameters were improved by separating organic carbon from the feed stream during the pre-flotation stage. In 2009 the separation of 30% C_{org} was accomplished, which translated into gold output increase in the CIL process by 1.5%.

Organic carbon removal in the Mt. Isa mine (Grano et al., 1991)

The Mount Isa mine, located in north-west part of Queensland, is one of the biggest underground copper, zinc and lead mines in the world. Copper and lead-zinc ores are mined and processed separately. The final concentrate produced in Mt. Isa mine's ore concentrator plants during standard flotation would have been heavily contaminated by naturally floating carbonate pyrite, talk and carbon shale. Due to this fact a pre-flotation in the Jameson cell has been applied, in which 2% of the feed mass is separated from the feed stream, of which 50% is actually a naturally hydrophobic material (containing organic carbon), with minimal losses of copper (~0.8%).

Organic carbon removal in KGHM POLSKA MIEDZ SA

The constantly increasing requirements, within the scope of the flash smelting furnace effectiveness in relation to the organic carbon content, were the impulse for undertaking appropriate steps during the processing stage within the framework of the KGHM Polska Miedź S.A. research and development activity. The aforementioned issue has been the subject of a complex research with the goal of developing a method that

would allow for economically and technologically effective production of concentrates featuring stable parameters, in light of present and future metallurgical requirements.

The segregation of the final concentrate into poor and rich in organic carbon via classification in hydrocyclones was performed in Rudna Concentrator Plant in years 2003–2007. This method of classification was causing problems with thickening and filter pressing of the concentrate rich in organic carbon. The product was causing difficulties in the gravity thickening process, resulting in the finest size fraction leaking into the thickeners' overflow, which in turn was causing significant disruptions in the technological process. The results of the conducted research were not satisfactory for the metallurgical industry. That was why the segregation of concentrate into “poor” and “rich” in organic carbon via classification in hydrocyclones was discontinued in 2007.

Due to the lack of possibility to increase the effectiveness of separating the concentrate into products featuring appropriate organic carbon contents and stable quality-quantity parameters in hydrocyclones, especially in the low-carbon concentrate, research has been started in order to develop alternative methods of their production.

Next works utilized differences in flotation kinetics between organic carbon and copper compounds. Due to these features it has been proved, that there is a possibility of segregating the concentrate using the flotation method. This issue became the basis for conducting tests of segregating the concentrate into poor and rich in organic carbon. Positive results allowed to justify the feasibility of conducting a full research cycle, in which research on an industrial scale regarding the diversification of calorific value of the concentrate in flotation process within the framework of a research and development (Trybalski et al., 2010) was conducted. The main goal of their research was to determine the technological possibilities of enhancing the concentrates quality through the reduction of C_{org} content to a level required by the flash smelting technology employed in Glogow Smelter. It has been proved, based upon the results of the research, that by using only the differences in the flotation kinetics of copper sulfides and organic substance a satisfying diversification of two concentrates in terms of the content of these components can be achieved, which satisfy the current needs of the flash furnace and Glogow shaft smelter technology. However, taking into account the continuing modernization of Glogow Smelter, consisting of replacing the shaft technology with the flash smelting technology, additional laboratory and industrial research has been conducted by using chemical reagents. Low-saccharification maltodextrin was used, among others, as an organic carbon depressor (Drzymala, et al., 2011). This test indicated great effectiveness of the reagent in the production of two kinds of concentrate with significant diversification of these components: one rich in Cu and poor in organic carbon and one poor in copper and rich in C_{org} (Foszcz and Drzymala, 2011). Further works in this matter were aimed at the improvement of the final concentrate in Rudna Concentrator Plant (Skorupska et al., 2011). The results of Rudna Concentrator Plant final concentrate flotation tests have confirmed the possi-

bility of producing concentrates featuring diversified chemical compositions, optimal for metallurgical processes (Skorupska et al., 2011).

The results of the mentioned papers, especially the performed economic analysis, has given the authorization to conduct industrial tests of segregating the concentrate with the application of maltodextrine as in the Wroclaw University of Technology patent (Drzymala, et al., 2007). The goal of these tests was to optimize the parameters of the process of increasing segregation in terms of Cu and C_{org} contents in the segregating flotation process and consumption of the reagent and to specify its effect on concentrate dewatering. While it is true that the conducted tests have resulted in having access to the appropriate technology, the broad range of feed variability makes it impossible to produce the concentrate of a stable composition. That is why Rudna Concentrator Plant has taken the different measures in this matter. In order to design the right technology, which would be appropriate from the point of view of processing capabilities and metallurgical requirements, research has begun on developing an optimal concentration variant in order to ensure the production of concentrate featuring reduced C_{org} content, based upon the results and experience of other world producers.

Therefore, the main objective of this paper is to determine the possibility of C_{org} separation during the pre-flotation stage, which may directly cause the reduction of C_{org} content in the scavenger flotation feed and indirectly cause the reduction of C_{org} content in the final concentrate to a level which is acceptable for the flash smelting process.

Experimental

A complex analysis of processing technologies used throughout the world has indicated that KGHM Polska Miedz S.A. is not the only plant struggling with-unwanted occurrence of organic carbon in the ore, and consequently, in the concentrate. The technologies of C_{org} removal outlined already of this paper have become the impulse to undertake appropriate actions in this matter in KGHM Polska Miedz S.A. Division of Concentrators. Several trials and tests were conducted and the results are presented below.

Laboratory flotation

Material from the Polkowice concentrator plant, line II (Fig. 1), was used. The first of the samples was extracted from the \varnothing 500 mm hydrocyclone overflow which is normally fed to the rougher flotation machine MF-222. To this research, the rougher flotation machine was the addition pre-flotation machine (and all required parameters like the collectors and no returned materials from the scavenger and cleaner flotation machines which contain collectors) were met.

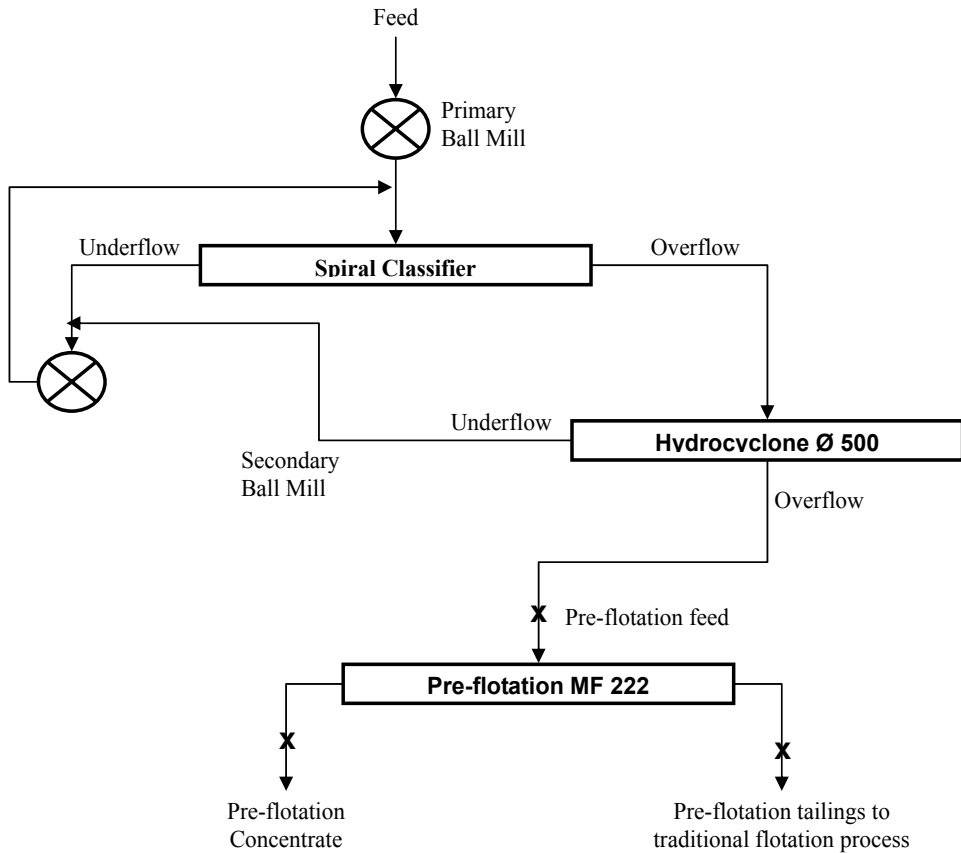


Fig. 1. Schematic block of line II of Polkowice concentrator plant

The scope of the experiments covered two stages: in the first one (experiment I) a comparative laboratory flotation was performed: Flotation A (pre-flotation feed) using Corflot frother (100 g/Mg) and Flotation B (pre-flotation feed) using Corflot frother (60 g/Mg) and collector (a mixture of ethyl and isobutyl sodium xanthate, 120 g/Mg).

The second material used in experiment II was the concentrate from rougher flotation machine MF-222 (obtained only with the application of Corflot frother (100g/Mg, reagent without collectors). The goal of the experiment were to determine the possibility of improved material separation in terms of C_{org} content, and to ensure the possibility of returning as great amount of Cu as possible from pre-flotation concentrate to traditional flotation circuit, thus reducing Cu losses.

The preliminary material extracted from pre-flotation was ground (15 min to 90% $>100 \mu\text{m}$) and a laboratory flotation was performed by adding only Corflot frother (100 g/Mg).

Both experiments were conducted using a Mechanbor laboratory flotation machine equipped with a 1 dm^3 cell. The time of fractional flotation in the experiments was

constant (5 min), while the concentrate was collected after $k_1 = 30$ s, $k_2 = 90$ s, $k_3 = 3$ min, and $k_4 = 5$ min.

The flotation products were dried, weighed and samples were taken for chemical analysis. The determination of Cu and C_{org} content was performed in Quality Control Laboratory, Lubin. Copper was analyzed by using the iodometric titration method, while the organic carbon was analyzed by using a spectrometric method. The results are compiled in Tables 1 and 2 and in Figs 2 to 4.

Research results

The results of conducted laboratory flotation are presented in the form of tables and the Mayer curves in Figs 2, 3 and 4 due to the fact, that the recovery (ε) and the yield (γ) play a significant role in the evaluation of the executed experiments. Because the Mayer curve is sensitive to the feed composition, the location of the upgrading curve depends on the feed. However, a similar content of both Cu and C_{org} in the feed allows a direct comparison of the flotation results of Cu and C_{org} on the same Mayer plot.

A comparison of the results shown in Figs 2 and 3 indicates that the addition of collector has a minimal effect on C_{org} flotation. The reverse situation is observed in case of copper. The addition of collector has a beneficial effect on flotation since it improves flotation selectivity, that is both concentrate recovery and yield. The difference in Cu and C_{org} floatability while using only frother during the pre-flotation stage may, by maintaining proper technological conditions, create a possibility for a satisfying separation of C_{org} from the feed directed for scavenger flotation.

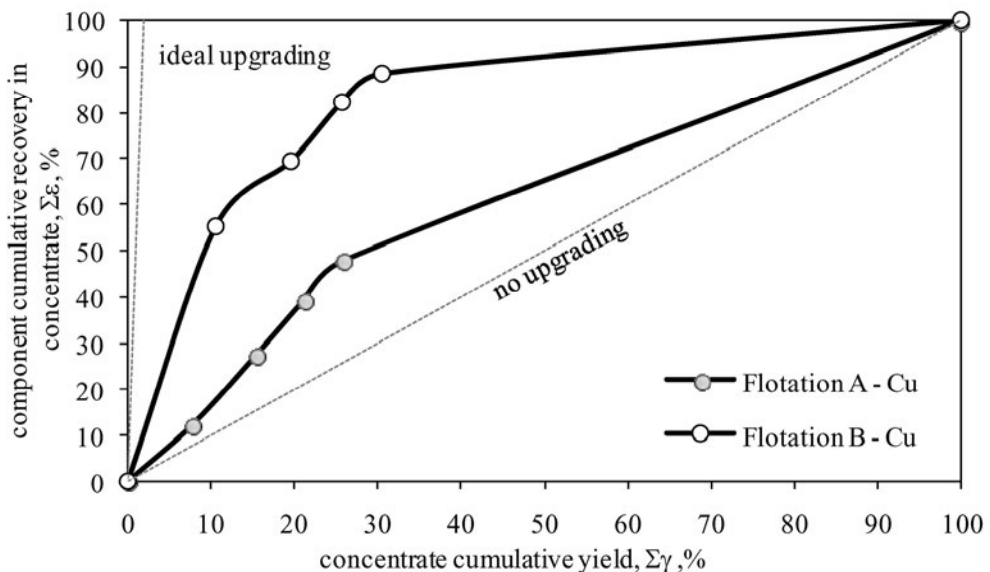


Fig. 2. Results of experiment I – flotation A and B, copper concentration curves

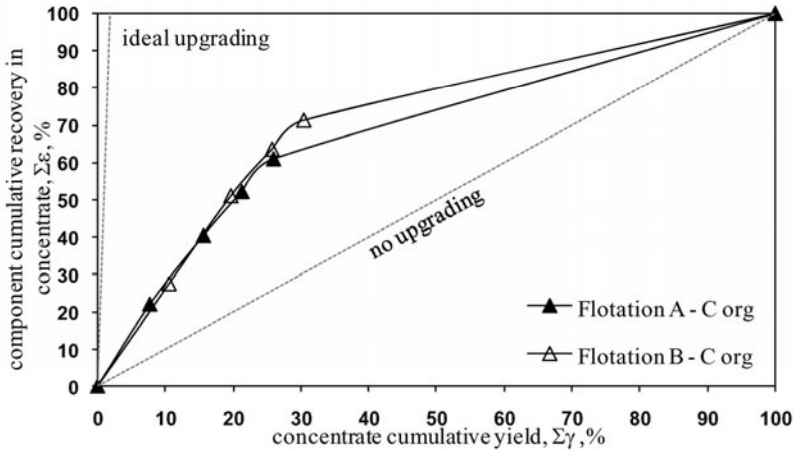


Fig. 3. Results of experiment I – flotation A and B, organic carbon concentration curves

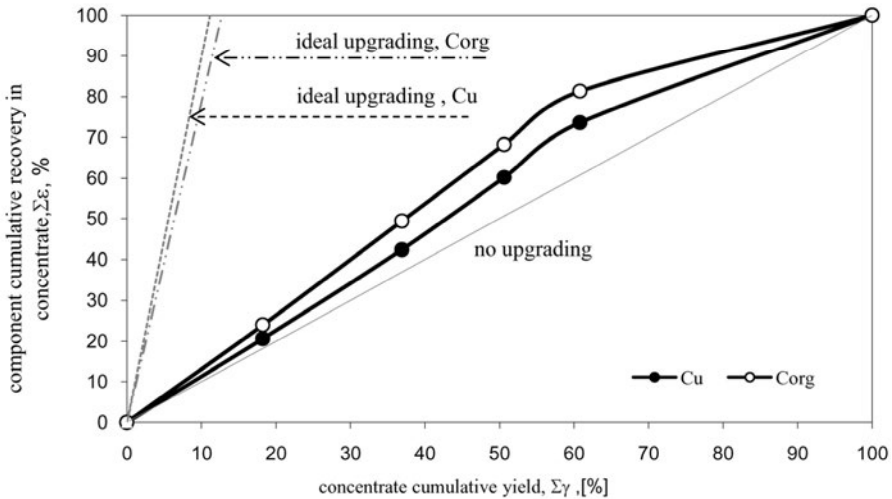


Fig. 4. Results of experiment II – laboratory flotation (Mayer's upgrading curve).
Pre-flotation concentrate with Corflot frother (100 g/Mg)

Figure 4 shows that regrinding and cleaner flotation of the pre-flotation concentrate is justified. Cleaner flotation allows to achieve greater C_{org} content compared to the feed and makes it possible to return about 27% of Cu to the traditional concentration circuit.

The results from experiment I and II confirm the differences in surface characteristics of carbon and copper sulfides, which is directly reflected in their flotation kinetics. Naturally hydrophobic carbon does not require surface modification with a collector,

therefore it floats by using only the frother in the process. Without collector, sulfides exhibit far worse flotation characteristics.

Table 1. Results of experiment I. Flotation A – laboratory flotation without collector. Frother addition (100 g/Mg). λ – content, ε – recovery, γ – yield

Product	Time	γ [%]	$\Sigma\gamma$ [%]	λ_{Cu} [%]	ε_{Cu} [%]	$\Sigma\varepsilon_{Cu}$ [%]	λ_{Corg} [%]	ε_{Corg} [%]	$\Sigma\varepsilon_{Corg}$ [%]
			0			0			0
A/k1	30"	7.72	7.72	3.02	12.21	12.21	4.99	22.01	22.01
A/k2	1'30"	7.81	15.53	3.78	15.46	27.67	4.12	18.38	40.39
A/k3	3'	5.65	21.18	3.94	11.66	39.33	3.68	11.88	52.27
A/k4	5'	4.69	25.87	3.52	8.64	47.97	3.27	8.76	61.03
A/c.		74.13	100.00	1.34	52.03	100.00	0.92	38.97	100.00
Σ		100.00		1.91	100.00		1.75	100.00	

Table 2. Results of experiment I. Flotation B – laboratory flotation with collector (120 g/Mg) and frother (60 g/Mg) addition). λ – content, ε – recovery, γ – yield

Product	Time	γ [%]	$\Sigma\gamma$ [%]	λ_{Cu} [%]	ε_{Cu} [%]	$\Sigma\varepsilon_{Cu}$ [%]	λ_{Corg} [%]	ε_{Corg} [%]	$\Sigma\varepsilon_{Corg}$ [%]
			0			0			0
B/k1	30"	10.58	10.58	8.36	55.31	55.31	4.27	27.69	27.69
B/k2	1'30"	9.02	19.60	2.53	14.28	69.59	4.26	23.57	51.26
B/k3	3'	6.12	25.72	3.35	12.82	82.41	3.29	12.34	63.59
B/k4	5'	4.78	30.50	2.10	6.28	88.69	2.68	7.86	71.45
B/c.		69.50	100.00	0.26	11.31	100.00	0.67	28.55	100.00
Σ		100.00		1.60	100.00		1.63	100.00	

Table 3. Results of experiment II. Laboratory flotation of concentrate from pre-flotation machines MF-222 (with Corflot 100 g/Mg). λ – content, ε – recovery, γ – yield

Product	Time	γ [%]	$\Sigma\gamma$ [%]	λ_{Cu} [%]	ε_{Cu} [%]	$\Sigma\varepsilon_{Cu}$ [%]	λ_{Corg} [%]	ε_{Corg} [%]	$\Sigma\varepsilon_{Corg}$ [%]
			0			0			0
II/k1	30"	18.23	18.23	12.63	20.64	20.63	16.76	24.01	24.01
II/k2	1' 30"	18.67	36.90	13.02	21.78	42.40	17.31	25.38	49.39
II/k3	3'	13.72	50.62	14.48	17.81	60.20	17.52	18.89	68.27
II/k4	5'	10.17	60.80	14.74	13.44	73.63	16.31	13.03	81.31
II/c.		39.20	100.00	7.51	26.38	100.00	6.07	18.69	100.00
Σ		100.00		11.16	100.00		12.73	100.00	

Industrial trials

The positive results of the experiments conducted on a laboratory scale have decided in favor of conducting the test on a technical scale. In order to determine the validity of the assumed thesis that there is a possibility of organic carbon separation during pre-flotation stage under KGHM Polska Miedz SA Division of Concentrators industrial conditions comparative tests of pre-flotation stage process effectiveness were conducted (Polkowice Concentrator Plant, line II, Fig.1).

The basis of the test is the comparison of the processes run under industrial conditions. The tests were conducted on three-cell flotation machine with an overall capacity of 144 m³ under comparable conditions. Analogous settings of froth level and air flows were used for both test stages, which were respectively 15 cm and 6 m³/min.

The effectiveness of the process while adding the reagents in normal way and while performing current production was analyzed in the first test – (Corflot, ~40 g/Mg) and collector (a mixture of ethyl and isobutyl sodium xanthate, ~60 g/Mg). The second stage of the experiment took place only in the presence of a frother (Corflot, ~80g/Mg).

Trial results

The analysis of product produced while conducting the experiments (feed α , concentrate β , tailings ν) is presented in from Figs 5 to 7.

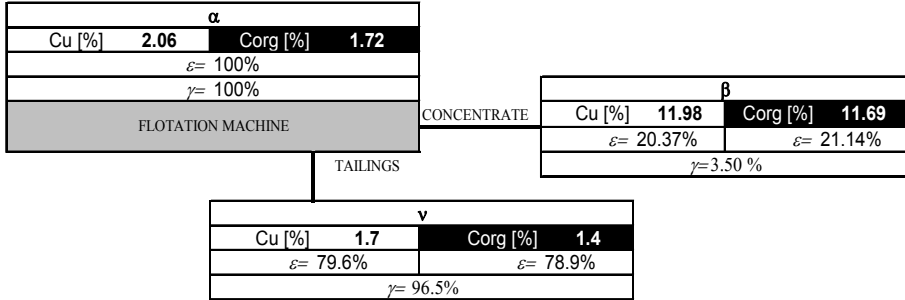


Fig. 5. Trial 1. Results of flotation machine sampling–test included collector and Corflot frother, ~40 g/Mg, xanthate, ~60 g/Mg

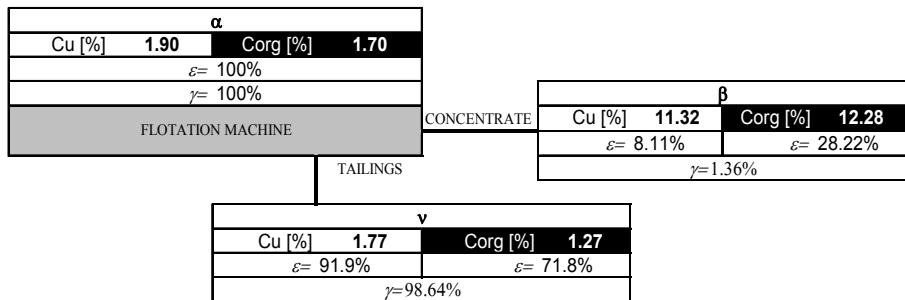


Fig. 6. Trial 2. Results of flotation machine sampling–test. Corflot frother only, ~80g/Mg

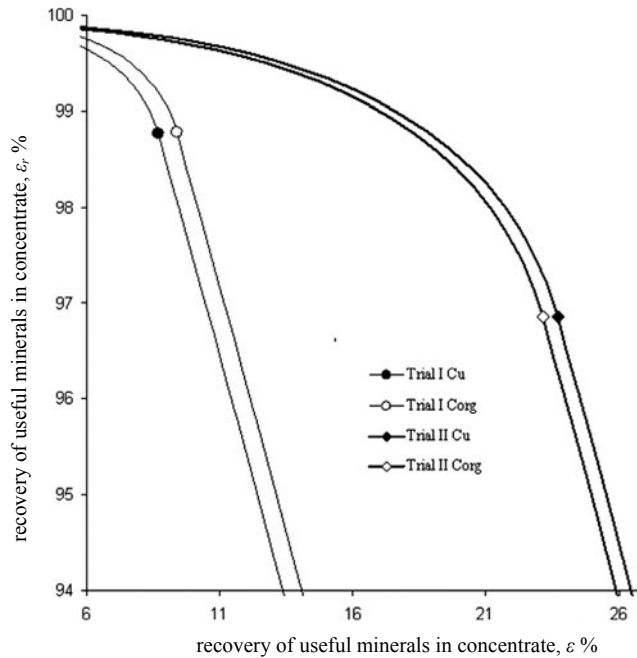


Fig. 7. The Fuerstenau curve for industrial trial of pre-flotation of Cu and C_{org}

Based upon the approximate results of the trials (Figs 5 and 6) also presented in Fig. 7, a comparison of C_{org} and Cu concentration performance under industrial conditions indicates noticeable differences in recovery and yields of the concentration process products (concentrate, tailings) in relation to the conditions of the conducted experiment i.e. the application of a collector reagent and its absence during the process.

Results and discussion

The analysis of the obtained results shows, that there is a possibility of separating significant amounts of organic carbon on the pre-flotation stage by applying only the frother. In comparison to flotation with collector, flotation in which a frother was used about 28% of organic carbon contained within the feed was successfully separated, thus reducing its content from 1.7 to 1.27% with minimal copper losses of 8.1%. The insubstantial yield of the concentrate and the organic carbon content of 12.26% has a beneficial effect on this process, which results from the further processing of the produced concentrate i.e. regrinding and purification in order to return as great amount of copper back to the process as it is possible.

The results of the conducted research allow for the following conclusion:

- flotation kinetics of the organic matter without application of collector is much better than the flotation kinetics of copper sulfides

- separation of organic carbon during the pre-flotation stage under KGHM Polska Miedz S.A. Division of Concentrators conditions is possible
- produced concentrate, featuring greater content of organic substance, can be made a subject to regrinding and cleaning flotation in order to return significant amounts of copper to the conventional concentration process
- Corflot frother used during the tests was applied in order to ensure the appropriate run of the process. Other frother, used for instance in coal flotation, will be tested.

Division of Concentrators is where solutions to the most important problems occurring in concentration technologies are being sought within the framework of research and development activity. However, the problem of organic carbon extends beyond the framework of processing technologies due to the fact, that it is a global problem, because it has an influence on the economic-technological effectiveness of the entire company. That is why this subject is researched in such a complex way and analyzed by the concentrator staff. In order to meet the expectations of present and future metallurgical requirements many possibilities of adapting the concentrate quality to metallurgical requirements were researched and tested, some of which are not possible to implement in current production. That is why the described here actions, which were initiated by the employees may be the turning point in the production of concentrate featuring appropriate quality both for the target technology in the form of flash smelting furnace technology. however, it requires further research due to the fact, that the results presented within this paper are of diagnostic nature.

References

- DOUCET D., GIRARD D., GRONDIN L., MATTE P., 2010, Technical Report on the December 31, 2009, *Mineral Resource and Mineral Reserve Estimate and the Suuri Extension Project, Kittila Mine, Finland*, March 4, 2010.
- DRZYMALA J., 2011, *Dekstryny jako reagent flotacyjny segregujący polskie przemysłowe koncentraty miedziane na dwa produkty o zróżnicowanej zawartości węgla organicznego*, *Przegląd Gorniczy*, 7/8, 104–107.
- DRZYMALA J., KAPUSNIAK J., TOMASIK P., 2007, *A method of production of copper concentrates rich in chalcocite*, Polish Patent PL 195693 B1.
- FOSZCZ D., DRZYMALA J., 2011, *Differentiation of organic carbon, copper and other metals content by segregating flotation of final Polish industrial copper concentrates in the presence of dextrin*, *Physicochemical Problem of Mineral Processing*, 47, 17–26.
- GRANO S.R., GRIFFIN L.F., JOHNSON N.W., SMART ST., RALSTON R.C., 1991, *Treatment of Naturally Hydrophobic Gangue Minerals at the Cooper Concentrator of Mt Isa Mines Limited*. 4th Mill Operators' Conference, Proceedings of the Australian Institute of Minerals and Metals, Burnie 10–14 March, 121–128.
- GREDELJ S., ZANIN M., GRANO S.R., 2009, *Selective flotation of carbon in the Pb-Zn carbonaceous sulphide ores of Century Mine, Zinifex*. *Mineral Engineering* 22 (2009), 279–288.
- KIJEWSKI P., LESZCZYNSKI R., 2010, *Organic carbon in copper ore – significance and problems*, *Scientific Papers of the Mineral and Energy Economy Research Institute of The Polish Academy of Sciences*, no. 79.

- SKORUPSKA B., WIENIEWSKI A., KUBACZ N. et al., 2011, *Attempts at concentrate segregation by using maltodextrine in Rudna Concentrator Plant and the evaluation of its effects on the pyrometallurgical processes' run in KGHM Polska Miedz S.A.*, INFM paper no. 1076 (not published).
- SKORUPSKA B., WIENIEWSKI A., KUBACZ N., 2011, *The possibilities of producing copper concentrates featuring diversified organic components content*, Mining and Geology, vol. 6, paper 2.
- SMITH T., LIN D., LACOUTURE B., ANDERSON G., 2008, *Removal of organic carbon with a Jameson Cell at Red Dog Mine*, 40th Annual Meeting of the Canadian Mineral Processing 22–24 January 2008, Ontario, Canada.
- TRYBALSKI K., FOSZCZ D., GAWENDA T., KRAWCZYKOWSKI D., 2010, *The development of concentrate production technology featuring diversified calorific values on the segregation flotation stage*, AGH University of Science and Technology paper, (not published).

Received March 16, 2012; reviewed; accepted July 8, 2012

BENEFICIATION OF ARSENIC BEARING COMPLEX SULPHIDE ORE BY FLOTATION

Alim GUL, Gulay BULUT, Ayhan Ali SIRKECI

Istanbul Technical University, Mining Faculty, Mineral Processing Division, Ayazağa, Istanbul, Turkey
gbulut@itu.edu.tr

Abstract: In this study beneficiation of a sulphide ore from the Gümüşhane-Black Sea Region of Turkey was investigated. Detailed flotation studies were carried out with the ore sample which contained 2.95% Pb, 6.72% Zn and 0.32% Cu. Mineralogical analyses showed that the sample includes pyrite, galena, sphalerite, chalcopyrite, tennantite, cerussite, anglesite and smithsonite. On the other hand, hematite, goethite, limonite, calcite and quartz were determined as gangue minerals. Selective sulphide concentrates with low arsenic content were tried to be produced by froth flotation. Individual concentrates of Pb, Zn and Cu assayed 67.54% Pb, and 61.49% Zn and 23.31% Cu where corresponding recoveries were 73.0% and 77.1% and 38.7%, respectively. Arsenic contents were less than 2000 ppm in the lead and zinc concentrates. Copper concentrate assayed 5.03% As since the major copper minerals were in tennantite form (copper arsenic sulphide mineral). In flotation tests, non-toxic reagents such as metabisulphite, caustified starch, and activated carbon were used to depress minerals in relevant circuits.

Key words: *arsenic, non-toxic depressants, sulphide minerals, flotation*

Introduction

The treatment processes for the beneficiation of copper-lead-zinc ores are generally complex. The methods used in the processing of copper-lead-zinc ore could be classified as follows (Bulatovic, 2007): a) sequential copper, lead, zinc flotation method where the copper, lead, and zinc are sequentially floated to produce separate copper, lead and zinc concentrates, b) bulk flotation of copper and lead followed by zinc flotation from the bulk tailings. The copper-lead separation is performed on the upgraded bulk concentrate. This is the most commonly used method in the treatment of copper-lead-zinc ores, c) bulk flotation of copper-lead-zinc minerals followed by a selective flotation of copper, lead and zinc from the bulk concentrate. This method is rarely used and is effective on the ores where the principal copper minerals are bornite, covellite and other secondary copper sulphides.

There is no general rule that can be prescribed as to which method is selected for the treatment of copper-lead-zinc ores.

Arsenic is one of the most hazardous inorganic pollutants for both the environment and human health. Therefore, discharge to the environment must be strictly controlled (Mandal et al., 2002). Minerals of copper with arsenic, which are enargite (Cu_3AsS_4), tennantite ($3\text{Cu}_2\text{S}\cdot\text{S}_{0.5}\cdot\text{As}_2\text{S}_3$), tetrahedrite ($3\text{Cu}_2\text{S}\cdot\text{Sb}_2\text{S}_3$), do not have significant economic values. Furthermore, the existence of As in the concentrates requires payment of a penalty to the smelter. It is of economic and environmental interest to remove arsenic bearing minerals at an early stage of the process such as flotation (Ma and Bruckard, 2009).

Enargite, tennantite and tetrahedrite are usually secondary minerals to other copper sulphides. Flotation mechanisms of these minerals are not well understood since there are limited studies involved (Fornasiero et al., 2001; Smith and Brucard, 2007; Sasaki et al., 2010; Benzaazoua et al., 2002). Laboratory and plant practices showed that the flotation behaviour of enargite is similar to that of chalcocite. Tennantite and tetrahedrite do not respond well to flotation using xanthate as a collector. Tetrahedrite floats well with aerophine and mercaptan type of collectors at a pH value between 8 and 10 (Bulatovic, 2007).

Selective separation of sulphide minerals can be achieved using a variety of collectors and modifiers to adjust surface properties (Finkelstein, 1997; Yamamoto, 1980; Shen et al., 2001; Chandra and Gerson, 2009; Laskowski et al., 1991; 2007). In practice, when treating complex sulphide ores, the use of two or more depressants is common, especially when a selectivity problem is present or separation of several valuable minerals is required (Bulatovic and Wysloulzil, 1995).

Sulphur-oxy depressants are added to the flotation pulp in the form of sodium sulphite, sodium bi-sulphite, sodium metabisulphite or sulphur dioxide for the depression of pyrite, sphalerite and galena (Grano et al., 1997; 1997a; 1997b; Khmeleva et al.; 2003; 2005; 2006). Gül (2007) studied the effects of sodium meta bisulphite and activated carbon on the selective flotation of chalcopyrite from pyrite and successfully depressed pyrite while producing a high grade copper concentrate. Gül et al. (2008) used non-toxic reagents such as zinc sulphate, sodium meta bisulphite, caustic starch and activated carbon instead of highly toxic reagents like potassium bichromate and sodium cyanide, they obtained successful results for the separation of chalcopyrite, galena and sphalerite selectively.

This investigation focuses on producing individual concentrates of Pb and Zn with low arsenic contents from a complex sulphide ore employing non-toxic depressants to achieve selectivity.

Materials and methods

The ore sample was taken from Gümüşhane in Black Sea Region of Turkey. Mineralogical analyses show that the ore contains sphalerite (ZnS), galena (PbS), tennantite

($\text{Cu}_{12}\text{As}_4\text{S}_{13}$), chalcopyrite (CuFeS_2), cerussite (PbCO_3), anglesite (PbSO_4) and smithsonite (ZnCO_3). On the other hand pyrite, hematite, goethite, limonite, calcite and quartz were determined as gangue minerals. Figure 1 shows the mineralogical structure of the ore sample. Pyrite is generally seen as free and to some extent as locked particles whose average size is around 60 μm . In some cases pyrite has transformed to limonite. Sphalerite particles are generally seen to form irregular shapes and rarely replaced by pyrite. Sphalerite is the most abundant mineral in the ore after pyrite and it has an average particle size of 70 μm . Galena has irregular particle shapes with an average size of 60 μm . In the advanced cases of the replacement tennantite particles were locked in galena. Galena itself, on the other hand, was replaced by pyrite. Tennantite is generally observed as irregular particles and in some cases forms aggregates with other minerals. It usually fills the voids between pyrite particles though may enclose fine pyrite grains. Particle size of tennantite may vary between 10 and 300 μm . In Table 1 the results of chemical analysis of the ore sample are given.

Selective flotation experiments were carried out to obtain lead, zinc, copper and pyrite concentrates. Tests were conducted with samples ground below 0.1 mm employing a laboratory size ball mill. The final flotation flowsheet is presented in Fig. 2.

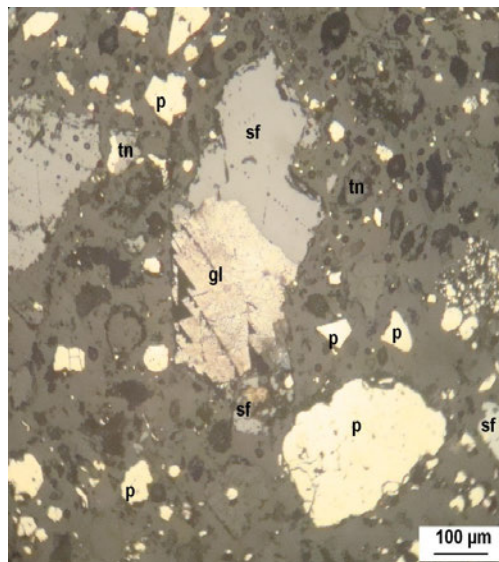


Fig. 1. Irregular shaped pyrite, sphalerite, galena and tennantite particles seen in the ore body

Table 1. Chemical analysis of the ore sample

Component	Assay, %
Pb	2.95
Zn	6.72
Cu	0.32
Fe	16.95
S	26.00
As	0.20
CaO	9.97
Al ₂ O ₃	2.38

It can be seen from Table 1 that the ore contains 2.95% Pb, 6.72% Zn, 0.32% Cu, and 0.20% As.

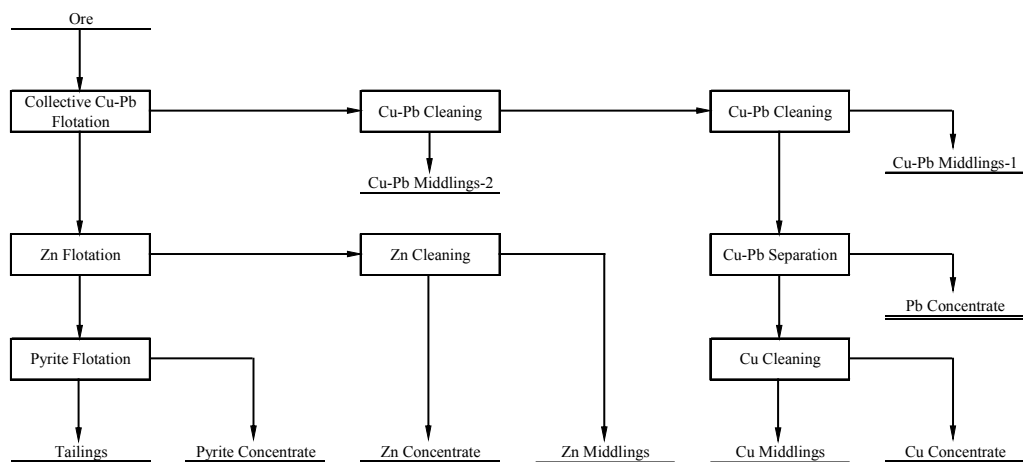


Fig. 2. Flotation flowsheet of experimental studies

Aerophine 3418-A was used as a collector in the Pb-Cu circuit whereas potassium amyl xanthate was the collector in the sphalerite-pyrite circuit. Sodium metabisulphite ($\text{Na}_2\text{S}_2\text{O}_5$) and ZnSO_4 were employed for the depression of sphalerite. Pyrite was deactivated by increasing pH by lime addition. Furthermore, $\text{Na}_2\text{S}_2\text{O}_5$ was added for the depression of pyrite. Sphalerite was later activated by CuSO_4 addition. In the selective flotation of copper minerals from galena the pulp was treated with activated carbon first and then sodium meta bi-sulphite and caustified starch were added to depress galena where copper was floated by the addition of small amounts of Aero 208. On the other hand, depressants like quebracho and S7260, that is a synthetic polymeric depressant were used in the Pb-Cu circuit to obtain selective concentrates (Cytac, 2002). Lime and sulfuric acid were the reagents to control the pulp pH. In this investi-

gation the effect of pH, collector dosage, the number of flotation stages, depressant type and dosage were studied on the selective concentration of Cu, Pb and Zn minerals in the ore sample.

Results and discussions

Flotation tests were carried out to obtain selective concentrates of Pb, Zn, and Cu. The procedure adopted was to float Pb-Cu collectively first leaving Zn in the sink and then to activate Zn using conventional methods. Pb-Cu separation from the bulk concentrate was achieved by depressing Cu and floating Pb minerals. The flotation conditions and test results are presented in Tables 2 and 3, respectively.

Table 2. Flotation test conditions

Collective Cu-Pb Flotation		Zn Flotation	
Na ₂ S ₂ O ₅ , g/Mg	1500	CuSO ₄ , g/Mg	300
ZnSO ₄ , g/Mg	2250	KAX, g/Mg	50
Aerophine 3418 A, g/Mg	35	MIBC, g/Mg	70
MIBC, g/Mg	80	pH	11.0
pH	9.0	Zn Cleaning	
Cu-Pb Separation		KAX, g/Mg	2.5
Quebracho, g/Mg	50	MIBC, g/Mg	10
S7260, g/Mg	25	pH	11.0
Aerophine 3418 A, g/Mg	5	Pyrite Flotation	
MIBC, g/Mg	2.5	KAX, g/Mg	200
pH	9.0	MIBC, g/Mg	60
		pH	4.5-5.0

Table 3. The results of selective flotation using Quebracho and S7260

Products	Weight %	Pb, %		Zn, %		Cu, %	
		Assay	Recovery	Assay	Recovery	Assay	Recovery
Pb Concentrate	3.0	52.44	51.7	7.08	3.3	5.05	43.1
Cu-Pb Middlings 1	0.9	44.03	13.0	8.34	1.2	2.40	6.1
Cu-Pb Middlings 2	2.4	19.30	15.2	7.39	2.7	1.88	12.8
Zn Concentrate	9.4	1.02	3.2	60.77	88.2	0.38	10.2
Zn Middlings	1.2	2.85	1.1	6.20	1.2	0.83	2.8
Pyrite Concentrate	36.5	0.57	6.9	0.36	2.0	0.19	19.7
Tailings	46.6	0.58	8.9	0.20	1.4	0.04	5.3
Total	100.0	3.04	100.0	6.48	100.0	0.35	100.0

S7260 and Quebracho were used to depress copper minerals and pyrite in the bulk Pb-Cu concentrate. However, the attempt to depress Cu minerals was not a success and consequently Pb concentrate assayed 5.05% Cu. Zinc concentrate, on the other hand, was obtained with 60.77% Zn content and 88.2% recovery. Since zinc was successfully concentrated with relatively high recoveries and grades, in the proceeding tests attention was given to the separation of Pb from Cu and As and conditions in the zinc circuit were not further studied.

In the following experiments alternative procedures were studied to obtain a clean Pb concentrate. The rougher Pb-Cu bulk concentrate was cleaned twice employing $ZnSO_4$ and $Na_2S_2O_5$ as depressants. In the separation of Pb from Cu, all minerals were depressed first using activated carbon, $Na_2S_2O_5$ and caustified starch and Cu was floated by the addition of small amounts of Aero 208 which is particularly synthesized for Cu. Flotation conditions and results of selective flotation for the Pb-Cu separation are given in Tables 4 and 5, respectively.

Table 4. Flotation conditions for separation of Pb from Cu

Collective Cu-Pb Flotation		Cu-Pb Separation	
$Na_2S_2O_5$, g/Mg	1500	Activated Carbon, g/Mg	250
$ZnSO_4$, g/Mg	2250	$Na_2S_2O_5$, g/Mg	500
Aerophine 3418 A, g/Mg	50	Caustified Starch, g/Mg	100
MIBC, g/Mg	60	Aero 208, g/Mg	6
pH	9.0	MIBC, g/Mg	6
Cu-Pb Cleaning		pH	6.0
$Na_2S_2O_5$, g/Mg	375		
$ZnSO_4$, g/Mg	750		
MIBC, g/Mg	2.5		
pH	9.0		

Table 5. Results of flotation for Pb-Cu separation

Products	Weight %	Pb, %		Zn, %		Cu, %	
		Assay	Recovery	Assay	Recovery	Assay	Recovery
Pb Concentrate	3.7	65.52	76.0	7.16	4.7	0.77	9.1
Cu-Pb Middlings	0.9	19.29	5.4	3.50	0.6	15.73	44.9
Cu-Pb-Zn Middlings 1	0.8	3.87	1.0	18.40	2.6	2.97	7.5
Cu-Pb-Zn Middlings 2	2.6	3.23	2.6	16.50	7.7	1.13	9.3
Tailings	92.0	0.52	15.0	5.14	84.4	0.10	29.2
Total	100.0	3.19	100.0	5.60	100.0	0.32	100.0

The lead concentrate produced meets the specifications of smelters in terms of Pb and Cu contents. Furthermore, Pb recovery is at an acceptable level. Therefore, the results in Table 5 prove that separation is successful between lead and copper. In order

to check the reproducibility of the experiment and to produce a copper concentrate another test was conducted under the experimental conditions seen in Table 6 and the results are presented in Table 7.

Table 6. Experimental conditions to produce selective Pb and Cu concentrates

Collective Cu-Pb Flotation		Cu-Pb Cleaning	
Na ₂ S ₂ O ₅ , g/Mg	1500	Na ₂ S ₂ O ₅ , g/Mg	375
ZnSO ₄ , g/Mg	2250	ZnSO ₄ , g/Mg	750
Aerophine 3418 A, g/Mg	50	MIBC, g/Mg	2.5
MIBC, g/Mg	60	pH	9.0
pH	9.0	Cu Cleaning	
Cu-Pb Separation		Without any reagents	
Activated Carbon, g/Mg	250	Zn Flotation	
Na ₂ S ₂ O ₅ , g/Mg	500	CuSO ₄ , g/Mg	300
Caustified Starch, g/Mg	100	KAX, g/Mg	40
Aero 208, g/Mg	6	MIBC, g/Mg	50
MIBC, g/Mg	6	pH	11.0
pH	6.0	Zn Cleaning	
Pyrite Flotation		KAX, g/Mg	2.5
KAX, g/Mg	200	MIBC, g/Mg	10
MIBC, g/Mg	60	pH	11.0
pH	4.5-5.0		

Copper was floated using Aero 208 from the bulk Pb-Cu concentrates and then cleaned without any reagents addition.

Table 7. Results of selective flotation

Products	Weight %	Pb, %		Zn, %		Cu, %		As, %	
		Assay	Rec.	Assay	Rec.	Assay	Rec.	Assay	Rec.
Pb Concentrate	3.7	67.54	73.0	8.72	5.3	0.59	6.0	0.16	2.9
Cu Concentrate	0.6	12.65	2.2	3.18	0.3	23.31	38.7	5.03	14.9
Cu Middlings	0.5	46.26	6.8	5.51	0.4	2.78	3.8	0.54	1.3
Cu-Pb Middlings 1	0.8	6.03	1.4	21.30	2.8	2.86	6.3	0.55	2.2
Cu-Pb Middlings 2	2.5	4.65	3.4	20.31	8.3	1.73	12.0	0.99	12.3
Zn Concentrate	7.7	0.58	1.3	61.49	77.1	0.28	6.0	0.05	1.9
Zn Middlings	1.6	1.97	0.9	10.89	2.8	1.39	6.2	0.49	3.9
Pyrite Concentrate	36.5	0.52	5.5	0.27	1.6	0.17	17.2	0.31	56.0
Tailings	46.1	0.41	5.5	0.19	1.4	0.03	3.8	0.02	4.6
Total	100.0	3.43	100.0	6.14	100.0	0.36	100.0	0.20	100.0

Rec.: Recovery

It can be seen from Table 7 that a Pb concentrate could be obtained with 67.54% content and 73.0% recovery. The relationship between Cu and As contents are seen in Table 7 hence As assay in the Pb concentrate is closely related to the Cu content. Zinc concentrate was produced with 61.49% content and 77.1% recovery. Copper content in Zn concentrate is 0.28%, and As is 0.05%. Copper minerals are seen to be depressed effectively, consequently arsenic content decreases in Pb and Zn concentrates. Furthermore a copper concentrate is obtained with 23.31% Cu content and 38.7% recovery while As content is 5.03% as expected. It is suggested that high As content copper concentrates could be heat treated to get rid of As. Therefore, the concentrate is roasted at low temperatures, so that the arsenic is selectively fumed off into a low-volume stream product leaving a calcined product rich in copper and sulphur. In the final stage, arsenic in the fumes is immobilised in a low temperature ceramic such that safe disposal back into the soil is possible (Jahanshahi et al., 2006; Bruckard et al.; 2010).

Some depressants used in the conventional selective flotation of sulphide ores are extremely toxic and must be avoided as much as possible. In this study the use of non-toxic reagents such as $ZnSO_4$, sodium metabisulphite ($Na_2S_2O_5$), caustified starch and activated carbon instead of highly toxic conventional reagents such as $K_2Cr_2O_7$ and NaCN provided successful results for the selective flotation of galena, sphalerite, tenatite and pyrite.

The mechanism of $ZnSO_4$ to depress sphalerite is well known. Possible deactivation mechanisms regarding sodium metabisulphite and caustified starch are presented in the introduction yet the usage of starch must be clearly monitored since excess amounts will depress all minerals. Starch deactivates minerals through reactions with metal oxides or hydroxides on the surface. It is also reported that it can attach to the surface by hydrophobic forces (Liu et al.; 2000; Bıçak and Ekmekci; 2005). Activated carbon, however, is not a direct depressant for sulphide minerals; it actually adsorbs excess amounts of collector species. Activated carbon in this study was used for the selective flotation of chalcopyrite from galena. When it was added to the flotation pulp, excess amount of collector was adsorbed thus reducing the concentration of collector in the solution. On decreasing the collector concentration in the solution by adding activated carbon, the collector desorbs off the surface of galena and hence depression is facilitated.

Conclusions

1. This investigation conducted with a Pb-Cu-Zn ore sample collected from Gümüşhane (Turkey) has proven that it is possible to selectively separate As containing copper minerals from galena and sphalerite using non-toxic reagents.
2. Separate lead and zinc concentrates were produced assaying 67.54% Pb, 61.49% Zn with 0.16% and 0.05% As, respectively, that are much lower than the smelter requirement of 2000 ppm.

3. As a result of this investigation As being an environmental pollutant was eliminated to acceptable levels in Pb and Zn concentrates employing non-toxic reagents as an alternative to high toxic conventional chemicals.

References

- BENZAAZOOUA M., MARION P., LIOUVILLE-BOURGEOIS L., JOUSSEMET R., HOUOT R., FRANCO A., PINTO A., 2002, *Mineralogical distribution of some minor and trace elements during a laboratory flotation processing of Neves-Corvo ore (Portugal)*, International Journal of Mineral Processing, 66, No. 1–4, 163.
- BICAK O., EKMEKCI Z., 2005, *Polisakkaritlerin flotasyonda bastırıcı olarak kullanımı ve soğurum mekanizmaları*, Madencilik, 44, No. 1, 19 (In Turkish).
- BRUCKARD W.J., DAVEY K.J., JORGENSEN F.R.A., WRIGHT S., BREW D.R.M., HAQUE N., VANCE E. R., 2010, *Development and evaluation of an early removal process for the beneficiation of arsenic-bearing copper ores*, Mining Engineering, 23, No. 15, 1167.
- BULATOVIC S., WYSLOUZIL D.M., 1995, *Selection and evaluation of different depressants systems for flotation of complex sulphide ores*, Minerals Engineering, 8, No. 1–2, 63.
- BULATOVIC S.M., 2007, *Handbook of flotation reagents, chemistry. theory and practice, flotation of sulfide ores*, Elsevier, Amsterdam.
- CHANDRA A.P., GERSON A.R., 2009, *A review of the fundamental studies of the copper activation mechanism for selective flotation of sulfide minerals, sphalerite and pyrite*, Advances in Colloid and Interface Science, 145, 97.
- Cytec mining chemical handbook*, 2002, Horton Printing Company, Meriden.
- FINKELSTEIN N.P., 1997, *The activation of sulphide minerals for flotation: a review*, International Journal of Mineral Processing, 52, No. 2–3, 81.
- FORNASIERO D., FULLSTON C.L., RALSTON J., 2001, *Separation of enargite and tennantite from non-arsenic copper sulfide minerals by selective oxidation or dissolution*, International Journal of Mineral Processing, 61, No. 2, 109.
- GRANO S.R., SOLLAART M., SKINNER W., PRESTIDGE., RALSTON J., 1997, *Surface modifications in the chalcopyrite-sulphite ion system. I. collectorless flotation, XPS and dissolution study*, International Journal of Mineral Processing, 50, No. 1–2, 1.
- GRANO S.R., JOHNSON N.W., RALSTON J., 1997a, *Control of the solution interaction of meta bisulphite and ethyl xanthate in the flotation of the Hilton ore of Mount Isa Mines Limited*, Australia, Mineral Engineering, 10, No. 1, 17.
- GRANO S.R., PRESTIDGE C.A., RALSTON J., 1997b, *Solution interaction of ethyl xanthate and sulphite and its effect on galena flotation and xanthate adsorption*, International Journal of Mineral Processing, 52, 161.
- GÜL A., 2007, *The role of Na₂S₂O₃ and activated carbon on the selective flotation of chalcopyrite from a copper ore using a dithiophosphine-type collector*, Mineral Processing, Extractive Metal.Rev., 28, 235.
- GÜL A., YÜCE A.E., SIRKECI A.A., OZER M., 2008, *Use of non-toxic depressants in the selective flotation of copper lead-zinc ores*, Canadian Metallurgical Quarterly, 47, No. 2, 111.
- JAHANSHAHI S., BRUCKARD W.J., CHEN C., JORGENSEN F.R.A., 2006, *Management of minor elements in the production of basemetals*, in: Green Processing 2006, 3rd International Conference on the Sustainable Processing of Minerals, Newcastle, Australia, The Australasian Institute of Mining and Metallurgy, Melbourne, 2006, 25.

- KHMELEVA T.N., BEATTIE D.A., GEORGIEV T.V., SKINNER W.M., 2003, *Surface study of the effect of sulphite ions on copper-activated pyrite pre-treated with xanthate*, Mineral Engineering, 16, 601.
- KHMELEVA T.N., SKINNER W.M., BEATTIE D.A., 2005, *Depression mechanisms of sodium bisulphite in the xanthate-collectorless flotation of copper activated sphalerite*, International Journal of Mineral Processing, 76, 43.
- KHMELEVA T.N., CHAPELET J.K., SKINNER W.M., BEATTIE D.A., 2006, *Depression mechanisms of sodium bisulphite in the xanthate-induced flotation of copper activated sphalerite*, International Journal of Mineral Processing, 79, 61.
- LASKOWSKI J.S., LIU Q., BOLIN N.J., 1991, *Polysaccharides in flotation of sulphides. Part 1. Adsorption of polysaccharides onto mineral surfaces*, International Journal of Mineral Processing, 33, No. 1–4, 223.
- LASKOWSKI J.S., LIU Q., O'CONNOR T., 2007, *Current understanding of the mechanism of polysaccharide adsorption at the mineral /aqueous solution interface*, International Journal of Mineral Processing, 84, 59.
- LIU Q., ZHANG Y., LASKOWSKI J. S., 2000, *The adsorption of polysaccharides onto mineral surfaces: an acid/base interaction*, International Journal of Mineral Processing, 60, p. 229.
- MA X., BRUCKARD W.J., 2009, *Rejection of arsenic minerals in sulfide flotation — A literature review*, International Journal of Mineral Processing, 93, No. 2,1, 89.
- MANDAL B. K., SUZUKI K. T., 2002, *Arsenic round the worlds: a review*, Talanta, 58, 201.
- SASAKI K., TAKATSUGI K., ISHIKURA K., HIRAJIMA T., 2010, *Spectroscopic study on oxidative dissolution of chalcopyrite, enargite and tennantite at different pH values*, Hydrometallurgy 100, 144.
- SHEN W.Z., FORNASIERO D., RALSTON J., 2001, *Flotation of sphalerite and pyrite in the presence of sodium sulfite*, International Journal of Mineral Processing, 63, No. 1, 17.
- SMITH L.K., BRUCKARD W. J., 2007, *The separation of arsenic from copper in a Northparkes copper–gold ore using controlled-potential flotation*, International Journal of Mineral Processing, 84, 15.
- YAMAMOTO T., 1980, *Mechanism of depression of pyrite and sphalerite by sulphite*, Complex sulphide ores, ed. M. J. Jones, London, Institute of Mining and Metallurgy, 71.

Received April 18, 2012; reviewed; accepted July 11, 2012

LEAD(II) REMOVAL FROM AQUEOUS SOLUTIONS BY SOLVENT EXTRACTION WITH TETRACARBOXYLRESORCIN[4]ARENE

Joanna KONCZYK¹, Cezary KOZŁOWSKI¹, Władysław WALKOWIAK²

¹ Institute of Chemistry and Environment Protection, Jan Długosz University of Częstochowa, 42-201 Częstochowa, Armii Krajowej 13/15, Poland, e-mail: j.konczyk@ajd.czest.pl

² Chemical Metallurgy Division, Faculty of Chemistry, Wrocław University of Technology, 50-370 Wrocław, Wybrzeże Wyspiańskiego 27, Poland

Abstract: A novel tetracarboxylresorcin[4]arene was synthesized and its selective complexing ability towards Pb(II) ions was examined. The influence of several parameters such as pH of aqueous phase, agitation time, extractant and modifier concentrations on solvent extraction of Pb(II) ions from the aqueous nitrate phase into chloroform organic phase was studied. The stoichiometry of the formed metal-ligand complexes was established by slope analysis. Pb(II) ions were quantitatively extracted in the form of 2:1 Pb(II)-resorcin[4]arene complex from aqueous solutions of pH 5.5 to the solution of ligand in chloroform. Competitive solvent extraction experiments in the presence of Zn(II) and Cd(II) ions were also carried out and high selectivity of the extractant towards Pb(II) over Zn(II) and Cd(II) was found. The selectivity order was: Pb(II) >> Cd(II) > Zn(II).

Keywords: solvent extraction, lead(II), zinc(II), cadmium(II), resorcinarene

Introduction

For many years solvent extraction has been one of the most used techniques for the removal and separation of heavy metal ions in the industrial scale processes. The general advantage of solvent extraction over traditional methods used for wastewaters treatment (chemical precipitation, coagulation-flocculation, ion exchange, adsorption, membrane filtration) is highly selective metal recovery from aqueous solutions (> 500 mg/dm³) during continuous operations. The efficiency of metal ion extraction depends on many parameters such as ligand structure, solution pH, type of solvent, temperature and time of process, however the extractant ability to form a metal-ligand complex has a crucial effect on the process selectivity. Therefore, results of wide studies dealing with extractive removal and separation of Pb(II) ions with the use of

commercially available chemicals *e.g.* di(2-ethylhexyl)phosphoric acid – D2EHPA (Holdich and Lawson, 1985; Gherasim et al., 2011), CYANEX (Menoyo et al., 2001; Kozłowska et al. 2007), tributyl phosphate – TBP (Arous et al., 2010), aromatic hydroxyoximes – LIX (Rodriguez et al., 1997) and newly synthesized macrocycles such as lariat and crown ethers (Kalmykov et al., 1998; Walkowiak and Kozłowski, 2009), calixarenes and calixcrowns (Roundhill et al., 2009) as extractants carried out in various extraction systems were reported.

Calix[n]arene-based compounds with different groups such as carboxylic, ester, amide, thioamide and acetylhydrazide moieties functionalizing phenolic oxygen atoms of calixarene or thiacalixarene platform were applied for Pb(II) extraction. It was noted that calixarenes functionalized with proton-ionizable groups such as carboxylic acids have a better complexing ability towards lead ions than their analogs with non-ionizable (*e.g.* ester) groups or non substituted hydroxyl groups (Toumi et al., 2008). Many researchers have found that carboxyl derivatives of calix[n]arenes are efficient extractants of lead ions and that the number of attached carboxylic groups, conformational structure of these ligands and cavity size of basic skeleton play a crucial role in a Pb(II) ions complexation. Mono-, di- (Yang et al., 2011; Park et al., 2010), tetra- (Ohto et al., 1999) and pentaacids (Adhikari et al., 2010) were used as a Pb(II) complexing agents and it was observed that incorporation of more proton-ionizable groups to the calixarene skeleton enhanced its binding affinity and selectivity towards Pb(II) ions. Ohto et al. (1999) reported high efficiency and selectivity of Pb(II) extraction over Zn(II), Cu(II), Fe(III) and Al(III) by tetracarboxylcalix[4]arene with following selectivity orders: Pb(II) > Fe(III) > Cu(II) > Zn(II).

The results presented by Park et al. (2010) show that the mixed calix[4]arene possessing two carboxylic and two butyloxy groups on the narrow rim occurring in 1,3-alternate, partial cone (with butyl groups up) and cone conformations was an efficient extractant of lead ions at equilibrium pH of aqueous phase equal to 5.0, but the change of isomeric forms to partial cone with carboxyl groups decreased the complexing ability of this ligand.

One of the most promising and intensively studied class of macrocycles related to calixarenes are calix[n]resorcinarenes, named also resorcin[n]arenes. They are products of the acid-catalyzed condensation reaction of resorcinol with an aldehyde. Resorcinarenes differ from calixarenes in the spacing of the phenolic hydroxyl groups (the upper wide rim) and have more functionalization sites in the molecule (from 2 to 16 sites for resorcin[4]arenes) than calixarenes, therefore the different extractive properties of resorcinarenes towards metal ions than those of calixarenes should be expected. Although many resorcin[n]arenes (usually $n = 4, 6$) were synthesized (Kozłowski et al., 2010), there are only very few examples of their separation properties towards metal ions, especially transition and post-transition metal ions (Jain and Kanaiya, 2011). Podychaev et al. (2009) quantitatively extracted Pb(II) ions from nitrate aqueous solution (pH = 6.0) containing $2.5 \cdot 10^{-4}$ M picric acid to chloroform phase with tetranonylcalix[4]resorcinarene bearing acetylhydrazone groups. Only non-

ionizable resorcin[4]arenes modified by methylene bridges were applied for Pb(II) ions removal in membrane extraction by using polymer inclusion membranes; in this process the transport of about 80% Pb(II) ions to nitric acid was observed (Benosmane et al., 2009; 2010). In the analogy to calixarenes, resorcinarenes with attached proton-ionizable carboxylic groups should be more efficient and selective extractants for Pb(II) ions in comparison to corresponding non-ionizable compounds.

We synthesized tetracarboxylresorcin[4]arene and studied its extraction behavior towards Pb(II) ions. The influence of parameters such as the agitation time, the ligand and modifier concentrations and pH of aqueous phase on process efficiency was discussed. Selectivity of the ligand towards Pb(II) was also evaluated by a competitive extraction with Pb(II), Zn(II) and Cd(II) ions.

Experimental part

Reagents

Tetracarboxylresorcin[4]arene $R(\text{COOH})_4$ was synthesized in two steps. In the first step involving the acid catalyzed condensation of resorcinol with dodecanal, the undecylresorcin[4]arene was obtained (Schantwinkel et al., 2008). This compound was functionalized by α -bromoacetic acid in the presence of NaH in dry THF, according to procedure similar to that described by Demirel et al. (2003). The structure of the compound presented in Fig. 1 was confirmed by ^1H NMR spectroscopy (500MHz, DMSO-d_6), δ : 0.825 (t, 12H, $J = 7,5$ Hz, CH_3), 1.12–1.125 (m, 72H, $\text{CH}_3(\text{CH}_2)_9$), 1.824 (m, 8H, CH_2CH), 4.24 (m, 4H, ArCHAr), 4.51 (s, 8H, OCH_2COOH), 6.30 (s, 4H, ArH), 6.38 (s, 4H, ArH), 8.80 (s, 4H, ArOH)

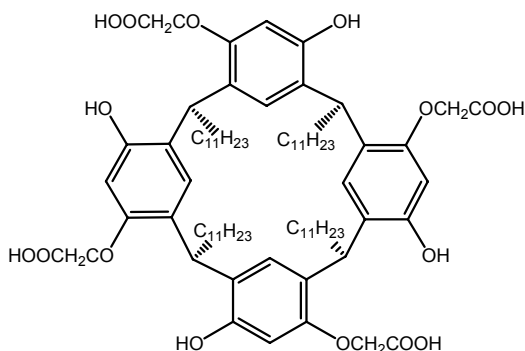


Fig. 1. Structure of $R(\text{COOH})_4$

The HPLC grade chloroform (CHCl_3) used as the ligand solvent was provided from POCH (Gliwice, Poland). The other organic chemicals were of commercially available reagent grade and were used without further purification.

All aqueous solutions were prepared using analytical reagent grade chemicals (POCH, Across) and deionized water (conductivity – 0.10 $\mu\text{S}/\text{cm}$). Solutions of Pb(II), Zn(II) and Cd(II) were prepared by dissolving appropriate amounts of $\text{Pb}(\text{NO}_3)_2$, $\text{Zn}(\text{NO}_3)_2 \cdot 6 \text{H}_2\text{O}$ and $\text{Cd}(\text{NO}_3)_2 \cdot 4 \text{H}_2\text{O}$ in water.

Solvent extraction procedure

The solvent extraction experiments were carried out at room temperature in a stopped glass flask at 1:1 volume ratio of aqueous and organic phases. The chloroform phase of $\text{R}(\text{COOH})_4$ and aqueous phase containing metal nitrate were agitated by mechanical shaker with a constant stirring rate 600 rpm. The phases were separated after the mixture was settled for 12 h and the metal ion concentrations were determined in aqueous phase using flame atomic absorption spectrometer (Solar 939, Unicam). Metal ion concentrations in the organic phase $[M^{2+}]_{org}$ were calculated from the difference of the metal ion concentrations in the aqueous phase before $[M^{2+}]_{aq,0}$ and after extraction $[M^{2+}]_{aq}$ and the following equations for the percent extraction %*E* (Eq. 1) and the metal distribution ratio between organic and aqueous phases *D* (Eq. 2) calculation were applied:

$$\%E = \frac{[M^{2+}]_{aq,0} - [M^{2+}]_{aq,eq}}{[M^{2+}]_{aq,0}} \cdot 100 \%, \quad (1)$$

$$D = \frac{[M^{2+}]_{aq,0}}{[M^{2+}]_{aq,eq}}. \quad (2)$$

The pH of aqueous phase was adjusted by adding a small amount of HNO_3 and measured with Elmetron CX-731 pH-meter. The pH value of aqueous solutions after solvent extraction was taken as the equilibrium pH.

Results and discussion

Effect of *n*-decanol

During preliminary experiments of solvent extraction from $5 \cdot 10^{-4} \text{ M}$ Pb(II) (pH = 5.0) aqueous nitrate solution by $\text{R}(\text{COOH})_4$ dissolved in CHCl_3 at $5 \cdot 10^{-4} \text{ M}$ concentration, the formation of emulsion at the interface of aqueous and organic phases was observed. This phenomenon in extraction systems is known and described in the literature, especially for alkali metal ions extraction from nitrate aqueous solutions with macrocycles (Delmau et al., 2005). Most of the available evidence on third phase formation suggests that it may be due to limited dissolution of extractant after its protonation when contacted with acidic aqueous phase and that the addition of a modifier, e.g. a long chain alcohol usually prevented the third phase appearance, therefore *n*-decanol

was added to organic phase. Our investigations revealed that the third phase can be removed after addition of 20% of n-decanol, but such modification resulted in a decrease of the extraction efficiency of Pb(II) ions. The effect of n-decanol content in organic phase on extractability of tetracarboxylresorcinarene was studied. Results are shown in Fig. 2.

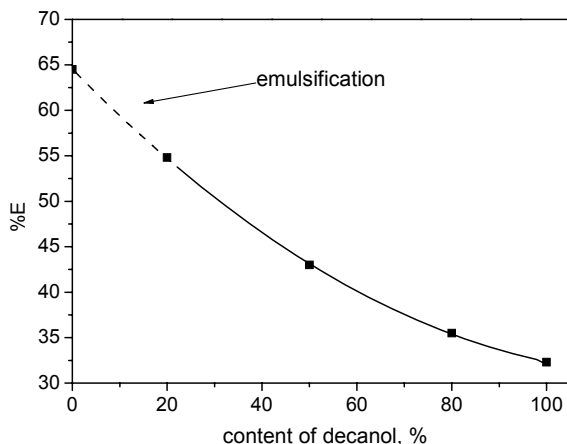


Fig. 2. Effect of n-decanol on percentage extraction of Pb(II) by $R(\text{COOH})_4$ ($[\text{Pb}(\text{II})] = 5 \cdot 10^{-4}$ M, $\text{pH} = 5.0$; $[R(\text{COOH})_4] = 5 \cdot 10^{-4}$ M; contact time: 1 h)

Effect of agitation time

The solvent extraction experiments were carried out for $1 \cdot 10^{-3}$ M $R(\text{COOH})_4$ solution in CHCl_3/n -decanol (4/1) and aqueous phase containing $5 \cdot 10^{-4}$ M Pb^{2+} (pH 5.5) at agitation times ranging from 5 to 180 min. The Pb(II) extraction percentage increased with the contact time and reached the plateau of 55% within 50–70 min. The further agitation of solutions caused the slight decrease of the extraction efficiency, nevertheless, these changes are within the range of the experimental error estimated to be approximately $\pm 2\%$. To ensure equilibrium, 1 h contact time was maintained during the extraction studies.

Effect of pH

The efficiency of extraction of metal cations by acidic-type extractants depends on the deprotonation of extractant molecules and the formation of metal-ligand complex. Extraction process for divalent metal ions with tetracarboxylresorcin[4]arenes at the aqueous/organic interface can be written as follows:



where $R(\text{COOH})_4$ and $[R(\text{COO})_4\text{H}_{4-2a}]\text{M}_a$ denote extractant and metal-ligand complex, respectively. This equation shows that the acidity of aqueous phase plays a significant role in extraction process, therefore the effect of initial pH of aqueous phase containing $5 \cdot 10^{-4}$ M Pb(II) in the range 1.5–6.0 was determined. The extraction of Pb(II) ions in the higher pH may not be precise because of the metal ions hydrolysis and the hydroxide precipitation that can interfere with the metal-ligand complex formation and cause decline of process efficiency. As shown in Fig. 3, the increase of pH to 5.5 caused the enhancement of process efficiency to ca. 60%, however with the further increase in pH efficiency slightly declines. Pb(II) extraction at low pH seems to be caused by the occurrence of strong intermolecular hydrogen bonding and protonation of most hydroxyl groups in the $R(\text{COOH})_4$ molecule. When there is sufficient excess of H^+ ions in the strongly acidic solution in comparison to metal ion, most of oxygen pair electrons coordinate rather with H^+ than with metal cations. In the case of the high pH of aqueous solution, where limited amount of H^+ ions is present, the interaction between oxygen lone pair electrons of $R(\text{COOH})_4$ and vacant orbital of Pb(II) is possible. Similar profile of percent Pb(II) loading to the organic phase versus pH of aqueous phase was found for dimetoxycalix[4]arene di(carboxylic acid) with cone conformation (Park et al., 2010). However, these results differ from those obtained by Ohto et al. (1999) for methylbutylcalix[4]arene with four acetic acid groups and Adikhari et al. (2010) for *t*-butylcalix[5]arene with five acetic acid moieties, where a quantitative removal of Pb(II) ions from acidic solutions of pH above 2.0 was observed. It is probably caused by the differences in the geometrical arrangement of carboxyl groups in calixarene and resorcinarene molecules and their dissociation.

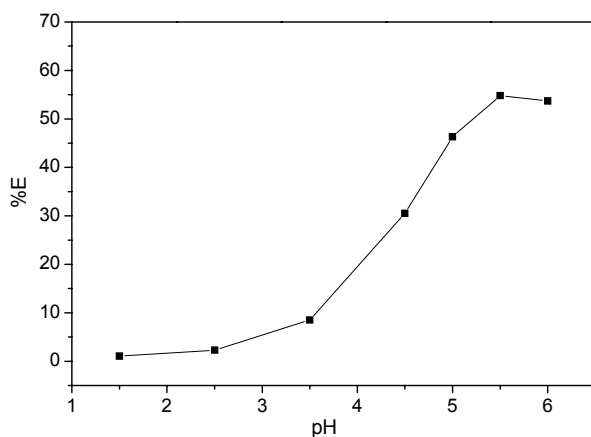


Fig. 3. Effect of pH on the Pb(II) extraction ($[\text{Pb(II)}] = 5 \cdot 10^{-4}$ M; $[\text{R}(\text{COOH})_4] = 1 \cdot 10^{-3}$ M; the contact time: 1 h)

Effect of extractant concentration

The solvent extraction of Pb(II) with extractant concentration in the range from $5 \cdot 10^{-4}$ to $1 \cdot 10^{-2}$ M under the best conditions of agitation time and aqueous phase pH was investigated. It was observed that the Pb(II) extraction efficiency increased with the resorcinarene concentration increase and reached maximum values of 99% for $R(\text{COOH})_4$ in $\text{CHCl}_3/\text{n-decanol}$ (4/1 vol.) mixture at the $1 \cdot 10^{-2}$ M concentration. Fig. 4 shows the logarithmic relation of the Pb(II) distribution ratio between aqueous and organic phases vs. extractant concentration. The slope of obtained straight line was determined to be 1.66 ± 0.04 what can indicate that two metal ions are extracted by one ligand molecule, and complexes $R(\text{COO})_4\text{Pb}_2$ are formed.

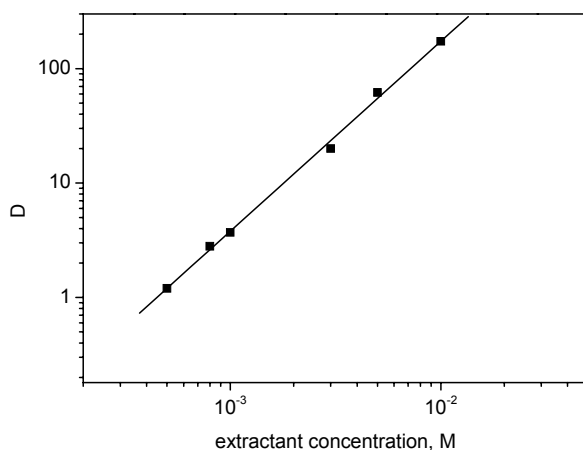


Fig. 4. Effect of extractant concentration on the distribution coefficient
 ($[\text{Pb}(\text{II})] = 5 \cdot 10^{-4}$ M, pH = 5.5)

The extraction ability of macrocyclic carrier is optimized by the structural modifications both within the ring and terminal groups, that can be either hydrophobic alkyl chains or ionizable, hydrophilic units. The complexation ability with metal ion may proceed by electrostatic interaction with aromatic rings (size-recognition) as well as by the cation- π interaction. For the explanation of Pb(II) complexation mechanism by $R(\text{COOH})_4$, a further evidence, e.g. by determination of crystallographic structure of the ligand and its complex with Pb ions is required.

Competitive solvent extraction of Pb(II), Zn(II) and Cd(II)

The competitive solvent extraction of Pb(II), Zn(II) and Cd(II) ions from $5 \cdot 10^{-4}$ M aqueous nitrate solutions into chloroform/n-decanol (4/1 vol.) phase containing $1 \cdot 10^{-3}$ M resorcinarene $R(\text{COOH})_4$ as an extractant was also carried out. The obtained values of percent extraction show that $R(\text{COOH})_4$ can be used for selective removal of Pb(II) over Cd(II) and Zn(II) ions. The relatively high separation of Pb(II) ions was observed

in the competitive solvent extraction from aqueous solution in pH range 4.0–6.0 (Fig. 5).

The efficiency and selectivity of metal ions extraction decreased in the order Pb(II) \gg Cd(II) > Zn(II). The selectivity coefficients S calculated as $D_{\text{Pb(II)}}/D_{\text{Cd(II) or Zn(II)}}$ at different pH's of aqueous phase are presented in Table 1.

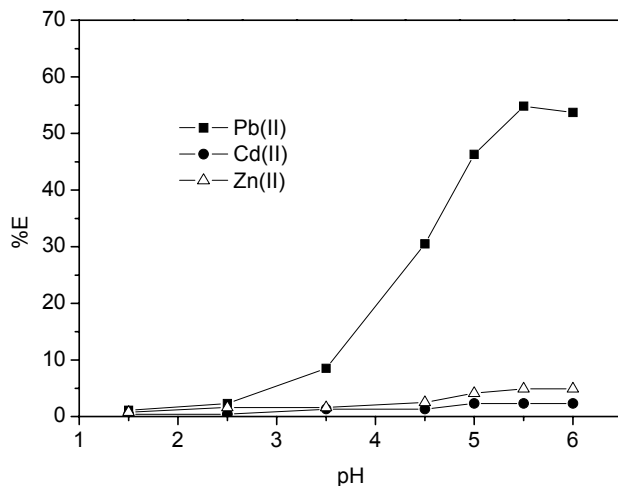


Fig. 5. Competitive solvent extraction of Pb(II), Cd(II) and Zn(II) ions, ($[M(\text{II})] = 5 \cdot 10^{-4}$ M; $[R(\text{COOH})_4] = 1 \cdot 10^{-3}$ M; the contact time: 1 h)

Table 1. Selectivity coefficients at different pH's of aqueous phase (process conditions in Fig. 5)

S	pH						
	1.5	2.5	3.5	4.5	5.0	5.5	6.0
$S_{\text{Pb/Cd}}$	1.38	1.39	5.56	17.41	20.20	23.44	22.40
$S_{\text{Pb/Zn}}$	2.97	6.01	6.81	32.30	36.68	51.53	49.24

The increase of pH resulted in higher selectivity coefficients. The highest S values were obtained for a pair Pb(II) / Zn(II) ions at pH 5.5. The successful separation Pb(II) by $R(\text{COOH})_4$ was achieved. The excellent extraction behavior of applied extractant towards Pb(II) ions results probably from better fitting of large Pb(II) cations to cavity size of resorcinarenes than in the case of smaller cations, *i.e.* Cd(II) and Zn(II).

Conclusions

The tetracarboxylresorcin[4]arene was found to be an efficient and selective extractant for lead(II) solvent extraction from nitrate aqueous solutions. The best efficiency of the solvent extraction was obtained for one-hour agitation time of aqueous phase at pH

5.5 and organic phase containing $R(\text{COOH})_4$ as the extractant ($5 \cdot 10^{-4}$ M), n-decanol (20% vol.) as the organic phase modifier and chloroform as the diluent. Under these conditions the separation of Pb(II) over Cd(II) and Zn(II) ions with high selectivity coefficients equal to 23.4 and 51.5, respectively, was achieved.

Acknowledgments

This work is part of the projects No. N N209 441539 and N N209 762940. The authors acknowledge Polish Ministry of Science and Higher Education and National Science Centre for financial support of these projects.

References

- ADHIKARI B.B., OHTO K., GURUNG M., KAWAKITA H., 2010, *Allosteric effect of the first lead on stepwise extraction of the second lead ion with p-t-butylcalix[5]arene pentacarboxylic acid derivative*, Tetrahedron Lett., 51, 3481–3485.
- AROUS O., AMARA M., TRARI M., BOUGUELIA A., KERDJOUJ H., 2010, *Cadmium (II) and lead (II) transport in a polymer inclusion membrane using tributyl phosphate as mobile carrier and CuFeO_2 as a polarized photo electrode*, J. Hazard. Mat. 180, 493–498.
- BENOSMANE N., GUEDIOURA B., HAMDI S. M., HAMDI M., BOUTEMEUR B., 2010, *Preparation, characterization and thermal studies of polymer inclusion cellulose acetate membrane with calix[4]resorcinarenes as carriers*, Mat. Sci. Eng. C, 30, 860–867.
- BENOSMANE N., HAMDI S.M., HAMDI M., BOUTEMEUR B., 2009, *Selective transport of metal ions across polymer inclusion membranes (PIMs) containing calix[4]resorcinarenes*, Sep. Purif. Technol., 65, 211–219.
- DELMAU L.H., LEFRANC T.J., BONNESEN P.V., BRYAN J.C., PRESLEY D.J., MOYER B.A., 2005, *Fundamental studies regarding synergism between calix[4]arene-bis(tert-octylbenzo-crown-6) and alcohol modifiers in the solvent extraction of cesium nitrate*, Solvent Extr. Ion Exch., 23, 23–57.
- DEMIREL N., MERDIVAN M., PIRINCCIOGLU N., HAMAMCI C., 2003, *Thorium(IV) and uranium(VI) sorption studies on octacarboxymethyl-C-methylcalix[4]-resorcinarene*, Anal. Chim. Acta, 485, 213–219.
- GHERASIM C.-V. I., BOURCEANU G., OLARIU R.-I., ARSENE C., 2011, *Removal of lead(II) from aqueous solutions by a polyvinyl-chloride inclusion membrane without added plasticizer*, J. Membr. Sci. 377, 167–174.
- HOLDICH R.G., LAWSON G.J., 1985, *The solvent extraction of lead from chloride solutions using di(2-ethylhexyl)phosphoric acid*, Hydrometallurgy, 14, 387–393.
- JAIN V.K., KANAIYA P.H., 2011, *Chemistry of calix[4]resorcinarenes*, Russ. Chem. Bull., 80, 75–102.
- KALMYKOV St.N., ARHIPOV A.Y., ABRAMOV A.A., IVANOVA N.A., IOFA B.Z., PRONINA O.P., SAPOZHNIKOV Yu.A., ANISIMOV A.V., 1998, *Extraction of Sr(II), Ag(I) and Pb(II) by some oxa-tia- and tia-crown ethers*, J. Radionucl. Nucl. Chem., 228, 33–35.
- KOZŁOWSKA J., KOZŁOWSKI C.A., KOZIOL J.J., 2007, *Transport of Zn(II), Cd(II) and Pb(II) across CTA plasticized membranes containing organophosphorous acids as an ion carriers*, Sep. Pur. Technol., 57, 430–434.
- KOZŁOWSKI C., KUDELSKA W., KONCZYK J., 2010, *New Trends in Modifications and Applications of Resorcinarenes*, in *Macrocyclic Chemistry: New Research Developments*, Nova Publisher.
- MENOYO B., ELIZALDE M.P., ALMELA A., 2001, *Extraction of lead by CYANEX 302 from phosphoric acid media*, 2001, Solv. Extr. Ion Exchange, 19, 677–698.

- OHTO K., FUJIMOTO Y., INOUE K., 1999, *Stepwise extraction of two lead ions with a single molecule of calix[4]arene tetracarboxylic acid*, *Anal. Chim. Acta*, 387, 61–69.
- PARK Ch., CHUN S., BARTSCH R.A., 2010, *Effect of conformation on metal ion extraction by calix[4]arene dicarboxylic acids*, *J. Incl. Phenom. Macrocycl. Chem.*, 66, 95–105.
- PODYACHEV S.N., BURMAKINA N.E., SYAKAEV V.V., SUDAKOVA S.N., SHAGIDULLIN R.R., KONOVALOV A.I., 2009, *Synthesis, IR and NMR characterization and ion extraction properties of tetranonylcalix[4]resorcinol bearing acetylhydrazone groups*, *Tetrahedron*, 65, 408–417.
- RODRIGUEZ DE SAN MIGUEL E., AGUILAR J.C., BERNAL J.P., BALLINAS M.L., RODRIGUEZ M.T.J., DE GYVES J., CHIMMEL K., 1997, *Extraction of Cu(II), Fe(III), Ga(III), Ni(II), In(III), Co(II), Zn(II) and Pb(II) with LIX® 984 dissolved in n-heptane*, *Hydrometallurgy*, 14, 19–30.
- ROUNDHILL D.M., SOLANGI I.B., MEMON S., BHANGER M.I., YILMAZ M., 2009, *Liquid-liquid extraction of toxic metals (Cd, Pb, Hg) by calixarenes*, *Pakistan J. Anal. Environ. Chem*, 10, 1–13.
- SCHNATWINKEL B., STOLL I., MIX A., REKHAVSKY M.V., BOROVKOV V.V., INOUE Y., MATTAY J., 2008, *Monomeric, dimeric and hexameric resorcin[4]arene assemblies with alcohols in apolar solvents*, *Chem. Commun.*, 3873–3875.
- TOUMI N., KAJO F., FOURNIER D., VOCANSON F., LAMARTINE R., DUMAZET-BONNAMOUR I., 2008, *A useful approach toward solid-liquid extraction of metal cations with unsupported calixarenes*, *Mat. Sci. Eng. C*, 28, 645–652.
- WALKOWIAK W., KOZŁOWSKI C., 2009, *Macrocycle carriers for separation of metal ions in liquid membrane processes – a review*, *Desalination*, 240, 186–197.
- YANG Y., KYUNG LEE E., ZHOU H., SUROWIEC K., BARTSCH R.A., 2011, *Synthesis and metal ion extraction of calix[4]arene mono- and diacids with 2-methoxyethoxy pendant groups*, *J. Incl. Phenom. Macrocycl. Chem.* 70, 197–204.

Received April 13, 2012; reviewed; accepted July 5, 2012

MICROBIAL TRANSFORMATIONS OF FOSSIL ORGANIC MATTER OF KUPFERSCHIEFER BLACK SHALE – ELEMENTS MOBILIZATION FROM METALLOORGANIC COMPOUNDS AND METALLOPORPHYRINS BY A COMMUNITY OF INDIGENOUS MICROORGANISMS

**Renata MATLAKOWSKA, Dariusz RUSZKOWSKI,
Aleksandra SKŁODOWSKA**

Laboratory of Environmental Pollution Analysis, Faculty of Biology, University of Warsaw,
Miecznikowa 1, 02-096 Warsaw, Poland, e-mail- rmatlakowska@biol.uw.edu.pl

Abstract: The presented article describes the role of community of indigenous microorganisms occurring in the Kupferschiefer black shale in elements mobilization from fossil organic matter of the deposit. The short description of metalloorganic compounds and metalloporphyrins extracted from black shale was presented as well as the characterization of indigenous microorganisms. The processes of fossil organic matter colonization, biofilm development and elements mobilization accompanying bacterial growth was summarized.

Keywords: *black shale, fossil organic matter, metalloporphyrins, metalloorganic compounds, biotransformation, microbial community*

Metalloorganic compounds and metalloporphyrins occurring in Kupferschiefer black shale

The ~256-million-year-old polymetallic Kupferschiefer black shale located in Fore-Sudetic Monocline is a sedimentary rock containing large accumulation of organic carbon. The concentration of organic carbon is between 7–16% and it is typically of marine origin. It represents kerogen type II and contains a mixture of three maceral groups: liptinite, vitrinite and inertinite, as well as other organic components such as amorphous sapropelic mass and solid bitumens (Oszczepalski, 1999). The organic carbon of the Kupferschiefer is mainly comprised of long-chain saturated and unsaturated aliphatic hydrocarbons and polycyclic aromatic hydrocarbons (Skłodowska et al., 2005).

A major part of metals present in black shale occur in organic compounds (Sawłowicz, 1985; 1989; 1991; Szubert et al., 2006). Two types of organic compounds containing metals were identified in black shale – metalloporphyrins and metalloorganic compounds. The first group is represented among other by: tetraphenyl porphyrin, tetramethoxyphenyl porphyrin, tetramethyl porphyrin and metalloporphyrins derivatives such as copro-porphyrin permethyl ester and azoporphyrates (Table 1). Among metalloorganic compounds determined in black shale organic matter were: sandwich type compounds, carbonyl and carbamate compounds (Table 1).

Table 1. The list of organic compounds containing metals detected in Kupferschiefer shale

Chemical compounds	Chemical formula
Metalloporphyrins and metalloporphyrins derivatives	
$\alpha, \beta, \gamma, \delta$ -tetraphenylporphyrin (nickel, lead cobalt copper)	$C_{44}H_{28}N_4Ni$ (or <i>Pb, Co, Cu</i>)
Magnesium 5, 10, 15, 20 – tetrakis chlorophenyl porphyrin	$C_{44}H_{24}Cl_4N_4Mg$
[Tetramethyl 3,8,13,18-tetramethyl-21H,23H-porphine-2,7,12,17-tetrapropoato[2-]-N21,N22,N23,N24]-(zinc, copper)	$C_{40}H_{44}N_4O_8Zn$ (or <i>Cu</i>)
Tetra[1,2-(4-t-butyl)-benzo]-tetra-azaporhinato-oxyvanadium	$C_{48}H_{48}N_8OV$
Tetra[1,2-(4-t-butyl)-benzo]-tetra-azaporhinato-chloroaluminium	$C_{48}H_{48}N_8AlCl$
Chloro-(5,10,15,20)-tetramesitylporphinato chromium (III)	$C_{56}H_{52}N_4ClCr$
Metalloorganic compounds	
Methyltriisopropyltine	$C_{10}H_{24}Sn$
Ditelluride, bis(2,4,6-trimethylphenyl)	$C_{18}H_{22}Te_2$
Tungsten,(2,3- eta)-bicyclo[2.2.1]hepta-2,5-diene]pentacarbonyl	$C_{12}H_8O_5W$
Platinum, dichloro[(1,1',2,2'-eta)-3,3'-oxybis[propene]]	$C_6H_{10}Cl_2OPt$
Tungsten, phenyltricarbonyl-pi-cyclopentadienyl	$C_{14}H_{10}O_3W$
Zirconium,bis(1,2,3,4,5-eta)-1-(1,1-dimethyl)-2,4-cyclopentadien-1-yl	$C_{23}H_{34}Zr$

Indigenous community of microorganisms isolated from Kupferschiefer black shale

A community containing eight bacterial strains were isolated from black shale in the Lubin copper mine using cultivation based methods (Matlakowska and Sklodowska, 2009). Phylogenetic analysis based on 16S rRNA gene homology showed that five strains belonged to the γ -Proteobacteria (*Pseudomonas* sp., *Acinetobacter* sp.), one to the Firmicutes (*Bacillus* sp.) and two to the Actinobacteria (*Microbacterium* sp.).

Detailed analysis of these isolates revealed the adaptation of indigenous bacteria to geochemical conditions of the examined environment. They exhibited such properties as:

- ability to transform black shale ore and use it as a carbon and energy source,
- extremely high-level resistance to metals and metalloids (As, Co, Cu, Ni and Zn),

- proficiency in assimilation of organic acids (capric, adipic malic acids, pyruvic acid, galacturonic acid, itaconic acid),
- the activity of esterase, lipase and dioxygenase,
- the ability to degrade some aliphatic and aromatic hydrocarbons,
- the production of siderophores and organic acids which showed the ability to complex elements from black shale,
- the transformation of synthetic metalloporphyrins.

Organic matter colonization and biofilm development

It was demonstrated that an enriched community of indigenous heterotrophic microorganisms isolated from black shale grown under aerobic conditions could utilize shale organic matter as the sole carbon and energy source.

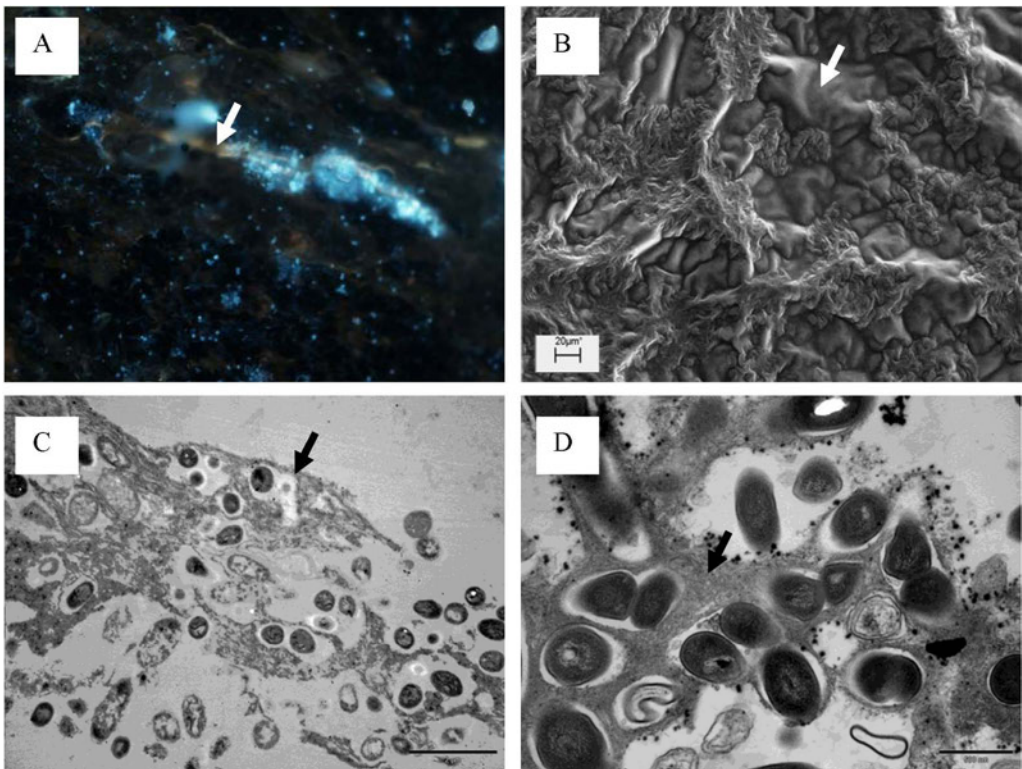


Fig. 1. (A) Epifluorescence micrograph of black shale sections showing the distribution of DAPI-stained microorganisms on the organic-rich laminae on the surface of black shale; (B) scanning electron microscopy (SEM) photomicrographs of bacterial colony-like form grown on a solid mineral medium covered with organic matter extracted from black shale as sole energy and carbon source. (C, D) Ultrathin section TEM photomicrographs of bacterial cells cultivated on mineral medium with organic matter extracted from black shale. The arrows indicate organic matter

Indigenous bacteria directly interact with black shale organic matter to produce a widespread biofilm on the Kupferschiefer shale surface (Matlakowska et al., 2012). They exhibit a specific affinity to fine laminae within the black shale that are rich in organic matter (Fig. 1A). The selective affinity was demonstrated by the localization of the biofilm along these strips oriented parallel to the lamination of the black shale.

Bacteria were able to grow in aerobic conditions on liquid mineral medium supplemented with organic matter extracted from black shale as the sole carbon and energy source. Figure 1B shows photomicrograph of a colony-like form from a mixed culture of bacteria growing on solid mineral medium overlaid with organic matter as the sole carbon and energy source. Colonization of shale extract is apparent and it is a direct evidence of capability of indigenous bacteria to use organic matter as energy and carbon source (Matlakowska and Skłodowska, 2011). Ultrathin cross and longitudinal sections of bacteria grown on solid mineral medium supplemented with organic matter were examined using transmission electron microscopy (TEM) (Figs 1C, D). A direct attachment of cells to organic matter is visible. Intracellular reserve material was also detected in bacterial cells. This material was identified as phosphorus by X-ray microprobe analysis (Matlakowska and Skłodowska, 2011).

Fossil organic matter biodegradation and elements mobilization

The study of biodegradation of black shale organic matter was based on the simultaneous analysis of the concentration of released organic carbon and the analysis of metal concentration mobilized to aqueous phase of cultures and chloroform extracts of this phase. The chemical analysis of biodegradation products was also performed.

Degradation of the black shale organic matter was clearly demonstrated by the release of organic carbon (DOC) into the aqueous phase of the cultures (Fig. 2). The level of DOC in the liquid phase reached a maximal concentration of 16 mg/dm³ after 25 days of cultivation.

It was confirmed that about 70% of organic matter was degraded after 30 days of experiment. The main biodegradation intermediates and products were identified as phosphonic acid dioctadecyl ester, cyclopropene butanoic acid, phthalic acid bis(methyl nonyl) ester, hexadecanoic acid, octadecanoic acid, hexadecanol and chloropropionic acid. At the end of the cultivation a part of these compounds completely disappeared indicating that they were metabolized and isoindole-1,3 was detected which is a well-known metabolite of i.e. pyrene, fluoranthene and phenanthrene produced by bacterial degradation (Matlakowska and Skłodowska, 2011).

Simultaneous analysis of metals in aqueous phase and chloroform extracts allowed comparing the total concentration of metals released from organic matter and their content in organic compounds. The concentration of cobalt, copper and nickel directly

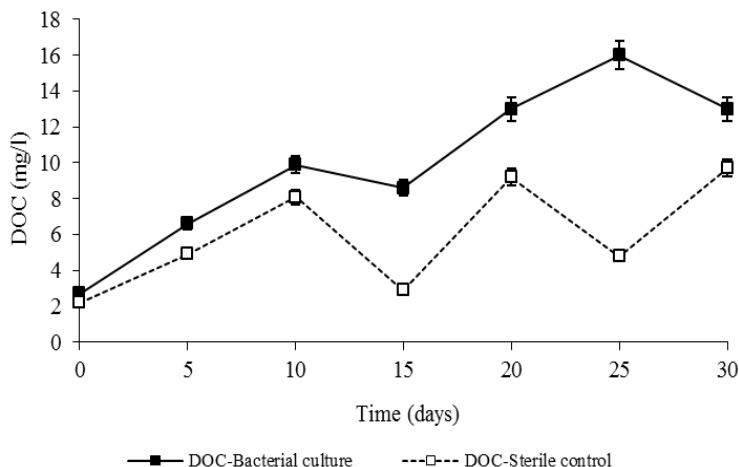


Fig. 2. Organic carbon mobilization from shale organic matter – the changes of the dissolved organic carbon (DOC) concentration in the aqueous phase of bacterial cultures during growth of microorganisms.

released from organic matter extracted from black shale to the aqueous phase of cultures and control as well as chloroform extract of this phase and are presented on Figs 3A, B, C. It was clearly showed that the biodegradation of organic matter cause the release of metals into the culture solution.

The concentration of cobalt, copper and nickel in organic fraction (chloroform extract) reached the highest value in bacterial cultures between 20 and 25 days what is in correlation with the concentration of organic carbon in the aqueous phase. At the end of experiment the concentration of these elements in chloroform extracts decreased. Simultaneously the increase of the concentration of cobalt and copper in the aqueous phase was observed (Figs 3 A, B).

Obtained results support the hypothesis that the biodegradation of organic compound leads to the release of chemical elements to the aqueous phase.

The most interesting results were obtained for copper. About 74% of copper present in black shale substrate was released to aqueous phase of bacterial culture after 30 days of cultivation. In the case of control copper extraction was about 10%. Interestingly, the percent of copper occurring in the form of organic compounds decreased from 19% to 0.15% in bacterial culture in the course of experiment, what confirmed the biodegradation of organic compounds containing this metal. In the case of control, the concentration of copper in chloroform extract was stable and represented the dissolved compounds. The concentration of cobalt and nickel release to aqueous phase of culture from black shale organic matter was 1.4% and 8.9% respectively, while in control 3.4% and 13.8%. The concentration of these metals in bacterial culture was lower than in control and indicated specific fluctuations during experiment. It was calculated that approximately 10% of cobalt and 20 % of nickel were accumulated by bacterial cells during experiment.

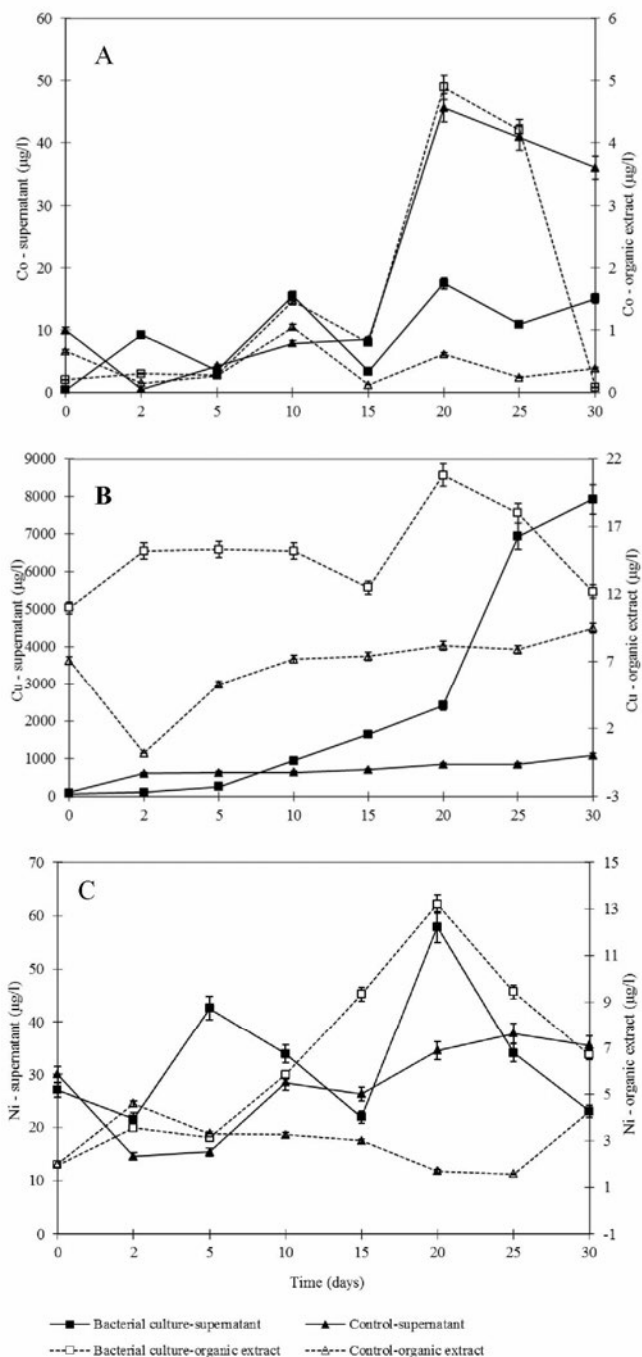


Fig. 3. Concentration of cobalt (A), copper (B) and nickel (C) in the aqueous phase and chloroform extracts of bacterial cultures and sterile controls over the 30 days of cultivation

The biodegradation of organic compounds containing metals were also confirmed by the analysis of UV-Vis spectra of chloroform extracts of aqueous phase. It revealed the significant differences between the bacterial cultures and the sterile control cultures as well as between the bacterial cultures at different days of cultivation (Fig. 4).

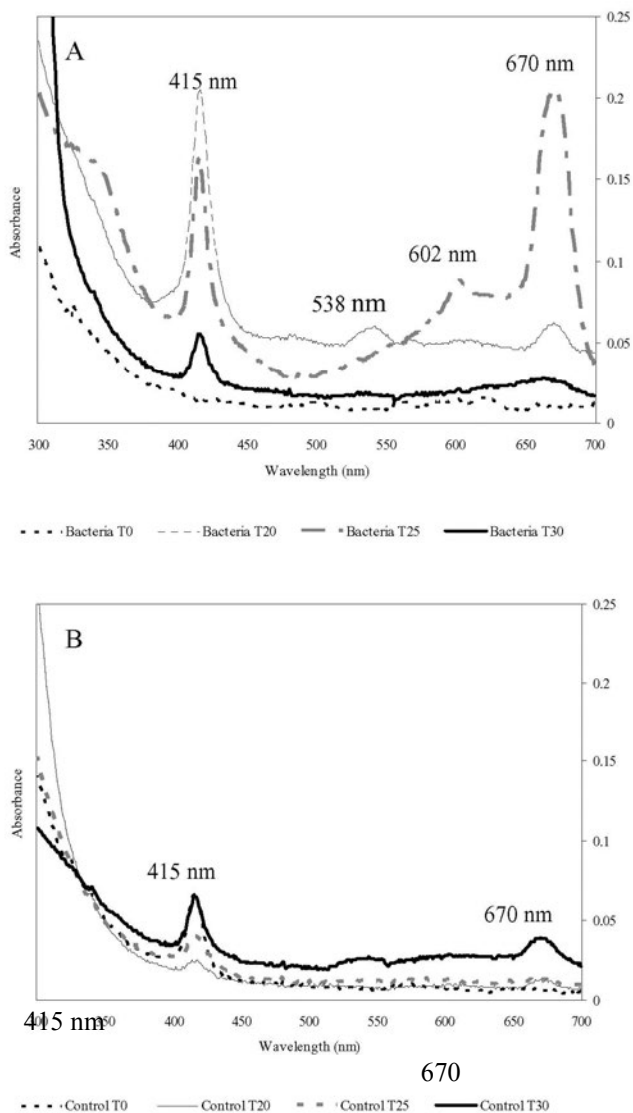


Fig. 4. UV-Vis spectra of chloroform extracts of the aqueous phase of bacterial cultures (A) and sterile control (B) containing organic matter extracted from black shale at the beginning of the experiment (T0), and after 25 (T25) and 30 days (T30) of cultivation

The spectrum of the sample after 20 and 25 days of bacterial treatment exhibited absorption bands typical for metalloporphyrins which is a Soret band (390–425 nm) and Q band (480–700 nm) (Kadish et al., 2000). An intense Soret band with maximum absorption at 415 nm and Q bands with maximum absorption peaks at 602 and 670 nm were apparent and they were considerably stronger than in the control samples. All of these peaks had decreased after 30 days of bacterial cultivation, indicating the degradation of these compounds. Similar results were obtained in earlier experiment in which the biodegradation of whole black shale and synthetic metalloporphyrins were studied (Matlakowska and Sklodowska, 2010, 2010a). The first step in synthetic metalloporphyrin biotransformation was identified as the highly efficient uptake of these compounds by bacterial cells and further degradation of them in bacterial cells (Matlakowska and Sklodowska, 2010a). The changes of UV-VIS spectra observed in this study also reflected the metalloporphyrins uptake and biodegradation.

Conclusions

- The results of this study confirm that indigenous bacteria play a role in the biotransformation of black shale and can influence the geochemical cycles of ancient organic carbon in the deep terrestrial subsurface.
- The biodegradation of organic matter was accompanied by the metal mobilization and release of organic compounds.
- Biodegradation of resistant compounds such as geoporphyrins was confirmed.
- The presence of phosphonic acid dioctadecyl ester in bacterial culture and intracellular reserve material containing phosphorus confirm the role of indigenous microorganisms in phosphorus mobilization from organic matter and simultaneous immobilization in cells.
- The capability of indigenous bacteria to degrade black shale organic matter may strongly influence carbon mobilization from deposit as well as shale fraction of tailings. This phenomenon may also cause the mobilization of potentially toxic compounds to the soil and groundwater.

Acknowledgements

This work was supported by a research grant from the Polish Ministry of Science and Higher Education (N N304 068635) and Bioshale (European project contract NMP2-CT-2004 505710). We wish to thank Dr. Krzysztof Nejbert from Institute of Geochemistry, Mineralogy and Petrology, Faculty of Geology, University of Warsaw (Poland) for his help in taking a picture 1A.

References

- KADISH K., SMITH K.M., GUILARD R., 2000, *The porphyrin handbook*. Academic Press, San Diego. vol. 1.
- MATLAKOWSKA R., SKLODOWSKA A., 2009, *The culturable bacteria isolated from organic-rich black shale potentially useful in biometallurgical procedures*. J. Appl. Microbiol. 107, 858–866.

- MATLAKOWSKA R., NARKIEWICZ W., SKŁODOWSKA A., 2010, *Biotransformation of organic-rich copper bearing black shale ore by indigenous microorganisms isolated from Lubin copper mine (Poland)*. Environ. Sci. Technol. 44, 2433–2440.
- MATLAKOWSKA R., SKŁODOWSKA A., 2010a, *Uptake and degradation of copper and cobalt porphyrins by indigenous microorganisms of Kupferschiefer*. Hydrometallurgy 104, 501–505.
- MATLAKOWSKA R., SKŁODOWSKA A., 2011, *Biodegradation of Kupferschiefer black shale organic matter (Fore-Sudetic Monocline, Poland) by indigenous microorganisms*. Chemosphere 83: 1255–1261.
- MATLAKOWSKA R., SKŁODOWSKA A., NEJBERT K., 2012, *Bioweathering of Kupferschiefer black shale (Fore-Sudetic Monocline, SW Poland) by indigenous bacteria: implication for dissolution and precipitation of minerals in deep underground mine*. FEMS Microbiol. Ecol. DOI:10.1111/j.1574-6941.2012.01326.x.
- OSZCZEPALSKI S., 1999, *Origin of the Kupferschiefer polymetallic mineralization in Poland*. Mineralium Deposita 34, 599–613.
- SAWŁOWICZ Z., 1985, *Significance of metalloporphyrins for the metal accumulation in the copper-bearing shales from the Zechstein copper deposits, Poland*. Mineral. Polon. 16, 35–42.
- SAWŁOWICZ Z., 1989, *Organic matter in the Zechstein Kupferschiefer from the Fore-Sudetic Monocline. I. Bitumen*. Mineral. Polon. 20, 69–86.
- SAWŁOWICZ Z., 1991, *Organic matter in the Zechstein Kupferschiefer from the Fore-Sudetic Monocline. II. Kerogen*. Mineral. Polon. 22, 49–67.
- SKŁODOWSKA A., MATLAKOWSKA R., BAL K., 2005, *Extracellular polymer produced in the presence of copper minerals during bioleaching*. Geomicrobiol J. 22, 1–9.
- SZUBERT A., SADOWSKI Z., GROS C.P., BARBE J.M., GUILARD R., 2006, *Identification of metalloporphyrins extracted from the copper-bearing black shale of Fore Sudetic Monocline (Poland)*. Mineral. Eng. 19, 1212–1215.

Received April 17, 2012; reviewed; accepted July 11, 2012

SEPARATION OF NICKEL AND ZINC IONS IN A SYNTHETIC ACIDIC SOLUTION BY SOLVENT EXTRACTION USING D2EHPA AND CYANEX 272

Mahdi GHARABAGHI¹, Mehdi IRANNAJAD², Amir Reza AZADMEHR²

¹ School of Mining Engineering, College of Engineering, University of Tehran, Tehran, Iran;
m.gharabaghi@gmail.com, gharabaghi@ut.ac.ir

² Department of Mining & Metallurgical Engineering, Amirkabir University of Technology, Hafez St, Tehran, Iran

Abstract: Solvent extraction was used to recover nickel and zinc from synthetic acidic solution. Many leaching solution and waste waters contain both zinc and nickel at the same time. Bis (2,4,4-trimethylpentyl) phosphinic acid (Cyanex 272) and Di(2-ethylhexyl) phosphoric acid (D2EHPA) were used to separate nickel and zinc. In the D2EHPA system, at equilibrium pH of 2, zinc extraction was more than 98% whereas nickel extraction was only 0.36%. The extraction of metals was found to increase with an increase of pH of the aqueous phase. At equilibrium pH 3.5, zinc extraction was completed and higher than 99% zinc was extracted using Cyanex 272. The maximum nickel extractions using D2EHPA and Cyanex 272 were achieved at equilibrium pH 4.5 and 7.5, respectively. Both extractants showed the relatively good separation levels between nickel and zinc. D2EHPA and Cyanex 272 isotherms for single metal solutions showed that the extraction order was $Zn^{2+} > Ni^{2+}$. $\Delta pH_{1/2}$ value showed that the separation of nickel and zinc using Cyanex 272 was simpler than D2EHPA system. The stripping study was performed using sulphuric acid and it was shown that above 98% zinc and nickel could be extracted. These results demonstrated separation of zinc and nickel from sulphate solutions to be favorable.

Keywords: D2EHPA; Cyanex 272; nickel extraction; zinc extraction

Introduction

In hydrometallurgical and environmental processing, selective recovery and removal of metals from industrial and waste solutions are very important and has been extensively studied (Gupta, 1990; Rotuska, 2008). Solvent extraction is a popular method for separation of metal ions from aqueous solutions which has been widely used in hydrometallurgical engineering for selective metals recovery from low-grade ores, complex ores and metallic wastes. This technology has been proposed as an efficient

separation method for waste treatment and metal recycling from industrial wastes (Sole et al., 2005).

Many solvents have been proposed for metals extraction in hydrometallurgical processes. Among these, organophosphorus-based extractants, oxime extractants and Cyanex extractants has been used for nickel extraction from acidic and alkaline solutions (CYANEX, 2007; Gotfryd, 2005; Grigorieva et al., 2010; Tanaka and Alam, 2010; Tsakiridis and Agatzini, 2004). Jakovljevic et al. (2004) used Cyanex 301 for nickel extraction from chloride medium. Tanaka and Alam (2010) have used LIX84-I for nickel extraction from ammoniacal–sulphate leach liquors.

Several researchers used di-2-ethylhexyl phosphoric acid (D2EHPA) for nickel and/or cobalt extraction from solutions. Separation of nickel from associated ions like Co is a major problem specially when choosing a single extracting agent like D2EHPA (Bhaskara Sarma and Reddy, 2002; Zhang et al., 2001). Versatic 10 acid and LIX 63 synergistic system was used to separate Ni and Co from the Zn, Cu, Mn, Mg and Ca in the synthetic laterite leach solution. However, the synergist was not commercially available (Cheng, 2006). Organophosphorus and its thio-analogs have used for the extraction of Ni and Co from a variety of synthetic solutions/leach liquors by Reddy and co-workers (Reddy et al., 2006, 2008).

Dithiophosphinic acid base extractants such as cyanex 301 are efficient solvents for nickel hydrometallurgy (CYANEX, 2007 ; Grigorieva et al., 2010). The possibility of nickel recovery from pregnant solutions using Cyanex extractant has been demonstrated in published papers (Agrawal, 2008; Gotfryd, 2005; Jakovljevic et al., 2004; Tsakiridis and Agatzini, 2004).

The separation of nickel from zinc has been encountered in materials such as hydrometallurgical zinc production, copper converter slag leaching, nickel laterite, etc. As seen from the above, in the most of reported studies, the main objective was to removal of these metals from the solution and limited amounts of data on the separation of nickel from zinc are available systematic investigation about nickel and zinc separation by solvent extraction is not abundant. Considering the importance of nickel and zinc mixtures, it is necessary to perform systematic investigations to search for effective extraction systems for nickel separation from zinc.

This paper presents the results of an investigation on the separation and recovery of nickel and zinc with different extractants (bis (2,4,4-trimethylpentyl) phosphinic acid (Cyanex 272) and di(2-ethylhexyl) phosphoric acid (D2EHPA)) diluted in hexane. The results focused on the determination of pH isotherms for metals separation. We systematically monitored the effects of important process parameters on nickel and zinc extraction and separation. The extracted ions were removed from the organic phase using sulphuric acid as an effective stripping agent.

Experimental

The stock solutions of zinc(II) and nickel(II) sulphate (0.5 M each) were prepared by dissolving analytical grade chemicals (Merck, Germany) in distilled water. Analytical grade Cyanex 272 (Cytec, Canada) and D2EHPA (Merck, Germany) were used as organic solvents without further purification whereas hexane was the diluent. Dilute H₂SO₄ and NaOH (Merck, Germany) solutions were used to adjust the pH of the aqueous solutions.

Perkin-Elmer atomic absorption spectroscopy was used to measure the nickel and zinc concentration in the solutions. The pH of the aqueous phase was measured using a pH meter (Fisher Scientific pH meter). The organic/aqueous mixture was agitated with a mechanical shaker.

Solvent extraction experiments were performed in flasks containing equal 50 cm³ volumes of aqueous and organic solutions. The pHs of aqueous solutions were kept constant by buffer solutions. The mixtures were agitated by mechanical shaker for 30 minutes, although the equilibrium conditions may have been reached in a few minutes. In each experiment, the organic phase contained 1M of the extractant (either D2EHPA or Cyanex 277) in hexane. Aqueous to organic phase ratio was 1:1 in all tests. After mixing the aqueous and organic solutions were separated by a separatory funnel. After phase separation for each test, about 10-cm³ aqueous solution was taken for chemical analysis. 40 cm³ of organic solution was taken for stripping using sulfuric acid solution. After stripping, the strip solution was taken for chemical analysis.

Results and discussion

Solvent extraction with D2EHPA

Distribution coefficient (D) is the ratio of metal concentration in organic phase to that in the aqueous phase at equilibrium. The extraction efficiency is commonly defined by equation 1:

$$\text{Extraction (\%)} = 100 \frac{[M]_{org}}{[M]_{aq}} = \frac{100D}{d + \frac{V_{aq}}{V_{org}}} \quad (1)$$

In the above equation, V_{aq} is the volume of aqueous phase and V_{org} is the volume of organic phase. In the solvent extraction process, the nickel and zinc solutes from the feed solution diffuse onto the interface of the emulsion globules and react with the carrier (reaction 1). The extraction of nickel and zinc by chelating extractants, can be represented by general equation 2 and 3 respectively:





Preliminary experiments showed that 1 M D2EHPA diluted with hexane was suitable for the extraction of copper from the concentrated aqueous feed solutions. The effects of equilibrium pH on the extraction of nickel and zinc from simulated acidic leaching solutions using D2EHPA is shown in Figs 1a and 1b respectively. In these experiments, aqueous solution containing different concentrations of nickel and cadmium shaken with 1 M D2EHPA at O:A ratio of 1:1 for 30 minutes at various equilibrium pH as shown in Fig. 1. The metals extraction increased with increasing aqueous pH for both extractant systems, particularly for nickel. At equilibrium pH of 2 zinc extractions was more than 98%, whereas nickel extraction was only 0.36%.

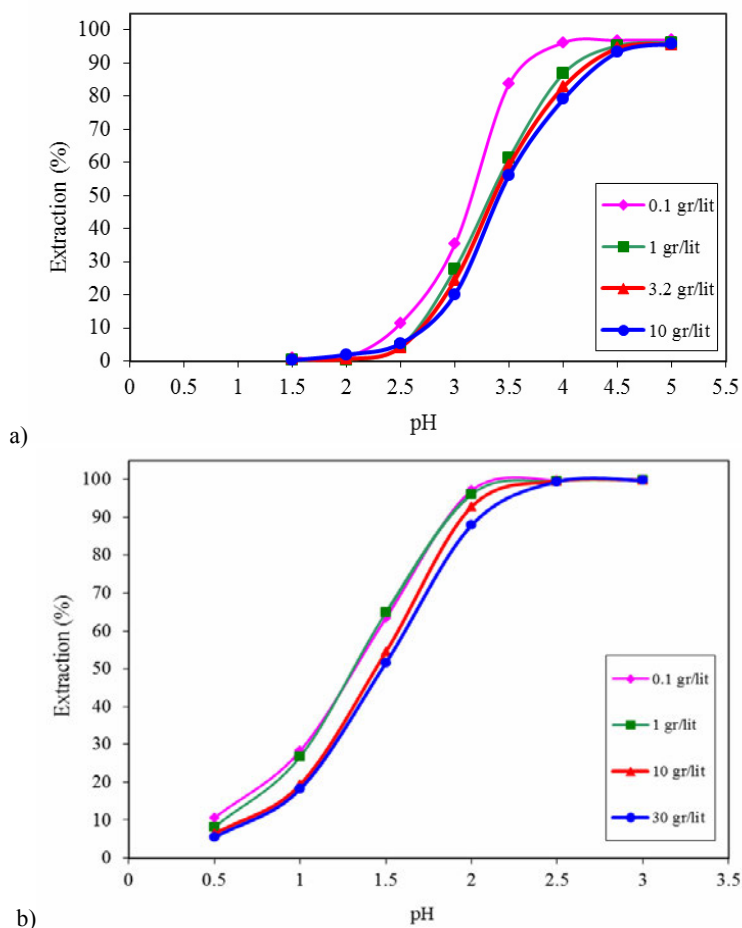
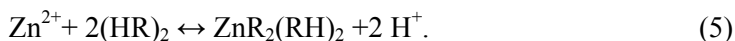
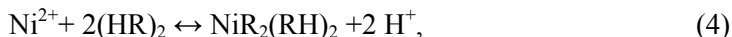


Fig. 1. Effects of aqueous phase pH on the extraction of nickel and zinc, 1 M D2EHPA, $t = 30$ minutes, $T = 25$, O/A phase ratio = 1:1: a) nickel, b) zinc

Solvent extraction with Cyanex 272

Nickel and zinc extraction from leaching solutions in different equilibrium pH was studied using Cyanex 272 as the extractant (figure 2). The results indicated that the nickel and zinc were extracted according to this sequence: $\text{Zn}^{2+} > \text{Ni}^{2+}$. The extraction equilibrium was as follows (Eqs 4 and 5):



The zinc and nickel extraction was found to increase with the increase in pH of the aqueous solution in the pH range 1–3 for zinc and 5–7.5 for nickel. This behavior is similar to results of pH effect of on the zinc extraction from aqueous waste solution using Cyanex (Ali et al., 2006). The same trend was obtained in the extraction of zinc from alloy electroplating wastewater using Cyanex 272 (Sze and Xue, 2003).

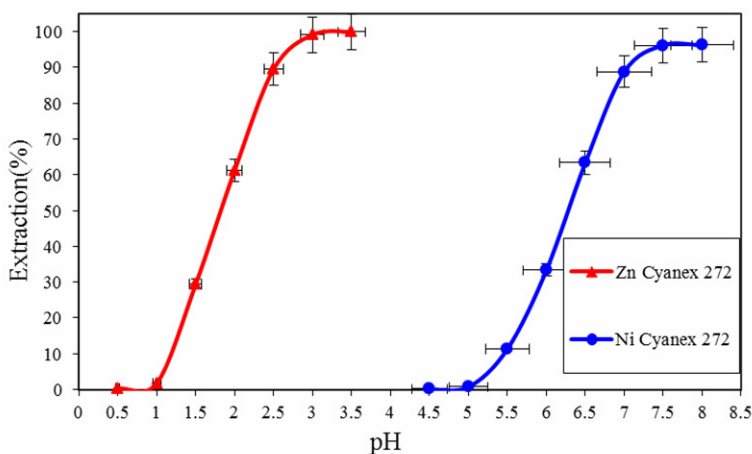


Fig. 2. Extraction percentages of nickel and zinc with 1 M Cyanex 272, as a function of the pH; initial aqueous solution: 1 g/l Ni, 1 g/l Zn; O/A = 1

Extraction mechanism

Plots of $\log D$ vs equilibrium pH for nickel and zinc extraction using D2EHPA are shown in Fig. 3. This figure gives a slope of 1.45 and 1.72 for nickel and zinc extraction respectively. These slopes indicated the release of 2H^+ leading to the extraction of nickel and zinc as NiHA_2 and ZnHA_2 in the organic phase as shown in Eqs 2 and 3 (Agrawal, 2008).

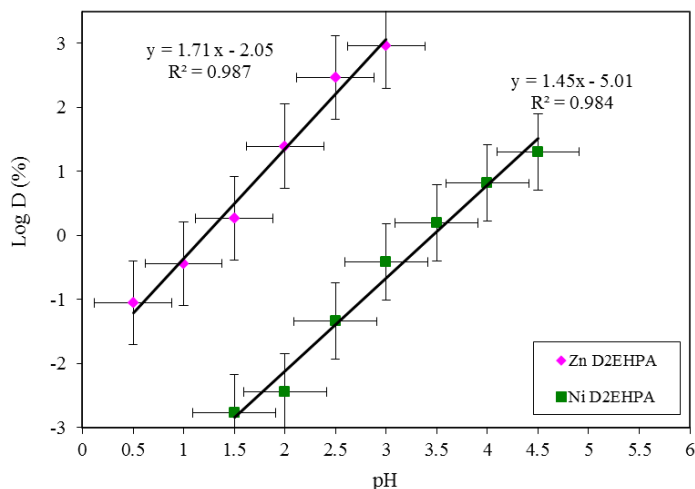


Fig. 3. $\log D$ for vs equilibrium pH for nickel and zinc extraction using D2EHPA

Figure 4 shows the plots of \log distribution coefficient vs equilibrium pH for nickel and zinc extraction by Cyanex 272. The slope for nickel extraction was 1.4, and for zinc extraction was 1.79. Similar to D2EHPA, these amounts of slopes showed that the release of 2H^+ leading to the extraction of nickel and zinc in the organic phase as shown in the equations 4 and 5.

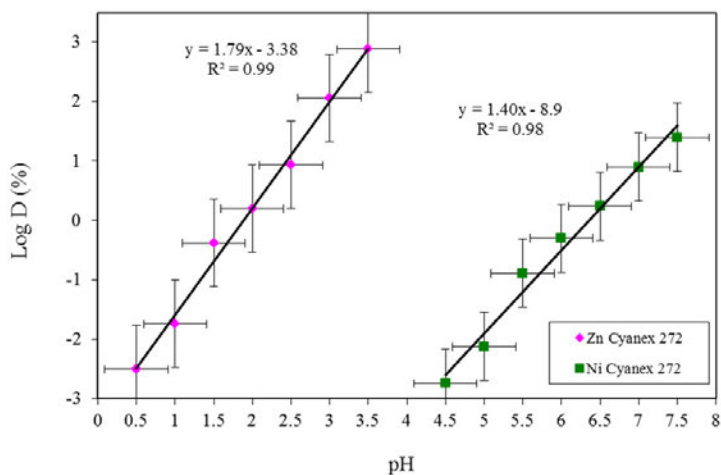


Fig. 4. $\log D$ for vs equilibrium pH for nickel and zinc extraction using Cyanex 272

Screening of extractants

In order to check the extractant capability for separation of nickel and zinc, the experiments were performed with a diluted solution containing 1 g/dm^3 of each metal

(Ni and zinc) using 1 M D2EHPA and 1 M Cyanex 272 as extractants. The effects of pH on the extraction efficiency are shown in the Fig. 5. The order of extraction for both solvents was Zn > Ni. The results showed that the D2EHPA was capable of extracting both metals at lower pH values. Regarding the selectivity, both extractants were selective for both metal but Cyanex 272 was more selective. In the metals separation by D2EHPA, Ni and Zn curves were closer. As it can be seen in Fig. 5a, by increasing pH from 0.5 to 2.5, zinc extraction using D2EHPA increased from about 11% to above 99%. In the Cyanex 272 extraction system, at equilibrium pH 3.5, zinc extraction was completed and was higher than 99%. In the case of nickel extraction by D2EHPA, 63.8% of nickel was extracted at pH 3.5. Using Cyanex 272, zinc ions had no effects on the nickel extraction. Similar behavior by Cyanex 272 was observed in zinc extraction(Salgado et al., 2003).

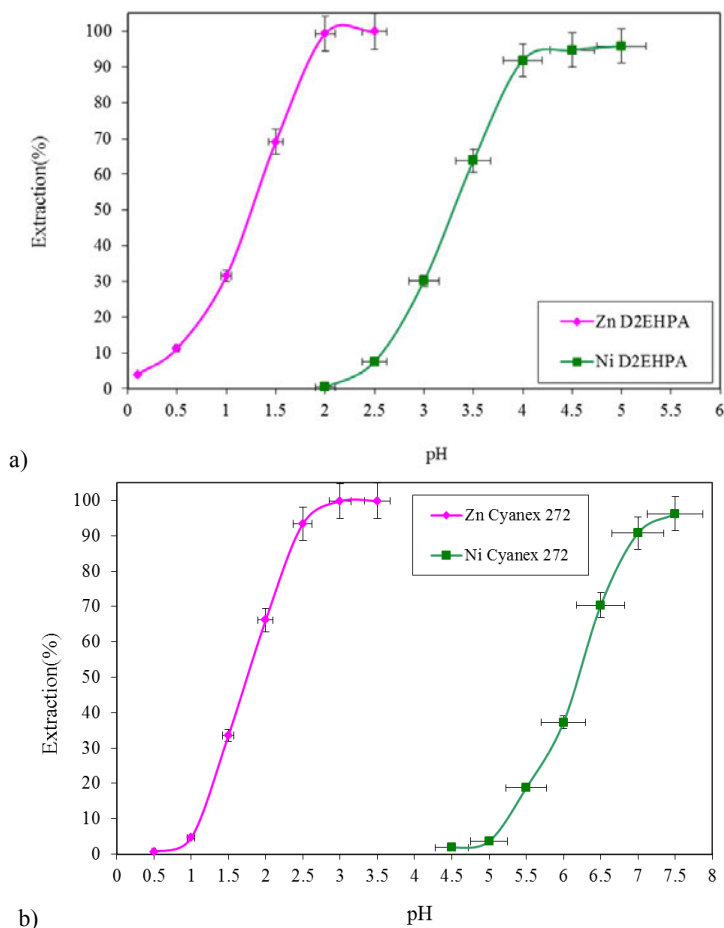


Fig. 5. The effects of pH on nickel and zinc separation; initial aqueous solution: 1 g/dm³ Ni, 1 g/dm³ Zn; O/A = 1, a) 1M D2EHPA, b) 1 M Cyanex 272

Extractant selectivity

The $pH_{1/2}$ values were used to show the separation selectivity for both extractant and Table 1 the $pH_{1/2}$ values for metals and respective differences. The difference in $pH_{1/2}$ values for nickel and zinc was used to identify the separation degree between nickel and zinc. If two metals have a greater $\Delta pH_{1/2}$ value, then they will have higher selectivity and better separation efficiency will be obtained. In our experiments, the $pH_{1/2}$ values obtained were 1.3 and 3.35 for zinc and nickel using D2EHPA extractant and 1.85 and 6.2 for zinc and nickel by Cyanex 272. The $\Delta pH_{1/2}$ value for the D2EHPA system was 2.05 and this difference shows that nickel separation from zinc can be performed 2 pH units higher than zinc. This amount indicated a relatively good separation level between nickel and zinc. In the Cyanex 272 extraction system, the $\Delta pH_{1/2}$ value was higher which showed that the separation of nickel and zinc using Cyanex 272 was simpler than D2EHPA system. Although Cyanex 272 exhibited simpler process and offered good separation of nickel and zinc, it is relatively expensive to be used commercially. D2EHPA is much less expensive, so D2EHPA was selected for further studies from the economical viewpoint, because D2EHPA is cheaper than Cyanex 272.

Table 1. $pH_{1/2}$ and respective differences ($\Delta pH_{1/2}$) for two solvent solutions

Extractant	$pH_{1/2}$		$\Delta pH_{1/2}$
	Zn	Ni	Zn–Ni
D2EHPA	1.3	3.35	2.05
1 M Cyanex 272	1.85	6.2	4.35

Comparison of extractant separation factor

The selectivity of extractant for desired metal separation can be quantified using separation factor β . The highest value of the separation factor corresponds to the highest selectivity in metals separation. Separation factor β is defined as follows (Reddy et al., 2008):

$$\beta = \frac{D_{Ni}}{D_{Zn}} \quad (6)$$

The separation factors β for both extractants were calculated and are plotted against pH (Fig. 6). It was shown that the both extractant had relatively good separation factor and the capacity of these extractants to separate nickel from zinc was apparent. Separation factor for D2EHPA was more dependent on pH. In D2EHPA system in the range pH of 2 to 2.5 the separation factor of nickel reached its maximum. In nickel and zinc separation using Cyanex 272, the separation factor of nickel reached its maximum in the pH range of 3.5–4.

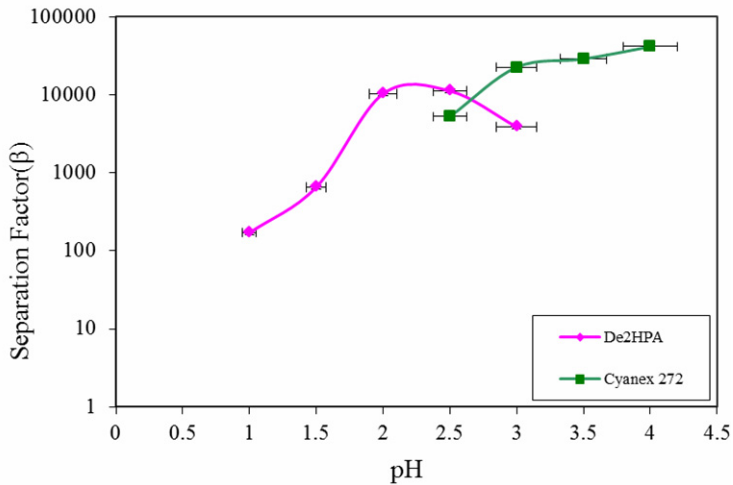


Fig. 6. Separation factors against equilibrium pH (1 M DEHPA and 1 M Cyanex 272, O/A = 1, 1 g/dm³ zinc and nickel concentration)

Stripping studies

The stripping investigations were performed using H₂SO₄ to for the stripping of zinc and Ni ions from the loaded D2EHPA solution. The stripping efficiencies of zinc with 2 and 5 M H₂SO₄ from a 1M DEHPA were 98.8 and 99.7% respectively. Nickel stripping from the loaded organic phase was studied using sulphuric acid. The results obtained indicated that the stripping percent nickel reached 98% using 2M sulphuric acid.

Conclusions

Nickel and zinc extraction and separation from sulphate solutions were carried out using D2EHPA and Cyanex 272 diluted with hexane. Using both extractants, the percentage extraction of both metals increased with the increase in pH of the aqueous phase. The observed $\Delta\text{pH}/2$ showed that the separation of nickel and zinc using both extractant was possible. The slope analysis studies of $\log D$ vs. pH plot gave a straight line, and its slope indicated that the releasing of 2H⁺ was the controlling mechanism in metal extraction. Separation factors obtained with combinations of two extractants showed that under experimental conditions, both extractants were capable of extracting nickel and zinc.

References

- AGRAWAL A., MANOJ M.K., KUMARI S., BAGCHI D., KUMAR V., PANDEY B.D., 2008. *Extractive separation of copper and nickel from copper bleed stream by solvent extraction route.* Minerals Engineering 21, 1126–1130.

- ALI A.M.I., AHMAD I.M., DAOUD J.A., 2006. *CYANEX 272 for the extraction and recovery of zinc from aqueous waste solution using a mixer-settler unit*. Separation and Purification Technology 47, 135–140.
- BHASKARA SARMA P.V.R., REDDY B.R., 2002. *Liquid-liquid extraction of nickel at macro-level concentration from sulphate/chloride solutions using phosphoric acid based extractants*. Minerals Engineering 15, 461–464.
- CHENG C.Y., 2006. *Solvent extraction of nickel and cobalt with synergistic systems consisting of carboxylic acid and aliphatic hydroxyoxime*. Hydrometallurgy 84, 109–117.
- CYANEX, 2007, ® Extractant, CYANEX® Extractant, Technical Brochure, Cytec Canada, Inc.
- GOTFRYD L., 2005. *Solvent extraction of nickel(II) sulphate contaminants*. Physicochemical Problems of Mineral Processing 39 117–128.
- GRIGORIEVA N.A., PASHKOV G.L., FLEITLIKH I.Y., NIKIFOROVA L.K., PLESHKOV M.A., 2010. *Nickel extraction from sulfate media with Cyanex 301 in the presence of electron donor additives*. Hydrometallurgy 105, 82–88.
- GUPTA C.K., MUKHERJEE T.K., 1990. *Hydrometallurgy in Extraction Processes*. CRC Press.
- JAKOVLJEVIC B., BOURGET C., NUCCIARONE D., 2004. *CYANEX® 301 binary extractant systems in cobalt/nickel recovery from acidic chloride solutions*. Hydrometallurgy 75, 25–36.
- REDDY B.R., PRIYA D.N., 2006. *Chloride leaching and solvent extraction of cadmium, cobalt and nickel from spent nickel-cadmium, batteries using Cyanex 923 and 272*. Journal of Power Sources 161, 1428–1434.
- REDDY B.R., RAO S.V., PRIYA D.N., 2008. *Selective separation and recovery of divalent Cd and Ni from sulphate solutions with mixtures of TOPS 99 and Cyanex 471 X*. Separation and Purification Technology 59, 214–220.
- ROTUSKA K., CHMIELEWSKI T., 2008. *Growing role of solvent extraction in copper ores processing*. Physicochemical Problems of Mineral Processing 42, 29–36.
- SALGADO A.L., VELOSO A.M.O., PEREIRA D.D., GONTIJO G.S., SALUM A., MANSUR M.B., 2003. *Recovery of zinc and manganese from spent alkaline batteries by liquid–liquid extraction with Cyanex 272*. Journal of Power Sources 115, 367–373.
- SOLE K.C., FEATHER A.M., COLE P.M., 2005. *Solvent extraction in southern Africa: An update of some recent hydrometallurgical developments*. Hydrometallurgy 78, 52–78.
- SZE Y.K.P., XUE L., 2003. *Extraction of Zinc and Chromium(III) and Its Application to Treatment of Alloy Electroplating Wastewater*. Separation Science and Technology 38, 405–425.
- TANAKA M., ALAM S., 2010. *Solvent extraction equilibria of nickel from ammonium nitrate solution with LIX84I*. Hydrometallurgy 105, 134–139.
- TSAKIRIDIS P.E., AGATZINI S.L., 2004. *Simultaneous solvent extraction of cobalt and nickel in the presence of manganese and magnesium from sulfate solutions by Cyanex 301*. Hydrometallurgy 72, 269–278.
- ZHANG P., YOKOYAMA T., SUZUKI T.M., INOUE K., 2001. *The synergistic extraction of nickel and cobalt with a mixture of di(2-ethylhexyl) phosphoric acid and 5-dodecylsalicylaldoxime*. Hydrometallurgy 61, 223–227.

Received June 15, 2012; reviewed; accepted July 15, 2012

DETERMINATION OF THE NIP ZONE ANGLE IN HIGH-PRESSURE GRINDING ROLLS

Daniel SARMAK¹, Zdzisław NAZIEMIEC²

¹ AGH University of Science and Technology, Faculty of Mining and Geoengineering, Department of Environmental Engineering and Mineral Processing, Mickiewicza 30 Av., 30-059 Krakow, Poland, Fax: +48 12 617 21 98, Mobile: +48 692 597 032, Email: dsaramak@agh.edu.pl

² Institute of Glass, Ceramics, Refractory and Building Materials, Department of Mineral Building Materials, Krakow, znaziemiec@immb.com.pl

Abstract: A proposal of the nip zone angle determination in high-pressure grinding rolls (HPGR) crushing process is presented in the paper. Knowledge of the nip zone angle value makes it possible to determine the real maximum pressing force in the high-pressure comminution. Two methods of determination of this maximum pressure were proposed and verified. The first method is based on the roll's geometry and the change of the HPGR chamber's volume together with the roll rotation, while the second one considers the outlet gap width. Results of the nip zone angle calculations according to both methods are similar and show that the nip zone angle is around 3°. The verification was carried out in a piston-die press and experimental results show that the product size distributions from HPGR and piston-die press are similar. The methodology of the nip zone angle determination presented in the paper has then its practical confirmation. A proper determination of the nip zone border makes it possible to calculate the comminution probability of given type of material and is a basis for the HPGR crushing process modeling and optimization.

Keywords: HPGR, comminution, nip zone, ore processing

Introduction

High-pressure comminution becomes more and more popular technology in industrial mineral processing operations, which can be applied both at secondary or tertiary crushing operations, and during the coarse grinding stage (Morell, 2008; Bearman, 2006; Morley, 2006). The HPGR devices are usually implemented into industry as a replacement of conventional tumble and semi-autogenous mills (SAG) due to considerable reduction of energy consumption and size reduction ratio improvement. HPGR presses find applications in many mining and mineral processing industry

areas like ore processing, cement clinker grinding or limestone flour and fine aggregates production.

The HPGR technology was introduced in the mid-eighties and originally applied in the cement industry (Schoenert, 1988; Maxton et al., 2003). In hard ore processing it was applied in diamond mines for kimberlite crushing. Constant investigations over the HPGR performance benefited in further modernization of technology (Daniel and Morell, 2004; Daniel, 2008; Gruendken et al., 2008; Bailey et al., 2009; Saramak et al., 2010) and since then presses have been gradually applied to harder and more abrasive materials like iron or non-ferrous metal.

The application of HPGR technology results in following advantages:

- lower energy consumption (Fuerstenau et al., 1991; Rule et al., 2008),
- reduced grinding media consumption,
- lower operating costs,
- finer product,
- low dust and noise pollution,
- faster equipment delivery schedules.

The main benefit results from the method of the feed material size reduction: a slow application and the gradual increase of the pressing forces. It causes the damage of the grain structure together with micro-crack formation, and the unfavourable phenomenon of the particle over-grinding is practically eliminated (Fuerstenau et al., 1991; Tromans and Meech, 2002; Morell, 2008; Saramak, 2011a)

The HPGR technology has also some limitations and still need investigations heading towards better understanding of the issue through the development of different HPGR-based flow-sheets (Powell 2010). An introduction of new research programmes significantly increases possibilities of the HPGR-based flow-sheet performance modeling (Daniel, 2004; Morell, 2008; Tumidajski and Saramak, 2009) and optimization (Gruedken et al. 2008; Saramak 2012; 2011b)). Considering the above, an extensive investigation of the wear of linings can be beneficial. Also issues connected with the bath-tub effect (an extensive wear of the central area of rolls) or the edge effect (at very sides of rolls the material breakage is lower than in the central area) are significant.

Principles of high-pressure comminution

The main part of the high-pressure grinding rolls press is a set of two counter-rotating rolls running in bearings and enclosed in the frame. One roll is settled in the frame in the fixed position (fixed roll), while the position of the second one (floating roll) is dynamic allowing the horizontal movement according to the variations in the feed and hydraulic pressure. Both rolls are separated with shims on ends, preventing the contact of the fixed and floating roll. The rolls are driven by two separate motors connected to the roll shafts with the use of gear reducers.

The crushing process in the HPGR crushing chamber is evoked by the pressing force from two rotating rollers. The ore is choke-fed and the material is dragged into the nip zone of working chamber and as the distance between the rolls is decreasing, the pressing force from the floating roller significantly increases, causing the failure of the individual particles structure and formation of micro-cracks. This results in a large reduction of the product particle size, which comes out during the next processes, usually the tertiary grinding in mills. Two zones can be distinguished in the working HPGR chamber: pre-compacting zone and the nip zone (Figure 1)

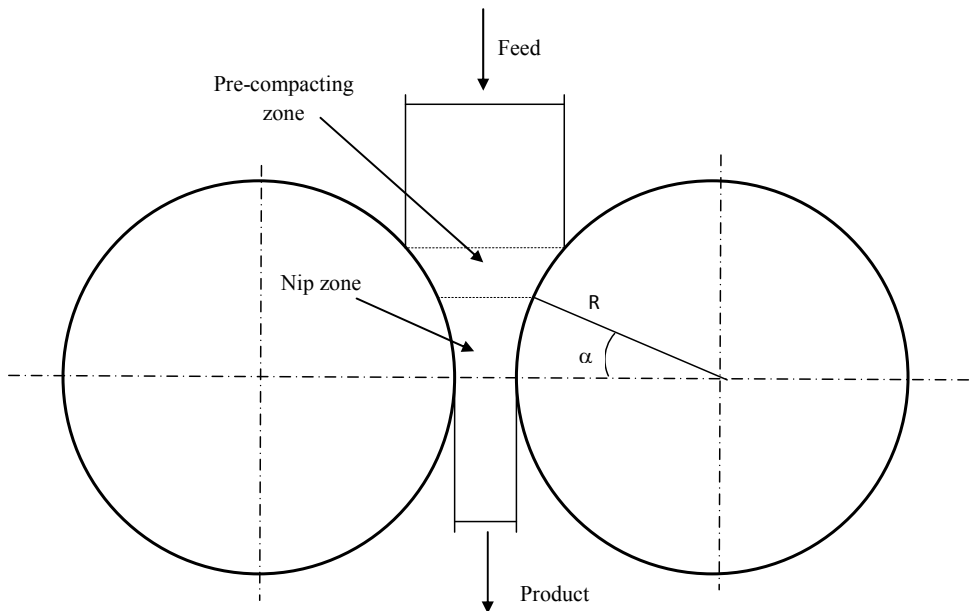


Fig. 1. HPGR crushing scheme

In the first zone the initial thickening of the material can be observed. The pressing force causes that most of inter-particle spaces are eliminated or at least minimized. The proper comminution takes place in the nip zone, because here the maximum pressing force is obtained. The product is usually in a solid sheet form, also referred as flake. The thickness of the flake generally depends on the feed properties and HPGR operating conditions. The micro-crack formation in single particles causes easier size reduction in downstream grinding processes. The Bond work index value in this case is reduced from 20 to 30% for limestone and 15 to 20% for harder minerals.

Methods of pressing force and pressure calculation

The pressing force (F) in HPGR can be calculated from equation (1):

$$F = \frac{D^2 \pi}{4} n P_h \quad (1)$$

where: F – pressing force, kN,
 D – roll's diameter,
 n – number of pistons,
 P_h – hydraulic pressure, kPa.

The pressure P is the most significant operating parameter, measured in MPa or N/mm²:

$$P = \frac{F}{1000 D l} \quad (2)$$

where: D – roll diameter, m,
 l – roll length, m.

The value of P is calculated per total working surface of rolls, but the feed material is comminuted only on certain section of rolls in working chamber, marked in Fig. 1. The real P value calculated from Eq. (2) is then only an approximate. The main crushing process takes part only in the nip zone (Fig. 1) where P_{max} (a maximum pressure value) occurs. Several different formulas can be applied. In order to calculate the maximum operating pressure in press (P_{max}) Schoenert (1988) proposed the following formula:

$$P_{max} = \frac{P}{k \alpha} \quad (3)$$

where: k – constant,
 α – nip zone angle (6–10 degrees).

Neumann (2006), in turn, proposed the following formula for the maximum pressing force:

$$F_{max} = c \frac{F}{\sqrt{s}} \quad (4)$$

where: c – constant related to the device and the feed material properties,
 F – pressing force, kN,
 s – gap width, mm.

Formula (4) does not consider the diameter–gap relationship in press. For the various relationship between the gap and roll diameter, the changeable degree of feed material compression is observed. The compression degree is higher for narrow gap s (Fig. 2a) because values of $\frac{s_1}{2R + s_1}$ are smaller than $\frac{s_2}{2R + s_2}$ (Fig. 2). The feed mate-

rial bed is then more compressed and greater values of pressing force are also expected.

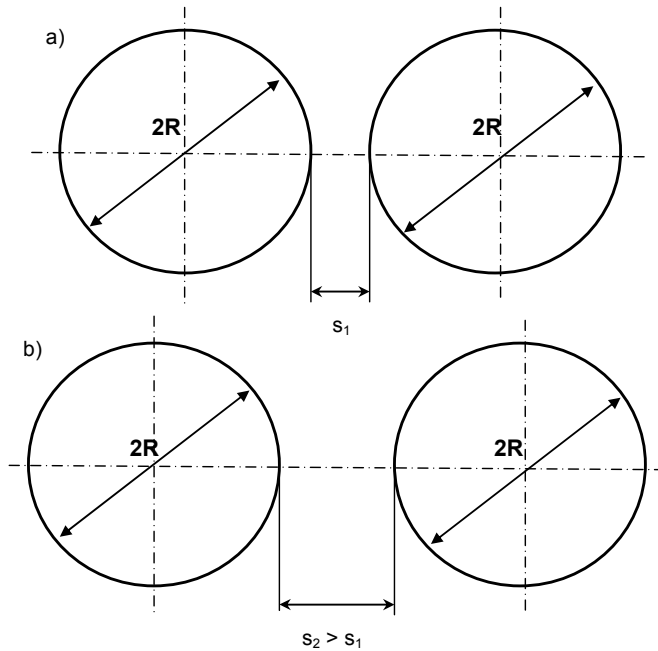


Fig. 2. Influence of relationship between gap s and the roller's diameter $2R$ on material's compression level in HPGR

Unland and Kleeberg (2006) proposed an empirical formula for P_{max} :

$$P_{max} = \frac{F}{Dl \sqrt{2 \frac{s}{D} \left(\frac{\rho_p}{\rho_n} - 1 \right) c}} \quad (5)$$

where: F – pressing force,
 s – gap width, mm,
 ρ_n – feed density, kg/dm³,
 ρ_p – density of compressed product, kg/dm³,
 c – constant,
 D – roll diameter,
 l – roll length.

Formula (5) allows for determination of the maximum pressure value as a function of the gap width, roll's pressing force and the feed and product densities. For the given type of material the feed density is constant, and only the product density will be a variable.

Other authors (Schwechten, 1987; Smitz, 1993) introduced into the formula for P_{max} , a φ parameter, which describes the feed compression ability:

$$P_{max} = \frac{F}{Dl\varphi\sqrt{\frac{s}{D}}} \quad (6)$$

where: F – pressing force,
 s – gap width,
 φ – feed compression ability,
 D – roll diameter,
 l – roll length.

Feige (1989) run an investigations over the pressing forces in roller crushers. As a result of the above, he proposed the owing formula for calculation the value of maximum pressure:

$$F_{max} = \frac{2F_r}{lL} \cong \frac{2D \int P(\alpha) d\alpha}{\sqrt{d(2D+d)}} \quad (7)$$

where: F_r – pressing force,
 L – a depth of the pressing force penetration into the feed material bed between the rolls, $L \cong \frac{1}{2}\sqrt{d(2D+d)}$,
 d – particle size.

Experimental

The real value of maximum pressure can be precisely calculated from the following formula:

$$P_{max} = \frac{F}{1000Dl\pi\frac{\alpha}{360}} = \frac{P}{\pi\frac{\alpha}{360}} \quad (8)$$

where: P_{max} – maximum pressure, MPa
 P – pressure, MPa,
 α – nip zone angle, [°], which, from the scope of the press geometry, is constant regardless the rolls diameter.

The value of pressure is increasing significantly in the nip zone, and rapidly decreased when the compressed material leaves the press working chamber ($\alpha < 0$). The pressure in nip zone is exerted by the floating roll tighten towards the fixed one with

four pistons, and through decreasing the volume of the space between the rolls as the feed material is dragged deeper into the crushing zone. The maximum pressure is expected to occur in the area, where the volume decreases are minimal. In order to find the border value of α , below which these minimal changes in the volume are observed, the nip zone volume should be determined as a function of α .

Considering the situation in the opposite direction to the process run, the lowest value of the space gap between the rolls is on the level zero, for $\alpha = 0$. Together with the increasing of α value, the volume of nip zone increases, but these changes are not large and approximately constant at the beginning. Together with the further increasing of α , the h value and distance between the rolls (see Fig. 2) increase as well and, as a result, the horizontal component of the pressing force F_x (Fig. 4) decreases too. The nip zone border is placed on the height h , where the working chamber volume starts to increase more rapidly. All necessary notations were given in Figure 3, and after suitable calculations, the nip zone value V as a function of α , can be described by the formula (9):

$$V(\alpha) = lR^2 \left(\sin \alpha - \frac{1}{4} \sin 2\alpha - \frac{\pi\alpha}{360} \right) \tag{9}$$

where: l – rolls length, m,

R – rolls diameter, m,

α – angle determining the nip zone border, degrees.

The pressing force value reaches maximum if the first derivative of $V(\alpha)$ heads towards zero:

$$F \rightarrow \max, \quad \text{when} \quad \frac{\partial V(\alpha)}{\partial \alpha} \rightarrow 0. \tag{10}$$

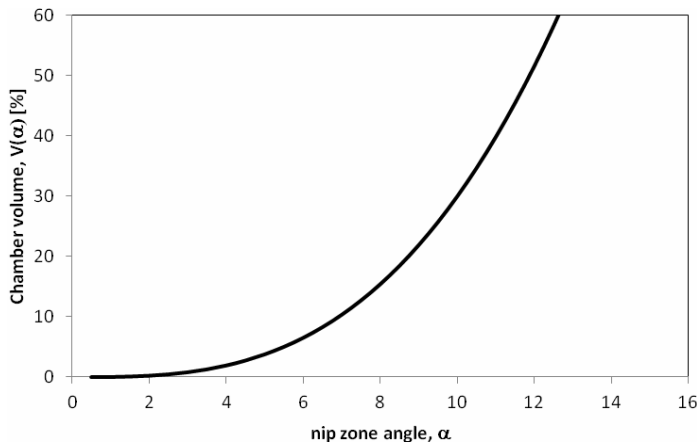


Fig. 3. The press working chamber volume course in relationship to α value

The $V(\alpha)$ function is presented in Fig. 3.

Analyzing Fig. 3, one can notice, that for $\alpha < 3$, chamber volume increases are insignificant. For $\alpha > 4$, in turn, the volume increases more rapidly, what results in decreasing the pressing force on the feed material bed and, in a consequence, the lower comminution intensity. The horizontal component \vec{F}_x of the force F decreases as well (Fig. 4). The curve presented in Fig. 3 can be very well approximated by using the exponential function:

$$\hat{V}(\alpha) = 0.03\alpha^3. \quad (11)$$

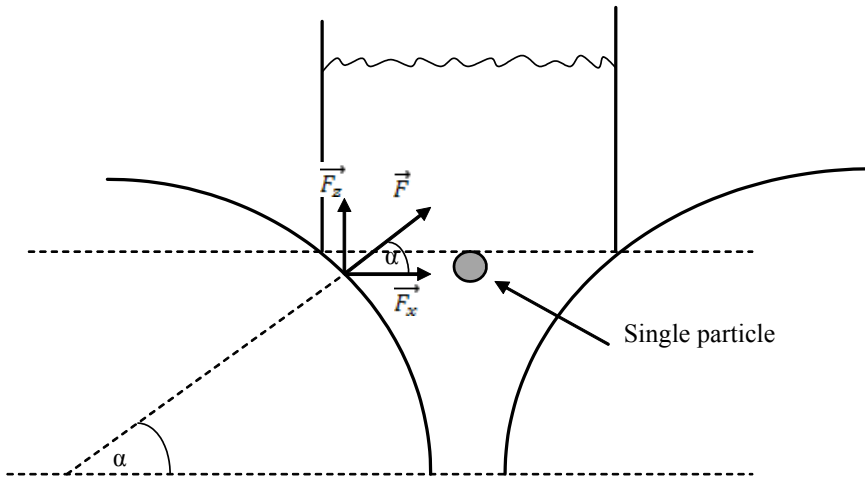


Fig. 4. Forces affecting the feed material between the rolls

The nip zone can be also alternatively determined, taking an advantage of the relationship between the gap and roll diameter. The above relationship is considered as constant, and according to various sources, is determined with following equation for ore processing:

$$s = 0.025R. \quad (12)$$

On the basis of the above, the nip zone is proposed to be described as a space between the rolls, limited by the height equal to s (Fig. 5).

It is possible to calculate the α value for the above nip zone from the formula:

$$\alpha = \arcsin\left(\frac{s}{R}\right). \quad (13)$$

Accepting formula (13) $\alpha = 2.87^\circ \approx 3^\circ$.

Results of calculations are convergent to those, obtained in the previous paragraph.

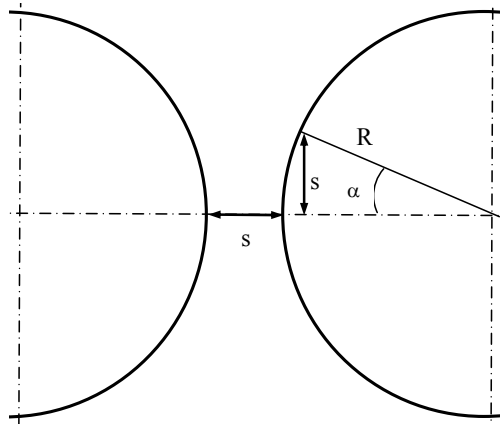


Fig. 5. The nip zone determined by using the gap width s

Verification and discussion

A verification covered an experimental programme of limestone crushing in pilot plant press (test 1) and in a laboratory piston-die press (test 2). Test 1 was run for following operating parameters:

- operating pressure $P = 3,16 \text{ N/mm}^2$,
- operating gap width $s = 22 \text{ mm}$.

The real operating pressure P_{\max} for the above parameters was calculated by using formula (9). For accepted angle of the nip zone $\alpha = 3^\circ$ (14), $P_{\max} = 120.7 \text{ MPa}$. For such a pressure value a laboratory test in piston-die press was run. Results of both experiments are presented in Fig. 6.

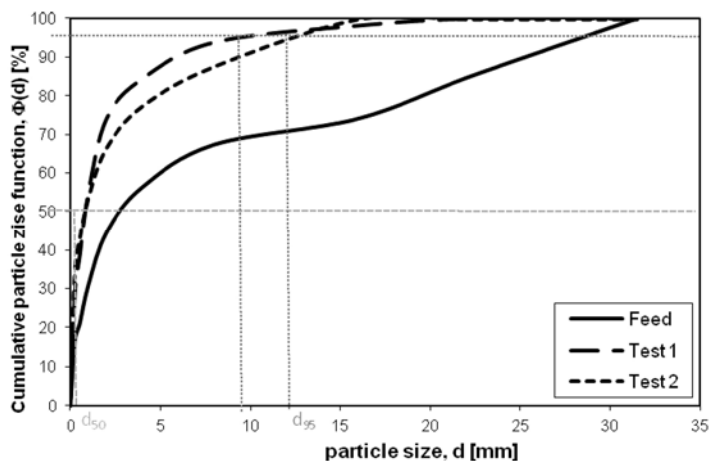


Fig. 6. A comparison of crushing results in plant HPGR (test 1) and piston-die press (test 2)

Average (d_{50}) and maximum (d_{95}) product particle size values were also determined, together with the weight recovery of the fine (i.e. below 0.3 mm) particle fraction $\gamma_{0.3}$. Results are presented in Table 1.

Table 1. Average and maximum particle size of crushing products from test 1 and test 2

Index	Test 1	Test 2
d_{50} [mm]	0.85	0.83
d_{95} [mm]	10.1	12.7
$\gamma_{0.3}$ [%]	30.9	36.9

where: d_{50} – average product's particle size, d_{95} – maximum product's particle size, $\gamma_{0.3}$ – weight recovery of -0.3 mm size fraction

Analyzing the crushing results one can see that an average graining obtained in both tests (d_{50}) is the same for both products, while the maximum particle size of product d_{95} and finest particle contents are quite similar. The greater differences were observed for the product size fractions between 5 and 10 mm, but they do not exceed 10%. This difference can be a result of various dynamics of a product breakage in both devices. In HPGR the particles move together with the rolls' revolution, and may settle down a position which makes easier the breakage. The particle movement in the piston-die test, in turn, occurs only to a limited degree. The content of particles over 3–4 mm is a rather of minor importance, however, because this fraction is anyway recycled to the crushing device.

Comparing the results of both tests, it can be stated, that the reduction ratio value obtained in piston-die test, corresponds to the real high-pressure comminution process. It is also convergent with the methodology of the nip zone angle determination, presented in "Experimental" section. The production of the finest particles is practically identical for both devices. The additional gain of the above verification is the possibility of application the piston-die press as a replacement of laboratory HPGR device, which is more favorable from economic scope.

Conclusions

Apart from the pressure, the high-pressure comminution efficiency is tied with other indices and process parameters, like the roll's surface profile, feeding system, recycle stream volume, device capacity, feed and product particle size and others. However, the real values of pressing force significantly influence not only the feed size reduction ratio, but also the material grindability in downstream grinding processes in ball mills. A determination of real operating pressure value can be helpful for selecting the optimal operating conditions of HPGR and is convergent with the main principle of mechanical processing: do not grind unnecessarily. The excessive pressure values produce more concised flakes, which need to be additionally de-agglomerated. Results

presented in the paper have their practical implementation in the optimization investigations, heading towards the improvement of the high-pressure grinding rolls operation efficiency.

Acknowledgments

The article was written within the frames of Ministry of Science research grant N N524 466139.

References

- BAILEY C., LANE G., MORELL S., STAPLES P., 2009, *What can go wrong in comminution circuit design?*, Proceedings of the 10th Mill Operators' Conference, Adelaide, SA.
- BEARMAN R., 2006: *High-Pressure Grinding Rolls – Characterising and defining process performance for engineers*. 3rd International Symposium “Advances in Comminution, Society for Mining, Metallurgy and Exploration (SME).
- DANIEL M.J., MORELL S., 2004: *HPGR Model verification and scale-up*, Minerals Engineering, vol. 17.
- DANIEL M.J., 2008: *Summary of research outcomes of the P9N project, incorporating mineralogical analyses, particle weakening and micro-cracked HPGR products*, Proceedings of 5th PROCEMIN seminar, Santiago, Chile.
- FEIGE F., 1989: *Measurement of pressure acting on layer of particle between two rollers*. Aufbereitungs-Technik 30 (1989), issue 10.
- FUERSTENAU D.W., SHUKLA A., KAPUR P.C., 1991: *Energy consumption and product size distribution in choke-fed high-compression roll mills*. Int. Journal of Mineral Processing, vol. 32.
- GRUENDKEN A., MATTHIES E., VAN DER MEER F.P., 2008: *Flowsheet considerations for optimal use of high pressure grinding rolls*, MEI Comminution '08 Conference, Falmouth, Cornwall, UK.
- MAXTON D., MORLEY C., BEARMAN R., 2003. *A quantification of the benefits of high pressure rolls crushing in an operating environment*. Minerals Engineering vol. 16.
- MORLEY C., 2006: *High-Pressure Grinding Rolls – A technology review*. 3rd International Symposium “Advances in Comminution, Society for Mining, Metallurgy and Exploration (SME).
- MORRELL S., 2008: *A method for predicting the specific energy requirement of comminution circuits and assessing their energy utilization efficiency*. Minerals Engineering, vol. 21, issue 3.
- NEUMANN E.W., 2006: *Some basics on High-Pressure Grinding Rolls*. 3rd International Symposium “Advances in Comminution, Society for Mining, Metallurgy and Exploration (SME).
- POWELL M., 2010: *Enlightened circuit design is essential to the take-up of new equipment*, Draft paper and presentation for Comminution'10 conference, Cape Town, South Africa, 13–16 April 2010.
- RULE C.M., MINNARR D.M., SAUREMANN, 2008: *HPGR – revolution in Platinum?* Third International Conference „Platinum in Transformation”, The Southern African Institute of Mining and Metallurgy.
- SARAMAK D., 2001a: *Technological issues of High-Pressure Grinding Rolls operation in ore comminution processes*, Archives of Mining Sciences, vol. 56, issue 3.
- SARAMAK D., 2011b: *The influence of chosen ore properties on efficiency of HPGR-based grinding circuits*, Gospodarka Surowcami Mineralnymi Mineral Resources Management, vol. 27, issue 4.
- SARAMAK D., 2012: *De-agglomeration in High-Pressure Grinding Roll based crushing circuits*, Physicochem. Probl. Miner. Process., vol. 48 (1).

- SARAMAK D., TUMIDAJSKI T., BROŻEK M., GAWENDA T., NAZIEMIEC Z.: Aspects of comminution flowsheets design in processing of mineral raw materials. *Gospodarka Surowcami Mineralnymi Mineral Resources Management*, vol.26 issue 4, 2010.
- SCHMITZ T.: *Modellierung der Zerkleinerung in der Gutbett-Walzenmühle und Verknüpfung mit dem Schuttgutverhalten zur Voraussage kritischer Betriebszustände*. Dissertation TU Clausthal.
- SCHOENERT K., 1993: *A first survey of grinding with high-compression roller mills*. *International Journal of Mineral Processing*, vol. 22.
- SCHWECHTEN D., 1987: *Trocken-und Nassmahlung sproeder Materialien in der Gutbett-Walzenmühle*. Dissertation TU Clausthal.
- TROMANS D., MEECH J.A., 2010: *A fundamental analysis of fracture mechanics of minerals during comminution, research being conducted at The Centre for Environmental Research in Minerals, Metals and Materials (CERM³)*, UBC, July 2010, www.mining.ubc.ca/cerm3/energy%20efficiency.html.
- TUMIDAJSKI T., SARAMAK D., 2009: *Methods and models of mathematical statistics in mineral processing* (in Polish), AGH University of Science and Technology Press, Krakow.
- UNLAND G., KLEEBERG J., 2006: *The normal load on roll surfaces of high pressure grinding rolls*. *Proceedings of XXIII International Mineral Processing Congress, Istanbul*.

Received May 15, 2012; reviewed; accepted July 13, 2012

COMPARISON BETWEEN NEURAL NETWORKS AND MULTIPLE REGRESSION METHODS IN METALLURGICAL PERFORMANCE MODELING OF FLOTATION COLUMN

Fardis NAKHAEI, Mehdi IRANNAJAD

Department of Mining & Metallurgical Engineering, Amirkabir University of Technology, Tehran, Iran
Iranajad@aut.ac.ir

Abstract: Artificial neural networks are relatively new computational tools which their inherent ability to learn and recognize highly non-linear and complex relationships makes them ideally suited in solving a wide range of complex real-world problems. In this research, different techniques (Linear regression, Non-linear regression, Back propagation neural network, Radial Basis Function for the estimation of Cu grade and recovery values in flotation column concentrate are studied. Modeling is performed based on 90 datasets at different operating conditions at Sarcheshmeh pilot plant, a copper concentrator in Iran, which include chemical reagents dosage, froth height, air and wash water flow rates, gas holdup and Cu grade in the rougher feed and flotation column feed, column tail and final concentrate streams. The results of models were also expressed and analyzed by intuitive graphics. The results indicated that a four-layer BP network gave the most accurate metallurgical performance prediction and all of the neural network models outperformed non-linear regression in the estimation process for the same set of data.

Keywords: *metallurgical performance; separation; neural networks; non-linear regression; prediction; flotation column*

Introduction

The flotation column was invented by the Canadian Pierre Boutin in the 1960s. The flotation column has continued to attract more and more attention with its wide use in the metal and non-metal mineral processing fields. It has many advantages including high separation efficiency, large production capacity, and low cost. The ability to operate columns with deep froth beds and to wash the froth was the main reasons cited for the improved metallurgical performance. Concentrate grade and recovery modeling is usually commenced at the mineral processing stage of a mining project and is continued throughout the life of a mine. The major focus of this task lies in recovery

and grade estimations, which are useful for mine investment decisions, plant design and control planning.

In recent years, many researchers have focused on the relationship between metallurgical performance and operation properties. These research results show that efficiency of process depends on its operation conditions and most effective parameters are feed grade, grain size, froth height and wash water and air rates and etc. Thus, some researchers by using classic statistical methods and recently by developing intelligent techniques have established models based on experimental conditions to estimate grade and recovery.

Zhang et al. (2007) implemented artificial neural networks (ANNs) for coal mining information fusion. They studied the parameters affecting the volume of a gas burst in Chinese coal mines. A total of 20 gas bursts and six different factors (working depth, seam thickness, gas content, mining intensity, adjacent layer spacing and adjacent layer gas content) were used to train and validate the network. Al Thyabat (2008) used neural networks (NN) for the optimization of froth flotation. A multi-layered feed-forward NN was used to study the effect of feed mean size, collector dosage and impeller speed on flotation recovery and grade. Gupta et al. (1999) also worked on this topic, focusing on phosphate flotation. In order to find some relationships between rate constants and operating variables, they suggested a hybrid model combining first principles and NNs. Once calibrated, the prediction of the effect of frother concentration, particle size, air flow rate and bubble diameter on phosphate recovery was made possible. Ozbayoglu et al. (2008) applied different techniques for the estimation of coal Hardgrove Grindability Index (HGI) values. Nonlinear regression and NN techniques are used for predicting the HGI values for the specified coal parameters. Results indicate that a hybrid network which is a combination of four separate NNs gave the most accurate HGI prediction and all of the NN models outperformed non-linear regression in the estimation process. Jorjani et al. (2007) investigated the application of NNs in organic and inorganic sulfur reduction from coal. This work is an attempt to solve the important question: with the use of experimental data resulted from laboratory level, can we predict directly the organic and inorganic sulfur reduction by means of NNs? In this context the present study, ANN and multivariate statistical models are presented which have potential of predicting with acceptable accuracy using some simple parameters. The aim of this work is to evaluate two models described in the literature to estimate Cu grade and recovery in the column flotation concentrate, and to identify which models and method give the best predictions.

The remainder of the paper is organized as follows. Section 2 provides a brief description of the pilot plant and the selection of data. Sections 3 introduce the architecture and learning algorithm of BPNN and RBFNN. Section 4 describes the result and discussion and section 5 concludes the presentation.

Pilot plant description

The Sarcheshmeh pilot plant has an identical circuit configuration compared to the plant and can process 1.6 Mg/h (tone/h) of ore. The rougher flotation bank consists of 14 cells (35 dm³ each) in three units (6cell–4cell–4cell) and the regrind mill is a 76.2 cm by 137.2 cm ball mill. The scavenger banks have 6 cells (30 dm³). The single stage flotation column operation which is employed in the cleaner circuit is composed of a column with 26 cm internal diameter and 540 cm height. Figure 1 shows the flotation circuit of the pilot plant. The column is fed by the mixture of rougher stage and scavenger stage concentrates, previously classified in cyclones. Column tailing is used as scavenger feed, and column concentrate is the plant final product.

The pilot flotation column is instrumented with flow meters for feed, wash water and air as well as with a conductivity profile. Local control loops are implemented to regulate feed, tails, wash water and air flow rates. Two 23 cm long spargers are used, made of PVC tubes. The holes of 1.5 mm in diameter in a grid with dimensions of 2.5 cm × 2 cm were drilled.

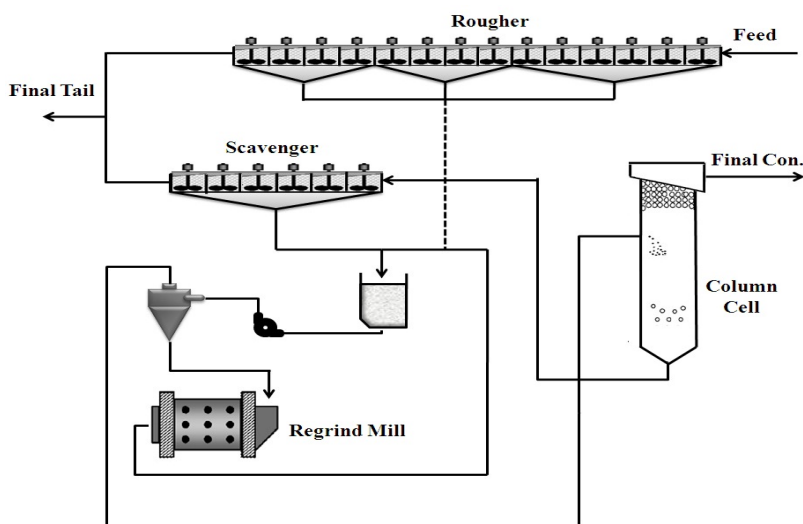


Fig. 1. The flow sheet of flotation circuit of the Sarcheshmeh pilot plant

The pulp–froth interface position is measured using a semi-analytical method based on the conductivity profile along the column. The non-floated flow rate is also controlled by a variable speed peristaltic pump driven by a frequency inverter. The pressure measurements are used to calculate the values of the air holdup and of the froth layer height. The data acquisition system is also connected via a port to a microcomputer.

Collecting data

The basic idea behind the current research is statement of ANN (artificial neural network) and MNL (multi non-linear regression) capability to estimate the Cu grade and recovery in flotation column concentrate. The most important step in developing an ANN and MNL is to assemble data that can be used for training and testing the model. Therefore, a series of reliable experimental data was collected in 4 tests. A total of 90 data pairs have been selected from the experimental database. Pilot plant data was collected, over a period of 13 min based on RTD (residence time distribution), in order to cover fluctuations in all the measured variables related to the concentrate grade prediction (Nakhaei, et al. 2012).

The simultaneous measured variables are chemical reagents dosage, froth height, air and wash water flow rates, gas holdup, Cu and grade in the rougher feed, flotation column feed, column tail and final concentrate streams. The sampling period was chosen as 13 min. The maximum, minimum, mean and standard deviation of variables are given in Table 1.

The pH was adjusted to 11.8 with lime. In all tests, the rougher feed flow rate was kept 1.6 tone/h. The particle size characterization and solid percent data are given in Table 2. The chemical reagents used for the flotation process include collector and frother. Frother and collector were added in rougher cells and ball mill (before flotation circuit), respectively. The reagent type and dosage (collector and frother) used in the flotation circuit are presented in Table 3. The chemical analysis and mineralogical composition of the samples show that in all samples, the ore consists of mainly 1.78% CuFeS_2 , 0.27% Cu_2S and 0.083% MoS_2 .

Table 1. The maximum, minimum, mean and standard deviation of variables in different operating conditions

Variable	Index	Maximum	Minimum	Mean	Standard deviation
Froth height (cm)	H_F	120	35	83.61	20.52
Air holdup (%)	ϵ_g	92	71	82.36	4.1
Cu grade in the rougher feed (%)	RF	0.93	0.77	0.82	0.04
Cu recovery in the flotation column (%)	Re	91.27	83.34	87.33	1.75
Cu grade in the flotation column feed (%)	CoF	11.96	6.95	8.89	1.22
Cu grade in the flotation column tail (%)	CoT	2.68	1.05	1.81	0.45
Cu grade in the flotation column concentrate (%)	FC	25.21	15.93	21.13	2.12
Frother dosage (g/Mg)	Fr	36	32	34	1.64
Collector dosage (g/Mg)	C	40	36	38	1.64
Wash water flow rate (cm/s)	Q_w	0.34	0.11	0.27	0.08
Air flow rate (cm/s)	Q_a	1.72	0.63	1.1	0.25

Table 2. Flotation conditions used in the experiments (pH=11.8)

Parameter	Rougher feed	Column feed	Final concentrate	Final tail
Solid (%)	27	14	14.5	28
# -325 (%)	48	85	74	54

Table 3. Reagents type was used in the flotation circuit

Reagents	Type and commercial name
Collectors	Z ₁₁ , Nascol 451
Frothers	MIBC, Dowfroth 250

Methods

Back propagation neural network architectures

Back propagation is the most commonly used neural network type due to its simplicity in implementation and its successful generalization capabilities for complex data sets. Back propagation neural network is a three-layered feed forward architecture. The three layers are input layer, hidden layer and output layer. Functioning of back propagation proceeds in three stages, namely learning or training, testing or inferences and validation. Figure 2 shows the p-q-1 (p input neurons, q hidden neurons, and 1 output neuron) architecture of a back propagation neural network model. Input layer receives information from the external sources and passes this information to the network for processing. Hidden layer receives information from the input layer, and does all the information processing, and output layer receives processed information from the network, and sends the results out to an external receptor. The input signals are modified

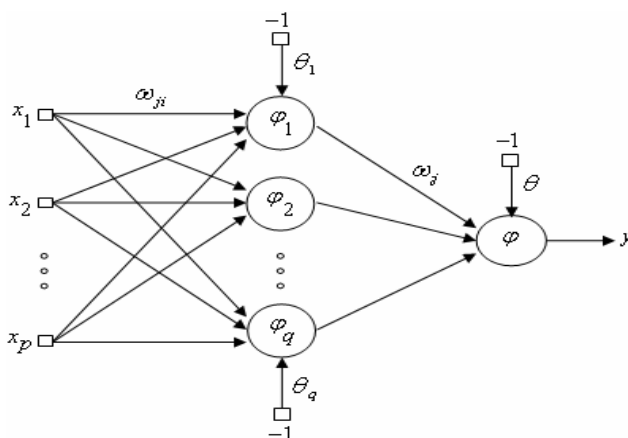


Fig. 2. A schematic diagram of multilayer feed forward neural network

by interconnection weight, known as weight factor w_{ji} , which represents the interconnection of i^{th} node of the first layer to j^{th} node of the second layer. The sum of modified signals (total activation) is then modified by a sigmoid transfer function (φ). Similarly, outputs signal of hidden layer are modified by interconnection weight (w_{ki}) of k^{th} node of output layer to j^{th} node of hidden layer. The sum of the modified signal is then modified by sigmoid transfer function and output is collected at output layer (Mosavi, 2011).

Output from a neuron in the input layer is

$$O_{pi} = x_{pi}, \quad i = 1, 2, \dots, p. \quad (1)$$

Output from a neuron in the hidden layer is

$$O_{pj} = \varphi(\sum_{i=0}^p w_{ji} o_{pi} + \theta_j), \quad j = 1, 2, \dots, q. \quad (2)$$

Output from a neuron in the output layer is

$$O_{pk} = \varphi(\sum_{i=0}^q w_{ki} o_{pj} + \theta) = y, \quad k = 1, 2, \dots, n. \quad (3)$$

Learning or training in back propagation neural network

Batch model type of supervised learning has been used in the present case, where interconnection weights are adjusted using delta rule algorithm after sending the entire training sample to the network. During training, the predicted output is compared with the desired output, and the mean square error is calculated. If the mean square error is more than a prescribed limiting value, it is back propagated from output to input, and weights are further modified till the error or number of iterations is within a prescribed limit. Mean square error, E_p for pattern p is defined as (Samanta et al., 2009):

$$E_p = \sum_{i=1}^n \frac{1}{2} (D_{pi} - O_{pi})^2 \quad (4)$$

where D_{pi} is the target output, and O_{pi} is the computed output for the i^{th} pattern. Weight change at any time t , is given by:

$$\Delta w(t) = -\eta E_p(t) + \alpha \Delta w(t-1) \quad (5)$$

η = learning rate ($0 < \eta < 1$); α = momentum coefficient ($0 < \alpha < 1$).

Radial basis function network

Architecture of radial basis function network

Basically radial basis function network is composed of large number of simple and highly interconnected artificial neurons and can be organized into several layer, i.e.

input layer, hidden layer, and output layer by Haykin (2004). These inputs are the non-linearly transformed by a set of RBFs, creating a new space, j , in the hidden layer. Through this non-linear transformation only, the network acquires the capability of non-linear function al mapping. The most commonly used non-linear RBF is the Gaussian function. Other types of non- linear functions such as multi quadratic and the thin-plate spline are alternately used (Haykin, 2004). The general consensus is that the type of the basis function does not have much impact on the general performance of the RBF network. The Gaussian RBFs of the network are characterized by two sets of parameters: radial basis centers, μ , and widths, σ . Hence, the different basis functions in the hidden layer are recognized by these parameters. The i^{th} basis function of the network can be expressed by the following mathematical formula

$$\Phi_i(x) = \exp\left(-\frac{\|x - \mu_i\|}{\sigma_i}\right) \tag{6}$$

where $\Phi_i(x)$ is the output from the i^{th} basis function, μ_i the center of the i^{th} basis function, σ_i the width of the i^{th} basis function and $\| \cdot \|$ the Euclidian distance of the input from the center. The outputs from the hidden layer are then linearly combined to produce the final output (y) of the network, which in the study is the Cu grade and recovery in flotation column concentration. This can be expressed as:

$$y = \sum_{i=1}^n w_i \cdot \Phi_i(x) \tag{7}$$

where y is the output of the network, w_i the weight associated with the i^{th} basis function and n the number of the basis functions. While the weight parameters of a feed-forward network are determined using a complex non-linear optimization algorithm, demanding expensive computational time, the weight parameters of a RBF network can be fixed by using a least square algorithm. This is the point where a RBF network gains substantial computational advantage over a feed-forward network.

Preparation of data sets

The normalized data sets are used for training the network. In the present case, the data are normalized between 0 and 1 to ensure that each input is represented in the network training as well as different kinds of input quantities are normalized in the same scale. The data sets are normalized in the range of 0 and 1 using (Nakhaei et al., 2010):

$$N_p = \frac{A_p - meanA_{ps}}{stdA_p} \tag{8}$$

where, A_p is actual parameter, $meanA_{ps}$ is mean of actual parameters, $stdA_p$ is standard deviation of actual parameter and N_p is normalized parameter.

Testing and validation of neural network

Entire experimental data set is divided into training set, testing set. The error on the testing set is monitored during the training process. The testing error will normally decrease during the initial phase of training, as does the training set error. However, when the network begins to overfit the data, the error on the testing set will typically begin to rise. When the testing error starts increasing for a specified number of iterations, the training is stopped; and the weights at the minimum value of the testing error are returned.

Results and discussion

All data analysis methods used 60 training and 30 testing data points. Different combinations of the data set are used during the process, so all the data points have eventually been tested. Eight input parameters were setup as network inputs to the input layer. These parameters are chemical reagents dosage (frother and collector), froth height, air and wash water flow rates, gas holdup, Cu grade in the rougher feed, flotation column feed streams are considered as input which have the influence on Cu grade and recovery in flotation column concentrate are considered as output parameter.

Multi linear regression

The same approach is used in linear and non-linear regressions as it was used in the neural network system training and testing. A statistical model of regression, the data of which is similar to that of NNs, had been employed to predict Cu grade and recovery. It should be mentioned that 60 sets of data were selected for simulating the regression model. Also, the 30 data were used to test the performance of the model where inputs are referred to independent variables which are the same as inputs used in NN. The MLR equations forecasted the Cu grade and recovery with correlation coefficients of 0.87 and 0.85 in testing stage respectively. The MSE between the estimated Cu grade and recovery and the desired data was 1 and 0.96 respectively. Results show that the average error for linear regression was considerably higher than the other models.

Multi non-linear regression

Two multivariable regression equations were developed for the prediction of the Cu grade and recovery, which were deduced for these results as the follows:

$$\begin{aligned}
 Fc = & 147.2951 - 0.0047H_f + 3.448 \cdot 10^{-4}H_f^2 - 0.0009C^2 + 0.1235Fr \\
 & - 1.7435\varepsilon_g + 0.01087\varepsilon_g^2 + 10.3393Q_a - 4.328Q_a^2 + 8.1804Q_w \\
 & + 6.434Q_w^2 - 184.757RF + 109.8199RF^2 + 1.3818CoF - 0.0596CoF^2
 \end{aligned} \tag{9}$$

$$\begin{aligned}
 Re = & 25.3116 - 0.0267H_f - 3.05 \cdot 10^{-4} H_f^2 - 0.0524C - 0.0027Fr^2 \\
 & + 0.6013\varepsilon_g - 0.0028\varepsilon_g^2 + 11.2774Q_a - 3.3297Q_a^2 - 5.9272Q_w \\
 & + 17.171Q_w^2 + 106.0232RF - 64.9079RF^2 - 2.3751CoF + 0.1408CoF^2
 \end{aligned}
 \tag{10}$$

All symbols used in equations were explained in Table 1.

The statistical significance of the regression coefficient is a test which indicates whether there is a relationship between independent variables effect and the dependent variable. To assess the significance of regression coefficients, one needs to set a risk level (called the P-value level). As the rule of thumb, in most cases the P-value is set at level 0.05 (for 95% confidence).

The regression coefficient obtained from equations 9 and 10 showed that the majority of independent variables and their interactions had a significant effect on the grades and recoveries in a way that the P-values were less than 0.05. The MNLN equations forecasted the Cu grade and recovery with correlation coefficients of 0.9 and 0.86, respectively

BP neural network

Best network architecture (i.e. number of hidden layers, number of neurons in the hidden layers, learning rate and momentum coefficient) has been obtained by trial and error based on mean square error MSE in training, MSE in testing, and the number of iterations. A feed-forward ANN was trained with the BP algorithm, the model of which was designed by software package MATLAB 2009. The best results were obtained with Feed-forward NN with 8-12-8-2 arrangement that was capable to estimate

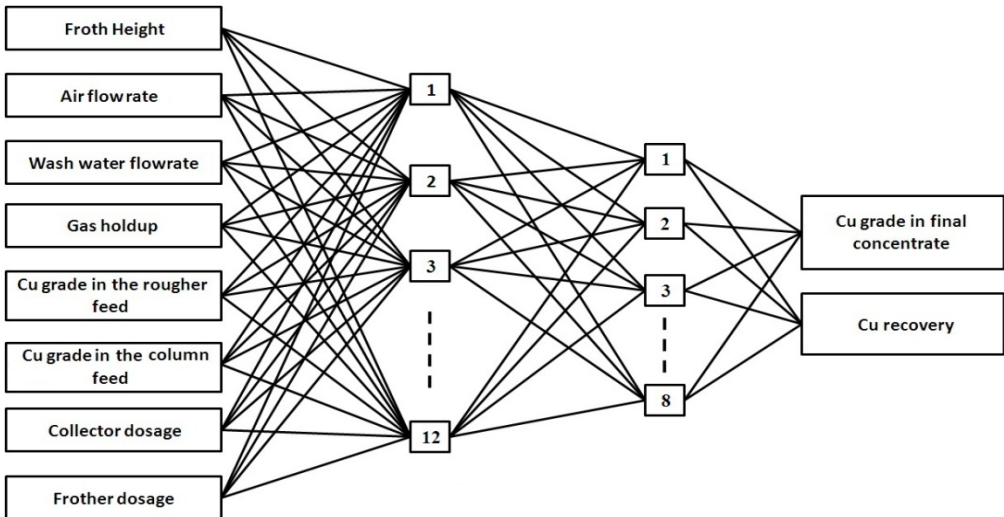


Fig. 3. Optimum structures of the proposed BPNN for estimating metallurgical performance of Cu in flotation column

metallurgical performance of Cu in flotation column (Fig. 3). Log-sigmoidal and linear were used as transfer functions in hidden layers and output layer, respectively. In NN modeling approach, a Levenberg-Marquardt training algorithm was used as a learning rule. The training process was stopped after 500 epochs for metallurgical performance of Cu. In this study, the associated ANNs analyses were carried out with an optimal value of learning rate of 0.2 and the momentum of 0.8. The R (correlation coefficient) values of testing set for Cu grade and recovery are 0.92 and 0.92, respectively.

RBF neural network

In this section an attempt has been made in selecting the methodology of the network. The present methodology is used with an advantage that hidden layer weights or centre vectors are optimized first then it forward the processes to the output layer. Hidden-output layer weights are further optimized using gradient descent technique. So there was no backflow at the input-hidden layer which reduces the simulation time of the code. Best network architecture (i.e. number of centre vectors in the hidden layers, learning rate and momentum coefficient) has been obtained by trial and error based on mean square error in training, testing, and the number of iterations.

Best network architecture (i.e. number of centre vectors in the hidden layers, learning rate and momentum coefficient) has been obtained by trial and error based on mean square error in training, testing, and the number of iterations. Number of centre vectors varies from 10 to 30 and range of η and α varies from 0.1 to 0.9. The best results were obtained with 8-30-2 arrangement that was capable to estimate metallurgical performance of Cu in flotation column. Also, the associated ANNs analyses were carried out with an optimal value of learning rate of 0.7 and the momentum of 0.9 with 1000 iterations.

Table 4. Metallurgical performance estimation results by various models

Std error	MIN error	MAX error	MSE	R	Index	Model
0.99	-2.07	1.63	1.00	0.87	FC	MLR
0.92	-2.44	2.09	0.96	0.85	Re	
0.84	-1.37	2.31	0.98	0.9	FC	MNLN
0.91	-2.41	1.26	1.09	0.86	Re	
0.73	-1.07	1.56	0.71	0.92	FC	BPNN
0.66	-1.3	0.82	0.48	0.92	Re	
0.83	-1.36	1.82	0.75	0.91	FC	RBFNN
0.73	-1.7	1.38	0.66	0.90	Re	

Comparison of Cu grade and recovery prediction by NN and statistical methods

Apparently, it has been observed from Table 4 as well as Figs 4 and 5 that Cu grade and recovery predicted by both BPNN and RBFNN is within a very good tolerance limit compared with the traditional regression method. Both the networks are well fitted with the data collected and show the least variation error in predicting the Cu grade and recovery. It has also been observed that BPNN shows better prediction accuracy compared to RBFNN but RBFNN converges faster compared to BPNN.

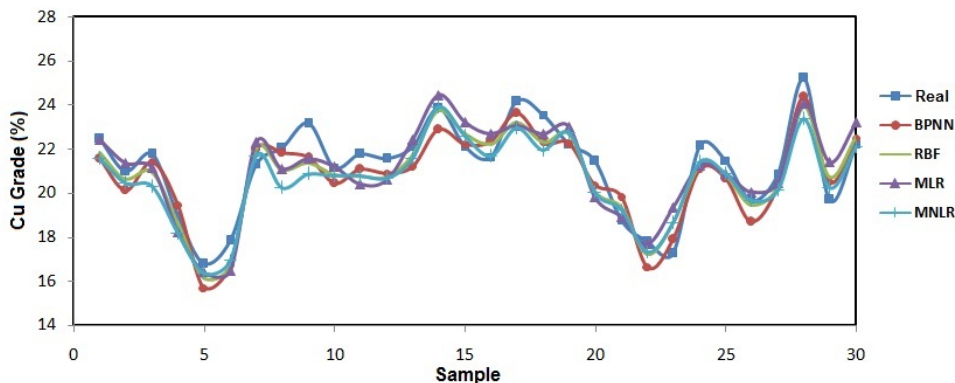


Fig. 4. NN values and regression values against observed (experimental) values in testing stage

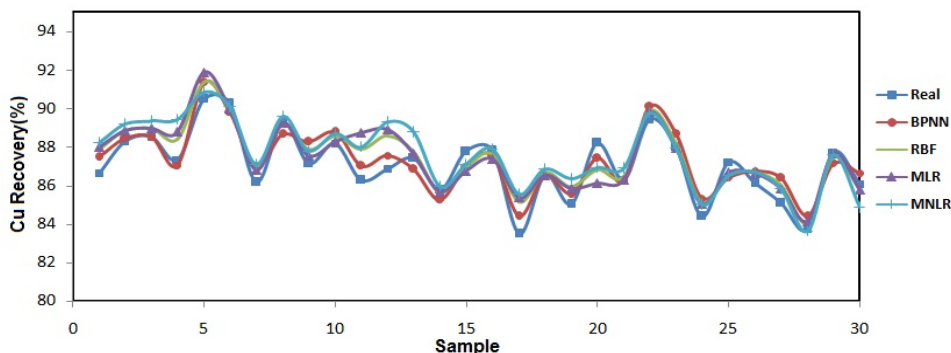


Fig. 5. NN values and regression values against observed (experimental) values in testing stage

Conclusion

This paper uses two techniques – ANN and statistical methods – to estimate Cu grade and recovery values in flotation column concentrate. This study has shown that BPNN is effective for predicting metallurgical performance of flotation column. Significant advantage of this model is that it can provide satisfactory predictions with short as well as large data. The experimental results suggest that BPNN models can offer reliable frameworks for modeling Cu grade and recovery in flotation column. Similarly it

has also been observed that RBFNN (radial basis function neural network) based prediction systems achieve faster convergence compared to BPNN (back propagation neural network) based system but with higher levels of prediction errors. Therefore, it can be a very powerful tool for treating the experimental data in other similar processes. Also, the model performance may be improved by considering additional program such as genetic algorithms (GA) and fuzzy systems.

Acknowledgments

The authors would like to acknowledge the support of Department of Research and Development of Sarcheshmeh Copper Plants for this research.

References

- AL THYABAT S., 2008. *On the Optimization of Froth Flotation by the Use of an Artificial Neural Network*. Journal of China University of Mining and Technology, 18, 418-426.
- HAYKIN S., 2004. *Neural Networks, A Comprehensive Foundation*, second ed. Prentice Hall, NJ, USA.
- JORJANI E.S., CHELGANI C., MESROGLI Sh., 2007. *Prediction of Microbial Desulfurization of Coal using Artificial Neural Network*. Journal of Minerals Engineering 20, 1285-1292.
- MOSAVI M.R., 2011. *Error reduction for GPS accurate timing in power systems using Kalman filters and neural networks*. J. Electr. Eng. 161–168 R. 87 NR 12.
- NAKHAEI F., SAM A. MOSAVI M.R., VAGHEI Y. 2012. *Recovery and Grade Accurate Prediction of Pilot Plant Flotation Column Concentrate: Neural Network and Statistical Techniques*, International Journal of Mineral Processing, In press.
- NAKHAEI F., SAM A. MOSAVI M.R., ZEIDABADI S., 2010. *Prediction of Copper Grade at Flotation Column Concentrate using Artificial Neural Network*. IEEE Conference on Signal Processing.
- OZBAYOGLU G., OZBAYOGLU A., OZBAYOGLU M., 2008. *Estimation of Hardgrove Grindability Index of Turkish coals by neural networks*. Int. J. Miner. Process. 85 (4), 93–100.
- SAMANTA B., BANDOPADHYAY S., 2009. *Construction of a radial basis function network using an evolutionary algorithm for grade estimation in a placer gold deposit*, Computers & Geosciences 35, 1592–1602.
- ZHANG X.Q., WANG H.B., YU H.Z., 2007. *Neural Network Based Algorithm and Simulation of Information Fusion in the Coal Mine*. Journal of China University of Mining and Technology, 17(4), 595-598.

Received April 30, 2012; reviewed; accepted July 11, 2012

SEPARATION OF LEAD(II) AND COPPER(II) BY PLASTICIZER MEMBRANES WITH SULPHUR ANALOGUS OF PHOSPHINIC ACIDS AS CARRIERS

Marta KOŁODZIEJSKA¹, Cezary KOZŁOWSKI², Malgorzata ULEWICZ¹

¹ Department of Metal Extraction and Recirculation, Czestochowa University of Technology, 42-200 Czestochowa, Armii Krajowej 19 Street, Poland

² Institute of Chemistry and Environment Protection, Jan Dlugosz University of Czestochowa, 42-201 Czestochowa, Armii Krajowej 13/15, Poland, e-mail: c.kozlowski@ajd.czest.pl

Abstract: Investigation of selective removal of Pb(II) and Cu(II) from acidic nitrate aqueous solutions using transport across polymer inclusion membranes PIMs was performed. The sulphur analogus of phosphinic acids, *i.e.* bis(2,4,4-trimethylpentyl)monothiophosphinic acid (**1**) and *tert*-butyl(phenyl)-phosphinothioic acid (**2**) as well as their mixture were incorporated into polymer inclusion membranes composed of cellulose triacetate as a support and *o*-nitrophenyl octyl ether as a plasticizer. In the experiments the transport of Cu(II) across PIM with **1** was rapid and complete, however the lead(II) removal increased with increased membrane saturation. Selective transport of Cu(II) over Pb(II) through PIMs with binary carrier system (**1** + **2**) was observed; the selectivity order was: Cu(II) >> Pb(II). At temperature of 50°C the selectivity coefficient Cu(II)/Pb(II) for membrane with binary carriers was the highest and was equal to 758.

Keywords: plasticizer membranes, organophosphorous acids, lead(II), copper(II)

Introduction

Recently polymer inclusion membranes (PIMs) represent an attractive alternative to liquid-liquid extraction for the selective removal and concentration of divalent metals ions from aqueous solutions. Transport of metal ions across PIM can be described as simultaneous extraction and back-extraction operations combined in a single stage. PIMs are formed by casting cellulose triacetate (CTA) from an organic solution to form a thin, stable film. The casting solution also contains an ion exchange carrier and a membrane plasticizer (Kislik, 2010, Nghiem et al., 2006).

As metal ion carriers in the liquid membrane processes very often the phosphoroorganic compounds are used. The separation of Co(II) and Ni(II) by sup-

ported and hybrid liquid membranes with Cyanex 301, Cyanex 302, Cyanex 272, and D2EHPA, was presented by Gega et al. (2001), whereas Ulewicz and Walkowiak (Ulewicz, 2004, 2007; Ulewicz and Walkowiak, 2003) studied separation of Zn(II), Cd(II), Cu(II), Co(II), and Ni(II) by polymer liquid membranes with D2EHPA, Cyanex 301 and Cyanex 272. Zinc(II) ions can be effectively separated from aqueous chloride solutions containing another metal ions, *i.e.* Cd(II), Cu(II), Co(II), and Ni(II), due to the transport across polymer inclusion membrane with D2EHPA or Cyanex 272 as the ion carrier, whereas Cyanex 301 used as ion carrier allowed much further transport of Cu(II) ions from mixture of metal ions solutions. Although the extraction of lead(II) using PIMs with tailor made carriers (Kozłowski et al., 2008) and commercial carriers (Salazar-Alvarez et al., 2005) has been reported previously, to our knowledge there are no experimental reports on the selective transport of Pb(II) with organophosphorous acids using PIMs.

The influence of natural extractants on cation transport selectivity and efficiency has been also explored by Kozłowski (2006) as well as Kozłowska et al. (2007). Cyanex 301 and 302 used as ionic carriers for competitive transport of Zn(II), Cd(II), and Pb(II) gave preferential selectivity order: Pb(II) > Cd(II) > Zn(II). They also proved that the addition of 3,7-dinonylnaphthalene-1-sulfonic acid into PIM with Cyanex 302 causes a synergetic effect on separation of Pb(II) and Cd(II) ions from Zn(II). From transport across PIM with mixture of carriers, the selectivity coefficient Pb(II)/Zn(II) and Cd(II)/Zn(II) was 3.5 whereas from transport across PIM containing only Cyanex 302 the selectivity coefficients Pb(II)/Cd(II) and Pb(II)/Zn(II) were 1.3 and 2.2, respectively. The synergistic membrane transport of Pb(II) across PIMs containing different crown ethers in the presence of dialkyl-naphthalenesulphonic acids was also reported by Nazarenko and Lamb (1997). A synergistic effect between the calixarenes and dinonylnaphthalenesulfonic acids, used as the counter-ions, was observed in transport of Cs(I) and Sr(II) ions across PIMs by Arena et al. (1998).

In this work the authors present the results for competitive transport of copper(II) and lead(II) ions from dilute aqueous solutions across polymer inclusion membranes with sulphur analogus of phosphinic acids. Also effects of temperature upon the efficiency and selectivity of ions transport with binary carriers is now reported.

Experimental part

Reagents

The inorganic chemicals, *i.e.* copper(II) and lead(II) nitrates were of analytical grade and were purchased from POCh (Gliwice, Poland). The organic reagents, *i.e.* cellulose triacetate (CTA), *o*-nitrophenyloctyl ether (*o*-NPOE) and dichloromethane were also of analytical grade and were purchased from Fluka and used without further purification. The ion carrier, *i.e.* bis(2,4,4-trimethylpentyl)monothiophosphinic acid (**1**) was obtained from Fluka. The sample of optically active *tert*-butyl(phenyl)phosphinothioic acid (**2**) having $[\alpha]_{589} = +5.3$ (MeOH) was prepared in the Centre of Molecular and

Macromolecular Studies in Lodz by the addition of elemental sulfur to secondary *t*-butylphenylphosphine oxide; unpublished results (Wang et al., 2001 cited in literature data). It should be noted here that both thiophosphinic acids exist as tautomeric mixtures (**1a** and **1b** or **2a** and **2b** respectively). For *tert*-butyl(phenyl)phosphinothioic acid the tautomeric form **2b** was found to predominate – Fig. 1. Extraction of Pb(II) and Cu(II) by phosphinothioic acid tautomeric form used in this study depends not only on the acidity strength, but also on the ion–dipole interaction between the hydroxyl and sulfur groups and the cations, steric (depth) effect of the substituent.

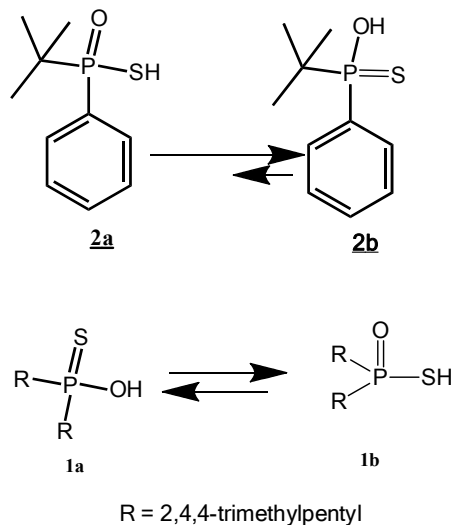


Fig. 1. Tautomeric structures of sulphur analogus of phosphinic acids

Polymer membrane preparation and characterization

The polymer membranes were prepared according to the procedure reported in the previous paper (Kozłowski, 2007). A solution of cellulose triacetate as the support, plasticizer and sulfur analogues of phosphinic acid as ion carrier in dichloromethane was prepared. A specified portion of this solution was poured into a membrane mould comprised of a 9.0 cm diameter glass ring placed on a glass plate with cellulose triacetate - dichloromethane glue. After slow solvent evaporation overnight the resulting membrane was peeled off from the glass plate by immersion in cold water. Then the membrane was soaked for 12 hours in distilled water to achieve their homogeneity.

The thickness of the PIM samples was measured using a digital micrometer (Mitutoyo) with an accuracy of 0.0001 mm. The thickness of membrane was measured 10 times for each case and shown as average value of these measurements with the standard deviation below 1%. The thickness of membrane before and after the transport was the same. The prepared membranes had thickness equal to 27 μm .

The each experiential point was repeated 4 times, *i.e.* formed membrane by immobilization, thickness measured and transport parameters calculated. Experimental reproducibility was high with standard deviation below 1% measured values.

Transport studies

Transport experiments were carried out in a permeation module cell described in our earlier paper (Ulewicz et al., 2007). The membrane film (at surface area of 4.9 cm²) was tightly clamped between two cell compartments. Both, *i.e.* the source and receiving aqueous phases (45 cm³ each) were mechanically stirred at 600 rpm. As the receiving phase the deionized water was used. The transport experiments were carried out at the temperature of 20 ± 0.2°C. Metal concentration was determined by withdrawing small samples (0.1 cm³ each) of the aqueous receiving phase at different time intervals and analyzing by atomic absorption spectroscopy method (AAS Spectrometer, Solaar 939, Unicam). The source phase pH was kept constant (pH = 5.0) and controlled by pH meter (pH meter, CX-731 Elmetron, with combine pH electrode, ERH-126, Hydromet, Poland). The permeability coefficient (P , m/s) of metal ions across membranes was described by the following equation (Danesi, 1984-85):

$$\ln\left(\frac{c}{c_i}\right) = -\frac{A}{V}Pt \quad (1)$$

where c is the metal ions concentration (M) in the source aqueous phase at some given time, c_i is the initial metal ions concentration in the source phase, t is the time of transport (s), V is volume of the aqueous source phase (m³), and A is an effective area of membrane (m²).

A linear dependence of $\ln(c/c_i)$ in the source phase versus time was obtained and the permeability coefficient was calculated from the slope of the straight line that fits the experimental data. The initial flux (J_i) was determined as equal to:

$$J_i = P c_i \quad (2)$$

The selectivity coefficient (S) was defined as the ratio of initial fluxes for $M1$ and $M2$ metal ions, respectively:

$$S = \frac{J_{i,M1}}{J_{i,M2}} \quad (3)$$

To describe the efficiency of metal removal from the source phase, the recovery factor (RF) was calculated:

$$RF = \frac{c_i - c}{c_i} \cdot 100\% \quad (4)$$

The reported values correspond to the average values of three replicates, with the standard deviation within 5%.

Results and discussion

The most important factors influencing the transport of metal ions through polymer inclusion membranes are the acidity of the ion carrier, kind of solvent (plasticizer) as well as the maximal concentration of carrier playing also an important role in saturation of membranes. In the first series of experiments, competitive transport of Cu(II) and Pb(II) from aqueous nitrate solutions containing the metal ion species at concentrations of 0.0010 M through PIM with organophosphorous acid (**1**) as the ionic carrier and *o*-NPOE as the plasticizer into 0.50 M HNO₃ aqueous solution was investigated. Membrane composition was: 80% *o*-NPPE, 15% CTA, and 5% ion carrier. The blank experiments for the transport when the ion carrier was absent, i.e. with membranes containing the support (CTA) and plasticizer (*o*-NPPE) only, show no significant flux across PIM.

Effect of carrier **1** concentration

The effect of the concentration of ion carrier **1** in the organic membrane phase on the copper(II) and lead(II) transport is given in Fig. 2. Showing the removal curves of metal ions transport through PIM with **1** at concentrations range from 0.10 to 1.0 M. The copper(II) ions were transported with a very high rate, and the selectivity order was as follows: Cu(II) > Pb(II). The process efficiency increased with the ionic carrier saturation of liquid phase membrane, especially for copper ions.

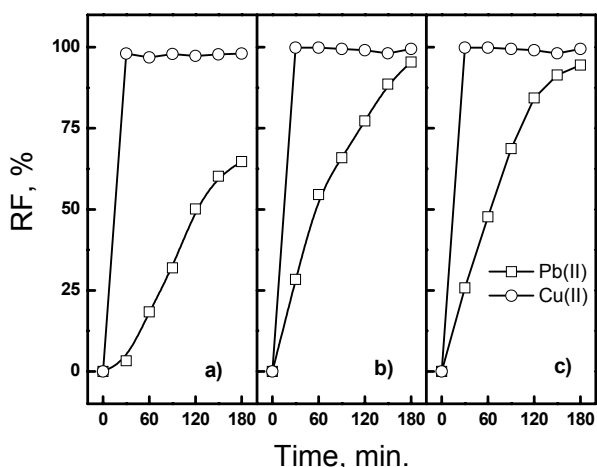


Fig. 2. The recovery factors of lead(II) and copper(II) vs. time of competitive transport across PIM with carrier **1**. Source phase: 0.0010 M for Pb(II) and Cu(II); receiving phase: 0.50 M HNO₃; membrane: 4.0 cm³ *o*-NPOE/1.0 g CTA, a) 0.10 M, b) 0.50 M, c) 1.0 M carrier **1** (based on plasticizer)

The aqueous source phase acidity constantly increases by protons and metal ions exchange during counter-transport in the membrane system, and is a significant factor determining the selectivity transport. We found that the source phase pH value in the process of transport through PIM containing **1** became stable on the level of 3.5 after 30 min of transport.

For copper(II) removal the optimum concentration range of the carrier was 0.1–1.0 M; in the experiments the transport of Cu(II) was rapid and complete. However the lead(II) removal increased with increase of membrane saturation. When the concentration of ion carrier **1** was 0.1 M, the best recovery factors for copper(II) and lead(II) were 99% and 65%, respectively. The examined cation permeation of PIM with **1** was found to be very efficient, also the permeation selectivity for this membrane was very poor. For this reason for next experiments the phosphinothioic acid derivative as a carrier of a lower acidity was applied.

Effect of binary carriers

The next series of experiments dealt with competitive transport of Pb²⁺ and Cu²⁺ cations from aqueous solutions containing the metal ions at concentrations of 1.0–10⁻³ M through PIM with organophosphoric acids **1** and **2** as well as the binary mixture as the ion carriers, and *o*-NPOE as the plasticizer into 0.5 M HNO₃. Figure 3 presents the recovery factor values of investigated metal ions from the source phase, determined after 2 hours of transport through PIM with carriers **1** and **2** and binary carrier system at the concentration of 0.10 M. The Cu(II) and Pb(II) ions were extracted more efficiently, since their RF values for the transport through PIM containing **1** were 98% and 55%.

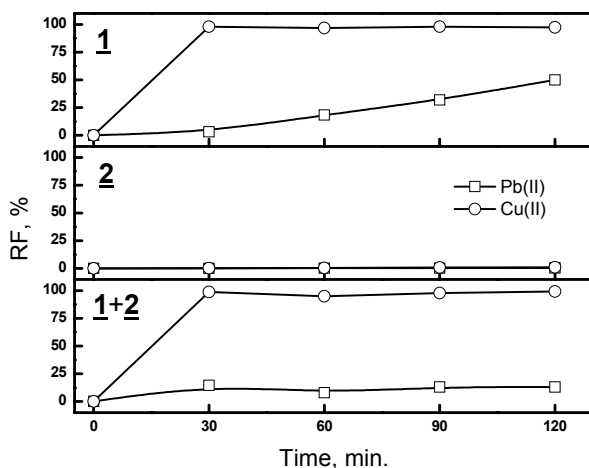


Fig. 3. The recovery factors of lead(II) and copper(II) vs. time of competitive transport across PIM with carriers **1**, **2**, and binary carrier **1** + **2**. Source phase: 0.0010 M for Pb(II) and Cu(II); receiving phase: 0.50 M HNO₃; membrane: 0.40 cm³ *o*-NPOE/1.0 g CTA, 0.10 M each carrier (based on plasticizer)

However carrier **2**, used for the Cu(II) and Pb(II) ions transport is a less acidic organic acid. The both metal ions were transported with a small rate and the selectivity order was as follows: Cu(II) > Pb(II); the process efficiency was determined by tendency to tautomeric reagouping ionic carrier **2** in liquid phase membrane as well as namely spherical hindrance *t*-butyl group. These factors interfere with ion exchange (deprotonation), resulting in a low affinity to form metal complexes.

After that time, metal ions were still transported due to the protonation and deprotonation reactions of the carrier which occurred because of the difference between the source phase pH and the receiving phase pH and because of the low protonation constant of the acidic carrier.

For membranes with 0.10 M of **2** the maximum value of the RF for Cu(II) ions was equal to 1.46% which practically suggests that carrier structure is not able to metal ion complexation.

In the case of transport by PIM with binary mixture of carriers **1** + **2** the separation of Cu(II) over Pb(II) was higher, compared to the membranes with alone **1** or **2**, the recovery factor values of investigated metal ions from the source phase determined after 2 hours transport through PIM with **1** + **2** were more efficient only for copper(II), since their RF values for Cu(II) and Pb(II) were 98% and 11%, respectively. Under conditions, the transport through the membrane with binary carrier shows a relatively high selectivity of Cu(II) over Pb(II) ions for 0.10 M **1** + **2**; the $S_{Cu/Pb}$ value was 11.4. The use of a mixture of carriers does not favor lead(II) complexation due to tendency of thiophosphinic acid and phosphinothioic acid to form hydrogen bonds, and the presence of the sterically hindered structures, *i.e.* *tert*-butyl group.

These large separation factors among Cu(II) over Pb(II) cations rival those reported by Hiratani et al. (1997). The separation of Pb(II) from Cu(II) in a liquid membrane transport system, as well as those reported by Molinari et al. (2005) and Sabry et al. (2007). Although these papers deal with the separation of some metal ions, they do not report on the selective separation of Cu(II) over Pb(II) from mixtures using organophosphoric acid as ion carriers.

The RF values recorded in this paper agree well with those reported by us for the removal of Pb(II), Zn(II) and Cu(II) (Ranpreet et. al., 2011) and are lower than those reported by Salazar-Alvarez et al. (2005).

Effect of temperature on transport with binary carriers

The complexing behavior towards copper and lead of binary organophosphorus acid was examined at temperature of 50°C. The influence of temperature on the selective transport of metal ions across PIM with **1+2** were determined. The competitive transport of copper(II) and lead(II) through PIM containing binary carriers showed higher selectivity than membranes with single carrier. Combination of **1** with **2** in the membrane also significantly improved selective removal of copper(II) when the PIM system at temperature 50°C was used. Initial fluxes, selectivity orders for PIM with carriers **1** and **2** and mixture **1+2** are shown in Table 1.

Table 1. Kinetics and selectivity parameters for competitive transport of copper(II) and lead(II) through PIM with organophosphorous acids as the ion carriers. Source phase: $1.0 \cdot 10^{-3}$ M Cu^{2+} and 0.10 M Pb^{2+} , pH = 3.0; Receiving phase: 0.5 M NaNO_3 ; Membrane: 75% *o*-NPPE, 15% CTA, and 10% carrier (4.0 cm^3 *o*-NPOE/1.0 g CTA, 0.10 M carrier based on plasticizer volume)

Ion carriers	Metal ions	Initial fluxes $\mu\text{mol}/\text{m}^2 \cdot \text{s}$	Selectivity orders and selectivity coefficients
<u>1</u>	Cu(II)	$85.2 \pm 0.05^*$	Cu(II) > Pb(II)
	Pb(II)	2.4 ± 0.03	36
<u>2</u>	Cu(II)	8.1 ± 0.04	Cu(II) > Pb(II)
	Pb(II)	0.80 ± 0.06	10
<u>1+2</u>	Cu(II)	83.4 ± 0.07	Cu(II) >> Pb(II)
	Pb(II)	0.11 ± 0.02	758

* Standard deviation values for 4 experiments

The initial fluxes for copper(II) are much higher for PIM with **1** and PIM with **1 + 2** than for membranes with **2**, but the selectivity of binary carriers is very high. Selectivity coefficients Cu(II)/Pb(II) for membrane with binary carriers was the highest and was equal to 758. On the other hand the highest value separation coefficient was found in the case in which practically negligible removal of Pb(II) was observed. In both experiments under temperatures 25 and 50°C the controllable factor of selectivity for binary carrier system was proton migration in each of tautomeric forms; as a consequence the best selectivity of copper(II) ions removal. High recoveries of copper(II) from dilute aqueous solution containing lead(II) were obtained by applying thio-phosphinic and phosphinothioic acids as carriers in transport across polymer inclusion membranes at relatively shorter times when comparing to other separation methods.

Conclusion

Polymer inclusion membranes containing organophosphorous acid, i.e. bis(2,4,4-trimethylpentyl)monothiophosphinic acid transfer Cu(II) and Pb(II) ions efficiently, at concentration of ion carrier in membrane equal to 0.5 M. With the use of the bis(2,4,4-trimethylpentyl)monothiophosphinic acid and *tert*-butyl(phenyl)phosphinothioic acid as an mixture of ionic carriers, the competitive transport of metal ions shows the preferential selectivity order: Cu(II) >> Pb(II).

The addition of *tert*-butyl(phenyl)phosphinothioic acid into PIM with bis(2,4,4-trimethylpentyl)monothiophosphinic acid plays a role of the factor which increases the selectivity in the membrane process. Competitive transport through polymer inclusion membranes containing above mixture of carriers was found to be an effective method for separation and recovery of copper(II) from solutions containing lead(II) ion, the selectivity factor Cu(II)/Pb(II) being over 750. The application of the proposed methods for the selective removal of ions from spent solutions, generated after the galvanizing process or hydrometallurgical ore process, has also been examined.

Acknowledgments

This work is a part of the projects No. NN209441539. The authors acknowledge Polish Ministry of Science and Higher Education and National Science Centre for financial support of these project.

References

- ARENA G., CONTINO A., MAGRA, SCIOTTO, D., LAMB, J. D., 1998, *Selective transport of cesium and strontium ions through polymer inclusion membranes containing calixarenes as carrier*, *Supramol. Chem.*, 10, 5-15.
- CHO M. H., CHUN H. S., KIM J. H., RHEE C. H., KIM S. J., 1999, *Study on separation of heavy metal ions in a natural macrocycle-mediated emulsion liquid membrane system*, *Bull. Korean Chem. Soc.* 12, 474-477.
- CHO M. H., SEON-WOO K. H., HEO M. Y., LEE I. C., YOON C. J., KIM S. J., 1988, *Studies on the macrocycles mediated transport in bulk liquid membrane system of transport metal ions*, *Bull. Korean Chem. Soc.*, 9, 292-295.
- DANESI P.R., 1984-85, *Separation of metal species by supported liquid membranes*, *Sep. Sci. Technol.*, 19, 857-894.
- GEGA J., WALKOWIAK W., GAJDA B., 2001, *Separation of Co(II) and Ni(II) ions by supported and hybrid liquid membranes*, *Sep. Purif. Technol.*, 22-23, 551-558.
- HIRATANI K., TAKAHASHI T., SUGIHARA H., KASUGA K., FUJIWARA K., HAYASHITA T., BARTSCH R. A., 1997, *Selective liquid membrane transport of lead(II) by acyclic polyether dicarboxylic acid ionophore*, *Anal. Chem.*, 69, 3002-3007.
- KISLIK V.S., 2010, *Liquid membranes. Principles and application in chemical separation and wastewater treatment*, Elsevier, UK.
- KOZŁOWSKA J., KOZŁOWSKI C.A., KOZIOL J.J., 2007, *Transport of Zn(II), Cd(II) and Pb(II) across CTA plasticized membranes containing organophosphorous acids as ion carriers*, *Sep. Purif. Technol.*, 57, 430-434.
- KOZŁOWSKI C.A., 2006, *Facilitated transport of metal ions through composite and polymer inclusion membranes*, *Desalination*, 198, 132-140.
- KOZŁOWSKI C.A., KOZŁOWSKA J., 2009, *PNP-16-crown-6 derivatives as ion carriers for Zn(II), Cd(II), Pb(II) transport across polymer inclusion membranes*, *J. Membr. Sci.*, 326, 215-221.
- KOZŁOWSKI C.A., WALKOWIAK W., GIREK T., 2008, *Modified cyclodextrin polymers as selective ion carriers for Pb(II) separation across plasticized membranes*, *J. Membr. Sci.*, 310, 312-320.
- KOZŁOWSKI C.A., 2007, *Kinetics of chromium(VI) transport from mineral acids across cellulose triacetate (CTA) plasticized membranes immobilized by tri-n-octylamine*. *Ind. Eng. Chem. Res.*, 46, 5420-5428.
- MOLINARI R., ARGURIO P., PIRILLO F., 2005, *Comparison between stagnant sandwich and supported liquid membranes in copper(II) removal from aqueous solutions: flux, stability and model elaboration*, *J. Membr. Sci.*, 256, 158-168.
- NAZARENKO A.Y., LAMB J.D., 1997, *Selective transport of lead(II) and strontium(II) through a crown ether-based polymer inclusion membrane containing dialkyl-naphthalenesulfonic acid*, *J. Inclusion Phenom. Mol. Recognit. Chem.*, 29, 247-258.
- NGHIEM L.D., MORNANE P., POTTER I.D., PERERA J.M., CATTRALL R.W., KOLEV S.D., 2006, *Extraction and transport of metal ions and small organic compounds using polymer inclusion membranes (PIMs)*, *J. Membr. Sci.*, 281, 7-41.
- SABRY R., HAFEZ A., KHEDR M., EL-HASSANIN A., 2007, *Removal of lead by an emulsion liquid membrane. Part I*, *Desalination*, 212, 165-175.

- SALAZAR-ALVAREZ G., BAUTISTA-FLORES A. N., RODRIGUEZ de SAN MIGUEL MUHAMMEDA M., de GYVES J., 2005, *Transport characterization of a PIM system used for the extraction of Pb(II) using D2EHPA as carrier*, J. Membr. Sci., 250, 247-257.
- SINGH R., MEHTA R., KUMAR V., 2011, *Simultaneous removal of copper, nickel and zinc metal ions using bulk liquid membrane system*, Desalination, 272, 170-173.
- TSUKUBE H., UENISHI J., HIGAKI H., KIKKAWA K., TANAKA T., WAKABOYASHI S., OAE S., 1993, *Side arm effects on cation binding, extraction, and transport functions of oligopyridine functionalized aza-crown ethers*, J. Org. Chem., 58, 4389-4397.
- ULEWICZ M., 2004, *Transport of transition metal ions through polymer inclusion membranes with Cyanex 301*, Ars Separatoria Acta, 3, 81-88.
- ULEWICZ M., 2007, *Transport jonów Zn(II) i Pb(II) przez polimerowe membrany inkluzyjne przy użyciu D2EHPA*, Przemysł Chemiczny, 86/9, 861-865.
- ULEWICZ M., SADOWSKA K., BIERNAT J.F., 2007, *Transport of Zn(II), Cd(II) and Pb(II) across polymer inclusion membrane doped with imidazole azacrown ethers*, Desalination, 214, 352-364.
- ULEWICZ M., WALKOWIAK W., 2003, *Separation of zinc(II) and cadmium(II) ions from sulfate solutions by ion flotation and transport through liquid membranes*, Physicochem. Probl. Min. Process., 37, 77-86.
- WANG F., POLAVARAPU P.L., DRABOWICZ J., MIKOLAJCZYK M., LYZWA P., 2001, *Absolute configurations, predominant conformations and tautomeric structures of enantiomeric tert-butyl-phenyl-phosphinothioic acid*, J. Org. Chem., 66, 9015-9019.

Received July 2, 2012; reviewed; accepted July 15, 2012

WETTING OF SURFACES WITH IONIC LIQUIDS

**Maciej POLESKI, Justyna LUCZAK, Robert ARANOWSKI,
Christian JUNGNIKKEL**

Department of Chemical Technology, Chemical Faculty, Gdansk University of Technology, 80-233 Gdansk, Poland, cjungnickel@googlemail.com

Abstract: The paper focuses on assessing wettability of surfaces modified with ionic liquid solutions. Dialkylimidazolium chlorides have been selected as the test group, because of their immediate availability and limited previous research. Contact angle of selected ionic liquid solutions have been measured with two methods: capillary rise test and simplified sitting droplet analysis, performed by means of digital camera. During tests the extremely high viscosity of dialkylimidazolium chlorides has been observed to drop rapidly with prolonged exposition to atmospheric moisture and measured experimentally with Karl-Fischer titration and viscosity measurements. Contact angles of selected ionic liquids have been presented.

Keywords: ionic liquid, wettability, contact angle, capillary rise, surface interactions

Introduction

Ionic liquids are a branch of novel, organic chemicals, distinguished by their unique properties. From a chemical point of view, ionic liquids are salts, composed most commonly of a large, organic cation and smaller, inorganic anion. However, unlike most of the salts, ionic liquids are, as the name suggests, liquid at low temperatures. They are most often defined as liquid salts with a melting point lower than 100°C, but remain liquid over a broad range of temperatures (Yang and Pan, 2005).

Ionic liquids (ILs) have been already utilized in many unit operations and processes and it was found out that may serve as substitutes for traditional solvents. However, the reason why ionic liquids find application in so many fields of research and industry is their extraordinary customization potential. Dialkylimidazolium cation-based ILs possess two alkyl chains that can be shortened, extended and branched with ease, and substitution of one anion with another can completely change physicochemical properties of the substance. Thousands of possible and useful configurations just wait to be discovered and implemented in new ways and they all differ in physicochemical

characteristics, like melting point, viscosity, surface tension, conductivity, reactivity or wettability.

The potential applications of ILs are numerous including usage as reaction media, extraction and separation technologies, electrochemistry and many others. For the applications involving heterogeneous systems and transport of ILs in capillary, fibrous, or porous environments, interfacial properties such as wettability has to be known.

Wettability is a tendency of a liquid to spread on a solid surface (Kumar and Prabhu, 2007). Measurement of the contact angle is the way to estimate wettability when the tested fluids are pure and the contact surface (solid or liquid) is perfectly flat, mainly because the surface tension of the interfaces is constant when no surfactants or other compounds are present to alter the wetting (Anderson, 1986). When using Young's equation it was assumed that the surface is rigid, homogeneous and perfectly flat – in such a case a single, specified contact angle for each three-phase system could be obtained. Estimation of contact angles for ionic liquids are, so far, very poorly investigated (Batchelor et al., 2009; Restolho et al., 2009), even though knowledge on their wettability is needed to select IL for many applications.

The surface tension is dependant on slight changes of temperature, surface characteristics or viscosity of the liquid, the equilibrium maintained by the interfacial tensions can be disrupted. The estimation of contact angles for given systems becomes useful only when the interaction potentials of two of those phases can be treated as constant or described numerically. Many simplistic models of wetting of solid materials, for example, have been developed for this purpose and when different surface types are used they are commonly described with their respective critical surface tensions (CST) (Zisman 1964).

The critical surface tension (CST) can be defined as a relative descriptor of wettability of solid surface (Zisman 1964). The test consists of plotting the cosine of the contact angles between several different liquids with defined, decreasing surface tensions on their interface with solid phase. CST is then defined by extrapolation of the line to $\cos \theta = 1$ (Ulosoy and Yekeler, 2004). However, this test can be applied only to low-energy solid surfaces (Sömnez and Cebeci, 2004), with CST values of the same magnitude as of the surface tensions measured in the tests.

Three common imidazolium-based species has been selected for this study, varying in alkyl chain length. This test group of chemicals has been chosen in a way that will permit correlation of obtained results with their molecular structure. All selected ionic liquids are dialkylimidazolium chlorides, which are also very hygroscopic and obtaining purified samples without detectable amounts of water is nearly impossible (Wassercheid and Welton, 2003). Therefore the influence of moisture has also been determined during this study.

Experimental

Reagents

All 1-alkyl-3-methylimidazolium chlorides were obtained from Merck KGaA, Darmstadt, Germany, with a purity of $\geq 98\%$. All samples were degassed and dried at 70°C under vacuum prior to use. Glass beads (Interminglass; Poland) with diameter 150–250 μm were used. Prior to use, the beads were thoroughly cleaned and degassed, with methanol:acetone:chloroform (1:1:1 by volume) and dried at 130°C .

Direct contact angle measurement. Sessile drop method

Ionic liquid has been placed inside the Hamilton syringe, which was then placed inside the grip of the component with micrometric screw. The droplet was placed on the microscopic cover glass surface placed atop the glass pedestal and its image has been taken with digital camera. For the contact angle was calculated from equation, assuming a non gravitationally distorted spherical cap formed by a liquid drop (Woodward, 1999)

$$\theta = 2 \tan^{-1} \frac{2h}{d} \quad (1)$$

where: h – height of the droplet profile [pixel], d – diameter of the droplet base [pixel]

Precision of this method was significantly high, obtained angles differ no more than 1° . However, the authors are aware that a number of other numerical solutions exist, which also take the gravitational effects into account (Allen 2003).

Capillary rise method

Wettability of glass beds was determined by capillary rise methods based on the Washburn equation described elsewhere (Washburn, 1921; Siebold, 2000; Wolfrom, 2002; Trong, 2006; Joskowska, 2012). The glass capillary filled with a bed of sorbent was attached to a movable grip, which could be lowered and raised smoothly. When the experiment was started, the capillary was slowly lowered to touch the surface of tested liquid. Readings of the scale were taken in regular intervals and the change of mass of liquid could be observed when the sorbent bed was penetrated. As reference liquids dichloromethane has been for hydrophilic glass beads and 1-hexanol for hydrophobic glass beads (Hołownia and Kwiatkowska et al., 2008). The references liquids were chosen (from 30 available), that are ideal wetting liquids (contact angle zero) by suspending the beads on the surface of each liquid. The various controversies regarding the reference liquids in capillary rise methods are discussed by Kowalczuk et al. (2012).

Viscosity

Viscosity of the samples has been measured by cone-plate method with Brookfield LV-III Rheometer with a CPE-40 type spindle. Tests were performed under the temperature of 25°C.

Karl-Fisher titration

Water content in ionic liquid samples was determined by coulometric titration method using 831 Karl-Fischer Coulometr, Metrohm.

Results and discussion

Ionic liquid hygroscopicity and its influence on the contact angle sessile drop method

The values of contact angle of three ionic liquids with different chain length on glass plate was presented in Table 1. The contact angle of microscopic glass cover was determined by the sessile drop method.

Table 1. Results and statistical analysis of contact angle measurements performed by means of photographic method on microscopic cover glass. Values of $\log K_{ow}$ taken from literature (Thöming, Cho et al., 2011)

Abbreviation	Θ , degree	Standard deviation	$\log K_{ow}$
[HMIM][Cl]	14.592 ± 0.539	0.507	-1.730
[OMIM][Cl]	10.815 ± 0.301	0.293	-0.600
[DMIM][Cl]	105.951 ± 1.295	0.949	0.311

Contact angle values of [HMIM][Cl] and [OMIM][Cl] were similarly low and both of these substances were found to almost wet microscopic cover glass effectively. However, contact angles for [DMIM][Cl] were extremely high, due to the inability of the molecule to interact with the glass surface. This was most probably caused by the alkyl chain, which at chain length 10 blocks the columbic interaction of the headgroup with the surface.

It was later assumed that the difference between observed contact angles for these samples may also related with different effects of moisture absorption into their structure. To compare the affinity of these ionic liquids towards water octanol water partition coefficient $\log K_{ow}$ (as shown in Table 1) may be used. For both [HMIM][Cl] and [OMIM][Cl], the $\log K_{ow}$ was found to be negative, proving their affinity towards water. Positive value found for [DMIM][Cl] is one of the reasons behind the extremely high contact angle observed in described procedure.

Ionic liquid hygroscopicity and its influence on the Washburn method

Contact angle values evaluated in the capillary rise test is dependant on the surface tension and viscosity of the tested liquid and the relation of these parameters with those exhibited by the reference wetting substance. The results are shown in Table 2. A number of researchers measured both viscosity and surface tension for a broad group of ionic liquids, determining them with different tools. Ghatee and Zolghadr (2008) measured surface tensions of several ionic liquids with modified capillary rise method utilizing digital cathetometer. Gomez et al., (2006) determined dynamic viscosities of few pure ionic liquids and their water solutions in various temperatures, by means of several commercially available viscosimeters. During the procedure it was observed that a small sample of tested ionic liquid becomes perceptibly less viscous after an hour of exposure to air, which proved that moisture is absorbed by these samples at a very high rate.

Table 2. Surface tension and viscosity values for pure ionic liquids used in this study

Abbreviation	Surface tension, mJ/m ² , 25°C,	Viscosity, cP, 25°C
[HMIM][Cl]	41.8 ^a	18089 ^b
[OMIM][Cl]	31.9 ^a	20883 ^b

a – (Ghatee and Zolghadr 2008), b – (Gómez, González *et al.* 2006)

An effort has been put into further investigation of surface tension and viscosity changes related with increasing water content within the tested liquids. Literature concerning surface tension variation in ionic liquids and absorbed moisture has been reviewed. Freire et al. (2007) measured surface tensions of two species of saturated 1-alkyl-3-methylimidazolium ionic liquids at 30°C and for water content up to 15% molar ratio. For more hydrophilic [BMIM][PF₆] non-linear surface tension variation of 6% was noted. For [OMIM][PF₆] such a variation was insignificantly smaller, less than 1% (Freire et al., 2007). They concluded that the influence of water content on surface tension of ionic liquids is significant only for hydrophilic ionic liquids, with shorter alkyl chain. Klomfar et al. (2010) obtained similar results and found no apparent correlation between water content and surface tension of ionic liquid samples.

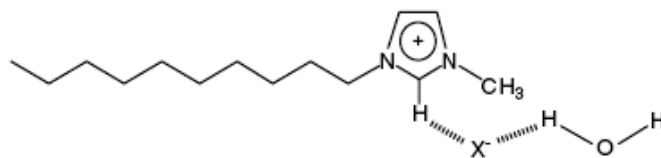


Fig. 1. Figure describing basis for networking of water molecules and ionic liquid. Both dialkylimidazolium cation and water form hydrogen bond with a given anion

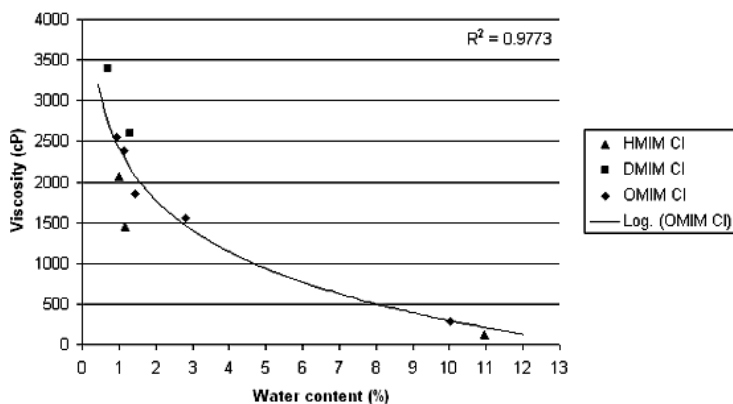


Fig. 2. Graph describing the relationship between increasing water content and viscosity of tested dialkylimidazolium chlorides

Viscosity of typical room-temperature ionic liquids rarely exceeds 200 cP. All dialkylimidazolium chlorides are exception to this rule and their extremely high viscosity is a result of hydrogen bonding between Cl^- anions and the hydrogen atoms (as shown in Fig. 1) on the imidazolium cation ring (Wassercheid and Welton, 2003). When water is introduced into such a structure, chloride anions bond with hydrogen in the water molecules, which, due to their smaller size when compared to dialkylimidazolium cation, are much more mobile. With the increase of water content, the process responsible for high viscosity in ionic liquids is disrupted and a rapid decrease of this parameter is observed. New bonding is strong enough to significantly hamper any procedures dedicated to removal of water content – even with prolonged vacuum drying used for samples tested in this paper, the water was still present in a quantity as high as 1% molar fraction.

As shown in Fig. 2 it was initially suspected, the viscosity was found to decrease rapidly with the increase of water content, giving us a strong, logarithmic correlation with the coefficient of determination as high as 98%. Data obtained for [HMIM][Cl] appears to further prove the validity of this correlation. Unfortunately, measurements for [DMIM][Cl] after more then 15 minutes were rendered impossible to performed due to gelation, whereby the liquid turned into a semi-solid matter.

This process has been observed and even induced earlier by many researchers, who investigated the nature of this and similar structures (Firestone et al., 2004; Kaper and Smarsly 2006; Inoue et al., 2007). This spontaneous self-organization is based upon formation of robust H-bonded network between dialkylimidazolium cation, chloride anion and water molecules (Fig. 1). Hydrophobic and hydrophilic segments of such a structure are segregated, which leads to formation of regions of confined water. Such a structure is one of the simplest forms of “ionogels”, physical gels based on ionic liquids (Firestone et al., 2004).

Uncertainty concerning the actual amount of water in samples during contact angle measurements is the source of greatest discrepancies in results presented in this paper. Viscosity data obtained for [HMIM][Cl] and [OMIM][Cl] after a three hour period was assumed to be the closest available estimation of viscosity observed during the capillary rise experiments. Although the capillary rise experiments took much less time than this, but the volume of liquids used in that procedure was approximately ten times smaller, while the area of exposure to moisture was the same in both cases.

The observed time of penetration indicate that the exact viscosity of [OMIM][Cl] during the test was significantly lower than the one estimated earlier. Moisture adsorbed on hydrophilic glass could have been the reason of such an occurrence. It should be noted, however, that the time of bead penetration for [OMIM][Cl] was slightly higher than the one for [HMIM][Cl] for the same beads, while this tendency is reversed in case of hydrophobic sorbent. This observation proves initial assumptions concerning hydrophobicity of both. Contact angle for [HMIM][Cl] on hydrophilic glass (Table 3) is close to the one observed during the photographic procedure. Very high contact angles exhibited by both ionic liquids on the hydrophobic glass prove that this type of sorbent is not wetted well by tested liquids, as shown in Table 4.

Table 3. Final results of contact angle measurements by means of capillary rise procedure for hydrophilic sorbent. Average times of penetration of bed by referential solvent (t_0) and tested liquid (t_1) have been used to calculate the final values, while highest and lowest values were used to estimate the margin of error

Series	[HMIM] [Cl]		[OMIM] [Cl]	
	t_0 [s]	t_1 [s]	t_0 [s]	t_1 [s]
1	2	360.5	2.5	388.5
2	2	365	3	392.5
3	1.5	327.5	2.5	379
Mean value	1.833	351	2.667	386.667
t_0/t_1	0.00522		0.00690	
$K \cdot t_0/t_1$	0.955		4.070	
θ	17.222 ± 8.862		–	

Table 4. Final results of contact angle measurements by means of capillary rise procedure for hydrophobic sorbent. Data analyzed analogically to Table 5

Series	[HMIM] [Cl]		[OMIM] [Cl]	
	t_0 [s]	t_1 [s]	t_0 [s]	t_1 [s]
1	1.5	665.5	3	503
2	3.5	701.5	2.5	411
3	5	635	2.5	395
Mean value	3.333	667.333	2.667	436.333
t_0/t_1	0.00500		0.00611	
$K \cdot t_0/t_1$	0.077		0.305	
θ	85.573 ± 1.441		72.254 ± 0.322	

Determination of contact angles

Results obtained with both photographic and capillary rise method have been summarized in the table below (Table 5). Values obtained for microscopic cover glass are difficult to compare to those relying on capillary rise measurements, as the two methods used are completely different, based on different principles. The quantity of water present in the samples played a significant role in determination of measured contact angles and no data have been obtained concerning its change during the actual experiments. Increasing length of the alkyl chain on the 1-alkyl-3-methylimidazolium cation increases the hydrophobic character of given ionic liquid. The extent of water-repelling properties of ionic liquids are less in the formation of stable contact angle then its type – [HMIM][Cl] and [OMIM][Cl] behave almost identically in all performed tests. Even only slightly hydrophilic ionic liquid, like [OMIM][Cl] will form a low contact angle on only slightly hydrophilic surface, like the microscopic cover glass. [DMIM][Cl] is barely hydrophobic and its contact angle observed on the identical surface is extremely high.

Table 5. Summary of contact angle results obtained for tested systems

Solid phase	[HMIM] [Cl] (degrees)	[OMIM] [Cl] (degrees)	[DMIM] [Cl] (degrees)
Microscopic cover glass	14.592 ± 0.539	10.815 ± 0.301	105.951 ± 1.295
Hydrophilic beads	17.222 ± 8.862	–	–
Hydrophobic beads	85.573 ± 1.441	72.254 ± 0.322	–

Conclusions

Wetting potential of ionic liquid group being the subject of this paper is related with many independent factors. Hydrophobicity of 1-alkyl-3-methylimidazolium ionic liquids is based on the length of an alkyl chain and has been described previously by log K_{ow} . The water content is crucial factor concerning wetting process of all ionic liquids with chloride anion, especially when their extremely hygroscopic character is taken into account. Completely water-free samples of ionic liquid are extremely viscous and could not be used to wet any kind of surface efficiently. Water molecules disrupt the hydrogen bonding between chloride anion and hydrogen atoms of imidazolium ring, rapidly decreasing the viscosity of ionic liquids (Wassercheid and Welton, 2003). This process influence contact angle values differently for hydrophilic and hydrophobic specimen. Water molecules diffuse in hydrophilic samples and decrease of viscosity result in an exceptionally good wetting observed for hydrophilic surfaces and increase contact angle for hydrophobic solids. In case of hydrophobic dialkylimidazolium ionic liquids, water molecules are trapped in liquid crystalline structure of an ionogel, which is a semisolid matter, unable to wet any surface. If an ionogel structure cannot be formed for given species of ionic liquid, it can be assumed that its viscosity will decrease after addition of water or after moisture absorption.

References

- ALLEN J.S., 2003. *An analytical solution for determination of small contact angles from sessile drops of arbitrary size*. Journal of Colloid and Interface Science 261: 481–489.
- ANDERSON W.G., 1986. *Wettability Literature Survey – Part 2: Wettability Measurement*. Journal of Petroleum Technology: 1246–1262.
- BATCHELOR T., CUNDER J., FADEEV A.Y., 2009. *Wetting study of imidazolium ionic liquids*. Journal of Colloid and Interface Science 330 415–420.
- FIRESTONE M.A., RICKERT P.G., SEIFERT S., DIETZ M.L., 2004. *Anion effect on ionogel formation in N,N'-dialkylimidazolium-based ionic liquids*. Inorganica Chimica Acta 357, 3991–3998.
- FREIRE M.G., VARVALHO P.J., FERNANDES A.M., MARRUCHO I.M., QUEIMADA A.J., COUTINHO J.A.P., 2007. *Surface tension of imidazolium based ionic liquids: Anion, cation, temperature and water effect*. Journal of Colloid and Interface Science 314: 621–630.
- GHATEE M.H., ZOLGHADR A.R., 2008. *Surface tension measurements of imidazolium-based ionic liquids at liquid-vapor equilibrium*. Fluid Phase Equilibria 263: 168–175.
- GÓMEZ E., GONZÁLEZ B., DOMÍNGUEZ Á., TOJO E., TOJO J., 2006. *Dynamic Viscosities of a Series of 1-Alkyl-3-methylimidazolium Chloride Ionic Liquids and Their Binary Mixtures with Water at Several Temperatures*. Journal of Chemical & Engineering Data 51: 696–701.
- HOŁOWNIA D., KWIATKOWSKA I., HUPKA J., 2008. *An investigation of wetting of porous materials*. Physicochemical Problems of Mineral Processing 42: 251–262.
- INOUE T., DONG B., ZHENG L.-Q., 2007. *Phase behaviour of binary mixture of 1-dodecyl-3-methylimidazolium bromide and water revealed by differential scanning calorimetry and polarized optical microscopy*. Journal of Colloid and Interface Science 307: 578–581.
- JOSKOWSKA M., KOPCZYNSKA I., DEBSKI B., HOŁOWNIA-KEDZIA D., ARANOWSKI R., HUPKA J., 2012. *Wetting of supports by ionic liquids used in gas separation processes*. Physicochem. Probl. Miner. Process. 48: 129–140.
- KAPER H., SMARSLY B., 2006. *Templating and Phase Behaviour of the Long Chain Ionic Liquid C₁₆mimCl*. Zeitschrift für Physikalische Chemie 220(10–11): 1455–1471.
- KLOMFAR J., SOUČKOVÁ M., PÁTEK J., 2010. *Surface tension measurements with validated accuracy for four 1-alkyl-3-methylimidazolium based ionic liquids*. Journal of Chemical Thermodynamics 42: 323–329.
- KOWALCZUK P.B., DRZYMAŁA J., 2012. *Surface flotation of particles on liquids. Principles and applications*. Colloids and Surfaces A: Physicochemical and Engineering Aspects 393: 81–85.
- KUMAR G., PRABHU K.N., 2007. *Review of non-reactive and reactive wetting of liquids on surfaces*. Advances in Colloid and Interface Science 133: 61–89.
- RESTOLHO J., MATA J.L., SARAMAGO B., 2009. *On the interfacial behavior of ionic liquids: Surface tensions and contact angles*. Journal of Colloid Interface Science 340: 82–86.
- SIEBOLD A., NARDIN M., SCHULTZ J., WALLISER A., OPPLIGER M., 2000. *Effect of dynamic contact angles on capillary rise phenomena*. Colloid and Surfaces A 161: 81–87.
- SÖMNEZ Í., CEBECI Y., 2004. *Investigation of relationship between critical surface tension of wetting and oil agglomeration recovery of barite*. Colloids and Surfaces A 234: 27–33.
- THÖMING J., CHO C.-W., PREISS U., JUNGnickel C., STOLTE S., ARNING J., RANKE J., KALMT A., KROSSING I., 2011. *Ionic Liquids: Prediction of Physicochemical Properties with Experimental and/or DFT-Calculated LFER Parameters To Understand Molecular Interactions in Solution*. Journal of Physical Chemistry B 115: 6040–6050.
- TRONG D., HUPKA J., DRZYMAŁA J., 2006. *Impact of roughness on hydrophobicity of particles measured by the Washburn method*. Physicochem. Probl. Miner. Process. 40: 45–52.

- UOSOY U., YEKELER M., 2004. *Variation of critical surface tension for wetting of minerals with roughness determined by Surtronic 3⁺ instrument*. International Journal of Mineral Processing 74: 61–69.
- WASHBURN E.W., 1921. *The dynamics of capillary flow*. Phys. Rev. 17: 273–283.
- WASSERCHEID P., WELTON T., 2003. *Ionic Liquids in Synthesis*. Weinheim.
- WOLFROM R.L., CHANDER S., HOGG R., 2002. *Evaluation of capillary rise methods for determining wettability of powders*. Miner. Metall. Proc. 19: 198–202.
- WOODWARD R.P., 1999, *Contact Angle Measurements Using the Drop Shape Method. First Ten Angstroms*. Portsmouth, VA, USA
- YANG Z., PAN W., 2005. *Ionic liquids: Green solvents for nonaqueous biocatalysis*. Enzyme and Microbial Technology 37: 19–28.
- ZISMAN W.A., 1964. *Relation of the Equilibrium Contact Angle to Liquid and Solid Constitution*. *Advance in Chemistry*. Washington DC, American Chemical Society.

Received June 24, 2012; reviewed; accepted July 22, 2012

PREPARATION AND PHYSICOCHEMICAL CHARACTERISATION OF CERAMIC SUPPORTS FOR SUPPORTED LIQUID MEMBRANES

**Iwona CICHOWSKA-KOPCZYNSKA, Monika JOSKOWSKA,
Anna WOJCIECHOWSKA, Robert ARANOWSKI**

Department of Chemical Technology, Chemical Faculty, Gdansk University of Technology,
80-952 Gdansk, Poland, aran@pg.gda.pl

Abstract: Supported liquids membranes are very promising products. They have been intensively investigated in last two decades and widely used in many technologies especially in gas separation and purification processes. A key aspect in obtaining satisfying effectiveness and long membrane lifetime is a proper choice of ionic liquid and polymeric or ceramic support. Properties of both affect the processes of obtaining useful supported ionic liquid membranes. In comparison to polymeric membranes, ceramic ones are slightly thicker, however they are thermally and mechanically more stable. Our research was aimed at sintering fine glass particles of 500 to 45 μm in size in order to prepare porous membranes which can be used as supports for liquid membranes. Dextrin and borax were used as pore-making agents. The membranes, as disks 35 mm in diameter and 3 mm of thickness, were prepared. The porosity was determined using absorption method. It was found, that the porosity could be controlled by changing the applied pressure from 1 to 5 MPa, particle size distribution, sintering temperature, type and amount of pore-enhancing agents.

Keywords: glass cullet, recycling, porous material, membranes

Introduction

Supported liquids membranes (SLMs) are very promising for separation and purification of gaseous streams because of their very small demand for the membrane phase. This feature is very important particularly in supported ionic liquid membranes (SILMs) due to a high cost of ionic liquids (ILs). The SLM is a two phase system of porous support and liquid phase kept in the membrane pores by capillary forces (Walczyk, 2006). However, one of the major obstacles to industrial applications is a limited lifetime (poor stability) of the membrane due to the loss of the organic solvent from the support pores.

The most popular materials for supported liquid membrane supports preparation are polymer and ceramic membranes. The latter are widely used in filtration and separation technologies. Microstructure, porosity, pore size and wettability have a great influence on their permeability (Weixing, 2006). Moreover, inorganic membranes gained a significant attention due to their high stability in organic solvents and high temperatures (Kuraoka, 2000). In comparison to polymeric membranes, ceramic supports have higher mechanical, chemical and thermal stability. Operational temperature for polymeric supports cannot exceed 100°C, whereas for ceramic ones it is nearly 700°C. They are also resistant for concentrated acids and can be used in contact with a broad spectrum of organic solvents without any changes in their structure and mechanical properties. Ceramic supports reveal the ability of long-term work and the cost of their preparation is relatively low. Usually, they are made of waste glass cullet. Glass has been also widely used to produce hollow fiber membranes (Kuraoka, 1998) and some of them present high selectivity for different gases (Sehelekhin, 1992; Way, 1992).

This work has been focused on the use of glass cullet to produce porous membranes, that can be applied in the supported ionic liquid membrane technology (SILMs). However, such application requires determination of products properties. The aim of this study was to investigate the factors influencing sinterability to improve the mechanical properties of ceramic bodies made from soda-lime glass cullet. Furthermore, the effect of the amount of pore-making organic and inorganic components was examined.

Properties mentioned above, give the SILMs predominance over traditional SLMs (Gamer, 2008, Hernandez-Fernandez, 2009, Letcher, 2007), as ionic liquids (ILs) have negligible vapor pressure, are non-flammable, liquid in a wide range of temperatures and solubilize many organic and inorganic species (Kittel, 2009, Pernak, 2000, Schaffer, 2011).

Experimental

Materials

Silicate-soda-lime colorless glass was used in this investigation. Pure dextrin and borax were obtained from POCH, Poland, with a purity of $\geq 95\%$. Five ionic liquids were used in this study: 1-ethyl-3-methylimidazolium bis(trifluoromethylsulfonyl)imide [EMIM][Tf₂N], 1-ethyl-3-methylimidazolium trifluoromethanesulfone [EMIM][TfO], 1-butyl-3-methylimidazolium bis(trifluoromethylsulfonyl)imide [BMIM][Tf₂N], 1-butyl-3-methylimidazolium trifluoromethanesulfone [BMIM][TfO], 1-hexyl-3-methylimidazolium bis(trifluoromethylsulfonyl)imide [HMIM][Tf₂N]. All chemicals were supplied by Merck Chemicals Company, Darmstadt, Germany, with purity higher than 99%. The molecular structures of ILs cations and anions used in this study are shown in Figs 1 and 2.

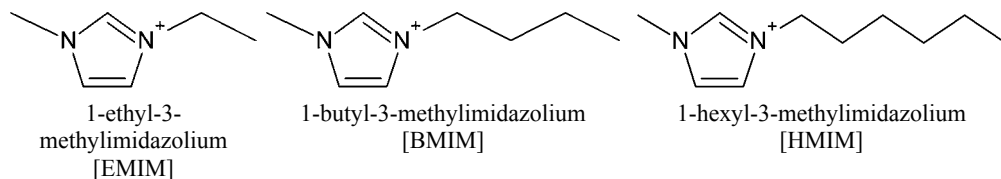


Fig. 1. Structure of ionic liquids cations used in the experiments

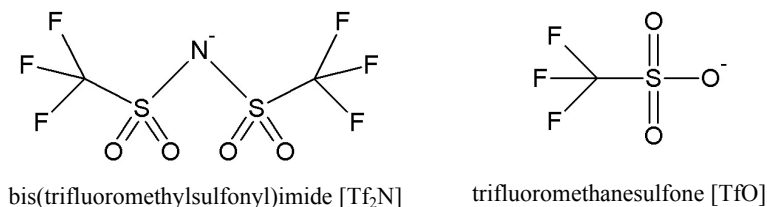


Fig. 2. Structure of ionic liquids anions used in the experiments

Preparation of glass matrix

The technology of producing glass porous materials requires the use of glass in the form of powder (Ciecińska, 2007). Glass samples were crushed in a jaw crusher and then ground using a disc mill and ball mill, for 2 hours, respectively. The maximum particle size of 500 μm was obtained. Particle-size distributions were determined with standard sieve analysis and the orbiting laboratory shaker (OS 10 basic, IKA) with frequency vibration of 450 rpm. Glass particles with the grain size distribution of: 250–500; 106–250; 63–106; 45–63 μm were used for preparation of porous discs, by sintering with pore-enhancing compound. The chemical composition of glass cullet used in the experiments was determined using an X-ray fluorescence spectrophotometer, according to the procedure described in PN-EN ISO 12677:2005 and is presented in Table 1. Into a disc shaped form, ceramic powder was pressed using a hydraulic

Table 1. Chemical composition of glass used for sintering

Compound	Weight percent [%]
SiO ₂	73.20
Na ₂ O	12.50
CaO	9.87
Al ₂ O ₃	2.62
MgO	0.96
K ₂ O	0.59
Fe ₂ O ₃	0.10
TiO ₂	0.07
SO ₃	0.06
MnO	0.02

press under pressure of 1 MPa to 5 MPa. The discs were then sintered at 700°C for 60 minutes in air atmosphere. A linear increase of temperature with 10°C/min rate was applied to obtain 700°C. Selected properties of membranes (specific density, apparent density, total porosity) were examined according to standard test method PN-EN 1389:2005 (Komitet, 2005). The structures of obtained porous membranes were observed with a scanning electron microscope (SEM).

Morphological characterization

Philips-FEI XL 30 ESEM (Environmental Scanning Electron Microscope) was used to determine morphological properties and the average pore size of ceramic supports. Before SEM observation, obtained samples of supports were coated with ultrathin gold layer.

Wetting of ceramic supports with ionic liquids

In order to determine the effect of chemical structure of the ionic liquids on ceramic supports wetting, cations differing in alkyl chain lengths and different anions were selected. In order to determine the wettability of various supports by ionic liquids, capillary rise method based on Washburn equation was used (Joskowska, 2012, Siebold, 2000, Studenbacker, 1955, Trong, 2006, Washburn, 1921, Wolfrom, 2002). Ceramic membrane samples sized 5×3×10 mm were used in the experiments. The time of penetration, increase in height of liquid penetrating into ceramic membrane and the decrease in mass of the liquid in a container was recorded every second using an electronic balance, attached to a computer. The time $t = 0$ approximately corresponded to the moment of membrane submersion in the wetting liquid. The experiments were repeated eight times and the mean value was calculated. On the basis of the Washburn equation, angle values were calculated. The results are shown in Table 7.

Results and discussion

Granular composition of glass powder obtained by milling is presented in Table 2.

Table 2. Granular composition of glass powder

Size of glass grains [μm]	Sifting [%]
>500	90.20
250–500	7.57
106–250	1.06
63–106	0.23
45–63	0.07
<45	0.88

During thermal analysis, the glass powder becomes soft at 700°C and melts at 810°C, whereas at 1020°C the samples flow. On the basis of thermal analysis, the optimal temperature of sintering was selected. It was found that addition of dextrin and borax slightly decreases the softening temperature, to 698°C and 695°C, respectively. However it can be roughly assumed that such amounts of compounds do not affect the softening temperature. To obtain the highest possible porosity, the samples were sintered at 700°C.

Tables 3–5 present the results obtained using different types of binder: 50% aqueous solution of dextrin, dry dextrin, 50% aqueous solution of borax and using various glass powder granulation, different amounts of binder and pressures in a range from 1 to 5 MPa.

Table 3. Properties of ceramic supports obtained using 50% aqueous solution of dextrin (15% m/m), at 700°C

Granulation [μm]	Pressure [MPa]	Bulk density [g/cm^3]	Effective porosity [%]	Total porosity [%]
250–500	1	1.75	23.2	30.3
250–500	3	1.81	23.7	27.9
106–250	1	1.85	20.6	26.3
106–250	3	1.89	21.0	24.7
63–106	1	1.96	14.8	21.6
63–106	3	1.97	17.4	21.3
45–63	1	2.06	15.9	17.8
45–63	3	2.07	14.7	17.3
<45	1	2.07	13.7	17.5
<45	3	2.07	13.3	17.1

Supports prepared using 50% aqueous solution of dextrin had a total porosity of 30.3% (granulation 250–500 μm). Still, the lower granulation of glass powder, the lower porosity of supports. Glass powder granulation of size less than 45 μm (in comparison to 250–500 μm grain size) decreases the total porosity from 30.3% to 17.5%. An increase in press pressure from 1 to 3 MPa decreases the total porosity from 30.3% to 27.9% (for grain size 250–500 μm). However, when using 5% m/m and 10% m/m of 50% aqueous solution of dextrin the total porosity is lower than for 15% m/m for each granulation used. For 250–500 μm granulation, the porosity is reduced from 30.3% (15% m/m of binder) to 27.8% (10% m/m of binder) and 25.3% (5% m/m of binder). Formulation of ceramic support occurred to be impossible when adding 50% aqueous solution of dextrin above 15% m/m. However, the porosity obtained using aqueous solutions of dextrin was not sufficient to obtain satisfying support for the liquid membrane. In order to increase the total porosity, the solution was substituted with dry dextrin in amounts of 10, 15 and 20% m/m. However, preliminary experiments revealed that 10 and 15% m/m is not enough for obtaining satisfying porosity.

Moreover, using more than 20% m/m prevented from obtaining stable discs. Table 4 presents characteristics of supports obtained using 20% m/m of dry dextrin.

Table 4. Properties of ceramic supports obtained using 20% m/m of dry dextrin

Granulation [μm]	Pressure [MPa]	Sintering temperature [$^{\circ}\text{C}$]	Bulk density [g/cm^3]	Effective porosity [%]	Total porosity [%]
250–500	1	700	0.86	65.4	65.7
250–500	3	700	0.87	64.6	65.2
250–500	5	700	1.32	45.6	47.3
250–500	1	810	1.28	44.8	48.5
106–250	1	700	0.92	62.7	63.2
106–250	3	700	0.94	61.8	62.6
63–106	1	700	0.95	61.1	61.9
63–106	3	700	1.02	58.3	59.4
45–63	1	700	0.99	59.3	60.6
45–63	3	700	1.06	56.1	57.6
<45	1	700	1.12	56.7	58.4
<45	3	700	1.20	50.2	52.9

For granulation of 250–500 μm usage of dry dextrin gives supports with 65.7% total porosity. As mentioned in the case of dextrin water solution, the porosity is lower when using fine glass powder. An increase in press pressure from 1 to 3 MPa slightly decreases the porosity for the 250–500 μm grain size. It decreases from 65.7% to 65.2%. Further pressure increase to 5 MPa reduces porosity to 47.3%. Moreover sintering at 810 $^{\circ}\text{C}$ also reduces the total pores volume to 48.5% (for granulation of 250–500 μm).

Experiments have been also conducted using borax as a binder. Table 5 presents characteristics of ceramic supports obtained using 10% m/m of 50% aqueous solution of borax for different grain sizes at 700 $^{\circ}\text{C}$.

Table 5. Characteristics of ceramic supports obtained using 50% aqueous solution of borax (10% m/m)

Granulation [μm]	Pressure [MPa]	Bulk density [g/cm^3]	Effective porosity [%]	Total porosity [%]
250–500	1	1.82	22.0	27.4
250–500	3	2.01	16.3	19.6
106–250	1	1.88	20.3	24.8
106–250	3	2.03	15.5	19.1
63–106	1	2.78	11.3	13.1
63–106	3	1.97	10.2	12.5
45–63	1	2.19	11.2	14.7
45–63	3	2.14	10.4	12.7
<45	1	2.18	11.8	13.6
<45	3	1.97	10.7	12.5

The 50% aqueous solution of borax gives 27.4% porosity (granulation of 250–500 μm). Still, the lower grain size is, the lower porosity is obtained. Using powder granulation of size less than 45 μm leads to 50% lower porosity in comparison to the 250–500 μm grain size. Again, an increase in press pressure reduces the porosity. Application of 5% m/m of 50% aqueous solution of borax reduces porosity from 27.4% to 18.3% (granulation of 250–500 μm).

Dry borax has been also used in the experiments. However, 10% m/m and 5% m/m occurred to be too much to obtain stable supports. Application of dry borax is not possible for such purposes. Figure 3 shows the dependence of granulation on porosity using different binder types at 700°C and press pressure of 1 MPa. It is clearly visible that the decrease in granulation causes the decrease in porosity for all the binders used in this study.

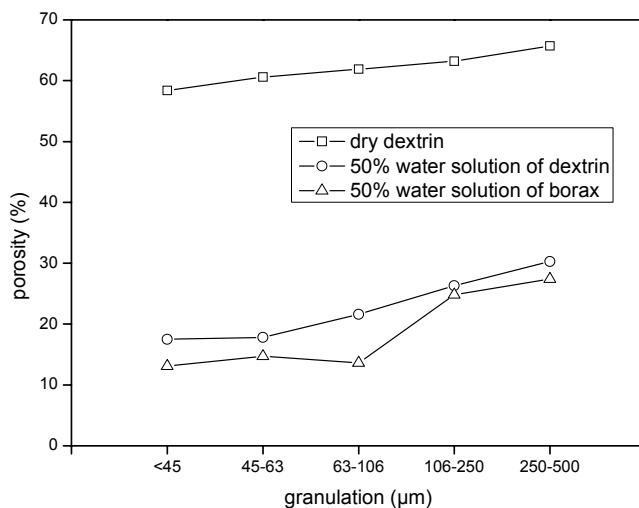


Fig. 3. Total porosity vs. granulation of glass powder

Press pressure of 1 MPa, sintering temperature of 700°C and addition of dextrin of 20% m/m gives the highest porosity for different grain sizes. Application of 50% aqueous solution of dextrin gives lower porosity than application of dry dextrin. Moreover, addition of dextrin water solution above 15% m/m prevents from obtaining stable support. The increase in pressure and sintering temperature also reduces the support porosity. Application of borax as binder does not improve properties of supports. Moreover, it is not possible to obtain any support using dry borax.

To summarize, the best properties of supports are obtained when using glass powder with granulation of 250–500 μm , 20% m/m of dextrin as binder and sintering temperature of 700°C. Porosity obtained using press pressure of 1 MPa and 3 MPa does not differ significantly, however, membranes prepared with 3 MPa of press pressure show higher mechanical stability.

The total porosity of obtained supports is at the level of 60% and it stays in correlation with values obtained by other authors that utilized saccharose as binder, sintering temperature of 1000°C and granulation of 45–100 μm (Ciecińska, 2007).

Kosmulski et al. (2009) used quartz sand, cryolite, glass cullet of 18% m/m and 40% water solution of dextrin to obtain 42% porosity (Kosmulskiet al., 2009). Porosity of 65% can be also obtained using water as a pore-forming agent. At 700°C water evaporates forming pores (Yanagisawa, 2006). Figure 4 presents the surface of ceramic supports obtained using glass powder with granulation of 250–500 μm , press pressure of 1 MPa and either 10% m/m addition of borax or 20% m/m addition of dextrin.

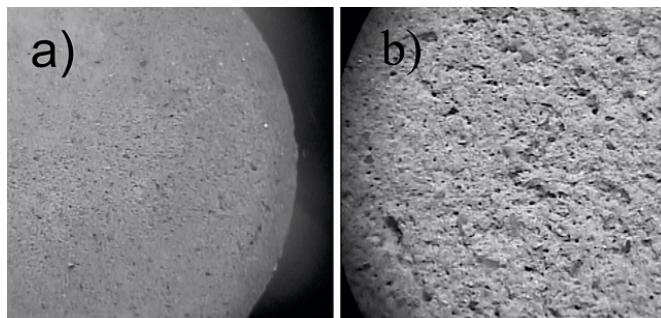


Fig. 4. Structure of ceramic supports obtained with a) 10% m/m of dry borax, b) 20% m/m of dry dextrin

Depending on the type of pore-forming agent used, supports demonstrate different textures. Surface of supports obtained using dextrin shows higher roughness. Figures 5-10 present SEM micrographs of ceramics formed using 500–250 μm glass particles.

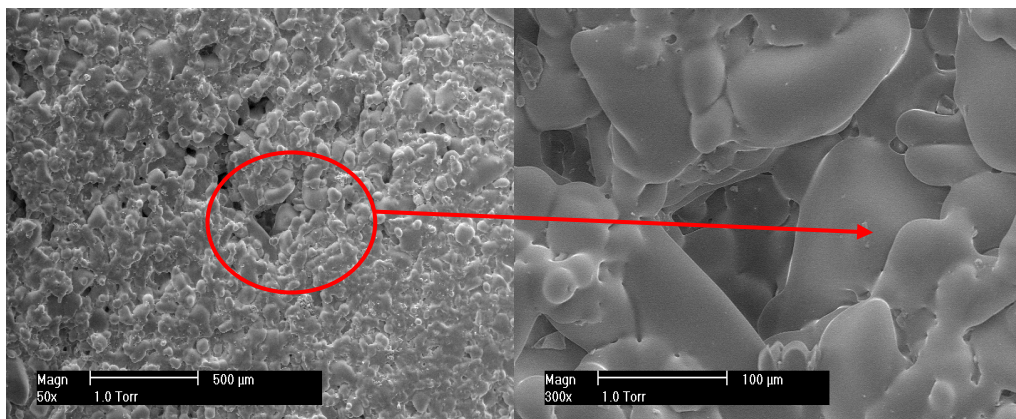


Fig. 5. SEM micrograph, 500–250 μm , 20% dry dextrin, 1 MPa, 700°C

Fig. 6. SEM micrograph, 500–250 μm , 20% dry dextrin, MPa, 700°C

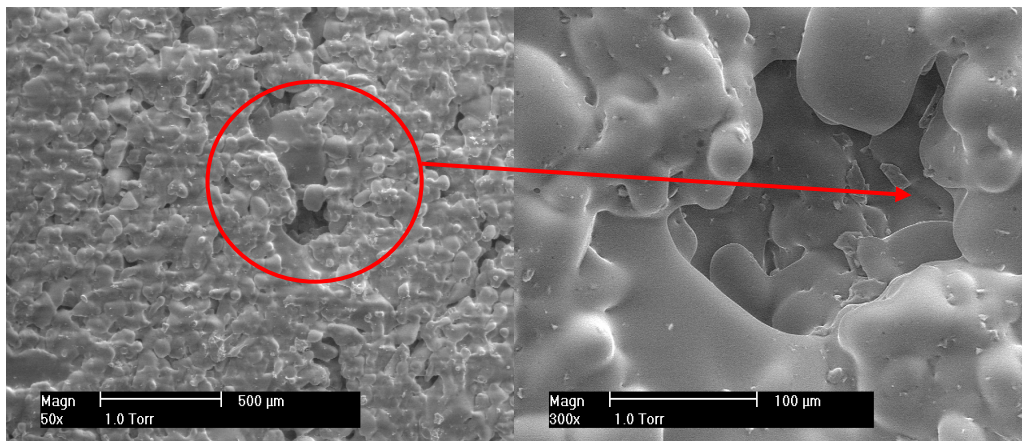


Fig. 7. SEM micrograph, 500–250 μm , 15% aqueous solution of dextrin, 1 MPa, 700°C

Fig. 8. SEM micrograph, 500–250 μm , 15% aqueous solution of dextrin, 1 MPa, 700°C

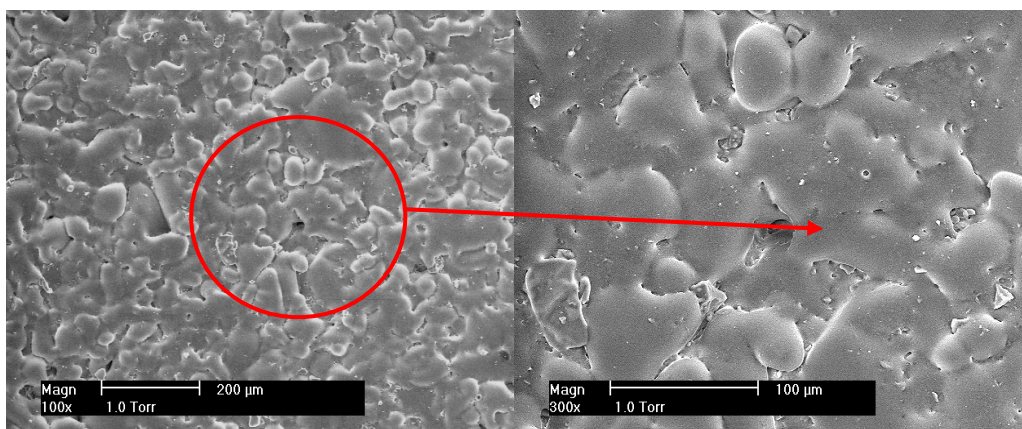


Fig. 9. SEM micrograph, 500–250 μm , 10% solution of borax, 1 MPa, 700°C

Fig. 10. SEM micrograph, 500–250 μm , 10% solution of borax, 1 MPa, 700°C

In both cases, using dextrin or borax, support structure is irregular and pores are heterogeneous. However, supports obtained using borax (Figs 9 and 10) are slightly more homogenous and the pores are rather closed. The matrix obtained using dextrin has larger amount of pores opened. This is confirmed by porosity experiments (Tables 3 and 4). The SEM micrographs allowed to calculate the average pores size which is $72 \pm 27 \mu\text{m}$ using 20% of dry dextrin.

The method using dextrin as a pore-making agent occurred to be suitable to prepare ceramic supports with porosity over 60%. Both substrates are easily available, not expensive and the supports obtained have repetitive properties.

Wetting experiments have been based on the mass increase measurements. A graph of square of mass increase vs. time is presented in Fig. 11.

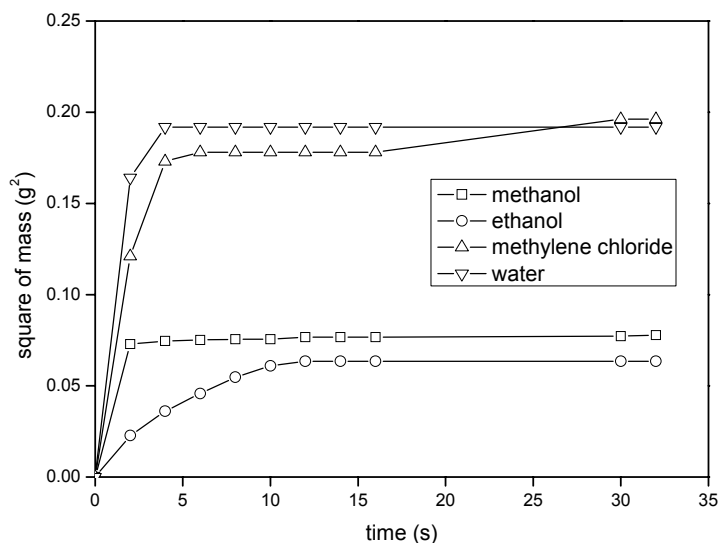


Fig. 11. Membrane wetting with reference liquids

Liquids wet ceramic materials in two steps. At first, liquid fills the pores rapidly, and afterward it moves in horizontal direction subsequently until the mass is constant. The rapidity of wetting is affected by liquid viscosity, density and surface tension. Table 6 presents physicochemical properties of reference liquids.

Table 6. Physicochemical properties, penetration time for reference liquids at 298K

Reference liquid	Density [kg/m ³]	Viscosity [mPa·s]	Surface tension [mN/m]	Penetration time [s]
Water	997	0.895	72.6	4
Methanol	793	0.584	23.0	1
Ethanol	789	1.190	22.0	10
Methylene chloride	1320	0.423	27.2	4

Among the examined liquids, methanol wets the ceramic matrix best, whereas ethanol penetrates the matrix the most slowly. In practice, the best wetting liquid is chosen on the basis of the highest value of $r \cos \theta$, so the ratio $m^2 \eta / (t \rho^2 \gamma)$ should be the highest among the examined liquids (Ayala, 1987).

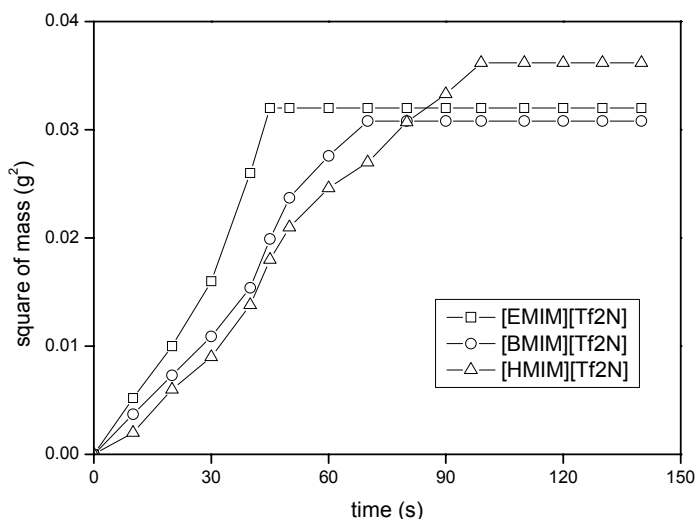
Methanol has been chosen as the reference liquid for further experiments, and the contact angle was assumed as 0 degree ($\cos \theta = 1$). On this basis contact angles for ionic liquids were calculated (Table 7).

Table 7. Physicochemical properties and contact angles of ionic liquids at 298 K

Liquid	Viscosity [mPa·s]	Surface tension [mN/m]	Penetration time [s]	K^*	$\cos\theta$	θ [deg]
Metanol	0.58	23.0	1	reference liquid	1	–
[EMIM][Tf ₂ N]	32.6	32.6	45	40.1	0.892	27
[BMIM][Tf ₂ N]	48.1	30.8	70	61.4	0.878	29
[HMIM][Tf ₂ N]	70.0	32.6	99	84.6	0.854	31
[EMIM][TfO]	40.4	37.8	45	42.1	0.935	21
[BMIM][TfO]	74.3	34.7	94	84.3	0.897	26

* K is the quotient of surface tension of methanol and viscosity of ionic liquid ratio and surface tension of ionic liquid and viscosity of methanol ratio.

A graph of ceramic matrix wetting with [Tf₂N] based ionic liquids is presented in Fig. 12.

Fig. 12. Square of mass vs. penetration time for [Tf₂N] based ionic

It can be seen that the time of penetration increases as the numbers of carbon atoms in alkyl chain in imidazolium cation increases. It is also confirmed with data obtained for ionic liquids with [TfO] as anion (Fig. 13).

The best wetting is observed for [EMIM][TfO] and [BMIM][TfO] ~ [EMIM][Tf₂N] > [BMIM][Tf₂N] > [HMIM][Tf₂N] respectively. Wettability of [Tf₂N] based ionic liquids is as following: [EMIM] > [BMIM] > [HMIM]. Increasing numbers of carbon atoms in hydrocarbon chain of ILs leads to an increase of contact angle

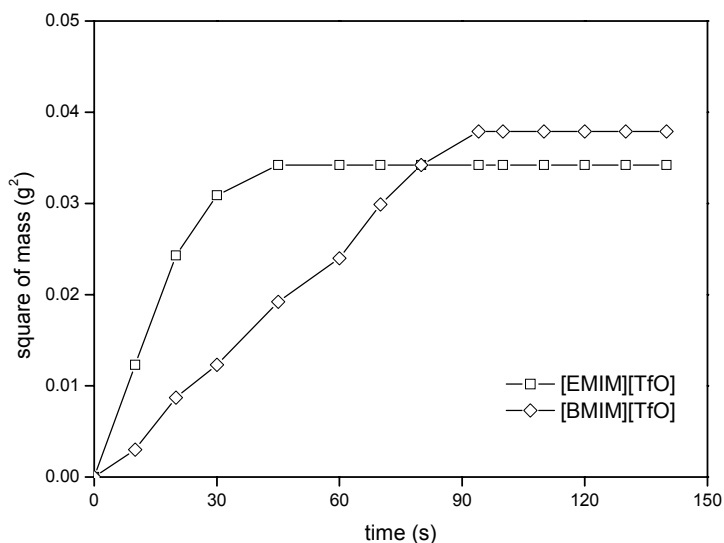


Fig. 13. Square of mass vs. penetration time for [TfO] based ionic

between ionic liquid and ceramic matrix, what is in correlation with the viscosity of ILs (the viscosity increases in the following order: [EMIM] < [BMIM] < [HMIM]). The dependence is observed for [TfO] based ionic liquids likewise. All of the values of contact angles are lower than 90 degree, so it can be concluded that the ceramic matrix is well wetted with examined ionic liquids and can be used as a membrane phase to obtain stable support for ionic liquid membranes.

Conclusions

In the present study, porous materials were prepared from glass powders by sintering at 700°C, with dextrin and borax as pore-making agents. The obtained porous materials had different bulk density and total porosity. The porosity could be controlled by changing the particle size distribution, kind and amount of pore-forming agents, applied pressure on preparation stage and sintering temperature. The glass porous materials obtained with pure dextrin exhibited higher porosity, comparing with sodium tetraborate. The maximum total porosity was obtained for the following parameters: 250–500 μm glass size fraction, the applied pressure 1 MPa, and sintering temperature 700°C (softening point for this glass cullet). As a result, porous materials of over 60% total porosity were obtained. Applying this method allows to prepare porous membranes which can be applied as supports for liquids. Moreover such supports are well wetted with commonly used ionic liquids. Due to this fact, formation of SILMs based on ceramic supports is reasonable by all means. Such membranes can be used in catalytic processes (where ionic liquids are used as catalysts), biological filtration (due to

antiseptic properties of some ILs) or separation and purification processes (for example separation of carbon dioxide from biogas).

Acknowledgements

This research was supported by the National Science Centre, grant No. 7563/B/T02/2011/40, Removal of Volatile Organic Compounds from Gas Phase using Ionic Liquids. Financial support of this work was provided also by the National Centre for Research and Development of Poland, grant 04/strategic program/2010 on Advanced Technologies of Energy Generation, Pilot Agricultural Biogas Microstation and Fermentation and Separation of Carbon Dioxide from Biogas with Ionic Liquids Application. We are very grateful for financial support provided by the National Science Centre, grant No. 1815/B/H03/2009/36.

References

- AYALA R.E., CASASSA E.Z., PARFITT G.D., 1987, *A study of the applicability of the capillary rise of aqueous solutions in the measurement of contact angles in powder systems*. Powder Technol., 51, 3–14.
- CIECIŃSKA M., 2007, *Szklą odpadowe do produkcji specjalnych materiałów porowatych*. Szkło i Ceramika, 58, 9–13.
- GAMER A.O., ROSSBACHER R., KAUFMANN W., VAN RAVENZWAAY B., 2008, *The inhalation toxicity of di- and triethanolamine upon repeated exposure*. Food Chem. Toxicol., 46, 2173–2183.
- HERNANDEZ-FERNANDEZ F.J., DE LOS RIOS A.P., ALONSO F.T., PALACIOS J.M., WILLORA G., 2009, *Preparation of supported ionic liquid membranes: Influence of the ionic liquid immobilization method on their operational stability*. J. Mem. Sci., 341, 172–177.
- JOSKOWSKA M., KOPCZYŃSKA I., DEBSKI B., HOLOWNIA-KEDZIA D., ARANOWSKI R., HUPKA J., 2012, *Wetting of supports by ionic liquids used in gas separation processes*. Physicochem. Probl. Miner. Process., 48, 129–140.
- KITTEL J., IDEM R., GELOWITZ D., TONTIWACHWUTHIKUL P., PARRAIN G., BONNEAU A., 2009, *Corrosion in MEA units for CO₂ capture: pilot plant studies*. Energy Procedia, 1, 791–797.
- PN-EN 1389:2005, 2005, *Techniczna ceramika zaawansowana – Kopozyty ceramiczne – Właściwości fizyczne – Oznaczanie gęstości i porowatości otwartej*.
- KOSMULSKI M., SANELUTA C., MARCZEWSKA-BOCZKOWSKA K., KURZYDŁOWSKI K., KONOPKA K., OZIĘBŁO A., SZAFRAN M., LIPIEC W., *Kompozyt ceramika ciecz-jonowa i sposób wytwarzania kompozytu ceramika-ciecz jonowa*, P. Warszawska, Editor. 2009: Warszawa, Polska, 1–6.
- KURAOKA K., AMAKAWA R., MATSUMOTO K., ZAYAWA T., 2000, *Preparation of molecular+sieving glass hollow fiber membranes based on phase separation*. J. Mem. Sci., 175, 215–223.
- KURAOKA K., QUN Z., KUSHIBE K., YAZAWA T., 1998, *Trail for preparation of glass capillary membranes by elution of alkali metal ions*. Sep. Purif. Technol., 33, 297–309.
- LETCHER T.M., *Thermodynamics, solubility and environmental issues*, ed. Elsevier. 2007, Amsterdam: Elsevier.
- PERNAK J., 2000, *Ciecze jonowe – rozpuszczalniki XXI wieku*. Przem. Chem., 79, 150–153.
- SCHAFFER A., BRECHTEL K., SCHEFFKNECHT G., 2011, *Comparative study on differently concentrated aqueous solutions of MEA and TETA for CO₂ capture from flue gas*. Fuel, doi:10.1016/j.fuel.2011.06.037.

- SEHELEKHIN A.B., DIXON A.G., MA Y.H., 1992, *Adsorption, permeation, and diffusion of gases in microporous membranes. II. Permeation of gases in microporous glass membranes*. J. Mem. Sci., 75, 233–244.
- SIEBOLD A., NARDIN M., SCHULTZ J., WALLISER A., OPPLIGER M., 2000, *Effect of dynamic contact angles on capillary rise phenomena*. Colloid and Surfaces A, 161, 81–87.
- STUDENBACKER M.L., SNOW C.W., 1955, *The influence of ultimate composition upon the wettability of carbon blacks*. J. Phys. Chem., 59, 973–976.
- TRONG D., HUPKA J., DRZYMAŁA J., 2006, *Impact of roughness on hydrophobicity of particles measured by the Washburn method*. Physicochem. Probl. Miner. Process., 40, 45–52.
- WALCZYK H., 2006, *Niskotemperaturowa kondensacja lotnych związków organicznych w obecności gazu inertnego w spiralnym wymienniku ciepła*. Prace Naukowe Instytutu Inżynierii Chemicznej PAN, 6, 7–127.
- WASHBURN, E.W., 1921, *The dynamics of capillary flow*. Phys. Rev., 17, 273–283.
- WAY J.D., ROBERTS D.L., 1992, *Hollow Fiber Inorganic Membranes for Gas Separations*. Sep. Purif. Technol., 27, 29–41.
- WEIXING L., WEIHONG X., NANPING X., 2006, *Modeling of relationship between water permeability and microstructure parameters of ceramic membranes*. Desalination, 192, 340–345.
- WOLFROM R.L., CHANDER S., HOGG R., 2002, *Evaluation of capillary rise methods for determining wettability of powders*. Miner. Metall. Proc., 19, 198–202.
- YANAGISAWA K., BAO N., SHEN L., ONDA A., KAJIYOSHI K., MATAMORAS-VELOZA Z., RENDON-ANGELES J.C., 2006, *Development of a technique to prepare porous materials from glasses*. J. Eur. Ceram. Soc., 26, 761–765.

Received April 30, 2012; reviewed; accepted July 17, 2012

KINETIC STUDIES ON SORPTION OF Ni(II) AND Cd(II) FROM CHLORIDE SOLUTIONS USING SELECTED ACIDIC CATION EXCHANGERS

Paulina OTREMBSKA, Jerzy GEGA

Czestochowa University of Technology, Department of Chemistry, 19 Armii Krajowej Str.,
42-200 Czestochowa, Poland, e-mail: potrembska@wip.pcz.pl

Abstract: Sorption of nickel(II) and cadmium(II) ions from chloride solutions was tested. Three different strongly acidic cation exchangers, i.e. Lewatit MonoPlus SP 112, Amberlite 200C and Amberlyst 15, were used. Effects of phase contact time, pH and initial concentration of metal ions on equilibrium and kinetics of sorption by batch methods were studied. It was showed that sorption of Ni(II) and Cd(II) could be described by the pseudo-second order equation. Experimental results data were analyzed using the Langmuir and Freundlich isotherms. Sorption of Ni(II) and Cd(II) onto investigated resins followed the Langmuir isotherm.

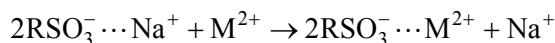
Keywords: sorption, nickel, cadmium, adsorption kinetics, adsorption isotherm

Introduction

Increasing industrialization can lead to several environmental problems. Heavy metals like Cd, Ni, Cr, Cu, Pb can contaminate groundwater, surface water or sea. They are harmful to life and became a serious public health problem. Heavy metals are non-degradable substances, long standing, which can accumulate in the environment.

There are many different methods of removal and recovery of metal ions from water and wastewater. These methods include ion-exchange (Pehlivan and Altun, 2006; Gega and Otrembska, 2011), electrodepositon (Rudnik and Nikiel, 2007), precipitation (Lewis, 2010; Provazi et al., 2011), flocculation (Dabrowski et al., 2004; Kurniawan et al., 2006), sorption (Lazaridis, 2003; Srivastava et al., 2008; Kilyushik et al., 2011), solvent extraction (Gega et al., 2010; Rodrigues and Mansur, 2010; Clegg et al., 2011), reverse osmosis (Qin et al., 2004), electro dialysis (Marder et al., 2004) and membrane separation (Walkowiak et al., 2000; Gega et al., 2001; Pospiech and Walkowiak, 2007; Chaudhari and Murthy, 2010). Among these methods, the ion-

exchange is very popular and has been widely used for Ni(II) and Cd(II) removal (Dizge et al., 2009; Zainol and Nicol, 2009). It is based on replacement of ions between insoluble substance – ion exchange resin and aqueous phases. Resin releases ions like hydrogen or sodium to solution and binds metal ions without any structural change. After separation process attached heavy metals are recovered in a more concentrated form by elution with appropriate reagents. The physicochemical reaction which occur during nickel(II) and cadmium(II) removal can be presented as (Kurniawan et al., 2006):



where RSO_3^- is the anionic group connected to the ion exchange resin, M^{2+} is Ni(II) or Cd(II) ion.

In recent years, a number of commercial resins such as Amberlite IRC-748 (Lin et al., 2008), Amberlite IR-120 (Demirbas et al., 2005), Lewatit CNP 80 (Demirbas et al., 2005), Purolite S930 (Deepatana and Valix, 2008) have been used to remove heavy metals from aqueous solutions. In comparison with other common methods, ion-exchange provides a lot of advantages. Wide application of this method was caused by invention and use of new organic and inorganic exchangers.

In this paper, the removal of Ni(II) and Cd(II) ions from chloride solutions using strongly acidic ion-exchange resins was investigated. The two main objectives of the study include: the study of the sorption mechanism of Ni(II) and Cd(II) ions on the resins under equilibrium conditions and the investigation of the kinetics characteristics. The effectiveness of sorption was studied as a function of pH, initial nickel(II) and cadmium(II) concentration and contact time in a batch system. The experimental results were fitted to the Langmuir and Freundlich adsorption isotherm models and were analyzed on the basis of Lagergren pseudo-first order and pseudo-second order equations.

Materials and methods

Ion-exchange resins

Commercial strongly acidic cation (SAC) exchange resins: Lewatit MonoPlus SP 112 (Lanxess), Amberlite 200C, Amberlyst 15 (Rohm & Haas) in sodium form were used. The physical and chemical characteristic of the resins are given in Table 1. Wet forms of resins were used for experimental studies.

Solution preparation and batch experiments

Solutions of metal ions were prepared by dissolving an appropriate salt, i.e. nickel(II) chloride hexahydrate and cadmium(II) chloride hemipentahydrate in deionized water.

The pH was adjusted by the addition of appropriate volume of hydrochloric acid or sodium hydroxide solutions.

Table 1. Characteristics of main properties of strongly cation exchanging resins (based on information from manufacturers)

Characteristics	LewatitMonoPlus SP 112	Amberlite 200C	Amberlyst 15
	Value		
Structure	Macroporous	Macroreticular	Macroreticular
Matrix*	PS-DVB	S-DVB	S-DVB
Functional group	Sulfonic acid	Sulfonic acid	Sulfonic acid
Ionic form as shipped	Na ⁺	Na ⁺	H ⁺
Total exchange capacity	1.7 val/dm ³	≥1.7 val/ dm ³	5 val/kg
Moisture content	53–55%	46–52%	10%
Particle size	660 μm ±70 μm	600–850 μm	400–500 μm
Temperature limitations	1–120°C	1–135°C	1–120°C

* PS-DVB – polystyrene-divinylbenzene, S-DVB – styrene-divinylbenzene

The sorption of nickel(II) and cadmium(II) onto resins was carried out by means of the batch method. The amount of 2.5 g of wet resin was contacted with 25 cm³ of the corresponding equimolar Ni(II) and Cd(II) solution for 30 min using a laboratory shaker (WU-4, Premed). A mixture of the metal ions was used. Initial concentration of both ions was changed in the range from 0.1 mM to 100 mM. After shaking, the solution was separated from the resin by filtration, and concentration of ions was determined by atomic absorption spectrometry (SOLAAR 939) with an air/acetylene flame and the appropriate hollow cathode lamps.

Data analysis

The sorption ability of resins was estimated by means of recovery R (%), the amount of ions sorbed at specific time t , q_t (mg/g) and sorption capacity SC (mval/g) which were calculated as follows:

$$R = \frac{c_0 - c_{eq}}{c_0} \cdot 100\% \quad (1)$$

$$q_t = \frac{c_0 - c_t}{w} V \quad (2)$$

$$SC = \frac{n_0 - n_{eq}}{m} \cdot 2 \quad (3)$$

where c_0 and c_{eq} are initial and equilibrium concentrations of nickel(II) and cadmium(II) ions, (mg/dm³), V is the volume of the solutions (dm³), w is exchanger

weight (g), n_0 and n_{eq} are initial and equilibrium number of moles of metal ions (mole), m is amount of resin (g). Total SC was calculated as summarized sorption capacity for Ni(II) and for Cd(II).

Results and discussion

Effect of pH and initial metal ions concentration on Ni(II) and Cd(II) sorption from aqueous solution

The pH of solution is a significant factor which controls the surface charge of the adsorbent and ionization of the adsorbate in solution (Dizge et al., 2009). The influence of pH on the sorption of nickel(II) and cadmium(II) from chloride solution was investigated in the range of 0 to 5 and is shown in Fig. 1. The results indicate that very high recovery were obtained for all resins. Recovery factor was the lowest at pH = 0 and almost 100%, at pH = 2 and higher for both ions, separation of these ions was not possible. At pH = 0 some differences between sorption of Ni²⁺ and Cd²⁺ were observed, what indicate possibilities of separation of both metal ions. Sorption at pH above 5 was not carried out to avoid any possible interference from metal precipitation in solution.

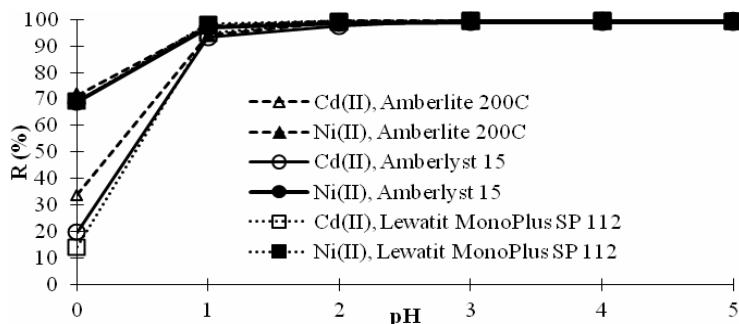


Fig. 1. Recovery of Ni(II) and Cd(II) as a function of pH in ion-exchange processes. Initial concentration of ions: 10 mM, volume: 25 cm³, pH = 0–5, amount of resin: 2.5 g, time: 30 min

Ion exchange is an equilibrium reaction that is dependent on the ionic concentrations of various ions both inside and outside of resin bead. Effect of initial concentration of Ni(II) and Cd(II) ions in aqueous solution on their sorption have been also studied. The results are presented in Fig. 2. The amount of adsorbed metal ions is dependent on the initial metal ion concentration. The calculated values of sorption capacity (SC) show that the best results are obtained for Lewatit MonoPlus SP 112: (1.70 mval/g), and for Amberlite 200C (1.64 mval/g), the lowest for Amberlyst 15 (0.97 mval/g).

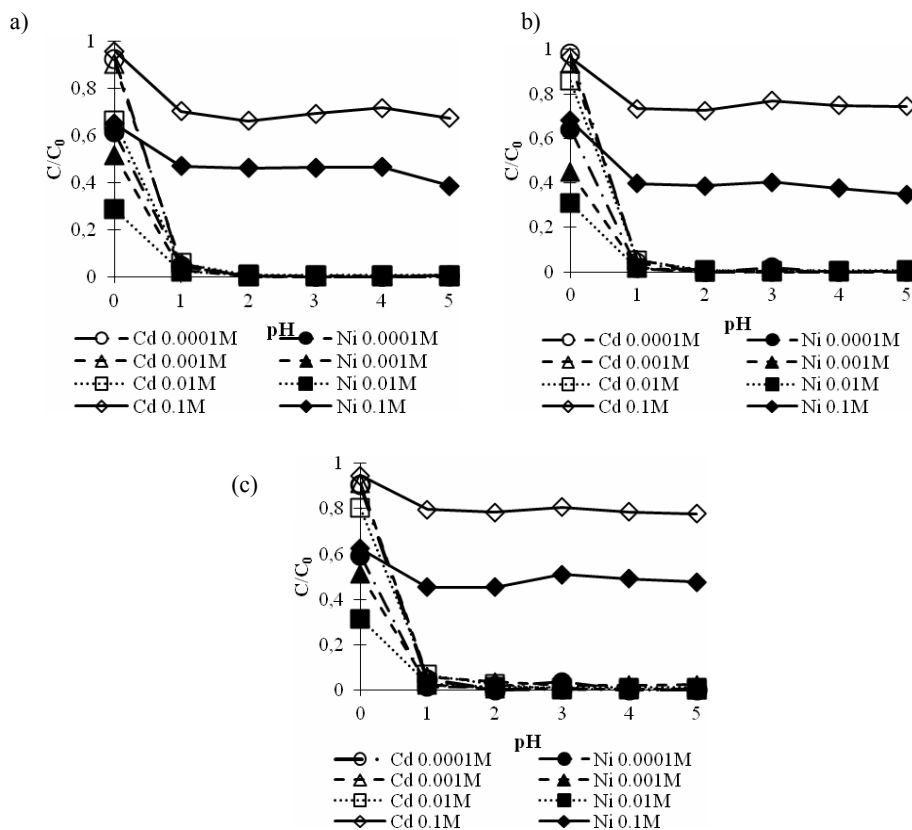


Fig. 2. Effect of initial concentration of Ni(II) and Cd(II) ions on the sorption effectiveness. Ion exchangers: (a) Amberlite 200C, (b) Lewatit MonoPlus SP 112, (c) Amberlyst 15. Initial concentration of metal ions: 0.1 mM – 100 mM, volume of solution: 25 cm³, pH = 0–5, amount of resin: 2.5 g, time: 30 min

Effect of agitation time on Ni(II) and Cd(II) sorption from chloride solution

Effect of agitation time on nickel(II) and cadmium(II) sorption on investigated ion-exchange resins has been studied. Figure 3 demonstrates that the amount of the adsorbed metal ions onto SAC exchange resins increases with time. The sorption of Ni(II) and Cd(II) was rapid for the first 5 min and equilibrium was reached after 20 min. Therefore, the period of 30 min was considered as the optimum time for all experiments presented in the paper.

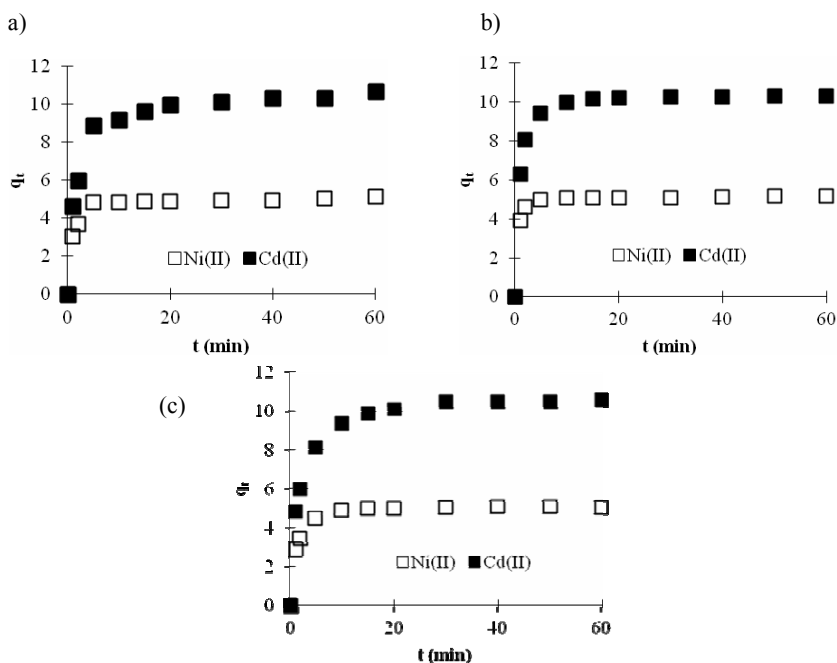


Fig. 3. Kinetic studies of Ni²⁺ and Cd²⁺ sorption process on (a) Amberlite 200C, (b) Lewatit MonoPlus SP 112, (c) Amberlyst 15 at pH = 1. Experimental conditions – see Fig. 1.

Kinetic modeling

There are two very important factors decisive for resins application in metal ion sorption: sorbate–sorbent interaction and experimental conditions. In ion exchange, the moving of ions is controlled by either intraparticle diffusion or boundary layer diffusion. The process of removing ions with and ion-exchange resin is followed by metal ions transfer from the bulk of the solution to a liquid thin layer which surrounds each resin particle, followed by diffusion of ions through liquid thin layer to the resin surface, thereafter intraparticle diffusion of ions through resin channels proceed then cationic exchange occurs (Hamdaoui, 2009; Plazinski et al., 2009). In some cases the first step can be neglected in controlling the overall sorption rate, e.g. in very fast mechanical mixing of sorbate–sorbent system. The most popular equations used in analysis of experimental results are the pseudo-first and pseudo-second order kinetic equations.

Pseudo-first order model

At the end of 19th century, Lagergren presented an empirical rate equation for adsorption of oxalic and malonic acid onto charcoal. It was the pseudo-first order kinetic equation which is called also the Lagergren equation and has been one of the most

often used kinetic equations to date. In the paper published by Lagergren the pseudo-first order kinetic equation was expressed as:

$$\frac{dx}{dt} = k(X - x) \quad (4)$$

where X and x (mg/g) are the adsorption capacity at equilibrium and at time t and k (1/min) is the rate constant of the pseudo-first order kinetic equation (Yuh-Shan, 2004). Today, the most popular form of this kinetic equation is:

$$\lg(q_e - q_t) = \lg q_e - \frac{k_1}{2.303} t \quad (5)$$

where q_e is the amount of metal ions adsorbed per unit weight of adsorbent at equilibrium (mg/g), q_t is the amount of metal ions (mg/g) adsorbed at specific time t and k_1 (1/min) is the rate constant. The value of k_1 (1/min) was calculated from the slopes of the linear plot of $\lg(q_e - q_t)$ versus t . The higher k_1 parameters indicate obtaining the equilibrium in shorter time.

Pseudo-second order model

The pseudo-second order model was proposed by Blanchard et al. (1984) to describe the kinetics of heavy metal ions removal by natural zeolites. This model is usually associated with the situation when the rate of direct adsorption/desorption process controls the overall sorption kinetics. The most frequently used form of the pseudo-second order equation is the one presented by Ho (Ho et al., 1996; Ho and McKay, 1999):

$$\frac{t}{q_t} = \frac{1}{k_2 q_e^2} + \frac{1}{q_e} t \quad (6)$$

where k_2 (g/(mg·min)) is the rate constant and can be determined from the plot of t/q_t versus t . The initial sorption rate, h (mg/(g·min)), can be calculated by using following formula:

$$h = k_2 q_e^2. \quad (7)$$

Kinetic analysis

The results which were subjected to the kinetic analysis were obtained by batch method and presented in Table 2. It was presented that correlation coefficient values of the pseudo-second order kinetic equation were higher than those of the pseudo-first order kinetic equation. Comparison of q_e values from kinetic equations and experimental results was done. The q_e values calculated from the pseudo-first order kinetic equation were meaningfully different than calculated from experiments as opposed to the

q_e values calculated from the pseudo-second order kinetic equation. Based on the agreement of the calculated q_e values with the experimental and high correlation coefficients sorption of nickel(II) and cadmium(II) on the SAC resins presented in this work was best described by the pseudo-second order kinetic equation. As it was showed in Table 2 the highest initial sorption rate was for Lewatit MonoPlus SP 112. It was possible to order the SAC resins with the h value decreasing: Lewatit MonoPlus SP 112 > Amberlite 200C > Amberlyst 15.

Isotherm modeling

In order to supply information about surface properties, resin affinities for Ni(II) and Cd(II) equilibrium isotherm equations are used. In this study the equilibrium isotherms are described by the Langmuir and Freundlich equations. Linear regression was used to determine the best fitting isotherm.

The best known and most widely applied adsorption isotherm is the Langmuir equation. The linearized Langmuir isotherm equation is:

$$\frac{c_e}{q_e} = \frac{1}{Q_0 b} + \frac{c_e}{Q_0} \quad (8)$$

where c_e is the equilibrium concentration of metal ions (mg/dm^3), q_e is the amount of metal ions adsorbed per unit mass of adsorbent at equilibrium (mg/g), Q_0 (mg/g) and b (dm^3/mg) are the Langmuir constants related with the monolayer sorption capacity and the free energy of sorption and can be calculated from the plot c_e/q_e versus c_e .

Table 2. Kinetic parameters comparison for SAC resins

Ion	Resin	Experimental q_e	Calculated from kinetic equation						
			Pseudo-first order			Pseudo-second order			
			q_e	k_1	R^2	q_e	k_2	h	R^2
Ni(II)	Lewatit MonoPlus SP112	5.10	0.72	0.24	0.911	5.15	0.88	23.43	1.000
	Amberlite 200C	4.93	1.13	0.21	0.827	5.03	0.40	10.04	1.000
	Amberlyst 15	5.06	2.02	0.21	0.950	5.22	0.23	6.33	1.000
Cd(II)	Lewatit MonoPlusSP112	10.26	3.94	0.27	0.992	10.49	0.17	18.54	1.000
	Amberlite 200C	10.17	5.00	0.16	0.945	10.61	0.07	7.83	1.000
	Amberlyst 15	10.48	5.57	0.15	0.982	10.99	0.06	6.95	1.000

q_e (mg/g); k_1 ($1/\text{min}$); k_2 ($\text{g}/(\text{mg}\cdot\text{min})$); h ($\text{mg}/(\text{g}\cdot\text{min})$)

The dimensionless constant separation factor (R_L) was also calculated. The R_L parameter is defined as:

$$R_L = \frac{1}{1 + bc_0} \quad (9)$$

where c_0 is the initial concentration of the adsorbate (mg/dm^3). The value of R_L indicates the shape of the isotherm: $R_L > 1$ – unfavorable, $R_L = 1$ – linear, $0 < R_L < 1$ – favorable, $R_L = 0$ – irreversible (Bulut et al., 2008; Wołowicz and Hubicki, 2011).

The Freundlich isotherm is used to describe the adsorption characteristics of the resin used in solutions. It is given in linear form by:

$$\ln q_e = \ln k_F + \frac{1}{n} \ln c_e \quad (10)$$

where k_F is the Freundlich constant connected with the sorption capacity of adsorbent (mg/g), $1/n$ is the Freundlich constant connected with the sorbent surface heterogeneity: $1/n = 0$ – irreversible, $0 < 1/n < 1$ – favorable, $1/n > 1$ – unfavorable. Freundlich constants were calculated from the plot of $\ln q_e$ versus $\ln c_e$.

The Langmuir and Freundlich isotherm parameters values obtained for all resins are shown in Table 3. The values of determination coefficient of the Langmuir isotherm are higher than those calculated from Freundlich isotherm. This means that the Langmuir isotherm represents a better fit of the experimental data than the other one. The sorption data obtained for Lewatit MonoPlus SP 112 was compared with the course of the Langmuir and Freundlich isotherms and the results are shown in Fig. 4.

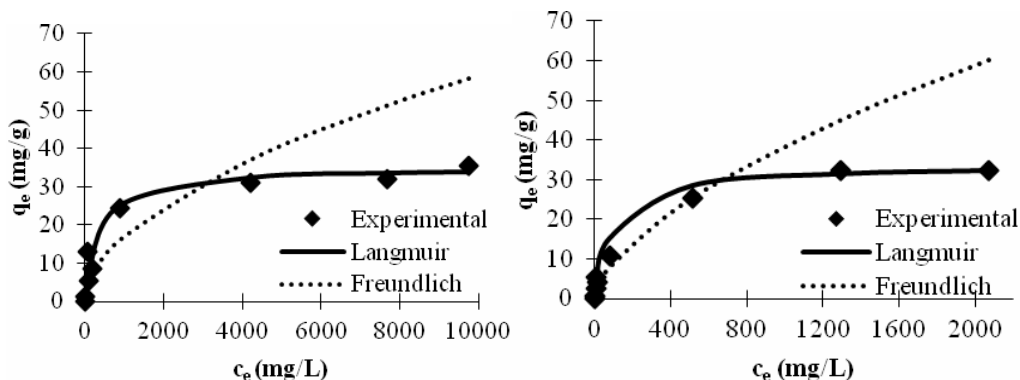


Fig. 4. Fitting of Freundlich and Langmuir isotherms to the experimental data obtained for the Lewatit MonoPlus SP 112: a) cadmium(II), b) nickel(II)

The Freundlich constant $1/n$ for all three resins was less than unity which means that the sorption of Ni(II) and Cd(II) ions is favorable. The Langmuir isotherm was found to be fitted with the determination coefficient in range of 0.992 to 0.999. The maximum monolayer capacity Q_0 was the highest for Amberlite 200C and it was 34.20 mg/g for Ni(II) and 39.47 mg/g for Cd(II). The R_L values (equilibrium parameter) for both ions were found to be in the range from 0 to 1 for all resins. It confirmed that the sorption of nickel(II) and cadmium(II) was favorable.

Table 3. Adsorption isotherm parameters for adsorption of Ni(II) and Cd(II) on SAC resins

Ion	Resin	Langmuir			Freundlich		
		Q_0	$b \cdot 10^3$	R^2	k_F	$1/n$	R^2
Ni(II)	Lewatit MonoPlus SP112	33.73	1.06	0.997	0.41	0.54	0.933
	Amberlite 200C	34.20	6.56	0.992	0.38	0.66	0.919
	Amberlyst 15	29.57	9.18	0.994	0.55	0.579	0.946
Cd(II)	Lewatit MonoPlus SP112	35.20	2.83	0.995	0.41	0.61	0.900
	Amberlite 200C	39.47	2.17	0.992	0.38	0.56	0.916
	Amberlyst 15	28.10	5.50	0.999	0.43	0.52	0.874

Q_0 (mg/g); b (dm³/mg); k_F (mg/g)

Conclusions

In this study, the potential of SAC exchange resins for nickel(II) and cadmium(II) sorption from chloride solutions was investigated. The amount of the adsorbed metal ions onto SAC exchange resins increases with time. The sorption process is fast. The experimental results show that 30 min is enough to reach the equilibrium. The amount of adsorbed ions is dependent on the initial metal ion concentration. The biggest sorption capacity (SC) was obtained for Lewatit MonoPlus SP 112: (1.70 mval/g), and for Amberlite 200C (1.64 mval/g), the lowest for Amberlyst 15 (0.97 mval/g). The main factor governing the effectiveness of sorption and separation of Ni(II) and Cd(II) is concentration of H⁺ in solution. To obtain separation of Ni(II) and Cd(II) appropriate pH of initial solution should be used (Gega and Otremska, 2012). The recovery was the lowest at pH = 0, higher at pH = 1 and almost 100% at pH = 2 and higher for both ions. It was found that Ni(II) and Cd(II) sorption on Lewatit MonoPlus SP 112, Amberlite 200C and Amberlyst 15 was very well described by the Langmuir isotherm (monolayer model). The kinetics of adsorption of metal ions onto SAC resins was studied by using pseudo-first and pseudo-second order equations. For studied system, the pseudo-second order kinetic model showed the best correlation with the experimental data.

References

- BLANCHARD G., MAUNAYE M., MARTIN G., 1984. *Removal of heavy metals from waters by means of natural zeolites*. Water Research 18(12): 1501–1507.
- BULUT E., ÖZACAR M., ŞENGİL İ.A., 2008. *Adsorption of malachite green onto bentonite: Equilibrium and kinetic studies and process design*. Microporous and Mesoporous Materials 115(3): 234–246.
- CHAUDHARI L.B., MURTHY Z.V.P., 2010. *Separation of Cd and Ni from multicomponent aqueous solutions by nanofiltration and characterization of membrane using IT model*. Journal of Hazardous Materials 180(1–3): 309–315.

- CLEGG J., ANTONIOLI B., BRAY D., GLOE K., GLOE K., JOLLIFFE K., KATAEVA O., MEEHAN G., WENZEL M., 2011. *Liquid-liquid extraction studies with 4,4'-biphenylene-spaced bis- β -diketones*. Journal of Inclusion Phenomena and Macrocyclic Chemistry 71(3): 319–329.
- DĄBROWSKI A., HUBICKI Z., PODKOŚCIELNY P., ROBENS E., 2004. *Selective removal of the heavy metal ions from waters and industrial wastewaters by ion-exchange method*. Chemosphere 56(2): 91–106.
- DEEPATANA A., VALIX M., 2008. *Comparative adsorption isotherms and modeling of nickel and cobalt citrate complexes onto chelating resins*. Desalination 218(1–3): 334–342.
- DEMIRBAS A., PEHLIVAN E., GODE F., ALTUN T., ARSLAN G., 2005. *Adsorption of Cu(II), Zn(II), Ni(II), Pb(II), and Cd(II) from aqueous solution on Amberlite IR-120 synthetic resin*. Journal of Colloid and Interface Science 282(1): 20–25.
- DIZGE N., KESKINLER B., BARLAS H., 2009. *Sorption of Ni(II) ions from aqueous solution by Lewatit cation-exchange resin*. Journal of Hazardous Materials 167(1–3): 915–926.
- GEGA J., WALKOWIAK W., GAJDA B., 2001. *Separation of Co(II) and Ni(II) ions by supported and hybrid liquid membranes*. Separation and Purification Technology 22–23(1–3): 551–558.
- HAMDAOUI O., 2009. *Removal of copper(II) from aqueous phase by Purolite C100-MB cation exchange resin in fixed bed columns: Modeling*. Journal of Hazardous Materials 161(2–3): 737–746.
- HO Y.S., MCKAY G., 1999. *Pseudo-second order model for sorption processes*. Process Biochemistry 34(5): 451–465.
- HO Y.S., WASE D.A.J., FORSTER C.F., 1996. *Kinetic Studies of Competitive Heavy Metal Adsorption by Sphagnum Moss Peat*. Environmental Technology 17(1): 71–77.
- GEGA J., OTREMBSKA P., 2012. *Separation of nickel(II) and cadmium(II) with ion-exchange process*. Separation Science and Technology 47: 1345–1349.
- GEGA J., WALKOWIAK W., OTREMBSKA P., POSPIECH B., KOSARGA E., 2010. *Separation of nickel and cadmium from synthetic spent battery leach solutions*. XXVth International Symposium on Physico-Chemical Methods of Separation, Ars Separatoria 2010, Toruń 359–362.
- KILYUSHIK Y., SMOLENSKAYA L., LEIKO A., DRUZHININA T., 2011. *Sorption of nickel and cadmium ions from aqueous solutions by a complexing resin based on modified polyamide fiber*. Fibre Chemistry 43(3): 239–244.
- KURNIAWAN T.A., CHAN G.Y.S., LO W.-H., BABEL S., 2006. *Physico-chemical treatment techniques for wastewater laden with heavy metals*. Chemical Engineering Journal 118(1–2): 83–98.
- LAZARIDIS N.K., 2003. *Sorption Removal of Anions and Cations in Single Batch Systems by Uncalcined and Calcined Mg-Al-CO₃ Hydrotalcite*. Water, Air, & Soil Pollution 146(1): 127–139.
- LEWIS A.E., 2010. *Review of metal sulphide precipitation*. Hydrometallurgy 104(2): 222–234.
- LIN L.-C., LI J.-K., JUANG R.-S. 2008. *Removal of Cu(II) and Ni(II) from aqueous solutions using batch and fixed-bed ion exchange processes*. Desalination 225(1–3): 249–259.
- MARDER L., BERNARDES A.M., ZOPPAS FERREIRA J., 2004. *Cadmium electroplating wastewater treatment using a laboratory-scale electro dialysis system*. Separation and Purification Technology 37(3): 247–255.
- PEHLIVAN E., ALTUN T., 2006. *The study of various parameters affecting the ion exchange of Cu²⁺, Zn²⁺, Ni²⁺, Cd²⁺, and Pb²⁺ from aqueous solution on Dowex 50W synthetic resin*. Journal of Hazardous Materials 134(1–3): 149–156.
- PLAZINSKI W., RUDZINSKI W., PLAZINSKA A., 2009. *Theoretical models of sorption kinetics including a surface reaction mechanism: A review*. Advances in Colloid and Interface Science 152(1–2): 2–13.

- POSPIECH B., WALKOWIAK W., 2007. *Separation of copper(II), cobalt(II) and nickel(II) from chloride solutions by polymer inclusion membranes*. Separation and Purification Technology 57(3): 461–465.
- PROVAZI K., CAMPOS B.A., ESPINOSA D.C.R., TENÓRIO J.A.S., 2011. *Metal separation from mixed types of batteries using selective precipitation and liquid–liquid extraction techniques*. Waste Management 31(1): 59–64.
- QIN J.-J., MAUNG NYUNT W., MAUNG HTUN O., LEE H., 2004. *A pilot study for reclamation of a combined rinse from a nickel-plating operation using a dual-membrane UF/RO process*. Desalination 161(2): 155–167.
- RODRIGUES L.E.O.C., MANSUR M.B., 2010. *Hydrometallurgical separation of rare earth elements, cobalt and nickel from spent nickel–metal–hydride batteries*. Journal of Power Sources 195(11): 3735–3741.
- RUDNIK E., NIKIEL M., 2007. *Hydrometallurgical recovery of cadmium and nickel from spent Ni–Cd batteries*. Hydrometallurgy 89(1–2): 61–71.
- SRIVASTAVA V.C., MALL I.D., MISHRA I.M., 2008. *Adsorption of toxic metal ions onto activated carbon: Study of sorption behaviour through characterization and kinetics*. Chemical Engineering and Processing: Process Intensification 47(8): 1269–1280.
- WALKOWIAK W., BARTSCH R., KOZLOWSKI C., GEGA J., CHAREWICZ W., AMIRI-ELIASI B., 2000. *Separation and Removal of Metal Ionic Species by Polymer Inclusion Membranes*. Journal of Radioanalytical and Nuclear Chemistry 246(3): 643–650.
- WOŁOWICZ A., HUBICKI Z., 2011. *Investigation of macroporous weakly basic anion exchangers applicability in palladium(II) removal from acidic solutions – batch and column studies*. Chemical Engineering Journal 174(2–3): 510–521.
- YUH-SHAN H., 2004. *Citation review of Lagergren kinetic rate equation on adsorption reactions*. Scientometrics 59(1): 171–177.
- ZAINOL Z., NICOL M.J., 2009. *Comparative study of chelating ion exchange resins for the recovery of nickel and cobalt from laterite leach tailings*. Hydrometallurgy 96(4): 283–287.

Received June 24, 2012; reviewed; accepted July 27, 2012

NON-AQUEOUS FRACTURING TECHNOLOGIES FOR SHALE GAS RECOVERY

Andrzej ROGALA, Jan KRZYSIEK, Maciej BERNACIAK, Jan HUPKA

Department of Chemical Technology, Chemical Faculty, Gdańsk University of Technology, Gdańsk, Poland,
jhupka@pg.gda.pl

Abstract: Fracturing technologies for shale gas production were developed mainly in the USA and are currently being adapted to geological conditions and environmental requirements in other countries. This paper presents literature on theoretical and practical aspects of gas production from shale with the emphasis placed on alternatives to hydraulic fracturing. Technical and environmental aspects of non-aqueous fracturing technologies are also considered.

Key words: shale gas, hydraulic fracturing, unconventional gas resources, explosive fracturing

Introduction

Hydraulic fracturing (HF) is a widely used method for fracturing rock during natural gas production. It is based on pumping fracturing fluid which contains proppant and other additives in order to stimulate oil and gas formations. Despite of HF advancement and its wide application in many world regions it is burdened with problems which need to be solved. Mentioned drawbacks consist of waste fluid management, investment costs, environmental costs, risk of surface and ground water contamination (USEPA, 2011), emission of methane and social disapproval/misunderstanding. All those shortcomings associated with HF resulted in developing new methods of shale gas production including fracturing with liquid carbon dioxide, carbon dioxide/nitrogen foams, and liquefied petroleum gas (LPG).

The all listed methods are designed to maintain compatibility of fracturing fluid and clay minerals consisting of expanding smectite [$\text{Na}_{0.3}\text{Al}_2(\text{Si}_{3.7}\text{Al}_{0.3})\text{O}_{10}(\text{OH})_2$] and swelling illite [$\text{K}_{0.7}\text{Al}_2(\text{Si}_{3.3}\text{Al}_{0.7})\text{O}_{10}(\text{OH})_2$] (Ahn and Peacor, 1986). This approach allows to eliminate potential fracture closing by smectite and illite, which decides about fracturing quality and gas productivity on perforations or created fractures.

As can be seen in Table 1, smectite has much greater surface area and CEC (cation-exchange capacity) than illite, and for both of them those properties are more pronounced than for other clay minerals like kaolinite and chlorite. CEC shows ability of clays to bond water. Greater CEC means that much more water can be trapped in the clay's structure and clay's swell or expansion will be greater. Expanding smectite (much) and swelling illite (less) cause troubles in shales so, we have an additional argument to search for technologies that do not use water as a base fluid (Lal, 1999).

Table 1. Surface area and CEC of clay minerals
(Eslinger and Pevear, 1988, after Martin and Dacy, 2004)

Type of mineral	Surface area [m ² /g]			CEC [meq/100 g]
	Internal	External	Overall	
Smectite	750	50	800	80–150
Illite	5	15	30	10–40
Kaolinite	0	15	15	1–10
Chlorite	0	15	15	<10

Mentioned above methods are similar to HF since they use fracturing fluids, thus arising many technological problems and hazards, both technical and environmental. An alternative is explosive/propellant fracturing technology (Snider et al., 1997) not requiring any fracturing fluid. Such pre-completion method stimulates the rock formation using a series of cumulative charges detonations in order to perforate the rock, and creates fractures with gases generated by burning high energy fuel – so called propellant. The main disadvantage is low range of occurring fractures, limiting performance and permeability of the rock. Technology using explosives became a tool allowing low pressure hydraulic fracture opening instead of only perforator being used. This method of perforation is used with limited success in some shale in the USA and Canada.

Technologies using non wetting fluid

Liquid CO₂

Fracturing with carbon dioxide is a method patented in the early 80's (Bullen and Lillies, 1982). The method is well-established and has been repeatedly modified. Commonly used for dry fracturing in water-sensitive formations. It involves injecting sand with liquid carbon dioxide (CO₂) as the carrier fluid of proppant without the addition of water or other auxiliary compounds. Proppant, in addition to naturally occurring sand grains is a man-made or specially engineered material, such as resin-coated sand or high-strength ceramic materials. CO₂ on the surface is a liquid at a pressure of 1.4 MPa and a temperature of –34.5°C. It uses specialized equipment to enable prop-

pant added directly to liquid CO₂ under these conditions on the surface. Liquid CO₂ viscosity is about 5 cP and therefore allows to increase viscosity to carry proppant in propagated fracture. After stabilization of temperature and pressure CO₂ partly dissolves in residual water and liquid hydrocarbon deposits

Biggest advantages of liquid CO₂ fracturing are: the elimination of potential formation damage normally associated with fracturing fluids, very rapid clean-up and evaluation of the well following the stimulation (Lillies and King, 1982). The technology has undergone many tests and improvements (Wright, 1998). By the end of the nineties of the twentieth century there were more than 1,200 successful CO₂ fracturings in Canada only. The technology was also used in the USA for Devonian shale in East Kentucky and West Pennsylvania, Texas and Colorado (Arnold, 1998). The results indicate, that the average gas production in some wells was as much as five-fold greater than the production from conventional HF treatments. If the wellhead pressure rapidly drops, CO₂ in such conditions may result in ice formation in a form of “X-mas tree” and tubing which eventually restricts the gas flow. Therefore, it was decided to optimize the process by adding nitrogen to the CO₂ gas which not only prevents ice build-up, but also reduces the cost of operating the well (Gupta et al, 1998).

The main problem associated with CO₂ or CO₂/N₂ gas mixture fracturing is their transport in the liquid state and storage in pressurized containers. In particular, the loss of CO₂ to the atmosphere should be avoided because of eventual impact on global warming. CO₂ fracturing keeps clays (smectite and illite) stabilized and prevents metal leaching and chemical interactions. Biggest successes in CO₂ fracturing were recorded in Canada and in the former Soviet Union in late eighties (Luk and Grisdale, 1994).

Nitrogen fracturing

Using nitrogen for oil and gas recovery from deposits of hydrocarbons dates back to year 1960 (Petty et al. 1967). At the beginning, nitrogen was commonly used as auxiliary fluid in first shale gas production process. Technologies using nitrogen as a fracturing fluid were developed in late seventies (Freeman et al. 1983). Previous attempts to employ nitrogen focused mainly on foam fracturing (see subpart Foams)). The initial successes associated with the elimination of large quantities of liquid and replacing them with gas did not eliminate all problems. The remaining amount of water and other additives were smaller, nevertheless, difficulties in the production process had occurred.

Solutions using nitrogen for the extraction of gas from Devonian shale in Washington County, OH, USA, dealt with the part of these problems (Gottschling et al., 1985). Applied technologies are based on trucks delivering liquid nitrogen, which after heating changes into the gaseous state. As a gas, nitrogen is pumped from numerous sources and injected under the pressure of 24 MPa (3500 psi) in shallow wells. Approximately 60% of the volume used for this operation is a pure nitrogen gas without proppant, designed to produce fractures in the stimulated formation. The remaining 40% is carrying 423–625 μm sand and is injected into the wellbore, where the sand

particles mixed with nitrogen were propagated into the fracture. During field tests 270 m³ of nitrogen per hole were used. Further tests followed to determine optimal conditions for fracturing various rock formations.

Another research on the application of nitrogen for rock fracturing using gas under high pressure was made by Lokhandwala and Jariwala (2005) who referred to many advantages both economical and ecological. Nitrogen as widely available and non expensive gas, reduces the cost of reservoir stimulation. It is an inert gas, therefore, it does not damage rock formation. Absence of water in the system excludes the possibility of rock swelling. In addition lack of water eliminates the formation W/O emulsion which otherwise requires the use of additional chemicals. Ease of removal of gas favors the clean-up processes, and thus prepares the well after fracturing into production. Gas can be removed easily and the clean-up process is fast.

All mentioned advantages would promote the gaseous nitrogen fracturing to be world's best solution for production of hydrocarbons. However, placing the proppant in high velocity gas stream is problematic, as well as resulting erosion. The size and geometry of fractures created during initial fracturing caused problems with proppant deposition from the carrying gas. This technology is limited to shallow wells as a result of reduction of hydrostatic pressure that affects bottom hole treating pressure (BHTP).

Foams

Shale reservoirs fracturing using foams exists for over 30 years (Harris et al., 1988). It is a modification of hydraulic fracturing which depends upon exchange of part of liquid with gas, usually nitrogen, rarely carbon dioxide (Chilingarian et al., 1989). The fracturing fluid consists of proppant, surfactants, and foam stabilizers. Chemicals are mixed with water and dispersed using gaseous nitrogen to create foam with various foam ratio (Gaydos and Harris, 1980). The advantage of using foams is less expanding smectite and swelling illite in comparison to HF. Unfortunately, it is not possible to totally eliminate clay swelling.

There are also other advantages of using foam fracturing (Phillips et al., 1987):

- foams have wide range of viscosities
- high efficiency of return fracturing foam to the surface
- less damage to the reservoir due to small volume of water remaining in the shales.

The disadvantages of this technology are:

- low proppant concentration in fluid
- very high costs of foam fluid systems
- less economical as compared to aqueous and oil-based fracturing fluids
- difficult rheological characterization of foams (Reidenbach, 1986),
- higher surface pumping pressure.

LPG fracturing

One of the most promising alternatives to HF is LPG fracturing (Loree and Mesher, 2007). LPG is applied as propane under high pressure in liquid form. LPG before the fracturing is gelled to allow the transport of proppant into the fracture. The main advantage of LPG for fracturing is to increase the productivity of the well. This is due to the different behavior of water and LPG in changed reservoir pressure. In the case of hydraulic fracturing, residual water in the narrow fracture is being held by closing fracture and capillary interactions. This causes a partial water block of the reservoir and reduces the gas flow. In the case of LPG, after pressure drop it changes the physical state from liquid to gas and freely flows through the fractures, without affecting smectite and illite (Taylor et al., 2005). Other advantages resulting from the use of LPG for fracturing include:

- lower viscosity, density and surface tension of the fluid, which results in lower energy consumption during fracturing
- full compatibility with reservoirs because LPG and hydrocarbons are mutually soluble,
- smaller volume of chemicals added to the fracturing fluid
- no fluid loss – possible 100% recover
- sustainable, recyclable and more environmentally friendly than HF. It is because there is no water use in fracturing operation, fracturing fluid is inert to reservoir minerals and can be recycled during operations
- numerous existing government and industry regulations and procedures about using LPG
- gaseous LPG is more dense than air, so there is no risk to air contamination and impact on global warming.

The use of LPG has its drawbacks:

- investment costs are higher than for HF, because LPG is pumped into well at a very high pressure, and after each fracturing it has to be liquefied again
- LPG must be stored in costly pressurize tanks (water in HF is stored in non-pressure tanks or in natural outdoor pools)
- LPG is explosive
- LPG is more dense than air and fills up the ground cavities.

These drawbacks cause LPG method has many opponents. especially in eco organizations. A letter to Commissioner of New York Department of Environmental Conservation was sent pertaining to LPG fracturing in New York to explore shale gas (Steven Russo et al., 2012). The views on the LPG fracturing negative impact on the environment were presented, followed by argument that it is against the law of New York. Unfortunately the sources refer to articles from newspapers and own speculations having no scientific base.

The greatest asset of LPG fracturing technology is its smaller environmental impact. This is due to the lack of use of frac water almost no chemicals, and thus lesser

risk of environmental pollution due to flowbacks. So far, LPG fracturing has been used where it is prohibited to use water-based fracturing fluids, like in New Brunswick, Canada (Le Blanc et al., 2011). However, due to cost and geological conditions, this method is not widespread.

Explosive/propellant system – EPS

Perforation with cumulative explosives and shale's reservoir fracturing using explosion gas under high pressure has been known for several decades (Howard, 1971). The technology using both explosives and rocket fuel to stimulate shale exists for more than 30 years and constantly is being improved (Gilliat et al., 1999). Stimulation using high pressure gases received from burning propellant is known for couple of years (Page and Miskimins, 2009). In the USA work on developing the system is undergoing. Perforation, however, hardly exceeds 0.3–0.5 m (1.0–1.5 ft), reaching 0.7 m (2.3 ft) under some conditions. Such short range of perforation does not allow the above mentioned method to fully replace hydraulic fracturing in shale gas production. Today, the EPS is used for preliminary fracturing with effectiveness oscillating around 5–10% due to ineffective flow control of gases generated during perforation. Perforation technology using propellant (rocket fuel) simultaneously for generating high pressure gas is patent pending by one of the leading oil companies (Snider, 1997). It is used for low-range fracturing, mainly in sandstone formations in the vicinity of the reservoir water retention. It is commonly used for initiation of fracture in all perforation for HF.

Currently used in the field Trade Mark systems are Stimgun, StimTube, Gasgun, Pulsefrac etc. and combined perforation/propellant, and propellant only for specific applications. Propellant is an explosive used to propel a projectile or missile, or to do other work by the expansion of high pressure gas produced by burning, e.g. rocket fuel (Bailey and Murray, 1989). The EPS has basic features of Stimgun and Gasgun with dramatically improved performance such as:

- fracture length at given wellbore depth and bottom hole stimulation pressure
- energized dual cumulated detonation
- prolonging tip of perforation tunnel into the fracture
- classic cumulated propellant impact and all direction fracture development
- a new concept of shock reduction.

The approach is considered as environmentally friendly for shale gas and oil fracturing solution for contributing to return on investment (ROI) at a new level. Fracture geometry monitoring will have range to be visible in tomography pictures. The major gas flow mechanism is to be from fracture, fracturing slippage and desorption. The EPS has no impact on formation fluid compatibility, wettability, formation heavy and light metal leaching, smectite expansion, illite swelling, formation frac stress development (tilting) that locks up the perforation nor created fractures in HF. When full length is perforated with EPS with its limited frac entry compared to HF, the overall

gas production is expected to be close to HF performance where induced formation stress affects perforation opening for fracture. The EPS is considered as a fraction of costs of HF.

Summary and final comments

The current fracturing technology is applicable to specific areas with fluid sensitive shale. Based on current hydraulic fracturing performances in Poland, shale has certain volume of low density smectite clay that has tendency to absorb frac water and to expand. It may also have impact on observed tilting effect caused by massive frac fluid and proppant injection and reorientation of existing formation stress by increasing dramatically its value. Increased formation stress and shale expansion in contact with water may cause both soft shale layers to move and plug perforation and close some

Table 2. Comparison of fracturing technologies (Krzysiek, 2012)

Consideration	Water Based	N ₂ Foam	CO ₂ Liquid	N ₂ Gas	LPG Liquid	EPS
Environmentally friendly	N	N	N	Y	N	Y
Fluid availability	?	Y	Y	Y	N	-
Fluid recycling	Y	Y	?	N	Y	-
Chemicals used	Y	Y	?	?	?	N
Reservoir compatibility	?	?	Y	Y	Y	Y
Fracture creation	Y	Y	Y	Y	Y	Y
Proppant carrying	Y	Y	Y	Y	Y	?
Recovery to pipeline	N	N	N	N	Y	N
Heavy metals flowback	Y	Y	N	N	N	N
Frac cost	1	>1*	>>1*	>>1*	>>>1*	<<<1*
Fluid left in formation	Y	Y	N	N	N	-
Well clean up	Y	Y	Y	N	N	Instant production
Frac geometry predictability	N	N	N	N	N	Y
Tilting stress development	Y	Y	Y	Y	Y	N
Zone water in flux risk	1	>1*	>1*	>1*	>1*	>>>1*
Fracture length	1	>1*	>1*	>1*	>1*	>>1*
Active flow frac perforation	?	?	?	?	?	Y
Frac well performance	1	<1*	<<1*	<1*	<<1*	>1*
Local road damage risk	Y	Y	Y	Y	Y	N
Environmental risk	Y	Y	Y	Y	Y	Y
NO _x and CO ₂ in pumping	Y	Y	Y	Y	Y	N
Return on investment	1	<1*	<1*	<1*	<1*	<<<1*

Y – yes, N – no

*Average data from field applied technology by Jan Krzysiek

fracture. Frequently, most of the perforation is inactive with extremely high frac initiation pressure, sometimes beyond pump capacity. Production log time (PLT) may precisely define it, if it is run in hole.

In non-aqueous fracturing technologies application of the EPS provides most cost-effective and environmentally-friendly attention despite of lower production performance. EPS allows to expect that all perforations are productive and with sustained gas production level which may reach HF production performance at lower cost. It is preferred that EPS is being run on tubing conveyed perforator (TCP).

Unit operations and features associated with discussed featuring technologies are summarized in Table 2.

Acknowledgements

Financial support by the Polish Statutory Research Grant No. 020222 is gratefully acknowledged.

References

- AHN J.H., PEACOR D.R., 1986. *Transmission electron microscope data for rectorite: Implications for the origin and structure of "fundamental particles"*. Clays and Clay Minerals, 34, 180–186.
- ARNOLD D.L., 1998. *Liquid CO₂-sand fracturing: the dry frac*. Fuel and Energy Abstracts, Volume 39, Number 3, pp. 185–185(1).
- BAILEY A., MURRAY S.G., 1989. *Explosives, Propellants and Pyrotechnics*, London: Brassey's (UK) April 1989, 180.
- BULLEN R.S., LILLIES A.T., 1982. *Carbon dioxide fracturing process and apparatus*. US Patent No 4374545.
- ESLINGER E., PEVEAR D., 1988. *Clay Minerals for Petroleum Geologists and Engineers*. SEPM Short Course Notes No. 22, Society of Economic Paleontologists and Mineralogists, Tulsa 1988.
- FREEMAN E.R., ABEL J.C., KIM C.M., HEINRICH C., 1983. *A Stimulation Technique Using Only Nitrogen*. Society of Petroleum Engineers, 35, 12, 2165–2174.
- GAYDOS J.S., HARRIS P.C., 1980. *Foam fracturing: Theories, Procedures and Results*. Society of Petroleum Engineers, DOI 10.2118/8961-MS, SPE Unconventional Gas Recovery Symposium, 18–21 May 1980, Pittsburgh, Pennsylvania.
- GILLIAT J., SNIDER P.M., HANEY R., 1999. *Field Performance of New Perforating/Propellant Technologies*. 1999 SPE Annual Technical Conference and Exhibition, Houston, 3–6 October.
- GOTTSCHLING J.C., ROYCE T.N., SHUCK L.Z., 1985. *Nitrogen Gas and Sand: A New Technique for Stimulation of Devonian Shale*. Journal of Petroleum Technology 37, 5, 901–907.
- GUPTA D.V.S., BOBIER D.M., 1998, *The History and Success of Liquid CO₂ and CO₂/N₂ Fracturing System*. SPE, Canadian Fracmaster Ltd., SPE Gas Technology Symposium, 15–18 March 1998, Calgary, Alberta, Canada.
- HARRIS P.C., KLEBENOW D.E., KUNDERT D.P., 1989. *Constant internal phase design improves stimulation results*. SPE Paper 17532.
- HOWARD G.C., 1971. *Explosively fracturing formations in wells*. US Patent No 3587743.
- KARGBO D.M., WILHELM R.G., CAMPBELL D.J., 2010. *Natural Gas Plays in the Marcellus Shale: Challenges and Potential Opportunities*. Environ. Sci. Technol. 2010, 44, 5679–5684.

- KRZYSIEK J., 2012. *Is Polish Shale Gas posing challenge to players and researchers?* Workshop Abstract Proceedings, Interfacial Phenomena in Theory and Practice, VII Summer School, Sudomie June 24th-30th 2012.
- LAL M., 1999. *Shale Stability: Drilling Fluid Interaction and Shale Strength*. SPE Paper 54356, SPE Latin American and Caribbean Petroleum Engineering Conference held in Caracas, Venezuela, 21–23 April 1999.
- LEBLANC D., MARTEL T., GRAVES D., TUDOR E., LESTZ R., 2011. *Application of Propane (LPG) Based Hydraulic Fracturing in the McCully Gas Field*, New Brunswick, Canada. Society of Petroleum Engineers. 10.2118/144093-MS.
- LILLIES A.T., KING S.R., 1982, *Sand Fracturing With Liquid Carbon*. Publisher Society of Petroleum, DOI 10.2118/11341.
- LOKHANDWALA K.A., JARIWALA A., 2005. *Natural gas treatment process for stimulated well*. US Patent No 7537641.
- LOREE D.N., MESHER S.T., 2007, *Liquefied Petroleum Gas Fracturing System*. US Patent Application No 2007204991.
- LUK S.W.M., GRISDOLE J.L., 1994. *High proppant concentration/high CO₂ ratio fracturing system*. US Patent No 5515920.
- MADER D. et al., 1989. *Hydraulic proppant fracturing and gravel packing*. Elsevier Science Publishers B.V., ISBN 0-444-87352-x (Volume 26), 0-444-41625-0 (series).
- MARTIN P., DACY J., 2004. *Effective Q_v by NMR core tests*. SPWLA 45th Annual Logging Symposium, June 6-9, 2004.
- Office of Research and Development, U.S. Environmental Protection Agency. 2011. *Draft Plan to Study the Potential Impacts of Hydraulic Fracturing on Drinking Water Resources*. Washington, D.C.
- PAGE J.C., MISKIMINS J.L., 2009. *A Comparison of Hydraulic and Propellant Fracture Propagation in a Shale Gas Reservoir*. Journal of Canadian Petroleum Technology, 48(5), 26–30.
- PETTY C.B., HENDRICKSON A.R., BROWN L.S., 1964. *Liquid Nitrogen In Well Operations*. US Patent No 3358763.
- PHILLIPS A.M., COUCHMAN D.D., WILKE J.G., 1987. *Successful Field Application of High-Temperature Rheology of CO₂ Foam Fracturing Fluids*. Society of Petroleum Engineers DOI 10.2118/16416-MS, Low Permeability Reservoirs Symposium, 18–19 May 1987, Denver, Colorado.
- REIDENBACH V.G., HARRIS P.C., LEE Y.N., LORD D.L., 1986. *Rheological Study of Foam Fracturing Fluids Using Nitrogen and Carbon Dioxide*. Society of Petroleum Engineers DOI 10.2118/12026-PA.
- SNIDER P.M. et al. 1997. *Apparatus and method for perforating and stimulating a subterranean formation*. United States Patent No. 5775426.
- TAYLOR R.S., FUNKHOUSER P., DUSTERHOFT R.G., LESTZ R.S., BYRD A., 2005. *Compositions and methods for treating subterranean formations with liquefied petroleum gas*. US Patent No 7341103.
- USEPA (United States Environmental Protection Agency), 2011. *Plan to Study the Potential Impacts of Hydraulic Fracturing on Drinking Water Resources*. U.S. Environmental Protection Agency, Office of Research and Development, Washington, D.C. [online], http://www.epa.gov/hfstudy/HF_Study_Plan_110211_FINAL_508.pdf.
- WRIGHT T.R., 1998. *Frac technique minimizes formation damages Dry Frac*. World Oil [online], http://findarticles.com/p/articles/mi_m3159/is_n1_v219/ai_20387355/.

Received May 14, 2012; reviewed; accepted July 19, 2012

UNUSUAL APPLICATION OF POROUS MATRIX MADE FROM QUARTZITE SCHIST

Tomasz MARCINISZYN

Institute of Physics, Wrocław University of Technology, Wybrzeże Wyspiańskiego 27, 50-370 Wrocław, Poland; tomasz.marciniszyn@pwr.wroc.pl

Abstract: Results of dielectric spectroscopy of quartzite slate are presented. New type of a porous matrix based on quartzite schist was described. The matrix was filled by a ferroelectric TGS-crystal. The phase transition of the TGS bulk was shown to occur and compared with the phase transition of the component quartzite schist filled with TGS (QSM-TGS). The resonance phenomena in the QSM were shown and described from the point of view filled material.

Key words: quartzite schist matrix, QSM, resonance

Introduction

Quartzite slates samples come from the Jegłowa mine located on the Strzelin Hills belonging to the foothills of the Sudety Block. Quartzite schists are situated about 15 meters below the ground level under the layer of quartzite (Fig. 1). The quartzite schist and quartzite occurring in the foothills of the Sudety Block was discovered and described in the XIX century (Lehmann, 1885). Properties of quartzite schist were described in the paper of Chmura (1967). Quartzite schist contains mainly SiO₂ (87–99%), Al₂O₃+TiO₂ (0.5–7%), Fe₂O₃ (0.1–2%), K₂O (0.2–3%) and Na₂O (0.02–1.5%), depending on the region of the Sudety Block and depth (Chmura, 1967). Density of quartzite schist equals 2.58–2.60 g/cm³. Quartzite schist has a wide range of effective porosity (open porosity), 0.5–9.3%, depending on depth (Chmura, 1967). Quartzite schist is a material with the temperature of the fire resistance $T = 1580–1710^{\circ}\text{C}$. In the twenty century quartzite was used mostly to build O.H. furnaces (Piech, 1999). Presently quartzite with quartzite schist is use in the construction industry (stone interior accessories, roads and so on).

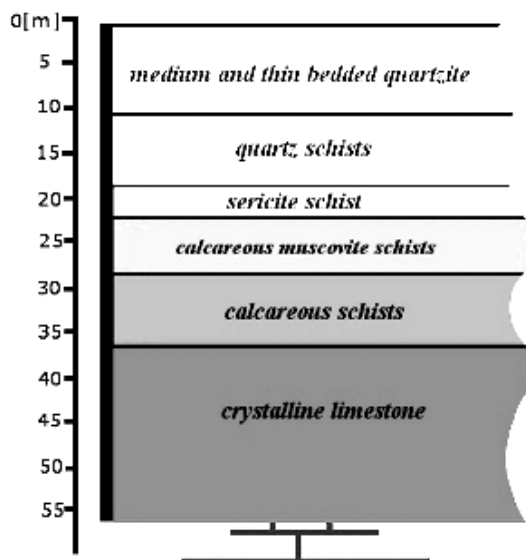


Fig. 1. Lithological profile of Jegłowa area vs depth

The aim of this work is to study dielectric spectroscopy of the empty and embedded with crystallites of tryglycine sulfate (TGS) quartzite schist matrix (QSM) and investigations of physical properties of this composite. The pores occurring in the quartzite schist matrix reduce the size of the introduced material. Embedded crystallite size reduction to nanocrystalline level results in surface effects domination which, in turns, starts to determine the physical properties of the material. There have been many theoretical and experimental studies on the size dependence of lattice dimensions of such compounds (Wang et al., 2011; Sieradzki et al., 2010, 2011; Rysiakiewicz-Pasek et al., 2010). To the authors knowledge, there is no previously documented case describing the possibility to use natural material-quartzite schist as a matrix.

The TGS has second order phase transition with the Curie point at 322 K. The TGS is applied to many applications such as infrared detectors, pyroelectric vidicon tubes operating at room temperature (Ashok et al., 2003; Balamurugan, et al., 2007). Additionally the TGS crystals are used in fabrication of capacitors, transducers and sensors.

Sample preparation and experimental

From the quartz schist, a cube of side 10 mm was prepared by cutting. Next the quartzite schist cube was heated at the high temperatures. After annealed, the matrix from the cube schist was developed. Precise chemical compositions of quartzite schist was determined using the XRF method and presented in the Table 1.

Table 1. Chemical composition of quartzite schist

	Compound	Composition [%]
	SiO ₂	88.8
	Al ₂ O ₃	7.07
	Fe ₂ O ₃	1.28
	CaO	< 0.01
	MgO	0.26
Spectral analysis (XRF)	Cr ₂ O ₃	0.04
	MnO	0.02
	K ₂ O	2.27
	P ₂ O ₅	< 0.01
	SO ₃	< 0.01
	Na ₂ O	< 0.01
	TiO ₂	0.23
	ZrO ₂	0.01

The TGS was introduced into QSM as an aqueous solution. The QSM was soaked in the saturated aqueous TGS solution at 320 K for 3 hour. Then the sample was taken out and dried. The process was repeated twice. The QSM surfaces were polished mechanically to remove small TGS crystals. The quartzite schist matrix filled with the TGS was marked as QSM-TGS.

To describe the properties of the quartzite schist matrix dielectric spectroscopy measurements of empty and filled with the TGS crystal matrix were performed. An automatic Novocontrol Alpha impedance analyzer in the frequency range from 10^1 to $5 \cdot 10^7$ Hz and temperature from range from 273 to 360 K was used in the measurements.

Results

Measurements in wide frequency range were performed at 293 K and 373 K. The frequency dependence of the real part of permittivity for the QSM and QSM-TGS at 293 K and at 373 K is shown in the Figs 2 a) and b), respectively. It is well visible that in both QSM and QSM-TGS at both measurement temperatures about $1.7 \cdot 10^7$ Hz permittivity rapidly increases. It can be explained by resonance phenomena, like in the case of quartzite (Marciniszyn et al., in press). The piezoelectric resonance in quartzite is caused by vibrations occurring inside SiO₂ grains with average size of 0.15 mm. The value of the maximum of the real part of permittivity is twentyseven-fold much higher then for QSM in comparison to QSM-TGS at 293 K and twice higher than for QSM measured at 373 K. The difference in the value of permittivity of the empty matrix at 293 K and 373 K can be caused by absorbed water. Additionally, the peak of

the real part of permittivity has become wider for QSM–TGS compared with QSM. The value of the peak of the real part of permittivity for QSM–TGS measured at 296 K exhibits the same value as for measurement at 373 K, which confirmed a good filling of QSM.

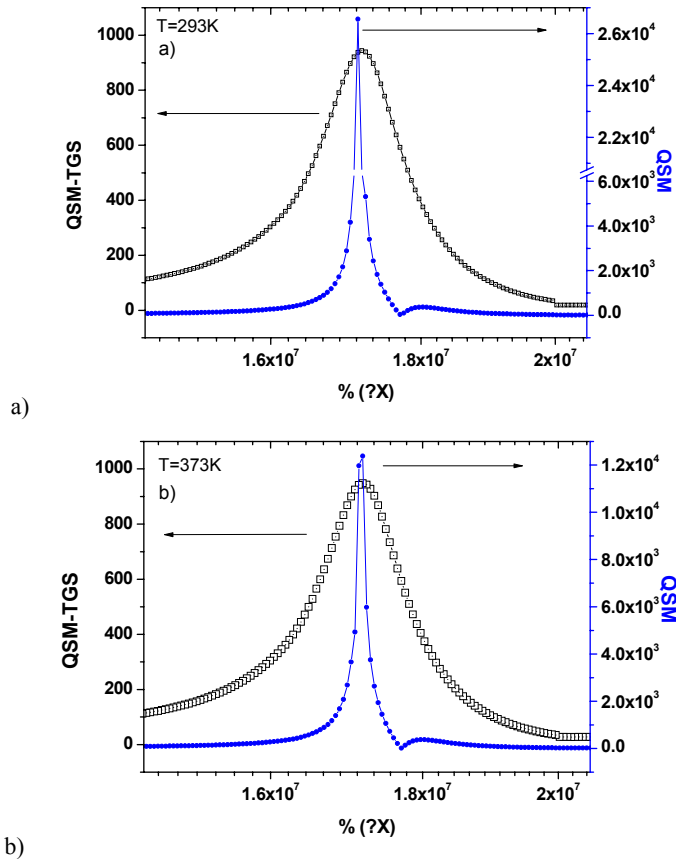


Fig. 2. Frequency dependence of the real part of the dielectric permittivity for QSM–TGS and QSM at 293 K (a) and 373 K (b)

To describe the influence of the matrix on the phase transition in TGS material dielectric spectroscopy test at different temperatures for 1 kHz frequency was performed and the result are shown in Fig. 3. From Fig. 3 it is well visible that for the bulk of TGS the second phase transition occurs at 321 K. For the QSM–TGS the phase transition become less sharp and the peak of the real part of permittivity disappears. The temperature of the phase transition is difficult to estimate. The matrix also caused reduction in the value of permittivity of the filled material.

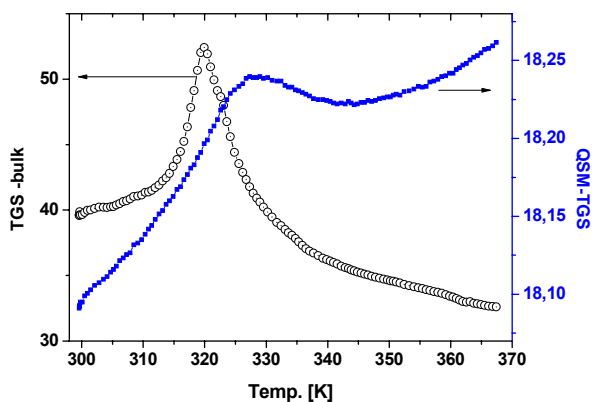


Fig. 3. The temperature dependence of the real part of the dielectric permittivity for TGS-bulk and QSM-TGS

Conclusions

In this paper dielectric spectroscopy of the empty and filled quartzite schist matrix was described. The resonance in QSM was shown. Filling material of QSM was crystalline TGS. It was shown that the filling material has significant influence on the resonance occurring in QSM. The TGS crystal introduced into matrix decreases the value of the maximum $\varepsilon'(f)$ and made the resonance peak smooth when compared to the empty quartzite schist matrix. QSM has large potential as a basic material in which we can control the resonance peak by the filling material. Additionally, is possible to get QSM with different size of pores.

Acknowledgments

This work was co-funded by the European Social Fund.

References

- BALAMURUGAN N., LENIN M., BHAGAVANNARAYANA G., RAMASAMY P., 2007, *Growth of TGS crystals using uniaxially solution-crystallization method of Sankaranarayanan-Ramasamy*, Crystal Res. Technol. 42, 151–156.
- BATRA A.K., AGGARWAL M.D., LAL R.B., 2003, *Growth and characterization of doped DTGS crystals for infrared sensing devices*, Materials Lett. 57, 3943–3948.
- CHMURA K., 1967, *Rozwój litograficzny Jęglowskiej serii kwarcytowej*, Rocznik Polskiego Towarzystwa Geologicznego, t. XXXVII, Kraków.
- LEHMANN J., 1885, *Dattelquarz von Krummendorf bei Strehlen*, Jb. Schles. Ges. 63, 144.
- MARCINISZYN T., SIERADZKI A., POPRAWSKI R., (paper in press), *Electrical properties and microstructure of quartzite from Jęglowa/Poland after thermal treatment*, Journal of Applied Geophysics.
- PIECH J., 1999, *Wyłożenia ogniotrwale pieców i urządzeń cieplnych*, Kraków.

- RYSIAKIEWICZ-PASEK E., KOMAR J., CIŻMAN A., POPRAWSKI R., 2010, *Calorimetric investigations of NaNO_3 and NaNO_2 embeded into porous glasses*, J. Non-Crystalline Solids, 356, 661–663.
- SIERADZKI A., KOMAR J., RYSIAKIEWICZ-PASEK E., CIŻMAN A., POPRAWSKI R., 2010, *Calorimetric Investigations of Phase transitions in KNO_3 embeded into Porous Glasses*, Ferroelectrics, 402, 60–65.
- SIERADZKI A., CIŻMAN A., POPRAWSKI R., MARCINISZYN T., RYSIAKIEWICZ-PASEK E., 2011, *Electrical conductivity and phase transitions in KDP- and ADP-porous glass nanocomposites*, Journal of Advanced Dielectrics, Vol. 1, No. 3, 337–343.
- WANG J., TAGANTSEV A.K., SETTER N., 2011, *Size effect in ferroelectrics: Competition between geometrical and crystalline symmetries*, Physical Review B, 83, 014104-5.

Received May 13, 2012; reviewed; accepted June 12, 2012

COPPER RECOVERY FROM CHALCOPYRITE CONCENTRATE ACID LEACH SOLUTIONS BY ACORGA M5397

Khalid EL AMARI¹, El-Aid JDID², Pierre BLAZY³

¹ Laboratoire Géoressources, Unité Associée au CNRST (URAC 42), Faculté des Sciences et Techniques Guéliz, B. P. 549, 40000 Marrakech, Maroc; elamari@fstg-marrakech.ac.ma

² LEM UMR 7569, Nancy Université, ENSG-INPL-CNRS, 15 avenue du Charmois, B.P. 54 501, Vandoeuvre-Les-Nancy, France

³ ENSG-INPL, Rue du Doyen Marcel Roubault, B. P. 40, 54501 Vandoeuvre, France

Abstract: Chalcopyrite concentrate from Hajar Mine, Morocco, was leached with nitro-fluosilicic acid leach solution. The pregnant leach solution obtained contained 19.3 g/dm³ Cu, 18.1 g/dm³ Fe, 4.5 g/dm³ Zn and 0.03 g/dm³ Pb. Copper recovery from this pregnant leach liquor was performed by solvent extraction using Acorga M5397 diluted in Escaid 110. McCabe–Thiele distribution isotherms showed that at pH 1.7 complete and selective copper extraction can be achieved with $\phi_o/\phi_a = 1.5/1$ in 3 stages of extraction. Stripping of the loaded copper by treating the organic phases by a fresh sulphuric acid solution was easily realized.

Keywords: *Copper solvent extraction, solvent extraction selectivity, nitro-fluorosilicic acid, AcorgaM5397*

Introduction

Metal copper production from ores can be performed by two main methods: conventional pyrometallurgical method (smelting/converting) and hydrometallurgical method (leaching followed by solvent extraction – electrowinning process, SX-EW) (Padilla et al., 2010).

Since 1900, when the world production was less than 0.5 teragrams (Tg) (500 thousand tonnes) world copper mining production has been growing by around 4% per year to reach nearly 16 Tg in 2009. SX-EW production, virtually non-existing before the 1960's, reached nearly 3.3 Tg in 2009 according to International Copper Study Group (2010). The ore quality is of increasingly lower grade with poor physical rock quality and high impurity level (Helle et al., 2010).

At the present pyrometallurgical route is the most frequently used technique to produce copper metal from chalcopyrite concentrates (Padilla et al., 2010; Habashi, 2007). However, copper production by heap leaching combined with SX-EW has become a gigantic operation (Habashi, 2007). According to Watling (2006), more than 20% of refined copper is produced via hydrometallurgy.

Other processes like bacterial leaching, roast-leach, chloride leaching, and pressure oxidation especially for dirty or low grade sulphide concentrates receive much more attention (Pradham et al., 2008; Dreisinger, 2004; Blazy and Jdid, 2002). However the importance of hydrometallurgical techniques involving SX - EW for recovery of copper from oxides and also some sulphide ores is growing rapidly (International Copper Study Group, 2010). They had gained wide acceptance as one of the new tools of hydrometallurgy, and are becoming the key processes in copper hydrometallurgy.

Copper solvent extraction from pregnant sulphuric acid leach solutions is widespread commercially with the use of LIX reagents (Suttill, 1989; Arbiter and Fletcher, 1994). It is also performed from chloride solutions in Cuprex process (Dalton et al., 1991) and ammoniacal solutions using some LIX reagents as LIX 54, 26, 34, 622N... (Arbiter and Fletcher, 1994; Dalton et al., 1991; Yoshinari and Katsutoshi, 1988; Henkel Corporation; Panigrahi et al., 2009).

Chalcopyrite is the most abundant copper sulphide mineral and most refractory regarding chemical leaching as well as bioleaching (Koleini et al., 2010) and the leaching of chalcopyrite remains the most difficult stage of the process. In the case of Hajar Mine copper concentrate, Morocco, leaching stage was performed using a complex acid leach medium, mixture of nitric acid and fluorosilicic acid (El Amari et al., 2000). Previous work performed by El Amari et al. (2006) showed that copper dissolution was non selective and the pregnant leach solution was rich in copper, iron, zinc and lead. In the case of this complex solution LIX 984 was efficient and selective in separation of copper from Zn, Pb and Fe.

For the purpose of the present study, copper solvent extraction was carried out on the same pregnant leach nitro-fluorosilicic acid solution as in previous work (El Amari et al., 2006), but using a modified nonylsalicyl aldoxime reagent (Acorga M5397) to evaluate its selectivity and loading capacity of copper. The copper loaded organic phases were then subjected to a stripping stage using a fresh sulphuric acid solution.

Experimental

Pregnant leach solution (PLS) used in this study was obtained by the treatment of a sample of copper concentrate from Hajar Mine (Morocco) in $\text{HNO}_3\text{-H}_2\text{SiF}_6$ mixture. Leaching tests were carried out according to El Amari et al. (2000). Principal characteristics of this solution are listed in Table 1.

Table 1. Characteristics of the feed solution (PLS)

	pH	Eh (mV/ENH)	Cu (g/dm ³)	Zn (g/dm ³)	Fe (g/dm ³)	Pb (g/dm ³)
PLS	0.6	580	19.3	4.5	18.1	0.03

Commercial extractant Acorga M5397, provided by ICI Specialty Chemicals, is a chelating agent belonging to the oximes family. It is a blend of 2hydroxy-5-nonylsalicylaldoxime, a long chain alcohol and a metallurgical grade diluent. Escaid 110 was used for the dilution of the Acorga solvent in this study with.

The equilibrium distribution of copper between the organic and aqueous phases was determined by mixing equal volumes (50 cm³) of the two phases by rapid stirring with magnetic stirrer. After each test both phases were separated and the concentration of the elements concerned (Cu, Fe, Pb and Zn) in the aqueous phase before and after extraction was determined by Inductive Coupled Plasma – Atomic Emission Spectroscopy (ICP-AES, to determine the rate of their recovery. Metal content in the organic phase was determined from the mass balance.

Results and discussion

To determine the effect of the most significant parameters governing the solvent extraction, namely: pH of the solution, the kinetics of the extraction, and extractant concentration in the solvent, the experiments were carried out at ambient temperature and atmospheric pressure, with organic phase (φ_o) to aqueous phase (φ_a) volume ratio of 1/1 ($\varphi_o/\varphi_a = 1/1$). The leach solution was rich in various metals. The concern of the study was to recover selectively copper, keeping the other elements in the initial PLS solution. The distribution isotherms of copper were established according to McCabe–Thiele diagrams that permit the determination of the theoretical number of counter-current stages of extraction.

The copper re-extraction from the loaded organic phase was carried out by a sulphuric acid solution. The studied parameters are the acid concentration of the stripping solution, the re-extraction kinetics and the φ_o/φ_a volume ratio.

Copper extraction from PLS

Effect of extractant concentration

Varying the concentration of the extractant in Escaid between 5 and 20% by volume, and keeping constant the other operational parameters: 15 minutes of contacting time, $\varphi_o/\varphi_a = 1/1$ and ambient temperature, the dependence of percentage extraction of copper on extractant concentration was established (Fig. 1). The results show the high extraction capacity of Acorga M5397 and the increases in the recovery of copper with extractant concentration. In spite of this good extraction capacity, the cop-

per distribution coefficient of 0.63 seems to be less important because of high concentration of this element in the initial aqueous solution. In the case of PLS Acorga M5397 is also very selective toward separation of copper from iron and zinc. Coextraction of lead reached about 17% at this Acorga concentration value. This could be due to the small concentration of lead in PLS. Taking into account lead/copper concentration ratio in PLS (less than 0.2%) one can neglect this coextraction. Loaded organic phase in these conditions contains 7.47g/L Cu and 5 mg/L Pb.

The rest of the experiments were performed at the extractant concentration of 20 vol%.

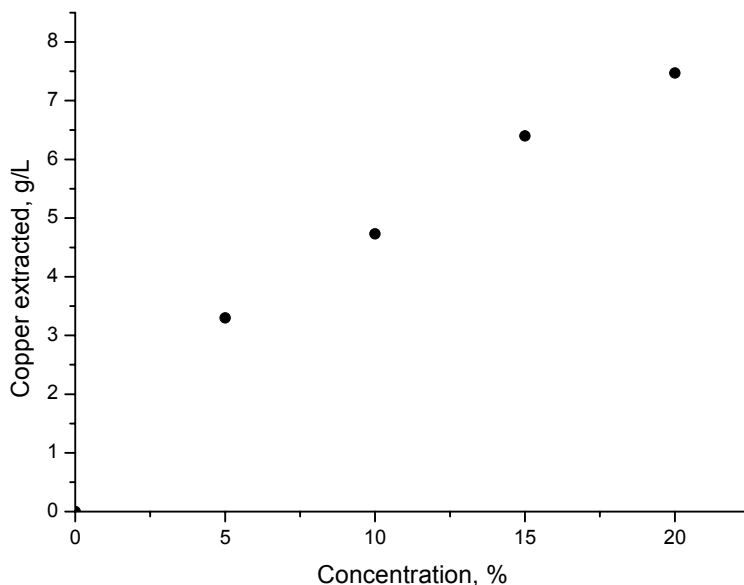


Fig. 1. Effect of concentration of Acorga M5397 on the copper extraction from PLS ($19.3 \text{ g/dm}^3 \text{ Cu}$) at $\text{pH} = 0.6$ and $\varphi_o/\varphi_a = 1/1$

Kinetics of extraction

The results presented in Fig. 2 were obtained at the concentration of the extractant of 20%, ambient temperature, φ_o/φ_a of 1/1, and the contact time varying from 2 to 15 minutes. Extraction reached the equilibrium in 10 minutes. The rate of extraction of copper amounted to about 38%. Iron and zinc remained in aqueous phase confirming the high selectivity of Acorga M5397 toward these elements. Lead was coextracted at the level of 15%.

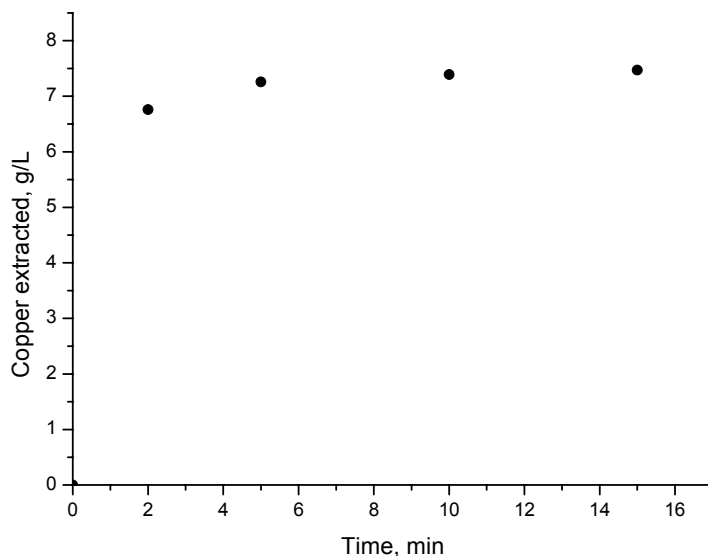


Fig. 2. Kinetics of copper extraction from PLS (19.3 g/L Cu) by Acorga M5397 20% at pH = 0.6 and $\varphi_o/\varphi_a = 1/1$

Effect of Organic/Aqueous ratio

The effect of φ_o/φ_a ratio was studied by varying the φ_o/φ_a from 1/2 to 10/1, with 20% Acorga M5397 (v/v) in Escaid 110, contact time 10 min and pH of 0.6. Results, listed in Table 2, suggest a decrease in copper raffinate with increase of φ_o/φ_a . Coextraction of iron and zinc did not exceed 3%. Coextraction of lead reached 43% for φ_o/φ_a of 10/1.

Table 2. Concentration of metals in raffinate (φ_a) and of Cu in the organic phase (φ_o) during extraction of copper with Acorga M5397 (pH 0.6)

φ_o/φ_a ratio	φ_a in equilibrium				φ_o in equilibrium
	Cu (g/dm ³)	Fe (g/dm ³)	Zn (g/dm ³)	Pb (g/dm ³)	Cu (g/dm ³)
Feed	19.30	18.10	4.50	0.03	
1/2	14.66	18.02	4.42	0.019	9.22
1/1	11.80	18.04	4.50	0.025	7.47
2/1	7.78	18.10	4.33	0.022	5.745
3/1	5.86	18.10	4.48	0.020	4.47
5/1	4.02	17.98	4.46	0.026	3.05
10/1	2.24	17.55	4.37	0.017	1.703

Based on data of Table 2, the McCabe–Thiele copper distribution isotherm (Fig. 3) shows that in such a very acidic solution more than 6 extraction counter-current stages with a φ_o/φ_a of 2/1 are necessary to recover 88% of copper from the PLS.

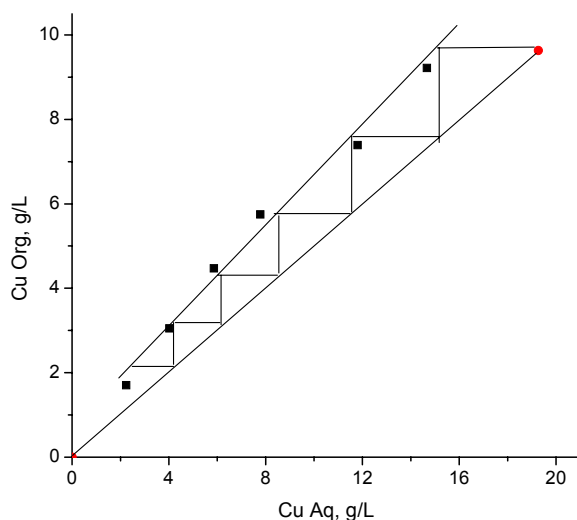
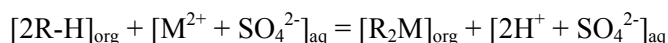


Fig. 3. The McCabe–Thiele diagram for copper extraction from PLS (19.3 g/dm³ Cu) with Acorga M5397 20% at $\phi_o/\phi_a = 2/1$ and pH = 0.6

According to the extraction and re-extraction mechanisms by oximes reagents, given by Rao et al. (2000) and Kitobo et al. (2010), it appears that pH of the solution is one of the most significant parameters controlling the extraction and the re-extraction of the metal ions.



where: M^{2+} – metallic ion in aqueous solution,

$[2R-H]_{\text{org}}$ – extractant dissolved in the organic phase,

$[R_2M]_{\text{org}}$ – charged metal organic complex dissolved in the organic phase.

The extraction coefficient can be determined as:

$$\log E = \log k + 2 \log [HR]_{\text{org}} + 2 \text{pH}$$

where k is the equilibrium constant.

To improve the copper extraction pH of the solution was adjusted to 1.7 by adding of NH_4OH to 28% by volume. This pH adjustment leads to the composition of the solution listed in Table 3. The decrease of Cu, Zn, Fe and Pb in the final solution is due to the formation of a white precipitate (El Amari et al., 2006).

Table 3. Characteristics of aqueous feed solution (PLS) after pH readjustment

	pH	Eh (mV/ENH)	Cu (g/dm ³)	Zn (g/dm ³)	Fe (g/dm ³)	Pb (g/dm ³ L)
PLS	1.7	506	16.28	3.92	16.15	0.027

The effect of φ_o/φ_a ratio on this solution is presented in Table 4. Compared with those obtained in the case of PLS at pH = 0.6, the distribution coefficient of copper was improved, reaching 1.63 with the increase of copper loading capacity of Acorga M5397 by a factor of about 1.4 (for φ_o/φ_a 1/1). Extraction rates of iron and zinc did not change confirming the high selectivity with respect to copper. Extraction of lead reached 15%.

Table 4. Concentration of metals in raffinate (φ_a) and of Cu in organic phase (φ_o) during extraction of copper with Acorga M5397 (pH 1.7)

φ_o/φ_a ratio	φ_a in equilibrium				φ_o in equilibrium
	Cu (g/dm ³)	Fe (g/dm ³)	Zn (g/dm ³)	Pb (g/dm ³ L)	Cu (g/dm ³)
Feed	16.28	16.15	3.92	0.027	
1/2	10.47	15.76	3.87	0.027	11.62
1/1	6.18	16.03	3.92	0.023	10.10
2/1	1.67	16.15	3.92	0.027	7.31
3/1	0.69	16.15	3.92	0.024	5.20
5/1	0.32	16.15	3.92	0.024	3.19
10/1	0.13	15.90	3.92	0.024	1.62

The distribution isotherm, measured under the same conditions of the solution but at pH = 1.7 (Fig. 4) from data of Table 4 shows that one can theoretically exhaust the solution in three counter-current stages by Acorga M5397 20% v/v using φ_o/φ_a of 1.5/1. In two stages 94% of copper could be recovered, the residual content of copper is less than 1 g/dm³.

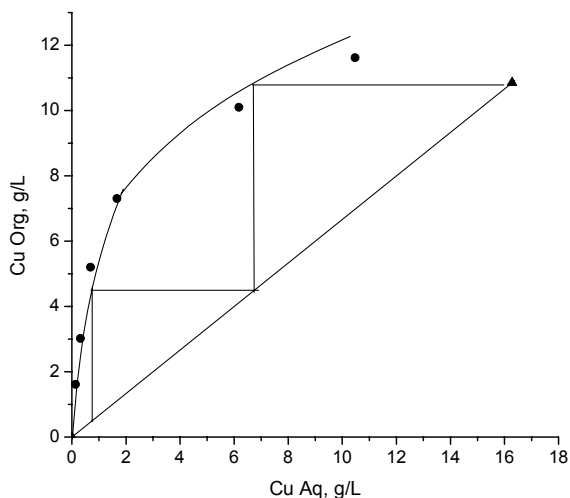


Fig. 4. The McCabe–Thiele diagram for copper extraction from PLS (16.28 g/dm³ Cu) with Acorga M5397 20% at $\varphi_o/\varphi_a = 1.5/1$ and pH = 1.7

Stripping of copper loaded Acorga M5397

Copper stripping was studied on organic phase charged by contact with the aqueous phase at pH of 1.7, $\varphi_o/\varphi_a = 1/1$, 15 minutes of contact time, ambient temperature, atmospheric pressure and 20% Acorga M5397 (v/v) concentration. The loaded organic phase contained 9.74 g/dm³.

At this stage of the study the stripping solution was made of sulphuric acid which is mostly used for the recovery of copper from oximes, and in which the recovery of copper by electrolysis is the conventional technique applied in the hydrometallurgy.

The variable parameters of the study were the concentration of the stripping solution, the kinetics of copper recovery and the φ_o/φ_a volume ratio. The constant parameters were the ambient temperature and the atmospheric pressure.

Tests were carried out with the variable concentration of the fresh sulphuric acid solution (0.5 M to 2 M), $\varphi_o/\varphi_a = 1/1$ and the contact time of 20 minutes. From the results presented in Fig. 5 one can deduce that copper recovery from the organic phase charged with 9.74 g/dm³ is complete only when the concentration of sulphuric acid reaches 2 M. Then, the kinetics of copper recovery was determined by varying the time of contact between 2 and 20 minutes, and fixing φ_o/φ_a to 1/1. Figure 6 highlights relatively fast kinetics for the copper stripping. For an equilibrium time of approximately 10 minutes one re-extracts 98% Cu.

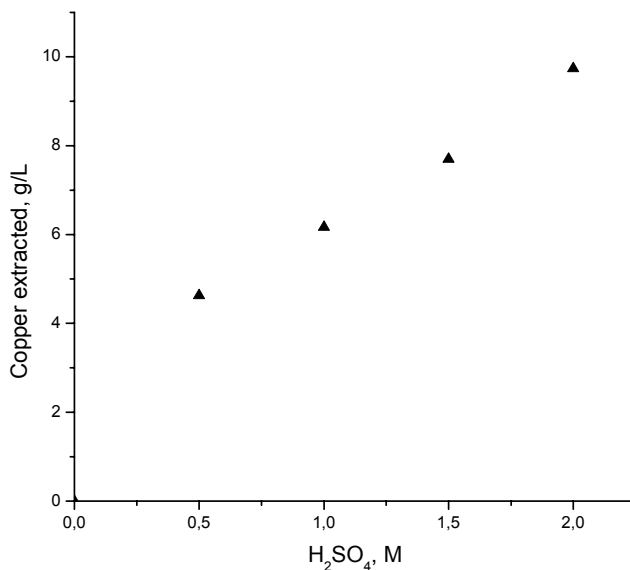


Fig. 5. Effect of H₂SO₄ concentration on copper stripping from loaded organic phase of Acorga M5397 (9.74 g/L Cu), $\varphi_o/\varphi_a = 1$, contact time 20 min

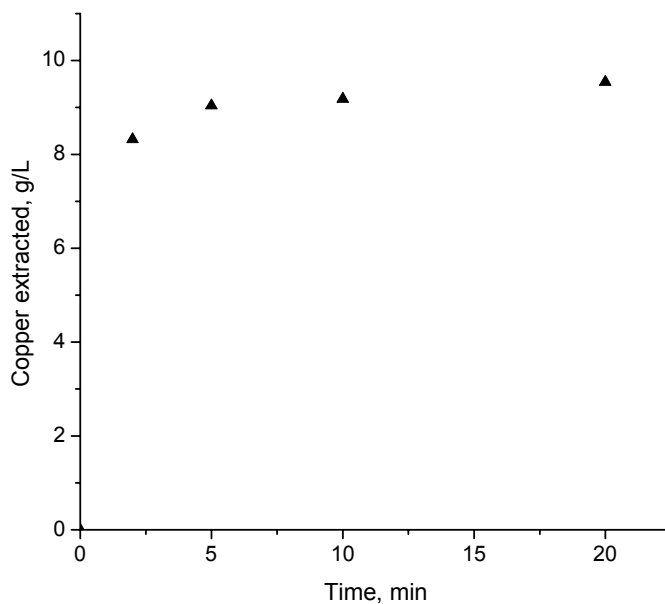


Figure 6. Kinetics of copper stripping from loaded organic phase of Acorga M5397 (9.74 g/dm³ Cu) at $\phi_o/\phi_a = 1$; 2M H₂SO₄

The effect of the variation of ϕ_o/ϕ_a , ranging between 0.5 and 3 was studied by working at a contact time of 10 minutes and 2 M H₂SO₄. Results are presented in Table 5. It can be seen that one can extract in only one contact stage all copper, when the ϕ_o/ϕ_a is between 0.5 and 1/1, with the corresponding copper contents in aqueous solutions attaining 4.88 g/dm³ and 9.75 g/dm³, respectively. With a high ϕ_o/ϕ_a (3/1) one can re-extract only 70% Cu in a single contact stage, but aqueous solution is more enriched in copper (20.42 g/dm³).

Table 5. Concentration of copper in the raffinate (ϕ_a) and in the organic phase (ϕ_o) during stripping with Acorga M5397 (pH 1.7)

ϕ_o/ϕ_a ratio	ϕ_a in equilibrium	ϕ_o in Equilibrium
	Cu (g/ dm ³)	Cu (g/ dm ³)
Feed		9.74
1/2	4.88	0
1/1	9.74	0
2/1	15.32	2.08
3/1	20.42	2.93

The plot of the Mc Cabe–Thiele diagrams (Fig. 7) from the data of Table 5 shows that by operating copper stripping at counter-current with a ϕ_o/ϕ_a of 3/1, total recovery

of copper can theoretically be reached in 3 stages of re-extraction. The obtained aqueous phase contains about 29 g/dm³ Cu.

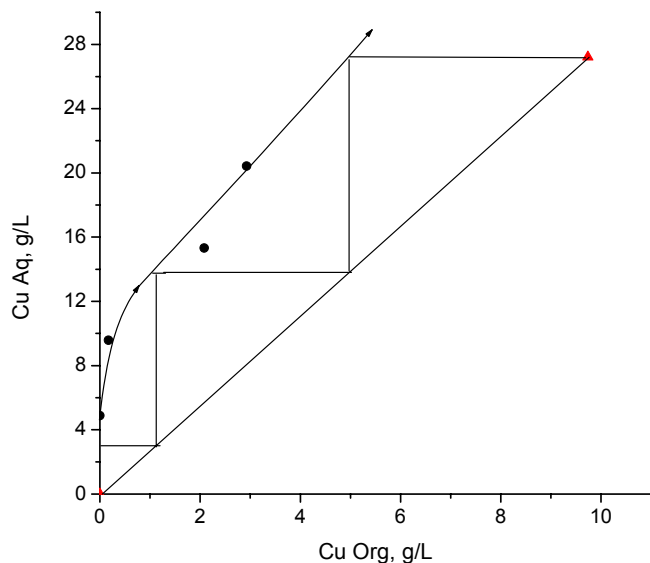


Figure 7. The McCabe–Thiele diagram for copper stripping from loaded organic phase of Acorga M5397 (9.74 g/L Cu) at $\phi_o/\phi_a = 3$

Conclusions

The complexity of the pregnant leach nitro-fluorosilic acid solution, obtained from the Hajar Mine Copper concentrate, is due to the difficulty of dissolving chalcopyrite by conventional agents. The good dissolution rates obtained by this leaching agent are affected by the weak selectivity toward copper (iron, zinc and lead are also leached). Nevertheless, the use of Acorga M5397 to extract selectively copper was effective. Coextraction of lead was noted, but can be neglected taking into account the lead/copper concentration ratio in the PLS (less than 0.2%).

Loading extractant capacity was improved by increasing the pH of the PLS. Compared to LIX 984, which belongs to the same solvent family, and used under the same conditions by El Amari et al. (2006), loading capacity of Acorga M5397 was higher without being less selective.

With pH 0.6, copper exhaustion of the solution by counter-current extraction requires more than 6 stages, whereas with a solution pH of pH 1.7, 94% of initial copper in the PLS could be recovered in only two counter-current extraction stages with Acorga M5397. The total extraction could be achieved in three stages.

The recovery of the copper contained in loaded organic phase Acorga M5397 was easily performed by sulphuric acid solution (2M H₂SO₄), allowing to obtain concentrated copper solution for electrowinning.

Acknowledgements

Authors would like to thank the Reminex Society (ONA; Morocco) for the financial support of this study.

References

- ARBITER N., FLETCHER A.W., 1994, *Copper hydrometallurgy-evolution and milestone*, Mining Engineering, 118–124.
- BLAZY P., JDID E.A., 2002, *Hydrométallurgie du cuivre*. Techniques de l'Ingénieur, M2242, 1–10.
- DALTON R. F., DIAZ G., PRICE R. ZUKEL A.D., 1991, *The cuprex metal extraction process: recovering copper from sulfide ores*. JOM, 51–56.
- DREISINGER D., 2004, *New developments in hydrometallurgical treatment of copper concentrates*. Engineering and Mining Journal, 205, 32–35.
- EL AMARI K., JDID E.A., BLAZY P., BOUHAFID A., EL MERAY M., AKALAY I., 2000, *Acid and Oxidizing Leaching of Chalcopyrite Concentrate by Ferric Sulphate and Fluorosilicic-Nitric Media*. Separation Science and Technology, 35 (13), 2143–2158.
- EL AMARI K., JDID E.A., BLAZY P., 2006, *Copper solvent extraction from chalcopyrite concentrate acid leach solutions by Lix 984*. Journal of Mining and Metallurgy, 42 B (1), 1–11.
- HABASHI F., 2007, *Copper metallurgy at the crossroads*. Journal of Mining and Metallurgy, 43 B, 1–19.
- HELLE S., JEREZ O., KELM U., PINCHEIRA M., VARELA B., 2010, *The influence of rock characteristics on acid leach extraction and re-extraction of Cu-oxide and sulphide minerals*. Minerals engineering, 23, 45–50.
- HENKEL CORPORATION, Private communication.
- INTERNATIONAL COPPER STUDY GROUP, 2010, *The World Copper Factbook*, 1–54.
- KITOBO W., GAYDARDZHIEV S., FRENAY J., BASTIN D., IIUNGA N., 2010, *Separation of copper and zinc by solvent extraction during reprocessing of flotation tailings*. Separation science and Technology, 45, 535–540.
- KOLEINI S.M.; JAVAD; AGHAZADEH VALEH, SANDSTRÖM A., 2011, *Acidic Sulphate Leaching of Chalcopyrite Concentrates in Presence of Pyrite*. Minerals Engineering, 24, 381–386.
- PADILLA R., RODRIGUEZ G., RUIZ M.C., 2010, *Copper and arsenic dissolution from chalcopyrite-enargite concentrate by sulfidation and pressure leaching in H₂SO₄-O₂*. Hydrometallurgy, 100, 152–156.
- PANIGRAHI S., PARHI P.K. NATHSARMA K.C., 2009, *A study on extraction of copper using LIX 84-I and LIX 622N*, Separation and Purification Technology. 70(1), 58–62.
- PRADHAM N., NATHSARMA K.C., SRINIVASA R., 2008, *Heap bioleaching of chalcopyrite: A review*. Minerals Engineering 21 (5), 355–365.
- SRINIVASA RAO K., DEVI N.B., REDDY B.R., 2000, *Solvent extraction of copper from sulphate medium using MOC 45 as extractant*. Hydrometallurgy, 57, 269–275.
- SUTTILL R. K., 1989, *Solvent extraction: a key in maintaining copper production*. EEMJ, 24–27.
- WATLING H.R., 2006, *The bioleaching of sulphide minerals with emphasis on copper sulphides – A review*. Hydrometallurgy, 84, 81–108.
- YOSHINARI B., KATSUTOSHI I., 1988, *Solvent extraction equilibria of copper (II) by carboxylic acids with high acid dissociation constants*. Hydrometallurgy, 21, 203–212.

Received May 16, 2012; reviewed; August 3, 2012

AN ANALYSIS OF EFFECT OF PARTICLE SIZE ON BATCH FLOTATION OF COAL

Marian BROZEK, Anna MLYNARCZYKOWSKA

AGH University of Science and Technology, Faculty of Mining and Geoengineering, Department of Environmental Engineering and Mineral Processing, Al. Mickiewicza 30, 30-065 Kraków, Poland,
tel/fax +48-12-617-21-98, e-mail: brozek@ach.edu.pl, mindziu@agh.edu.pl

Abstract: This paper presents the analysis of the batch flotation with regard to the size of the floated particles with coal as an example. Empirical studies were conducted on samples of bituminous coal from the Jankowice coal mine (33 type in Polish classification). Experimental includes fractional flotation of coal samples with various particle size, the float and sink analysis of flotation products and determination the ash content in each flotation and densimetric fractions. The evaluation of flotational upgrade was based on the partition curve and value of heterogeneity index (standard deviation) with the division into concentrate and tailings as a measure of flotation efficiency. From the partition curve, partition size, which is assumed in flotation as the maximum size of floatable particles under the given physicochemical conditions, was calculated. On the basis of float and sink analyses, it was found that floated particles are particles with hydrophobic properties corresponding to the density (related to the mineral matter content) below 1.6 Mg/m^3 . In this connection, the probability of detachment of a particle from a given particle size fractions, was calculated as a relation between the mass of particles with the density below 1.6 Mg/m^3 in tailings and the mass of particles with this density in the feed. With the increase in particle size, the degree of heterogeneity increases and reaches the maximum value for particle size fractions $0.315\text{--}0.4 \text{ mm}$, then decreases for larger particles. The characteristics of the dependence of the degree of heterogeneity on particle size is analogous as in many flotation processes – the dependence of the flotation rate constant flotation on particle size.

Key words: *flotation, float and sink analysis, probability of detachment, indices flotation processing*

Introduction

Flotation is the most common and widely accepted method of enrichment of fine coal below 0.5 mm and even below 1 mm . This method has been used to enrich several million tones of coking and power coal in Poland.

Coal is a heterogeneous material of two kinds. The petrographic composition and content of mineral matter cause changes in particle hydrophobic properties, and actu-

ally generate their distribution. The organic coal matter has hydrophobic properties, while the degree of hydrophobicity, measured by the contact angle, varies with the maceral composition. The components of the mineral matter, however, are hydrophilic. With the increase in the coverage rate of the particle by the mineral matter, the contact angle, the value of which depends also on the degree of surface roughness and the presence of microcracks, decreases. The relation between volume and surface properties for coal was proved and described with the use of deterministic and stochastic models of batch flotation (Brożek and Młynarczykowska, 2006, 2007, 2009).

The flotometric equation is also known which is based on the balances of forces acting in the three-phase particle-air bubble-liquid system, solved only numerically at the moment of particle detachment. This equation in the form of polynomial of 3rd degree has been presented as a trigonometric function with only one solution. The team of Drzymala (Watanabe et al., 2011) presented the analytical form of an equation, connecting the maximum size of floating particle and its hydrophobicity, expressed as a contact angle.

A significant aspect in flotation upgrading is constituted by the analysis of elementary phenomena occurring at phase boundaries, which have a decisive effect upon the process effectiveness. These problems have been widely described in the literature (Hukki, 1953; Kelsall, 1960; Bogdanov et al., 1964; Laskowski and Iskra, 1970; Woodburn et al., 1971; Bartlett and Mular, 1974; Jiang and Holtham, 1986; Flynn, 1987; Laskowski et al., 1991; Jiang, 1991; Laskowski, 2002; Vianna et al., 2003; Honaker and Ozsever, 2003).

A variable content of useful component, especially in the ores upgraded by flotation, requires deep milling for liberation of the minerals. Flotation comprises very fine particles (from a few to several tens microns) which, in given physicochemical and hydrodynamic conditions, either are able to make up a stable flotation aggregate or are taken by the rotating medium and are mechanically transported into the concentrate. In numerous works concerning both ores and coal the authors are still trying to describe the effect of the finest particles upon upgrading effectiveness, both theoretically and technologically. They are explaining the mechanisms which determine forming of flotation aggregates, simultaneously setting the limits of particle sizes which are subjected to classical flotation (De Bruyn and Modi, 1956; Collins and Jameson, 1976; Trahar and Warren, 1976; Scheludko et al., 1976; Bustamante and Warren, 1983; Crawford and Ralston, 1988; Drzymala, 1994a; 1994b; Malysa, 2000; Miettinen et al., 2010; Kowalczyk et al., 2011; Chipfunhu et al., 2011).

The analysis of the effect of particle size on flotation properties of coal in the batch flotation process is presented in this article.

The use of partition curves for the analysis of enrichment results is a common method of the separation accuracy evaluation and parameters calculated on the basis of those curves are the indicator of separation devices' quality.

Flotation enrichment in a machine with mechanical agitation of flotation pulp, occurs inherently in turbulent conditions (Mika and Fuerstenau, 1968).

Such a regime of separation leads to the phenomenon of particle detachment and transition the rules of useful components to tailings. In connection with this, the separation process is subject to the probability calculus. The statistical character of the separation process is expressed numerically by the partition function and its graphical representation – the partition curve (Tromp's curve), determining the probability of finding a particle with specific properties occurring in a given separation product.

The separation efficiency in industrial practice as said above, is measured by probable error. In flotation conditions the value of probable error depends on factors related to physical and physicochemical properties of particles, flotation machine characteristics and parameters related to the reagent regime in the flotation chamber.

The consequence of particle scattering is consist in their transition to improper products and this fact depends on the relation between forces acting on each particle. These comprise forces facilitating particle detachment from the air bubble and the particle adhesion force to an air bubble.

The partition number (recovery) for particles of the cell product (tailings) is expressed by the following formula:

$$T = \frac{n_k}{n_k + n_p} \quad (1)$$

where: n_k – the number of floatable particles of a narrow size fraction with given flotation properties occurring in the cell product, n_p – the number of particles with given flotation properties occurring in the froth product.

Formula (1) presents a fraction of the total number of floatable particles with given flotation properties which remained in a cell science they were subject to detachment. It may also determine the probability of a particle to occur in the cell product (tailings). This probability is equivalent to the probability of particle detachment from an air bubble, so in the case of flotation the partition number for tailings is the probability of particle detachment from the air bubble.

The analysis of the effect of particle sizes, on flotation properties of coal in the batch flotation process is presented in this article.

Empirical studies were conducted on samples of bituminous coal from the Jankowice coal mine (33 type in Polish classification). They include performing fractional flotation of the raw material samples with various particle size, the float and sink analysis of separation products and determination of the ash content in all density fractions.

The evaluation of the enrichment process was based on the partition curve and the value of heterogeneity index (standard deviation) with the splitting into the concentrate and tailings.

Experimental

Method of samples preparation

The coal sample was crushed in two stages, at first in a jaw crusher and then in a roll crusher to the particle size below 0.63 mm. The purpose of such a method of crushing was to limit the yield of the finest particles, below 0.1 mm, in the crushing product. The obtained crushing product was sieved to obtain the following size fractions: 0.1–0.2 mm, 0.2–0.315 mm, 0.315–0.4 mm, 0.4–0.5 mm and 0.5–0.63 mm. A sample with a wide range of particle sizes of 0.1–0.63 mm was made up from the narrow size fractions and with equal weight yield of respective size fractions in order to determine the degree of independence of the narrow particle size flotation process. The ash content was determined in all samples. Each sample was washed on a screen 0.063 mm before flotation in order to remove fine dust which could have affected the flotation results.

Fractional flotation

Flotation tests were carried out in a Denver type mechanical flotation machine with flotation cell volume of 1 dm³. *n*-hexanol was used as a collecting-frothmaking reagent. It does not change pulp pH but only reduces the surface tension on the gas–liquid phases boundary, increasing at the same time air dispersion in the suspension. Also the adsorption of alcohol occurs on the surface of air bubbles which ensures their stabilization and prevents coalescence (Malysa, 2000; Krzan and Malysa, 2002). A solution with concentration of 0.08 g/dm³ of hexanol was prepared. The solids content of 80 g in 1 dm³ of the flotation suspension, is equivalent to the consumption of the reagent in the amount of 1000 g per 1 Mg of dry feed. Low concentration of flotation pulp was kept because of practical reasons because favourable coal flotation results can be achieved at low pulp density (Sablík, 1998).

A sample with the mass of 80 g was moistened in 1 dm³ of solution in the flotation cell for 15 minutes, with the impeller off. Then the suspension was agitated for 5 minutes without the air inflow to the flotation cell, which facilitated better reagent adsorption on the surface of floated particles. After turning the air inflow on, fractional flotation was conducted, gathering subsequent fractions of the froth product for: 15 s, 15 s, 30 s, 60 s and 60 s. Total flotation time was equal to 180 s (up to white froth). The tailings product comprised the remains in the flotation cell.

Flotation of all six samples was conducted in the same conditions. The ash content was determined in flotation products.

Float and sink analysis of flotation products

All products of fraction flotation were subject to the float and sink analysis in carbon tetrachloride solutions were performed. The liquid maximum density was equal to the density of pure CCl₄, that is 1.60 Mg/m³. Lower values of liquid density; 1.35 and 1.225 Mg/m³, were obtained by dilution with anhydrous ethyl alcohol. The choice of liquid density was conditioned by the mass of the obtained densimetric fractions in

each flotation product, which should be large enough to enable the ash content determination. The lowest particle density was equal to 1.20 Mg/m^3 , because all particles a in the liquid to occur such density. In the fraction with density higher than 1.60 Mg/m^3 , the average density of particles was determined by the pycnometer method, the values of which were given in the brackets. The ash content was determined in all densimetric fractions.

Results and discussion

Flotation kinetics

The fractional flotation results are presented in Table 1, in which the cumulative yields, the ash contents in the fractions and coordinates of the upgrading curve are concentrate grade θ , tailings grade β , recovery combustible and volatile matter in the concentrate ε and ash recovery in tailings ε' (Figs 1–6).

Flotation kinetic curves of the tested size fractions are illustrated in Fig. 7. Their analysis indicates that for all size fractions, apart from the largest size fraction (0.5–0.63 mm), in the time interval from 0 to about 20 s, the flotation kinetics proceeds according to the $\frac{1}{2}$ order kinetics equation (Bogdanov 1959, Brozek and Mlynarczykowska, 2006). With the increase in flotation time, the order of flotation kinetics increases (Pogorelyj, 1962). It can be the sum of orders of kinetics $\frac{1}{2}$ and 1 or $\frac{1}{2}$ and $\frac{3}{2}$. For the size fraction 0.5–0.63 mm, most probably it is a sum of orders of kinetics $\frac{1}{2}$ and $\frac{3}{2}$ in the whole flotation time interval. The $\frac{1}{2}$ order kinetic curve is represented by a sector of parabola. The limit of the derivative of the function of the concentrate yield dependence to time $\gamma_k(t) = R(t)$, for the $\frac{1}{2}$ order kinetics is equal to (Brozek and Mlynarczykowska, 2007):

$$\lim_{t \rightarrow 0} \frac{dR}{dt} = \frac{k}{\sqrt{C_0}} \quad (2)$$

where: R – recovery of flotation, k – flotation rate constant of the $\frac{1}{2}$ order, C_0 – the initial concentration of particles under flotation in the flotation cell, t – time of flotation.

The limit of the derivative, given by equation (2), presents the slope of the flotation kinetics curve at the point $t = 0$. As it can be seen from Fig. 7, the slope of the flotation kinetics of the initial time of flotation decreases with the increase of particle size. Respectively for the constant value of the solids concentration in suspension $C_0 = \text{const}$. ($80 \text{ g/dcm}^3 = 0.074$), with a decreasing slope of the function $R(t)$ at the point $t = 0$, the flotation rate constant for the $\frac{1}{2}$ order kinetics decreases with the increase of particle size.

The exact determination of the kinetics equations, including the flotation of order changes during the process, will be subject to separate discussions and publication.

Table 1. The results of fractional flotation and indices of flotation upgrading

Particle size [mm]	Produkt name	Flotation time [s]	Ash A [%]	$\sum \gamma \downarrow$ [%]	θ [%]	$\sum \gamma \uparrow$ [%]	β [%]	ε' [%]	ε [%]	σ_0 [-]	σ_{th} [-]	σ_0/σ_{th} [-]
0.1–0.63	K1	15	12.40	32.06	12.4	100	37.93	100	45.24	0.237	0.604	0.39
	K2	30	17.01	41.39	13.44	67.94	49.97	89.52	57.72			
	K3	60	19.85	49.90	14.53	58.61	55.22	85.33	68.70			
	K4	120	28.81	57.03	16.32	50.10	61.22	80.88	76.87			
	K5	180	53.66	59.93	18.13	42.97	66.60	75.46	79.04			
	Tailings		67.53	100	37.93	40.07	67.53	71.35	100			
	Feed		100									
0.5–0.63	K1	15	7.99	11.37	7.99	100	33.51	100	15.73	0.161	0.472	0.34
	K2	30	6.91	17.61	7.61	88.63	36.79	97.29	24.47			
	K3	60	10.71	24.36	8.47	82.39	39.05	96.00	33.53			
	K4	120	11.08	31.78	9.08	75.64	41.58	93.85	43.46			
	K5	180	12.22	36.45	9.48	68.22	44.90	91.39	49.62			
	Tailings		47.3	100	33.51	63.55	47.30	89.69	100			
	Feed		100									
0.4–0.5	K1	15	8.17	23.3	8.17	100	42.16	100	36.99	0.273	0.635	0.43
	K2	30	13.01	30.93	9.36	76.70	52.48	95.49	48.47			
	K3	60	16.49	38.97	10.83	69.07	56.84	93.13	60.07			
	K4	120	22.73	45.33	12.50	61.03	62.16	89.99	68.57			
	K5	180	36.25	49.20	14.37	54.67	66.74	86.56	72.84			
	Tailings		69.07	100	42.16	50.80	69.07	83.23	100			
	Feed		100									
0.315–0.4	K1	15	10.47	32.69	10.47	100	40.14	100	48.89	0.287	0.632	0.45
	K2	30	17.67	42.62	12.14	67.31	54.56	91.48	62.55			
	K3	60	20.00	51.64	13.52	57.38	60.94	87.11	74.62			
	K4	120	32.08	58.49	15.69	48.36	68.58	82.61	82.39			
	K5	180	50.58	61.60	17.45	41.51	74.61	77.14	84.96			
	Tailings		76.55	100	40.14	38.40	76.55	73.22	100			
	Feed		100									
0.2–0.315	K1	15	12.60	45.47	12.60	100	37.36	100	63.43	0.260	0.484	0.54
	K2	30	23.84	56.56	14.81	54.53	57.99	84.66	76.92			
	K3	60	31.92	65.85	17.22	43.44	66.71	77.58	87.02			
	K4	120	56.59	72.42	20.79	34.15	76.18	69.64	91.57			
	K5	180	63.86	75.43	22.51	27.58	80.85	59.69	93.30			
	Tailings		82.93	100	37.36	24.57	82.93	54.55	100			
	Feed		100									
0.1–0.2	K1	15	16.46	50.47	16.46	100	36.89	100	66.80	0.245	0.482	0.51
	K2	30	23.38	62.05	17.75	49.53	57.71	77.48	80.87			
	K3	60	31.39	70.46	19.38	37.95	68.18	70.14	90.01			
	K4	120	59.60	77.16	22.87	29.54	78.65	62.99	94.30			
	K5	180	71.51	80.03	24.62	22.84	84.24	52.16	95.59			
	Tailings		86.07	100	36.89	19.97	86.07	46.60	100			
	Feed		100									

To determine the degree of independence of flotation of particles of different sizes, the flotation of the wide size fraction 0.1–0.63 mm was conducted and compared with

the kinetic curve for this particle size reproduced from the sum of curves for narrow size fractions with the weight of 0.2 for each of them. Figure 8 presents both kinetics curves. As it can be seen, the kinetics course is similar and these curves practically overlap. On this basis a conclusion can be drawn that particular particle size fractions float independently from each other.

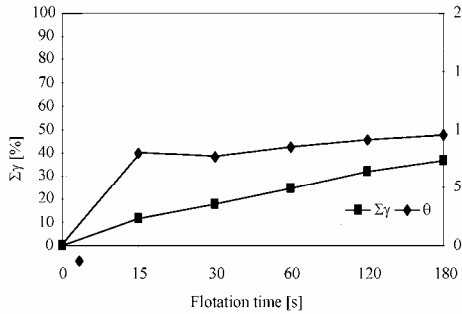


Fig. 1. Flotation yield and ash content in the concentrate in the function of time for particle size 0.5–0.63 mm

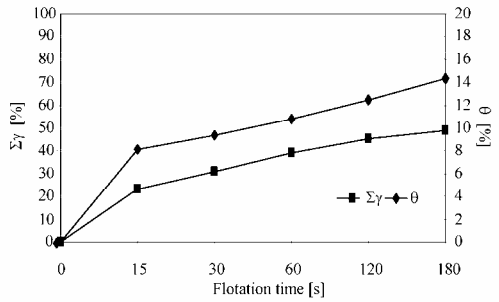


Fig. 2. Flotation yield and ash content in the concentrate in the function of time for particle size 0.4–0.5 mm

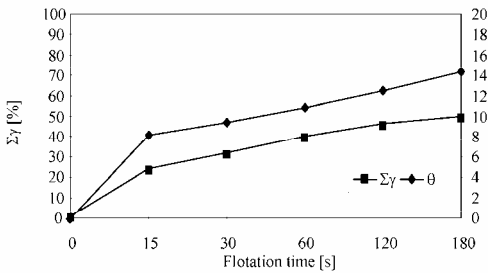


Fig. 3. Flotation yield and ash content in the concentrate in the function of time for particle size 0.4–0.315 mm

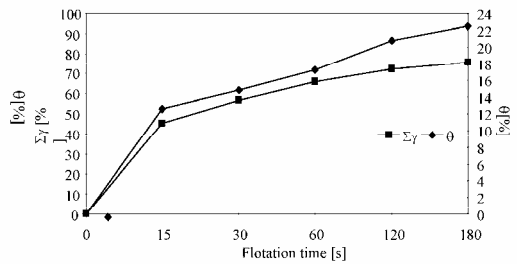


Fig. 4. Flotation yield and ash content in the concentrate in the function of time for particle size 0.2–0.315 mm

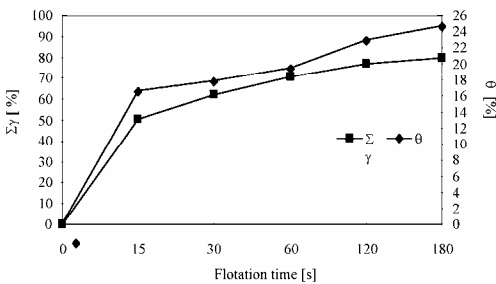


Fig. 5. Flotation yield and ash content in the concentrate in the function of time for particle size 0.1–0.2 mm

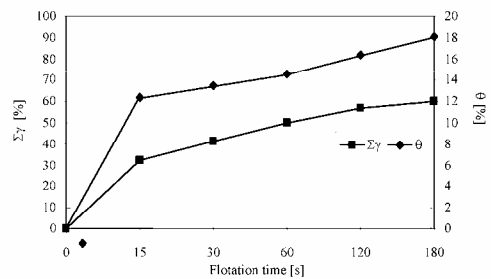


Fig. 6. Flotation yield and ash content in the concentrate in the function of time for particle size 0.1–0.63 mm

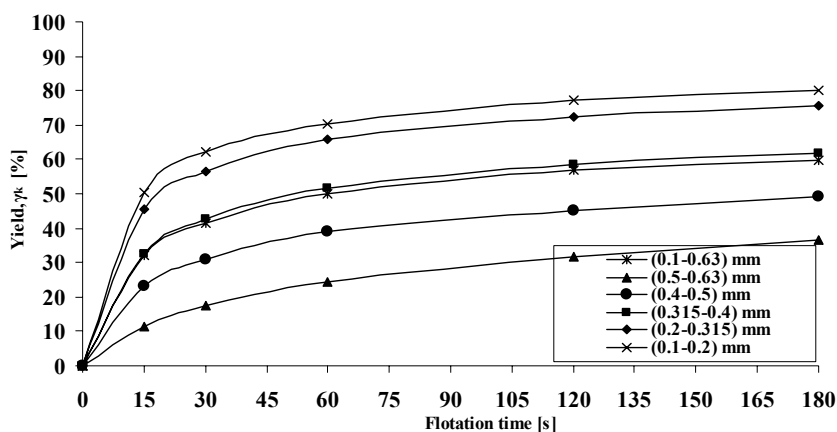


Fig. 7. Flotation kinetic curves of narrow size fractions

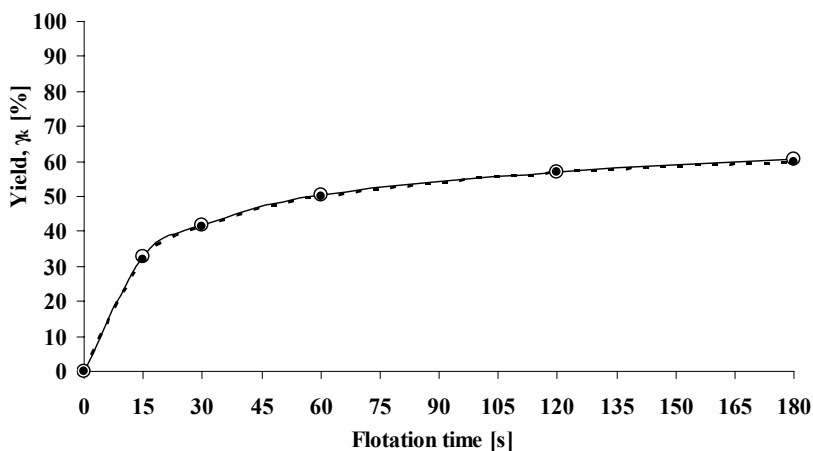


Fig. 8. Comparison of flotation kinetics of wide size fraction and sums of flotation of all narrow size fractions

Float and sink analysis of flotation products

The results of the float and sink analysis of concentrates and tailings of respective size fractions, in the liquid of density 1.6 Mg/m^3 , are presented in Table 2.

The results given in Table 2 will be used to calculate, the probability of particle detachment from an air bubble in the next section.

As it results from the experimental data contained in Figures 9-13, in all cases the ash content in the flotation concentrate is higher than the ash content in the heavy liquid concentrate at the same yield. Differences in ash contents are generally larger for fine grain classes to the disadvantage of flotation. As it will be discussed in the next

part of the paper, it is the result of the phenomenon of floating of hydrophilic particles with the high mineral substance content to the froth product.

Table 2. Results of float and sink analysis in the liquid of density of 1.6 Mg/m³

Size fraction [mm]	Density CC ₁₄ [Mg/m ³]	Products name	Density fraction [Mg/m ³]	Mass [g]
0.5–0.63	1.6	concentrate	< 1.6	50.95
			> 1.6	3.60
		tailings	< 1.6	38.72
			> 1.6	60.93
0.4–0.5	1.6	concentrate	< 1.6	66.05
			> 1.6	7.30
		tailings	< 1.6	8.96
			> 1.6	70.65
0.315–0.4	1.6	concentrate	< 1.6	80.65
			> 1.6	13.41
		tailings	< 1.6	2.09
			> 1.6	57.11
0.2–0.315	1.6	concentrate	< 1.6	87.49
			> 1.6	27.12
		tailings	< 1.6	0.20
			> 1.6	37.27
0.1–0.2	1.6	concentrate	< 1.6	99.77
			> 1.6	18.36
		tailings	< 1.6	0.68
			> 1.6	29.63

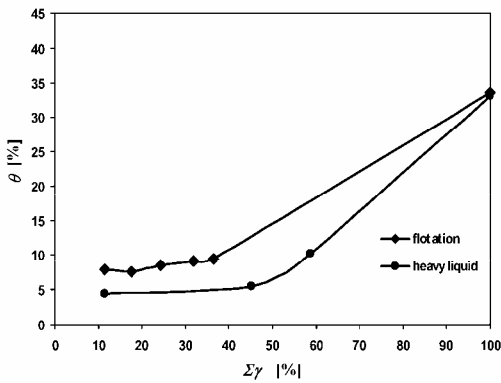


Fig. 9. Ash content in concentrate as a function of yield for particle size 0.5–0.63 mm

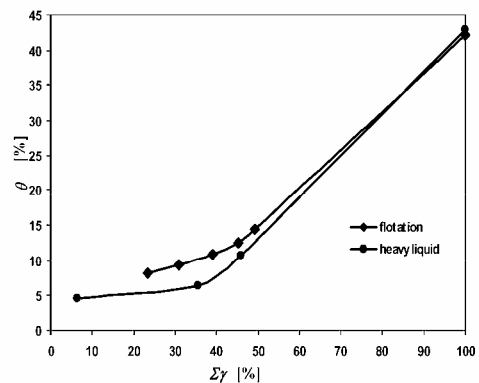


Fig. 10. Ash content in concentrate as a function of yield for particle size 0.4–0.5 mm

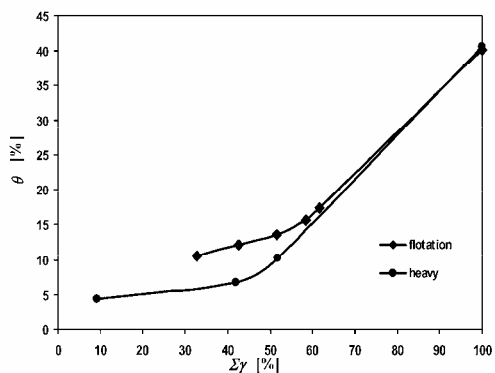


Fig. 9. Ash content in concentrate as a function of yield for particle size 0.315–0.4 mm

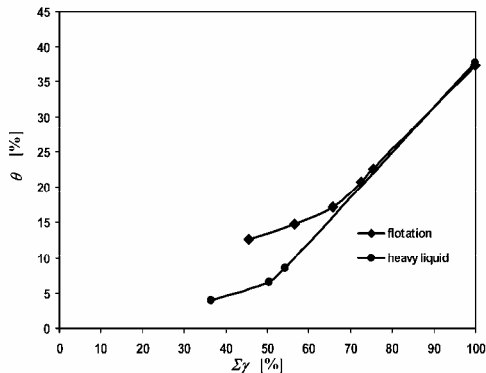


Fig. 10. Ash content in concentrate as a function of yield for particle size 0.2–0.315 mm

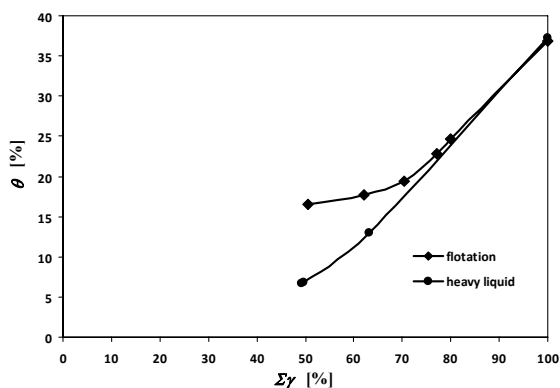


Fig. 13. Ash content in concentrate as a function of yield for particle size 0.1–0.2 mm

Evaluation of flotation

Partition curve

According to the dependence of the flotation rate constant on particle size, the yield of K1 product, as shown in Table 1, after flotation time of 15 s, decreases with the increase in size fraction from the value of 50.47% for the size fraction 0.1–0.2 mm to the value of 11.37% for the size fraction 0.5–0.63 mm.

The concentrate yield after flotation time of 180 s (up to empty froth) decreases with the increase in particle size from the value of 80.03% for the size fraction 0.1–0.2 mm to the value of 36.45 % for the size fraction 0.5–0.63 mm. The decrease in the concentrate yield with the increase in particle size is equivalent to the increase in the tailings yield. The increase in the tailings yield is related to the increase in the probability of particle detachment.

As it result from comes out of the data (Table 2), the flotation tailings of the finest particle size fraction 0.1–0.2 mm, contain merely 0.68 g of fraction with the density below 1.6 Mg/m³, while the concentrate contains 99,77 g. For this reason, it was as-

sumed that floated particles are these with hydrophobic properties corresponding to the density (related to the mineral matter content) below 1.6 Mg/m^3 . It is coal for which the density of particles is connected with the content of mineral matter which can be described by means of ash content. The lower the density of particles, the higher the content of organic coal matter, low ash content and better floatability. The mutual relations of the mentioned features have been described in the following works Brozek (1995a, b, c), Brozek and Mlynarczykowska (2005).

Therefore, the probability of detachment of a particle from a given particle size fraction, according to formula (1), was calculated as a relation between the mass of particles with the density below 1.6 Mg/m^3 in tailings and the mass of particles with this density in the feed. Particle size, being the arithmetic mean of lower and upper limit of the size fraction, was assigned to the probability calculated in this way. The particle size 0.2–0.315 was omitted due to too weak partition for tailings. The detachment probability are as follows:

- for the size fraction 0.1–0.2 mm

$$P_d(0.15 \text{ mm}) = \frac{0.68 \text{ g}}{100.45 \text{ g}} \cdot 100\% = 0.68\% \quad (3a)$$

- for the size fraction 0.315–0.4 mm

$$P_d(0.357 \text{ mm}) = \frac{2.09 \text{ g}}{82.74 \text{ g}} \cdot 100\% = 2.52\% \quad (3b)$$

- for the size fraction 0.4–0.5 mm

$$P_d(0.45 \text{ mm}) = \frac{8.96 \text{ g}}{75.01 \text{ g}} \cdot 100\% = 11.94\% \quad (3c)$$

- for the size fraction 0.5–0.63 mm

$$P_d(0.57 \text{ mm}) = \frac{38.72 \text{ g}}{89.67 \text{ g}} \cdot 100\% = 43.17\% \quad (3d)$$

In Fig. 14, the dependence of detachment probability on particle size and at the same time the partition curve giving the probability for a particle with the density below 1.6 Mg/m^3 of getting to tailings was plotted. The partition size approximated from the partition curve and simultaneously maximum floatable particle size in the physico-chemical conditions in the flotation cell, assumed in this paper, is equal to $d_{50} = 0.58 \text{ mm}$.

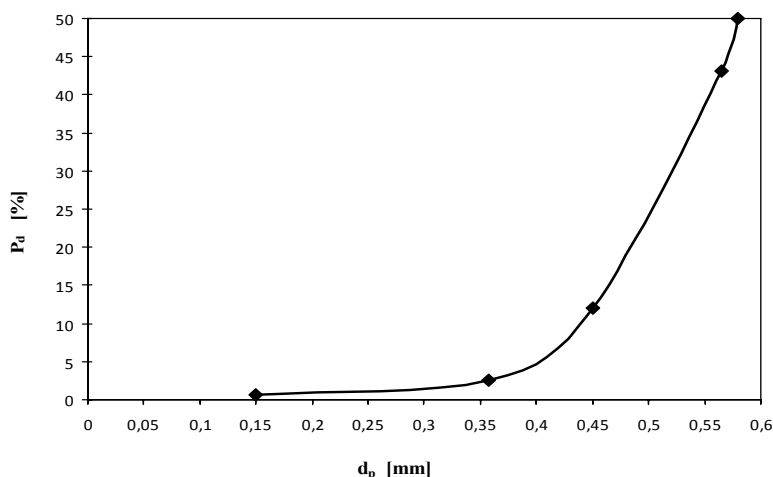


Fig. 14. Dependence of the detachment probability on particle size

Qualitative evaluation of flotation effectiveness

The qualitative data of flotation products are given in Table 1. This is the ash content in respective fractions A , concentrate grade θ , the yield of concentrate $\sum \gamma \downarrow$, recovery of combustible and volatile matter in the concentrate ε , tailings grade β , the yield of tailings $\sum \gamma \uparrow$ and recovery of ash in tailings ε' . On the basis of this data, the following observations can be found. The ash content in tailings decreases with the increase in particle size. It is caused by the fact that particles with the low ash content of the density below 1.6 Mg/m^3 get to tailings as a result of detachment, intensity of which increases with the increase in particle size (as shown in Fig. 14). Also, for this reason the yield of tailings increases with the increase in particle size. With the increase of particle size, the recovery of ash in tailings increases as well. This happens at the expense of a significantly greater increase in the yield of tailings (through the phenomenon of detachment) with the increase of particle size (from 19.97% for the size fraction 0.1–0.2 mm to 63.55% for the size fraction 0.5–0.63 mm, that is the increase by 3.18 times) than the decrease in the ash content with the increase in particle size (from 86.07% for the size fraction 0.1–0.2 mm to 47.30 for the size fraction 0.5–0.63 mm, that is the decrease by 1.8 times). This is, with the increase in particle size, tailings with relatively low, in comparison to the feed, the ash content (upgrade ratio $\beta/\alpha = 1.4$ for the size fraction 0.5–0.63 mm) but with high yield are obtained. On the other hand, for the finest particle fraction, tailings with the high ash content (upgrade ratio $\beta/\alpha = 2.33$) and low yield are obtained. Such a situation causes the increase in the combustible and volatile matter loss in tailings with the increase in particle size from 4.61% for the size fraction 0.1–0.2 mm to 50.38% for the size fraction 0.5–0.63 mm. As shown in Table 1, with the increase in particle size, the yield of the concentrate decreases as well as the ash content decreases in the concentrate. The decrease in the yield is re-

lated to the phenomenon of low-ash particles' detachment, which get to tailings and increase the loss of combustible and volatile matter in tailings. On the other hand, the decrease of the concentrate grade with the increase of particle size or, the other way round, the increase of the concentrate grade with the decrease of particle size is the result of entrainment, called mechanical flotation of gangue particles (hydrophilic particles) to the concentrate (Konopacka, 2005). The intensity of this phenomenon increases with the decrease in floated particle size as well as with the increase in flotation rate. Mechanical flotation causes deterioration of the concentrate quality and increase in ash remnants in the concentrate at decreasing the floated particle size from 10.31 % for the size fraction 0.5–0.63 mm to 54.40% for the size fraction 0.1–0.2 mm. To sum up, it can be said that the phenomenon of detachment concerns larger particles and causes the loss in combustible and volatile matter in tailings; on the other hand, the phenomenon of entrainment, characteristic of smaller particles, increases ash remnants in the coal concentrate. Both phenomena decrease the flotation effectiveness.

For determining the optimum enriched particle size, because of the phenomena of large particles detachment and entrainment of fine particles, on the basis of the results given in Table 1, the degree of heterogeneity was calculated for flotation of particular size fractions with splitting into the concentrate and tailings. The degree of heterogeneity can be the measure of differentiation of a certain feature or the component content (characteristic of a given raw material) in the separation products. With the splitting into the concentrate and tailings, the degree of heterogeneity is expressed by the following formula (Stepinski 1964):

$$\sigma_a = \sqrt{\gamma_k(\theta - \alpha)^2 + (1 - \gamma_k)(\beta - \alpha)^2} \quad (4)$$

where: γ_k – the yield of the concentrate, α – feed grade, θ – the concentrate grade, β – the tailings grade.

From the mathematical point of view, this is the standard deviation of a random variable, such as the ash content in the case of coal. The larger value of the heterogeneity index, the more diverse the separation products, i.e. the better separation. With the accurate separation, the ash content in the concentrate and tailings, respectively, are equal to: $\theta = 0$ and $\beta = 1$.

In this case the degree of heterogeneity is as follows:

$$\sigma_a = \sqrt{\beta^2 + \alpha^2 - 2\beta\alpha - \gamma_k\beta^2 + 2\beta\alpha\gamma_k} \quad (5)$$

On the basis of the balance equation

$$\alpha = \gamma_k\theta + (1 - \gamma_k)\beta \quad (6)$$

for the ideal separation $\alpha = (1 - \gamma_k) = \gamma_o$ and $\gamma_k = (1 - \alpha)$ the degree of heterogeneity has the maximum value and is equal to:

$$\sigma_{th} = \sqrt{\alpha - \alpha^2}. \quad (7)$$

With the lack of separation $\theta = \alpha$ and $\beta = \alpha$ and from the formula (4) it follows that $\sigma_a = 0$.

On the basis of flotation results given in Table 1, the real σ_0 and theoretical σ_{th} degree of heterogeneity and the relation of those values σ_a / σ_{th} as a measure of flotation efficiency. The calculation results are included in Table 1. With the increase in particle size, the degree of heterogeneity increases and reaches the maximum value for particle fractions 0.315–0.4 mm, and then it decreases for larger particles. The characteristics of the dependence of the degree of heterogeneity on particle size is analogous with many flotation processes – the dependence of the flotation rate constant on particle size.

A similar tendency is demonstrated by the dependence of flotation efficiency on particle size. The relation σ_a / σ_{th} has the maximum value for particles from the fraction 0.2–0.315 mm. Thus, it can be said that within this particle size interval, because of the low probability of detachment, there is low scattering of hydrophobic particles to tailings.

Conclusions

1. From the comparison of flotation kinetics of wide particle fractions to kinetics obtained from the sum of kinetic curves for narrow size fraction, with appropriate weights, it appears that particles with different sizes float independently from each other. Knowing the particle size distribution of the feed and flotation kinetics of each size fractions, the flotation course of the feed can be forecast.
2. The ash content in tailings decreases with the increase in particle size. It is caused by the fact that particles with the low ash content with the density below 1.6 Mg/m³ get to tailings as a result of detachment, intensity of which increases with the increase in particle size. This causes the increase in the loss of combustible and volatile matter in tailings with the increase in particle size.
3. The yield of the concentrate decreases with the increase in particle size. The decrease in the yield is related to the phenomenon of detachment of low-ash particles, which get to tailings increasing by this the loss of combustible and volatile matter in tailings.
4. The ash content increases in the concentrate with the decrease in particle size. It is related to the effect of entrainment of gangue (hydrophilic particles) to the concentrate. The intensity of this phenomenon increases with the decrease in floated particle size as well as with the increase in the flotation rate. This causes the increase in ash remnants in the concentrate.
5. To sum up, it can be said that the phenomenon of detachment concerns larger particles and causes the increase in the loss of combustible and volatile matter in tailings; nevertheless, the phenomenon of mechanical flotation, characteristic of

smaller particles, increases ash remnants in the coal concentrate. Both phenomena decrease the flotation effectiveness.

6. The degree of heterogeneity increases with the increase in particle size and reaches the maximum value for particles of the size fraction 0.315 – 0.4 mm, then decreases for larger particles. The characteristics of the dependence of the degree of heterogeneity on particle size is analogous as in many flotation processes – the dependence of the flotation rate constant on particle size.

Acknowledgements

The paper has been supported by the statutory project No 11.11.100.276

References

- BARTLETT D.R., MULAR A.L., 1974, *Dependence of flotation rate on particle size and fractional mineral content*. Int. J. Miner. Proces., 1, 277–286.
- BOGDANOV O.S., HAINMAN V.J., MAXIMOV I.I., 1964, *On certain physical – mechanical factors determining the rate of flotation*. Proc. VII IMPC, New York, Gordon & Breach, 169–174.
- BUSTAMANTE H., WARREN L.J., 1983, *Relation between the relative density of composite coaly grain and their flotation recovery*. Int. J. Miner. Process., 10, 95–111.
- BROŽEK M., MLYNARCZYKOWSKA A., 2005, *Distribution of adhesion rate constant in the coal sample*. Acta Metallurgica Slovaca; ISSN 1335–1532.
- BROŽEK M., MLYNARCZYKOWSKA A., 2006, *Application of the stochastic model for analysis of flotation kinetics with coal as an example*. Physicochemical Problems of Mineral Processing, 40, 31–44.
- BROŽEK M., MLYNARCZYKOWSKA A., 2006, *Analysis of kinetics models of batch flotation*. Physicochemical Problems of Mineral Processing., 41, 51–65.
- BROŽEK M., MLYNARCZYKOWSKA A., 2009. *Kinetic flotation*. Wyd. IGSMiE PAN, Cracow.
- CHIPFUNHU D., MASSIMILIANO Z., STEPHEN G., 2011, *The dependency of the critical contact angle for flotation on particle size – Modelling the limits of fine particle flotation*. Minerals Engineering 24, 50–57
- COLLINS G.L., JAMESON G.J., 1976, *Experiment on the flotation of fine particles. The influence of particle size and change*. Chem. Eng. Sci., 31, 985–991.
- CRAWFORD R., RALSTON J., 1988. *The influence of particle size and contact angle in mineral flotation*. Int. J. Miner. Process., 23, 1–24
- DE BRUYN P.L., MODI H.J., 1956. *Particle size and flotation rate of quartz*. Trans. AIME, 205, 415–419.
- DRZYMAŁA J., 1994a. *Characterization of materials by Hallimond tube flotation. Part 1: maximum size of entrained particles*. Int. J. Miner. Process., 42, 139–152.
- DRZYMAŁA J., 1994b. *Characterization of materials by Hallimond tube flotation. Part 2: maximum size of floating particles and contact angle*. Int. J. Miner. Process., 42, 153–167.
- FLYNN S.A., 1987. *A froth ultra-fine model for the selective separation of coal from mineral in a dispersed air flotation cell*. Pow. Techn., 49, 127–142
- HONAKER R.Q., OZSEVER A.V., 2003. *Evaluation of the selective detachment process in flotation froth*. Minerals Engineering, 16, 975–982
- HUKKI R.T., 1953, *measurement and evaluation of the rate of flotation as a function of particle size*. Trans. AIME, 196, 1122–1123.

- JIANG Z.W., HOLTHAM P.N., 1986. *Theoretical model of collision between particles and bubbles*. Trans. IMM, 95, 187–194.
- JIANG Z.W., 1991. *Modelling of flotation process by quantitative analysis of the collision and adhesion between particles and bubbles*. Proc. XVII IMPC, Dreseden, vol. 2, 429–440.
- KELSALL D.F., 1960. *Application of probability in the assessment of flotation system*. Trans. IMM, 70, 191–204
- KONOPACKA Ż., 2005. *Mechanical flotation*. Publishing House of Technical University of Wrocław, Wrocław
- KOWALCZUK P. B., SAHBAZ O., DRZYMALA J., 2011, *Maximum size of floating particles in different flotation cells*. Minerals Engineering, 24 8, 766–771
- KRZAN M., MAŁYSA K., 2002, *Profiles of local velocities of bubbles in n-butanol, n-hexanol, n-nonanol solution*. Coll. Surfaces. A: Physicochemical and Engineering Aspects, 207, 279–291.
- LASKOWSKI J., ISKRA J., 1970. *Role of capillary effects in bubble-particle collision in flotation*. Trans. IMM, 79, 6–10.
- LASKOWSKI J.S., XU Z, YOON R.H., 1991. *Energy barrier in particle-to-bubble attachment and its effect on flotation kinetics*. Proc. XVII IMPC, Dresden, vol. 2, 237–249.
- LASKOWSKI J.S., 2002. *Fundamental and engineering aspects of coal surface heterogeneity*. Proc. XIV ICPC, Johannesburg, 265–271.
- MAŁYSA E., 2000, *Floatability of coals as a function of surfactant activity of the alcohols*. Gospodarka Surowcami Mineralnymi, 16, 45–54.
- MIETTINEN T., RALSTON J., FORNASIERO D., 2010, *The limits of fine particle flotation*, Minerals Engineering 23, 420–437.
- SABLIK J., 1998, *Flotacja węgla kamiennych*. Główny Instytut Górnictwa. Katowice, Poland.
- MIKA T., FUERSTENAU D.W., 1968. *Pogorelyj microscopic model of the flotation process*. Proc. VIII IMPC, Leningrad, vol. II, 246–269.
- SCHELDUDKO A., TOSHEV B.V., BOJADJIEV D.T., 1976. *Attachment of particles to a liquid surface capillary theory of flotation*. Journal of the Chemical Society, Faraday Transactions 1: Physical Chemistry in Condensed Phases 72, 2815–2828.;
- SCHULZE H.J., 1977. *New theoretical and experimental investigations on stability of bubble particle aggregates in flotation: a theory on the upper particle size of floatability*. Int. J. Miner. Process., 4, 241–259.
- SCHULZE H.J., 1992. *Interface actions in mineral processes*. Aufbereitungs Technik, 33, 434–443.
- STĘPIŃSKI W., 1964. *Gravitational processing*. PWN Warsaw.
- TRAHAR W.J., WARREN L.J., 1976. *The floatability of very fine particles – a review*. Int. J. Miner. Process., 3, 103–131.
- WATANABE M., KOWALCZUK P. B., DRZYMALA J., 2011. *Analytical solution of equation relating maximum size of floating particles and its hydrophobicity*. Physicochemical Problems of Mineral Processing, 46, 13–20
- WOODBURN E.T., KING R.P., COLBORN R.P., 1971, *The effect of particle size distribution on the performance of a phosphate flotation process*. Metall. Trans., 2, 3163–3174.
- VIANNA S.M., FRANZIDIS J.P., MANLAPING E.V., SILVESTER E.S., FU PING-HAO, 2003, *The influence of particle size and collector coverage on the floatability of galena particles in a natural ore*. Proc. XXII IMPC, Cape Town 2003, 816–826.

Received July 1, 2012; reviewed; accepted August 10, 2012

SOLVENT EXTRACTION OF COPPER(II) FROM CONCENTRATED LEACH LIQUORS

Katarzyna OCHROMOWICZ, Tomasz CHMIELEWSKI

Wroclaw University of Technology, Faculty of Chemistry, Division of Chemical Metallurgy
Wybrzeze Wyspianskiego 27, 50-370 Wroclaw, Poland, e-mail:tomasz.chmielewski@pwr.wroc.pl

Abstract: Hydrometallurgical treatment of complex copper sulfidic ores, by-products and concentrates requires aggressive, oxidative leaching methods and application of Fe(III) ions and oxygen or bacteria assisted environment. Leach liquors generated in the process are usually copper and iron-rich solutions of high acidity. Such conditions require the application of suitably strong and selective reagent to extract copper in SX operations. This paper discusses the copper extraction behavior of commercial copper reagents: LIX 984N, LIX 612N-LV and Acorga M5640. Aqueous feed solutions used in SX studies were PLS' generated in atmospheric leaching of commercial flotation concentrate, produced at Lubin Concentrator (KGHM). McCabe-Thiele diagrams were generated and copper net transfer values were compared and discussed. It was shown that stronger modified aldoxime reagents (Acorga, LIX 612) are superior over non-modified salicylaldoxime/ketoxime mixture (LIX 984N). Particularly, the ester modified Acorga M5640 showed advantages in recovery and copper net transfer values.

Keywords: *copper ore, hydrometallurgy, separation, Acorga, LIX*

Introduction

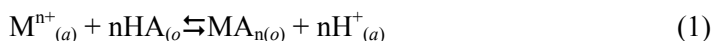
Solvent extraction (SX) has been recognized as a one of the most important separation techniques for metals in solutions. The technology is increasingly being used in hydrometallurgy to separate, purify and concentrate metals such as nickel, cobalt, copper, zinc, uranium and rare earths. In the meantime a considerable amount of work has been carried out and reported (Szymanowski, 1993; Habashi, 1999; Ritcey, 2006; Flett, 2005; Apostoluk et al., 2009). A number of plants have been designed and operated to extract copper from leach solutions of various composition. Until recently typical pregnant leach solutions (PLS) contained from 0.5 to 4 g/dm³ Cu. Such leach liquors are usually generated in heap and dump leaching of copper oxide ores or by-products, which are readily leached under ambient conditions.

In recent years, there has been a considerable development of hydrometallurgical processes for copper extraction applying SX combined with electrowinning (EW) for the production of high-grade electrolytic copper. As a result, more than 20% of world copper production is currently produced from heap leaching–SX operations of oxide copper ores. The low capital and operating costs of SX plants together with the easy operation and the production of top quality electrolytic metals close to the mine site make the economics of the SX processes very attractive, being suitable and feasible in the range of small to medium capacities, where conventional smelting process is not applicable.

Copper flotation sulfide concentrates are mainly processed by means of smelting, converting and electrorefining, the unit operations that have dominated the World copper industry for technical and economic reasons. Research and development for hydrometallurgical alternatives to traditional pyrometallurgical processes has remarkably intensified in the recent years. A wide range of chemical and biological processes for copper recovery from concentrates has been developed (Dreisinger, 2006; Gupta, 1990; Habashi, 1999; 2005; 2007; Jansen and Taylor, 2000; Marsden, 2007; Peacey et al., 2003; Ramahadran et al., 2007). These processes appeared to be successful in leaching of copper from polymineral and chalcopyrite concentrates, purifying the leach solutions (PLS) using modern separation processes, mainly solvent extraction, and recovering a high value, high purity copper metal product. Chmielewski (2012) discussed the possible role of hydrometallurgy in more effective processing of poly-metallic concentrates or by-products from Polish copper industry.

In the past ten years, a great deal of attention has been paid to development of hydrometallurgical treatment of complex copper sulfidic ores, by-products and concentrates (Hyvärinen and Hämäläinen, 2005; Dreisinger, 2006). This type of material requires more aggressive, oxidative leaching methods and application of Fe(III) ions and oxygen or bacteria assisted environment. Higher grades of solids are employed in the leaching operations resulting in more concentrated leach liquors with higher metal content than those produced in heap leaching. Usually leaching of sulfide concentrates is realized with the use of iron(III) salts and sulfuric acid as a leaching medium. Leach liquors generated in the process can contain from 20 to 80 g Cu/dm³, from 0 to 30 g Fe/dm³ and other metal values which have to be sequentially recovered (Kordosky, 2002). Moreover, the acidity of leach liquors changes in the pH range from below 1 to around 2.

According to Eq. (1)



the extraction reaction of metal cations M^{n+} by extractant HA is reversible towards hydrogen ions. It means that for each mole of copper extracted, the raffinate acidity is increased by one mole. In solutions where copper concentrations can be in excess of 40 g/dm³ a significant amount of acid is generated to the raffinate. This in turn can shift the equilibrium towards stripping reaction. A solution is to use a stronger copper

extractant, which will be able to extract copper at higher acidity, but which in turn requires more acid to be stripped. One can also increase the concentration of extractant in order to extract more copper. This can in turn result in more viscous organic phases, particularly the loaded organic, leading to poorer phase separation performance with increased entrainment losses, and increased impurity transfer to the strip side. One can also operate at a higher organic to aqueous phase ratio (O/A). The choice of parameters depends on how high the copper concentration is and what else is in the ore or in the feed (Molnar and Verbaan, 2003).

Presented paper discusses the copper extraction behavior of commercial copper reagents with copper sulfide concentrate leach solutions. The performance of LIX 984N, LIX 612N-LV and Acorga M5640 in Escaid 100 diluent were investigated. McCabe–Thiele diagrams were generated, copper net transfer values were compared and discussed.

Experimental

Reagents and solutions

Aqueous feed solutions used in SX studies were PLS' generated in atmospheric leaching of commercial flotation concentrate, produced at Lubin Concentrator (KGHM). Leaching with sulfuric acid solution resulted in a leach liquors (PLS) containing 25–27 g/dm³ Cu, ~30 g/dm³ total Fe, 1.4–1.9 g/dm³ Zn, 0.06–0.1 g/dm³ Co and 0.02–0.03 g/dm³ Ni. The solution was highly acidic, H₂SO₄ concentration varied between 20 and 30 g/dm³.

LIX[®]984N and LIX[®]612N-LV, applied in SX laboratory tests, were manufactured by Cognis and supplied by Cognis Ireland Ltd., Acorga M5640 were manufactured by Cytec Canada Inc. and supplied by Cytec Netherlands. LIX[®]984N was a mixture of oximes: 5-nonylsalicylaldoxime and 2-hydroxy-5-nonylacetophenone oxime. LIX[®]612N-LV was a proprietary mixture of 2-hydroxy-5-nonylbenzaldehyde oxime and a high flash point hydrocarbon diluents with low viscosity. The active substance of Acorga M5640 reagent is 5-nonylsalicylaldoxime and a fatty ester 2,4,4-trimethyl-1,3-pentanediol diisobutyrate (modifier).

Escaid[®]100, used as a diluent, was supplied by Exxon Mobil Chemical. This is kerosene type diluent containing 19% of aromatic compounds. In copper extraction systems alky-aromatic diluents, containing below 20% of aromatics are preferred because of better solubility of formed complexes. Moreover, in some cases when such diluents are used the modifier content may be reduced or even eliminated.

Analytical methods

The aqueous solutions were analyzed for metals concentration by AAS using a Varian SpectrAA 20Plus. The free acid content in the leaching solution was determined by the titration method with pH control. The concentration of copper in organic phase was

calculated from a difference between its initial concentration in PLS and its concentration in raffinate at fixed O/A phase ratios. Measurements of the pH were carried out with Elmetron CX-731 pH-meter using a Hydromet glass electrode.

Results and discussion

Aqueous phase pretreatment

Leaching of sulfide flotation concentrates from Lubin Concentrator with oxygenated ferric sulfate solutions acidified with sulfuric acid results in highly acidic pregnant leach solutions. Therefore, neutralization of the acid before copper extraction is required, considering lowering extraction efficiency with increase in acidity of the aqueous PLS phase. It is preferable to neutralize feed solution and start extraction at pH 1.5–2, depending on the applied extractant.

Table 1. Composition of PLS and SX feed solutions after neutralization with dry/wet flotation concentrate

Feed composition	Cu g/dm ³	Fe g/dm ³	Zn g/dm ³	Co mg/dm ³	Ni mg/dm ³	pH	volume cm ³
PLS	26.9	30.7	1.81	98.0	21.9	0.3	1000
PLS I neutr (dry)	35.2	28.4	1.67	95.0	21.9	2.4	750
PLS	24.8	24.2	1.43	31.5	28.5	0.6	1000
PLS II neutr (wet)	26.0	23.8	2.04	29.0	26.3	2.2	1030

Flotation concentrates (dry or wet) of known moisture and carbonates (Ca, Mg) content were used for initial aqueous phase neutralization. In the first case, material was dried in laboratory dryer at 105°C for 24 h. Then, the small portions of dried solids were added to the pregnant leach solution and pH was measured. After stabilization of pH next portion was added until pH 2 was reached. Similarly, the neutralization of PLS with wet concentrate was realized. The content of aqueous phases before and after neutralization with dry/wet concentrate is given in Table 1.

After neutralization with dry concentrate one can observe increase in copper concentration. This is partially due to Cu leaching taking place during this step and partially because of solution losses in the filtration step. One can also notice the increase of copper and zinc concentrations in PLS after neutralization with wet concentrate, which was probably due to leaching of the material. The pre-neutralized leach solutions were used as feed solutions in solvent extraction step.

Extraction

All extraction agents were used as received by diluting them to the desired concentration with Escald100 diluent. The extraction data were obtained by vigorously contacting barren organic and aqueous at various A/O phase ratio in laboratory shaker for 5

min at 25°C. After the phases separated, the copper(II) concentration in the aqueous phase was determined by AAS using standard methods.

The effect of extractant type on Cu-SX

Significant copper(II) concentrations in SX aqueous feed solutions enforce the application of organic phases containing high extractant concentrations. For this reason 30%(v/v) extractant solutions in Escaid 100 were used as an organic phase in all SX experiments. In the first place, extraction isotherms were generated for Cognis reagents. Based on the obtained results McCabe-Thiele diagrams were constructed and are presented in Fig. 1. Data on copper net transfer in organic are plotted as a function of overall O/A ratio in Fig. 2 for PLS I. The net transfer per unit of extractant is the g/L of solute removed from the aqueous feed per % extractant.

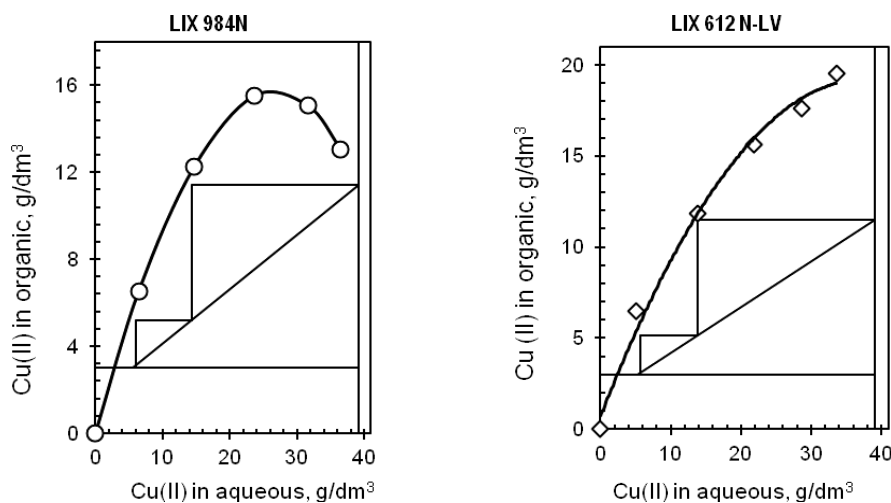


Fig. 1. The McCabe-Thiele diagram for 30 vol% of LIX 984 N and LIX 612 N-LV in Escaid 100, feed: PLS I, pH 2.2, O/A 4.0

From the results presented in Fig. 1 it is seen that in both cases about 86% of copper was extracted after two extraction steps at O/A ratio exceeding 4. Under virtually identical conditions raffinates with copper concentration of 5.5 and 5.2 g/dm³ can be obtained for LIX 984N and LIX 612N-LV, respectively. However, the equilibrium curve obtained for LIX 984 N is not as smooth as that generated for LIX 612. This is probably due to impurity (Fe) that is co-extracted with copper resulting in decreasing loading of Cu. Moreover, the organic phase containing LIX 612N-LV can be loaded up to 20 g Cu/dm³, whereas the other phase can only reach level of 16 g Cu/dm³. Thus, LIX 612 have greater extraction capacity what is an advantage over LIX 984N. Only very slight difference in copper net transfer values can be observed between investigated extractants (Fig. 2).The presented comparison of copper net transfer for LIX 612 and LIX 984 N shows decreasing copper loading capacity with increasing O/A ratios.

Better performance of LIX 612 can be explained by the fact that this reagent is modified with additives ensuring low viscosity of organic phase, thus guaranteeing better extraction and stripping efficiency comparing to regular extractants. For this reason, LIX 612N-LV was selected for further comparison with Cytec reagent – Acorga M5640.

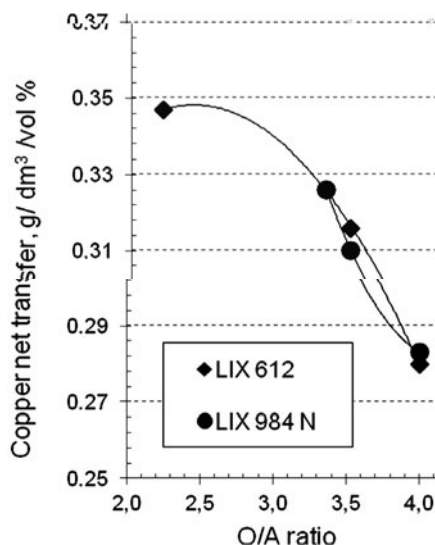


Fig. 2. Copper net transfer in organic phase at 30 vol % of reagent as a function of overall extraction O/A ratio, PLS I

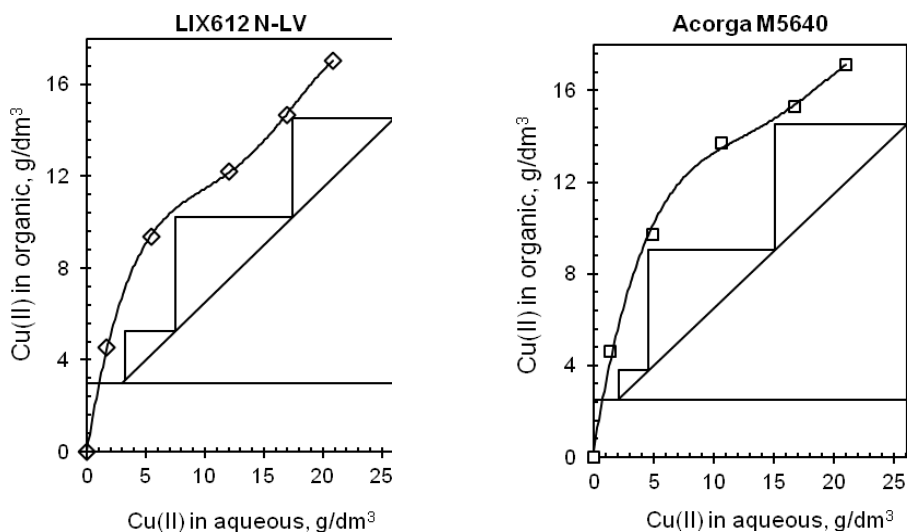


Fig. 3. The McCabe–Thiele diagram for 30 vol% of LIX 612 N-LV and Acorga M5640 in Escaid 100, feed: PLS II, pH 2.0, O/A 2.0

In subsequent experiments the extraction behavior of LIX 612 N-LV was compared with Acorga M5640 reagent. Pregnant leach solution pre-neutralized with wet flotation concentrate was contacted with 30% (v/v) solutions of extractants at various phase ratios. The obtained extraction isotherms are presented in Fig. 3. Data on copper net transfer in organic is plotted as a function of overall O/A ratio for PLS II (Fig. 4).

The obtained results show that it is possible to remove about 88% and about 92% of Cu(II) from PLS with the use of LIX 612 and Acorga M5640, respectively. In both cases three extraction stages at an excess of organic phase of 2 are required. However, in the case of Cytec extractant lower raffinate can be obtained (2 g/dm^3) comparing to LIX reagent (3 g/dm^3). Both of investigated phases have similar capacity and can be loaded up to $\sim 17 \text{ g/dm}^3 \text{ Cu}$.

A comparison of the net transfer values (Fig. 4) shows a slight advantage of Acorga M5640 over LIX 612 N-LV. As before, a decrease in copper net transfer with increasing O/A ratio can be observed.

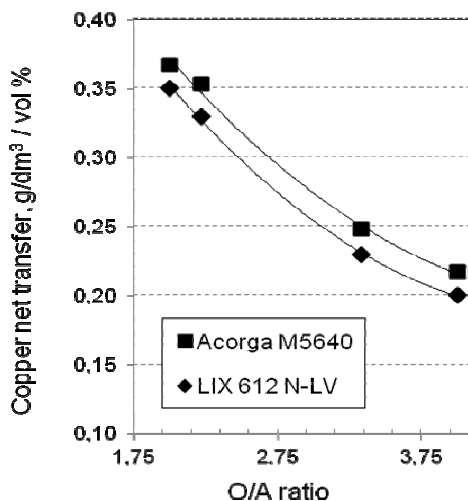


Fig. 4. Copper net transfer in organic at 30 vol % of reagent as a function of overall extraction O/A ratio, PLS II

Both extractants were further compared in terms of their extraction behavior with less concentrated and more acidified solutions. Mixed raffinate solutions after single extraction with copper concentration level of 10 g/dm^3 and $\text{pH} \sim 0.75$ were used as SX feed (marked as Raffinate I). Organic and aqueous phases were contacted at various A/O ratios. Extraction isotherms and generated McCabe-Thiele diagrams for Cognis and Cytec extractants are presented in Fig. 5. Additional comparison of SX circuit recovery vs. pH and copper net transfer values are plotted in Figs 6 and 7.

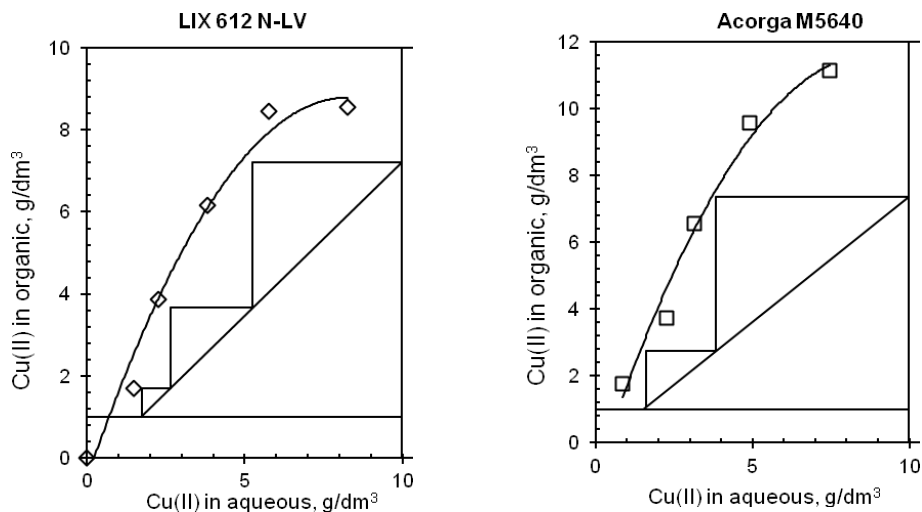


Fig. 5. The McCabe-Thiele diagram for 30vol% of LIX 612 N-LV and Acorga M5640 in Escaid 100, feed: raffinate I, pH 0.75, O/A 1.33

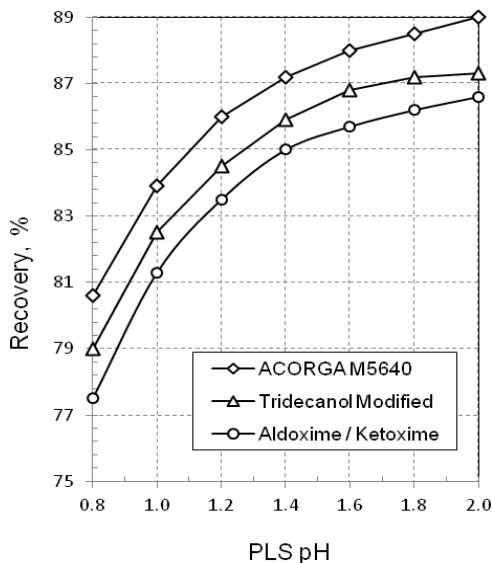


Fig. 6. SX circuit recovery comparison (30 vol % extractant, 25 g/dm³ of copper in PLS) (Moore et al., 1999)

The obtained results show that the application of Acorga provides much better copper recovery than the use of LIX reagent. The following extraction efficiencies and organic phase capacities were found: 73% and 8.5 g/dm³ for LIX, 83% and 11.1 g/dm³

for Acorga. Both experiments were performed at a small excess of organic phase ($O/A = 1.33$) and high acidity of aqueous phase. Copper recovery at the indicated level with organic phase containing LIX reagent requires three stages of extraction ending up with $1.7 \text{ g/dm}^3 \text{ Cu}$ raffinate, whereas the other reagent is able to reach lower raffinate ($1.5 \text{ g/dm}^3 \text{ Cu}$) after two extraction steps.

It is clear that Acorga M5640 ensures better copper recovery under identical conditions. This is consistent with the results presented in Fig. 6 (Moore et al.1999). Authors demonstrated that across the whole pH range, the ester modified Acorga M5640 provided the highest copper recovery of all the reagents tested, compared at the same reagent strengths.

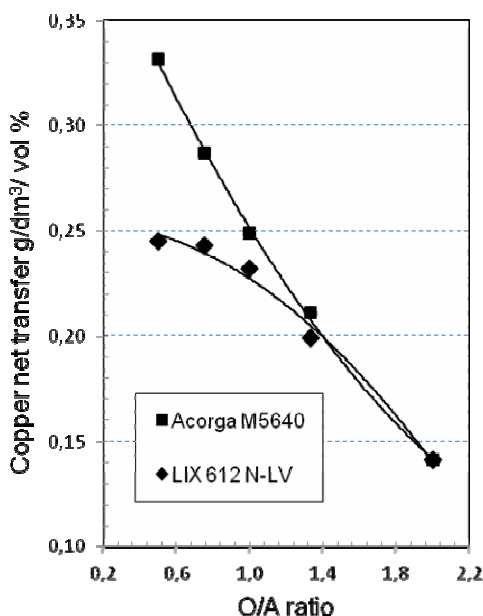


Fig. 7. Copper net transfer in organic phase at 30 vol % of reagent as a function of overall extraction O/A ratio, raffinate, pH 0.75

A graphical comparison of the copper net transfer values (Fig. 7) confirms previous observations and shows a decrease organic phase capacity with growing O/A ratio. Moreover, it reconfirms limited copper loading capacity of LIX 612 N-LV reagent.

It is also important to note the net transfer changes for reagents under different conditions (Table 2). It can be seen that the copper net transfer can be quite high (case 3, 4) or satisfactory (case 1, 2) at higher O/A ratios and lower acidity of the feed solution. In such cases reagent can achieve quite good copper recovery. However, when a reagent needs to make a comparatively high copper recovery but at higher acidity of

the feed solution, the work that reagent is doing is much poorer. It results in lower net transfer values, regardless of much beneficial O/A ratio (case 5,6).

Table 2. Summarized extraction data

	Feed g/dm ³ Cu	Reagent 30 vol%	Advance O/A	Recovery %	PLS pH	Copper net transfer g/dm ³ /vol %
1.	39.1	LIX 984 N	4.0	86.0	2.2	0.280
2.	39.1	LIX 612 N-LV	4.0	86.7	2.2	0.283
3.	26.0	LIX 612 N-LV	2.0	88.5	2.0	0.383
4.	26.0	Acorga M5640	2.0	92.3	2.0	0.400
5.	9.97	LIX 612 N-LV	1.33	82.9	0.75	0.207
6.	9.97	Acorga M5640	1.33	84.9	0.75	0.212

Considering all the results presented in this paper the investigated reagents can be ranked regarding their suitability for copper extraction from concentrated solutions. Starting from the best the order is following: Acorga M5640, LIX 612 N-LV, LIX 984N.

Conclusions

The obtained results demonstrated that investigated copper solvent extraction reagents are suitable for application to concentrated feed solutions from atmospheric or pressure leaching of copper concentrate. Among the reagent properties examined in this paper, the stronger modified aldoxime reagents (Acorga, LIX 612) was shown to be superior over non-modified salicylaldoxime/ketoxime mixture (LIX 984N). In particular, the ester modified Acorga M5640 showed advantages in recovery and copper net transfer values.

Acknowledgements

This work was carried out in the frame of HYDRO project (Polish NCBiR project contract ZBP/56/66309/IT2/10). Authors acknowledge the financial support given to this project by the NCBiR (National Center for Research and Development) under the IniTech Enterprise. We also wish to thank our various partners of the project for their contributions to the work reported in this paper.

References

- APOSTOLUK W., WALKOWIAK W., DUDA L.L., 2009, *Rola procesów rozdzielczych we współczesnej hydrometalurgii*, XII Seminarium "Metody hydrometalurgiczne a rozwój produkcji w KGHM „Polska Miedź” S.A. Lubin, 77–100.
- CHMIELEWSKI T., 2012, *Hydrometalurgia in KGHM Polska Miedz SA – Circumstances, Needs and Perspectives of Application*, *Separ. Sci. Technol.*, 47, 1264–1277.
- DREISINGER D., 2006, *Copper leaching from primary sulfides: Options for biological and chemical extraction of copper*, *Hydrometalurgy* 83, 10–20.

- FLETT D.S., 2005, *Solvent extraction in hydrometallurgy: the role of organophosphorus extractants*, J. Organometallic Chem., 690, 2426–2438.
- GUPTA C.K., MUKHERJEE T.K., 1990, *Hydrometallurgy in extraction processes*, Vol. I and II, CRC Press.
- HABASHI F., 1999, *Textbook of Hydrometallurgy*, 2nd Ed. Quebec.
- HABASHI F., 2005, *Recent Advances in the Hydrometallurgy of Copper*, Proc. Int. Copper Hydrometallurgy Workshop “Hydrocoper 2005” (Menacho J.M., Casas de Prada J.M., Eds.), Santiago, Chile, 43–55.
- HABASHI F., 2007, *Abandoned but not forgotten – the recent history of copper hydrometallurgy*, The John Durtizac Symposium on Copper Hydrometallurgy, Proceedings 6th International Copper-Cobre International Conference, August 3–20, 2007, Toronto, Canada, vol. IV, Met. Soc.
- HYVÄRINEN O., HÄMÄLÄINEN M., 2005, *HydroCopperTM – a new technology producing copper directly from concentrate*, Hydrometallurgy, 77, 61–65.
- JANSEN M., TAYLOR A., 2000, *Key elements in the selection of sulphide leach processes for copper concentrate leaching*, Alta Cu 2000, August 2000, Int. Proj. Dev. Serv. Pty Ltd.,
- KORDOSKY G.A., 2002, *Copper solvent extraction for concentrate leach solutions*, (Paper presented at ALTA Conference 2002), May 2002.
- MARSDEN J.O., 2007e, *Sulphate-based flowsheet options for hydrometallurgical treatment of copper sulphide concentrates*, The John Durtizac Symposium on Copper Hydrometallurgy, Proceedings 6th International Copper-Cobre Conference, August 25–30, 2007, Toronto, Canada, vol. IV, Met. Soc., 77–100.
- MARSDEN J.O., WILMOT J.C., 2007a, *Medium-temperature pressure leaching of copper concentrates – Part I: Chemistry and initial process development*, Min. Metall. Processing, 24(4) 193–204.
- MARSDEN J.O., WILMOT J.C., 2007b, *Medium-temperature pressure leaching of copper concentrates – Part II: Development of direct electrowinning and acid-autogenous process*, Min. Metall. Processing, 24(4) 205–217.
- MARSDEN J.O., WILMOT J.C., 2007c, *Medium-temperature pressure leaching of copper concentrates – Part III: Commercial demonstration at Bagdad, Arizona*, Min. Metall. Processing, 24(4) 218–225.
- MARSDEN J.O., WILMOT J.C., 2007d, *Medium-temperature pressure leaching of copper concentrates – Part IV: Application at Morenci, Arizona*, Min. Metall. Processing, 24(4) 226–236.
- MOLNAR R.E., VERBAAN N., 2003, *Extraction of copper at elevated feed concentrations*, materials presented at Hydrometallurgy 2003 – Fifth International Conference, Vol. 2: Electrometallurgy and Environmental Hydrometallurgy.
- MOORE T., TOWNSON B., MAES CH., TINKLER O., 1999, *Solvent Extraction of Copper from Concentrated Feed Solutions*, paper presented at ALTA Copper 1999.
- PEACEY J.I., GUO X.J., ROBLES E., 2003, *Copper Hydrometallurgy – Current Status, Preliminary economics, Future Direction and Positioning versus Smelting*, Copper 2003 – Cobre 2003, vol. VI, (Book 1) Santiago – Chile (Riveros P.A., Dixon D., Dreisinger D., Eds.), 205–222.
- RAMACHADRAN V., LAKSMANAN V.I., KONDOS P.D., 2007, *Hydrometallurgy of copper sulphide concentrate*, The John Durtizac Symposium on Copper Hydrometallurgy, Proceedings 6th International Copper-Cobre Conference, August 25–30, 2007, Toronto, Canada, vol. IV, Met. Soc., 101–128.
- RITCEY G.M., 2006, *Solvent Extraction in Hydrometallurgy: Principles and Application to Process Metallurgy*, 2nd Ed., Ottawa, Canada.
- SZYMANOWSKI J., 1993, *Hydroxyoximes and Copper Hydrometallurgy*, CRC Press, Boca Raton, FL.

Received May 23, 2012; reviewed; accepted August 10, 2012

ADSORPTIVE REMOVAL OF COLOUR PIGMENT FROM PALM OIL USING ACID ACTIVATED NTEJE CLAY. KINETICS, EQUILIBRIUM AND THERMODYNAMICS

Regina O. AJEMBA, Okechukwu D. ONUKWULI

Department of Chemical Engineering, Nnamdi Azikiwe University, P. M. B. 5025, Awka, Anambra, Nigeria,
ginaajemba@rocketmail.com

Abstract: The kinetics of colour pigment removal from palm oil using acid activated clay from Nteje has been investigated. To determine the equilibrium adsorption capacity, the effects of temperature, contact time, adsorbent dosage and particle size were studied. The experimental adsorption data were analyzed using pseudo-first order, pseudo-second order, and Elovich kinetic models. The pseudo-second order model fitted very well to the kinetic experimental data. Equilibrium isotherms were analyzed by Langmuir and Freundlich adsorption models. The data was in line with the Freundlich isotherm indicating a monolayer adsorption. The activation energy was calculated as 12 kJ/mol, and other thermodynamic parameters were determined as $\Delta S^\circ = 0.063$ J/mol, $\Delta H^\circ = -34.994$ J/mol, and $\Delta G^\circ = -58.606$ kJ/mol. These values indicate that the adsorption of colour pigment from palm oil onto acid activated clay was exothermic and can be attributed to physico-chemical adsorption process.

Keywords: *adsorption, kinetics, isotherm, activation, colour pigment, palm oil, bleaching*

Introduction

Acid activated clays (bentonite) have been employed as catalysts for a number of reactions of industrial interests (Didi, et al., 2009; Foletto et al., 2003; Breen et al., 1997; Mokaya et al., 1995). Activated clays have also been used in the paper industry, in the chemical industry, for environmental protection and in the foodstuff industry, for sulphur production, forest and water conservation (O'Driscoll, 1988), as well as bleaching of vegetable oils (Kirali and Lacin, 2006; Christidis et al., 1997; Makhoukhi et al., 2009; Selvaraji et al., 2004; Bakhtyar et al., 2011). Bleaching involves solely the removal of variety of impurities like fatty acids, gums, trace metals, phosphatides etc., followed by decolourization. Bentonites are found in nature abundantly. However, most of them should undergo appropriate physical or chemical treatments such as acid activation, ion exchange and heating in order to promote their surface properties

(Rossi et al., 2003; Rozic et al., 2010; Foletto et al., 2011; James et al., 2008; Taha et al., 2011). Acid activation of clays is one of the most important processes that have been performed to achieve structural modifications in the clays for edible oil bleaching. Activated clays show a much higher bleaching capacity when compared to natural clays. During acid activation, initially interlayer cations are replaced with H^+ ions followed by partial destruction of aluminum octahedral sheets with subsequent dissolution of structural cations. The desired changes in the physicochemical properties of clay occurring as a result of acid activation depend considerably on the condition of acid activation such as acid concentration and the duration and temperature of the activation process (Motlagh et al., 2008, 2011).

There are few researches on the kinetics of the bleaching process. Topallar (1998), studied the kinetics of sunflower seed oil bleaching and proposed a rate formula of $\log(A/A_0) = -k\sqrt{t}$, according to absorbance measurement. Nwankwere et al. (2012) investigated the kinetics of B-carotene removal from palm oil using unmodified natural clay, and they concluded that the adsorption followed the zero order kinetic equation. Al-Zahrani et al. (2000), investigated the kinetics of sulphuric acid activation of Saudi bentonite and found out that it followed the zero order kinetic equation.

In this work, the main objective was to investigate the equilibrium and kinetic parameters of the application of acid activated Nteje clay in the bleaching of palm oil.

Materials and methods

The clay used in this study was mined at Nteje (N: 6° 16' 00"; E: 6° 55' 00"; A: 118 m) in Aniocha local government area, while the palm oil was obtained from a local palm oil mill in Isuofia (N: 6° 1' 60"; E: 7° 2' 60"; A: 361 m) in Aguata local government area, both in Anambra state of Nigeria. All the chemicals used were analytical grade reagents.

Clay preparation and activation

The mined clay was sun-dried for 24 hours and grinded to smaller particles using mortar and pestle. The ground samples were sieved to remove impurities and then oven dried at 105°C. The samples were then put in contact with hydrochloric acid in a 250 cm³ flask placed in a regulated water bath. The flask was heated while continuously being stirred. To study the effect of activation variables, the experiment was repeated at various concentrations (0.5–5 mol/dm³), temperatures (50–120°C), for various contact times (2–6 h). At the completion of the heating time, the slurry was removed from the bath and allowed to cool. After the cooling, the slurry was filtered via a Buchner funnel and the clay residue was washed several times with distilled water, followed by filtration until the filtrate was neutral to pH indicator paper. The prepared wet sample was then dried in an oven at 120°C over night. The lumps of the prepared clays were crushed and sieved again into various particle sizes ranging from 0.045 to 0.408 mm

and stored for further use in the bleaching process. The activated clay samples were labeled as follows: NT0.5, NT1, NT2, NT3, NT4 and NT5, where the numbers denote the acid concentration. The activated clays were then characterized.

Adsorption Experiment

A 100 g sample of the refined unbleached palm oil was measured out into a 250 cm³ conical flask and heated on a magnetically-stirred hot plate to 90°C while stirring continuously. A 2 g sample of the sized activated clay was then added to the heated oil and stirred continuously via a magnetic stirrer carefully inserted into the beaker. The whole mixture was heated to a temperature of 130°C for 45 minutes. At the completion of the time, the hot oil and clay mixture was filtered under gravity using Whatman filter paper No. 42 (15 cm diameter), before measuring the absorbance. The bleaching/adsorption efficiency of the activated clay samples was then determined by measuring the colour of the bleached oil using UV-VIS Spectrophotometer (Model WFJ 525) at 450 nm. The bleaching efficiency is defined by the following expression in this study:

$$BE(\%) = \frac{A_{\text{unbleached}} - A_{\text{bleached}}}{A_{\text{unbleached}}} \cdot 100 \quad (1)$$

where $A_{\text{unbleached}}$ and A_{bleached} are absorbencies of unbleached and bleached palm oil, respectively, at 450 nm, BE is bleaching efficiency.

To study the effect of process variables on the bleaching efficiency of the activated clay samples the above experimental procedure was repeated at different adsorbent dosage (0.5, 1, 1.5, 2.0, 2.5, 3.0, 3.5, and 4.0 g); reaction temperatures (30, 70, 80, 100, and 120°C); particle size (0.045, 0.075, 0.106, 0.212, and 0.408 mm) and reaction time (20, 40, 60, 80, 100, 120, and 150 min). The effect of activation parameters on the bleaching efficiency of the clay samples was investigated by using the samples activated with different acid concentrations bleach palm oil.

Results and Discussion

Physical characterization

The results of the physical characterization of the raw and activated clays are summarized in Table 1. The results show that the acid activation of the clay caused some modifications in the structure of the clays. With an increase in concentration of hydrochloric acid, the activated samples showed a gradual increase in surface area until treatment with 3 mol/dm³ HCl. In treatment with 4 mol/dm³ HCl, a decrease of surface area was observed in comparison with the surface area of sample treated with 3 mol/dm³ HCl. The increase in the surface area from natural to activated samples is related to the elimination of the exchangeable cations, de-lamination of clays, and the generation of micro-porosity during the activation process (Dias et al., 2003). The

decrease observed at higher acid concentrations could be explained by the process of “passivation” (Pesquera et al., 1992). The octahedral sheet destruction passes the cations into the solution, while the silica generated by the tetrahedral sheet remains in the solids, due to its insolubility. Pesquera et al. (1992) suggest that this free silica generated by the initial destruction of the tetrahedral sheet, is polymerized by the effect of such high acid concentrations and is deposited on the undestroyed silicate fractions, protecting it from further attack and thereby resulting to a decreased surface area. The CEC values of the samples also displayed similar behaviour. With the increase of concentration of HCl, the samples showed a gradual decrease in CEC until treatment with 3 mol/dm³ HCl. In treatment with 4 mol/dm³ HCl, an increase of the CEC was observed in comparison with the CEC of sample treated with 3 mol/dm³ HCl and this could also be explained by the process of passivation.

Table 1. Physical properties of raw and activated clay

Properties	Clay type					
	NT0	NT0.5	NT1	NT3	NT4	NT5
Surface area (m ² /g)	88.4	127.6	186.7	296.3	207.5	199.5
Bulk density (kg/m ³)	1058.9	987.5	964	721.2	853.6	877.3
Oil retention (%)	22	27.4	33.6	54.5	41.8	38.7
Acidity	0.01	0.05	0.09	0.15	0.11	0.08
pH	8.1	6.8	4.4	2.8	3.9	4.1
Cation Exchange Capacity CEC (meg/100g)	89	80	71	50	64	67

Effect of time and acid concentration on the bleaching efficiency

To study the effect of time on the bleaching efficiency of the activated clay samples, the adsorption test was performed at different times ranging from 20–150 minutes. It was observed that adsorption efficiency of the samples increased as time increased

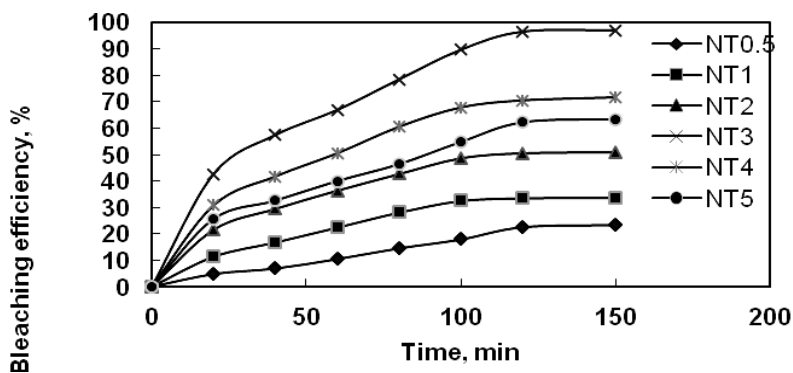


Fig. 1. Effect of bleaching time and acid concentration on bleaching efficiency

with the sample activated with 3 mol/dm^3 HCl (NT3) having the highest efficiency as shown in Fig. 1. Also, the figure shows the effect of varying the concentration of the acid used. It shows that bleaching efficiency increases with increase in acid concentration up to 3 mol/dm^3 above which the efficiency dropped drastically as a result of destruction of the clay structure by the excess acid.

Effect of temperature on bleaching efficiency

Figure 2 shows that the bleaching efficiency is favoured by an increase in reaction temperature. From the figure it is obvious that bleaching does not proceed to any appreciable degree at low temperatures. But as the temperature is increased from 30°C to 120°C , the bleaching efficiency increased showing that temperature promotes access to further adsorption sites in the adsorbent. The bleaching efficiency increased with reaction time at high temperature until it reaches a maximum, then it starts to decrease with increasing reaction time.

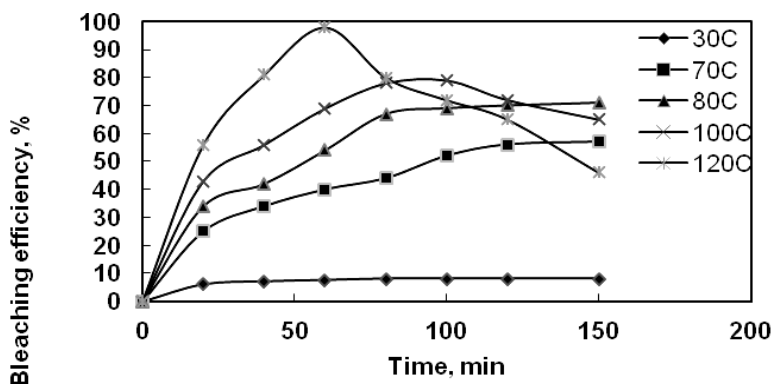


Fig. 2. Variation of bleaching efficiency with time at different temperatures

Effect of adsorbent dosage

Figure 3 represents the plot of bleaching efficiency versus adsorbent dosage. The clay dosage was varied from 0.5 to 4 g. It was observed that increasing the clay dosage increased the bleaching efficiency. The results clearly indicate that the bleaching efficiency increases to an optimum value at adsorbent dosage of 1 g above which further increase in adsorbent dosage has no significant effect on it, but the value remains constant. This could be explained by the fact that adsorption equilibrium has been reached between the adsorbent/oil mixtures, thereby, preventing further pigment removal by the excess adsorbent dosage.

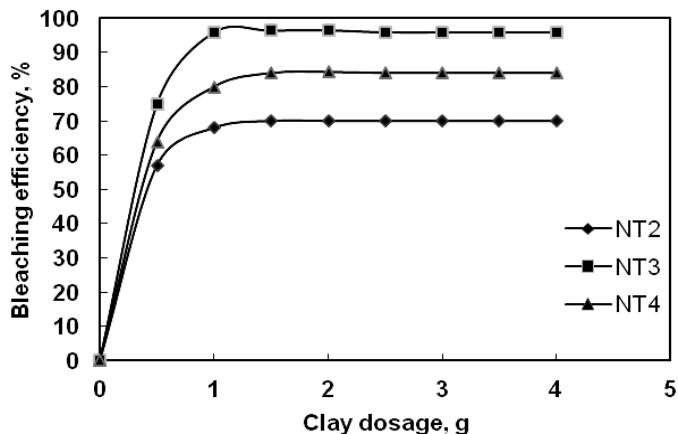


Fig. 3. Variation of bleaching efficiency with clay dosage

Effect of particle size of the adsorbent

To study the effect of particle size on the bleaching efficiency of the adsorbent, the experiment was performed at different particle sizes of 0.408, 0.212, 0.106, 0.075, and 0.045 mm. The results are shown in Fig. 4. The figure shows that the bleaching efficiency of the activated clay was increased as the particle size decreased; this is as a result of increased surface area, pore volume, and pore size of the particles. Reduced particle size creates more adsorption sites/cation exchange sites that are exposed to the sorbate. But, this positive effect of particle size reduction resulted to difficulty filtration because the oil retention of the adsorbent increased.

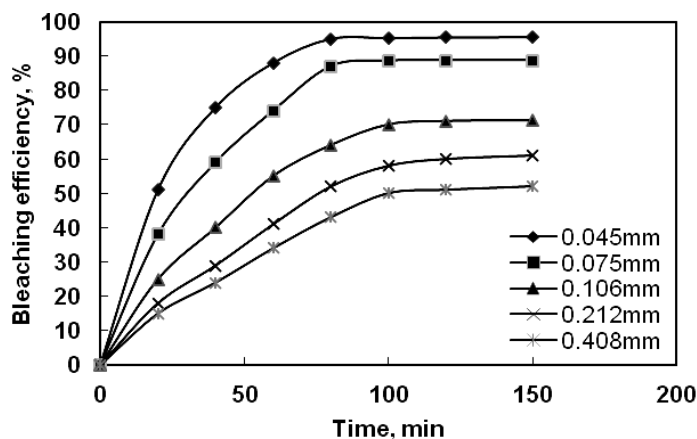


Fig. 4. Variation of bleaching efficiency with time at different particle sizes

Kinetics of bleaching

The effect of temperature on the bleaching efficiency of Nteje clay activated with 3 mol/dm³ hydrochloric acid as reflected in Fig. 2, were tested with several kinetic models in order to describe the adsorptive interaction between the colour pigment and the activated clay. The kinetic models used in the analysis of the data are as follows: Pseudo-first order, pseudo-second order, and Elovich kinetic equations. The respective linear forms of the equations are as given below:

$$\log (q_e - q_t) = \log q_e - k_1 t \quad (\text{pseudo-first order model}) \quad (2)$$

$$\frac{1}{q_t} = \frac{1}{k_2 q_e^2} + \frac{t}{q_e} \quad (\text{pseudo-second order model}) \quad (3)$$

$$q_t = \frac{1}{\beta} \ln(\alpha\beta) + \frac{1}{\beta} \ln t \quad (\text{Elovich model}). \quad (4)$$

Table 2. The kinetic parameters evaluated for colour pigment adsorption onto activated Nteje clay

Kinetic models	Parameters	Temperature (°C)				
		30	70	80	100	120
Pseudo first order	K_1	$1.16 \cdot 10^{-2}$	$1.38 \cdot 10^{-2}$	$1.61 \cdot 10^{-2}$	$1.84 \cdot 10^{-2}$	$1.15 \cdot 10^{-2}$
	q_e (mg/g)	6.98	7.23	8.93	8.67	7.53
	R^2	0.984	0.985	0.960	0.983	0.988
Pseudo second order	K_2	$1.246 \cdot 10^{-3}$	$1.947 \cdot 10^{-3}$	$3.300 \cdot 10^{-3}$	$2.600 \cdot 10^{-3}$	$2.353 \cdot 10^{-3}$
	q_e (mg/g)	8.31	9.35	10.75	11.24	9.09
	R^2	0.999	0.999	0.997	0.998	0.997
Elovich	α (mg/g min)	0.3146	0.4235	0.8195	0.7278	0.4565
	β (mg/g min)	0.5842	0.5504	0.4165	0.4083	0.5339
	R^2	0.987	0.977	0.990	0.991	0.979

The associated kinetic parameters have been evaluated from the slopes and intercepts of the respective linear plots of the kinetic equations, and the values are shown in Table 2. Comparison of the analyzed data based on the linear regression coefficient (R^2) values as shown in the table, showed that the experimental data is best described by the pseudo-second order equation (Eq. 3), which has the most linear fit with correlation coefficient $R^2 > 0.997$. Hence, the plot of the linear form of the pseudo-second order kinetic equation is shown in Fig. 5.

Adsorption isotherm

It was observed that as the temperature increased the amount adsorbed on the surface of the adsorbent increased. This change occurs as a result of increase in kinetic energy of the colour pigment particles, which increases the frequency of collisions between

the adsorbent and the particles and thus enhances adsorption on the surface of the adsorbent.

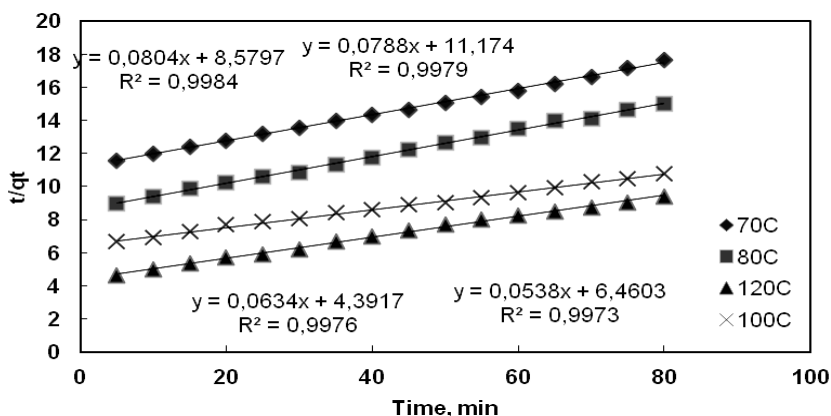


Fig. 5. Pseudo-second order kinetic fit for colour pigment removal from palm oil at different temperatures

Two main types of adsorption may usually be distinguished on surfaces. In the first type, the forces are of a physical nature and the adsorption is relatively weak. The forces in this type of adsorption are known as van der Waals forces and this type of adsorption is called van der Waals adsorption, physical adsorption or physisorption. The heat evolved during van der Waals adsorption is usually small, less than 20 kJ/mol. In the second type of adsorption, first considered in 1916 by Langmuir, the adsorbed molecules are held to the surface by covalent forces of the same general type as those occurring between bound atoms in molecules. The heat evolved during this type of adsorption, known as chemisorption, is usually comparable to that evolved during chemical bonding, namely 300–500 kJ/mol.

Langmuir considered adsorption to distribute molecules over the surface of the adsorbent in the form of a uni-molecular layer and for the dynamic equilibrium between adsorbed and free molecules, he proposed the following relation:

$$\frac{P}{X/m} = \frac{1}{a} + \frac{a}{b} P \quad (5)$$

where P is equilibrium pressure for a given amount of substance adsorbed, X is the amount of substance adsorbed, m is the amount of adsorbent, a and b are constants.

The mathematical expression relating adsorption to residual solute concentration was developed by Freundlich:

$$\frac{X}{m} = KC^n \tag{6}$$

where C is the amount of residual substance, and K and n are constants.

Since the absorbance measurements are taken in all experiments for the bleaching process, the relative amount of pigment adsorbed (X) and the residual relative amount at equilibrium (X_e) are obtained from Eqs 5 and 6:

$$X = \frac{A_0 - A_t}{A_0} \tag{7}$$

$$X_e = \frac{A_t}{A_0} = 1 - X \tag{8}$$

where A_0 is the absorbance of unbleached (crude) palm oil and A_t is the absorbance of bleached oil at time t . Thus, by means of Eqs 7 and 8, by writing X_e instead of equilibrium pressure P and the residual substance C , Eqs 5 and 6 are rearranged as follows (Topallar, 1998):

$$\frac{X_e}{X/m} = \frac{1}{a} + \frac{a}{b} X_e \tag{9}$$

$$\log \frac{X}{m} = \log K + n \log X_e . \tag{10}$$

To evaluate the nature of adsorption, the experimental data of Fig. 2, was analyzed by the established isotherm equations viz; Langmuir and Freundlich adsorption models.

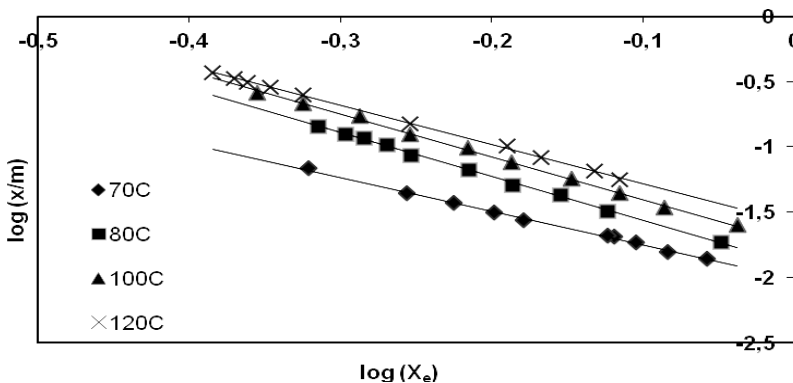


Fig. 6. Freundlich isotherm plot using NT3 for bleaching

Linear plots (Freundlich) obtained are shown in Fig. 6. The Freundlich and Langmuir model parameters and the statistical fits of the adsorption data to these models as calculated from the respective plots are presented in Table 3. It was observed that the Freundlich model adequately described the adsorption data with regression coefficient values greater than 0.997.

The values of the constant K_f increased with increasing temperature, indicating increasing access to adsorption sites.

Table 3. The isotherm parameters obtained from linear analysis of colour pigment adsorption onto Nteje clay activated with 3 mol/dm³ HCl

Isotherm models	Parameters	Temperature (°C)			
		70	80	100	120
Freundlich	K_f	$9.886 \cdot 10^{-3}$	$12.560 \cdot 10^{-3}$	$18.664 \cdot 10^{-3}$	$26.002 \cdot 10^{-3}$
	n	-0.3894	-0.2974	-0.3054	-0.3330
	R^2	0.997	0.998	0.998	0.999
Langmuir	K_a	-0.0635	-0.0318	-0.0366	-0.0437
	q_m	-5.1636	-2.8688	-2.8551	-2.8985
	R^2	0.985	0.986	0.980	0.989

Adsorption thermodynamics

Thermodynamic considerations of an adsorption process are necessary to conclude whether the process is spontaneous or not. The Gibbs free energy change, ΔG° , is an indication of spontaneity of a chemical reaction and therefore is an important criterion for spontaneity. Both energy and entropy factors must be considered in order to determine the Gibbs free energy of the process. Reactions occur spontaneously at a given temperature if ΔG° is a negative quantity. The free energy of an adsorption, considering the adsorption equilibrium constant K_f is given by the following equation:

$$\Delta G^\circ = -RT \ln K_f \quad (11)$$

where ΔG° is the standard free energy change (J/mol), R the universal gas constant (8.314 J/mol K), and T is the absolute temperature (K). Considering the relationship between ΔG° and K_f , change in equilibrium constant with temperature can be obtained in the differential form, and

$$-RT \ln K_f = \Delta H^\circ - T\Delta S^\circ \quad (12)$$

The above equation can then be written in the following forms

$$\Delta G^\circ = \Delta H^\circ - T\Delta S^\circ \quad (13)$$

or

$$\ln K_f = \frac{\Delta S^\circ}{R} - \frac{\Delta H^\circ}{RT} \quad (14)$$

The values of ΔH° and ΔS° are calculated from the slope and intercept of the plot of $\ln K_f$ versus $1/T$ (not shown). The values of the thermodynamic parameters are shown in Table 4. As can be seen from the table, the values of the Gibbs free energy change of adsorption, ΔG° , are all negative and show a decrease in the negative value as the temperature increases. According to Saha and Chowdhury (2009), a decrease in the negative value of ΔG° with an increase in temperature indicates that the adsorption process is more favourable at higher temperatures. This is possible because the mobility of adsorbate ions/molecules in the solution increases with increase in temperature and the affinity of adsorbate on the adsorbent is higher at high temperatures. This postulation was confirmed in this study as can be seen in the effect of temperature on the adsorption efficiency. As the temperature of the reaction was increased, the adsorption of the colour pigments onto the adsorbent increased. The values of the enthalpy, ΔH° , and entropy, ΔS° , as calculated from the plot of $\ln k_f$ versus $1/T$, are also presented in Table 4. The value of the enthalpy is negative and this implies that the adsorption process of colour pigments from palm oil onto locally activated clay is exothermic. In an exothermic process, the total energy absorbed in bond breaking is less than the total energy released in bond making between adsorbate and adsorbent, resulting in the release of extra energy in the form of heat. The magnitude of ΔH° gives an idea about the type of sorption. The heat evolved during physical adsorption falls in the range of 2.1–20.9 kJ/mol while that evolved during chemical sorption is in the range of 80–200 kJ/mol. Therefore, as seen from Table 4, it is deduced that the adsorption of colour pigments onto acid activated Nteje clay can be attributed to a physico-chemical adsorption process rather than a pure physical or chemical adsorption process (Saha and Chowdhury, 2010). The value of ΔS° as presented in Table 4 is positive and this reflects the affinity of the adsorbent towards the adsorbate species. A positive value of ΔS° suggests increased randomness at the solid/solution interface with some structural changes in the adsorbate and the adsorbent. The adsorbed solvent molecules, which are displaced by the adsorbate species, gain more translational entropy than is lost by the adsorbate ions/molecules, thus allowing for the prevalence of randomness in the system.

Table 4. Adsorption thermodynamic parameters

Temp. (K)	$\ln K_f$	ΔG° (kJ/mol)	ΔH° (J/mol)	ΔS° (J/mol)
343	-4.61664	-56.707	-34.994	0.063
353	-4.37724	-57.339		
373	-3.98116	-57.973		
393	-3.64958	-58.606		

Conclusion

The kinetic and equilibrium studies of the adsorptive purification of palm oil using acid activated Nteje clay have been successfully investigated. The adsorption of colour pigments into the clay surfaces increased with temperature, clay dosage, contact time, and decreasing particle size. The kinetic data agree very well with the pseudo-second order equation, and the rate is film diffusion controlled. The linear isotherm analyses indicated that the equilibrium data describe the Freundlich isotherm model very well. The thermodynamic parameters evaluated reveal the spontaneous and exothermic nature of colour pigment adsorption onto acid activated Nteje clay, and the adsorption takes place with increase of entropy.

References

- AL-ZAHRANI A.A., AL-SHAHRANI S.S., AL-TAWIL Y.A., 2000, *Study on the activation of Saudi bentonite, part II: characterization of the produced active clay and its test as an adsorbing agent*, J. King Saud Univ., 13, Eng. Sci. (2), 193–203.
- BAKHTYAR K.A., MUHAMMAD A.A., KARIM J.J., 2011, *Acid activation and bleaching capacity of some local clays for decolourizing used oils*, Asian J. Chem., 23 (6).
- BREEN C., ZAHOOOR F.D., MADEJOVA J., KOMADEL P., 1997, *Characterization and catalytic activity of acid-treated, size-fractionated smectites*, J. Phys. Chem. B, 27, 5324–5331.
- CHRISTIDIS G.E., SCOTT P.W., DUNHAM A.C., 1997, *Acid activation and bleaching capacity of bentonite from the Islands of Milos and Chios*, Aegean, Greece, Appl. Clay Sci., 12, 329–347.
- DIAS M. I., SUAREZ BARRIOS M., PRATES S., MARTIN POZAS J.M., 2003, *Characterization and acid activation of Portuguese special clay*, Appl. Clay Sci., 18, 537–549.
- DIDI M., MAKHOUKHI B., AZZOUZ A., VILLEMIN D., 2009, *Colza oil bleaching through optimized acid activation of bentonite: A comparative study*, Appl. Clay Sci., 42, 336–344.
- FOLETTTO E.L., COLAZZO G.C., VOLZONE C., PORTO L.M., 2011, *Sunflower oil bleaching by adsorption onto acid-activated bentonite*, Brazilian J. Chem. Eng., 28 (1), 169–174.
- FOLETTTO E.L., VOLZONE C., PORTO L.M., 2003, *Performance of an Argentinian acid-activated bentonite in the bleaching of soybean oil*, Brazilian J. Chem. Eng., 20, 139–145.
- JAMES O.O., MESUBI M.A., ADEKOLA F.A., ODEBUNMI E.O., ADEKEYE J.I.D., BALE R.B., 2008, *Bleaching performance of a Nigerian (Yola) bentonite*, Lat. Am. Appl. Res., 38, 45–49.
- KIRALI E., LACIN O., 2006, *Statistical modeling of acid activation on cotton oil bleaching by Turkish bentonite*, J. Food Eng., 75, 137–141.
- MAKHOUKHI B., DIDI M. A., VILLEMIN D., AZZOUZ A., 2009, *Acid activation of bentonite for use as a vegetable oil bleaching agent*, Grasasy Aceites, 60 (4), 343–349.
- MOKAYA R., JONES W., DAVIES M., WHITTLE M., 1993, *Chlorophyll adsorption by alumina pillared acid-activated clay*, J. American Oil Chem. Soc., 70, 241–244.
- MOTLAGH M.M., RIGI Z.A., YUZBASHI A.A., 2008, *To evaluate an acid activated bentonite from Khorasan (Iran) for use as bleaching clay*, IUST Int. J. Eng. Sci., 19 (5-2), 83–87.
- MOTLAGH M.M., YOUZBASHI A.A., RIGI Z.A., 2001, *Effect of acid activation on structural and bleaching properties of bentonite*, Iranian J. Mat. Sci. Eng., 8 (4), 50–56.
- NWANKWERE E.T., NWADIOGBU J.O., YILLENG M.T., EZE K.A., 2012, *Kinetic investigation of the adsorptive removal of B-carotene pigments from palm oil using unmodified natural clay*, Adv. Appl. Sci. Res., 3 (2), 1122–1125.

- O'DRISCOLL M., 1988, *Bentonite: over capacity in need of markets*, Industrial Minerals, 250, 43–67.
- PESQUERA C., GONZALEZ F., BENITO I., BLANCO C., MENDIOROZ S., PAJARES J., 1992, *Passivation of a montmorillonite by the silica created in acid activation*, J. Mat. Chem., 2(9), 907–911.
- ROSSI M., GIANAZZA M., ALAMPRESE C., STANGA F., 2003, *The role of bleaching clays and synthetic silica in palm oil physical refining*, Food Chemistry, 82, 291–296.
- ROZIC L., NOVAKOVIC T., PETROVIC S., 2010, *Modeling and optimization process parameters of acid activation of bentonite by response surface methodology*, Appl. Clay Sci., 48, 154–158.
- SAHA P., CHOWDHURY S., 2010, *Insight into adsorption thermodynamics*, Desalination, 250, 349–363.
- SELVARAJ R., YOUNGHUN K., CHEOL K. J., KYUNGHEE C., JONGHEOP Y., 2004, *Batch adsorptive removal of copper ions in aqueous solutions by ion exchange resins: 1200H and IRN97H*, Korean J. Chem. Eng., 21 (1), 187–194.
- TAHA K.K., SULEIMAN T.M., MUSA M.A., 2011, *Performance of Sudanese activated bentonite in bleaching cotton seed oil*, J. Bangladesh Chem. Soc., 24 (2), 191–201.
- TOPALLAR H., 1998, *Bleaching kinetics of sunflower seed oil*, J. American Oil Chem. Soc., 75 (4), 531–533.